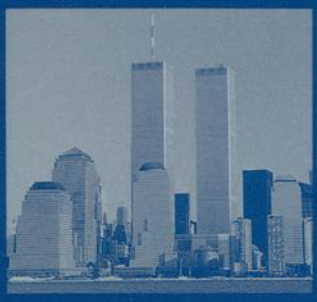


Corrosion Forms & Control for Infrastructure

Victor Chaker, editor

ASTM STP 1137



STP 1137

Corrosion Forms and Control for Infrastructure

Victor Chaker, editor

ASTM Publication Code Number (PCN)
04-011370-27

ASTM
1916 Race Street
Philadelphia, PA 19103

Library of Congress Cataloging-in-Publication Data

Corrosion forms and control for infrastructure / Victor Chaker, editor.
(STP ; 1137)
"ASTM publication code number (PCN) 04-011370-27."
"Papers presented at the symposium held in San Diego, CA on 3-4 November 1991"--Foreword.
Includes bibliographical references and index.
ISBN 0-8031-1432-X
1. Reinforcing bars--Corrosion--Congresses. 2. Reinforced concrete--Corrosion--Congresses. 3. Corrosion and anti-corrosives--Congresses. I. Chaker, Victor. II. Series: ASTM special technical publication ; 1137.
TA445.5.C673 1992
620.1'723--dc20 92-35015
CIP

Photocopy Rights

Peer Review Policy

Each paper published in this volume was evaluated by three peer reviewers. The authors addressed all of the reviewers' comments to the satisfaction of both the technical editor(s) and the ASTM Committee on Publications.

The quality of the papers in this publication reflects not only the obvious efforts of the authors and the technical editor(s), but also the work of these peer reviewers. The ASTM Committee on Publications acknowledge with appreciation their dedication and contribution to time and effort on behalf of ASTM.

Printed in Ann Arbor, MI
October 1992

Foreword

This publication, *Corrosion Forms and Control for Infrastructure,* contains papers presented at the symposium held in San Diego, CA on 3-4 Nov., 1991. The symposium was sponsored by ASTM Committee G-1 on Corrosion of Metals, Subcommittee G1.10 on Corrosion in Soils, and G1.14 on Corrosion of Reinforcing Steel. V. Chaker, Port Authority of NY and NJ in New York, NY was the Symposium Chairman. Symposium session chairmen were N.S. Berke of W.R. Grace and Co. in Cambridge, MA and E. Escalante of the National Institute of Standards and Technology (NIST) in Gaithersburg, MD.

About the Cover

The art work is by Melanie Wilson-Ligh of the Port Authority of NY and NJ, New York, NY.

The design concept shows that by using available technology, corrosion of the infrastructure can be controlled and that the life expectancy of both the existing and new infrastructure can be extended indefinitely.

The bottom pictures depict the corrosion impact on infrastructure. The middle pictures represent the state-of-the-art in sensors and computers to help control the corrosion of the infrastructure. The top pictures represent well-maintained infrastructures.

Contents

Overview

The symposium, Corrosion Forms and Control for Infrastructure was organized to gather the state-of-the-art information in several fields directly related to the corrosion of infrastructure. The accelerated rate of deterioration of this national asset is well recognized. Since the cost of its replacement is prohibitive, its maintenance and the extension of it's life expectancy are mandatory. To achieve this goal, new life prediction tools are needed, sensors for testing and monitoring must be developed, and artificial intelligence will have to be used for speed and accuracy.

The papers presented at the symposium and included in this volume met their purpose. The papers covered most of the topics targeted and publicized in the Call For Papers. The topics covered areas such as highway and bridge deterioration, numercial analysis, atmospheric corrosion, electrochemical impedance applications, stray current control, innovative solutions for pipes, corrosion of rebar in concrete, life cycle analysis, sensors for monitoring infrastructure corrosion, and corrosion forms in transportation infrastructure.

This book is useful to both the practicing engineer and the scientists, since it covers numerous practical experiences and applications as well as new concepts for sensors, tools, and computerized techniques. It offers facts and figures for modes of deterioration as well as new solutions for extending the life expectancy of structures. In addition, it gives innovative applications of existing technology to predict and control corrosion of many structures. This book will serve the engineering and scientific community in promoting the use of innovative successful techniques for solving some of the corrosion problems of infrastructure. It will also stimulate the manufacturing community to take some risks in developing needed tools for this important field.

This publication deals with the current problems facing the engineering community, with all its daring challenges. It contains new solutions for current problems and pioneer methodology to avoid future problems. In summary, it could be conceived as the link between the past, present, and future of corrosion control of infrastructure.

Acknowledgment

The Symposium Chairmen, the Officers, and Members of Committee G-1 on Corrosion of Metals, express their appreciation for the contributions of the authors, the reviewers, and symposium participants. A special acknowledgment of appreciation for the efforts of the ASTM staff in the development, follow up, and delivery of this special technical publication (STP). Some editing was done courtesy of Joan Regen of The Port Authority of NY and NJ, New York, NY.

Victor Chaker, P.E.
The Port Authority Of NY and NJ, New York, NY; symposium chairman and editor.

E.J. Fasullo[1]

INFRASTRUCTURE: THE BATTLEFIELD OF CORROSION

REFERENCE: E.J.Fasullo, "Infrastructure: The Battlefield Of Corrosion", Corrosion Forms and Control For Infrastructure, ASTM STP 1137, Victor Chaker, Ed., American Society for Testing and Materials, Philadelphia,1992.

ABSTRACT: Our nation's decaying infrastructure and its associated cost have put the engineering community on the alert. All responsible parties must cooperate to save and extend the life expectancy of these vital structures. Innovative ideas for the accurate prediction and determination of the condition of the various structures is needed badly. New testing techniques that use state-of-the-art, computerized equipment need to be developed.
Time is running out. We can no longer postpone the maintenance of our infrastructure. Thus, new financial ways and means have to be developed to pay the cost. The public and private sectors have to join forces to get the job done quickly and at an affordable cost.Our educational institutions also have to take a very active role to educate future generations and engrave in their minds the importance of preserving and maintaining existing structures. New approaches to educating engineers may be needed. Innovation in engineering design solutions must be encouraged by dealing with the issues of professional liability and establishing an engineering fee structure that rewards new ideas.

KEYWORD: cathodic protection, deicing salt, dredged material, precast concrete, satellite relay, radar, laser optics, ultra sound, remote sensing, value engineering.

---

[1]. E.J. Fasullo, P.E. Deputy Director of Engineering/Deputy Chief Engineer, Port Authority of New York & New Jersey, New York, NY 10048.

NATIONAL AND LOCAL UPDATE

NATIONAL

Our nation must confront a crisis that has been precipitated by years of underinvestment in the maintenance of its public works facilities. Beyond the clamor in the press, we know very little regarding the extent of the problem. One study has estimated that we will need to spend an additional $3 trillion during the next decade simply to halt the rate of deterioration. This would entail a 40% increase in all state and local taxes a move that would be legally impossible in many jurisdictions and politically impossible in all of them. Clearly, the problem is much more than money.[1]

If the federal government wants to provide additional funds to state and city governments to repair and replace deficient bridges, roads,water systems, sewers, and public buildings, it must improve the planning techniques, the inventories, and the capital budgeting procedures that it uses to ensure that money flows where it is most needed and in a manner that makes best use of scarce public dollars.

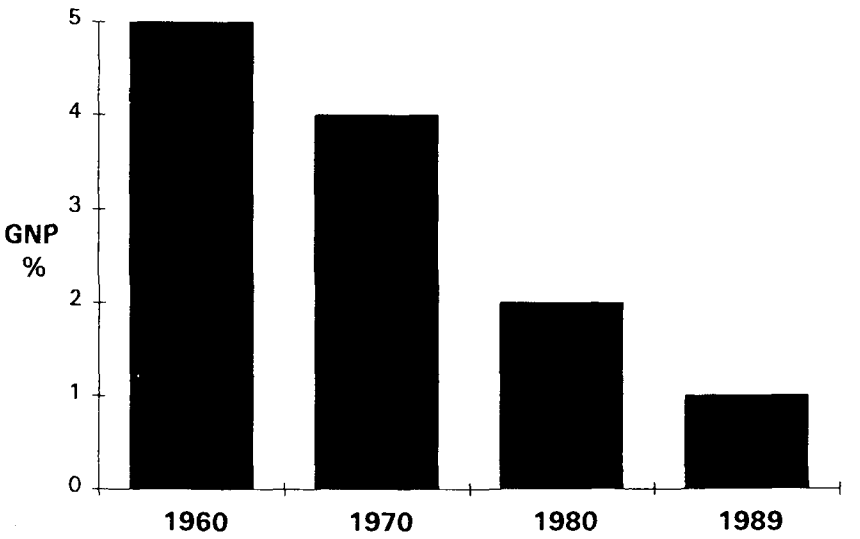

Figure 1 Infrastructure Cost

Lack of money is only part of the problem. Between 1965 and 1980, the share of the gross national product (GNP) devoted to investments in public works fell from 5% to only 2% as shown in fig. 1 and fell again from $30 billion in 1980 to $24 billion in 1989 as shown in fig. 2.[2] During the 1980s, the Federal Government has reduced investment in public works by about 22 percent.

The list of deficient structures and major problems has grown. Of the nation's 564,999 bridges, 17% are in critical or basically intolerable structural condition, and 8% of the interstate highway surfaces are at substandard. Boston loses 43% of its water supply through leaks.

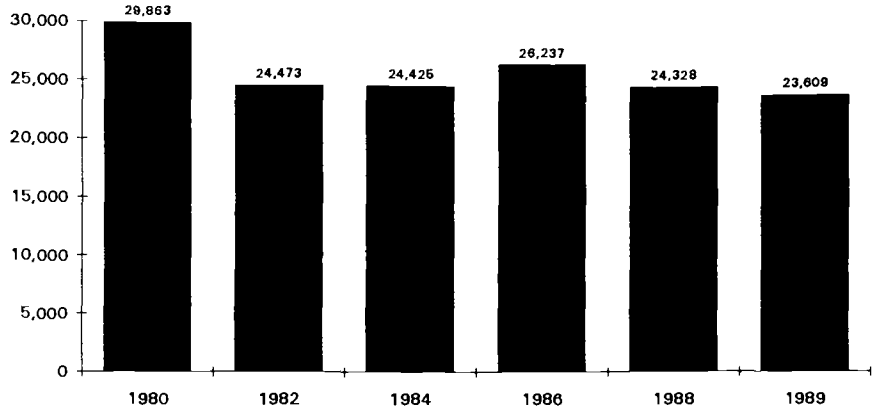

Figure 2 Federal Infrastructure Expenditures (in millions of 1982 adjusted dollars)

BACKGROUND

The absence of recordkeeping is a prime culprit. Until all levels of government agree to present capital budgets that include careful documentation of the rate of depreciation of public capital, we will not be able to resolve the basic infrastructure problem.

We have emphasized expansion and growth rather than the prudent use of public resources. With the massive population movement westward during the 19th century, the shift from rural to urban areas during the first half of this century, and the rapid suburbanization since World War II, our public works problems have been those of accommodating growth. Federal grants from the land grants to the railroads to rural electrification and wastewater

treatment projects have reflected this focus. We need to develop a more balanced public investment strategy that weighs the need to build for growth with the need to conserve what we have already constructed.

The short term outlook: Repair projects are not sufficiently glamorous. A major new project offers convenient media opportunities; a highway resurfacing does not. Squeezed by demands for every conceivable type of public service, state and local officials defer routine maintenance and rehabilitation of vital infrastructure systems for years. If these factors have contributed to a chronic underinvestment problem, other factors have created a crisis in recent years. The combination of rapid suburbanization, the energy crisis, inflation, and prolonged recession have robbed state and local governments of the revenues needed to make capital investments. If New York City and Cleveland suffered the most publicized brush with bankruptcy, many other jurisdictions were not far behind. Taxpayers placed constitutional or legal limits on the amount their governments could spend, borrow, or raise in revenues. Capital projects were the most vulnerable budget item: It is much easier to cancel a project to reline a sewer pipe than to lay off teachers and police.

The federal government has contributed to the problem. During the 1960's and 1970's, Congress seemed ready to come to the assistance of cities if they could document a severe problem. Between 1970 and 1980 the share of state and local governments' capital budgets that was subsidized by federal grants rose from 20% to 40%.

Most of the federal government's programs paid only for new construction and major rehabilitation, leading many recipients to defer maintenance until the public works had decayed badly enough to be eligible for federal funds. Federal-aid highway grants pay for 90% of the costs of construction of interstate highways, 75% for primary, secondary, and urban roads, and 80% for bridge replacement. This bias runs across many federal programs. In a survey of state and local governments conducted by the American Public Works Association, 90% of the respondents indicated that federal capital funds caused them to lower the priorities they attach to maintenance and repair. Additional federal money will not solve the problem.

THE ROLE OF CORROSION IN THE INFRASTRUCTURE ARENA

Corrosion has a major impact on the economy of the United States. The magnitude of corrosion is astounding: In 1949 Uhlig estimated the annual cost of corrosion in this country to be $5.5 billion. In 1972, a task group of the

Federation of Materials Societies estimated that cost at $15 billion. In 1978, the U.S. Department of Commerce, National Bureau of Standards estimated the cost of metallic corrosion to be $82 billion. This number was later revised to $120 billion. More recently it climbed to about $150 billion.

All of the above costs did not include the cost of rebar corrosion which is estimated at $150 to 200 billion per year. Thus, the total combined cost is estimated to be over $300 billion annually. On the positive side, approximately 40 percent of these costs are avoidable by the application of present available technology.

The potential savings to the United States economy by applying known corrosion control techniques are well recognized.

Causes of corrosion

1. Surface condition
   a) Partially covered with mill scale
   b) Impurities occluded in the metal surface
   c) Contact of dissimilar metals

2. Corrosive environment
   a) High-salt content
   b) High-acidity media
   c) High-oxygen content
   d) High-temperature media
   e) High-fluid velocity
   f) Bacteria in anaerobic environment
   g) Ammonia, chlorides, H_2S or other atmospheric environments which may lead to s.c.c. of metals

3. Stray currents
   a) D.C. electrified railways
   b) Cathodic protection systems
   c) D.C. welding operation

Corrosion prevention methods

1. Material selection
2. Environmental modification
3. Corrosion inhibitors
4. Coatings
5. Cathodic protection

Corrosion prevention methods are often used in conjunction with one another. Example, coatings are used with cathodic protection to present the most economical system.

Concrete and steel will continue to be essential materials for infrastructure construction for the forseable future. Recent research identified new additives, coatings, and applications for these materials to improve their durability and resistance to operating stress. Concrete is considerably stronger under compression than under tension. To compensate for its low tensile strength, concrete is reinforced with steel. Concrete is also porous and acts like a sponge in the presence of water and liquids. Under normal conditions concrete is an alkaline environment. In this case steel rebars form an oxide film that prevents further corrosion while this film remains intact. When this protective layer is disturbed, corrosion of steel begins and continues until it causes deterioration of the concrete. The main reason for the deterioration: The corrosion products occupy a much larger volume than the steel, which leads to cracks and delamination followed by spalling.

Main causes of rebar corrosion

1. Chloride ions cause the breakdown of the protective layer and the start of the corrosion process. Research determined that a content of 1.0 to 1.4 pounds of chloride per cubic yard of concrete is enough to destroy the passivity of steel and promote active corrosion.

2. Differences in chloride ion concentration lead to a difference in potential, creating anodic and cathodic areas of steel.

3. Oxygen is another important contributor to corrosion of steel in concrete.

4. A drop in the pH to a level of 11 to 12 is another contributor to rebar corrosion. This can be the result of the concrete absorbing carbon dioxide.

5. Stray D.C. currents entering a steel reinforced concrete structure create cathodic areas; when they leave the steel becomes anodic causing it to corrode.

Techniques to protect concrete structures against chloride contamination include dense concrete, liners, and corrosion inhibitors. Cathodic protection has been proven by the Federal Highway Administration to be the only rehabilitation technique to stop corrosion in salt-contaminated bridge decks regardless of the chloride content. [3]

INFRASTRUCTURE CHALLENGES AND ADVANCED TECHNOLOGY

INFRASTRUCTURE ASSETS

FORM	ASSETS	
TOTAL PUBLIC HIGHWAYS	3,874,000	miles
TOTAL AIRPORTS	17,327	number
TOTAL AIRWAYS	384,691	miles
TOTAL MOTOR BUSES	2,671	systems
TOTAL RAPID AND LIGHT RAIL	27	systems
TOTAL COMMUTER RAIL	12	systems
TOTAL RAILROADS	99,700	miles
TOTAL PORTS	1,109	Ports
TOTAL WATERWAYS	25,777	miles

INFRASTRUCTURE MAJOR PROBLEMS

FORM	PROBLEM
HIGHWAYS AND BRIDGES	10 percent of highways deficientient 42 percent of bridges deficient
MASS TRANSIT	Structural deterioration of rail systems in older urban areas
RAIL	Problems due to deferred maintenance
PORTS	Localized problems due to deferred maintenance
AIRPORTS	No major problems.

TRANSPORTATION

Most infrastructure for transportation is supplied and managed by the public sector. When demand exceeds supply,

congestion is likely to create air quality problems. Building new structures has been an attractive cost-effective option. However, this is no longer true in many of the large urban areas, because of large upfront capital expenses, insufficient land, and community opposition to the expected impact on the environment and quality of life.

One possible solution is to provide other travel alternatives. New technology includes tiltrotor aircraft and high-speed rail or magnetic levitation rail. However, new technologies will not be ready for at least another decade.

Nearly 42 percent of the nation's bridges are rated as unable to handle traffic demand or structurally deficient as shown in fig. 3.[2] Costs for repairing and replacing these are estimated at $70 billion.

Condition of Highways

Over 10 percent of the nation's roads have enough potholes, cracks, ragged shoulders, ruts, and washboard ridges to be classified as deficient. Heavy axle weights, such as those of large trucks and the stresses caused by freezing and thawing of harsh weather are the major causes of pavement damage.

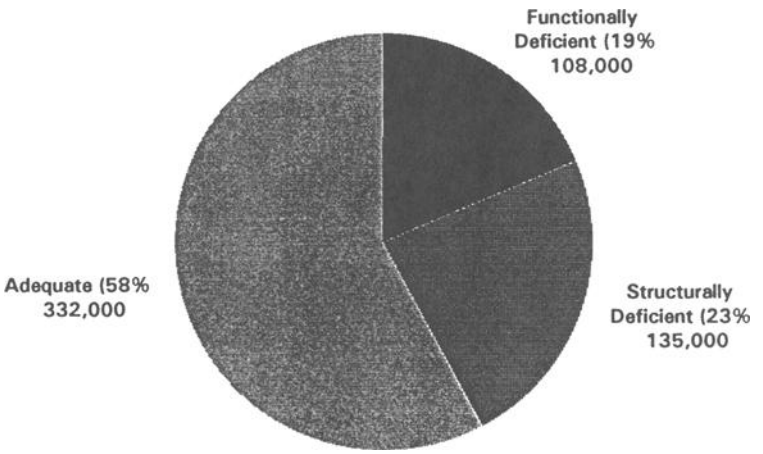

Figure 3 Conditions of U.S. Bridges

ADVANCED TECHNOLOGY FOR HIGHWAYS & BRIDGES

Technologies can make substantial contributions in solving the problem of improving the physical condition of highways and bridges to a satisfactory level.

1) Advances in electronic sensors and system management software permit automated data collection and analysis. These technologies have great potential to speed up and standardize the condition assessment process and help set priorities for repair.

2) Computerized bridge inventory systems can coordinate bridge condition analyses, set priorities, and budget for maintenance and repair. The data help the engineers determine the rating for every bridge and classify them according to their deficiency.

3) Pavement additives for deicing include ground rubber or calcium chloride covered with linseed oil. These additives can double or triple paving material costs and are not effective in all climates or under all highway conditions.

SOME MASS TRANSIT PROBLEMS

Public mass transit is not a self supporting venture. On the average revenues cover less than 40 percent of the operating costs. They are usually subsidized from State or local general funds and earmarked taxes. Buses receive substantially higher subsidies than rail transit systems.

Bus transit systems, especially operators of smaller buses, encounter problems with break wear, corrosion, electrical and air conditioning systems, wheelchair lifts, and vehicle handling. Maintenance costs are very high for these small operators.

Rail transit systems need to rehabilitate or replace railcars, power stations, overhead power wires or third rail, maintenance facility buildings, and storage yards and bridges.

The cost for rehabilitation and modernization of the mass transit system is estimated at $18 billion.

ADVANCED TECHNOLOGY FOR MASS TRANSIT

BUSES

1) Automatic vehicle monitoring systems can locate transit buses and communicate information to drivers, dispatchers, central traffic control computers, and passengers.

2) Electronic control systems can reduce emissions, smooth shifting, increase acceleration, and quiet operations of engines and transmissions. This should reduce maintenance costs and allow vehicles to be in service longer.

3) The use of Methanol or Natural Gas could reduce the emission of harmful exhaust to the environment.

RAIL

1) Track inspection technologies include the following elements:

   a) Automated track measurement systems. The equipment uses electro-optical or electromagnetic methods to give dynamic measurement of track geometry under loaded conditions.

   b) Dedicated rail flaw detection cars are used to test rails ultrasonically for defects resulting from fatigue. Track data can be stored in computerized form to help future maintenance.

2) New Rail Propulsion Technologies such as AC traction motors can save substantial energy costs.

3) Most modern train control systems now use pulsed currents through the track circuit to communicate allowable speed information and signaling rather than wayside signaling.

PORTS AND WATERWAYS' PROBLEMS

1) Limited fiscal resources to maintain and expand the system created a problem that needs a quick solution.

   Of the total U.S. freight ton-miles, 15 percent are produced by commercial barges and tows, which carry bulk commodities such as petroleum, grain, and coal.

Waterway transport offers the lowest ton-mile costs to shippers. The largest ocean and freshwater port facilities are owned and managed by public or quasi-public agencies such as the Port Authority of New York and New Jersey.

2) Despite the importance of ports to local economic development, few cities have integrated transportation systems that link ports to pipeline, rail, and truck services.

3) The most prevalent single environmental issue facing ports in this country is the proper disposal of dredged material. Dredged material is disposed of in the open ocean because of population growth in coastal areas and wetlands protection requirements.

Gaining approval for dredging projects from a long list of government and environmental groups can take years.

Maintenance restrictions have caused waterways to become shallower and narrower, severely limiting the types of vessels they can accommodate.

ADVANCED TECHNOLOGY FOR PORTS AND WATERWAYS

1) Non-destructive evaluation can give managers more extensive information about structural conditions and maintenance needs.
Sonar is used to find defects on underwater surfaces.
Electromagnetic sensors and pulse/echo ultrasound devices are used to probe inside solid structures.

2) Techniques for modeling local circulation and sedimentation can help design engineers to locate and orient piers, wharves, and other pile-supported structures.

3) Precast concrete for lock wall rehabilitation, in situ repair of deteriorated concrete, and roller compacted concrete for dams are examples of field tested projects.

4) Articulated concrete slabs and gravel prevent channel migration and permit self-dredging channel designs. Dikes and other structures deflect or stabilize currents within a channel.

5) New forms and locations for ports and vessel design modifications are alternatives for economic marine transportation.

AVIATION PROBLEMS

1) Aircraft noise is a serious problem for airport operators and airlines. The intensity of sound can be measured precisely; however, determining objectionable noise levels is more subjective. New technology has lowered noise levels, but additional reduction may be limited creating controversial issues.

2) Annual airline travel depends on the strength of the economy and generally follows trends in the Gross National Product (GNP). Current forecasts indicate that increasing numbers of United States and foreign airports will have traffic demand exceeding their capacity for longer periods of time each day.

3) Airline operations can place a severe burden on ground capabilities. Ground access to and from airports depends entirely on local planning and transportation management. No single agency or organization is responsible for research or planning for enhancing the capacity of ground facilities.

ADVANCED TECHNOLOGY FOR AVIATION

1) Analytic tools can help air traffic decision makers make rational system choices. The F.A.A. has some computer-based models for quantifying the effects of changes in equipment, procedures, airspace configurations, and user demand on system performance. Dynamic simulation laboratories to increase the system analysis capability, modeling, and simulation technologies are being added to the agency's traffic management facilities.

2) One of the most promising technologies for improving instrument flight rules (IFR) capacity at airports upgrades the secondary surveillance system to give faster radar data updates as well as larger and clearer controller displays.

3) Satellite-based systems offer the greatest potential for aviation navigation enhancement.

4) Advanced weather radar systems that can measure winds and other automated weather observing systems are being deployed.

5) Data link and satellite relay are two communications developments for aircraft.

6) New technologies for baggage screening include x-ray tomography devices, electromagnetic, and nuclear-based

systems to identify atomic elements. Vapor detection techniques will recognize and evaluate trace organic materials present in explosives.

7) New test programs are being initiated by ASTM Committees E24 on Fracture Testing and G01 on Corrosion of Metals to obtain the corrosion fatigue life of critical aircraft sections.

IDENTIFYING INFRASTRUCTURE NEEDS

While many innovative technologies are available to help infrastructure managers, their acceptance requires a sharing of the financial and technical risks among designers, manufacturers, builders, and government agencies that finance and operate these technologies.

Some of the currently available technologies used in private industry are not used widely in public works. Since the need to maintain and repair our infrastructure has reached its peak, advances in technology and materials can provide greater efficiency and higher operating standards. The following are some examples of such technologies:

1) NON-DESTRUCTIVE EVALUATION TOOLS

a) High speed, non-contact sensing technologies radar, infrared thermography, laser optics, ultra sound and others may be utilized to survey hundreds of miles of pavement, piping, or numerous bridge decks accurately in a single day.

b) Sound, temperature, pressure and others can be measured precisely with currently available sensors. They are accurate and small because of the use of silicon microchips.

c) Remote sensing and automatic control are now available and used in many fields such as marine dredging, automatic railroad track measurement, and cathodic protection.

2) MANAGEMENT AND DECISION MAKING TOOLS

a) Maintenance Management Information Systems allow managers to set priorities and schedule preventive maintenance. Computers are making the use of such systems available to public works operators.

b) Artificial intelligence and computers are used to provide automated reasoning such as:

   (i) Expert systems that duplicate a professionals' reasoning to solve problems in a given field.

   (ii) Computer vision, which analyzes a visual image in real time. A natural application would be highway cracking, patching, and potholes.

Many new technologies are still too expensive to be used daily in the field. In addition the expertise that is needed to use the sophisticated tools and interpret the test results requires upgrading of most state and government agencies.

DESIGN ISSUES

Designers use existing standards and previous experience to reduce the financial and professional risks. Neither government agency engineers nor consultants have an incentive to introduce new technologies. Many public officials are not interested in being the first owner of a new technology. Designers also rely on engineering standards and specifications to prevent unexpected failures. Since the design determines what the contractor will construct, opportunities for introducing new techniques are limited. Adding a metalurgical failure analysis unit to a design division would provide meaningful limitations.

Legal restrictions often prevent a designer from working with a contractor to develop a better or less costly project. Thus, proprietary and sole source technologies which may encourage innovative technology, are frowned upon by the current system.

Design, construction, operations, and maintenance responsibilities are fragmented in most organizations.

Design on the basis of system performance is not a widely used method. Good performance specifications require a thorough knowledge of the problem and the technologies available to solve the problem, as well as motivation and experience.

Design professional liability is a major inhibitor limiting the introduction of innovative ideas. There is virtually no financial reward incentive for construction engineers to innovate: If they have a new cost saving idea, the owner

benefits and the engineer assumes the risk if it does not work out.

Value engineering is a very specific cost control methodology for evaluating a design on the basis of its functional purpose and capital, operating, and maintenance costs. This method will identify cost items unnecessary for the proposed function of the facility and should be encouraged.

MANAGEMENT ISSUES

- Most public works projects are purchased under a system of competitive bidding. Selection on the basis of low bid is common for these projects. Choices on the basis of lowest initial cost ignore options that could have higher quality and long-term economy.

- Public decision makers are reluctant to approve new technology. New technology is surrounded by risk due to uncertainty. Public works projects are not suited for trial and error management. However, risk sharing arrangements can open the door to advanced technology. Engineers are selected and compensated on the basis of a fixed fee, sometimes on a fee proposal. There is no room for studying numerous alternatives as the standard solution that was used last time will probably be used again. Forms of selection and contracts that reward innovation must be developed and used on infrastructure projects.

PERSONNEL ISSUES

- The Public Works field is losing its well-trained people to the private sector and to early retirement incentives.

- Many new technologies require new skills and competitive salary with private industry. The current need for rehabilitation in Public Works magnifies these problems. Very little engineering education and training includes new technologies. Improved education and training are necessary to allow advanced technologies to be introduced more quickly. While the average age of infrastructure managers increases, the number of graduates from relevant engineering fields are insufficient to replace the retiring personnel.

EDUCATION ISSUES

Educating engineers cannot be left to professors alone. Leading engineers and design professionals must participate in the education process. Students must be taught an expanded view of the role of engineers in rebuilding our country. Leadership in the decision making, policy making, priority setting, and funding design process is equally the role of the engineer. [4]

CONCLUSION

Our infrastructue is currently plagued with pervasive problems. Ignoring them could cause large economic losses, jeopardize safety, and create delays in introducing new technology.

A challenge and an opportunity to our engineering societies, universities, scientists, and constructors will be to offer innovative solutions that will benefit future generations.

REFERENCES

[1] Aan H. Molof and Carl J. Turkstra, Ed., Anals of the New York Academy of Sciences, Infrastructure-Maintenance and Repair of Public Works, New York, 1984.

[2] Office of Technology Assessment, Public Works Technologies, Management and Financing, Delivering the Goods, U.S. Government Printing Office, April 1991.

[3] Federal Highway Administrator, "Memorandum - FHWA Position on Cathodic Protection Systems" Memorandum, April 23, 1982.

[4] Armando I. Perez, and A. Kurt Ardaman, "New Infrastructure: Civil Engineer's Role" Journal of American Society of Civil Engineering, vol.114,No.2,1988,PP.61-72.

Robert Baboian

SYNERGISTIC EFFECTS OF ACID DEPOSITION AND ROAD SALTS ON CORROSION

REFERENCE: Baboian, R., "Synergistic Effects of Acid Deposition and Road Salts on Corrosion", Corrosion Forms and Control for Infrastructure, ASTM STP 1137, Victor Chaker, Ed., American Society for Testing and Materials, Philadelphia, 1992.

ABSTRACT: The interaction of our natural environment (rain, snow, humidity) with chemicals introduced to the environment (road salts, emissions) provides a complex chemistry. During the past three decades, this chemistry throughout the world has changed drastically. Use of sodium chloride and calcium chloride for ice and snow removal has increased to an extremely high level. Emissions of SO_2 and NO_x have also risen to such levels. These emissions convert to sulfuric and nitric acids and are deposited over large areas by precipitation. The combination of protective film disruption on metals by chlorides and the deposition of reducible hydrogen ions by acid precipitation provides a synergistic effect on corrosion of infrastructure metals. Results of laboratory and field tests show that steel is much more susceptible to corrosion in this type of environment.

KEYWORDS: Acid deposition, road salts, marine salts, steel, reinforcing steel, bridges, storage tanks, synergistic corrosion, electrochemical theory, infrastructure, atmospheric corrosion, poultice corrosion, soil corrosion.

INTRODUCTION

The importance of corrosion in our modern, high-tech society can be measured by the magnitude of the direct and indirect problems which result from this degradation process. Certainly, the effects on our infrastructure are

Robert Baboian is Principal Fellow and Head of the Electrochemical and Corrosion Laboratory at Texas Instruments Inc., Attleboro, MA, 02703

a great contributor because of the magnitude of the problems which exist today. Throughout the World, elements of infrastructures are deteriorating to such a degree that it is considered of critical importance. Included here are highways, bridges, parking garages, water distribution systems, waste water collection and treatment systems, harbors, reservoirs, and railway and subway systems. Of particular importance is the problem of corrosion of reinforcing steel in concrete (rebar) not only because of the cost and safety concerns, but also because of the inconvenience that comes in making repairs.

ENVIRONMENT

The magnitude of infrastructure corrosion problems has increased significantly over the past 3 decades. This is due to the fact that the environment has become more aggressive due to a number of factors. For example, Figure 1 shows the annual use of road deicing salts in the United States to be almost non-existent before 1950.[1] The annual usage increased significantly during the 1960's and 1970's and it has leveled off at 10 million tons per year. These salts, sodium chloride and calcium chloride, are extremely corrosive due to the chloride ion's disruptive effect on protective films on metals as well as the increased conductivity of these electrolyte solutions. Accelerated corrosion by salt occurs due to the effects of direct splash and spray, contamination in natural waters such as streams, lakes, and drinking waters, leaching into soils, and by forming salt aerosols in the atmosphere. Thus, all of the elements of the infrastructure are exposed to this environment.

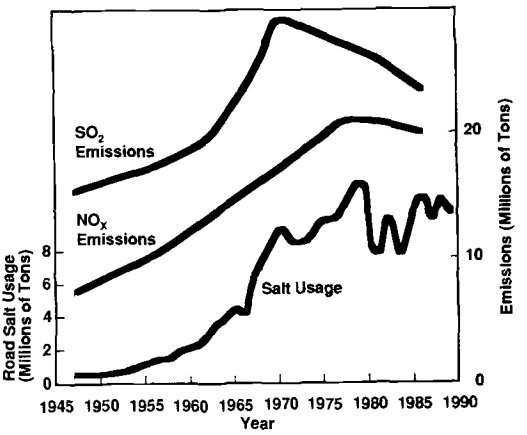

FIGURE 1 Annual Deicing Salt Usage, SO_2 and NO_x Emissions in the United States

The upward trend in SO_2 and NO_x emissions in the United States is also shown annually in Figure 1.[1] The level of SO_2 peaked at 30 million tons in 1970 and for NO_x peaked at 23 million tons in 1978. These pollutants are corrosive because they convert to acids either directly on the metal surface in contact with moisture, or, in the upper atmosphere.[2] For example, acid rain and snow are the result of long-range transport of SO_2 and NO_x, which convert to sulfuric acid and nitric acid in the upper atmosphere. These acids are then deposited as rain and snow in areas remote from the emissions source. However, localized emissions produce acid fog, acid dew, and dry acid deposits. The degradation caused by these effects therefore are due to local emissions rather than long range transport.

The effects of acid deposition have been the subject of intense study. Measurements of pH of deposition (such as acid rain) have yielded average values for large areas of the World.[2] This data is shown on the map in Figure 2 along with a keyed corrosivity indication. In general, corrosive areas in North America and Europe, are areas where marine salts or road salts are present. The most corrosive areas are those having a combination of these salts and acid precipitation.

FIGURE 2 Worldwide Corrosion Environment Map

CORROSION THEORY

Corrosion of metals can be treated by application of the mixed potential theory first described by Wagner and Traud.[3] The theory is based on two simple hypotheses. First, any electrochemical reaction can be divided into two or more oxidation or reduction reactions, and second, there can be no net accumulation of electrical charge during an electrochemical reaction. That the various partial reactions can be treated separately, as stated in the first hypothesis is only satisfied when the total rate of oxidation (corrosion) equals the total rate of reduction.

The anodic (oxidation) reaction occurs when electrons are removed from an area on the metal surface and positively charged ions go into solution. It can be represented by the equation:

$$(1)\quad M \longrightarrow M^{+} + e^{-}$$

The electrons flow to other areas on the metal surface where they are consumed by the cathodic reaction. There are several different cathodic (reduction) reactions which occur. The most common ones are:

$$(2)\quad 2H^{+} + 2e^{-} \longrightarrow H_2$$
(Hydrogen Evolution)

$$(3)\quad O_2 + 4H^{+} + 4e^{-} \longrightarrow 2H_2O$$
(Oxygen reduction: acidic solutions)

$$(4)\quad O_2 + 2H_2O + 4e^{-} \longrightarrow 4OH^{-}$$
(Oxygen reduction: neutral solutions)

$$(5)\quad M^{+n} + e^{-} \longrightarrow M^{+}\ (n-1)$$
(Metal ion reduction)

A combination of these reactions can occur providing that the net total reduction rate equals the net total oxidation rate. A number of factors including solution composition, pH, aeration, diffusion, and catalytic properties of the metal surface determine which reactions predominate.

Electrochemical techniques are most commonly used to study these reactions.[4] Use of the mixed potential theory is demonstrated by the activation polarization curves for a reversible electrode in Figure 3. When an electrochemical reaction is forced away from equilibrium, it is termed polarization and one reaction (either oxidation or reduction) proceeds faster than the other. The potential change due to polarization is n, defined as overvoltage and the current applied to polarize the

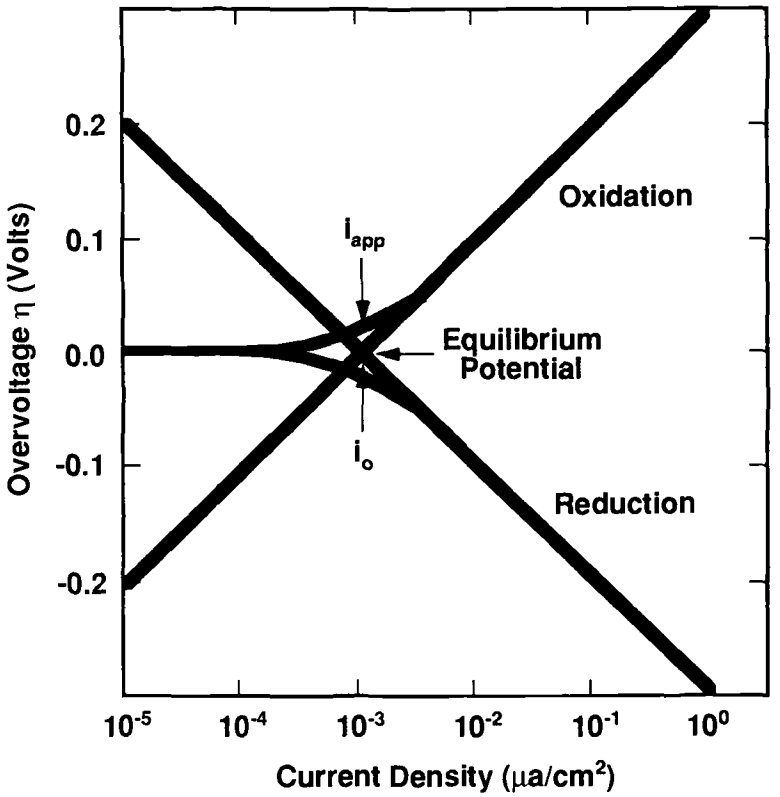

FIGURE 3 Schematic Activation Polarization Curve For a Reversible Electrode

potential away from equilibrium is the net rate of reaction. The expression relating reaction rate and overvoltage for activation polarization is:

$$(6)\quad n = +/- B \log i/i_o$$

Equation 6 is called the Tafel equation where io is the exchange current density and B is the Tafel constant (or Tafel slope). This equation is valid when the applied current is a linear function of overvoltage on a logarithmic scale such that i is a measure of the oxidation (for example, corrosion) or reduction (for example, hydrogen reduction) current.

The Tafel equation is valid when reactions are under activation control. In many cases, diffusion control plays an important part is the system, i.e., the rate of reaction is limited by diffusion. Polarization curves demonstrating both activation and diffusion control are shown in Figure 4.

In Figure 4, the anodic polarization curve for the corrosion reaction (equation 1) is characterized by the Tafel equation (equation 6). The corrosion rate, i_C, is calculated by use of the Tafel equation (i.e. extrapolating the Tafel region back to E_1, the equilibrium potential).

The cathodic polarization curve in Figure 4 is complex in that activation and diffusion controlled reactions occur. Close to the equilibrium potential, E_1, oxygen reduction occurs (equations 3 or 4) and the current is diffusion limited. At higher polarization potentials, hydrogen reduction under activation control occurs according to equation 2, in addition to oxygen reduction. The rate of hydrogen reduction, i_H, is calculated from the Tafel equation (equation 6) i.e. extrapolation of the Tafel slope to E_1. The total reduction rate is the sum of i_H and i_d and this sum is equal to the total oxidation rate (i_C) at the equilibrium potential, E_1.

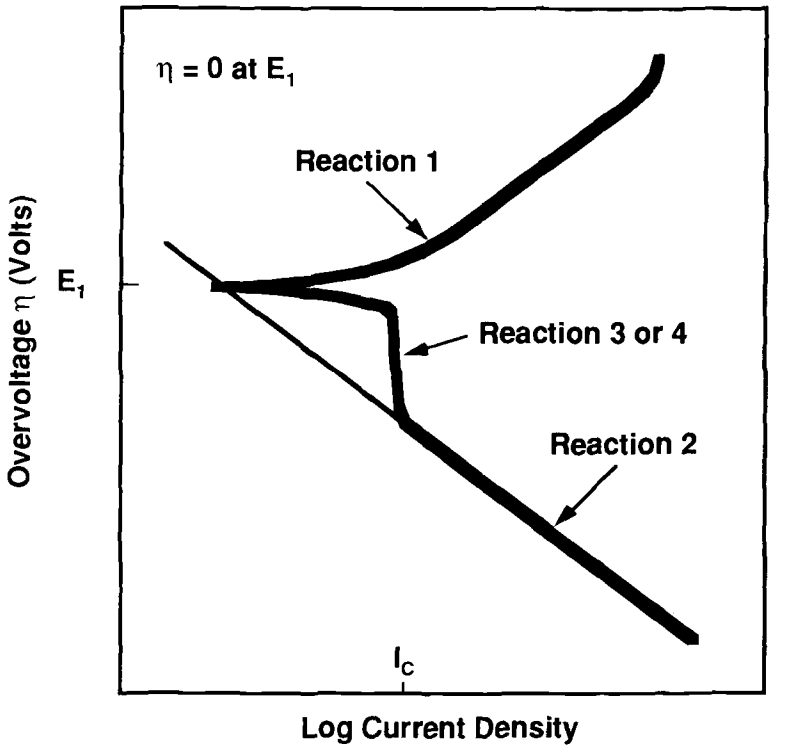

FIGURE 4 Schematic Polarization Curve For Electrode Under Activation and Diffusion Control

The most important points to be made here is that corrosion reactions are affected by the nature of both anodic and cathodic polarization curves. The anodic (corrosion) reaction rate may be reduced significantly by diffusion limited processes. Thus, formation of films on the surface of a metal can significantly reduce the corrosion rate. This is demonstrated by the anodic polarization curves for steel in Figure 5 in chloride containing, and inhibited electrolyte. The presence of a film forming inhibitor limits the anodic current over a wide range of potentials. However, in a chloride electrolyte, the film disruption mechanism yields a polarization curve which shows an increasing corrosion rate as the potential is changed in the more noble direction. But in the absence of reducible species, the cathodic current is low and therefore, according to the mixed potential theory, the corrosion rate (anodic current) will be low. The opposite is true with the introduction of reducible species.

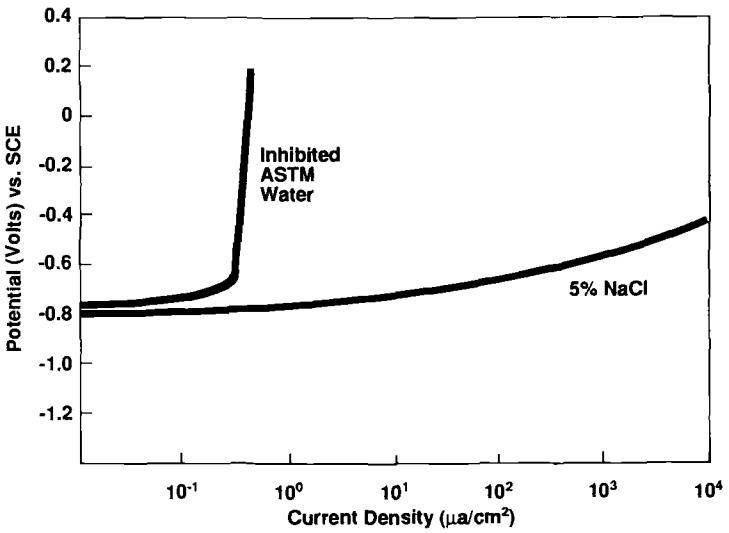

FIGURE 5 Anodic Potentiodynamic Polarization Curves For Steel in Inhibited and Chloride Electrolytes

The effect of oxygen on the cathodic polarization curve for steel is shown in Figure 6. Notice that at pH=8, the cathodic current at -1.0 volts vs. the SCE is much lower in deaerated electrolyte (ASTM Corrosive Water). The presence of oxygen thus increases the cathodic current on steel at its corrosion potential and therefore increases the anodic (corrosion) current at this pH.

It is well known that as the hydrogen ion concentration is increased (lower pH) equivalent hydrogen reduction occurs at more noble potentials. Thus, although hydrogen reduction on steel is limited at pH=8, significant hydrogen reduction can occur at lower pH values. This is demonstrated in Figure 7 which shows that for steel in ASTM Corrosive Water acidified to pH=2 with synthetic acid rain, the high cathodic current is not significantly different in aerated or deaerated electrolyte at the corrosion potential. Thus, when an electrolyte is acidified with acids (such as acid rain, acid snow, acid dew, acid fog, and dry acid deposits), the presence of oxygen is not required to have a high cathodic current and therefore increased corrosion rates can be observed in the absence of oxygen.

SYNERGISTIC EFFECTS

The synergistic effect of salts (such as sodium chloride and calcium chloride) and acids on metallic corrosion has been previously documented. Turcotte, Comeau, and Baboian showed the effects of calcium chloride and acid rain on the corrosion of steel in a poultice environment.[5] To reproduce poultice corrosion in the laboratory, steel samples were immersed in washed sand saturated with a solution of interest. Steel samples were tested in poultice with acid rain (distilled water adjusted to pH = 4 with a ratio of 3:7 nitric acid to sulfuric acid mixture) and 1% calcium chloride solution. The data in Table 1 shows that calcium chloride is more aggressive than acid rain but that the combination is much worse than the separate effects added. Thus, a synergistic effect on the corrosion of steel in poultice type environments is observed. It is important to note that this synergistic effect was not observed under alternate wetting and drying conditions.

A wide range of atmospheric exposure studies have demonstrated the synergistic effects of salts and acid deposition on metallic corrosion. In general, industrial areas, or areas subject to severe acid deposition are more corrosive when marine salts or road salts are present. The atmospheric exposure results for zinc and iron in Table 2 demonstrate the variation in corrosion rate for rural, urban, industrial, and marine sites.[6] For example, corrosion rates at an urban site in Halifax are much lower than those for the industrial site in Halifax. This industrial site has chlorides as well as an extremely high level of SO_2 in the atmosphere and an acidic precipitation pH. The marked effect of distance from the ocean on the corrosion rate can be observed in the data for the two Cape Kennedy sites and the two Kure Beach sites. The lowest rates are observed at the dry Arizona site.

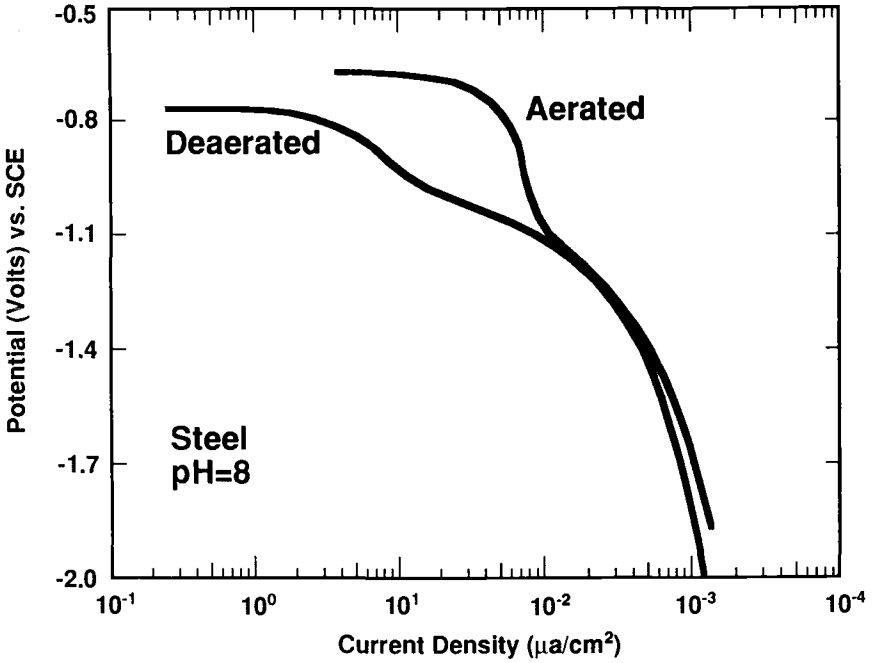

FIGURE 6 Cathodic Potentiodynamic Polarization Curves in ASTM Corrosive Water

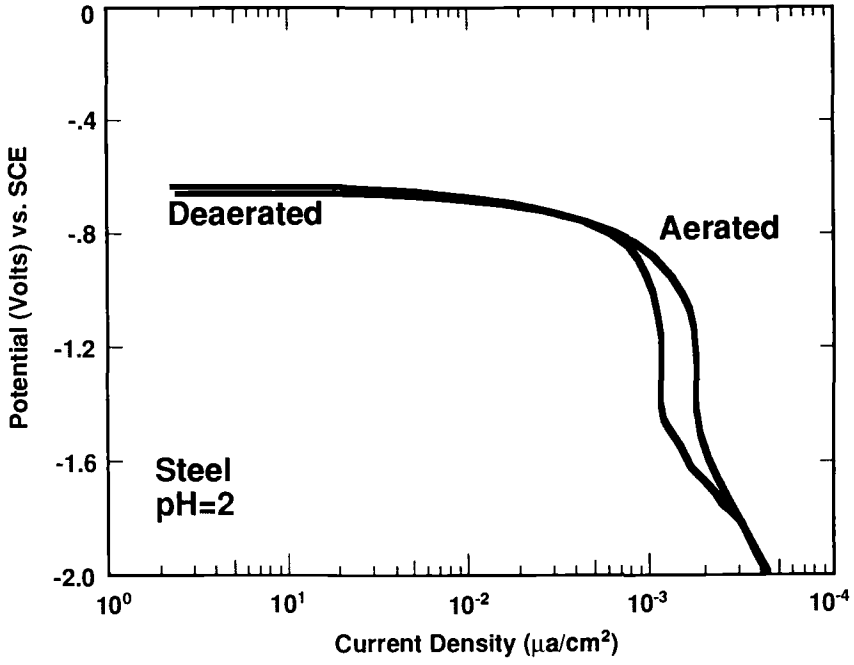

FIGURE 7 Cathodic Potentiodynamic Polarization Curves in ASTM Corrosive Water Acidified With Synthetic Acid Rain

TABLE 1

Corrosion Data for Steel in Poultice Test

Reference 5

	Acid Rain	$CaCl_2$	Acid Rain and $CaCl_2$
Avg. Penetration 2 weeks; no drying (mpy)	1.3	12.5	26.3
Avg. Penetration 12 weeks; drying and wetting (mpy)	19.3	87.4	82.8

TABLE 2

ATMOSPHERIC CORROSION RATES FOR ZINC AND IRON
(2 YEARS EXPOSURE) AT VARIOUS SITES

(REFERENCE 6)

SITE	CLASSIFICATION	CORROSION RATE (μm/Yr) ZINC	IRON
PHOENIX, AZ	RURAL	0.305	4.6
OTTAWA, ONT	URBAN	1.118	19.7
CAPE KENNEDY (0.8 Km FROM OCEAN)	MARINE	1.143	86.0
STATE COLLEGE, PA	RURAL	1.168	22.9
DETROIT, MI	INDUSTRIAL	1.321	14.4
POINT REYES, CA	URBAN	1.524	500.2
HALIFAX, NS	URBAN	1.575	26.6
KURE BEACH (240 M FROM OCEAN)	MARINE	2.017	145.4
DUNGENESS, UK	INDUSTRIAL/MARINE	3.632	487.9
NEWARK, NJ	INDUSTRIAL	3.683	50.6
CAPE KENNEDY (54 M FROM OCEAN)	MARINE	4.140	440.8
KURE BEACH (24 M FROM OCEAN)	MARINE	6.350	533.0
HALIFAX, NS (FEDERAL BUILDING)	INDUSTRIAL	7.417	113.4

The data in Table 2 shows that marine and industrial locations are more aggressive for zinc and iron corrosion. The introduction of salts over large areas through road deicing and dust control superimposed on existing environmental conditions provides the most aggressive corrosion conditions. In order to compare the corrosivity of the environment in Boston, Dallas, Detroit, and Montreal, field exposure tests have been conducted by mounting bare steel and galvanized steel coupons on the front bumpers of automobiles in these cities.[5] The corrosion rates in Table 3 can be compared with the pH of rainfall (Figure 2) and automobile poultice compositions (Table 4) for these cities.[1] The highest corrosion rates for bare steel and for zinc in galvanized steel were

TABLE 3

AVERAGE CORROSION RATES (μm/Yr)
FOR AUTO BODY STEELS

(REFERENCE 5)

CITY	BARE AUTO BODY STEEL	GALVANIZED AUTO BODY STEEL
Boston	57	2.92
Dallas	2.90	0.54
Detroit	45	1.31
Montreal	65	6.60

TABLE 4

AVERAGE COMPOSITION (PPM) OF POULTICES
FROM 50 AUTOMOBILES

(REFERENCE 1)

CITY	AVERAGE POULTICE COMPOSITION (ppm)			
	Cl^-	SO_4^{-2}	Ca^{+2}	Na^+
Boston	33	150	63	42
Dallas	23	133	348	82
Detroit	679	531	431	140
Montreal	63	3390	1404	77

observed in Montreal and Boston. These two cities have the lowest pH and highest relative sulfuric acid content in rainwater. Also, the relative sulfate and calcium concentrations in automobile poultices from these two cities are the highest, indicating the presence of large amounts of hygroscopic salts and acid deposition. This is very evident for Montreal, where the highest corrosion rates were observed. The drier Dallas environment produces the lowest corrosion rates.

The above data showing the synergistic effect of acid deposition and salts on metallic corrosion is important to understanding and solving problems of infrastructure degradation. Corrosion mechanisms can be more fully understood so that realistic and successful solutions to infrastructure corrosion problems can be developed.

In the specific example of corrosion of reinforcing steel (rebar) in concrete, oxygen access to the rebar can be limited due to the configuration. However, hydrogen ion deposition is increased by ten thousand times during a pH=3 acid precipitation event. The introduction of large amounts of this reducible species negates the requirement for oxygen in the corrosion process.

The placement of buried pipelines, and underground storage tanks along highways and streets subjects these steel structures to salts and acids which leach into the ground. The presence of oxygen in the corrosion process is not necessary due to hydrogen ion deposition by acid precipitation.

Finally, a large part of the infrastructure consists of painted steels exposed to the atmosphere. Corrosion and paint disbondment are accelerated by the combination of salts and acids which are in direct contact with these structures along roadways and in marine environments.

CONCLUSIONS

The combination of film disruption due to the presence of chlorides, and increased cathodic currents due to acidification yields a serious destructive force on steel. The data showing synergistic effects of acid deposition and marine and road salts on metallic corrosion is important to understanding and solving infrastructure degradation. Marine and road salts alone are extremely aggressive to infrastructure materials. However, acidification by acid deposition yields a most destructive environment: one which is difficult to duplicate for purposes of testing and development. If we are to solve the most serious infrastructure problems, the effect of the "real world" environment must be considered so that the solutions are the most economic as well as safe and sound.

REFERENCES

[1] Baboian, R., Mechanism of Automobile Corrosion and Prevention, Proceedings of the 11th International Corrosion Congress, Vol. 2, AIM, Milan, 1990.
[2] Baboian, R., Editor, Materials Degradation Caused by Acid Rain, American Chemical Society, SS 318, Washington, DC, 1986.
[3] Wagner, C., and Traud, W., Zeitschrift fur Electrochemie, Vol. 44, p. 391, 1938.
[4] Baboian, R., Editor, Electrochemical Techniques for Corrosion Engineering, NACE, Houston, TX, 1987.
[5] Turcotte, R.C., Comeau, T.C., and Baboian, R., Effects of Acid Deposition on Poultice-Induced Automotive Corrosion, in Materials Degradation Caused by Acid Rain, R. Baboian, Editor, American Chemical Society, SS 318, Washington, DC, 1986.
[6] Ailor, W., and Coburn, S., Metal Corrosion in the Atmosphere, ASTM STP 435, Philadelphia, 1968.

Thomas R. Menzies

NATIONAL COST OF DAMAGE TO INFRASTRUCTURE FROM HIGHWAY DEICING

REFERENCE: Menzies, T. R.. "National Cost of Damage to Infrastructure from Highway Deicing," Corrosion Forms and Control for Infrastructure, ASTM STP 1137, Victor Chaker, Ed., American Society for Testing and Materials, Philadelphia, 1992.

ABSTRACT: This paper draws on findings from a study of the full cost of highway deicing salt by a National Research Council committee. Cost estimates are presented for bridges, other highway components, and parking structures. Summation of the more reliable cost items, for which supporting data are dependable and relatively complete, suggests a national cost of $200 million to $500 million per year. Inclusion of cost items based heavily on committee judgment suggests a national cost of about $400 million to $900 million per year.

KEY WORDS: infrastructure, highway deicing, road salt, winter maintenance, bridge decks, parking structures, cost

During the past 20 years, the condition of the nation's infrastructure has received intense public and legislative attention. In particular, much of this attention has focused on the repair and maintenance problems associated with the deterioration of concrete bridges caused in large part by chloride deicing salts.

The effect of deicing salts (e.g., sodium chloride and calcium chloride) on bridges is well understood. During the 1950s and 1960s, thousands of bridges were constructed, many of them on newly constructed Interstates, using cast-in-place concrete heavily reinforced with steel. Subsequently, the decks of many of these bridges developed pores or fine cracks that allowed water

---

Mr. Menzies is a research associate at the Transportation Research Board, National Research Council, 2101 Constitution Avenue, Washington, D.C. 20418.

Although this paper draws heavily on the report of the National Research Council study committee, the views represented are those of the author and not necessarily those of the National Research Council.

and corrosive chlorides to reach the underlying steel bars. As the steel bars corrode, the resultant rust product expands, exerting pressure on the surrounding concrete and causing it to crack and fragment around the steel. In turn, these damaged areas provide free access to additional salt and moisture, which aggravates the destructive processes already caused by freeze-thaw, vibrations, and impact loadings from traffic.

Although bridge decks are the principal recipient of salt's adverse effects, various other bridge and infrastructure components are affected as well. For instance, corrosion of bridge joints and bearings, steel framing, and other bridge structural elements can be accelerated when exposed to salt from leaking decks and traffic splash and spray. Salt can also damage reinforced concrete pavement, pavement joints, highway drainage systems, and roadside hardware (e.g., guardrails, traffic signal circuitry). Additionally, long-term exposure to salt has been linked to the premature deterioration of hundreds of concrete parking structures in the northeastern and midwestern United States.

In recent years, a number of highway agencies have tried to control these adverse side effects by experimenting with noncorrosive deicers as alternatives to salt. Compared with these alternative materials, however, salt is inexpensive to purchase, and is easier to handle, store, and apply. As a result, highway agencies need to know the true cost of salt, including the cost of its adverse side effects, in order to determine the cost-effectiveness of higher-priced alternatives. Unfortunately, the last major studies to determine the true cost of salt were conducted nearly 20 years ago.

Recognizing the need for up-to-date cost information, Congress called on the Department of Transportation to sponsor a study of the full cost of salting, and identified the National Academy of Sciences as an organization to conduct the study. The National Research Council, which is the principal operating agency of the Academy, convened a special committee of experts in economics, chemistry, materials science, environmental science, and highway operations and maintenance. This paper draws on findings from the report of the committee, which was completed in October 1991. Specifically, the paper addresses costs related to bridges, other highway components, and parking structures.

BRIDGE DECKS

As discussed above, road salt is particularly detrimental to bridge decks because the chloride ions in salt, along with moisture, penetrate concrete and cause the rusting of reinforcing steel bars. Although this damage seldom affects the structural integrity of the deck, it can nevertheless cause extensive potholing of the deck surface, which can seriously degrade ride quality. Because bridge decks often lack full shoulders and have limited maneuvering room,

even minor irregularities and potholes can result in safety hazards that require prompt repair.

Deck Repair Costs

Conventional methods of deck repair range from patching of individual potholes to complete deck replacement. Because of its low cost, patching is the most common repair, although its effectiveness is usually only temporary. To provide longer-lasting repair, the damaged concrete must be removed and replaced with new concrete and special waterproof membranes or sealers that prevent further intrusion of salt and moisture. Such partial restoration, however, is seldom completely successful in halting the corrosion process, because unrestored sections often begin to corrode shortly after the deck has been repaired.

A disadvantage of partial restoration is that signs of corrosion, such as potholes, may not become evident until well after a large portion of the deck has become critically contaminated with chloride. Once this critical, or threshold, contamination level has been reached, deck deterioration usually continues, regardless of the subsequent use of salt or noncorrosive deicers. In many northern cities, where road salt is applied frequently and in large quantities, unprotected decks reach this threshold contamination level within 10 to 15 years after construction.

According to data from the National Bridge Inventory file, about 55 percent of concrete decks in the United States are in sound condition (Table 1). In particular, the heavy salt-using regions of the Northeast and Upper Midwest have a noticeably smaller share of sound decks than do other areas of the country. For instance, among 11- to 20-year old decks, only 75 percent are in sound condition in these salt-using regions, compared with about 85 percent elsewhere. Moreover, among 21- to 30-year old decks, only 45 to 60 percent are in sound condition, compared with 65 to 75 percent elsewhere.

Regional variations in deck condition are useful reference points for estimating the effect of continued salting on future deck repair costs. For example, in the Northeast, Midwest, and Mountain regions--where the majority of deicing salt is used--approximately 60,000 decks less than 20 years old are now in sound condition and potentially vulnerable to chloride contamination from continued salting (Table 2). On the basis of historical rates of deck deterioration in these salt-using regions, one would expect about 15 percent, or 10,000, to become seriously damaged during the next 10 years because of continued salting. Alternatively, however, if the lower rates of deck deterioration in the low-salt regions of the South and West are used instead, in order to determine how much deck damage would occur in the absence of road salt, then only 5 percent of these 60,000 decks, or 3,000, would become damaged--which is 7,000 fewer (Table 2).

This rough calculation suggests that about 7,000 decks will become damaged during the next 10 years because of continued salting. As a practical matter, however, deck damage will probably

TABLE 1 HISTORICAL RATES OF DECK DETERIORATION BY REGION (National Bridge Inventory file)

Region	Share of Decks in Sound Condition After 1-10 yrs	After 11-20 yrs	After 21-30 yrs
New England	93%	77%	47%
Upper Mid-Atlantic	94%	74%	47%
Lower Mid-Atlantic	91%	72%	58%
Great Lakes	92%	80%	58%
Upper Plains	90%	70%	64%
Lower Plains	95%	88%	74%
Mountain	91%	83%	64%
South, Pacific, and West	92%	85%	74%

Excluding Florida, Alaska, and Hawaii, which have exceptional environments.

be much less severe than experience suggests, mainly because of recent advances in bridge deck protection (discussed below). Because of these advances, it is more likely that this 7,000 figure represents a high-end estimate, and that as a low-end estimate, as few as half this many, or 3,500, will become damaged.

To estimate the average annual cost of repairing these damaged decks, it can be assumed (for simplicity) that about 1 in 10, or 350 to 700, will need to be rehabilitated each year during the 10-year period. The typical surface area of a deck is 7,000 ft^2. Multiplying this figure by 350 to 700 damaged decks yields between 2.5 million and 5 million ft^2 of deck surface that will need to be rehabilitated each year. According to estimates provided by the California and New York state highway departments, the average cost of rehabilitating a concrete deck, whereby the concrete is completely removed and replaced and the reinforcing steel is cleaned, is between $20 and $40/$ft^2$. Multiplication of this cost range by the 2.5 million to 5 million ft^2 of deck surface that would need to be repaired each year results in a total repair cost of between $50 million and $200 million per year.

Deck Protection Costs

During the past 20 years, the premature deterioration of concrete decks has challenged highway agencies to not only save the

TABLE 2 -- ESTIMATED NUMBER OF DECKS DAMAGED BY ROAD SALT DURING NEXT 10 YEARS

Region	Current Number of Sound Decks[a] (1)	Number of Sound Decks Damaged Over Next 10 years: Continued Road Salting (2)	Number of Sound Decks Damaged Over Next 10 years: Absence of Road Salt[b] (3)	Difference (4)=(2)-(1)	Average Deck Surface Area (ft^2) (5)	Total Deck Surface Area (ft^2) (6)=(4)x(5)
New England	2,100	500	200	300	7,600	2.3 million
Mid-Atlantic (Upper and Lower)	22,000	4,200	1,000	3,200	7,300	23.3 million
Great Lakes	20,400	4,000	1,700	2,300	7,100	16.3 million
Plains (Upper only[c])	11,900	1,000	200	800	6,800	5.4 million
Mountain	6,200	800	500	300	6,600	2.0 million
Total	62,600	10,500	3,600	6,900	7,100	49.3 million

[a]Includes only the population of bridges that are less than 20 years old, because these bridges may not already be contaminated with chlorides.
[b]Calculated by applying historical deck deterioration rates in the South and West to the existing population of sound decks in salt-using regions.
[c]Lower Plains states have deterioration rates similar to those of the South and West and therefore were excluded from the analysis.

SOURCE: Computer analysis of National Bridge Inventory file.

thousands of decks that are already critically contaminated with chloride but also to design and construct more durable decks that are more resistant to salt-induced corrosion. Because bridge decks are complex systems, this challenge involved many elements of the deck, ranging from improved deck drainage and joint sealants to special deck overlays systems that impede migration of chlorides into the concrete.

Since 1984, FHWA has required protection on all new Federal-aid bridges built in salt-using regions. The types of protection used, however, vary among states, depending on individual needs and the performance and cost of each protective system. In a TRB survey of state highway agencies, 40 of 48 responding states reported that they routinely use some type of protective system on bridges built where road salt is frequently used. By far the most common is epoxy-coated reinforcing steel, the use of which is standard practice in at least 25 states. Other types of protection range from waterproof membranes and special deck overlays to additional concrete cover over the reinforcing steel. Of the 25 states that routinely use epoxy-coated steel, 18 combine it with a waterproof membrane, additional concrete cover, a special deck overlay, or other protective systems.

The cost of installing and maintaining these protective systems has been studied by the National Cooperative Highway Research Program (NCHRP) [1]. According to that study, epoxy-coated steel combined with a special deck overlay is the most expensive system, costing about $\$5.50/ft^2$ more to install than a basic unprotected deck. The least expensive is an additional 2 inches of concrete cover, which adds about $\$2.15/ft^2$ to new deck construction costs. The average incremental cost of these systems is about $\$4/ft^2$ more than a basic concrete deck.

This average cost of deck protection is useful for projecting the future cost of protecting newly constructed decks. An analysis of the National Bridge Inventory file indicates that between 3,000 and 4,000 new decks are constructed each year in salt-using regions, where deck protection is necessary. Multiplied by the average deck surface area of 7,000 ft^2, the total area of these 3,000 to 4,000 new decks range between 20 million and 30 million ft^2. Hence, given an incremental protection cost of $\$4/ft^2$, the total annual cost of new deck protection is $75 million to $125 million (rounded to the nearest $25 million).

Summary of Bridge Deck Costs

After decades of salting, thousands of older decks in salt-using regions are now critically contaminated with chloride and will continue to deteriorate, regardless of the future use of salt or noncorrosive deicers. Accordingly, a priority of many highway agencies is to protect newer decks that are not already contaminated with chlorides. In recent years, important advances have been made in deck protection that reduce both the incidence and severity of deck damage. During the next 10 years, the total cost of protecting

newly-constructed decks and restoring currently sound (and uncontaminated) decks that become damaged by salting will be roughly $125 million to $325 million per year.

OTHER BRIDGE COMPONENTS

Much of the research that has been devoted to developing methods for repairing and protecting bridges from salt damage has focused on concrete bridge decks. Road salt, however, can also contribute to the deterioration of other bridge components, including steel grid decks, deck joints, drainage systems, and elements of the bridge structural system that are exposed to salt from faulty drainage and splash and spray from adjacent roadways.

Grid Decks, Joints, and Drainage Systems

In addition to its use in reinforced concrete, steel is the primary material in various other components of the deck system, including grid decks, joint devices, and drainage systems. These components are vulnerable to corrosion from road salt, but numerous other factors affect their durability as well.

Most steel decks are made of grid mesh, accounting for about 5 percent of all deck surfaces. These decks provide drainage of water, dirt, debris, and deicing salt through the grid openings. However, most older grid decks have a framework of steel beams and stringers to support the mesh panels. Salt-laden snow, mud, sand, and other debris that is tracked onto the deck will often drop onto the supporting structures, increasing their susceptibility to corrosion. Accordingly, grid decks and their supporting structures must be regularly cleaned and painted as a precaution against rusting, which can be exacerbated by frequent exposure to road salt [2].

Joint devices, likewise, require vigilant maintenance. Joints allow for movements of the deck caused by traffic loadings and thermal expansion and contraction. They are often made of metal formed into finger bars or plates, and are therefore susceptible to rusting, especially if they are improperly sealed and become clogged with moisture- and salt-retaining dirt and debris [2]. Rusted joints that do not perform properly can generate stresses on the deck that result in pavement fracturing or buckling, or cracking of the bridge approach slab. Road salt is therefore a factor that can affect joint corrosion and durability.

Much like joints, deck drainage systems require frequent maintenance. The drainage system is vital to the bridge because it eliminates trapped or ponded water, which can be hazardous to traffic and contribute to deterioration of the bridge understructure. Most drainage systems use metal pipes that funnel water from the deck to the ground. Poor drainage is usually caused

by dirt and debris clogging the pipes [2]. When drainage systems fail, backed-up water, which may be contaminated with salt and debris, can corrode the pipes, allowing salt and moisture-retaining debris to attack the bridge's structural components.

Bridge Structural Components

Because decks are secondary members of the bridge structure, damage or failure of deck components seldom has serious implications for bridge safety. By comparison, failure of structural components could result in sudden bridge collapse.

Structural elements vary according to bridge design, but usually include superstructure members, such as girders, stringers, and arches that support vertical loads; substructure members, such as abutments and piers, which transmit loads from the superstructure to the ground; and bearings, which transmit loads from the superstructure to the substructure, while allowing the bridge to undergo necessary movements without harmful stress. Most bridge structural elements are made of steel, reinforced concrete, or prestressed concrete, which, if exposed to road salt--because of either traffic splash and spray, faulty drainage, or leaky joints--are susceptible to corrosion and premature deterioration.

Bearings: Bearings serve an important function by allowing structural elements to undergo stress movements without damage. Bearings are often located where the bridge superstructure (e.g., girders) and substructure (e.g., pile caps) meet. Most bearing devices are constructed of steel, neoprene, bronze, or a combination of these materials [2]. The steel portions of bearings are normally protected by paint or galvanization. However, sand, dirt, debris, and road salt can accumulate around the bearing, causing corrosion and "freezing" of the device, especially if the protective system is poorly maintained.

Steel Framing and Supports: Corrosion is a problem for most steel frames and supports [2]. The corrosive action of atmospheric pollutants, sea spray, and moisture all make regular cleaning and painting of steel necessary in most regions of the country. Corrosion of steel is usually detected before it becomes a serious hazard. Repairs are made by removing the rust and applying a protective paint or coating or by replacing the rusted steel section with metal plating. Corrosion is accelerated by dirt, debris, and moisture that become trapped in pockets and crevices created by the framing and connection of steel members. The addition of salt to this environment increases the potential for more frequent and severe corrosion, especially if bridge cleaning and painting are lax.

Reinforced Concrete Supports: Road salt is frequently associated with deterioration of bridge structural support elements made of reinforced concrete [2]. The problem is similar to that of concrete decks; chlorides from road salt, along with moisture, migrate to the reinforcing steel, inducing corrosion and causing the

surrounding concrete to crack and fragment. Reinforced concrete box beams, stringers, pile caps, and support columns are among the structural elements affected. Leaky joints, poor drainage, and splash and spray from traffic provide avenues for salt access.

Because road salt is not applied directly on these support elements, salt damage takes longer to be identified and is generally not as extensive as salt-induced damage to decks. However, because of cramped working conditions and the need for falsework and scaffolding, even minor damage to concrete supports can prove very difficult and expensive to repair. Research is currently under way to develop less costly maintenance and repair treatments, such as cathodic protection and electrochemical chloride removal. These treatments, along with greater attention to deck drainage and corrosion protection (such as epoxy-coating steel) should help reduce the severity and incidence of this damage. Nevertheless, because repair of the concrete supports of just one long-span bridge can cost several million dollars, the total cost of salt-related damage is likely to be high.

Prestressed Concrete Supports: There is limited evidence that long-term exposure to road salt can damage prestressed concrete beams commonly found on segmental bridges. Prestressing improves the strength characteristics of bridge structural components by the tensioning of steel strands in the concrete. Because prestressed segments can be strung together with minimal intermediate support, this design is popular for long-span bridges crossing stretches of rough terrain, bodies of water, and congested urban areas. Because the steel strands are vital to structural integrity, the consequences of corrosion are far greater than the consequences of rusting reinforcing steel.

According to the National Bridge Inventory, there are some 25,000 prestressed bridges in the United States, accounting for about 5 percent of all bridges. To date, surveys of the condition of these bridges have found few corrosion-related problems. More than 12,000 prestressed concrete bridges were built in the United States between 1951 and 1966. According to an NCHRP study, highway agencies in 14 states that collectively contain more than half of these bridges report no significant problems [3]. In addition, a survey conducted by the American Concrete Institute found that of more than 30 million strands installed between 1950 and 1977, only 200 were affected by corrosion, usually due to corrosive environments involving seawater, poor design details, or faulty construction [4].

The sudden collapse of a 30-year old prestressed bridge in the United Kingdom in 1985, which was attributed to road salt-induced corrosion, renewed debate about the potential for corrosion of prestressed bridges [5]. Of particular concern is that corrosion of prestressing strands may take several decades to occur, because the strands are often embedded in special ducts or grout. Most prestressed bridges are relatively new, constructed during the past 35 years. Corrosion protection in many of these structures was

provided by the use of high-quality concrete and additional concrete cover. Because of the potentially catastrophic consequences of corrosion, most highway agencies now take extra precautions by coating and protecting the strands, ducts, and anchoring hardware in new prestressed bridges [4].

Because road salt's effect on prestressed concrete is uncertain, projections of future damage or costs due to salt would be speculative. The only cost that can clearly be associated with road salt is the added expense of corrosion protection. However, should significant corrosion of prestressed bridges be discovered in the future, the total cost would be considerably higher.

Summary of Other Bridge Component Costs

The effects of road salt on non-deck bridge components are frequently obscured by durability and maintenance factors that are unrelated to salt. Compared with deck damage, however, deterioration of other bridge components can be very expensive and difficult to repair, especially if the damage involves structural support elements. Although insufficient information is available to estimate these costs reliably, the committee believes that collectively they are as large as deck costs, and as a rough approximation, fall within the same range of $125 million to $325 million per year.

OTHER HIGHWAY COMPONENTS

Whereas road salt is clearly a principal factor in bridge durability, its impacts on other highway system components, such as pavements, drainage systems, and roadside hardware, are more uncertain and difficult to isolate from other durability factors.

Pavement

Pavement--both concrete and asphalt--is the single most expensive component of the highway system, accounting for about one-fifth of all highway expenditures [6]. In recent years, interest in reducing these expenditures has spurred considerable research aimed at improving pavement designs, materials, and maintenance practices. The impact of road salt, however, is not an area of major concern.

Perhaps the best-known effect of road salt on pavement is the aggravation of surface scaling in poor quality portland cement concrete. When improperly cured, over finished, or inadequately entrained with air--whereby microscopic air bubbles are mixed in with the concrete--concrete pavement is vulnerable to stress damage caused by trapped moisture that freezes and expands. Road salt can exacerbate this problem, both by increasing freeze-thaw cycles and by forming expanding crystals in the concrete. This effect,

however, is no longer a serious concern for most highway agencies, because air entrainment has been a standard construction practice for many years.

A more practical concern has to do with the performance and durability of expansion joints found in concrete pavement. These joints are used to control stresses; yet, the joints themselves require considerable maintenance. Cracks in jointed pavements are sometimes caused by corrosion of steel dowels that are installed in the joint. The purpose of these devices is to transfer loads across joints while allowing the joints to open and close freely in response to slab movements. When these dowels corrode, however, they may restrain joint movement, resulting in slab faulting and cracking. The use of road salt is a factor considered by highway agencies when selecting metals and coatings used in joint devices [7]. Yet, because joints are sometimes unsealed and exposed to numerous corrosion sources--such as moisture, dirt, and debris--it is difficult to attribute a portion of this pavement to road salt.

The corrosion of reinforcing steel bars and wire sometimes used in concrete pavement is another potential adverse effect of road salt. According to the Concrete Reinforcing Steel Institute, there are about 30,000 lane-miles of reinforced concrete pavement in the United States, mostly on freeways and other heavily traveled highways [8]. Reinforcing steel eliminates the need for joint devices and provides additional concrete tensile strength. Like concrete decks, reinforced pavement is susceptible to spalling and cracking caused by rebar corrosion. Overall, however, the extent and severity of this damage does not approach that of bridge decks, and the general condition of these pavements is thought to be well within the normal bounds for pavements serving high volumes of traffic [7]. During the 1970s, several incidents of severe spalling of reinforced pavements were linked to the use of deicing salts in Minnesota [7]. Since that time, however, few other serious problems have been reported, although some states, such as Wisconsin, are now using epoxy-coated steel in some new concrete pavement.

Drainage Systems

A portion of the salt spread on highways is ultimately washed through highway drainage and storm sewer systems, consisting of reinforced concrete culverts, metal pipes, catch basins, grates, manhole covers, curbs, and gutters. Because drainage systems account for about 10 percent of highway construction and maintenance expenditures and are important to highway operations and safety, their performance and durability are critical [9].

A severely deteriorated drainage system can be very difficult and expensive to repair. Conventional treatments, such as applying coatings and linings to pipes, are often costly and in some cases conflict with the original design objectives of the structure [9]. Hence, to prevent damage, new culvert pipes are often installed with extra wall thickness, galvanized coatings, and protective paving materials. Additionally, to prevent scaling and cracking due to

freeze-thaw cycles, air-entrained concrete and stone are used for curbs and grate spacers.

Although high chloride concentrations can enter highway drainage systems, the flow is usually rapid. High chloride concentrations that are sustained for a long period of time may accelerate the corrosion of drainage pipes by interfering with the natural formation of protective films and increasing the conductivity of water [10]. In addition, salt may contribute to scaling and cracking in improperly cured or over finished concrete grout, curbs, and grate spacers by aggravating freeze-thaw effects. In general, however, road salt is not considered a significant factor affecting the durability of drainage systems. During the past 30 years, several states have studied the performance of highway drainage systems. These studies have led highway agencies to conclude that the major factors affecting durability are: soil type, water chemistry (especially alkalinity and softness), traffic stress and vibration, silting, road settlement, erosion, and water abrasion [7, 10].

Roadside Hardware

Sign posts, light columns, circuitry in traffic signals, guardrails, wire fencing, retaining walls and noise barriers, as well as their concrete bases and connection hardware, are vulnerable to damage from road salt. Many highway fixtures and appurtenances are specially painted or constructed with corrosion-resistant materials. For example, wiring and fences are made of galvanized steel, light and sign supports are constructed of aluminum alloy tubing and anchored with stainless steel bolts, and guardrails are often painted with zinc-rich primer [11]. However, in general, the factors with the greatest affect on maintenance and replacement schedules of these components are normal wear, vehicle collisions, vandalism, obsolescence, and vibrations from traffic [11].

Sidewalks and Driveways

Public and private sidewalks and driveways may be exposed to salt from direct application, splash and spray from traffic, pedestrian and vehicle tracking, and runoff from salt-laden snowbanks. Because the concrete used in some sidewalks and driveways is poorly finished or improperly air entrained, it may scale and deteriorate more rapidly from freeze-thaw action when exposed to salt. Most damage to sidewalks and driveways, however, stems from settlement, erosion, growth of vegetation, and traffic stress [11]. The damaging effects of salt are likely to be minor compared with these other sources of damage.

Summary of Impacts on Other Highway Components

The durability of most highway components is affected by a number of factors, usually related to the quality of original

construction, maintenance practices, and the environment in which they are located. Road salt, therefore, is one of many factors affecting the condition of highway components. On the basis of the limited evidence available, the committee believes that salt-related costs of damage to highway components are sizable, but probably an order of magnitude smaller than total bridge costs, totalling to less than $100 million per year.

PARKING STRUCTURES

According to estimates derived from Census Bureau data [12], there are some 10,000 multilevel parking structures in the United States. About half of these structures are located in the salt-using regions of the Northeast and Midwest. Although they vary in type from freestanding facilities to multilevel decks integrated into other buildings, most are made of either cast-in-place or precast reinforced concrete. Many of these structures were built during the 1960s and 1970s, when concerns about salt-related corrosion were minimal. Most were originally designed for 40-year service lives without major deck repairs or renovation. During the past 10 to 15 years, however, hundreds of these structures have been deteriorating prematurely, in much the same manner as bridge decks.

During the winter months, road salt is dropped by cars onto the concrete flooring of parking structures. Over time, the chloride ions from the salt drippings seep into the flooring, reach the reinforcing steel, and induce corrosion. The process is similar to that of bridge deck corrosion; the rust product expands and exerts pressure, causing the surrounding concrete to crack. These cracks allow more moisture, salt, and oxygen to reach the embedded steel, further accelerating the corrosion process. Untreated, some of these cracks may expand to form delaminations that can lead to progressive structural weakening and losses in structure serviceability. In addition, leaky joints and faulty drainage systems can result in salt-induced corrosion and subsequent deterioration of underlying walls, electrical conduits, and concrete beams and support columns.

Parking Structure Repair Costs

As a result of decades of heavy salting, hundreds of parking structures have undergone major repair and rehabilitation during the past 20 years. The most common method of repair is simple patching and surface sealing, which is often combined with waterproof membranes. This treatment may postpone the need for additional repair by 2 to 6 years [13]. By the time numerous potholes appear, however, the garage deck is usually critically contaminated with salt, so continued corrosion and deterioration are inevitable unless more extensive repairs are made [14]. Longer-lasting repairs usually involve removal of the unsound concrete, cleaning of the reinforcing steel, and placement of a modified concrete that reduces

moisture penetration. This method of repair is about twice as expensive as simple patching but may postpone the need for more extensive repair by 10 years or more [13]. Other methods of repair include cathodic protection and injection of epoxy or other penetrants into cracks to serve as sealers.

According to estimates derived from Census Bureau data, about 5,000 parking structures are located in the salt-using regions of the Northeast and Midwest [12]. Many of these structures, especially older ones built during the 1950s and 1960s, have already undergone major rehabilitation because of salt damage. Meanwhile, many newer structures built during the 1980s, are equipped with state-of-the-art corrosion protection. Although it is difficult to project how many of these 5,000 garages will be damaged by continued salting, the most likely candidates are those built during the 1970s. Most of the roughly 500 to 1,500 garages built during that period (in salt-using regions) lack protective systems, and in recent years have started to show signs of salt-related decline.

Insufficient information is available to estimate precisely how many of these 500 to 1,500 garages will be seriously damaged during the next 10 years because of continued salting. However, if it is assumed for simplicity that 1 in 10 will become damaged each year, then 50 to 150 will need to be rehabilitated annually. The cost of the most common rehabilitation treatment--which involves concrete removal and replacement, cleaning of the reinforcing steel, and application of a special deck overlay--is about $\$7.50/ft^2$ [13]. The total surface area of a typical parking garage is about 150,000 ft^2. Hence, the average cost of rehabilitating a single parking garage damaged by salt is approximately $1 million ($\$7.50 \times 150{,}000\ ft^2$), and the total cost of rehabilitating 50 to 150 structures per year is $50 million to $150 million.

Parking Structure Protection Costs

In recent years, as corrosion damage has become more evident, most new parking garages have been built with design features and protective systems intended to reduce salt-related damage. About 90 percent of new parking structures are built with one or more protective systems [15]. Conventional systems--used in three-quarters of new structures--are penetrating sealers, membranes, and other surface treatments. Other systems include the use of galvanized or epoxy-coated reinforcing steel, additional concrete cover, and corrosion-inhibiting concrete additives [15]. In addition, much more attention is now paid to design and construction details, such as sloped floors for better drainage and proper concrete curing and finishing.

Corrosion protection increases the cost of constructing a new parking garage by about 1.5 percent, or on average, by about $100,000 [15]. Approximately 300 parking structures are built each year in the United States, resulting in annual spending on protection of approximately $30 million.

Summary of Parking Structure Costs

There are some 5,000 parking garages in the Northeast and Midwest. Like bridge decks, many older parking garages are critically contaminated with salt and will need to undergo major rehabilitation in the near future. Accordingly, a priority of the parking garage industry is to protect newer garages not already critically contaminated with chloride. During the next ten years, the total cost of protecting new garages ($30 million) and rehabilitating currently sound garages that become damaged by continued salting ($50 million to $150 million) will be roughly $75 million to $175 million per year.

SUMMARY OF INFRASTRUCTURE COSTS

Great strides have been made in the past 10 years in reducing the adverse side effects of salting by protecting infrastructure from corrosion. Advances are continuing and the outlook for further reductions in salt damage is promising. Collectively, however, the true cost of salting remains high, because of both corrosion protection costs and salt-related damage that persists despite this protection.

The committee's estimates of annual infrastructure costs are summarized in Table 3. The reliability of these estimates varies by cost item. Some cost items, such as bridge deck protection, can be quantified largely on the basis of available data. Summation of these more reliable cost estimates suggests a minimum infrastructure cost of between $200 million and $400 million per year. Several other cost items for which limited supporting data are available, such as damage to non-bridge highway components, can be approximated only on the basis of committee judgement. Inclusion of these items results in a less precise, although more complete, cost estimate of $400 million to $900 million per year (rounded to the nearest $100 million).

TABLE 3 SUMMARY OF ANNUAL COSTS TO INFRASTRUCTURE FROM SALTING

Cost Item	Annual Cost ($ millions)
Category I: Data are Relatively Reliable and Complete	
Bridge Decks	125 to 325
Parking Structures	75 to 175
Total	200 to 500
Category II: Estimates Based on Committee Judgement	
Bridge Non-Deck Components	125 to 325
Other Highway Components	100
Total	225 to 425
Total	425 to 925

REFERENCES

[1] Babaei, K., Hawkins N., NCHRP Report 297: Evaluation of Bridge Deck Protection Strategies, Transportation Research Board, National Research Council, Washington, D.C., 1987.

[2] American Association of State Highway and Transportation Officials. Manual for Bridge Maintenance, Washington, D.C., 1976.

[3] Perenchio, W., Fraczek, J., Pfeifer D., NCHRP Report 313: Corrosion Protection of Pre-stressing Systems in Concrete Bridges, Transportation Research Board, National Research Council, Washington, D.C., 1989.

[4] Shupack, M., "A Survey of the Durability Performance of Post-Tensioning Tendons," in American Concrete Institute Journal, October 1978, pp. 501-510.

[5] Woodward, R.J., "Collapse of a Segmental Post-Tensioned Concrete Bridge," in Transportation Research Record 1211, Transportation Research Board, National Research Council, Washington, D.C., 1989.

[6] Transportation Research Board, Special Report 202: America's Highways: Accelerating the Search for Innovation, National Research Council, Washington, D.C., 1984.

[7] Transportation Research Board, NCHRP Synthesis 60: Failure and Repair of Continuously Reinforced Concrete Pavement, National Research Council, Washington, D.C., 1979.

[8] Concrete Reinforcing Steel Institute, Construction of Continuously Reinforced Concrete Pavements, Schaumburg, Illinois, 1983.

[9] Transportation Research Board, NCHRP Synthesis 50: Durability of Drainage Pipe, National Research Council, Washington, D.C., 1978.

[10] Bednar, L., "Plain Galvanized Steel Drainage Pipe Durability Estimation with a Modified California Chart," in Transportation Research Record 1231, Transportation Research Board, National Research Council, Washington, D.C, 1989.

[11] American Public Works Association, Street and Highway Maintenance Manual, Chicago, Illinois, 1985.

[12] U.S. Department of Commerce, 1987 Census of Service Industries: Geographic Area Series, Report No. SC87-A-52, Bureau of the Census, 1989.

[13] Tighe, M., Van Volkinburg, D., "Parking Garage Crisis," Civil Engineering, September, 1989.

[14] American Concrete Institute, State-of-the-Art Report on Parking Structures, Report No. 362R-85, Detroit, Michigan.

[15] Parking Market Research Company, What's Going On Out There: A Statistical Analysis of Parking Construction in the United States, 1986-1989, McLean, Virginia, 1987.

Richard H. McCuen,[1] Pedro Albrecht,[1] and Jianguo Cheng[2]

A New Approach to Power-Model Regression of Corrosion Penetration Data

REFERENCE: McCuen, R. H., Albrecht, P., and Cheng, J. G. **"A New Approach to Power-Model Regression of Corrosion Penetration Data,"** *Corrosion Form and Control for Infrastructure, ASTM STP 1137*, Victor Chaker, Ed., American Society for Testing and Materials, Philadelphia, 1992.

ABSTRACT: Corrosion penetration data have traditionally been fit with the power model using a log transformation of both the exposure time and the penetration. The transformation has several disadvantages, including (1) the resulting model gives biased estimates of the penetration, (2) the sum of the squares of the errors in penetration are not minimized even though the sum of the squares of the logarithmic errors are minimized, and (3) the logarithmic transformation results in greater emphasis being placed on the penetration for the shorter exposure times.

An alternative method of fitting power models is discussed. The numerical calibration method is shown to produce better fitting and more rational power models than is provided with a logarithmic transformation. Unbiased power models can also be fitted. The fitting procedure is more complex than that for the log transform method.

The two fitting methods were compared using 32 sets of corrosion penetration data. The average standard error ratio for the numerical procedure was 58 percent of that for the logarithmic analyses, which suggests that the numerical procedure consistently produced better penetration estimates for the largest measured exposure time. Thus, more accurate 75-year projections of penetration should be expected with the numerical model. Analyses of the records suggest that record lengths of at least 10 years are necessary to produce accurate model coefficients.

KEYWORDS: Atmospheric corrosion, penetration, structures, weathering steel, power model, numerical optimization.

[1]Professor, Department of Civil Engineering, University of Maryland, College Park, MD 20742.

[2]Professor, Department of Mechanical Engineering, Nanjing Institute of Chemical Technology, Nanjing, China.

The interest in estimating the corrosion penetration at the end of the service life arose in civil engineering with the increased use of atmospheric corrosion-resistant steels for structural applications. Foremost among those steels are the ASTM High-Strength Low-Alloy Structural Steel (A242) and ASTM High-Strength Low-Alloy Structural Steel with 345 MPa Minimum Yield Point to 100-mm Thick (A588). Both are commonly referred to as *weathering steels*. Those steels have enhanced atmospheric corrosion resistance and are commonly used in a bare, unpainted condition. Therefore, engineers need to know how much steel will be lost to corrosion during the service life.

Two other steels have been exposed, along with weathering steel, in atmospheric exposure tests: *carbon steel*, with a maximum copper content of 0.04 percent; and *copper steel*, a carbon steel with about 0.20 percent copper. Copper steel is similar in composition to the old A440 structural steel, which has been deleted from the ASTM book of standards. The carbon and copper steels serve as references against which the corrosion penetration data for weathering steel have been compared. Neither should be used unpainted in structures. Lacking maintenance funds, highway and railway bridge owners are often unable to properly maintain paint systems. As a result, some carbon-steel bridges have corroded to a point where estimates of corrosion loss are needed to assess their remaining strength.

CORROSION ALLOWANCE

Engineers can compensate for the loss of strength by adding a corrosion allowance to the member thickness obtained from stress calculations. Domestic steel producers do not recommend such a corrosion allowance for bare, exposed weathering steel members because the small corrosion loss produces a negligible strength loss. This might be justified if weathering steel corroded at the rates of 0.51 and 1.3 lm/year/surface that the product literature advertises for Cor-Ten (™) and Mayari (™) weathering steels [*1,2*]. Engineers are cautioned that these rates were derived from atmospheric exposure tests of grades of A242 weathering steel of chemical compositions richer than those in use today for the same steel. Furthermore, most weathering steel structures are built from A588 steel, which is less corrosion resistant than A242 steel.

Faced with mounting evidence of much greater in-service corrosion losses than has been advertised, several specification-writing bodies are requiring corrosion allowances for bare, exposed weathering-steel structures. For example, the British Department of Transport calls for an increase of 1.0 mm/surface in rural and 2.0 mm/surface in industrial atmospheres. The German Institute of Steel Construcation, in its Guideline 007, calls for an increase in thickness of 0.8 mm/surface in rural, 1.2 mm/surface in urban, and 1.5 mm/surface in industrial and marine atmospheres, for a 60-year service life.

Albrecht et al. [*3*] have found that the corrosion penetration of weathering steel for bridges located in the contiguous United States can be contained by the upper bound

$$p = 50 + 7.5(t - 1) \quad (1)$$

where p = average corrosion penetration per surface in lm and t = exposure time in years. The corrosion rate of 7.5 lm/year/surface in Eq 1 is equal to the average steady-state corrosion rate of weathering steel falling in the ISO high corrosivity category [4]. Eq 1 implicitly assumes that the bridge is exposed to an environment in which the weathering steel can develop a protective oxide coating. It is based on corrosion penetration data from atmospheric exposure tests of A588 weathering steel coupons exposed in industrial environments [3,5,6] and measurements of corrosion loss in A588 steel bridges in rural and urban environments not exposed to salt-bearing traffic spray [7]. Substituting a service life of, say, t = 100 years gives a corrosion allowance of 0.6 mm/surface. This addition is not meant to compensate for such corrosion losses as would occur in very high corrosivity environments where weathering steel would not develop a protective oxide coating.

Clearly, to predict the corrosion loss at the end of the service life so that an allowance can be added to member thickness, one must be able to accurately extrapolate corrosion penetration data.

LOG-LOG FITTING OF POWER MODEL

Corrosion penetration data has typically been modeled using the power model structure:

$$\hat{p} = b_o t^{b_1} \quad (2)$$

in which $\hat{p}$ is the predicted value of the corrosion penetration p, t is the time, and b_o and b_1 are the regression coefficients. Equation 2 is used as the sample estimator for one of two population models:

$$p = \beta_o \, t^{\beta_1} \, e_i \quad (3)$$

or

$$p = \beta_o \, t^{\beta_1} + e_i \quad (4)$$

in which b_o and b_1 are the partial regression coefficients of the population, and e_i is the residual for observation i. Equation 3 is a multiplicative error model, while Eq 4 is an additive error model.

Equation 2 is typically fitted to measured data by taking logarithms of the two variables and expressing the logarithms of the variables in a relationship with a linear structure:

$$\log \hat{p} = \log b_o + b_1 \log t \quad (5)$$

Making the transformations $\hat{y} = \log \hat{p}$, $c = \log b_o$, and $x = \log t$ gives the standard form for linear regression analysis:

$$\hat{y} = c + b_1 x \quad (6)$$

The value of b_o is obtained for Eq 2 by the retransformation

$$b_o = 10^c \quad (7)$$

The least squares evaluation of Eq 6 gives an unbiased log-log model in that the resulting coefficients yield $Re_i = 0$, where e_i is the sample estimate of e_i. The coefficients c and b_1 of Eq 6 are unbiased estimators for Eq 5; the coefficients of Eq 5 are not necessarily unbiased estimators of the coefficients of Eqs 3 and 4. Goodness-of-fit statistics, such as the correlation coefficient, R, and the standard error of estimate, S_e, obtained from the fit of Eq 6 are often incorrectly used to reflect the accuracy of Eq 2.

In assessing the accuracy and applicability of prediction equations, the characteristics of the residuals are important. The error terms of Eqs 6 and 4 are additive, while for Eq 3 the error term is multiplicative. Thus, the errors for Eq 6 have constant variance in terms of y but not necessarily in terms of p.

To summarize the problem, the fitting of the power model of Eq 2 using the logarithmic transform of Eq 5 leads to an equation that has biased partial regression coefficients (i.e., b_1 is a biased estimator of b_1) and provides biased estimates of p. Furthermore, the goodness-of-fit statistics (i.e., R and S_e) for the logarithmic form in Eq 5 do not reflect the accuracy of predictions made with Eq 2. The objective herein is to briefly discuss a method of obtaining better estimates of the partial regression coefficients b_i of Eq 4, and estimates of p that are unbiased and have a smaller error variance than those obtained using a logarithmic transformation for Eq 5.

INDICES FOR ASSESSING MODELS

In engineering design, decisions are based on the $\hat{p}$ of Eq 2 rather than the log $\hat{p}$ of Eq 5. Therefore, one should be concerned about the accuracy of estimates $\hat{p}$, not log $\hat{p}$. Specific goodness-of-fit indicators are the mean error, which is a measure of the bias, and the mean square error, which is a measure of the accuracy of prediction. The mean error is the bias defined as:

$$\bar{e} = \sum_{i=1}^{n} e_i = \sum_{i=1}^{n} (\hat{w}_i - w_i) \tag{8}$$

in which w can be either log p or p, depending on whether the bias is calculated in the log p-space or the p-space, where $\hat{w}$ is the predicted value of w. The standard error of estimate, S_e, is the standard deviation of the errors, with the mean square error adjusted using the appropriate number of degrees of freedom m:

$$S_e = \left[\frac{1}{\nu} \sum e^2\right]^{0.5} = \left[\frac{1}{n-2} \sum (\hat{w}_i - w_i)^2\right]^{0.5} \tag{9}$$

When Eqs 8 and 9 are computed with the errors in the logarithmic space, then $\bar{e}$ and S_e apply only to log $\hat{p}$, not $\hat{p}$.

The correlation coefficient is a measure of the accuracy for a linear unbiased model and is computed by:

$$R = \left[\frac{\sum_{i=1}^{n} (\hat{w}_i - \bar{w}_i)^2}{\sum_{i=1}^{n} (w_i - \bar{w}_i)^2} \right]^{0.5} \quad (10)$$

in which $\bar{w}$ is the mean of w. Equation 10 can be applied to the power model, whereas the more commonly used form for computing R only applies to the linear model. Fitting Eq 5 using ordinary least squares provides unbiased estimates of log $\hat{p}$ and estimates of log $\hat{p}$ that have the minimum expected variation in the log p-space. Thus, the correlation coefficient reflects the accuracy of the unbiased estimates of log $\hat{p}$. However, when Eq 2 is fitted using the logarithmic transformation, it is not unbiased and does not have the minimum expected error variance in the y-space; thus, the correlation coefficient computed with the logarithmically transformed data for Eq 5 does not apply to Eq. 2 because the model is nonlinear and the estimates $\hat{y}$ are biased. One additional problem with the transformed calibration of Eq 5 is that the fitted coefficients reflect the sensitivity of log p to log t and not the sensitivity of p to t. Thus, the logarithmically derived coefficients are not unbiased estimators for assessing the effects of the predictor variable t on p.

NUMERICAL FITTING OF POWER MODEL

The problems associated with fitting Eqs 3 and 4 using a logarithmic transformation of Eq 2 can be overcome with a numerical fitting method that obtains values for the coefficients of Eq 2 directly, i.e., without a logarithmic transformation. A number of such methods are described in the literature. For example, McCuen and Snyder [*8*] fitted functionals with a nonlinear least squares method described briefly in the Appendix. Readers can obtain an executable program for this method, called NUMOPT, by sending to the first author a disk formatted for IBM compatible computers. Alternatively, data can be fitted numerically with any steepest descent or conjugate gradient method [*9,10*]. Numerically based pattern search methods minimize the sum of squares of the errors, just as is done in the least squares solution of Eq 6. The computer efficiency of the numerical methods can be enhanced with such aides as acceleration, deceleration, and pattern memory [*8*].

The numerical approach has several advantages for the additive model of Eq 4. Numerical fitting can lead to unbiased estimates in the p-space rather than the log p-space and can yield a smaller error variance in the p-space than is possible for the model fit it in the log p-space. Thus, the coefficient b_i will be the most efficient estimator of b_i in a statistical sense. Numerical fitting can also be used to fit other nonlinear functional forms, and fitting criteria other than minimizing the sum of the squares of the errors can be used.

Numerical fitting is not without disadvantages. First, the fitting algorithm is more complex. However, this is not an important problem since prepared computer programs are readily available.

Second, the computation time for numerical solutions is greater than that for analytical solutions such as ordinary least squares; however, with the availability of computers, this is also not a major problem. Third, numerical solution algorithms require initial estimates of the unknowns, which for the case of the model of Eq 2 would be the b_i coefficients. When using numerical fitting, the values of the coefficients from the analytical solution with the logarithmic transformation of Eq 6 can be used as the initial estimates for the numerical solution. The most significant problem with the numerical fitting is that the bias (measured in the y-space) is not a criterion function, so several trials may be necessary to reduce the bias to the point where it is essentially zero.

ATMOSPHERIC EXPOSURE TESTS

Albrecht and Lee [*6*] compiled corrosion penetration data for 104 sets of carbon, copper, A588, and A242 steel coupons that other investigators had exposed to the atmosphere at different sites across the United States. Each set consisted of multiple specimens of one type of steel exposed at one site. The 32 sets with the longest exposure times were retained for analysis in the present study. Table 1 summarizes the following information for each set: reference number, exposure site, type of environment, type of steel, exposure time at end of test, and number of data points.

The tests were performed at sites broadly classified by type of atmosphere as follows:

- *Rural environments*: South Bend and Saylorsburg, Pennsylvania.
- *Industrial environments*: Bayonne, Kearny, and Newark, New Jersey; Rankin, Bethlehem, and Monroeville, Pennsylvania; and Columbus, Ohio.
- *Marine environments*: Kure Beach, North Carolina, 25- and 250-m lots.

Semi-rural South Bend was included with the rural environments, and semi-industrial Monroeville with the industrial environments. The atmosphere in South Bend is more aggressive than is typical of rural atmospheres. The Kure Beach lots located 25 and 250 m from the shore line represent severe and moderate marine environments.

The longest exposure times were 10 to 20 years in rural and industrial environments and 7.5 to 16 years in marine environments.

Most specimens consisted of 150-mm long by 100-mm wide by 0.75-mm thick coupons. Some investigators tested other types of specimens such as 300-mm long strip tensile specimens of 22 gauge sheet [11,12] and 300-mm by 300-mm coupons of 0.8-mm to 6.3-mm thickness [*13*].

To minimize the corrosion penetration, most specimens were mounted on racks at an angle of 30 deg, facing south, as is recommended in the ASTM Standard Practice for Conducting Atmospheric Corrosion Tests on Metals (G50). The exception to this standard exposure were the specimens that faced the ocean at the 25-m lot in Kure Beach [*14-16*].

TABLE 1--Atmospheric exposure tests.

Set No.	Reference No.	Exposure Site	Type of Environment	Exposure Time at End of Test t_{end} (yr)	No. of Data Points n
		Carbon Steel			
1	11,12	Rankin, PA	Industrial	10.0	12
2	11,12	Bethlehem, PA	Industrial	10.0	12
3	11,12	Columbus, OH	Industrial	10.0	11
4	19,20	Saylorsburg, PA	Rural	16.0	5
5	17,24	Newark, NJ	Industrial	16.0	5
6	19,20	Bethlehem, PA	Industrial	16.0	5
7	14,15,16	Newark, NJ	Industrial	15.5	5
8	14,15,16	Kure Beach, NC	Marine (250 m)	7.5	4
9	13,18,22	Kearny, NJ	Industrial	20.0	5
		Copper Steel			
10	11,12	Rankin, PA	Industrial	10.0	12
11	11,12	Bethlehem, PA	Industrial	10.0	12
12	11,12	Columbus, OH	Industrial	10.0	11
13	19,20	Saylorsburg, PA	Rural	16.0	5
14	13,18,22	Kearny, NJ	Industrial	20.0	5
15	21	Bayonne, NJ	Industrial	18.1	6
16	21	Kure Beach, NC	Marine (250 m)	7.5	4
		A588 Steel			
17	19,20	Saylorsburg, PA	Rural	16.0	5
18	19,20	Bethlehem, PA	Industrial	16.0	5
19	19,20	Kure Beach, NC	Marine (250 m)	16.0	5
20	17,24	Newark, NJ	Industrial	16.0	5
21	14,15,16	South Bend, PA	Semi-rural	15.5	4
22	14,15,16	Monroeville, PA	Semi-industrial	15.5	4
23	14,15,16	Newark, NJ	Industrial	15.5	5
24	14,15,16	Kure Beach, NC	Marine (250 m)	15.5	5
25	14,15,16	Kure Beach, NC	Marine (25 m)	7.5	4
		A242 Steel			
26	11,12	Rankin, PA	Industrial	17.0	12
27	11,12	Columbus, OH	Industrial	10.0	11
28	19,20	Saylorsburg, PA	Rural	16.0	5
29	19,20	Bethlehem, PA	Industrial	16.0	5
30	14,15,16	South Bend, PA	Semi-rural	15.5	4
31	14,15,16	Kure Beach, NC	Marine (250 m)	15.5	5
32	13,18,22	Kearny, NJ	Industrial	20.0	5

Replicate specimens were removed from the racks at predetermined exposure intervals. The removal schedules were: 0.5, 1, 1.5, 2, 3, 4, 5, 6, 7, 8, 9, 10, and 17 years [*11,12*]; 1, 2, 4, 8, and 16 years [*17-20*]; 0.5, 1.5, 3.5, 7.5, and 15.5 years [*14-16,18,21*]; and 1, 2.5, 5, 10, and 20 years [*13,18,22*]. The specimens were chemically stripped of corrosion products. The corrosion penetration was calculated from the measured mass loss as is recommended in the ASTM Standard Practice for Preparing, Cleaning, and Evaluating Corrosion Test Specimens (G1). All values of corrosion penetration and corrosion rate are per exposed surface.

The corrosion penetrations of the replicate specimens that were exposed for the same length of time were then averaged, and the mean value at each exposure interval was reported. This practice is inadmissible from the viewpoint of statistical analysis. All values must be reported, and a corrosion penetration versus exposure time curve must be fitted through all data points, not just through the points for averages of replicate tests.

COMPARISON OF FITTING METHODS

Thirty-two sets of corrosion penetration data were fitted with the power model of Eq 2. In the log-log method, the coefficients b_0 and b_1 were fitted to minimize the sum of the squares of the errors. In the NUMOPT method, the coefficients were fitted to provide zero bias, with the sum of the squares of the errors being a minimum for the zero-bias constraint. Tables 2 and 3 list the regression coefficients, b_0 and b_1, for all 32 sets of data fitted with the log-log and NUMOPT methods, respectively. The fitting methods are compared in Figs. 1 through 3 for steels exposed in Rankin, Saylorsburg and Kure Beach. As is apparent from the figures, the NUMOPT method fitted the data consistently better than did the log-log method. Relative to the data points and the curves predicted with the NUMOPT method, the log-log method underestimated the penetration for some combinations of steel and environment and overestimated it for others.

The accuracy of the fitting methods was determined by comparing the standard error ratio, S_e/S_y, the mean prediction error (bias), $\bar{e}$, and the prediction error at the end of the test, e_{end}. The results are summarized in Tables 2 and 3 for the log-log and NUMOPT methods.

The standard error ratio, S_e/S_y, indicates the overall accuracy of prediction and reflects both the precision and the bias of the method. For every set, the standard error ratio was lower for the NUMOPT method (see fourth column in Table 3) than for the log-log method (Table 2), which indicates that the error variation from the NUMOPT method is always smaller than that from the log-log method. On the average, the standard error ratio for the NUMOPT method was 58 percent of the standard error ratio for the log-log method, calculated as the average of the ratio of standard error ratios listed in the last column of Table 3. The minimum value of the ratio of standard error ratios was 39 percent for A242 steel exposed in Kearny (set 32); and the maximum was 79 percent for carbon steel exposed in Bethlehem and Columbus (sets 2 and 3). Clearly, the NUMOPT method is consistently more accurate than the log-log method.

TABLE 2--Results of regression analysis; log-log method.

Set No.	Regression Coefficients		Standard Error Ratio	Mean Error (Bias)	Error at End of Test
	b_0	b_1	S_e/S_y	$\bar{e}$ (μm)	e_{end} (μm)
			Carbon Steel		
1	72.03	0.6156	0.194	-2.2	-36.8
2	71.87	0.4595	0.116	-0.1	2.0
3	55.15	0.5059	0.140	-0.3	-2.8
4	32.43	0.6573	0.136	0.6	12.6
5	50.73	0.3358	0.044	0.0	1.7
6	75.01	0.3125	0.078	-0.0	2.4
7	48.17	0.3893	0.137	0.1	6.0
8	40.36	0.7203	0.481	0.8	29.3
9	58.96	0.3355	0.076	0.0	-3.9
			Copper Steel		
10	59.00	0.5917	0.191	-1.2	-31.0
11	62.48	0.4245	0.098	-0.0	6.1
12	48.79	0.5022	0.282	-1.1	-11.9
13	28.62	0.5827	0.115	-0.1	7.0
14	29.06	0.3529	0.167	-0.2	-5.3
15	52.24	0.4216	0.080	-0.2	-5.1
16	33.32	0.6620	0.260	0.7	12.5
			A588 Steel		
17	28.37	0.4294	0.157	0.1	5.3
18	42.12	0.3035	0.189	0.0	3.7
19	28.96	0.6197	0.097	-0.5	-7.6
20	36.14	0.2784	0.049	-0.0	-0.8
21	29.07	0.4538	0.092	0.1	1.2
22	30.86	0.3838	0.074	-0.0	-1.4
23	33.53	0.3055	0.065	-0.0	-1.2
24	35.73	0.5491	0.163	-0.8	-14.1
25	109.95	1.0051	0.456	7.7	147.1
			A242 Steel		
26	29.72	0.3506	0.238	0.0	9.3
27	35.73	0.3557	0.238	-0.1	3.8
28	21.06	0.3590	0.136	0.0	1.0
29	32.65	0.1982	0.047	-0.1	-0.4
30	21.46	0.2853	0.113	-0.0	-1.1
31	23.08	0.5435	0.186	-0.4	-8.6
32	15.75	0.1755	0.244	-0.0	-1.4

TABLE 3--Results of regression analysis; NUMOPT method.

Set No.	Regression Coefficients		Standard Error Ratio	Mean Error (Bias)	Error at End of Test	Ratio of Errors at End of Test (NUMOPT/ log-log)	Ratio of Standard Error Ratios (NUMOPT/ log-log)
	b_0	b_1	S_e/S_y	$\bar{e}$ (μm)	e_{end} (μm)		
				Carbon Steel			
1	59.69	0.7356	0.119	0.0	-9.3	0.25	0.61
2	72.11	0.4501	0.092	0.0	-1.7	0.85	0.79
3	53.82	0.5242	0.111	0.0	0.8	0.29	0.79
4	36.14	0.5984	0.074	0.0	1.8	0.14	0.54
5	51.24	0.3297	0.023	0.0	0.9	0.53	0.52
6	75.27	0.3105	0.045	0.0	2.1	0.88	0.58
7	50.51	0.3586	0.072	0.0	1.0	0.17	0.53
8	50.44	0.5413	0.268	0.0	7.1	0.24	0.56
9	58.00	0.3445	0.044	0.0	-2.4	0.61	0.58
				Copper Steel			
10	50.84	0.6873	0.131	0.0	-13.5	0.44	0.69
11	63.08	0.4185	0.075	0.0	5.4	0.89	0.77
12	44.97	0.5639	0.218	0.0	-2.3	0.19	0.77
13	30.88	0.5399	0.060	0.0	1.0	0.14	0.52
14	27.35	0.3861	0.091	0.0	-2.0	0.38	0.54
15	52.85	0.4353	0.050	0.0	-2.6	0.51	0.62
16	37.79	0.5566	0.123	0.0	2.0	0.16	0.47
				A588 Steel			
17	29.98	0.3970	0.087	0.0	2.1	0.40	0.55
18	43.61	0.2821	0.093	0.0	1.5	0.41	0.49
19	26.72	0.6641	0.053	0.0	-0.5	0.07	0.55
20	35.96	0.2816	0.026	0.0	-0.5	0.62	0.53
21	29.83	0.4399	0.051	0.0	0.1	0.08	0.55
22	30.48	0.3906	0.039	0.0	-0.8	0.57	0.52
23	33.31	0.3102	0.040	0.0	-0.8	0.67	0.62
24	31.74	0.6180	0.099	0.0	-2.3	0.16	0.61
25	159.88	0.7317	0.246	0.0	12.4	0.08	0.54
				A242 Steel			
26	31.21	0.3192	0.161	0.0	6.2	0.67	0.68
27	36.06	0.3503	0.169	0.0	3.6	0.95	0.71
28	21.65	0.3430	0.077	0.0	0.0	0.00	0.57
29	32.65	0.2004	0.019	0.0	-0.3	0.75	0.40
30	21.06	0.2960	0.048	0.0	-0.6	0.55	0.42
31	20.92	0.6010	0.131	0.0	-2.3	0.27	0.70
32	15.42	0.1881	0.096	0.0	-0.9	0.64	0.39

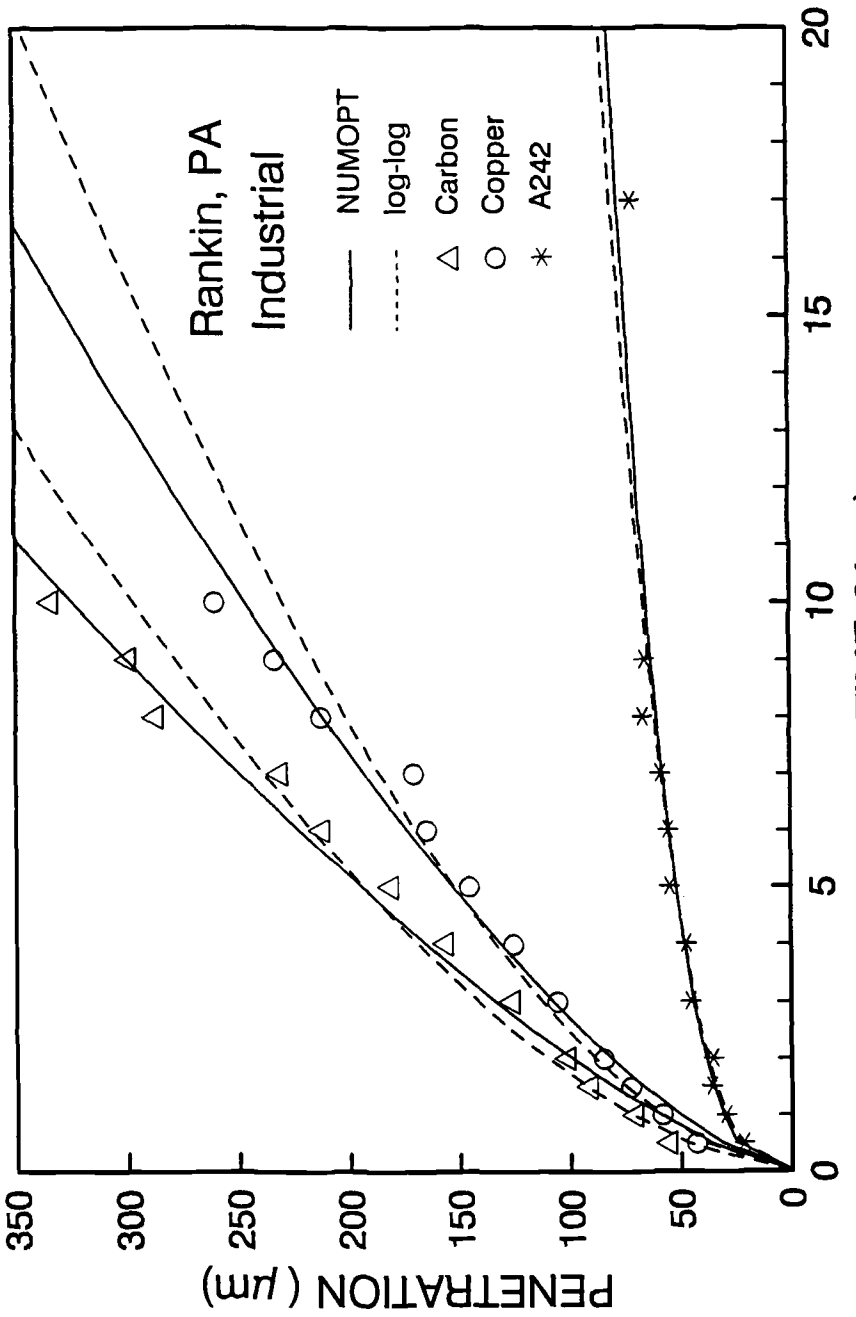

FIG. 1--Corrosion Penetration of Carbon, Copper and A242 Steels Exposed to Rankin, Pa., Industrial Atmosphere [11,12]

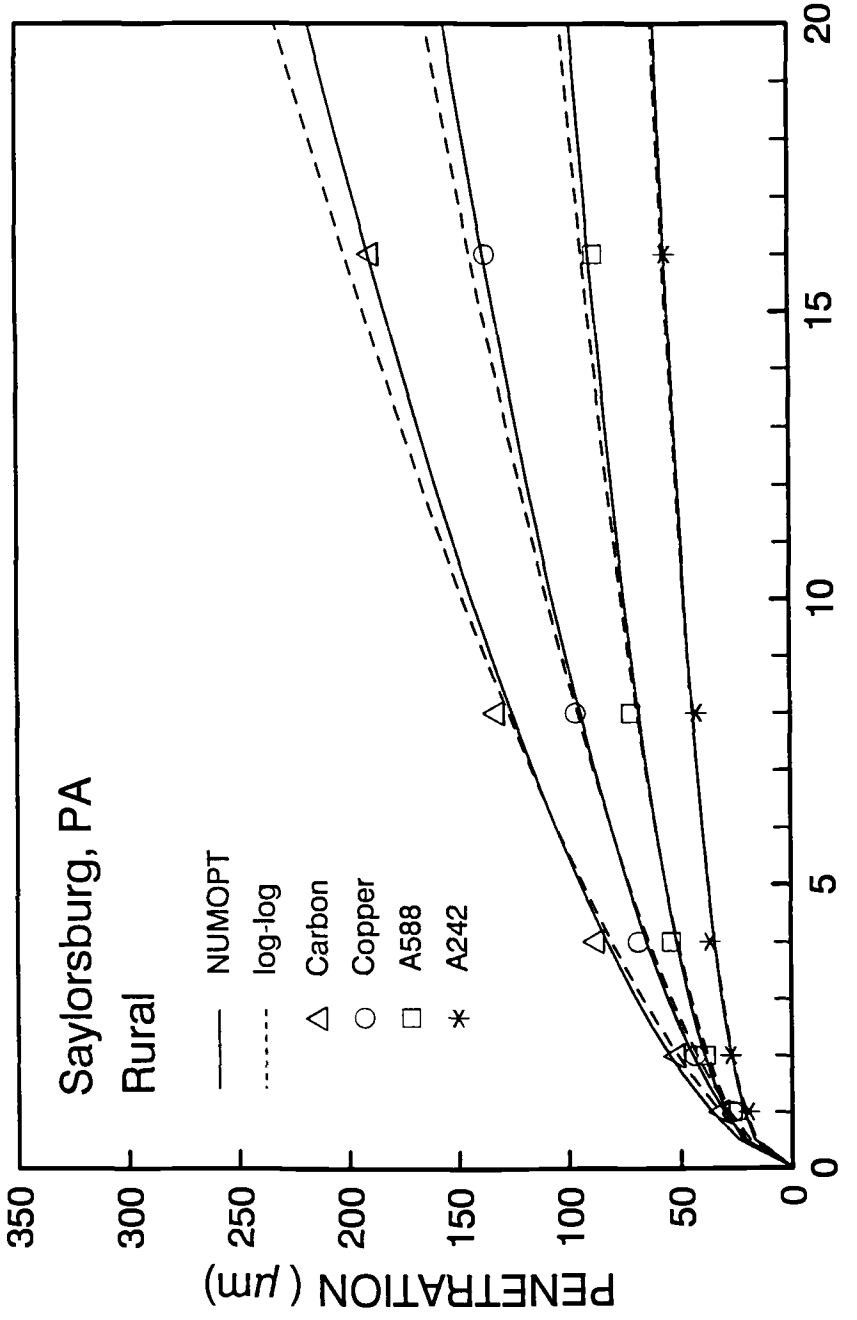

FIG. 2--Corrosion Penetration of Carbon, Copper, A588 and A242 Steels Exposed to Saylorsburg, Pa., Rural Atmosphere [19,20]

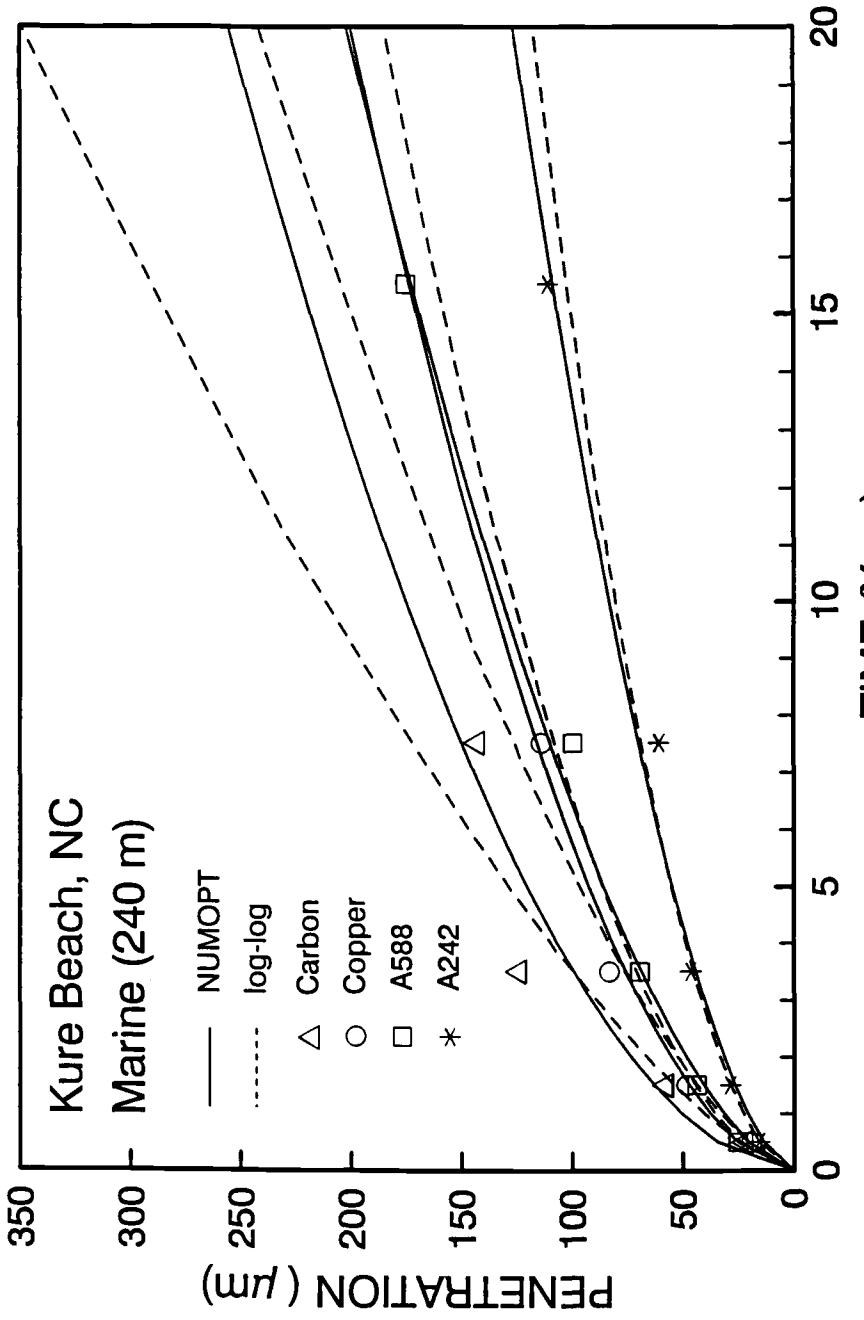

FIG. 3--Corrosion Penetration of Carbon, Copper, A588 and A242 Steels Exposed to Kure Beach, NC, Marine Atmosphere [14,15,16]

TABLE 4--Predicted corrosion penetration.

Set No.	Penetration at End of Test			Penetration at 75 Years		
	Log-log Method p (μm)	NUMOPT Method p (μm)	Ratio (NUMOPT/ log-log)	Log-log Method p (μm)	NUMOPT Method p (μm)	Ratio (NUMOPT/ log-log)
			Carbon Steel			
1	308	336	1.09	1069	1430	1.34
2	210	210	1.00	535	539	1.01
3	173	177	1.02	473	504	1.06
4	201	190	0.95	554	479	0.86
5	129	128	0.99	216	213	0.98
6	178	178	0.10	289	288	1.00
7	140	135	0.96	259	238	0.92
8	172	150	0.87	905	522	0.58
9	161	163	1.01	251	257	1.02
			Copper Steel			
10	239	256	1.07	798	1000	1.25
11	164	164	1.00	383	380	0.99
12	147	164	1.12	396	554	1.40
13	144	138	0.96	354	318	0.90
14	84	87	1.04	133	145	1.09
15	184	186	1.01	335	346	1.08
16	127	116	0.92	581	418	0.72
			A588 Steel			
17	93	90	0.97	181	166	0.92
18	98	95	0.98	156	147	0.94
19	161	169	1.04	421	470	1.12
20	78	79	1.00	120	121	1.01
21	101	100	0.99	206	199	0.97
22	88	89	1.01	162	165	1.02
23	78	78	1.01	125	127	1.01
24	161	173	1.07	383	458	1.20
25	833	699	0.84	8430	3765	0.45
			A242 Steel			
26	78	75	0.97	130	121	0.93
27	82	83	1.00	171	169	0.99
28	57	56	0.98	99	95	0.96
29	57	57	1.00	77	77	1.01
30	47	47	1.01	74	76	1.03
31	102	109	1.06	241	280	1.16
32	27	27	1.02	34	35	1.08

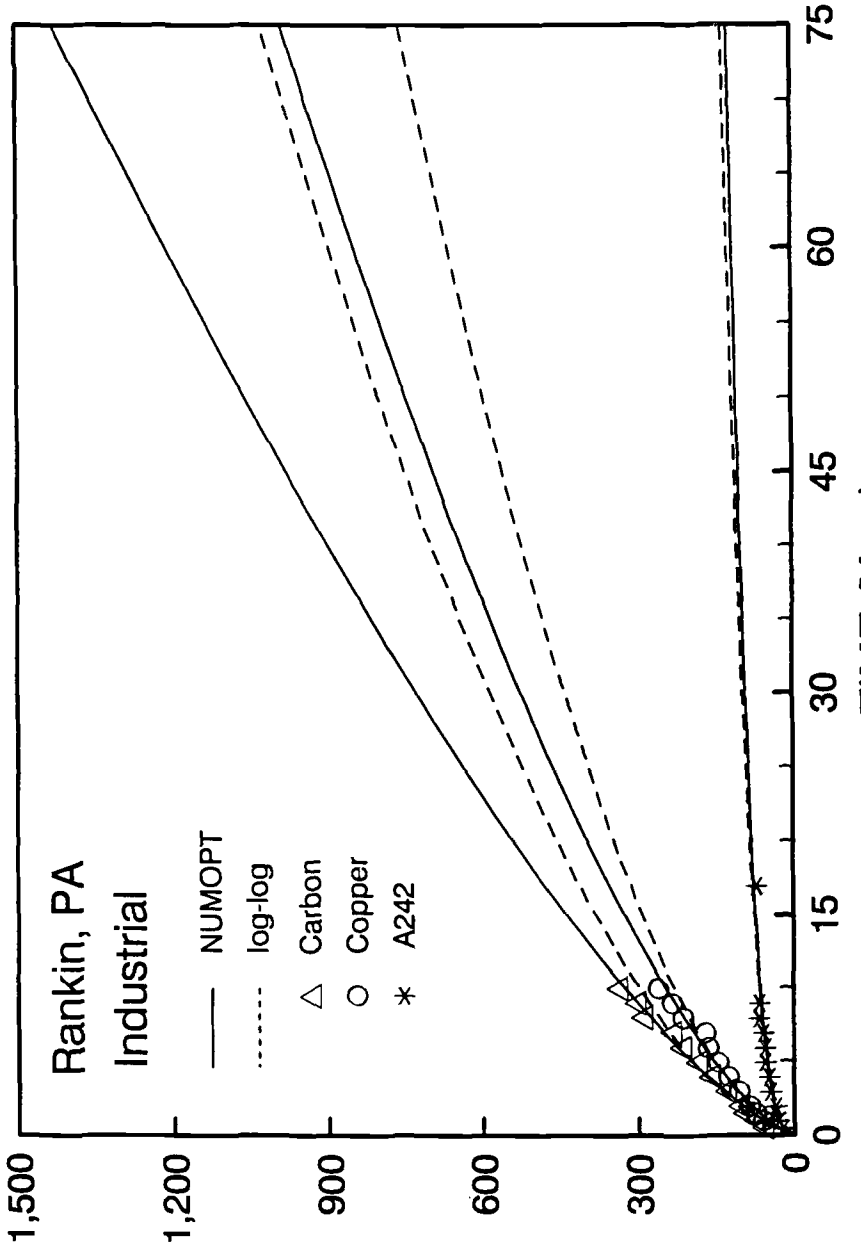

FIG. 4--Estimated Corrosion Penetration at End of 75-Year Service Life; Carbon, Copper, and A242 Steels Exposed to Rankin, Pa., Industrial Atmosphere [11,12]

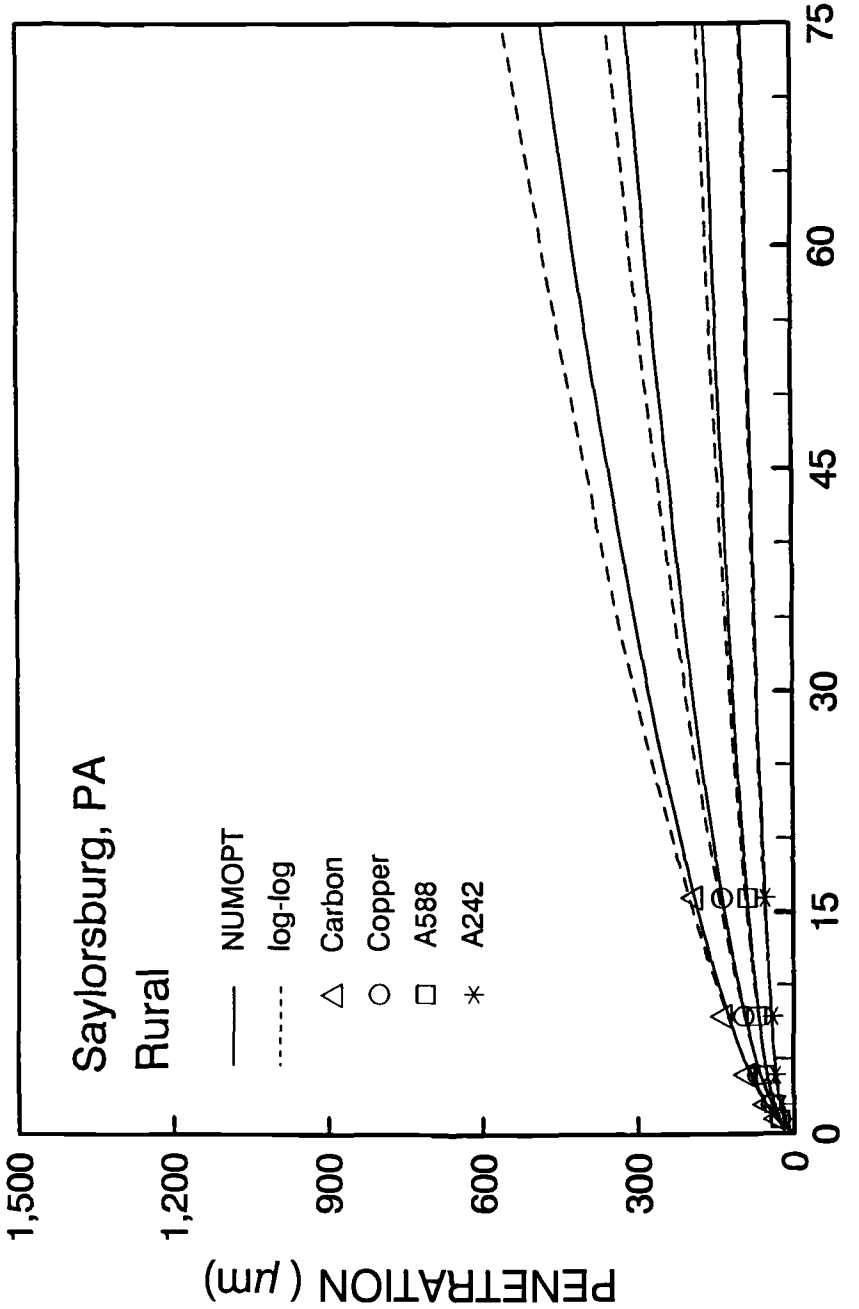

FIG. 5--Estimated Corrosion Penetration at End of 75-Year Service Life; Carbon, Copper, A588 and A242 Steels Exposed to Saylorsburg, Pa., Rural Atmosphere [19,20]

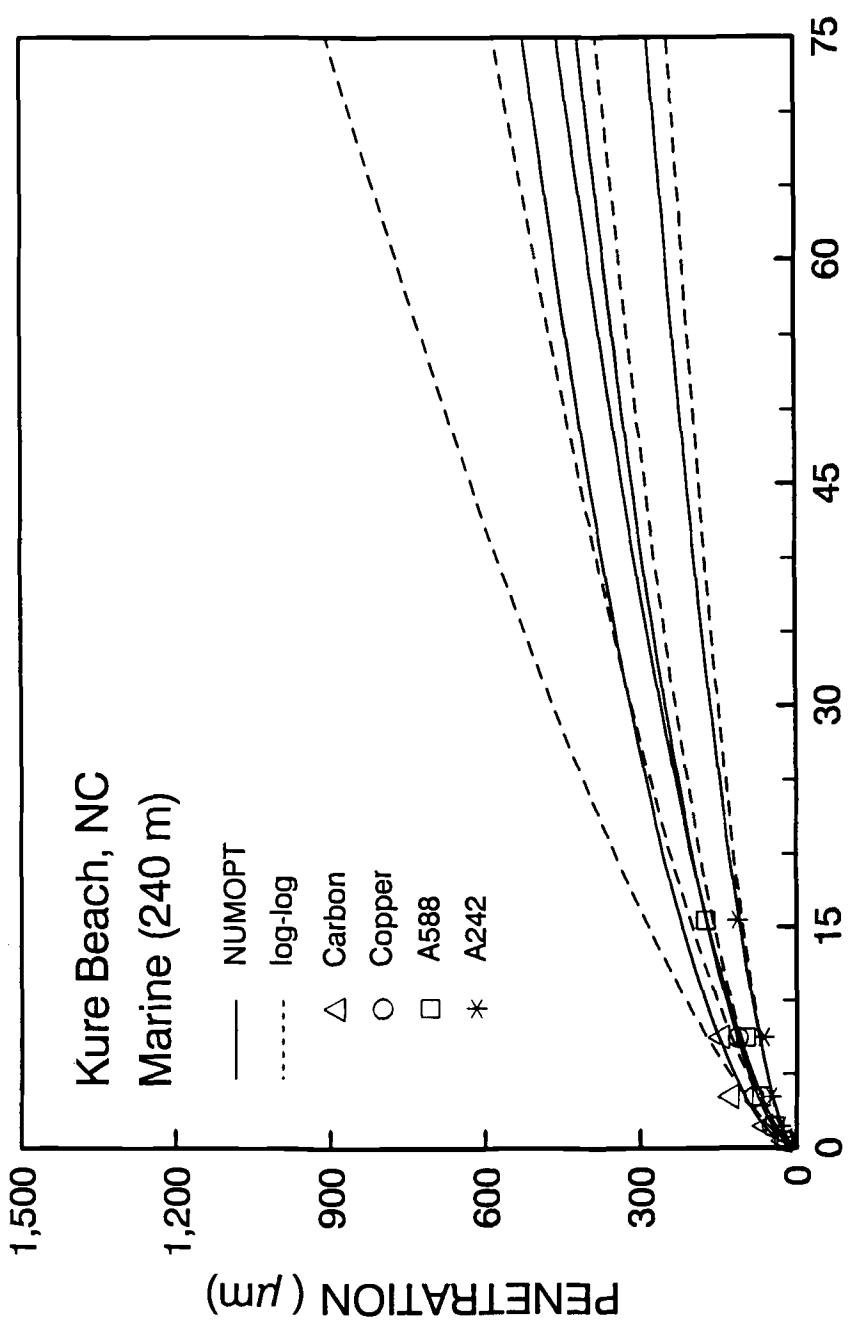

FIG. 6--Estimated Corrosion Penetration at End of 75-Year Service Life; Carbon, Copper, A588 and A242 Steels Exposed to Kure Beach, NC, Marine Atmosphere [14,15,16]

Although the biases were small for the log-log method, they were not zero. The largest value was $\bar{e}$ = 7.7 lm for A588 steel exposed in the 25-m lot in Kure Beach (set 25 in Table 2), which means that the log-log method overpredicted the penetration on average by 7.7 lm. The second largest value was $\bar{e}$ = -2.2 lm for carbon steel exposed in Rankin (set 1). In this case, the log-log method underpredicted the penetration. The bias was positive for some sets of data and negative for other sets, with no clear trend. In contrast, the NUMOPT method provided unbiased estimates of penetration, $\bar{e}$ = 0.0 for all sets of data in Table 3.

The prediction error at the end of the test, e_{end}, is indicative of how accurately the method can be expected to extrapolate the penetration to the end of the service life of the bride. This value was computed at the exposure time, t_{end}, at which the last specimens in a set were removed from the rack. The seventh column in Table 3 lists the ratio of the NUMOPT to log-log errors at the end of the test. All ratios were less than 1.0, indicating that the NUMOPT method consistently estimated the penetration more accurately than did the log-log method. Likewise, one can expect that the NUMOPT method would more accurately extrapolate the penetration to the end of the service life.

Logarithmic transformation of the data gives more weight to the penetration at shorter exposure times and less weight to the penetration at longer times. This is evident in Figs. 1 through 3. The log-log method fits the data better at short exposure times, while the NUMOPT method is more accurate at long exposure times. Since long-term data are more reliable, it does not seem rational to underweigh the larger penetrations as does the log-log method.

COMPARISON OF 75-YR PENETRATIONS

Estimates of corrosion penetration at the end of the service life of a bridge are needed to predict the remaining strength of corroded steel members. Table 4 summarizes for all 32 data sets the penetrations at the end of the test and at the end of a 75-year service life as predicted with the log-log and NUMOPT methods. Figs. 4 through 6 show the predicted penetration curves for steels exposed in Rankin, Saylorsburg, and Kure Beach, respectively. The data suggest three general conclusions.

First, the differences in predicted penetrations increase the farther the data are extrapolated. This trend is readily apparent for the 11 sets of data fitted in Figs. 4 through 6 in which the curves predicted with the log-log and NUMOPT methods diverge as exposure time increases. Another way of showing this trend is to calculate the ratio of the penetrations predicted with the NUMOPT and log-log methods, first at the end of the test and then at 75 years. The results are listed in columns four and seven of Table 4. They show that for all sets of data, without exception, a ratio of predicted penetrations greater than one at the end of the test becomes even larger at 75 years. Conversely, a ratio less than one at the end of the test becomes even smaller at 75 years. Since prediction errors are magnified in time, engineers are advised to fit corrosion penetration data with the more accurate NUMOPT method.

Second, the differences decrease as steel becomes more corrosion resistant, that is, in the order of carbon, copper, A588, and A242 steel. Indeed, the average absolute difference between the 75-year penetrations predicted with the log-log and NUMOPT methods (column five minus column six in Table 4) is: 104 lm for carbon steel, 70 lm for copper steel, 20 lm for A588 steel, and 9 lm for A242 steel. Assuming a corrosion allowance of, say, 1.0 mm over the service life, the method of fitting can account for as much as 10 percent of the allowance. Clearly, the method of fitting is important for some types of steel.

Third, the differences in predicted penetrations are positive for some data sets and negative for others. This is also evident from the ratio of predicted 75-year penetrations (see last column of Table 4), which varies from values smaller to larger than 1.0 for all types of steel. There appears to be no trend between the sign of the difference and type of steel or environment.

Finally, sample size contributes to the variation of the predicted 75-year penetration. Most sample sizes are small, meaning that the sampling variation of the coefficients is quite large. Inaccurate coefficients can contribute significantly to inaccurate estimates. The former practice of reporting only the average penetration of replicate coupons exposed for the same length of time compounds this problem. The available data are not sufficient to draw conclusions regarding the effect of sample size.

Other factors that contribute to the accuracy of predicting 75-year penetrations are the duration of the exposure test and the part of the record that is retained for analysis. These effects are examined in the following sections.

EFFECT OF ADDING LONG-TERM EXPOSURE DATA

The corrosion penetration at the end of a 75-year service life must often be estimated based on data from exposure tests of short duration. Since the duration of a test is typically much shorter than the service life of a bridge, engineers should clearly understand the reliability of extrapolating short-term exposure data.

The effect of test duration was examined by analyzing six data sets for carbon and weathering steels exposed in Rankin, Saylorsburg, and Kure Beach. All data were fitted with the NUMOPT method, with zero bias. As an example, for carbon steel exposed in Rankin the 0- to 2-year data were fitted first. Thereafter, data for progressively longer exposure durations were added -- 0 to 4 years, followed by 0 to 8 years -- until the sample contained all data from 0 to 10 years. The results of the analyses are given in Table 5 and plotted in Figs. 7 through 9.

The results show that exposure duration has a large and quite unpredictable effect on the estimated 75-year penetration. The effect appeared to be greater for steels of lower corrosion resistance, such as carbon steel, and for environments of higher corrosivity, such as the marine environment of Kure Beach. Conversely, it was smaller for weathering steel and the rural environment of Rankin.

For example, the estimated 75-year penetration of carbon steel exposed in industrial Rankin was 535 lm for the 0- to 2-year data

TABLE 5--Effect of adding long-term exposure data on predicted 75-year penetration.

Exposure Time (yr)	No. of Data Points n	Regression Coefficients b_0	b_1	Standard Error Ratio S_e/S_y	Mean Error (Bias) $\bar{e}$ (μm)	Penetration at 75 Years p (μm)
		Carbon Steel, Rankin, PA (Set No. 1)				
0- 2	4	73.78	0.4587	0.060	0.0	535
0- 4	6	72.58	0.5319	0.079	0.0	721
0- 8	10	63.60	0.6886	0.139	0.0	1243
0-10	12	59.69	0.7356	0.119	0.0	1430
		A242 Steel, Rankin, PA (Set No. 26)				
0- 2	4	29.36	0.3557	0.125	0.0	136
0- 4	6	29.50	0.3608	0.106	0.0	140
0- 8	10	29.26	0.3763	0.100	0.0	149
0-17	12	31.21	0.3192	0.161	0.0	121
		Carbon Steel, Saylorsburg, PA (Set No. 4)				
0- 2	2	31.00	0.7182	0.000	0.0	689
0- 4	3	30.57	0.7536	0.014	0.0	791
0- 8	4	31.66	0.6750	0.049	0.0	602
0-16	5	36.14	0.5984	0.074	0.0	479
		A588 Steel, Saylorsburg, PA (Set No. 17)				
0- 2	2	27.00	0.5305	0.000	0.0	267
0- 4	3	27.35	0.4930	0.020	0.0	230
0- 8	4	28.08	0.4563	0.036	0.0	201
0-16	5	29.98	0.3970	0.087	0.0	166
		Carbon Steel, Kure Beach, NC (Set No. 8)				
0- 1.5	2	40.58	0.8767	0.000	0.0	1787
0- 3.5	3	40.49	0.8930	0.005	0.0	1913
0- 7.5	4	50.44	0.5413	0.268	0.0	522
		A588 Steel, Kure Beach, NC (Set No. 24)				
0- 1.5	2	35.87	0.4980	0.000	0.0	308
0- 3.5	3	35.94	0.5226	0.016	0.0	343
0- 7.5	4	36.29	0.5029	0.021	0.0	318
0-15.5	5	31.74	0.6180	0.099	0.0	458

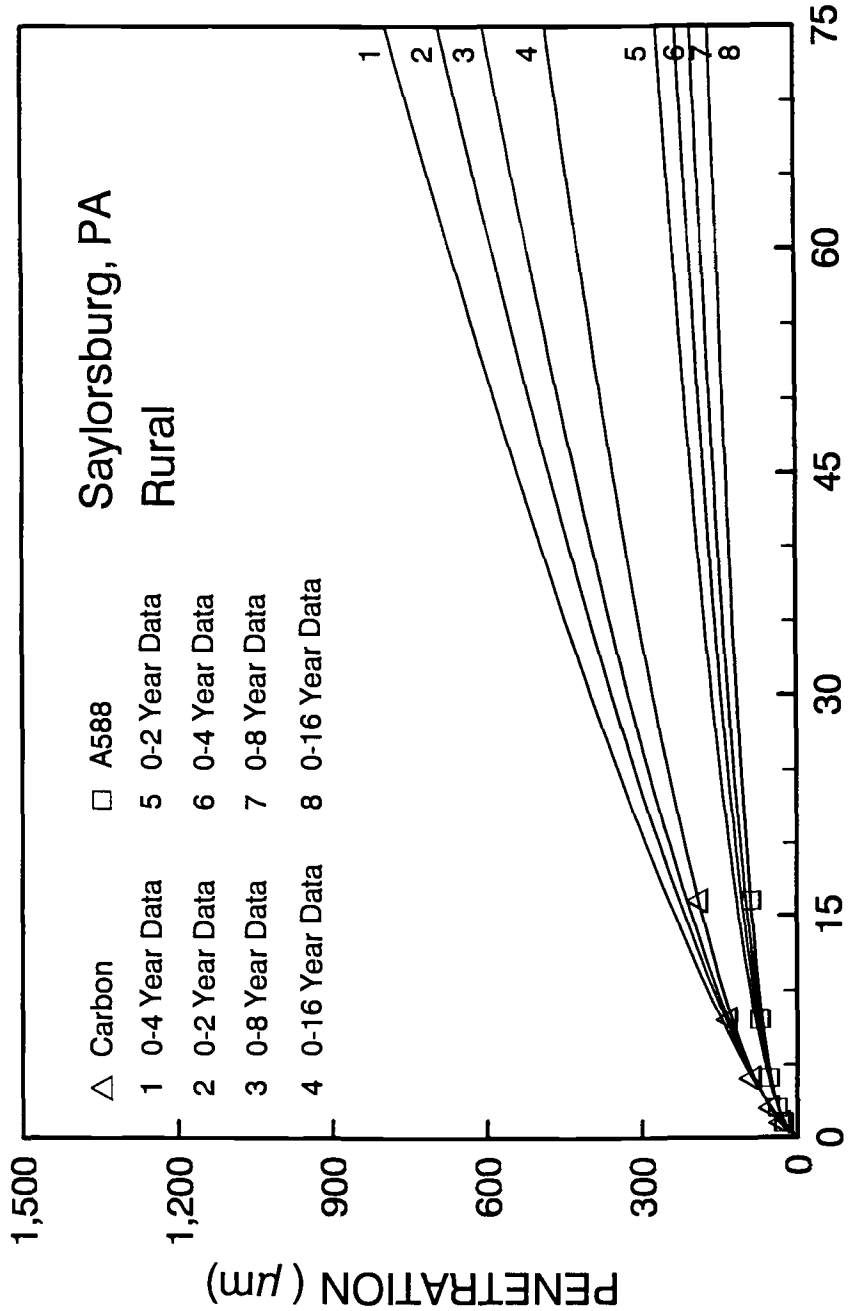

FIG. 7--Effect of Adding Long-Term Exposure Data on Estimated Penetration; Carbon and A242 Steels Exposed to Rankin, Pa., Industrial Atmosphere [11,12]

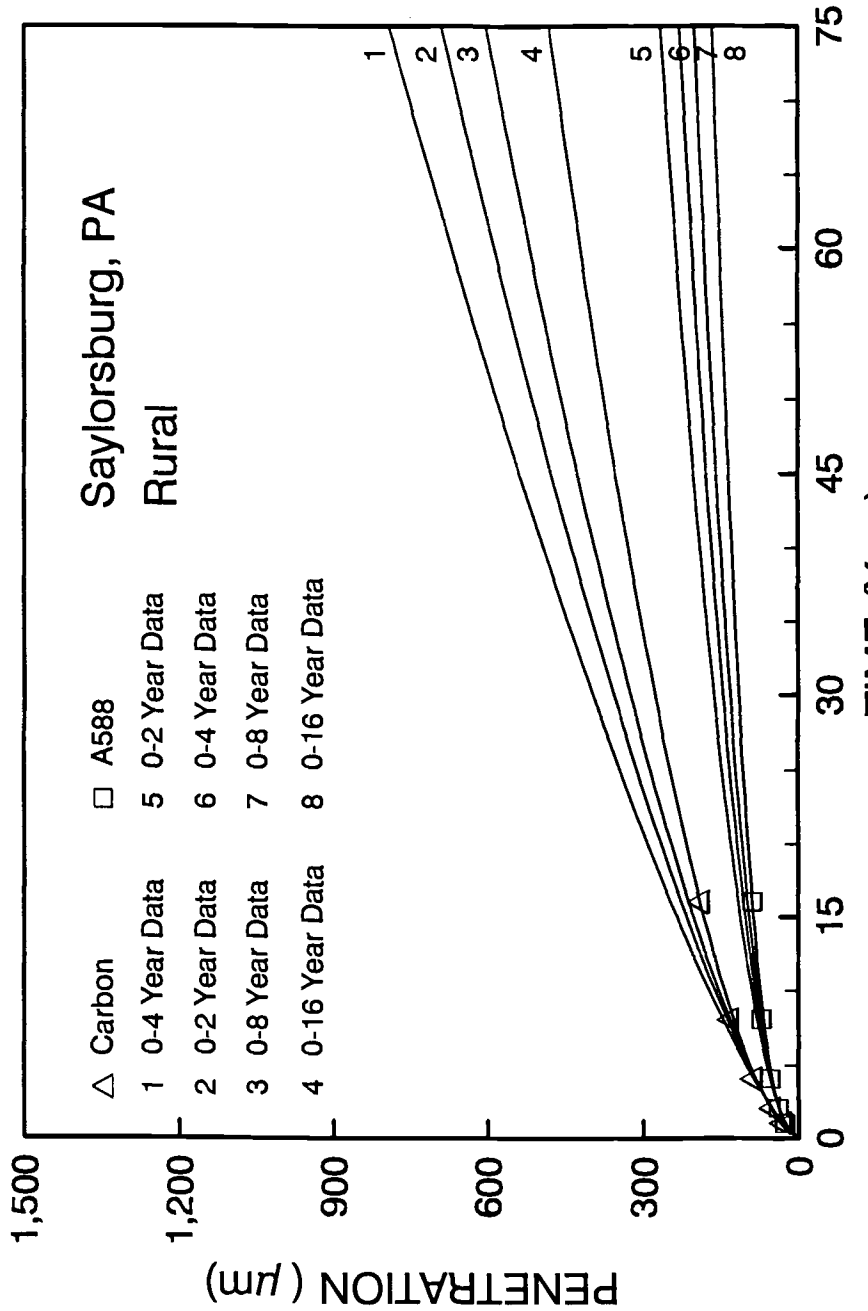

FIG. 8--Effect of Adding Long-Term Exposure Data on Estimated Penetration; Carbon and A588 Steels Exposed to Saylorsburg, Pa., Rural Atmosphere [19,20]

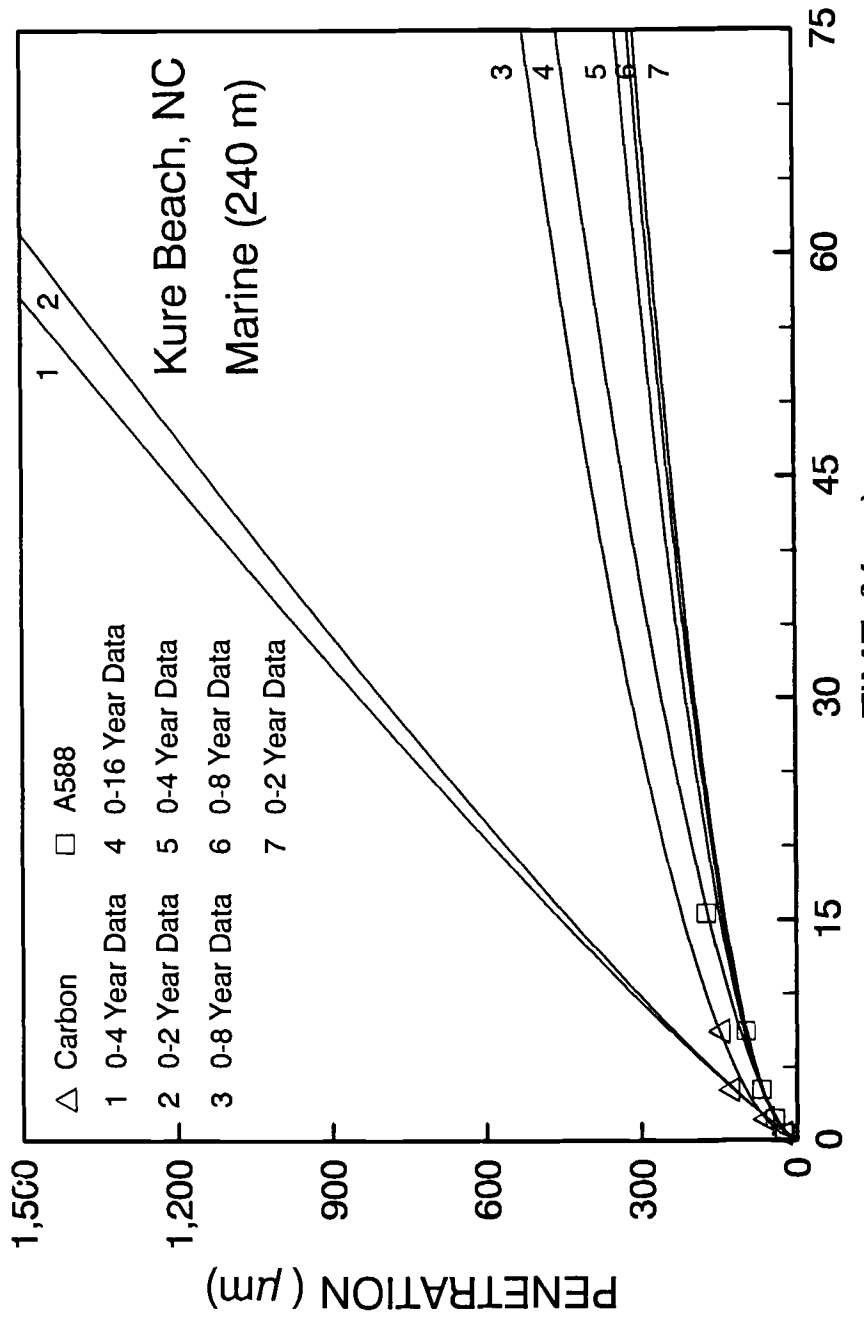

FIG. 9--Effect of Adding Long-Term Exposure Data on Estimated Penetration; Carbon and A588 Steels Exposed to Kure Beach, NC, Marine Atmosphere [14,15,16]

(Table 5 and Fig. 7). It progressively increased with exposure time to a value 1,430 lm for the 0- to 10-year data. On the other hand, the 75-year penetration of carbon steel exposed in marine Kure Beach was 1,787 lm for the 0- to 1.5-year data, increased to 1,913 lm for the 0- to 3.5-year data, and then dropped to 522 lm for the 0- to 7.5-year data (Table 5 and Fig. 9).

In an example for weathering steel, the estimated 75-year penetration of A588 steel exposed in rural Saylorsburg gradually decreased from 267 lm for the 0- to 2-year data to 166 lm for the 0- to 16-year data (Table 5 and Fig. 8). However, in marine Kure Beach, the 75-year penetration of A588 steel increased from 308 lm for the 0- to 1.5-year data to 458 lm for the 0- to 15.5-year data, while alternately rising and falling for intermediate exposure times.

Estimates of 75-year penetration are more accurate for long-term than short-term exposure data. Using the former as the norm, the 75-year penetrations calculated on the basis of short-term data were as much as 2.7 times smaller and 3.7 times larger for carbon steel; they were as much as 1.5 times smaller and 1.2 times larger for weathering steel. Such large errors are of concern when a bridge is built from bare weathering steel and will remain exposed to the environment for the entire service life, without protection.

If no applicable corrosion penetration data were available and the corrosivity of the environment at a specific bridge site were difficult to evaluate, the engineer could order a short-term exposure test. Given the time needed to plan and design a bridge, the engineer could then have up to, say, two years to decide whether to build the bridge from bare weathering steel or ordinary painted steel of equal strength. Judging by the results reported in Table 5, reliable estimates of 75-year penetration require eight years of data. For most bridges, there will be not enough lead time to perform corrosion penetration tests.

EFFECT OF DELETING SHORT-TERM EXPOSURE DATA

Models should represent the physical principles that underlie the corrosion process. In reviewing the data and the errors from the power model, it appears that the structure of Eq 2 is not sufficiently flexible to take the form of the data. The slope of a typical penetration curve for weathering steel is high during the first few years and then rapidly decreases with exposure time. Since the short-term exposure data are less important, it is of interest to examine its effect on the penetration at the end of the service life. This was done for the carbon and A242 steels exposed in Rankin. The full set was analyzed first, and then a progressively larger portion of the short-term data was deleted. The data were fitted with the NUMOPT method,

The results are summarized in Table 6 and Fig. 10. Deleting the short-term data gradually increased the penetration of carbon steel from 1,430 lm to 2,036 lm, by a factor of up to 1.43 for the 5- to 10-year data. It gradually decreased the penetration of A242 steel from 121 lm to 100 lm, by a factor of up to 0.83 for the 5- to 17-year data.

TABLE 6—Effect of deleting short-term exposure data on predicted 75-year penetration.

Exposure Time (yr)	No. of Data Points n	Regression Coefficients b_0	Regression Coefficients b_1	Standard Error Ratio S_e/S_y	Mean Error (Bias) $\bar{e}$ (μm)	Penetration at 75 Years p (μm)
		Carbon Steel, Rankin, PA (Set No. 1)				
5.0–10	6	42.31	0.8973	0.159	0.0	2036
3.0–10	8	47.55	0.8427	0.118	0.0	1808
1.5–10	10	54.57	0.7773	0.129	0.0	1565
0.5–10	12	59.69	0.7356	0.119	0.0	1430
		A242 Steel, Rankin, PA (Set No. 26)				
5.0–17	6	39.84	0.2125	0.491	0.0	100
3.0–17	8	35.36	0.2627	0.370	0.0	110
1.5–17	10	32.64	0.2984	0.285	0.0	118
0.5–17	12	31.21	0.3192	0.161	0.0	121

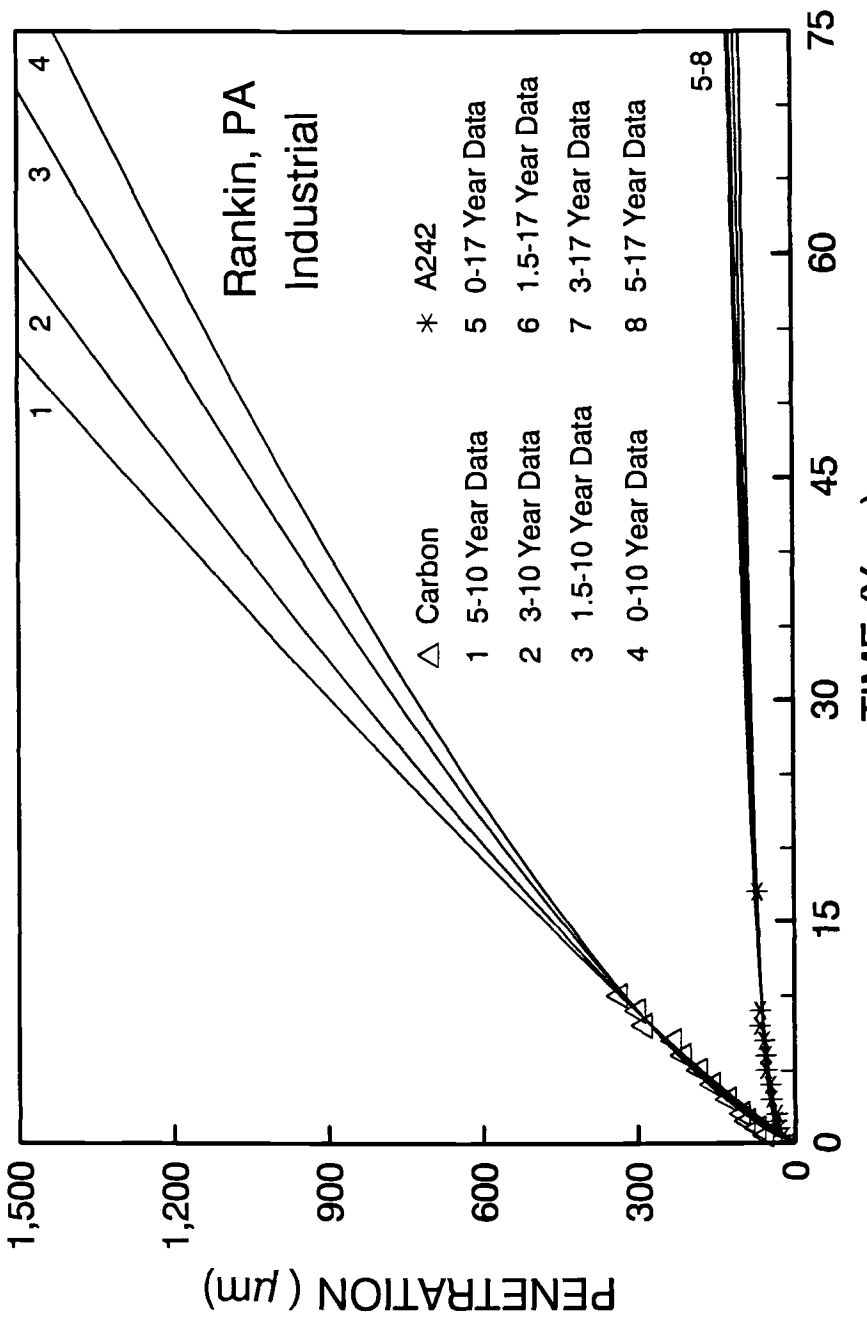

FIG. 10--Effect of Deleting Short-Term Exposure Data on Estimated Penetration; Carbon and A242 Steels Exposed to Rankin, PA, Industrial Atmosphere [11,12]

The radius of curvature of corrosion penetration curves is initially small and rapidly increases with exposure time. This corresponds to a change in the corrosion mechanism from film building to steady-state kinetics. The power model is not sufficiently flexible to represent this change in the physical processes. The long-term data better represent the steady-state corrosion portion of the penetration curve. Therefore, deleting the short-term data and fitting the power model to the long-term data leads to more accurate extrapolations of the penetration to the end of the service life. More flexible models are needed for fitting the entire set of data.

CONCLUSIONS

Engineering data can often be represented by one of the power models of Eqs 3 and 4. If the errors are multiplicative (Eq 3), the method of Bradu and Mundlak [23] yields unbiased, minimum variance estimators. When the data suggest an additive error term (Eq 4), the method provided herein should be used. The following conclusions apply to the problem of fitting corrosion penetration data with the power model:

1. A logarithmic transformation of the power model provides neither unbiased nor minimum error variance estimators of the regression coefficients.

2. Goodness-of-fit statistics (such as the correlation coefficient) obtained from the linear model based on logarithms, Eq 5, do not reflect the prediction accuracy of the nonlinear model of Eq 2, which is the model used for design. Furthermore, the correlation coefficient as traditionally calculated should only be applied to linear unbiased models, not to the power model of Eq 2.

3. The numerical fitting of the coefficients of the power model with NUMOPT improves the statistical efficiency of the coefficients and provides an unbiased model.

4. A numerically fitted model more accurately estimates penetration for longer exposure times.

5. Penetration data for exposure times of at least ten years are needed to reliably estimate the penetration at the end of a 75-year service life. For data sets with only short exposure times (i.e., 4 years and less), the power model does not appear to accurately estimate penetration at long-term exposure times.

6. The power model is not sufficiently flexible to represent the change in corrosion processes from film building at short exposure durations to steady-state kinetics at longer exposure times. More flexible models are needed such as the one presented by McCuen and Albrecht [26].

NUMERICAL FITTING OF POWER MODEL

In regression analysis such as that performed on the logarithms of data, the sum of the squares of the errors, F, are minimized by taking the derivatives $\partial F/\partial b_i$ where b_i is the i-th unknown. For nonlinear models such as the power model, it is not practical to analytically evaluate the derivatives. Instead, the error function can be numerically approximated with a Taylor series expansion [8]:

$$F = \Sigma e^2 = \Sigma (\hat{p}-p)^2 = \Sigma\left[h_o\left(\frac{\hat{p}_o-\hat{p}}{\Delta b_o}\right) + h_1\left(\frac{\hat{p}_1-\hat{p}}{\Delta b_1}\right)\right]^2 \qquad (11)$$

in which h_o and h_1 are the step sizes for coefficients b_o and b_1, respectively; $\hat{p}_o$ and $\hat{p}_1$ are the predicted values of p when b_o and b_1 are incremented by Db_o and Db_1, respectively, with the other coefficient held constant; and $\hat{p}$ is the predicted value of p for estimates b_o and b_1. The error function of Eq. 11 is iteratively calculated until F is minimum. Iteration is required because b_o and b_1 are incremented to find the steepest gradient of F and the step sizes are pre-set. Equation 11 forms the basis for the NUMOPT program.

The NUMOPT-power model is easily fitted with any numerical least-squares program. Such programs are referred to by any one of a number of names, including steepest descent, pattern search, nonlinear least squares, and conjugate gradient algorithms. They should yield the same results as long as the program minimizes the sum of the squares of the errors. Values of b_o and b_1 for Eq 2 can be estimated with the following procedure [25]:

1. Estimate initial values of b_o and b_1 with a standard program for linear regression analysis of the logarithms of the data (minimize Σe^2 in the log p-space).

2. Find the optimum values of b_o and b_1 with the NUMOPT program (minimum Σe^2 in the p-space); several executions of NUMOPT may be needed.

3. Using the response surface option, unbias the model such that the Σe^2 is a minimum for any unbiased solution.

REFERENCES

[1] *"Cor-Ten High-Strength Low-Alloy Steel,"* Brochure ADUSS 88-7888-01, United States Steel, Pittsburgh, Pennsylvania, 1980.

[2] *"Mayari R Weathering Steel for Bridges,"* Booklet 2858, Bethlehem Steel, Bethlehem, Pennsylvania.

[3] Albrecht, P., Coburn, S.K., Wattar, F.M., Tinklenberg, G.L., and Gallagher W.P., *"Guidelines for the Use of Weathering Steel in Bridges,"* NCHRP Report 314, Transportation Research Board, National Research Council, Washington, D.C., 1989.

[4] *"Corrosion of Metals and Alloys - Classification of Corrosivity of Atmospheres,"* Draft Proposal DP 9224, International Standards Organization, 1988.

[5] Albrecht, P. and Naeemi, A.H., *"Performance of Weathering Steel in Bridges,"* NCHRP Report 272, Transportation Research Board, National Research Council, Washington, D.C., 1984.

[6] Albrecht, P. and Lee, H.Y., "Corrosion Performance of Boldly Exposed Weathering Steel," Civil Engineering Report, University of Maryland, College Park, Maryland, 1989.

[7] McCrum, R.L., Arnold, C.J., and Dexter, R.P., *"Current Status Report, Effect of Corrosion on Unpainted Weathering Steel Bridges,"* Michigan Department of Transportation, Testing and Research Division, Lansing, Michigan, 1985.

[8] McCuen, R.H. and Snyder, W.M., *"Hydrologic Modeling,"* Prentice Hall, Inc., Englewood Cliffs, N.J., 1986.

[9] Monro, J.C., *"Direct Search Optimization in Mathematical Modeling and a Watershed Model Application,"* NOAA Technical Memorandum, NWS HYDRO-12, Silver Spring, Maryland, 1971.

[10] Rosenbrock, H.H., *"An Automatic Method of Finding the Greatest or Least Value of a Function,"* The Computer Journal, Vol. 3:175, 1960.

[11] Horton, J.B., *"The Composition, Structure and Growth of Atmospheric Rust on Various Steels,"* Ph.D. Dissertation, Lehigh University, Bethlehem, Pennsylvania, 1964.

[12] Horton, J.B., *"The Rusting of Low Alloy Steels in the Atmosphere,"* Presented at San Francisco Regional Technical Meeting, American Iron and Steel Institute, 1965.

[13] Larrabee, C.P., *"Twenty-Year Results of Atmospheric Corrosion Tests on USS Cor-Ten Steel, Structural Copper Steel, and Structural Carbon Steel,"* Applied Research Laboratory, United States Corporation, Monroeville, Pennsylvania, 1959.

[14] Gallagher, W.P., *"Long-Term Corrosion Performance of USS COR-TEN B Steel in Various Atmospheres,"* Technical Report, Research Laboratory, United States Steel Corporation, 1976.

[15] Komp, M.E., *"Atmospheric Corrosion Ratings of Weathering Steels - Calculation and Significance,"* Materials Performance, National Association of Corrosion Engineers, CORROSION/87, Paper No. 423, San Francisco, California, 1987, 42-44.

[16] Schmitt, R.J. and Mullen, C.X., *"Corrosion Performance of Mn-Cr-Cu-V Type USS COR-TEN High-Strength Low-Alloy Steel in Various Atmospheres,"* Technical Report, Applied Research Laboratory, United States Steel Corporation, Monroeville, Pennsylvania, 1965.

[17] Cosaboom, B., Mehalchick, G., and Zoccola, J.C., *"Bridge Construction with Unpainted High-Strength Low-Alloy Steel, Eight-Year Progress Report,"* New Jersey Department of Transportation, Division of Research and Development, Trenton, New Jersey, 1979.

[18] Cruz, I.S. and Mullen, C.X., *"The Architectural Application of Bare USS COR-TEN High-Strength Low-Alloy Steel,"* Technical Report, Applied Research Laboratory, United States Steel Corporation, Monroeville, Pennsylvania, 1962.

[19] Shastry, C.R., Friel, J.J., and Townsend, H.E., *"Sixteen-Year Atmospheric Corrosion Performance of Weathering Steels in Marine, Rural and Industrial Environments,"* Degradation of Metals in the Atmosphere, ASTM STP 965, S.W. Dean and T.S. Lee, Eds., American Society for Testing and Materials, Philadelphia, Pennsylvania, 1988, 5-15.

[20] Townsend, H.E. and Zoccola, J.C., *"Eight-Year Atmospheric Corrosion Performance of Weathering Steel in Industrial, Rural, and Marine Environments,"* Atmospheric Corrosion of Metals, ASTM STP 767, S.W. Dean, Jr., and E.C. Rhea, Eds., American Society for Testing and Materials, Philadelphia, Pennsylvania, 1982, 45-59.

[21] Copson, H.R., *"Long-Time Atmospheric Corrosion Tests on Low-Alloy Steels,"* American Society for Testing and Materials, 60, 1960, 650-667.

[22] Larrabee, C.P., and Coburn, S.K., *"The Atmospheric Corrosion of Steels as Influenced by Changes in Chemical Composition,"* First International Congress on Metallic Corrosion, London, 1962, 276-285.

[23] Bradu, D. and Mundlak, Y., *"Estimation in Log-Normal Linear Models,"* Journal of the American Statistical Association, Vol. 65 (329), March, 1970, 198-211.

[24] Mottola, V.E., *"Sixteen-Year Corrosion Penetration Data for A242 and A588 Steels in Newark, New Jersey,"* Private Communication, New Jersey Department of Transportation, Trenton, New Jersey, 23 January 1989.

[25] McCuen, R.H., *"Microcomputer Applications in Statistical Hydrology,"* Prentice-Hall, Englewood Cliffs, New Jersey, 1993 (in press).

[26] McCuen, R.H. and Albrecht, P., *"Composite Modeling of Corrosion Penetration Data,"* Symposium on Accelerated Corrosion Tests to Service Life Prediction of Materials, American Society for Testing and Materials, Miami, Florida, November, 1992.

V. Gensheimer DeGiorgi[1], A. I. Kaznoff[2]

A REVIEW OF COMPUTATIONAL SIMULATION TECHNIQUES

REFERENCE: DeGiorgi, V. G. and Kaznoff, A. I., **"A Review of Computational Simulation Techniques,"** Corrosion Forms and Control for Infrastructure, ASTM STP 1137, Victor Chaker, Ed., American Society for Testing and Materials, Philadelphia, 1992.

ABSTRACT: Accurate computational simulations require combining established numerical procedures, including modeling techniques, with accurate material characterizations. Accurate computational simulations also require an understanding of the physical phenomenon represented in a particular problem. The current work defines the steps required for the creation of an accurate computational simulation. A review of existing corrosion related computational simulations is incorporated into the discussion. An example case history of the creation of a computational simulation of a prototypical surface ship impressed current cathodic protection system is presented.

KEYWORDS: computational simulation, corrosion, cathodic protection, galvanic corrosion, boundary element, finite element, corrosion analysis

Corrosion is a complex synergistic problem. Fabrication materials, electrolyte compositions, changing material characterization with time and advancing degrees of corrosion, temperature and other environmental effects all contribute to the state of corrosion present at any point in time. The wide variety of structures subject to corrosion is a challenge to the researcher in that there is no simple definition of a typical problem.Computational simulations have been used successfully to predict structural integrity

[1]Research Engineer, Mechanics of Materials Branch, Naval Research Laboratory, Washington, DC 20375.

[2]Director, Materials Subgroup, 514, Naval Sea Systems Command, Washington, DC, 20362.

predict structure behavior for several decades. The mathematical and

material structural behavior for several decades [1] and have recently been successfully incorporated into analytical and computational evaluations of corrosion. The purpose of computational simulations is to bridge between analytical solutions and observations. A combination of computational, analytical and experimental data is required to properly bridge the gap.

The current work contains an outline of the requirements of an accurate computational simulation. Emphasis is placed on two major higher order computational simulation methods; finite element and boundary element. Examples cited in the work are not meant to be an exhaustive review of the subject but are rather meant to give the reader an idea of the diversity of problems to which computational simulations techniques have been applied. Detailed theoretical discussions of the two methods can be found in standard textbooks such as Cook [2] and Brebbia [3] and are not incorporated in the discussion. An example, presented in the latter part of this paper, illustrates the formation of a computational simulation using boundary element techniques.

COMPUTATIONAL SIMULATION OUTLINE

Despite the diversity of problems, programs and modeling techniques used there are factors which are common to all computational simulations. The basic steps in the development of a computational simulation are:

choice of a computational procedure
model development
material characterizations
model verification
simulation completion

Each of the basic steps will be discussed in detail.

Choice of Computational Procedure

The conservation of charge within an electrolyte is the basis of the mathematical formulation used in corrosion computational simulations. Numerical solutions for the equations governing electrochemical behavior have been developed. Detailed derivations of the governing differential equation for electrochemical applications can be found in standard textbooks such as Reference [3].

The choice of computational procedure will depend on problem definition as well as available computational and personnel resources. The advantages and disadvantages of using commercial codes will have to be considered during the initial planning stage. Also, decisions will be required with respect to model simplification. The choice of what aspects of a problem can be simplified must be made with an understanding of the physical phenomenon being analyzed and of computational simulation techniques. It is important to remember that all computational simulations involve some simplifications in order to create workable models.

One of the first general computational simulation methods to be applied to corrosion problems was the finite difference method [4]. Finite difference methods are best suited for geometrically simple

structures. As the need became apparent for computational simulations of more complex structures more advanced computations simulation methods are required.

The current work focuses on two major advanced computational simulation techniques; the finite element and boundary element methods. Both methods allow for the modeling of complex geometries. Both methods have been demonstrated to be numerically robust for a variety of problems. Because commercial codes exist for both methods the analyst has the option to use a commercial code or to develop his own corrosion problem code.

The finite element method is a versatile analysis procedure which can be applied to almost any structure. In a finite element analysis, as in any corrosion analysis, the region which must be discretized is the electrolyte surrounding the structure. Complex structures may require large numbers of 3-D elements to accurately model the structural details and a significant volume of the electrolyte surrounding the structure. The volume of electrolyte modeled must be sufficient for the development of the analog current and potential fields without imposing artificial boundary effects. Finite element method has been applied to a variety of corrosion problems including a galvanic study of tube to tubesheet connections [5], simple galvanic cells [6,7] and storage tanks with sacrificial anode protection systems [8]. Detailed evaluations of existing ship cathodic protection systems have also been performed [9,10].

Typical of work done with finite element method is an analysis performed by Helle in 1980 to determine the electrochemical potential around a ship [9]. Two depth configurations were considered; the first places the ship near the bottom of the sea and the second places the ship far from the seabed. The potential fields resulting from galvanic interactions of the ship hull, propellor and zinc anodes as well as cathodic impressed current system anodes were examined. The generalized effects of scratches and wear on the painted hull are included in the analysis by consideration of an average resistance for new and damaged paint. The cathodic polarization response of the painted hull is represented by an exponential potential function. The polarization behavior of the zinc anodes was assumed to be linear. An iterative solution procedure was used. The finite element results reported were in terms of the propellor potential as a function of sea water boundaries and the position of zinc anodes.

The work by Helle [9] is cited as an example of finite element application because it demonstrates the overall versatility of the method. Linear and non-linear polarization characteristics for different materials are incorporated in the model for an accurate representation of material response. The ability to combine sacrificial anodes and impressed current conditions, each defined by a different type of boundary condition, is demonstrated.

The boundary element method is based on the solution of boundary integral equations [6]. The governing differential equations are manipulated so that volume integrals are reduced to surface integrals in 3-D problems. Use of the boundary integral equation requires that only the boundary of the electrolyte be discretized. The boundary of the electrolytes consists of the structure-electrolyte interface and an outer boundary. In the case of a structure surrounded by a nearly

infinite medium such as seawater or soil, the outer boundary is an artificial boundary placed a significant distance away from the structure; a distance large enough so that it does not interface with the potential and current density fields at the structure-electrolyte interface. The volume of electrolyte modeled can be very large without significantly affecting the number of elements and nodes required for discretization. A boundary element model of structure submerged in an electrolyte will, in general, be much simpler than finite element model of the same region.

Like the finite element method, the boundary element method has been applied to many types of corrosion related problems. The boundary element method is often chosen because of it's applicability to unbounded domains such as the sea or large volumes of soil. Variations in numerical solution technique on the accuracy of results obtained from the boundary element method have been examined by Chuang, Zamani and Husing [11]. Simple galvanic cells [12,13] and offshore structures [14,15] have been analyzed by various researchers. Zamani and Chuang [16] have used the boundary element method to determine optimal current levels required in impressed current cathode protection systems for simple cells. Ship structures have been examined in detail by Zamani [17] and DeGiorgi, Thomas and Kaznoff [18].

A typical boundary element application involving the evaluation of the corrosion characteristics of a semi-submersible offshore platform was performed in 1990 by Telles et al [16]. A special purpose boundary element program was developed for this analysis. The choice of boundary element approach was based primarily on the unbounded domain of the sea. The platform analyzed had a combination protection system which incorporated both sacrificial and impressed current anodes. The program assumes a nonlinear cathodic polarization relationship. The analysis performed estimated the potential profile of the structure based on defined anode voltage values and locations. The authors make specific note of future plans which include analyses using different polarization curves and in-situ measurements of potential for verification of the computational simulation.

The cited reference demonstrates that the boundary element method is as versatile as the finite element method. The ability to include multiple material characteristics in a single model and the ability to define an infinite domain of seawater are demonstrated. The ability to model sacrificial and impressed current anodes by defined boundary conditions in the same analysis is also demonstrated.

While it is possible to use different techniques to obtain equally valid and accurate results, some techniques are inherently more adaptive to particular class of problems. Comparisons of the finite element and boundary element methods and their applicability to electrochemical corrosion problems have been discussed by Adey and Niku [19], Fu [20] and Zamani, Porter and Mufti [4]. In an early comparison evaluation Fu [21] created a simple one-dimensional cell and performed evaluations using hand calculations based on graphical methods, the finite element method and the boundary element method. It has been the consensus of reviewers that the boundary element method is better suited to infinite domain problems. The finite element method is still a vital method and must be considered in the selection of a computational simulation technique.

Model Development

Once the numerical simulation technique has been selected, the actual computational simulation model must be developed. Basic considerations such as the definition of the governing equations and the unknowns to be determined must be defined. The choice of appropriate boundary conditions is essential in the accurate computational simulation of the physical problem. Advanced computer codes allow for a wide variety of mixed, both potential and current density, unknowns. In addition to boundary condition definitions, there are different methods of modeling available to the analyst which combine geometric features and boundary conditions. For example, Zamani [17] modeled the rudder and propellor components of a surface ship by defining a cathodic region on the ship hull with a surface area equal to that of the rudder and propellor. In contrast, DeGiorgi, Thomas and Kaznoff [19] created separate geometric representations of the rudder and propellor which resulted in a multiple part model.

After the variables and method of modeling have been determined, the actual finite element or boundary element must be created. Numerous geometric modeling programs exist for a wide variety of computers ranging from PC's to workstations. The use of this type of software greatly enhances the analyst's ability to create an accurate 2-D or 3-D representation of the structure in a timely manner. To aid the novice analyst, general guidelines for finite element and boundary element mesh generation can be found in standard textbooks. Typically a much finer mesh is required for finite element evaluation than is required for boundary element evaluation.

Dimensional variations in structural features can introduce additional levels of complexity to the generation of finite element and boundary element meshes. In many structures, the region of concern with respect to corrosion is only a small fraction of the overall structure. It is possible for many orders of magnitude in scale to exist between the entire structure and the region of interest. In these cases global and regional models are combined in order to provide an computational simulation of the material response while using a reasonable amount of computer resources. The analyst must decide the most effective modeling approach for the particular problem. Both finite element and boundary element methods allow for use of global models and local detailed models of a smaller region.

Material Characterization

An issue which is common to computational simulations in many fields is the selection of the most appropriate material characterization. The adequacy of the material characterization will have an impact on the overall accuracy of the computational simulation.

Examples of the effects of material characterization appropriateness are easily drawn from structural integrity evaluations. It is accepted that the linear elastic stress-strain constitutive relationship is a valid material response representation prior to material yielding. Once the stress and strain have surpassed yield a variety of constitutive responses have been proposed. A recent review of tensile specimen phenomenology cited over 20 theoretical and

computational studies on constitutive modeling [22]. The uncertainty of the "correct" material characterization is not limited to corrosion analyses.

Polarization curves are specific to material and environmental effects such as, but not limited to, temperature, salinity, pH and flow rate will effect the polarization response of a material. Changes in material surface conditions, perhaps due to calcareous deposits or the collection of corrosion products, will also affect the polarization response. Time effects are also important if, for example, the surface effects described are time dependent. Temperature variations also fluctuate with time, either on a seasonal or daily basis. There are two basic methods to incorporate time effects; explicit inclusion of a time dependent polarization curve into the analysis would be the preferred manner of solution.

Because of the environmental dependence exhibited by polarization data in-situ measurements of current density and potential have been used in computational simulations. One example is a simulation of an offshore structure by Strommen et al [14]. The authors incorporated a time dependent polarization response determined from in-situ measurements from a offshore structure similar to that modeled.

Polarization data gathered from controlled experiments has shown a range of variation [23]. Scatter and variation in material characterization data should not discourage the use of computational simulations. It simply points out the care which must be exercised in the selection of the appropriate polarization curve. A knowledge of testing procedures is essential in order to determine the most appropriate experimental polarization curve for use in a particular computational simulation.

When it is considered appropriate to include the variation in polarization data into the computational simulation maximum and minimum response curves can be identified. Once identified these curves can be used in two independent computational simulations establishing a range of solutions values. While not offering a single solution value, this procedure should result in solution values which bracket actual structure behavior.

Another approximation approach is to establish an average or some other statistical significant material behavior response curve. Average material response is well suited for instances when the experimental polarization curves are consistent and do not show an extreme variation in potential for a given current density. Typical curves can also be chosen to perform computational simulations which will show performance trends. Typical curves are suited for structural design type of analyses in which the effects of changes in geometry are of interest.

Often the experimentally determined polarization curves extend over several orders of magnitude of current density. Inclusion of the entire response spectrum may result in numerical difficulties. One major commercial code requires that the slopes and changes in slopes be reasonable on a linear scale [24]. Obviously if this code, or codes written using similar algorithms are used, inclusion of a multi-order of magnitude response curve may result in unnecessary solution convergence problems. The analyst's knowledge of the problem should be sufficient to estimate the possible range of current density which will

occur in the particular simulation. In this manner the range of current density represented in experimental data may be truncated to one which can be reasonably represented on a linear scale if necessary.

The resistance of the electrolyte is also a required material property. In many cases single value definitions of resistance can be determined from laboratory data. Resistance may vary with time as in the case of bays or other water inlets. Variation in resistance with time requires a multiple analyses approach similar to that required to account for time effects on polarization data. In the case of buried structures, resistance of the soil may vary in space around the structure. This variation must be incorporated into the computational simulation.

In summary, one of the major challenges for the analyst in any computational simulation is the choice of an accurate and appropriate material characterization.The analyst must carefully match environmental conditions for the structure with environmental conditions associated with experimental results.

Model Verification

One of the least documented steps in the development of a computational simulation is the verification of the model. Once the numerical procedure has been chosen, the model created and material characterizations defined, the computational simulating must be verified. In all computational simulations there is a degree of simplification incorporated into the model and their effects must be evaluated. Verification of model may take one of several forms. Two methods are the use of simple problems which can be compared with closed form analytical solutions and the use of comparisons with experimental or in-situ collected data. Use of established "rules of thumb" to evaluate analysis results can also be used as a partial verification of the computational simulation.Once a simple boundary condition problem has compared favorably with the analytical solution, the boundary conditions can be changed so that the more complex physical problem is accurately modeled.

A typical model verification was performed as part of a galvanic analysis in 1984 by Bardal, Johnsen and Gatland [12]. The boundary element method was used to determine the galvanic corrosion rates and distribution in a simple electrochemical cell. Galvanic corrosion rates and distribution are accepted as being functions of the electrochemical properties of the two materials, the conductivity of the electrolyte, and the geometry of the cell. Computational and experimental work was performed offering a direct verification comparison of results. It is noted by the authors that variations between experimental and computational results can often be explained in terms of parameters, such as surface conditions, not included in the computational model. The need to have an understanding of the physical as well as the computational is emphasized in the comparison of results.

While it is not always possible for an analyst to perform both experimental work and computational simulations, some sort of computational simulation verification should be undertaken. It is essential that the computational simulation model and procedure be verified in some manner.

Simulation Completion

Once the model and material characterizations have been verified, actual service conditions can be evaluated. The material data required for evaluation of corrosion performance is typically potential and current density levels. A wide range of graphical programs exist which allow for the viewing of the simulation results as contour plots superimposed on the structure geometry.

EXAMPLE

As part of a developmental program, the computational simulation model of impressed current cathodic protections (ICCP) systems on for a prototypical ship has been developed. Preliminary model verification procedures have been completed[20].

The ability for ICCP systems to reduce the effects of corrosion on structures is well established. The ability to design more efficient ICCP systems using computational simulation techniques is one need which may be met by use of computational simulations. Computational simulations are seen as a supplemental design tool to be used in conjunction with scale model testing and other design expertise. The eventual goal is to use simulations in situations which are too complex to be accurately addressed by either of those methods.

Following the computational simulation outline presented earlier the ICCP system design outline with additional information is:

choice of a computational procedure (boundary element)
model development (multiple part ship model)
material characterizations (average value polarization curves from testing facility)
model verification (two part)
simulation completion

The boundary element method was chosen because it was felt to be well suited to the infinite domain problem represented by the surface ship. The electrolyte domain to be modeled is the sea surrounding the ship. A commercial computer code was chosen to be used in the analysis. Use of a commercial code will allow for a smooth transition from developmental to design applications.

As part of the model development a particular ship and ICCP system design to be simulated was selected. The verification analysis prototypical ship is a U. S. Navy CG-47 with a 6 anode ICCP system. The boundary element model developed is shown in Figure 1 and consists of 389 nodes and 319 elements. The ship model consists of three components: the hull, the propellor and the rudder. The propellor and rudder of the ship are modeled as separate geometric features. Nonlinear cathodic polarization data is used to characterize the material behavior. The number and placement of anodes is fixed. Dielectric shielding of fixed dimensions is included for each anode. Each anode is a current source and is represented by an element with prescribed boundary conditions. Elements which make up the dielectric shields are assigned zero current density. The hull, rudder and propellor can be assigned different material characteristics. The

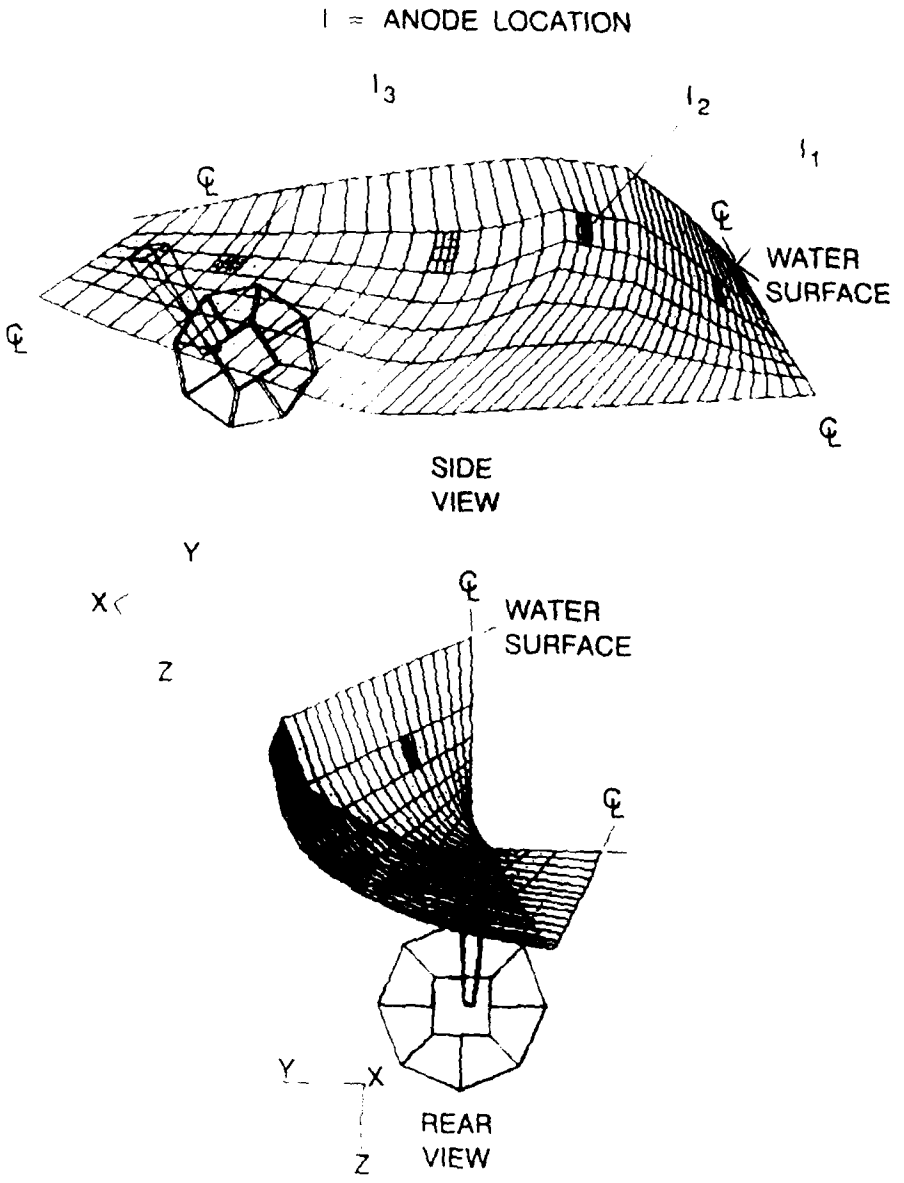

Figure 1 - Boundary Element Model of Surface Ship

infinite seawater domain is approximated by a box created from constant value elements used to enclosed the ship model. The edges of the box are a large distance, 20 times the ship's length, from the ends of the ship. Box elements are defined with zero current density to approximate the correct boundary conditions at infinity.

Model verification for the prototypical surface ship is divided into two parts: mathematical capability and comparison of scale model testing results.The mathematical capability phase of the verification procedure consists of the evaluation of the surface ship model with all components fabricated of bare steel. This phase verified the capability of the boundary element method and the program used to accurately assess ICCP system operation for a multiple part model. Use of bare steel as the material for all three components resulted in extreme conditions. Much higher levels of current are required to maintain protection for the bare steel structure than for a fully or partially painted hull. The results obtained will not be indicative of a full scale ship system but can be compared with current requirements based on simple analytical or graphical calculations. The first phase of the verification procedure was defined as such because it was felt that if the computer modeling techniques perform accurately for extreme conditions, normal operational conditions and materials may be accurately modeled using the same techniques. An average value polarization curve was used since the results would be compared to analytical estimates based on accepted values of current requirements [25,26]. It was reasoned that an average response would more closely approximate "rule of thumb" estimates than would a maximum or minimum data curve.

The bare steel hull analysis resulted in a total current requirement of 693 Amperes (A). to maintain adequate protection from corrosion. This compares favorably with analytical estimates of 757 A. The boundary element predicted current is within 8.4% of the analytical estimated value.

The second phase of the verification procedure will consist of comparing computational simulation results with results obtained from experimental evaluation of ship ICCP system performance using scale models. In the second phase, the hull, propellor and rudder will be assigned realistic material characterizations. Various paint damage patterns will be evaluated. Computational simulation results will be compared in detail with scale model test data.

For this particular analysis program the final stage of a computational simulation, simulation completion, is identical to the model verification stage. The two phase model verification will accredit the solution procedure and model as being able to accurately predict ship behavior.

CONCLUSIONS

The essential steps to the creation of an accurate computational simulation of a corrosion related problem have been outlined. Each step has been discussed in some detail. The existing finite element and boundary element models of corrosion problems can be used as examples to aid the analyst in the creation of a new computational simulation.

In reviewing the steps in creating an accurate computational simulation it is apparent that the analyst must have an understanding of the corrosion process modeled as well as the computational simulation procedure used.

REFERENCES

[1] Peterson, M. H., "Physical and Mathematical Modeling of Current Distribution and Cathodic Protection," The 8th Inter-Naval Corrosion Conference Proceedings, Plymouth, England, 1988.

[2] Cook, R. D., Concepts and Applications of Finite Element Analysis, John Wiley and Sons, New York, NY 1981.

[3] Brebbia, C. A. and Dominquez, J., Boundary Elements - An Introductory Course, McGraw-Hill, New York, NY, 1989.

[4] Zamani, N. G., Porter, J. F. and Mufti, A. A., "A Survey of Computational Efforts in the Field of Corrosion Engineering," International Journal of Numerical Methods in Engineering, Vol. 23, 1986, 1295-1311.

[5] Scully, J. R. and Hack, H. P., "Prediction of Tube-Tubesheet Galvanic Corrosion Using Finite Element and Wagner Number Analysis," Galvanic Corrosion, ASTM STP 978, Philadelphia, PA, 1988, 136-157.

[6] Kasper, R. G. and April, M. G., "Electrogalvanic Finite Element Analysis of Partially Protected Marine Structures," Corrosion, Vol. 39, No. 5, 1983, 181-188.

[7] Kasper, R. G. and Crowe, C. R., "Comparisons of Localized Ionic Currents as Measured from 1-D and 3-D Vibrating Problems with Finite Element Predictions for an Iron-Copper Galvanic Couple," Galvanic Corrosion, ASTM STP 978, Philadelphia, PA 1988, 118-135.

[8] Munn, R. S., "Analysis of Current and Potential Distribution in an Internal Shipboard Seawater Tank," Computers in Corrosion Control, NACE, Houston, TX, 191-200, 1986.

[9] Helle, H. P. E., "The Electrochemical Potential Distribution Around Ships," Royal Institute of Naval Architects, 1980, 253-263.

[10] Forrest, A. W. Jr. and Bicicchi, R. T., "Cathodic Protection of Bronze Propellers for Copper Nickel Surfaced Ships," Corrosion, Vol. 37, No. 6, 1984, 349-357.

[11] Chuang, J. M., Zamani, N. G., Hsiung, C. C., "Some Computational Aspects of BEM Simulation of Cathodic Protection Systems," Applied Mathematical Modelling, Vol. 11, 1987, 371-379.

[12] Bardal, E., Johnsen, R., and Garland, P. O., "Prediction of Galvanic Corrosion Rates and Distribution by Means of Calculation and

Experimental Models," Corrosion, Vol. 40, No. 12, 1984, 628-633.

[13] Zamani, N. G., Chuang, J. M., and Hsiung, C. C.,"Numerical Simulation of Electrodeposition Problems," International Journal for Numerical Methods in Engineering, Vol. 24, 1987, 1479-1497.

[14] Stommen, R., Kein, W., Finnegan, J. and Mehdizadeh, P., "Advances in Offshore Cathodic Protection Modeling Using the Boundary Element Method," Materials Performance, Feb., 1987, 23-27.

[15] Telles, J. C. F.,. Mansur, W. J., Wrobel, L. C., and. Marinho, M. G., "Numerical Simulation of a Cathodically Protected Semisubmersible Problem Using the PROCAT System," Corrosion, Vol. 46, No. 6, 1990, 513-518.

[16] Zamani, N. G. and Chuang, J. M., "Optimal Control of Current in a Cathodic Protection System: a Numerical Investigation," Optimal Control Applications and Methods, Vol. 8, 1980, 339-350.

[17] Zamani, N. G., "Boundary Element Simulation of the Cathodic Protection System in a Prototypic Ship," Applied Mathematics and Computation, Vol. 26, 1988, 119-134.

[18] DeGiorgi, V. G.,Thomas, E. D. II and Kaznoff, A. I., "Numerical Simulation of Impressed Current Cathodic Protection (ICCP) Systems Using Boundary Element Models," Computer Modeling for Corrosion, ASTM STP 1154, 1991, In Press.

[19] Adey, R. A. and Niku, S. M., "Computer Modeling of Galvanic Corrosion," Galvanic Corrosion, ASTM STP 978, Philadelphia, PA, 1988, 96-117.

[20] Fu, J. W., "Galvanic Corrosion Prediction and Experiments Assisted by Numerical Analysis." Galvanic Corrosion, ASTM STP 978, Philadelphia, PA, 1988, 78-85.

[21] Fu, J. W., "Numerical Methods for Galvanic Corrosion and Cathodic Protection Analyses," Computers in Corrosion Control, NACE, Houston, TX, 1986, 161-175.

[22] Matic, P. Kirby G. C. II and Jolles, M. I., "Determination of Ductile Alloy Constitutive Response by Iterative Finite Element and Laboratory Video Image Correlation," Engineering Fracture Mechanics, 1991, In Press.

[23] Hack, H. P. and Scully, J. R., "Galvanic Corrosion Prediction Using Long and Short-Term Polarization Curves, Corrosion, Vol. 43, No. 3, 1986, 79-90

[24] Computational Mechanics, "BEASY-CP User's Manual", Computational Mechanics Intl., Billerica, MA, 1990.

[25] Peadboud, A. W., "Principles of Corrosion," NACE Basic Corrosion Course, NACE, Houston, TX, 1970, 5-1 - 5-37.

[26] Laque, F. L, Marine Corrosion, Causes and Prevention, John Wiley and Sons, New York, NY, 1975.

Fred H. Haynie[1]

EVALUATION OF AN ATMOSPHERIC CORROSION RATE MONITOR

REFERENCE: Haynie, F. H.,"**Evaluation of an Atmospheric Corrosion Rate Monitor,**" Corrosion Forms and Control for Infrastructure, ASTM STP 1137, Victor Chaker, Ed., American Society for Testing and Materials, Philadelphia, 1992.

ABSTRACT: An Atmospheric Corrosion Rate Monitor (ACRM) with an improved polarization resistance type sensor design was evaluated. A year of hourly average sensor data were correlated with simultaneously collected environmental data and corrosion data measured by mass loss and a rain runoff technique. The study was done at an exposure site in the Research Triangle Park, NC. Sensor responses to wetness were reproducible. Although the sensors were sensitive enough to detect environmental changes other than wetness, these changes are apparently affecting cell resistance rather than polarization resistance. The ACRM may be modified to measure polarization resistance.

KEY WORDS: Atmospheric corrosion, time-of-wetness (TOW), environmental effects, sensors, polarization resistance, acid rain.

Predicting or even measuring the atmospheric corrosion behavior of complex structures is a difficult task. Wind and rain patterns around buildings, bridges, and tanks are not the same as those around standard size corrosion specimens exposed on standardized racks. Extrapolating the corrosion behavior of standardized coupons to predict the corrosion behavior of infrastructure is a very risky procedure.

[1]Atmospheric corrosion consultant, formerly with the U. S. EPA. Present address: 300 Oakridge Rd. Cary, NC 27511.

A device that could be attached to a point on a structure and measure corrosion rate as a function of time would be a valuable tool for the corrosion engineer to use. Through an EPA contract, Mansfeld, et. al. designed and tested an atmospheric corrosion rate monitor (ACRM) for this purpose [1]. The polarization resistance technique was used. Mansfeld and others have evaluated such sensors for reproducibility and ability to measure instantaneous corrosion rates [2]. Sensor design affects both. This paper describes the results of an experiment designed to evaluate the corrosion monitoring effectiveness of a sensor with approximately ten times the area of the original design.

EXPERIMENTAL PROCEDURE

The experiment was performed at an atmospheric monitoring site on the campus of Research Triangle Institute, beginning in April, 1988, and ending in April, 1989. Three types of zinc corrosion monitoring were done simultaneously with atmospheric monitoring; 1) mass gain and loss on 10- by 15-cm coupons, 2) zinc accumulation in rain runoff from similar coupons, and 3) recording instantaneous current changes on zinc corrosion sensors using the polarization resistance technique (atmospheric corrosion rate monitor - ACRM).

Atmospheric Monitoring

Hourly averages of ambient temperature, dew point, relative humidity, wind speed and direction, sulfur dioxide, ozone, nitrogen dioxide, and rainfall amount were continually recorded [3] .Particulate matter was measured on a weekly basis [4].

Mass Gain and Loss

Galvanized steel coupons (10- by 15-cm with chromate film removed) were exposed vertically and at 30 degrees to the horizon, facing south. The lower side of the 30° coupons and the northern side of the 90° coupons were protected from the environment with tape. Triplicate specimens at each angle were removed after 1, 2, 3, 4, 5, 6, and 9 months. At 12 months, sixteen 30° specimens and ten 90° specimens were removed. Corrosion film mass was determined by weighing the coupons before removing the film using ASTM Recommended Practice G-1. Thus, both film mass and total corrosion loss were determined.

Rain Runoff

Plastic troughs at the bottoms of duplicate 10- by 15-cm galvanized steel specimens at 30° and 90° were used to collect runoff from each major rain event. The bottom side

of the 30° specimens and the northern side of the 90° specimens were covered with tape. A total of 44 collections from each of the four specimens were made during the year. The pH of the ambient rain was determined each time a collection was taken. The collected volumes were measured and the concentrations of zinc and other ions were determined using atomic adsorption and ion chromatography.

ACRM

An atmospheric corrosion rate monitor (ACRM) was developed by Mansfeld, et al [1] under contract to the U. S. Environmental Protection Agency (EPA). The zinc-zinc polarization resistance sensor developed with this instrument used the same geometry as sensors specified by ASTMG84-84. EPA designed a sensor with ten times the area (Figure 1) to improve reproducibility between sensors. Figure 2 is a simplified diagram of the atmospheric corrosion rate monitoring system and the potentiostatic cycle used to measure polarization resistance. A more detailed description of the system and its use in this experiment has been reported [5].

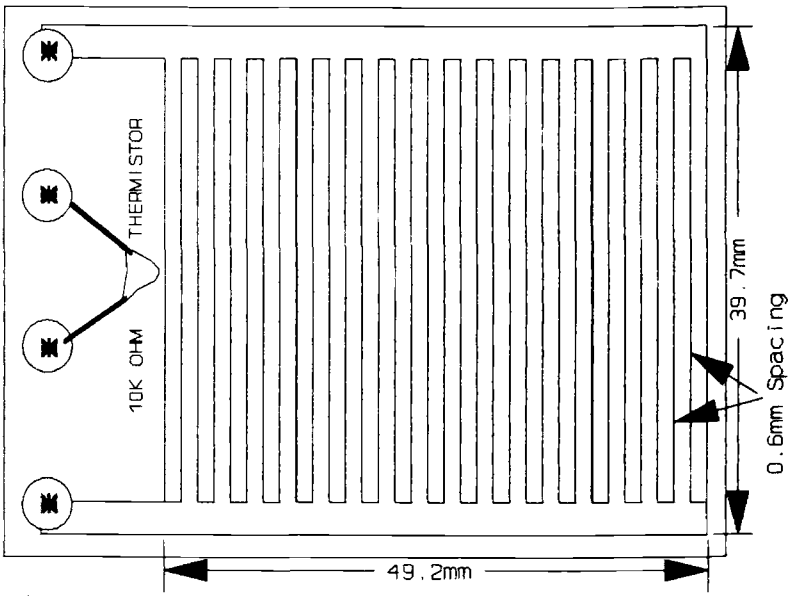

Fig. 1.--Configuration of zinc polarization sensor.

Two pairs of sensors were glued to each of two 10- by 15-cm galvanized steel specimens. One specimen with duplicate sensors on it was boldly exposed at an angle of 30° to the horizon facing south. The other was exposed at 90° to the horizon. A thermistor was mounted on one

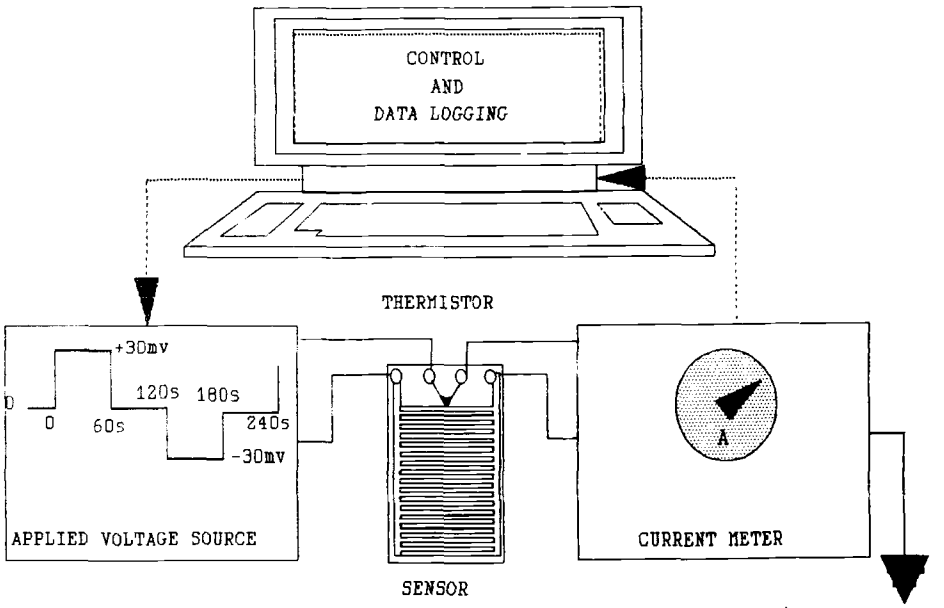

Fig. 2.--Atmospheric corrosion rate monitor (ACRM).

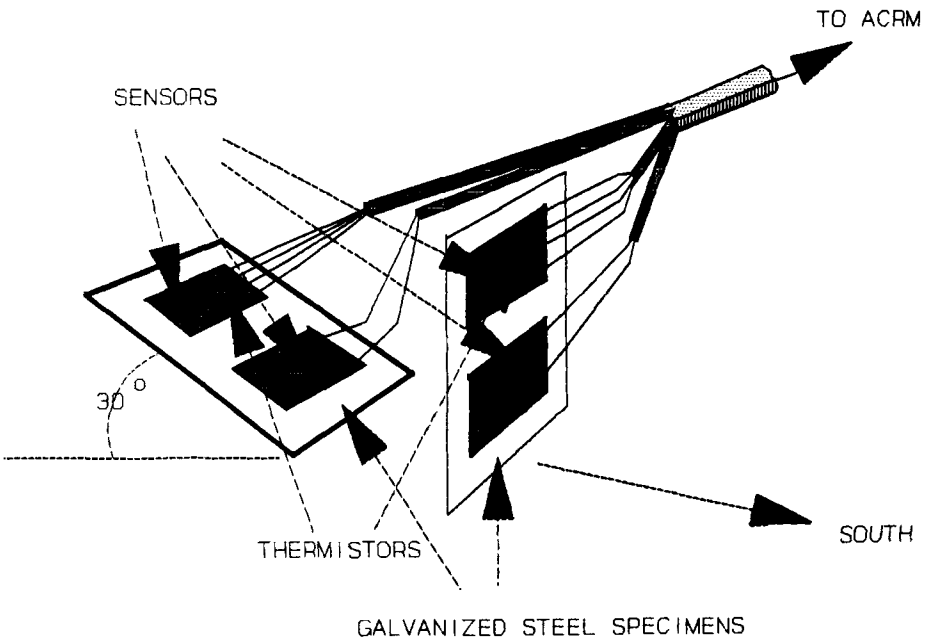

Fig. 3.--Arrangement of exposed sensors.

sensor exposed at each angle. This arrangement is shown in Figure 3. The data acquisition system was programmed to record hourly average resistances of both thermistors and sensors (six resistances each hour). After the study, all data recorded on the laptop microtapes were transferred to files on a desktop computer for analysis.

RESULTS AND ANALYSIS

The objective of this study was to compare the ACRM responses to environmental changes and with other methods of measuring corrosion. The analyses of different methods, however, are interdependent. For example, mass loss coupons corrode as a function of time-of-wetness (TOW) and the ACRM is a good instrument for measuring that parameter [5]. Thus, TOW determination will be discussed first.

TOW

The evaluation of the ACRM as a TOW meter has been reported[5]. Figure 4 shows that measured resistances of sensors have definite modes indicating dry and wet conditions. These responses are reproducible between sensors exposed at the same angle. Other than when it was raining, the sensors being wet was a function of the difference between the surface temperature and the ambient dew point and was not directly related to the ambient relative humidity. Exposure angle and sun angle affect specimen surface temperature. The average surface temperature below the ambient dew point when the sensors indicated going from dry to wet was 1.66° C with a standard deviation of the mean of plus or minus 1.85° C. This standard deviation is about the same magnitude as the accuracy of dew point measurements.

In this study, the surface was considered to be wet if the hourly average resistance of either sensor at the same exposure angle was less than one million ohms. In addition, the surface was considered to be wet when the average resistance was greater than one million ohms and rainfall was measured during the hour. Some rains contained very low conductivity water. Based on these criteria, the 30° specimens were wet 2477 hours while the 90° specimens were wet for only 1723 hours. The total exposure time for the experiment was 8805 hours.

Mass Loss and Gain

Mass was measured to the nearest milligram per panel. Mass was converted to equivalent zinc thickness using 150 cm^2 (the lower and northern surfaces were sealed from

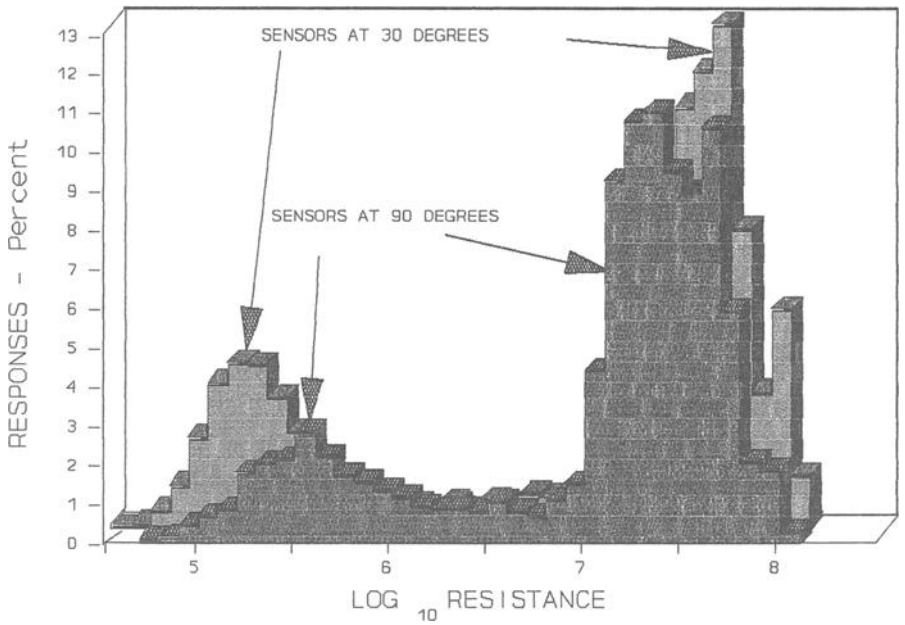

Fig. 4.--Distribution of sensor responses.

exposure with tape) for panel area and 7.14 gm/cm^3 for zinc density. Corrosion film mass was converted to equivalent units of penetration depth as if all the film were zinc. The results based on mass loss as a function of exposure time is shown in Figure 5. The differences in corrosion between the 30° and 90° coupons are large. Figure 6 shows that as a function of TOW, corrosion rates (slopes) on the coupons exposed at the different angles are similar. The lines in Figure 6 represent least squares fits of the corrosion model [6]:

$$C = Bt_w + (A/B)(1 - \exp(-BC/A)) \qquad (1)$$

where C is corrosion penetration, t_w is TOW, A and B are empirical constants. The first term is the corrosion lost to dissolution and the second term is the metal remaining on the surface in the corrosion product film. The constants A and B are respectively 1.14 μ^2/y and 2.78 μ/y for 30° coupons and 0.61 μ^2/y and 2.71 μ/y for 90° coupons. The A term has units of diffusivity and the B term represents the average rate of film dissolution.

The second term in Equation 1 represents the amount of zinc in the corrosion product film. A multiple linear

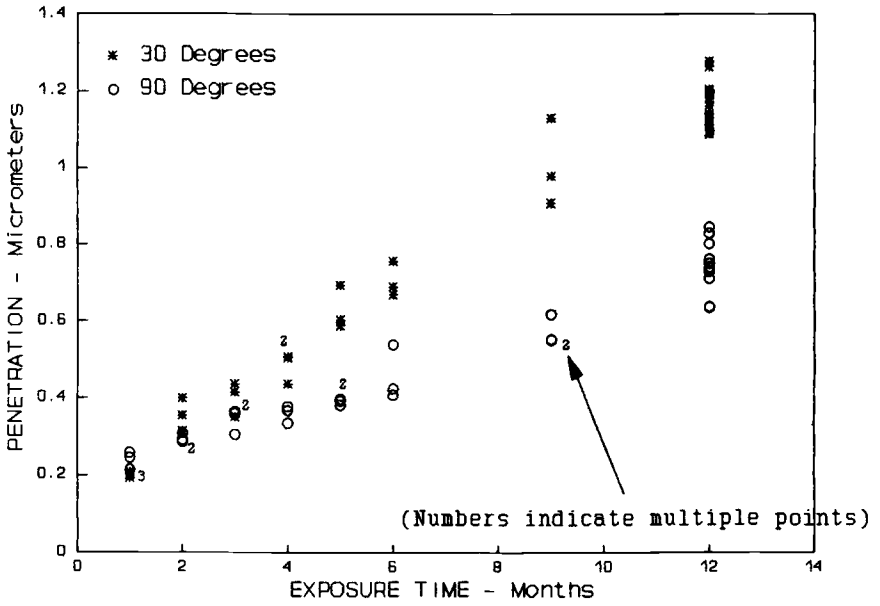

Fig. 5.--Corrosion of galvanized steel coupons.

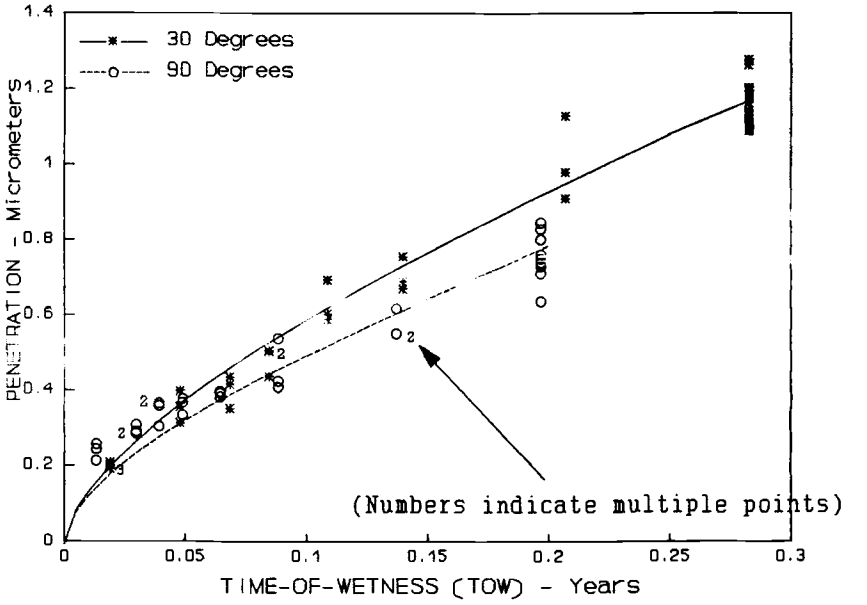

Fig. 6.--Corrosion of galvanized steel coupons as a function of TOW.

regression of penetration on TOW and film mass expressed as zinc thickness penetration, through the origin, yields values for the dissolution rate (B) and the fraction of film mass that is zinc. The resulting 30° and 90° values for B are, respectively, 2.03±0.22 μ/y and 1.71 μ/y± 0.24. The respective fractional amounts of zinc in the films are 0.69±0.07 and 0.59±0.07. The regressions for the two exposure angles are not statistically different from each other at the 95% confidence level. Neither are the coefficients representing the fractional amounts of zinc in the film significantly different from the value of 0.5955 for zinc in basic zinc carbonate. Based on measured concentrations of zinc in 30 samples of stripping solution, the average fraction of zinc in the film is 0.62±0.11.

By assuming the film is basic zinc carbonate, the amount of zinc dissolved can be calculated as total corrosion less 0.5955 times the film mass. Figure 7 is a plot of these results as a function of TOW. The slopes of the lines are regression obtained dissolution rates. These are believed to be the best estimates of average dissolution rates for the two exposure angles. For the 30° and 90° angles, respectively, the values for B are 2.33±0.05 μ/y and 1.71±0.08 μ/y. These values are statistically different from each other.

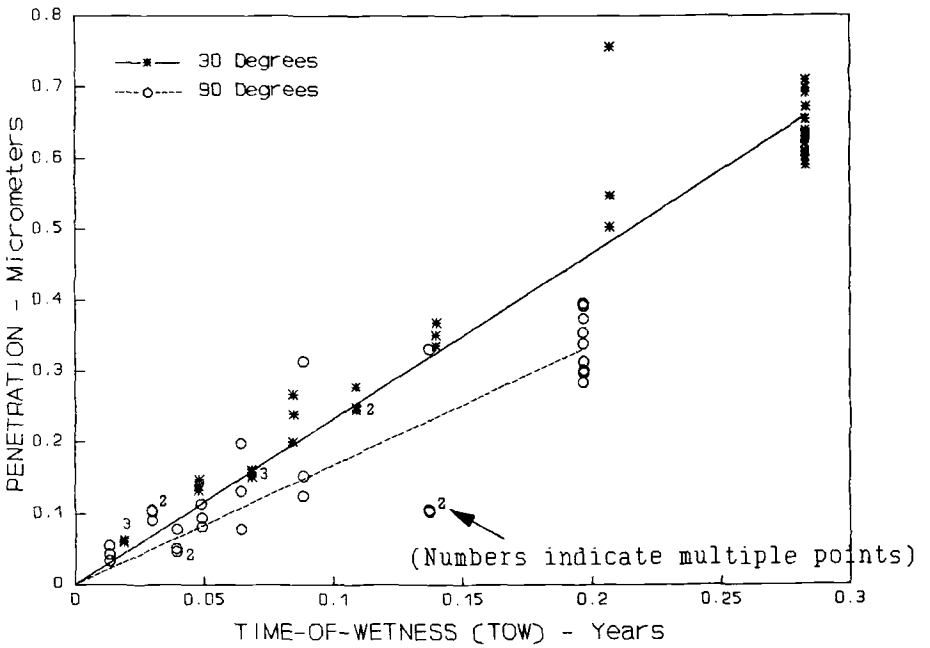

Fig. 7.--Penetration associated with dissolution of galvanized steel coupons as a function of TOW.

Runoff

Measuring the amount of zinc in rain runoff from coupons is part of an input-output analysis of the corrosion process. The runoff from small 10- by 15-cm coupons, however, is subject to splash losses [7]. In this experiment, the collected runoff volumes from the 30° coupons, averaged 57.3 % of a calculated volume expected to fall vertically on the coupons based on measured rain volume. Since the amount of zinc dissolved is the product of measured concentration and measured runoff volume, more than 40% of the zinc may not be accounted for. Figure 8 confirms these losses. The accumulated zinc in the runoffs from the four coupons is compared with the linear regression dissolution lines calculated from the mass loss coupons. The amount of zinc accumulation in runoffs averages 57.20±0.02 % of the amounts calculated for comparably exposed mass loss coupons.

The curves for duplicate specimens follow each other very closely. The variability is much less than that for

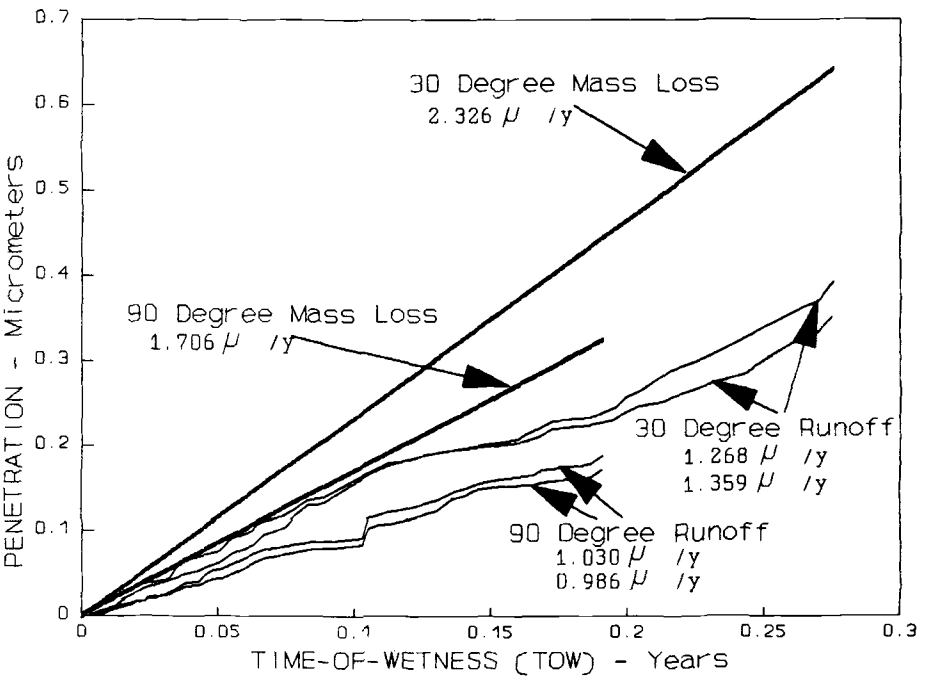

Fig. 8--Calculated penetration based on accumulated zinc in runoff compared with zinc mass loss as a function of TOW.

mass loss coupons, thus, corrosion rate changes with time are more easily determined. Part of the observed differences in corrosion behavior of the 30° and 90° exposed coupons is attributable to the difference in rainfall striking the specimens. The volumes collected from the 90° coupons averaged 25 % of the volumes collected from the 30° coupons. The difference in corrosion rates is not that large because most of the corrosion occurs when the coupons are wet with dew.

Effects of Environmental Changes

A model for dissolution of zinc as a function of environmental conditions has been developed [6]. There are three components to the model: 1) corrosion due to gaseous deposition of sulfur dioxide (SO_2), 2) corrosion due to rain acidity, and 3) corrosion caused by dissolved carbon dioxide in rain. The first term is:

$$C_d = 0.045V_d(SO_2)t_w + 1.29 \times 10^{-4}N \quad (2)$$

where C_d = zinc corrosion (penetration) due to deposition of SO_2, µm,
V_d = deposition velocity, cm/s
= 0.73 x square root of windspeed in m/s for standard coupons,
SO_2 = ambient sulfur dioxide concentration, µg/m^3,
t_w = time of surface wetness, years,
N = number periods between periods of surface wetness.

The second term is:

$$C_{RA} = 46R_r10^{-pH} \quad (3)$$

where C_{RA} = zinc corrosion (penetration) due to H^+, µm, and
R_r = total rainfall during exposure, cm.

For standard panels exposed at 30° from the horizontal, the average corrosion to the top side is multiplied by a factor of cos30°. From the runoff results, the 90° coupons would be 25 % of that amount.

The third term is:

$$C_{RC} = 91.56(rR_r)\exp(-21.34 + 3651/T) \quad (4)$$

where C_{RC} = zinc corrosion (penetration) due to carbon dioxide in rain, µm,
r = residence time factor,
R_r = rainfall, cm, and,
T = absolute temperature, °K.

As with the effect of rain acidity, the fraction of

rain striking the surface must be considered. The 30° calculations are multiplied by cos30° and the 90° calculations are multiplied by .25cos30°. From previous experience [7], the residence time factor (r) on standard coupons is about 0.2.

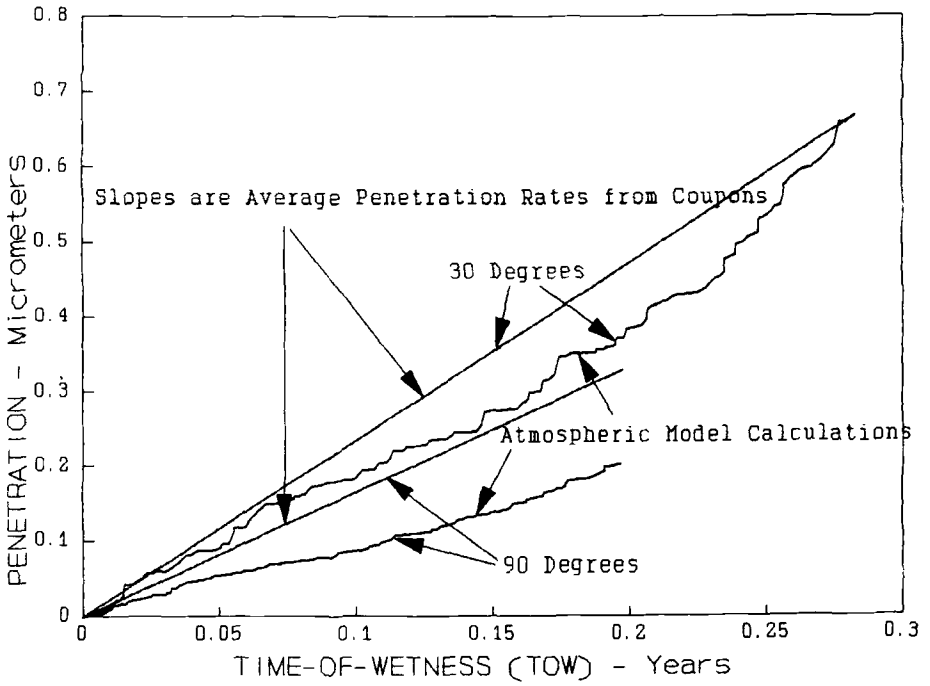

Fig. 9.--Zinc dissolution calculated from atmospheric effects model compared with average coupon results.

All of the components of these equations were measured during this experiment except the residence time factor. The surface temperature is used for T. Thus, the expected dissolution of coupons exposed at both angles can be calculated. The results of model calculations are shown in Figure 9. The calculated dissolution from 30° exposures after a year of exposure is the same as the average based on mass loss data. The average of the calculated dissolution rates for 90° exposures is about 60 % of the average based on massloss from coupons. The estimated fraction of rain striking the 90° coupons may be too low. In both cases, however, the calculated lines are within the 95 % confidence limits for the mass loss coupon data. The major slope changes in the calculated lines are due to differences in rainfall and are comparable to those observed from runoff measurements shown in Figure 8. Concentrations of SO_2 and wind speeds were low during periods of wetness and calculated effects of differences, therefore, are small

compared with the effects of rain. There are changes in the slopes of both curves from the first half (summer) to the last half (winter) that are attributable to the deposition of SO_2.

ACRM

The ACRM measured currents through the sensors resulting from potentiostatically applied 30 mv potentials. Resistances (dE/dI) were calculated and averaged for each hour. These resistances include cell resistances as shown in the model in Figure 10.

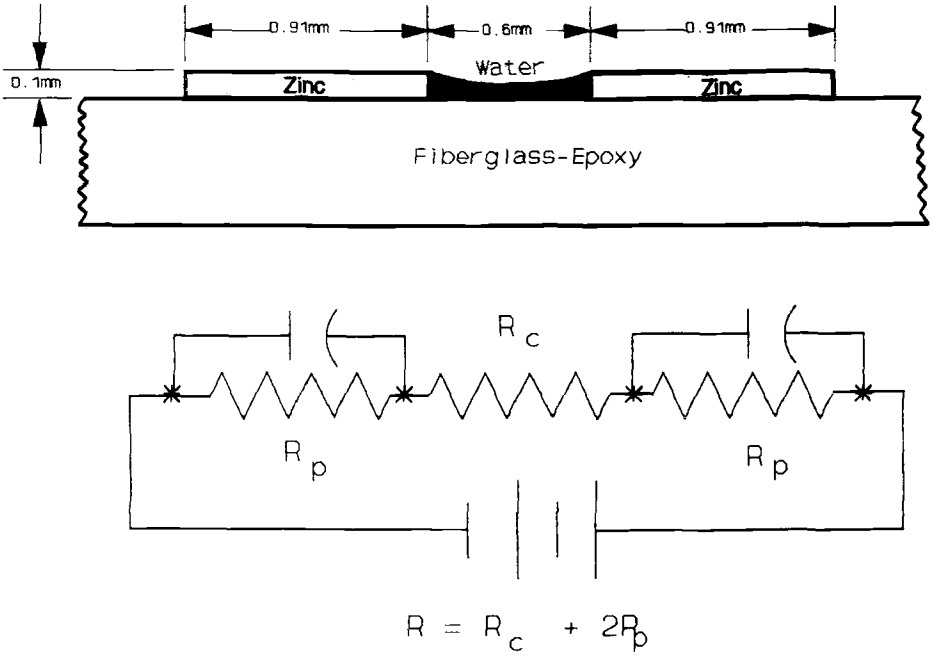

Fig. 10.--Polarization resistance cell model.

The polarization resistance is:

$$R_p = 6(R - R_c)/2 \quad (5)$$

where R_p = polarization resistance on 6 cm^2 half cell, ohm cm^2,
R = measured resistance, ohms, and
R_c = unmeasured cell resistance, ohms.

Although the cell area that is wet during periods of wetness varies, to analyze the data, the sensors were assumed to be completely wet. Also, the unmeasured cell resistance was assumed to be negligible (although actually

it is significant most of the time). Assuming an anodic Tafel slope (b_a) of 60 mv, the calculated corrosion current is:

$$I_c = 0.026/R_p \quad (6)$$

where I_c = corrosion current, amps/cm^2.

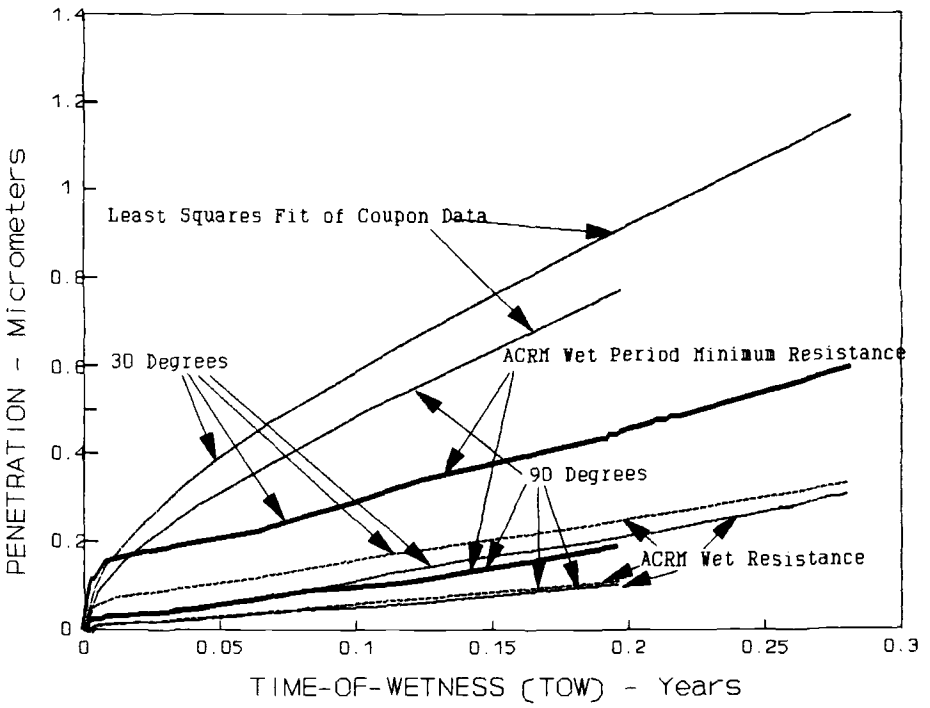

Fig. 11.--ACRM results compared with best fit coupon results.

Therefore, zinc corrosion is calculated to be $44.4/R_p$ μ/hr or 14.8/R μ/hr. The accumulated results are presented in Figure 11. The curves, based on measured average resistances for each hour of wetness, are consistent between sensors exposed at the same angle but indicate much lower corrosion rates than calculated for mass loss coupons. After the first month of exposure, these curves are almost linear and do not reflect the environmental changes that have occurred. The respective apparent corrosion rates for the 30° and 90° sensors are approximately 1 μ/y and 0.5 μ/y. These rates are equivalent to resistances of about 130,000 ohms and 260,000 ohms respectively. A corrosion rate of 2 μ/y would be expected to have a polarization resistance of about 65,000 ohm cm^2. Based on the dissolution rates for 30° and 90° coupons, the respective average cell resistances

R_c are approximately 105,000 ohms and 235,000 ohms during hours of wetness. From this analysis, cell resistance is much greater than polarization resistance during most wet hours. Cell resistance should be least when the sensors are fully wet. Sensors are more likely to be fully wet during long periods of wetness. Considering this probability, corrosion was calculated from the minimum resistance on either sensor exposed at the same angle any time during the wetness period and that resistance was assumed to be inversely proportional to the corrosion rate during the entire period of wetness. These results are plotted as accumulated corrosion in Figure 11. The relatively linear slopes of the curves indicate corrosion rates of about 1.5 μ/y and 1 μ/y for the 30° and 90° sensors respectively. Even with these assumptions the rates are considerably lower than rates calculated from mass loss coupons. The linear behavior suggests that cell resistances are larger than polarization resistances and that environmental effects on corrosion are not detectable with such high cell resistances. The cell resistance in ohms should be less than the expected polarization resistance in ohm cm^2 before significant effects of environmental changes may be apparent.

A subset of low resistance ACRM data were statistically analyzed to determine probable responses to environmental changes. The first 600 hours of exposure when there is a rapid buildup of corrosion product film was excluded and only those hours when the average resistance was less than 100,000 ohms were analyzed. Meeting these criteria were 790 hours for the 30° sensors and 102 hours for the 90° sensors. Multiple linear regressions on environmental parameters were performed in analyzing each set of data and both sets combined. The environmental parameters considered as independent variables were SO_2, windspeed, ambient temperature, dew point, relative humidity, hourly rainfall, surface temperature, and previous TOW. The analyses produced statistically significant coefficients for three of the variables; surface temperature, hourly rainfall, and TOW. The coefficients were statistically different from zero at confidence levels exceeding 95%. The same analysis was performed on 30° and 90° data sets and with both combined. Comparable coefficients were not statistically different from each other at similar confidence levels. The resulting coefficients from the combined analysis of 892 hours of data are; -7.80 ± 0.90 ohms/hr for TOW, -693 ± 88 ohms/°C for surface temperature, and 1518 ± 371 ohm hr/mm for hourly rainfall. These variables can affect both polarization resistance and cell resistance.

Polarization resistance is expected to increase with increasing TOW as a corrosion product film builds up and decreases the corrosion rate. A significant decrease in total resistance suggests that increasing surface area

causes decreasing cell resistance. Increasing amounts of rain can dilute concentrations of species reacting with the zinc and the basic zinc carbonate film and thus increasing polarization resistance. The dilution effect can also increase cell resistance. The decrease in resistance with increasing temperature is consistent with both a change in polarization resistance and a change in cell resistance. The magnitude of the change, however, suggests that it is a reaction effect rather than a conductivity effect.

DISCUSSION WITH RESPECT TO INFRASTRUCTURE CORROSION

In this study, four methods were used to estimate the corrosion behavior of zinc from thin galvanized steel coupons. Each has advantages and disadvantages as they may be applied to corrosion of infrastructure. The experimental results will be discussed with respect to their application to infrastructure corrosion.

Mass Loss Coupons

Standardized testing of coupons has been a valuable tool used to compare the relative corrosion behavior of different alloys in different atmospheric environments. The wealth of data accumulated by this method is often used as a basis in selecting construction materials for infrastructure. Metals in infrastructure, however, are not exposed as thin small coupons, 30° facing south, to the same environmental conditions. Thus, extrapolating coupon testing results to infrastructure corrosion is a long and difficult step that is subject to considerable error.

In this study, replicate specimens produced results with variability typical of standard testing. This variability is attributable to the fact that small specimens exposed at the same angle, on the same rack are not exposed to the same exact environmental conditions. Wind and rain patterns differ between locations on a rack and these patterns affect the corrosion behavior of coupons. Such patterns are even more variable around infrastructure exposed to ambient environments. The collected data were not sufficiently reproducible to detect environmental changes within the time frame of the experiment. Year to year changes in environmental effects may be detectable using this method after an initial exposure period of two to three years.

Runoff

The runoff method of monitoring corrosion has not been used extensively and has not been standardized. It, however, is a technique that could be applied to the monitoring of infrastructure corrosion. Based on this study, the results are much more reproducible than those

from mass-loss coupons and can detect environmental changes within the time frame between rain events. Only soluble losses are measured, however, and small surface areas may have relatively large splash losses. For large surfaces of metals that produce protective corrosion product films, these technique disadvantages are not applicable after the film has reached a relatively steady state thickness.

The technique can be modified to measure corrosion in areas protected from rain but subject to condensation of moisture. A corroded area can be periodically rinsed with deionized or distilled water and the rinse analyzed for ions.

Modelling the Effects of Atmospheric Changes

Some type of model is required to predict the corrosion behavior of a metal structure in its environment. Prediction accuracy is a function of how well the model simulates real corrosion behavior, the accuracy of the predicted values for environmental parameters, and the sensitivity of the model to changes in those parameters. Environmental effects of corrosion of complex structures is difficult to simulate mathematically. In model simplification, some times parameters that can cause significant effects are ignored.

The model used to calculate environmental effects in this experiment is for a well defined system on a simple structure. It, however, can be modified to be applicable to galvanized steel structures of different shapes and sizes in less well defined environments. Extrapolating the model to other metals is possible but is more difficult and is subject to greater potential for error.

ACRM

The intended purpose of the ACRM was to monitor corrosion rates "instantaneously" rather than over periods of exposure of weeks, months, or years. Using the polarization resistance technique, it is possible to estimate corrosion currents in a matter of minutes which is relatively "instantaneous". The ACRM can be used to reproducibly measure TOW, which is the most important parameter in atmospheric corrosion. Although this experiment has shown that the ACRM can detect environmental changes other than wetness, those changes appear to be affecting cell resistance rather than polarization resistance.

It is possible that through changes in hardware, software, or both, polarization resistance can be measured with the ACRM. Increasing the metal thickness and reducing the distance between sensor fingers can reduce cell

resistance. Reducing the distance between fingers increases the probability that the cell may be shorted by corrosion product buildup.

The ACRM can be modified to measure high and low frequency AC impedance and record the difference as polarization resistance [8]. Another approach is to program the ACRM to extrapolate measured DC resistances over a one minute period to zero and infinite times and take the difference as polarization resistance.

CONCLUSIONS

The conclusions derived from this study are:

1. The ACRM can reproducibly measure TOW within a period of a few hours rather than days.

2. Although the ACRM can detect environmental changes other than surface wetness, those changes appear to be affecting cell resistance rather than polarization resistance.

3. It is possible that hardware and software changes to the ACRM can be made so that polarization resistance can be measured.

ACKNOWLEDGEMENTS

This experimental work was done by the Environmental Protection Agency when the author was an EPA employee. David C. Stiles of Northrop Services Inc. - Environmental Sciences, performed the experimental work and the author greatly appreciates both the quality and quantity of his contributions to this study.

REFERENCES

1. Mansfeld, F., Jeanjaquet, S. L., Kendig, M. W., and Roe, D. K., Development and Evaluation of an Instantaneous Atmospheric Corrosion Rate Monitor, Project Report EPA/600/3-85/048, Unites States Environmental Protection Agency, Research Triangle Park, NC. 1985, July.

2. Mansfeld, F., Tsai, S., Jeanjaquet, S., Meyer, E., Fertig, K., and Ogden, C, Atmospheric Corrosion of Metals, ASTM 767, American Society for Testing and Materials, Philadelphia, 1982, p 309.

3. Tang, R., Barlow, P. M. and Waldruff, P., Materials Aerometric Database for Use in Developing Materials Damage Functions, Project Report, EPA/600/3-89/031, United States Environmental Agency, Research Triangle Park, NC, 1989, September.

4. McElhoe, B, Journal of the Air Pollution Control Association, Vol. 23, 1988, p. 1171.

5. Haynie, F. H., and Stiles, D. C., Materials Performance,Vol 30, No. 8, 1991, p. 58.

6. Spence, J. W., and Haynie, F. H., Corrosion Testing and Evaluation: Silver Anniversary Volume, STP 1000, American Society for Testing and Materials, Philadelphia, 1990, p. 208.

7. Haynie, F.H., Spence, J. W., Lipfert, F. W.,Cramer, S.D., and McDonald, L. G., Corrosion Testing and Evaluation: Silver Anniversary Volume, STP 1000, American Society for Testing and Materials, Philadelphia, 1990, p. 225.

8. Scully, J. R., Corrosion Testing and Evaluation: Silver Anniversary Volume, STP 1000, American Society for Testing and Materials, Philadelphia, 1990, p. 351.

Pedro Albrecht[1]

CORROSION CONTROL OF WEATHERING STEEL BRIDGES

REFERENCE: Albrecht, P., "**Corrosion Control of Weathering Steel Bridges**," *Corrosion Forms and Control for Infrastructure, ASTM STP 1137*, Victor Chaker, Ed., American Society for Testing and Materials, Philadelphia, 1992.

ABSTRACT: Bare exposed weathering steel is an economical alternative to ordinary painted steel if the weathering steel develops a protective oxide coating, meaning that the bridge need not be painted during its service life. To ensure satisfactory corrosion performance, engineers should follow the guidelines for the use of weathering steel in bridges described in this paper.

KEYWORDS: Weathering steel, bridges, atmospheric corrosion, design

This paper describes the corrosion forms found in highway bridges made of bare exposed weathering steel and how the corrosion affects the performance of the bridges. The designer must clearly understand the conditions that interfere with the proper development of the oxide coating to successfully apply the material. An evaluation of the macroenvironment and the simple substitution of weathering steel for ordinary steel in a set of standard engineering drawings is simply not sufficient.

Several examples of excessive corrosion of bridges in service illustrate conditions under which weathering steel does not develop a protective oxide coating. These examples form the basis for recommending guidelines for the design, fabrication, maintenance, and rehabilitation of weathering steel bridges.

For more detail on the information presented herein the reader is referred to Refs. *1* and *2* which, in turn, contain numerous references to the pertinent literature.

CHARACTERISTICS

Weathering steel is a term applied to a carbon steel base that is alloyed with about two percent of alloying elements such as copper,

[1] Professor, Department of Civil Engineering, University of Maryland, College Park, MD 20783

nickel, chromium, and silicon. This addition inhibits the steel's tendency to rust continuously in the atmosphere. When the structural details are properly designed and the bridge is located in a suitable environment, weathering steel forms a protective oxide coating and need not be painted.

The main advantage of using weathering steel is the potential it offers for savings in life cycle costs by eliminating the need for the initial painting and the periodic repainting of the bridge superstructure. These procedures are required for bridges made of ordinary steels that do not have enhanced atmospheric corrosion resistance. There are other advantages of not having to paint a bridge weathering steel bridge. For example: traffic lanes on highways passing under the bridge need not be closed; painters and motorists are not exposed to hazardous conditions; and expensive paint jobs over difficult terrains, bodies of water and electrified railways are avoided.

However, weathering steel bridges are not maintenance free. Proper detailing and choice of a suitable environment can reduce the need for some, but not all, maintenance.

SPECIFICATIONS

Weathering steel is supplied to the requirements of the following ASTM standard specifications:

- High-Strength Low-Alloy Structural Steel (A242)
- High-Strength Low-Alloy Steel with 345 MPa Minimum Yield Point to 100 mm Thick (A588)
- Structural Steel for Bridges (A709)
- Quenched and Tempered Low-Alloy Structural Steel Plate with 485 MPa Minimum Yield Strength to 100 mm Thick (A852)

It comes in yield strengths of 345 to 690 MPa. A242 steel is used only for architectural applications because the high phosphorus content impairs the weldability and toughness required of bridge steels. A588 steel is now available in five proprietary grades. Each grade is a variation of the same basic chemical composition which contains copper, chromium, nickel, and silicon for enhanced atmospheric corrosion resistance. A709 is a general specification for bridge steels. The two grades with enhanced atmospheric corrosion resistance, 50W and 100W, correspond to A588 steel and a modified A514 alloy steel. A852 steel is a new quenched and tempered weathering steel with 485 MPa minimum yield strength and a generic chemical composition.

The weathering steel specifications A242, A588, A709, and A852 were first issued in 1941, 1968, 1974, and 1986, respectively, and have undergone a number of changes over the years. The most important change affecting the corrosion resistance was made in the mid 1970's when it became apparent that the results of long-term exposure tests failed to confirm the claim that weathering steel has four times the atmospheric corrosion resistance of structural carbon steel without copper (0.02 % Cu max) and two times the corrosion resistance of structural steel with copper (0.2 % Cu min). These two reference steels are hereafter simply called carbon and copper steels. The compositions of A588 Grade A to E steels were then enriched with nickel, chromium, and silicon. At the

same time the atmospheric corrosion rating of A242 steel was lowered from "at least" to "approximately" four times that of carbon structural steel without copper.

APPLICATIONS

According to a 1987 telephone survey, some 2,300 weathering steel bridges were built on state highway systems alone. Not included in this number are weathering steel bridges on mass transit systems and on county, city and toll roads. Among the 50 states and the District of Columbia there are 4 nonusers of weathering steel, 14 former users, and 33 remaining users. The four states that do not have weathering steel bridges are Arizona, Hawaii, Nevada, and South Dakota. Hawaii has not used it because concrete is more economical than steel and its severe marine environment is too corrosive for steel. The climate in the other three states is so dry that paint systems on their ordinary steel bridges last 30 years. Moreover, weathering steel in these arid states would not develop an oxide coating of uniform appearance for a long time because precipitation and relative humidity are very low.

The 14 former users no longer build weathering steel bridges for the following reasons:

- Excessive corrosion of bridges in their state - Indiana, Iowa, Michigan, Washington, and West Virginia.
- Concern over the experience in other states - Alabama, Florida, Georgia, Oklahoma, and South Dakota.
- Aesthetic considerations - New Mexico and South Carolina.
- Economic factors - California and North Dakota.

Some states have more than one reason for not using weathering steel. For example, New Mexico and North Dakota also have a semi-arid climate in which paint systems on ordinary steel last a long time.

Among the 33 remaining users there is a great variety in degree of usage for new bridges, from almost exclusively (Vermont) to practically none (Pennsylvania and Tennessee). Recognizing the limitations of the material, most remaining users now follow their own design criteria for enhancing the corrosion performance such as:

- Using weathering steel mainly in rural areas, remote areas, or where the bridge is not visible to the public (8 states).
- Using it mainly over streams (5 states) and over railroad tracks (3 states).
- Not using it for grade separation structures (4 states), nor in cities and where the average daily traffic exceeds 10,000 (1 state).
- Not using it along the coast (6 states), on heavily salted highways (4 states), or high humidity areas (3 states)
- Painting steel 1.5 to 3 m on each side of joints (10 states).
- Blast cleaning all steel before erection (2 states).
- Keeping drainage water from running over substructure and protecting concrete against rust staining (5 states).
- Galvanizing scuppers, bearings, and expansion devices (1 state); and galvanizing finger plates (1 state).

- Not using hinges or sliding plates (1 state).
- Making decks jointless, and building bridges integrally with abutments where conditions permit (1 state).

The successful application of weathering steel for bridges requires on the part of the designer a clear understanding of the type of detail and microenvironment that initiate and support corrosion at a specific bridge site. An evaluation of the macroenvironment and the simple substitution of weathering steel for ordinary steel in a set of standard design drawings is simply not sufficient. This point must be emphasized.

EXPERIENCE

Experience with weathering steel bridges over the last 27 years -- the first three bridges were built in 1965 -- has revealed many satisfactory applications as well as problems with several bridges located in the snowbelt states of the Midwest and Northeast, in Gulf Coast states, and in high rainfall and foggy regions along the West Coast. The problems were generally caused by contamination of the steel structure with deicing salts, exposure to onshore breezes laden with sea salt, extended periods of wetness in areas of persistent high relative humidity, low clearance over bodies of water, and structural details that trap moisture. These types of problems have raised questions concerning the long term performance of weathering steel bridges.

As a result of poor performance, several states have remedially painted some bridges (Iowa, Louisiana, Michigan, and Ohio) or are in various stages of planning such work (Alaska, Indiana, Texas, and Washington). In other states where weathering steel bridges are excessively corroding only in limited areas, all steel within a certain distance of joints was remedially painted (Kentucky, Maryland, Massachusetts, Missouri, and New Jersey Turnpike).

Past experience has also shown that weathering steel is not a maintenance free material and has distinct limitations with regard to the environmental conditions under which it can be used. In essence, weathering steel does not develop a protective oxide coating if the steel remains wet for a long time or is contaminated with salt from any source.

Moisture Deposition

Direct precipitation of rain or snow is not needed for a steel surface to become wet. Weathering steel bridges can become wet in the following ways:

- Moisture condenses during the night when the surface temperature of the steel falls below the dew point.
- Radiant cooling of the skyward deck surface in a clear night causes moisture to condense on the upper portions of the steel girder and run down the web along drip lines.
- Capillaries in the porous oxide coating and crevices in structural details absorb moisture.

- Corrosion products adsorb moisture particularly in the presence of salt.
- Runoff water leaks through joints and cracks in the concrete bridge deck.
- Traffic spray is kicked up in the wake of high-speed traffic and settles on the overhead members of a bridge.

High relative humidity, nightly fog, moisture evaporating from bodies of water, and poor air circulation enhance the deposition of moisture.

Salt Contamination

Salt is deposited on bridges built in marine environments or where salt is spread on highways to melt ice and snow.

Oceanic air contains residual salt particles from evaporated droplets that form when waves breaking on the open sea surface release bubbles. These particles are mixed upwards 2 km into the marine atmosphere over the ocean. Onshore winds carry the salt-laden air inland, where the particles are deposited by wind impingement, gravitational fall-out and diffusion, or are washed out by precipitation. As a result, the salt concentration in the air and the rate of deposition diminish as the distance from the sea increases.

Waves breaking along the beach also release many bubbles. The larger bubbles are rapidly deposited by gravitational fall-out, making the marine environment more severe near the shore line than away from it.

Deicing salt is deposited on weathering steel bridges by salt-laden runoff water leaking through the deck joints and by salt-laden traffic spray that is kicked up behind trucks and settles on the overhead bridge members.

Salt deposition by traffic spray poses a severe corrosion hazard under combinations of low clearance, high traffic speed, and heavy usage of deicing salt. Its effect is particularly severe in depressed and half-tunneled highways where the lateral confinement helps to direct the spray onto the overpass bridge and prevents winds from clearing the spray. Traffic spray deposits deicing salts on large areas of all steel members, with larger amounts being deposited over the traffic lanes and smaller amounts over the shoulders.

CORROSION PERFORMANCE

Unpainted weathering steel resists only specific types of atmospheric corrosion in a limited range of environments. Therefore, the proper design of bridges must be based on a clear understanding of how chemical composition and environment influence the material's performance.

An important requirement for the satisfactory performance of weathering steel is an adequate content of alloying elements that help the steel form a protective oxide coating and hence reduce corrosion rate. The most important elements for increased corrosion resistance are copper, nickel, chromium, and silicon.

It is possible to develop weathering steels with higher alloy contents that would resist atmospheric corrosion in much more aggressive atmospheres. However, the available grades of weathering steel have limited atmospheric corrosion resistance because an increase in alloy content that improves corrosion resistance adversely affects other required properties such as toughness and weldability. The practical upper limit on alloy content restricts the types of environments in which weathering steel can be used for bridges.

For weathering steel to perform satisfactorily, the environment must provide adequate periods of drying, must not provide excessive periods of wetting, and must not contain excessive amounts of corrosive contaminants. The environment of a bridge is a combination of factors related to the general climate of the region (macroenvironment) plus factors related to the specific bridge site (microenvironment). Both must be considered in the selection of a suitable site and the design of the bridge.

An adequate design is necessary to ensure a protective oxide film develops on members exposed to the specific microenvironment. The design must allow for alternate wetting and drying cycles, must not create prolonged conditions of wetness, and should avoid connections and details subject to crevice and galvanic corrosion.

Atmospheric corrosion data are useful in determining the effects of types of atmospheres and exposure conditions on corrosion of weathering steel. However, such data do not usually reflect the corrosion rate of weathering steel in bridges exposed to the same type of atmosphere. This is so because most test data were obtained from small coupons exposed fully to the sun and precipitation -- called *boldly exposed* in the corrosion literature. In contrast, bridge members have greater mass and hence different thermal behavior than test coupons. In addition, most bridge members are not boldly exposed and are subjected to other environmental factors such as spray from roadway water. Finally, the atmospheric corrosion data reported in product literature are for A242 steel. This type of weathering steel has a higher alloy content and exhibits lower atmospheric corrosion rates than the A588 steel commonly used in bridges.

In addition to the effects of the atmosphere types in the macroenvironment, the corrosion performance of weathering steel bridges is also affected by several factors of the microenvironment such as shelter, orientation, contamination with local airborne pollutants, accumulation of debris, deposition of moisture, structural details, and geometry. The combined effects of the micro- and macroenvironments reduce the corrosion resistance of weathering steel in bridges to values lower than are measured with boldly exposed test coupons.

Weathering steel performing satisfactorily in a variety of bridges in the contiguous United States corrodes at a rate of 7.5 lm/yr/surface or less. Weathering steel corroding at a higher rate cannot be expected to develop a protective oxide coating and should be painted.

SITE ANALYSIS

To determine if weathering steel is suitable for use in a bridge at a specific site, the engineer must evaluate the corrosivity of both the macro- and microenvironments. The factors that play a critical role

in the corrosivity of a macroenvironment are climate, atmospheric pollutants originating from industrial activity, and airborne chlorides. Among the important factors to be considered in an evaluation of the corrosivity of the microenvironment are the performance of existing steel structures, site topography, local industrial plants, and deicing salt usage. A study of the microenvironment must include a site visit.

Since several years are needed to plan and design highways and bridges, there is sufficient time to measure the corrosivity of the environment and determine if weathering steel will perform satisfactorily. The most helpful tests are those that sample the atmosphere for the presence of salinity, and monitor time-of-wetness of the steel and sulfur dioxide content of the atmosphere. Instead of measuring the corrosivity of the environment, the corrosion penetration of weathering steel may be determined from exposure tests of coupons. At least two-year data are needed for this purpose. There are ASTM standards for all tests cited above.

If short time-of-wetness and low contamination of the steel are found to create favorable conditions for the formation of a protective oxide coating, then unpainted weathering steel may be specified.

ECONOMIC ANALYSIS

In choosing a type of steel, engineers should consider the life cycle cost of the structure. Calculations of life cycle cost must include the initial cost of the bridge, the cost of maintaining it, the repainting interval, and the time value of money. Life cycle costs were calculated for three bridges, each having five alternate systems of steel type and corrosion protection. The results showed that bare and maintenance-free A588 steel (initial cost only) would be the most economical. But experience with bridges in service and current manufacturers' literature show that weathering steel is not a maintenance free material. Of the other four systems considered, painted High-Strength Low-Alloy Columbium-Vanadium Steels of Structural Quality (A572) was the least expensive, followed by remedially painted A588 steel, painted Structural Steel (A36), and bare periodically hosed A588 steel. Engineers should perform such cost analyses to determine the most economical alternate for a specific bridge.

DESIGN DETAILS FOR ENHANCED CORROSION PERFORMANCE

The most important considerations in designing a weathering steel bridge are to prevent water ponding, divert the flow of runoff water away from the steel superstructure, prevent the accumulation of debris that traps moisture, and avoid environments in which the bridge would be contaminated with salt. Under conditions of prolonged wetness or contamination with salt, weathering steel does not form a protective oxide coating. In fact, it corrodes at about the same rate as carbon steel and, thus, offers no advantage in corrosion resistance.

Deck Joints

Leaking joints are the most serious and common cause of corrosion problems in weathering steel bridges. Runoff water leaking through the deck joints persistently wets the bearings, flanges, webs, stiffeners, and diaphragms in the vicinity of the joint. The runoff water migrates for long distances along the bottom flange and wicks about 150 mm up the web. The resulting excessive corrosion of the superstructure and the freezing of expansion bearings created major bridge maintenance problems. To avoid the problems created by leaking joints, the steel girders and concrete deck should be continuous over the piers and the girder ends should be built integrally with the abutments if soil conditions permit. There should be no expansion joints unless absolutely necessary. When expansion joints cannot be avoided, they should be sealed and maintained properly. Hanger plate-and-pin connections of girders at open deck joints must not be used. They are susceptible to crevice corrosion and are costly to maintain.

Box and Tubular Members

Whenever possible, box and tubular members for truss bridges should be constructed air-tight. If tight construction is not feasible, a sufficient number of hatches, vents, or openings should be provided to create a draft. The inside surfaces should be painted, and the coating around the openings should be extra heavy.

Box girders cannot be sealed against moisture entry. Therefore, the box must be adequately drained and ventilated to reduce the potential for moisture entrapment and accelerated corrosion. Furthermore, if the box girder is inaccessible for inspection and maintenance, the interior surfaces must be painted. Accessible box girders may be left bare but the inside must be periodically inspected for evidence of corrosion. Owing to its smooth contour, the exterior of a box girder is less prone to corrosion than an I-girder on which debris, moisture, and salt spray accumulate more easily.

Water Ponding and Debris Accumulation

In I-girder bridge members, water ponds and debris accumulates on horizontal surfaces and in corners formed by horizontal and vertical plates (reentrant corners), fostering excessive corrosion. The most susceptible locations are bottom flanges, gusset plates for horizontal bracing, longitudinal stiffeners, bolted splices of horizontal and sloped members, and intersections of bearing and intermediate stiffeners with flanges and gusset plates. To avoid water ponding and debris accumulation, it is important to: minimize the number of horizontal surfaces on which water can pond and debris can accumulate, minimize the number of reentrant corners that may entrap windblown dust and debris that prevent drainage, design details for self cleaning and easy discharge of water, and avoid crevices. Similar design criteria apply for truss bridge members.

Water Drainage

Water on the approach roadway must be intercepted before it flows onto the bridge deck. Downspouts for deck drains must be located such that runoff water is discharged away from any part of the bridge, and must extend below the adjacent members. Bridge decks should be drained with downpipes only when no acceptable alternative is available. Downpipes must be of rigid corrosion-resistant material and have cleanouts in sufficient numbers and at convenient locations to permit access to all parts of the downpipe system. Drain pipes must not be routed through box members.

Concrete Staining

Runoff water carrying suspended particles of iron oxide released by weathering steel will stain concrete surfaces if it is allowed to drain over abutments and piers, particularly during the early years of exposure. For aesthetic reasons, every effort should be made to minimize unsightly rust staining of concrete supports visible to the public by preventing runoff water from draining over the weathering steel and onto the concrete. Continuous jointless decks and integral abutments are most effective in preventing such staining.

Vertical Clearance

Combinations of high speed traffic, low clearance, and heavy usage of deicing salt on the lower roadway pose a severe corrosion hazard, as the spray plume kicked up by passing trucks is about twice as high as the truck. Grade separation structures must have adequate clearance to keep most spray from reaching the bridge. It is equally important to provide adequate clearance over bodies of water so that vapor emanating from the water surface does not condense on the weathering steel. The required clearance depends on the degree of air circulation and the topography at the site.

Guardrails

The lapped surfaces of guardrails are susceptible to crevice corrosion. The crevices accumulate salt, soak up moisture by capillary wicking, and corrode at a much faster rate than the freely exposed surfaces. Guardrails may be built from weathering steel, but the contact surfaces at the lap joints should be painted to protect them against crevice corrosion.

CORROSION RESISTANCE

The ASTM specifications A242, A588, and A709 state that the atmospheric corrosion resistance of weathering steel is approximately equal to two times that of carbon structural steel with copper, which is said to be equivalent to four times that of carbon structural steel without copper (max. 0.02 percent Cu).

The ASTM requirement is based on analysis of pre-1968 data for which the corrosion resistance was calculated as the ratio of the

corrosion rate of the reference steel (carbon or copper steel) to that of weathering steel, over an increment of exposure time. This rating criteria was shown to be unreliable and misleading because it did not consistently discriminate between good and poor performance of weathering steel in a variety of environments ranging from rural to moderate marine. The rating numbers do not reliably reflect the actual corrosion resistance of a weathering steel in a given environment. Thus, statements of relative corrosion rates are not helpful for purposes of stress analysis of weathering steel members. Instead, members must be designed for average, uniform corrosion penetration (loss of metal thickness) per surface expected at the end of the service life of the bridge.

Weathering steel performing satisfactorily can be expected to corrode at a rate not exceeding 7.5 lm/year/surface, depending on the type of exposure. For members 38 mm or greater in thickness, production tolerances will provide sufficient steel to compensate for these corrosion rates. For members less than 38 mm thick, the thickness should be increased by 0.8 mm per exposed surface above that arrived by stress calculation. Where corrosion rates greater than 7.5 lm/year are anticipated, weathering steel should not be used in bare condition.

It has recently been shown that A242 steel does not have four times the corrosion resistance of carbon steel [*3*]. Also, A588 steel has neither four times the corrosion resistance of carbon steel nor two times the corrosion resistance of copper steel. As a result, ASTM is now deleting the corrosion resistance statements from all weathering steel specifications and will refer the reader instead to the Standard Guide for Estimating Corrosion Resistance of Low-Alloy Steels (G101). The Guide quantifies the atmospheric corrosion resistance in terms of an index number that is of no help in designing bridges. Instead, engineers should refer to the corrosion penetration data for A588 steel exposed in rural, industrial, and marine environments [*2*].

WELDING

The welding procedure for weathering steel is similar to that for ordinary steels of comparable strength. The main difference is that the rust color and corrosion resistance of the weld metal must match those of the base metal. As with any other structural steel, good shop or field practice must be followed to obtain sound welds of desired strength and ductility.

Combinations of any approved grades of weathering steel may be welded together. Any grade of weathering steel may also be welded to ordinary steels such as the A36, A572, and A514 steels. In this case, however, the steels should be painted to prevent galvanic corrosion.

A588 steel and A709 Grade 50W steel are weldable by the prequalified procedures of ANSI/AWS D1.1 Structural Welding Code -- Steel. The weldability of A242 steel must be investigated by the engineer and that of A709 Grade 100W must be established by the producer.

Shielded metal arc (SMAW), submerged arc (SAW), gas metal arc (GMAW), and flux cored arc (FCAW) welding procedures, which conform to the provisions of AWS D1.1, may be used for welding weathering steel.

Electroslag and electrogas welding procedures may be used only for weldments of A242 and A588 steel members subjected to compressive stresses. These procedures must not be used for welding A709 Grade 100W steel nor for welding bridge members of any steel that are subjected to tensile stresses or reversal of stresses.

Unpainted A242 and A588 steel structures must be welded with electrodes or electrode-flux combinations matching the strength, corrosion resistance, and color of the base metal. In multiple-pass welds only the two outer layers on all exposed surfaces and edges must match the strength and corrosion resistance of weathering steel, provided the underlying layers are deposited with a filler metal matching the strength but not the corrosion resistance of weathering steel.

In single-pass welds, absorption of alloying elements from the steel base may give the weld metal a corrosion resistance and coloring similar to that of the steel base. Accordingly, filler metal matching the strength but not the corrosion resistance of weathering steel may be used for single-pass SMAW welds up to 6 mm and SAW, GMAW, and FCAW welds up to 8 mm in size.

Unpainted A709 Grade 100W steels must be welded with filler metal containing one or more of the elements Ni, Cr, Cu, and Si in quantities sufficient to match the corrosion resistance and color of the base metal.

The allowable stresses for the static design of welds for weathering steel bridges are the same as those for ordinary steel bridges. Reductions in allowable stress range are recommended for the fatigue design of welded details.

Joints must be continuously welded on all sides to prevent moisture intrusion and corrosion in the crevice formed by the contact surfaces. Fillet welds in built-up members must also be continuous.

BOLTING

Mechanical fasteners are supplied to the requirements of the ASTM Specifications for High-Strength Bolts for Structural Steel Joints (A325) and Heat Treated Steel Structural Bolts with 1,035 Minimum Tensile Strength (A490). The bolts designated Type 3 in these specifications are made of steels whose chemical compositions provide atmospheric corrosion resistance and weathering characteristics comparable to those of the A242, A588, and A709 weathering steels. The mechanical requirements for A325 and A490 Type 3 bolts are identical to those of their Type 1 and 2 counterparts which do not have atmospheric corrosion resistance.

Other types of fasteners such as regular bolts, unfinished bolts, and rivets may not be readily available in weathering steel grades.

Zinc and cadmium coated bolts, including galvanized steel bolts, should not be used in weathering steel bridges because in time the coating is sacrificed through cathodic corrosion, leaving an exposed carbon-steel bolt less resistant to atmospheric corrosion than the weathering steel.

The tightening of high-strength bolts must be controlled by (a) the turn-of-the-nut method, (b) with a calibrated wrench, or (c) with a load indicating device. The load indicating devices available for use in

bolted joints are the load indicator washer and the tension-control bolt.

Load indicator washers with epoxy coated and either mechanically galvanized or mechanically cadmium coated surfaces are supplied for use with Type 3 high-strength bolts. The gap between the washer and the bolt head, which is maintained by the flattened protrusions on the washer, may act as a crevice that serves as a path for water ingression to the shank and threads of the bolt. This condition may lead to accelerated crevice corrosion of the weathering steel bolt and plates particularly in the presence of salt water. Lacking long-term exposure data, load indicator washers are not recommended for use in joints of unpainted weathering steel bridges.

Tension control bolts conforming to the requirements of Specification A325 are available in Type 1 alone. They do not have the atmospheric corrosion resistance and weathering characteristics of Type 3 bolts and must, therefore, be painted.

Bolted joints of weathering steel members perform satisfactorily if: the bolts are initially tensioned to 70 percent of the tensile strength; the pitch on a line of fasteners adjacent to a free edge does not exceed 14 times the thickness of the thinnest part joined, nor 175 mm; and the distance between the center line of any bolt and the nearest free edge does not exceed 8 times the thickness of the thinnest part joined, nor 125 mm. Under these conditions the joint remains tight, and the space between the contact surfaces of two weathering steel plates seals itself with corrosion products that form around the plate edges. The contact surfaces of bolted joints that do not meet the aforecited guidelines must be painted.

High-strength bolts in tension or bearing may be designed to the allowable stresses given in the AASHTO specifications. Bolts in slip-critical connections of mill-scaled weathering steel members must be designed to lower allowable shear stresses corresponding to a slip coefficient of 0.23. This reduction is needed because the mill scale is more slippery and adheres more tightly to the underlying weathering steel base that does the mill scale of an ordinary steel base. If the mill scale is removed, the allowable shear stress for slip-critical connections of weathering steel members is the same as that for ordinary steel members.

Good detailing of bolted connections is important. Any detail that traps water and debris facilitates accelerated pitting or crevice corrosion. The designer must, therefore, detail such elements with extreme care to ensure there is no possibility of moisture entrapment. If this condition cannot be avoided all such unexposed surfaces, including the contact surfaces between the plies of the connection, are to be treated like ordinary steel and must be painted.

FATIGUE

Unlike painted bridges in which the steel is protected against the environment, weathering steel bridges are concurrently exposed to aqueous environments and subjected to truck-induced stress cycling during their service life. The combinations of exposure and loading are complex. Before the bridge is opened to traffic and during the initial years of service, weathering creates rust pits from which cracks may

eventually initiate. During the service life the aqueous environment enhances crack initiation and accelerates the rate of crack propagation. Therefore, the exposure conditions of a weathering steel bridge lead to a reduction in fatigue strength caused by the effect of weathering and corrosion fatigue on the crack initiation life plus the effect of corrosion fatigue on the crack propagation life. The effects are cumulative. These findings are supported by a vast amount of data on weathering fatigue, corrosion fatigue crack initiation life, corrosion fatigue crack growth rate, and corrosion fatigue life.

Based on a careful analysis of all data, the following reductions in allowable stress range are recommended for unpainted weathering steel bridges, depending on the type of detail and the type of environment to which a bridge is subjected.

- For environments of medium corrosivity in which members corrode at a rate of 1 to 5 lm/year/surface: A -- 34%, B -- 24%, C -- 13%, and D through E' -- 10%.
- For environments of high corrosivity in which members corrode at a rate of 5 to 10 lm/year/surface: A -- 44%, B -- 34%, C -- 23%, and D through E' -- 20%.

The reductions should be applied to the allowable stress ranges for painted bridges made of ordinary steels.

The recommended reductions in allowable stress range are not applicable to weathering steel structures exposed to environments of very high corrosivity in which long periods of wetness or high levels of contamination with salt deeply pit the surface and significantly reduce a member's net section. Recent work has shown that such severe corrosion reduces the fatigue strength of category A base metal and category B welded beams to that of category E [4].

The allowable stress ranges need not be reduced for painted weathering steel bridges whose paint system is properly maintained.

CONSTRUCTION

Exposed weathering steel must be handled carefully in shipment, storage, and erection. It should be treated with the amount of care required by a finished architectural product. To prevent damage from occurring during handling, members must be padded in appropriate places, blocked in transit, and handled with slings instead of chains.

Weathering steel members are best stored at the construction site in bold exposure and on an incline so as to facilitate drainage of any rainwater, melted snow, or condensed dew. To prevent unsightly and excessive corrosion, the following conditions should be avoided or minimized: long transit times in railcars or open trucks; ponding of water at the construction site; contact with the soil; and entrapment of water through nesting of I-beams, girders, angles, gusset plates, and the like. Intimate contact with treated or untreated lumber used in blocking or support must be avoided by inserting a plastic sheet at the contact points. Care must be taken to avoid deposits of soil and other surface contaminants.

The color and texture of the mill scale do not match those of the corroded steel surface. Unless the mill scale is removed, the steel

surface will appear mottled, flaky, and nonuniform for several years depending upon the degree of exposure and the aggressiveness of the local environment. Therefore, all surfaces visible to the public should be blast-cleaned to a near-white condition for aesthetic reasons.

The mill scale should also be removed when parts of, or the entire, structure may be exposed to long periods of wetness or contaminated with salt. Under these conditions the less noble weathering steel corrodes galvanically along the numerous cracks in the mill scale and where flecks of scale are missing. As a result, deep corrosion pits forming at the scale-free anodic sites may lead to large reductions in fatigue strength. In this case, commercial blast cleaning suffices for surfaces not visible to the public.

Foreign substances that adhere to the steel and inhibit the formation of the protective oxide must be removed soon after erection. Some materials such as mud, concrete dust, etc., will normally be displaced by the corrosion products during the natural weathering process. Paint or wax-based crayons should not be used for marking weathering steel, because these materials do not wash or weather away even after many years of exposure. Oil, grease, cutting compounds, and similar insoluble contaminants can be removed from steel surfaces by solvent cleaning.

Minor contamination of the steel surface with salt and other water soluble compounds during the early stages of exposure can be removed by fresh water hosing. More severe contamination requires steam cleaning, using detergents and cleaners, followed by a steam or fresh water wash to remove detrimental residues.

Water insoluble material such as loose mill scale, loose rust, loose paint (markings), rust scale, and weld slag can be removed by hand or power tool cleaning.

During construction, before the concrete deck is cast, water running over the weathering steel superstructure and onto the piers and abutments will stain the concrete. To prevent staining during this period, the vulnerable concrete surfaces should be draped, wrapped, or otherwise sheltered with heavy-gage plastic sheeting. After construction and during the service life of the bridge, the concrete surfaces continue to be rust stained for an indefinite period if water running or dripping off the girders reaches the piers and abutments. To reduce the penetration by rust particles, the concrete can be coated with liquid silicone-based sealers. Rust stains on concrete surfaces can be removed with proprietary chemical stain removers or, if the stained areas are large, by abrasive blast cleaning.

INSPECTION

An effective inspection and maintenance program is essential to ensure a weathering steel bridge reaches its design life. The inspection differs from, and is more difficult than, that of a painted ordinary steel bridge. Rust spots in a painted steel bridge are visible from afar and serve as a warning of paint failure. In contrast, the entire weathering steel bridge is covered with rust, and areas of severe corrosion can be detected only at close range.

Weathering steel bridges must be inspected at least every two years as is required for painted bridges. More frequent inspections may be warranted if the bridge is corroding severely.

The principle signs of existing or impending distress that the inspector should look for are the appearance of a nonprotective oxide film; accumulation on horizontal surfaces and in sheltered corners of windblown dust, debris, and oxide particles shed during weathering; water streaks and drain patterns on vertical and sloped surfaces; leaky expansion joints; and rust packout in crevices.

The inspector must be familiar with the colors and textures that the oxide film assumes when exposed to different macro and microenvironments. They indicate whether the oxide that forms on weathering steel is protective. The colors are indicative of the following conditions: yellow or orange -- initial stage of exposure, light brown -- early stage of exposure, chocolate brown to purple brown -- protective oxide, and black -- nonprotective oxide.

However, visual appearance alone can be deceptive. In addition, the oxide film must be tapped with a hammer and vigorously wire brushed to determine if it still adheres to the underlying steel base or has debonded. Loose oxide granules are indicative of problems, depending on the age and location of the structure. Nodules, flakes of 6-mm and greater diameter, and laminar sheets are all indicative of nonprotective oxide and severe corrosion.

When the appearance suggests the oxide film is nonprotective, the uniform corrosion penetration and pit depth should be measured with an ultrasonic thickness gage or a depth gage at selected locations on a member.

The visual detection of fatigue cracks in painted steel structures is made easier by the contrast between the color of the paint and the streak of moisture-laden rust oozing from the crack. This advantage is absent in weathering steel structures. Furthermore, rust fills the crevice formed by the crack in a weathering steel member during the long service exposure, thus hiding the crack from view. As a result, fatigue cracks in weathering steel bridges are not likely to be found by visual inspection until the member has fractured. The reliability of detecting cracks in weathering steel members with other methods such as ultrasonics, acoustic emission, and radiography has not yet been evaluated.

MAINTENANCE

Weathering steel is not a maintenance free material. Experience has shown that highway bridges, by their nature and use, accumulate much debris; become wet from condensation, leaky joints and traffic spray; and are exposed to salts and atmospheric pollutants. Different combinations of these three major factors may create exposure conditions under which weathering steel cannot form a protective oxide coating. Therefore, the bridges must be maintained properly. The following examples illustrate the type of periodic maintenance that is needed:

- Remove loose debris with a jet of compressed air or vacuum cleaning equipment.
- Scrape off sheets of delaminated rust.

- High-pressure hose wet debris and aggressive agents from the steel surfaces.
- Trace leaks to their sources.
- Repair leaky joints.
- Install drainage systems, drip plates, and deflector plates to divert runoff water away from the superstructure and abutments.
- Clean drains and downspouts.
- Clean and caulk all crevices.
- Remedially paint areas of excessive corrosion.

Washing bridges does remove debris and contaminants from the surface, but it cannot wash out the salt that typically migrates to the interface between the oxide film and the underlying steel.

REHABILITATION

Severely corroding weathering steel bridges must be remedially painted to protect the affected areas against further section loss. Similar to the repainting of ordinary steel bridges, this involves the following steps: selecting a coating system, developing sound and practical specifications, estimating the cost of painting, inspection of the painting job by an expert, and proper maintenance after the painting is completed.

Coating systems for remedially painted weathering steel must tolerate large dry film thickness variations caused by the roughness of the steel substrate, be insensitive to residues of rust and chemical contaminants that are difficult to remove from the deeply pitted surface, and have a low water vapor transmission rate to prevent osmotic blistering of the film.

The roughness of the surface and the presence of numerous pits make it very difficult to remove all visible rust products. Some rust products often remain at the bottom of the pits even after the surface has been thoroughly cleaned. Since specifications for painting steel structures usually require near-white blast cleaned surfaces, meaning removal of all visible rust products, the difficulty in achieving this condition must be addressed in the specification. One method is to specify that the surface meet the requirements of the Steel Structures Painting Council (SSPC) visual standards at a viewing distance of 0.6 m, deleting the verbal description of near-white blast cleaning.

A large quantity of primer is required to fill the pits of a corroded surface. Experience with remedially painted weathering steel bridges has shown that one gallon of primer covers only about one-fourth of the area given in the manufacturers' product data sheet.

Performance testing of generic paint systems that were applied on hanger plates, which had been removed from severely corroded joints on weathering steel bridges in Detroit, Michigan, has shown the following ranking, from best to worst: (1) multi-component organic zinc-rich, (2) single-component organic zinc-rich, (3) single-component inorganic zinc-rich, (4) moisture-cured urethane, (5) epoxy primer, (6) chlorinated rubber, and (7) alkyd systems.

A similar study on remedial painting of A588 steel panels that were exposed six months atop a bridge near the Gulf Coast in southern Texas showed that: overall, the organic zinc-rich systems (epoxy primer,

epoxy intermediate coat, and vinyl topcoat) were the best; the barrier type systems (e.g. those that did not contain zinc) were the best over flash rusted panels; flushing with water improved overall performance; only zinc-rich systems were not undercut; and it is more difficult to clean weathered A588 steel than A36 steel.

To summarize the results of the paint studies, coating systems with demonstrated good performance over weathered A588 steel consist of an epoxy zinc-rich primer, an epoxy polyamide intermediate coat, and either a urethane or vinyl topcoat. This hybrid system of galvanic and barrier protection has good tolerance to film thickness variation, surface contaminants, and application errors.

A comparative cost analysis of painting bridges in service, performed in 1988 dollars, yielded a unit cost of $\$2.29/ft^2$ for repainting an A36 steel bridge and $\$3.55/ft^2$ for remedially painting an A588 steel bridge. The Michigan experience with remedially painting four weathering steel bridges confirmed those estimates.

The major section losses result from accelerated corrosion in crevices and exposure to long periods of wetness. Both can be compounded by chloride contamination. The crevices that are formed between back-to-back angles, intermittently welded members, and between hanger plates and the web at some expansion joints are particularly vulnerable. The corrosion rate is much higher within crevices than on exposed surfaces of the steel. Crevices must be rehabilitated before the structure is remedially painted.

CONCLUSIONS

Bare exposed weathering steel is an economical alternative to ordinary painted steel, if the weathering steel develops a protective oxide coating and, as a result, the bridge need not be painted during its service life. To ensure satisfactory corrosion performance, engineers should follow the guidelines for the use of weathering steel in bridges described in this paper.

ACKNOWLEDGEMENT

The author greatfully acknowledges the contributions of A.M. Naeemi, S.K. Coburn, F.M. Wattar, G.L. Tinklenberg, and W.P. Gallagher in the preparation of NCHRP Reports 272 and 314 [*1*,*2*]. The information presented in this paper was taken from those reports.

REFERENCES

[*1*] Albrecht, P. and Naeemi, A. H., *Performance of Weathering Steel in Bridges*, NCHRP Report 272, Transportation Research Board, National Research Council, Washington, D.C., July, 1984.

[*2*] Albrecht, P., Coburn, S. K., Wattar, F. M., Tinklenberg, G. L., and Gallagher, W. P., *Guidelines for the Use of Weathering Steel in Bridges*, NCHRP Report 314, Transportation Research Board, National Research Council, Washington, D.C., June, 1989.

[3] Albrecht, P. and Lee, H.Y., "Evaluation of Rating Numbers for Atmospheric Corrosion Resistance of Weathering Steel," *Journal of Testing and Evaluation,* JTEVA, Vol. 19, No. 6, Nov. 1991, 429-439.

[4] Albrecht, P., Li, W.L., Shabshab, C.F., and Wright, W., *Fatigue Strength of Weathered A588 Steel Beams,* Report No. FHWA/MD-89/01, Department of Civil Engineering, University of Maryland, College Park, Maryland, September, 1991.

Jean-Jacques Hechler

WETNESS MONITORING ON THE EXTERIOR OF INFRASTRUCTURES

REFERENCE: Hechler, J.J., "Wetness Monitoring on the Exterior of Infrastructures," Corrosion Forms and Control for Infrastructure, ASTM STP 1137, Victor Chaker, Ed., American Society for Testing and Materials, Philadelphia, 1992.

ABSTRACT : The ASTM G-84 time-of-wetness sensor was used to study the moisture deposition on the exterior of a large building for an autumn and a winter period. It was possible to detect the presence of all types of moisture deposition and to measure the time-of-wetness at any location on the building. The influence of such parameters as orientation, design, and temperature on the moisture deposition is discussed.

KEYWORDS : time-of-wetness, TOW, moisture, condensation, atmospheric corrosion, building materials.

Atmospheric deterioration, corrosion and weathering of building materials are the results of a complex interaction of different physical, chemical and mechanical factors. One of the most important factors is humidity. It is now well established for metallic materials that this factor can be represented by what is now called time-of-wetness (TOW), the time during which the material is covered by a layer of moisture, when establishing damage functions [1]. Using electrochemical techniques, several sensors have been developed to measure TOW values [2, 3, 4]; among them the ASTM G-84 TOW sensor [5] is the most common, being commercially available [6]. Using climatic parameters, ISO also defines the TOW as the time for which the relative humidity is higher than 80% when the temperature is higher than 0°C [7].

The ASTM sensor was essentially developed to measure moisture on buildings, but strangely enough, with the exception of two very limited and not very recent studies [1], it has never been used to monitor the wetness outside a whole building. Some other uses are described by Yamasaki et al. [8] and by Yamasaki [9]. The results on the TOW presented here are part of a more comprehensive study on the effects of the design and orientation on the corrosion of metals on a building [10, 11] and are intended to establish the usefulness of this sensor in this field.

Dr. Hechler is a Senior Research Officer and Program Manager at the Industrial Materials Research Institute, National Research Council of Canada, 75, Boulevard de Mortagne, Boucherville, Province of Québec, Canada J4B 6Y4.

EXPERIMENTAL

The sensor described in ASTM G-84 consists of a copper and a gold electrode. When covered with moisture, it develops a galvanic voltage which can be as high as 500 mV but most of the time lies between 0 and 100 mV. The TOW is defined as the time for which the voltage is higher than 10 mV (20 mV can also be taken but leads to a smaller value of the TOW). Discussions on the significance of this threshold can be found in Sereda et al. [2] and in Hechler et al. [11]. Several problems have been encountered with these sensors, which at times give very different values for the TOW. A study of a large number of these sensors revealed that most of the problems arise from their different sensitivities to dew [11]. With a standard deviation of 7% for the rain TOW and 40% for the dew TOW, they behave very well in atmospheres with little dew compared to rain. For atmospheres where dew is important when compared to rain, a special selection of the sensors is recommended and was performed to select the sensors used in this study. A special measuring system was developed [12] in order to measure the small voltages from the sensors over the large distances represented by buildings, with only two wires running over the building on which the measuring electronics and the sensors are connected. The whole system is driven by a microprocessor which also stores the data on floppy disks. The total TOW is measured by continously scanning the sensors placed at 44 locations on the chosen building. Each 1/2 hour the voltage of each sensor is stored on the floppy disks and printed along with its total TOW for further data treatment.

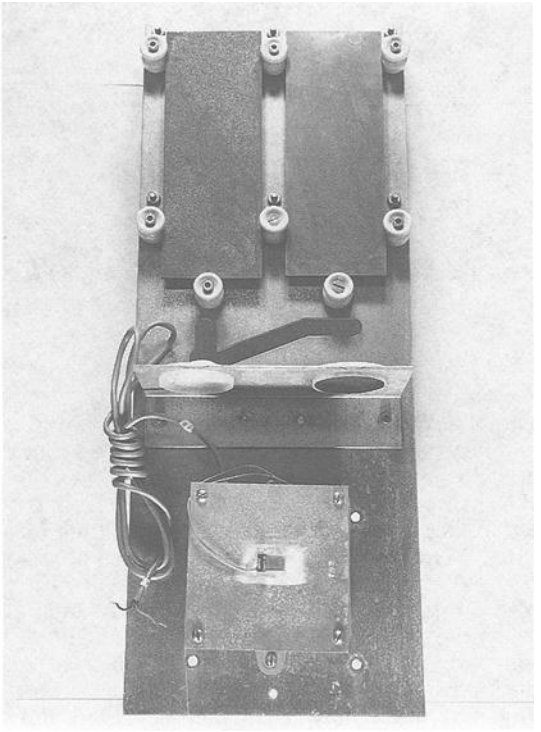

FIG. 1 - The mini-rack .

Fig. 1 shows the mini-rack used at each of the 44 locations. This rack was fastened to the exterior frame of the windows. The TOW sensor is glued on an aluminum plate which is fastened to a plastic box containing the electronics. At five locations (NE, SE, SW, NW and on the roof), this mini-rack also had a temperature sensor glued on the same aluminum plate as the TOW sensor, thus giving the temperature of the sensor. The measured temperature is thus also the temperature of the aluminum plate, which is different from the temperature of the bricks used on the building. This arrangement was preferred since one purpose of this study was to determine the parameters responsible for the corrosion of metals and not bricks. The values of other climatic factors mentioned in the text were measured by Environment Canada at a nearby airport, some 15 km east of the building. This rack also contained two metallic samples to determine the corrosion rates and passive and two passive monitors (sulfation and nitration plates) to assess the pollution deposition. Corresponding results are presented elsewhere [10, 11].

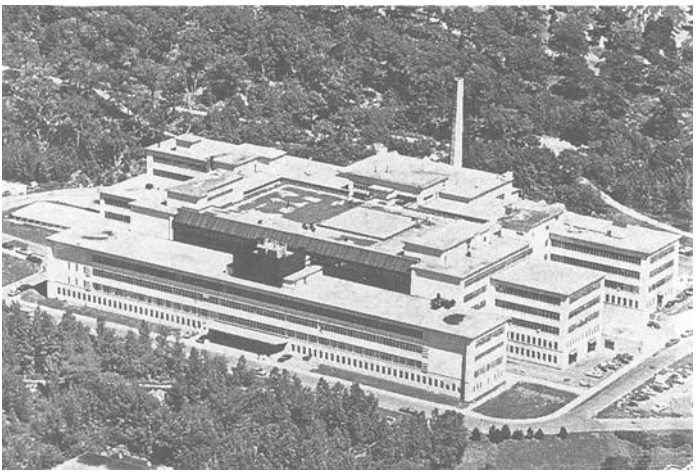

FIG. 2 - Aerial view of the buiding

Fig. 2 shows an aerial view of the chosen building. It is the Ecole Polytechnique, the engineering school of the Université de Montréal in Montréal, Canada. This building is located on the western slope of Mount Royal and is a free-standing building. Its only protection from the wind comes from the slope of Mount Royal on its southeastern face. It is basically a 4-story building (around 160 metres long, 80 metres wide and 30 metres high) with three external blocks on the north and south faces (Fig. 3). In its length it is oriented NE-SW. The difference in height between the NW and SE faces, due to the slope of the mountain, is equal to two stories. The mini-racks were placed on each wall at two different heights : on the second and fourth floor when possible, on the first and third floor when not possible. An ASTM G-90 rack with the same measuring devices was placed on the roof.

The monitoring took place between September 1986 and April 1987 and covers two seasons: autumn 1986, a period of 91 days, and winter 1987, a period of 114 days. Construction work on the building prevented the monitoring over a longer period.

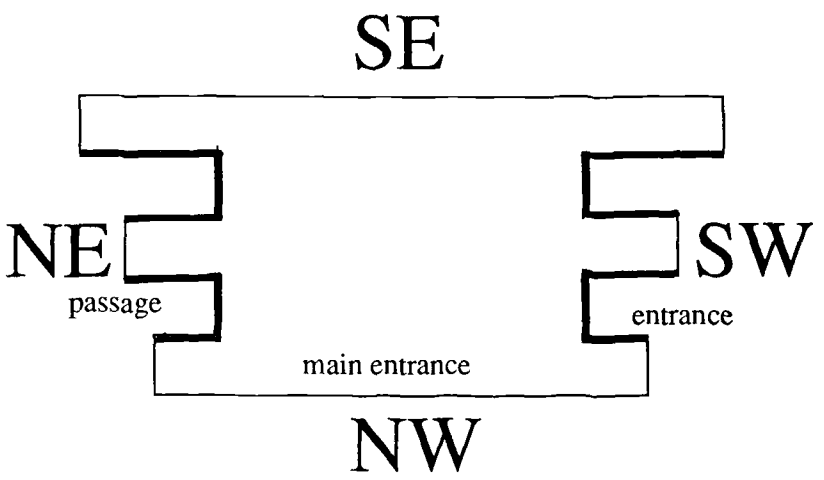

FIG. 3 - Orientation of the building. In the text, the (——) walls are caller the outermost walls and the (▬) walls the particular walls.

RESULTS AND DISCUSSION

Response of the sensors for different climatic conditions.

Heavy rain : Fig. 4 (1/10/86) gives the response of two sensors facing NE and SW for almost two identical periods of rain in October. The wind came from SW and W at around 20 km/h, causing wetting of the SW wall while the NE wall remains dry. The NE sensor develops only 2 or 3 mV due to the high ambient relative humidity, showing only traces of absorbed humidity coming from the high ambient relative humidity (around 90%). The change of the voltage with time is characteristic of a rain period : a very sharp increase of the voltage (up to 50-100 mV) then a small decrease during the rainfall followed by a slow decrease to zero during the drying period.

Dew and fog : Fig. 5 (21/9/86) shows some interesting correlations between temperature, orientation, wind direction and deposited moisture in September. Through a slow decrease in temperature during the night (12 p.m. to 7.00 a.m.), dew appears on all locations except on some SW locations. During that time, the wind blew from NNE. The NW, SW and SE sensors show the typical shape of the sensors' response during a dew period : a slow and small increase of the voltage (up to 10 mV) during the gradual appearance of the dew (4 a.m. to 7 a.m.), followed by a slow decrease to zero of the voltage due to drying when the temperature increases at the appearance of the sun (7 a.m. to 10 a.m.). During that time, the sensors exposed NE all developed a much higher voltage, up to around 40 mV, which is close to the voltage developed for thick humidity layers, as for rain. These sensors are exposed to the direction of the wind and such a high wetness can be explained by the deposition of some fog which was also present at that time. It is also interesting to note that one out of two NE sensors remained somewhat wet during the remaining of the day for two reasons. Firstly, they are not exposed to the sun and are much colder (14°C max.) than the SW sensors (32°C max.). Secondly, after 12 a.m., the wind changed

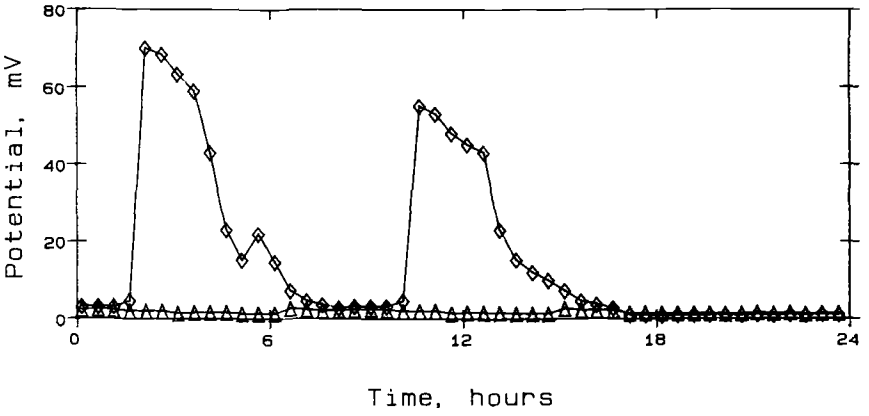

FIG.4 - Response of two sensors to rain (NE : Δ , SW : ◇)

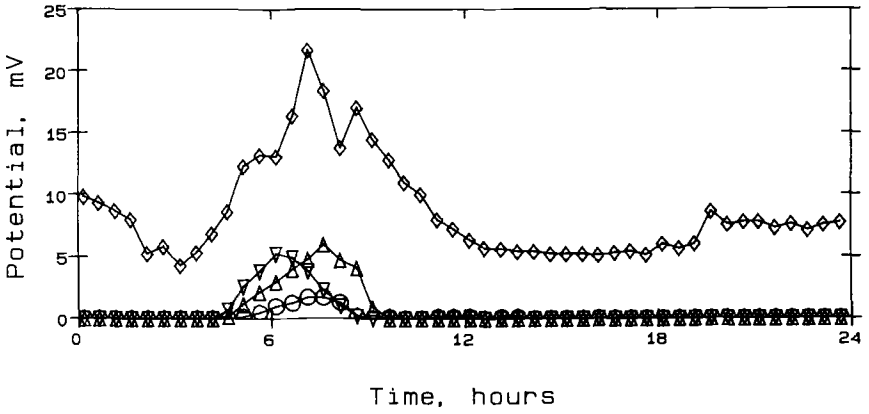

FIG. 5 - Response of the sensors to morning dew (NE: ◇ , NW: Δ , SE: O , SW: ▽)

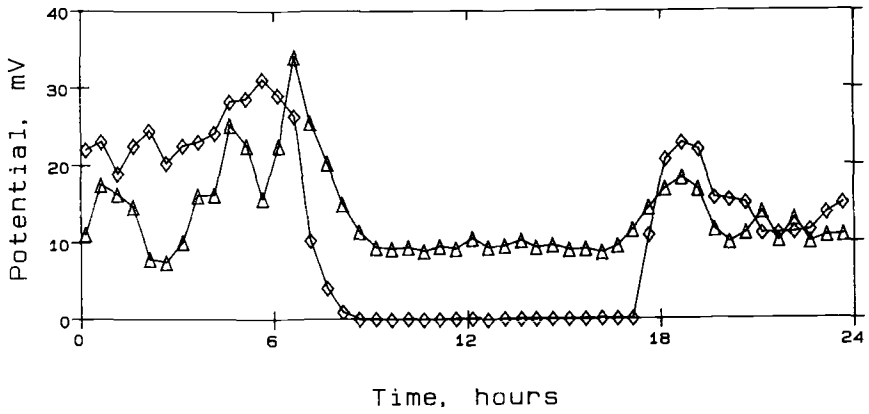

FIG. 6 - Response of two sensors to hoarfrost (NE : Δ , SW : ◇)

gradually to the SW, which slowed down the drying of the NE wall. This clearly shows the difference in condensed moisture which can prevail on different locations, some locations being wet all day while some other locations hardly see any moisture.

Low temperature and high humidity: Fig. 6 (18/2/87) shows some typical behaviour associated with subzero temperatures in winter. While the ambient temperature in this case remains below - 10°C, the three NW, SW and SE walls have periods with temperatures above zero and therefore experience very different humidity conditions than the NE wall, whose temperature remains close to the ambiant temperature. This particular day was sunny and calm. A decrease in the temperature in the morning created hoarfrost on most locations, the exceptions being some of the lower sensors. This hoarfrost disappeared around 8 a.m. as soon as the sun appeared, raising the temperature of the walls, except for the NE walls where nearly all sensors remained somewhat wet during the afternoon. At the disappearance of the sun and the decrease of the temperature, hoarfrost appeared again as in the morning.

Low temperatures and wet snow: Fig. 7 (30/3/87) corresponds to a cloudy day, with high winds from the south and with a period of wet snow in the afternoon. All sensors more or less see the two periods of wetness : hoarfrost in the morning and wet snow in the afternoon. The responses of the two sensors shown here are the two extremes observed; the NE sensor sees the hoarfrost, but being on the wall protected from the snow does see the snow only through a small increase of the ambient relative humidity, which causes a very small increase of the voltage; the SW sensor sees mainly the wet snow and almost does not detect the hoarfrost, probably due to a drying effect from the south wind.

Low temperatures and conditions close to condensation: Fig. 8 (4/1/87) shows a very close relationship between the temperature variations and the voltage of the sensor. A small decrease in the temperature increases the ambient relative humidity and the humidity absorbed on the electrodes, resulting in an increase of the voltage. This happens generally for this sensor when the relative humidity is close to 45% [11]. The same behaviour occurs on the five locations where temperature was measured.

These few examples have shown that, if properly selected, this sensor follows very closely any type of humidity, at any temperature even down to - 25°C, which appeared to be, at least at that location, the lowest temperature where a TOW can be measured.

Time-of-wetness changes with time

When one particular wetness event is analysed, it is more or less easy, when the wind direction is known, to follow the location and the appearance of the wetness. In the case of a rainfall, the first locations to become wet are usually on the side facing the wind, although due to the complex geometry of the building and due to the turbulence created, unexpected points downwind become wet as soon as the event starts. Other points become wet just by adsorbing humidity due to the increase of relative humidity at the start of the rain. Some other points protected by some structural design (i.e. roof overhang) seldom became wet and their behaviour can easily be predicted. Each event has its own particularities which influence the wetness and its appearance on a particular location on the building, and examples have already been shown above. More general tendencies on the building appear when the occurence of the TOW is studied over longer periods of time, one season, for example.

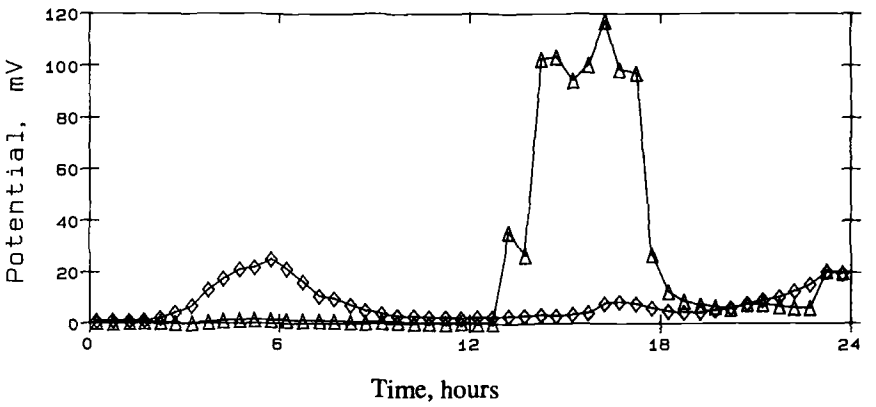

FIG.7 - Response of two sensors to hoarfrost and wet snow (NE : ◇ , SW : △)

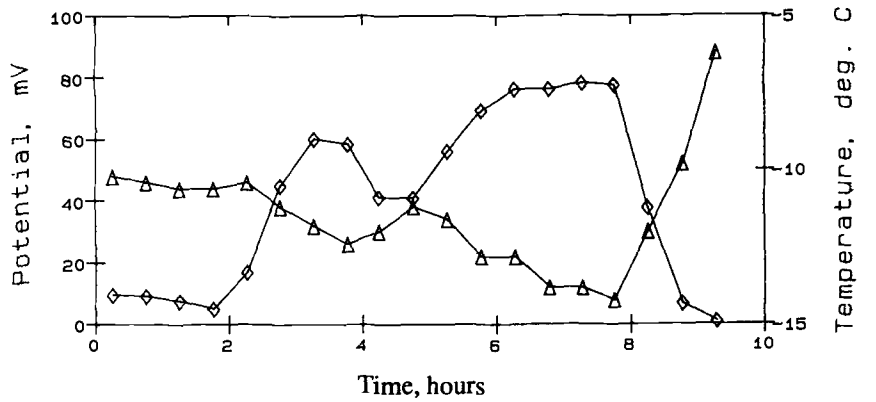

FIG. 8 - Temperature (△) and voltage (◇) for conditions close to condensation.

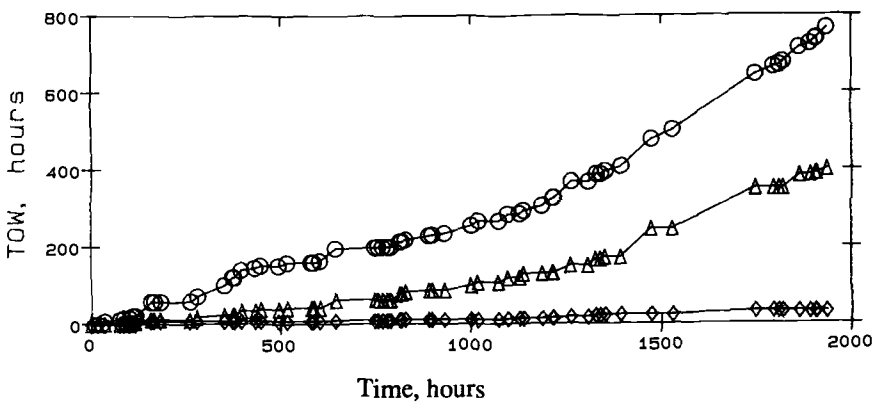

FIG. 9 -TOW evolution during the autumn period for three sensors having the highest, the lowest and an intermediate TOW (○ is the sensor on the roof, ◇ a sensor below the roof overhang and △ a sensor on the SW wall)

Fig. 9 shows this evolution for selected sensors during the autumn period. These curves all have the same shape and, with few exceptions, one curve never crosses another one. This shows that during the chosen period the same general parameters responsible for the wetness pattern on the building do not change appreciably. The same is true for the winter period. The highest TOW at any moment of the period is the ASTM location on the roof. This result was more or less expected since this unprotected location is exposed to all wind directions. It will therefore be important to compare all locations on the building to the roof location.

Outermost walls : By looking at all these curves, no very distinctive pattern on the building appears. This is certainly due to the complicated air flow, resulting from the geometry of the building, carrying the rain on the building in a very different manner from one point to another of the building [13] [14]. When only the outermost walls are considered a certain trend appears which is given in Table 1. This table gives the mean value of the total TOW for the main orientations including the value for the roof. For the autumn period, the NW and the SW faces of the building are the wettest, and for the winter period the wettest faces are NW and SE. By assuming that the air flow on the outermost walls can be represented mainly by the wind direction and wind speed, these two faces should be on the side of the prevailing winds. This is indeed the case : for the autumn period the wind direction was most of the time between west and south, and between west and north for the winter period. The relationship is good for the autumn period. For the winter period, the relationship with the prevailing wind is less clear : the mean values of the TOW are much closer one to another than for the summer period. This can be accounted for by the fact that during the winter period, with mainly subzero temperatures, the wetness is largely due to adsorbed moisture (as in Fig. 7) rather than to moisture (i.e. wet snow) driven on the walls by the wind.

Particular walls : Again it is very difficult to find a general trend on these walls, even if the study is restricted to three adjacent walls. For locations at the same height on these walls and on those on the adjacent outermost walls, when one compares the TOW, the values can be equal, higher or lower. The only common point that is observed is that generally the highest TOW on a wall is given by the lowest location for autumn while in winter this is only true for around half of the walls. This difference from one season to another reflects certainly the different predominant type of moisture present : in autumn the highest location is somewhat protected from the rain by the roof overhang, which in winter does not provide protection from absorbed moisture.

The TOWs of the three particular walls on the NE face close to the N corner can nevertheless be explained. One of these walls has on the ground floor a passage (see Fig. 3) as wide as the wall to permit access to a small interior space which is not covered by a roof. This design is responsible for the existence of a permanent draft through this passage. Table 2 gives the TOW values for these walls and for the adjacent outermost walls. It can be seen that the three lowest locations surrounding the passage have in autumn much higher TOW values than the higher locations and those on the adjacent outermost walls. During several rain events, these three locations also are amongst the first wet, even when the wind comes from the south. This shows clearly how, due to a special design, a resulting air flow increases the wind driven rain. During the winter, the highest locations on these walls are wetter than the lowest, again reflecting the different kind of moisture deposition (rain or hoarfrost) in autumn and in winter.

TABLE 1 - Mean TOW values for the outermost walls

Orientation	Mean TOW (hours)	Mean TOW/roof TOW
a) Autumn		
NW	632 (160)	0.70
SW	525 (170)	0.58
SE	418 (69)	0.46
NE	322 (177)	0.36
Roof[a]	899 (84)	1.00
b) Winter		
NW	1628 (231)	0.92
SE	1450 (99)	0.82
SW	1382 (224)	0.78
NE	1339 (220)	0.76
Roof[a]	1762 (116)	1.00

[a] The roof TOW is also the ASTM TOW.
Standard deviations are given in parentheses.

TABLE 2- TOW values for the N corner of the building
(all values in hours)

Walls	Higher locations	Lower locations
a) Autumn		
Particular walls	410	783
	459	704
	515	764
Adjacent outermost walls	339	386
	65	600
b) Winter		
Particular walls	1913	1614
	1914	1600
	1339	1496
Adjacent outermost walls	1296	1277
	994	1394

Wetness frequency.

Having measured every half an hour the voltage of every sensor, it is therefore possible over any period of time to determine for any location its "wetness frequency". This frequency is defined as the percentage of the number of days during which a location is wet at a certain time of the day (for instance, if location 34 is wet at noon during 30 days out of 60, the frequency of that location for noon is 50%).

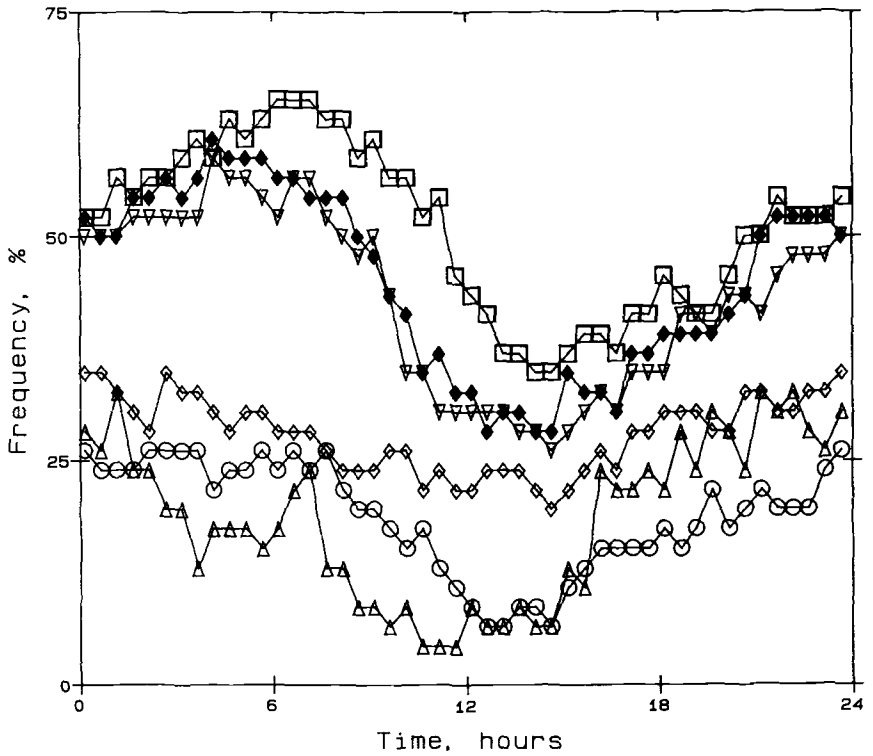

FIG. 10 - Wetness frequencies for the particular walls close to the N corner.

Influence of location and time of day : Fig. 10 shows some examples of how this frequency changes with location and time of the day. All curves have the same shape with a maximum between 4 a.m. and 8 a.m., reflecting the presence of the dew, and a minimum between noon and 2 p.m., which is the warmest part of the day corresponding to the least moisture on the exposed surfaces. These curves are very useful to detect any difference in behaviour within a wall or between walls. The curves presented in Fig. 10 are those for the three particular walls on the NE corner of the building. The three top curves shown in the figure correspond to the lower locations and the bottom curves to the higher locations. The three top curves are closely grouped and well separated from the three bottom curves which are also closely grouped. Again there can be seen very clearly the influence of the passage mentioned previously : it doubles the wetness frequency of the lower surrounding parts of the building. This is a good example of the usefulness of the sensor (and the notion of wetness frequency) in studying the effect of the design on the wetness outside a building. When all curves are similarly grouped for all the other walls, the figures are similar to Fig. 10 with no special features and with well distributed values of the frequency.

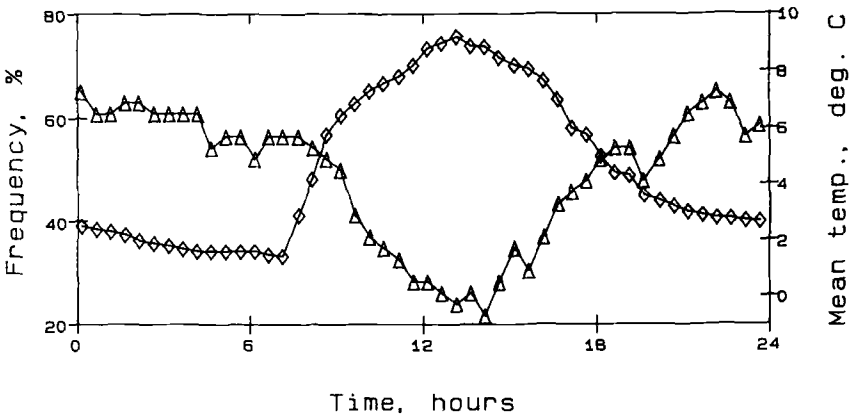

FIG. 11 -Wetness frequency ( ) and temperature ( ) on the roof for the autumn period.

Influence of the temperature : This influence can be determined only on the 5 locations having both a temperature and a TOW sensor. Fig. 11 shows the wetness frequency and the mean temperature versus the time of the day for autumn for the roof location. This location has the widest range of temperature and wetness frequency. The curves for the other four locations are similar; the NE location, having no sun, has the smallest range of temperature and wetness frequency. The relationship between wetness frequency and temperature is obvious. Fig. 12 shows this relationship for the SW location. Except for the NW wall, there is a good linear relationship between the frequency and the temperature. It would be interesting to know what the slope represents, being the change in wetness frequency induced by a change of one degree in the mean temperature. This slope is around - 3.3 for the SW, NW and SE walls, - 4.5 for the roof and - 6.4 for the NE wall. It depends certainly on parameters like wind direction and speed, orientation, close architectural features and surrounding structures, etc... More measurements are needed to assess its meaning. It is hoped that the wetness monitoring of three bridges in Québec currently underway will bring some additional information on that subject [15].

Time-of-wetness and total time.

Wetness occurs only during a fraction of the total real time. Its percent of the total time can not only vary greatly from one climate to another, but also, as has been shown here, between two locations very close on a building. Table 3 gives some values for the two periods. The roof TOW, measured on an ASTM rack which is the TOW usually reported in the literature, is 41% of the total time for autumn and 64% for winter. This value is around 35% over a whole calendar year for similar geographical locations [1]. It can be seen that some locations chosen here almost never get wet during the autumn period, but, due to the different type of moisture deposition, do get wet in the winter. Again it can be seen that due to this difference, the values are higher in winter and their range is much narrower than in autumn. Thus, in this particular study, the % of time when the building is wet varied from 0 to 64%, depending on the location where it is measured.

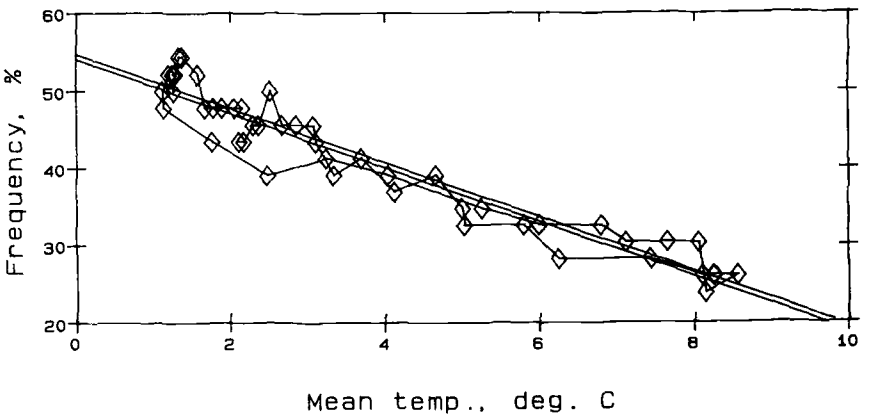

FIG. 12 - Relationship between wetness frequency and the mean temperature for the SW location.

TABLE 3 - TOW values as a percentage of the total time for selected locations of the building

Location	Autumn	Winter
NE, under the roof overhang	3	36
NE, under the roof overhang	8	62
NE, lower location	21	56
NW, higher location	24	67
SW, lower location	31	39
SE, higher location	36	50
Roof, ASTM rack	41	64

CONCLUSION

This study has shown that measuring the wetness on large buildings is not only possible but also that it provides especially a better understanding of its deposition. Information on how, where and when moisture presence develops can be easily obtained. The particular sensor used here also provides information on the nature of the wetness (rain, dew, hoarfrost, etc..) and on the speed of deposition and of drying, just by looking at the shape of the plot of its potential with time. As such, it should continue to prove itself very useful in any study related to degradation, restoration, design, etc...

ACKNOWLEDGMENTS

The author gratefully acknowledges the help of J. Boulanger and D. Noël for the computer handling of the huge amount of data and C. Pinon and the late R. Dufresne for the TOW measuring system.

REFERENCES

[1] Sereda, P.J., "Weather Factors Affecting Corrosion of Metals," in Corrosion in Natural Environments, ASTM STP 558, American Society for Testing and Materials, Philadelphia, 1974, pp. 7-22.

[2] Sereda, P.J., Croll, S.G. and Slade, H.F., "Measurements of the Time-of-Wetness by Moisture Sensors and their Calibration," in Atmospheric Corrosion of Metals, ASTM STP 767, American Society for Testing and Materials, Philadelphia, 1982, p. 267-283.

[3] Strekalov, P.V., Mikhailovkii, Y.N., Dzincharadze, G.K., Knotkova, D. and Vlachova, Y., "Monitoring the Time of Retention of a Phase Moisture Film on Metals during Atmospheric Corrosion, " Protection of Metals, Vol. 22, 1987, pp. 397-404.

[4] Kucera, V. and Mattson, E., "Electrochemical Technique for the Determination of the Instantaneous Rate of Atmospheric Corrosion," in Corrosion in Natural Environments, ASTM STP 558, American Society for Testing and Materials, Philadelphia, 1974, pp. 239-260.

[5] Anon.. "Standard Practice for Measurement of Time-of-wetness on Surfaces Exposed to Wetting Conditions as in Atmospheric Corrosion Testing," Annual Book of ASTM Standard, Vol. 03.2, 1989. American Society for Testing and Materials, Philadelphia, Pa.

[6] The Sereda Miniature Moisture Sensor, Model SMMS-01 manufactured by Epitek Electronics, 100 Schneider Road, Kanata, Ontario, Canada K2K 1V2 or Commerce Park, Ogdenburg, New York 13669, USA.

[7] Anon., "Corrosion of Metals and Alloys - Classification of Corrosivity of Atmospheres," International Organization for Standardization, Standard # 9223, 1990.

[8] Yamasaki, R.S., Slade, H.F. and Sereda, P.J., "Determination of Time-of-wetness due to Condensed Moisture," Durability of Building Materials, Vol. 1, 1983, pp. 353-361.

[9] Yamasaki R.S. , "Characterization of Wet and Dry Periods of Plastic Surfaces during Outdoor Exposures," Durability of Building Materials, Vol. 2, 1984, pp.155-169.

[10] Hechler, J.J., Boulanger, J., Dufresne, R. and Pinon, C., "Variation in Metallic Atmospheric Corrosion and its Parameters on a Building," Proceedings of the 9th European Congress on Corrosion, Utrecht, The Netherlands, October 1989, paper # 032, vol. 2.

[11] Hechler, J.J., Boulanger, J., Noël, D., Dufresne, R. and Pinon, C. "A Study of Large Sets of ASTM G 84 Time-of-Wetness Sensors", Corrosion and Evaluation: Silver Anniversary Volume, ASTM STP 1000, R.Baboian and S.W. Dean, Eds., American Society for Testing and Materials, Philadelphia, 1990, pp. 260-278.

[12] April, G.E., Pinon, C., Dufresne, R. and Hechler, J.J., "Atmospheric Corrosion Studies With Microcomputer Monitoring", Proceedings, Software and Hardware Applications of Microcomputer, Beverley Hills, CA, International Society for Mini and Microcomputer (ISMM), Anaheim CA, 1986, pp. 212-215.

[13] Hosker, R.P. Jr., "Flow Around Isolated Structures and Building Clusters : a Review," Transactions, ASHRAE, vol. 91, 1986, pp. 58-79.

[14] Robinson, G. and Baker, M.C., "Wind Driven Rain and Buildings," Division of Building Research, National Research Council of Canada, Ottawa, 1975, Technical Paper No 449.

[15] Hechler, J.J. and Thinh, T.P., "Projet de recherche, énoncé de travail : Dégradation atmosphérique des ponts : causes et remèdes," Laboratoire Central, Ministère des Transports du Québec, Sainte-Foy, Province of Québec, Canada and Industrial Materials Institute, National Research Council of Canada, Boucherville, Province of Québec, Canada. March 1990.

Khossrow Babaei[1] and Neil M. Hawkins[2]

PERFORMANCE OF REHABILITATED/PROTECTED CONCRETE BRIDGE DECKS

REFERENCE: Babaei, K., and Hawkins, N.M., **"Performance of Rehabilitated/ Protected Concrete Bridge Decks,"** Corrosion Forms and Control for Infrastructure, ASTM STP 1137, Victor Chaker, Ed., American Society for Testing and Materials, Philadelphia, 1992.

ABSTRACT: This paper is based on a research study aimed at determining the relative effectiveness of three bridge deck protective systems (i.e., latex-modified concrete (LMC) overlay, low-slump dense concrete (LSDC) overlay, and cathodic protection (CP) in preventing or halting reinforcing steel corrosion and corrosion-induced deterioration in salt-contaminated concrete. The paper documents the results of testing five LMC, five LSDC, and two CP bridge decks. The test bridges had experienced severe corrosion-induced deterioration and/or severe salt contamination before protection. At the time of testing the average age of both the LMC and LSDC overlays was about seven years, and the average age of the CP installations (slotted system) was five years. Also, among the concrete overlaid decks, seven had been subjects of previous similar investigations. Thus, the study determined changes in the effectiveness of concrete overlay protective systems with time.

The mode of internal concrete fracture caused by reinforcing steel corrosion and its magnitude were determined. Performance information was expressed in terms of corrosion-induced deterioration as well as rate of corrosion-induced deterioration. A criterion was established for the condition beyond which deterioration impairs deck serviceability. Accordingly, the effective service lives of the rehabilitated/protected decks were estimated. Also, the performance information was analyzed for factors affecting the condition of a rehabilitated/protected deck. Overlay surface cracking and overlay thickness were found to affect the corrosion-induced deterioration in the concrete overlaid decks. Correlations were made between those factors and the deterioration. In CP decks various types of concrete deterioration were found, their magnitudes were measured, and their causes were identified. Those types of deterioration, generally, were not related to corrosion of reinforcing steel. The cost-effectiveness of concrete overlay and cathodic protection strategies were determined on the basis of bridge deck life-time costs and compared.

KEY WORDS: bridge deck, concrete, reinforcing steel, corrosion, overlay, cathodic protection, rehabilitation, protection, cost-effectiveness

[1] Senior Engineer, Wilbur Smith Associates, BTML Division, 2921 Telestar Court, Falls Church, Virginia 22042.

[2] Head, Department of Civil Engineering, University of Illinois at Urbana-Champaign, 205 N. Mathews Avenue, Urbana, Illinois 61801-2397.

The protection of reinforced concrete bridge decks against corrosion of reinforcing steel has been a major effort for highway agencies in the United States. The majority of bridge decks were originally constructed according to design practices that did not provide sufficient protection against reinforcing steel corrosion. As a result, the application of deicing salt on some bridge decks during winter, or salt from marine environments, have caused embedded reinforcing steel to corrode and expand and therefore have caused the concrete to crack and deteriorate internally.

The rehabilitation of deteriorated bridge decks usually does not include the complete removal of salt contaminated, but sound, concrete. The contaminated concrete that remains in place has the potential to continue to corrode the embedding reinforcing steel. A bridge deck with salt contaminated, but sound, concrete may be protected against the occurrence of reinforcing steel corrosion. One of the most frequently used protective strategies has been the application of special concrete overlays (i.e., latex-modified concrete (LMC) and low-slump dense concrete (LSDC)). Those overlays are used to seal the underlying salt-contaminated bridge deck against the penetration of moisture and oxygen, the two elements that promote corrosion. Cathodic protection is another strategy. In this strategy, sufficient current in the proper direction is applied to the reinforcing steel to reverse the galvanic corrosion process. The corroding metal, which previously had been anode, becomes a non-corroding cathode.

This paper is based on a research study aimed at determining the relative effectiveness of three bridge deck protective systems (i.e., LMC overlay, LSDC overlay, and CP) in preventing or halting reinforcing steel corrosion and corrosion-induced deterioration in salt contaminated concrete. To pursue the project goal, the research team selected five LMC, five LSDC, and two CP (slotted system) bridges on which to conduct detailed field investigations and determine the relative performance of the systems.

SELECTED TEST SITES

All of the test bridges were located in the state of Washington. The test bridges had experienced severe corrosion induced deterioration and/or severe salt contamination before rehabilitation and protection. The nominal thicknesses of LMC and LSDC overlays were 38 mm (1 1/2 in.) and 51 mm (2 in.), respectively. Both CP systems were slotted systems built into the bare decks. In both decks the slots were primarily longitudinal. They were about 19 mm (3/4 in.) deep, 25 mm (1 in.) wide, 0.3 m (1 ft.) apart, and filled with a conductive polymer. Field testing of the test bridge decks was conducted during the summer/fall of 1988 and spring/summer of 1989. At the time of the testing, the average age of both the LMC and LSDC overlays was about seven years, and the average age of the CP installations was about five years. The test areas on each deck comprised the driving lane and the adjacent shoulder.

Tables 1 and 2 provide pre-rehabilitation/protection data on the five LMC and five LSDC bridge decks, respectively. Also, included in Tables 1 and 2 is post-rehabilitation/protection test data for four LMC bridge decks and three LSDC bridge decks. The test data were collected by the Washington State Department of Transportation in 1986 as part of a bridge deck research program (1). Table 3 lists background information on the two bridge decks protected with CP systems. Unlike all other bridge decks in the research program, the site of Bridge 104/5 (CP installation) was a marine environment rather than a deicer environment. That bridge was a pontoon bridge, and the CP system of that bridge was located on a relatively small section of its lower deck. The lower deck was exposed to a heavy salt spray from the adjacent water.

Table 1. Latex-Modified Concrete Overlays, Background Information

									Condition (1986)						
Bridge No. & Name	Year Built	Type of Structure	Length (ft) / Width (ft.)	Year Overlaid	(1) Cl contamination before overlaid	Conc. repair before overlaid (% of area)	Type of Conc. repair	ADT (1983)	(2) Cracking (% of area)	Pull-out Bond (psi)	Max. / Avg. / Min.	Debonding (% of area)	Half-Cell (3) (% of readings) <0.20 (V)	0.20-0.35 (V)	>0.35 (V)	Delamination (% of area)
20/211 S Swinomish D. Berentson Bridge	1972	16-Span prestressed beams, & 5-span steel beams	3,259 / 33	(4) Aug., Sept. 1981	83% (8-19-80) (test section)	1% (overall)	Monolithic	7,950	2%	>398 / 185 / 8		0%	100%	0%	0%	0%
90/510 S Medical Lake Road OC	1966	3-Span prestressed beams, (cont.)	130 / 36	June, 1982	50% (1-3-80)	14.97%	Monolithic	5,850	40%	382 / 251 / >159		0%	69%	30%	1%	4.38%
90/512 S N.P. Ry OC	1966	3-Span prestressed beams, (cont.)	150 / 38	June, 1982	30% (1-3-80)	1.7%	Monolithic	8,750	35%	>199 / 165 / 127		0%	77%	22%	2%	3.88%
2/311 Pine Cr.	1949	3-Span concrete T beam (cont.)	209 / 26	June, 1979	80%	9.9%	Monolithic	1,380	14%	462 / 329 / >159		0.01%	100%	0%	0%	0%
90/154 N Yakima River	1967	Concrete box (cont.)	588 / 30	(5) 1985	64%	>5% Extensive Rehab.	Patch	7,225	—	—		—	—			—

(1) Percent of concrete samples having more than 2 lb/cy chloride content
(2) Percent of cracked 5' x 5' grid squares
(3) Negative sign eliminated, measured on a 5' x 5' grid
(4) 300 ft. test section over partially continuous prestressed beams starting from span 15, from West
(5) 245 ft.test section between two mid-span hinges

(1 ft = 0.3 m; 1 psi = 6.4 kPa; 1 lb/cy = 0.59 kg/m^3)

Table 2. Low-Slump, Dense Concrete Overlays, Background Information

									Condition (1986)						
Bridge No. & Name	Year Built	Type of Structure	Length (ft) / Width (ft.)	Year Overlaid	(1) CT contamination before overlaid	Conc. repair before overlaid (% of area)	Type of Conc. repair	ADT (1983)	(2) Cracking (% of area)	Pull-out Bond (psi)	Max. / Avg. / Min.	Debonding (% of area)	Half-Cell (3) (% of readings) <0.20 (V)	0.20-0.35 (V)	>0.35 (V)	Delamination (% of area)
90/124 S Lake Valley Rd OC	1962	3-Span prestressed beams, (simple)	104 / 38	Aug., 1979	100% (5-14-79)	13.4%	Monolithic	5,950	28%		446 / 233 / 143	0%	100%	0%	0%	1.04%
90/150 S Taneum Cr.	1965	1-Span prestressed beams, (simple)	108 / 38	June - Aug., 1983	90% (12-9-81)	9.73%	Patch	7,550	84%		326 / 143 / 8	0%	53%	46%	1%	2.00%
90/162 N Wilson Cr.	1967	3-Span concrete slab (cont.)	118 / 38	Oct., 1981	50% (10-22-80)	17.75%	Monolithic, and patch	7,650	65%		>428 / 210 / 111	0%	64%	34%	2%	5.88%
90/134 N Cle Elum Rd	1962	Steel Truss & concrete Tee beam	297 / 31	1983	100%	>5%	Patch	5,950	—	—		—	—			—
970/5 NPRYC OC	1966	3-span prestressed concrete beam (cont.)	145 / 36.5	1982	60%	>5%	—	2,600	—	—		—	—			—

(1) Percent of concrete samples having more than 2 lb/cy chloride content
(2) Percent of cracked 5' x 5' grid squares
(3) Negative sign eliminated, measured on a 5' x 5' grid

(1 ft = 0.3 m; 1 psi = 6.4 kPa; 1 lb/cy = 0.59 kg/m^3)

Table 3. *Cathodically Protected* Decks, Background Information

						Pre-protection Condition				
Bridge No. & Name	Year Built	Type of Structure	Length (ft) ----- Width (ft.)	ADT	Year Protected	(1) $\overline{CT}$ contamination	Half-Cell (% of readings) <0.20 (V)	0.20-0.35 (V)	>0.35 (V) (2)	(6) Rehabilitation (% of area)
522/30 ES Woodinville Interchange	1968	Conventional conc box girder	300 ----- 35	5,800	1985	64%	10%	0%	0%	1.10%
104/5 Hood Canal Bridge	1961	Concrete floating pontoon	(3) 100 ----- 50	(4) 0	1983-84	(5) 56%	74%	23%	3%	33.16%

(1) Percent of concrete samples having more than 2 lb/cy chloride content at rebar level.
(2) Negative sign eliminated, measured on a 5' x 5' grid.
(3) Length and width of cathodically protected section.
(4) Lower deck of Pontoon Bridge not exposed to traffic.
(5) Data belongs to the upper deck which is exposed to salt from marine environment. The condition of the lower deck, where the test site is located, is likely worse than the upper deck due to a greater level of exposure.
(6) Measured in the current study in the test areas.

(1 ft = 0.3 m; 1 psi = 6.4 kPa; 1 lb/cy = 0.59 kg/m^3)

TESTING AND INTERPRETATION OF TEST RESULTS

In the following sections, the research findings are analyzed and interpreted for evidence that protected bridge decks may develop reinforcing steel corrosion and corrosion induced deterioration or that the protective systems themselves may deteriorate when exposed to a bridge environment.

Corrosion-Induced Deterioration in Overlaid Decks

Corrosion-induced deterioration was detected by chain dragging the overlays and was verified by the half-cell corrosion detection testing (ASTM Test Method C876), as well as spot coring. Table 4 gives the magnitude of the post-overlay deterioration, based on the percentage of deck area, of each overlaid deck in the study at the time the tests were conducted (i.e., 1988-89). For comparison, Table 4 also gives the magnitude of the deterioration of the overlaid decks in 1986 and the magnitude of the deterioration of the decks just before they were overlaid, if such data were available. Note that one of the LSDC bridge decks (90/134 N), because of its size, comprised two segments with two different types of construction. Those two segments were treated as different test decks in the study. Thus, the total number of LSDC test sites was six.

The magnitude of post-overlay deck deterioration may not convey much meaning unless accompanied by information about the overlay service life. In other words, the important factor for performance is the rate of deterioration, rather than the magnitude of deterioration. Plots of post-overlay deterioration versus overlay service period for the deteriorating decks are given in Figure 1. Those plots indicate that the deterioration rate varied significantly among the bridge decks. Also, the limited data in Figure 1 indicates that the deterioration rate tends to remain about the same, or decrease, for an individual deck up to nine years after an overlay has been placed.

Table 4 lists the deterioration rate, based on the percentage of deck area per year, of each overlaid deck in the study's 1988-89 survey. For comparison, Table 4 also lists the deterioration rate of the overlaid decks in the 1986 survey. The rate of post-overlay deterioration for each survey was calculated by dividing the magnitude of deterioration found in that survey by the age of the overlay at the time of that survey. While three LMC decks showed either no deterioration or insignificant deterioration for up to nine years after overlaying had occurred, two LMC decks showed deterioration rates of about 1 percent of the deck area per year seven years after they had been overlaid. The average deterioration rate for LMC decks was about 0.4 percent of deck area per year. Among the LSDC decks, one deck showed no deterioration five years after overlaying had occurred, but two decks showed deterioration rates of about 1 percent of deck area per year up to eight years after they had been overlaid. The average deterioration of the remaining three LSDC decks was about 0.25 percent of deck area per year. The overall average deterioration rate of the LSDC decks was about 0.5 percent of deck area per year.

Predicting Effective Service Lives of Overlaid Decks

The previous section described the performance of the concrete overlaid bridge decks and showed that performance trends can vary substantially from one site to another. However, the effective service lives of the concrete overlaid bridge decks have yet to be estimated and evaluated.

To determine the effective service life, a criterion is needed for the condition beyond which frequent maintenance will require deck rehabilitation. The following criterion is appropriate for concrete overlaid decks: 90 percent or more of the underlying deck area should remain free of corrosion-induced deterioration for the effective service life of the overlay. The conditions of the overlaid decks of this study support that criterion. The effective service life of an overlaid deck can be estimated by dividing

Table 4. Extent of Pre- and Post-Overlay Corrosion-induced Concrete Deterioration for Latex-modified and Low-slump Dense Concrete Overlaid Decks

Type of Overlay	Bridge Number	Deterioration, % of Deck Area			Deterioration Rate, % of Deck Area per Year			Estim. * Effective service life (yrs.)
		Before Overlaying	After Overlaying		Before Overlaying	After Overlaying		
			1986	1988-89		1986	1988-89	
LMC	20/211S	1	0	0 89	0.11	0	0	∞
	90/510S	14.97	4.38	7.68 89	0.93	1.10	1.10	9
	90/512S	1.7	3.88	6.87 89	0.11	0.97	0.98	10
	2/311	9.9	0	0 88	0.33	0	0	∞
	90/154N	>5	–	0.10 89	>0.27	–	0.03	333
LSDC	90/124S	13.40	1.04	1.23 88	0.79	0.15	0.14	71
	90/150S	9.73	2.00	2.97 88	0.54	0.67	0.59	17
	90/162N	17.75	5.88	7.47 89	1.27	1.18	0.93	11
	90/134N Mid-span	>5	--	0 88	>0.23	--	0	∞
	Two end spans		–	5.46 88		–	1.09	9
	970/5	>5	–	0.69 88	>0.31	–	0.12	83

*Assuming maintenance-free corrosion-induced deck deterioration is 10%, or less, of deck area

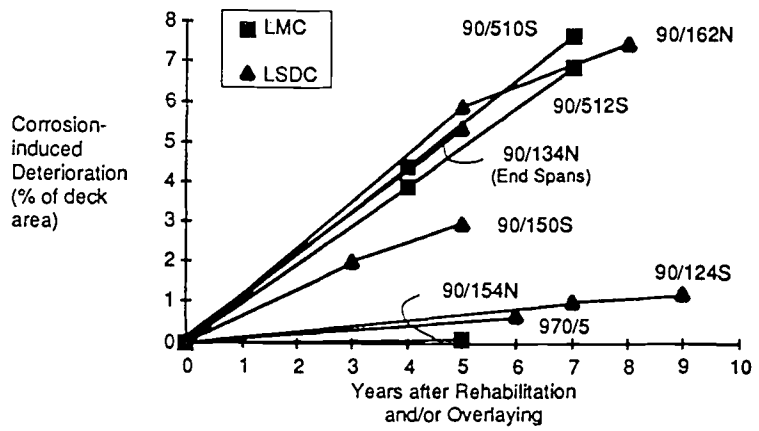

Figure 1. Relation between Post-Overlay Corrosion Induced Deterioration and Overlay Service Period for Latex-Modified Concrete and Low-Slump Dense Concrete Bridge Decks

"10% deterioration" by the deck's deterioration rate, expressed in terms of percentage of deck area per year. This has been done in Table 4. The deterioration rates used are those of 1988-89 survey.

As shown in Table 4, the effective service lives of both the LMC and LSDC overlaid decks are predicted to vary from nine years to infinity. However, the effective service life of a concrete overlaid deck is also limited by the durability of the overlay, which is typically about 25 years (2), depending on weathering and exposure to traffic. At the end of that period the overlay should be removed and replaced, or partially removed (scarified) and resurfaced. Considering that 25 years is the effective service life limit, two of the LMC and Three of the LSDC decks shown in Table 4 would be likely to need rehabilitation while their overlays were still in good shape. For maximum cost effectiveness, it is important that the underlying deck does not deteriorate critically before the overlay does so that the rehabilitation of the underlying deck, if any, and the overlay resurfacing can be done at the same time. On the basis of this concept, two of the LMC and three of the LSDC sites out of 11 sites in Table 4 were not performing satisfactorily. However, expressed differently, 55 percent of the test sites were satisfactorily retarding the continued corrosion of the reinforcing steel.

Factors Influencing the Effectiveness of the Overlay

Within the limited number of test bridges available, an effort was made to identify the factors (or factor) contributing to the differences in the performance of overlaid decks with respect to corrosion-induced deterioration in the concrete. Factors considered were: environment (humid versus relatively dry), traffic impact (driving lane versus shoulder), structure type (flexible versus rigid), magnitude of pre-overlay repair, and finally, overlay surface cracking. There were indications that the post-overlay deterioration rates increased with increases in the magnitude of the overlay surface cracking. Overlay surface cracking has the potential to accelerate corrosion-induced deterioration by wetting the deck (decreasing concrete electrical resistivity) and by periodically facilitating, through drying, the intrusion of new water and oxygen (mixed with that water) into the originally chloride contaminated deck. Generally, the depth of surface cracks in the bridges tested, as discussed later, was sufficient to allow penetration of water deep into the body of the underlying decks. Also, traffic impact affected deterioration. Impact from wheel loads can greatly contribute to the growth of incipient deterioration induced initially by corrosion. The deterioration in the overlaid decks occurred mainly in the roadway and rarely extended into the shoulder.

Nature of Concrete Overlay Surface Cracking

The extent of overlay surface cracking on each deck was quantified by designating any 1.5 m (5 ft.) by 1.5 m (5 ft.) grid square on the deck as a cracked area when cracking had occurred in that area. The results of this survey are given in Table 5 under "1988-89" column. As Table 5 shows, the worst cracking of an LMC overlay was 50 percent of the deck area, and the worst cracking of an LSDC overlay was 84 percent of the deck area. However, nationwide surveys of bridge decks have indicated that both LMC and LSDC overlays have the potential to develop surface cracking over 100 percent of the deck (2). Causes of cracking in concrete bridge decks and concrete overlays and methods of minimizing cracking are discussed in References 1 and 2.

In the bridges tested, the widths of the overlay cracks at the surface generally varied from 0.03 mm (1/32 in.) to 0.06 mm (1/16 in.) for both LMC and LSDC overlays. However, cracks as wide as 6 mm (1/4 in.) were found on two LSDC overlays. On the other hand, Three overlays (one LMC and two LSDC) had only narrow cracks of widths less that 0.03 mm (1/32 in.). Coring was used to determine the depth of the overlay cracks at several locations on each overlay. Generally, the cracks penetrated into the underlying decks to the level of the reinforcing steel. However in three overlays (one LMC and two LSDC) a number of cracks were shallow. The shallow cracks did not reach the overlay/deck interface.

Table 5. Extent of Surface Cracking in Latex-Modified and Low-Slump Dense Concrete Overlays

Type of Overlay	Bridge Number	Cracking, % of Deck Area		Deterioration Rate, % of Deck Area per Year 1988-89
		1986	1988-89	
LMC	20/211S	2	2 89	0
	90/510S	40	50 89	1.10
	90/512S	35	37 89	0.98
	2/311	14	21 88	0
	90/154N	--	24 | 9* 89	0.03
LSDC	90/124S	28	41 88	0.14
	90/150S	84	84 88	0.59
	90/162N	65	79 89	0.93
	90/134N Mid-span	--	41 | 29* 88	0
	Two end spans	--	58 88	1.09
	970/5	--	53 | 40* 88	0.12

* Surface cracks after excluding shallow longitudinal cracks

Effects of Overlay Cracking on Corrosion-Induced Deterioration

As shown in Table 5, the deterioration rates of both the LMC and LSDC decks, as measured in the 1988-89 survey, relate directly to the magnitudes of their overlay surface cracking, as determined in the same survey. This relationship becomes clearer when shallow surface cracks are excluded from the crack survey of 1988-89. The adjustment for shallow cracks has been made in Table 5.

Linear regression analyses were conducted to obtain the relation between the rate of corrosion-induced deterioration and deep overlay surface cracking. The results are plotted in Figure 2. The results indicate that for LSDC overlaid deck, cracking of up to 24 percent of the deck may be insignificant for the development of corrosion-induced deterioration, and that a maximum deterioration rate of about 1 percent of the deck area per year may be expected with cracking of 100 percent of the deck. For LMC overlaid decks, cracking of up to 8 percent of the deck may be insignificant for the development of deterioration, and a maximum deterioration rate higher than 1 percent of the deck area per year may be expected in conjunction with cracking of 100 percent of the deck.

The effect of cracking on the deterioration of decks overlaid with LMC seems to be more severe than the effect of cracking on the deterioration of decks overlaid with LSDC. This difference in behavior is probably related to the thickness of the overlay. LSDC overlays were thicker than LMC overlays. The thicker the overlay is, the smaller the width of the crack is at the level of the reinforcing bar, and that smaller width may reduce the ability of the crack to convey moisture and oxygen.

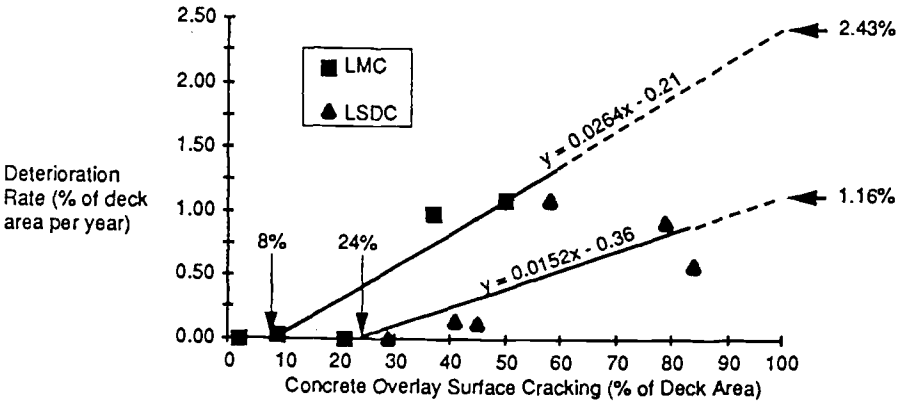

Figure 2. Correlation between Cracking in Concrete Overlays and Corrosion-Induced Deterioration of Bridge Decks

Mode of Corrosion-Induced Deterioration in Overlaid Decks

The results of a coring program showed that after the concrete surrounding a corroding bar has cracked, the internal cracks propagate diagonally toward the overlay interface (Figure 3). Once at the overlay interface, which is usually weaker than either the overlay or the underlying deck, the corrosion-induced cracks turn and subsequently extend along the overlay interface. This condition causes the overlay to debond near the corroding bar, delaying the crack from reaching the overlay surface and spalling the concrete. Corrosion-induced debonding was a characteristic of large deteriorated areas (i.e., greater than 0.45 m^2, or 5 $ft.^2$). Smaller corrosion-induced deteriorated areas generally did not show corrosion-induced debonding. In other words, they represented the early stage of concrete deterioration in which the internal fracture had not reached the overlay interface. The final stage of deterioration is predicted to be primarily stripping of pieces of the debonded overlay from the deck after they have developed fatigue cracking.

Nature of Overlay Surface Cracking in Deteriorated Areas

The deteriorated areas of the decks studied almost always coincided with surface cracking. However, surface cracking was also found in sound areas indicating that surface cracking was not necessarily caused by concrete deterioration. Generally, two types of overlay surface cracking were found in the deteriorated areas. The first type extended into the overlay and stopped at the overlay interface. This type of cracking generally coincided with overlay debonding, which had occurred around the corrosion cell (Figure 3). This type of cracking must have reached the interface after the debonding has occurred so that it could not propagate into the underlying deck. Note that aside from the various causes of concrete overlay surface cracking, debonding of the overlay itself can cause overlay surface cracking because of the lack of composite action between the overlay and the deck and exposure to traffic. After this form of cracking (fatigue cracking) has developed in debonded areas, overlay stripping can begin at any time.

The second type of overlay surface cracking in the deteriorated areas extended deep into the underlying deck. This type of cracking existed in areas that had not debonded (in the early stage of deterioration at the corroding bar, Figure 3). Also, the second type of cracking existed in sound

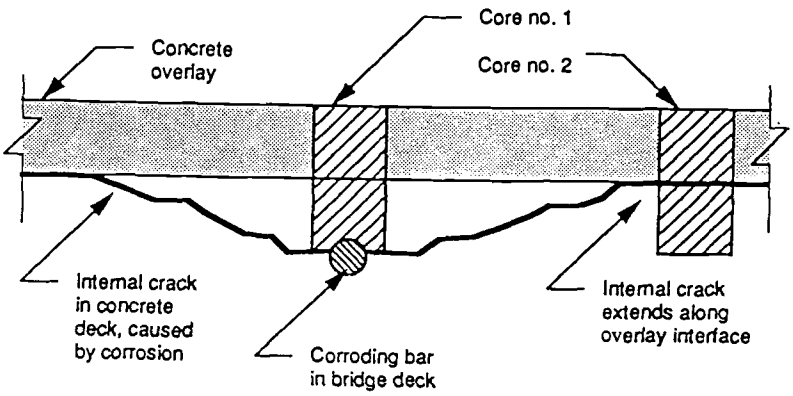

Figure 3. Mode of Internal Concrete Fracture in Concrete Overlaid Bridge Decks

concrete. This situation implies that the second type of cracking had occurred before "corrosion-induced debonding" and before the early stage of corrosion-induced deterioration, and that it had contributed to corrosion of the reinforcing steel.

Effectiveness of Cathodic Protection with Respect to Bar Corrosion

The effectiveness of the two cathodically protected bridge decks (Table 3) was determined by chain dragging the bare decks of the slotted CP systems. Four to five years after their rehabilitation and cathodic protection, neither site showed any significant amount of deterioration. The post-protection deterioration was 0.06 percent for Woodinville Interchange and 0.15 percent for the cathodically protected section of Hood Canal Bridge. The deterioration of the former bridge had occurred along the slots and, as discussed in the next section, is attributed to the durability of the slotted system, rather than corrosion of the reinforcing steel. On the other hand, the deterioration of the latter bridge had occurred in and around the repair areas. A half-cell potential survey of the deteriorated areas of Hood Canal Bridge showed that the average difference between the most negative potential in the deteriorated areas and the least negative potential in the adjacent sound areas was 357 mV for the deterioration adjacent to the repairs but only 24 mV for the deterioration within the repairs. These results indicate that in Hood Canal Bridge the deterioration adjacent to the repairs was probably caused by corrosion, whereas the deterioration within the repairs was probably the result of the repair concrete debonding from the underlying concrete. Although the half-cell potentials were polarized, the difference in potential may not have been significantly affected by the polarization. The average "most negative" and "least negative" polarized potentials in the deterioration adjacent to the repairs were -759 mV and -402 mV, respectively, and they were -393 mV and -369 mV, respectively, in the deterioration within the repair areas. Note that the lower deck of Hood Canal Bridge is continuously exposed to an extremely humid marine environment, an ideal condition for steel corrosion in salt contaminated concrete.

Another indication of the satisfactory performance of the CP system was that in Hood Canal Bridge the section of the deck next to the cathodically protected section had developed relatively extensive internal concrete cracks (delamination). Those sections were rehabilitated at the same time the cathodically protected section was rehabilitated, but they were coated with a polymer material with sand broadcast over it. Also, in Woodinville Interchange, regardless of the 25 percent of surface cracking in the bare deck, no sign of corrosion-induced deterioration was found. The cracks were deep transverse cracks caused by negative moment, and they ran directly over the top transverse bars. In bare decks, this type of cracking is usually the most harmful in facilitating corrosion of the reinforcing steel.

Durability of Cathodic Protection

Three types of problems with the durability of the slotted CP system were found. The first type had occurred in Woodinville Interchange. Visual survey of the deck of that bridge showed spalls of about 25 mm (1 in.) by 76 mm (3 in.) in many locations along and adjacent to the slots. Their density was nine spalls per 93 m^2 (1,000 $ft.^2$) of deck area. The spall depths, however, were shallow and did not exceed 6 mm (1/4 in.). It is possible that while the deck was being saw cut to build the slots, the weak layer of concrete at the surface developed horizontal cracks. Later, traffic impact caused the cracked concrete to spall. This type of problem was not found in the CP system of Hood Canal Bridge. That CP system is not exposed to traffic.

The second problem had also occurred in Woodinville Interchange. Chain dragging of that bridge deck detected delaminations (internal concrete cracks) along, and attached to, the slots in many areas. The delaminated areas constituted 0.06 percent of the deck area, and they were on the average 203 mm (8 in.) long and 102 mm (4 in.) wide. The density of the delamination was about three delaminations per 93 m^2 (1,000 $ft.^2$). Coring of the concrete in a delaminated area showed that the internal crack had initiated at the edge of the bottom of the slot (Figure 4) and had propagated diagonally. That internal crack was probably initiated by the stress concentration caused by the impact of wheel loads. The conductive polymer in the slot is more flexible than the concrete. Under this condition, the wheel load forces are resisted primarily by the concrete. The irregularity in the shape of the concrete, created by the slot, then causes a crack to initiate from the corner of the slot. This type of problem was not noticed in the CP system of Hood Canal Bridge, which does not carry traffic. Also, both the first and second problem types were concentrated in the negative moment area of the deck of Woodinville Interchange, indicating that tensile stresses in the concrete aggravated cracking.

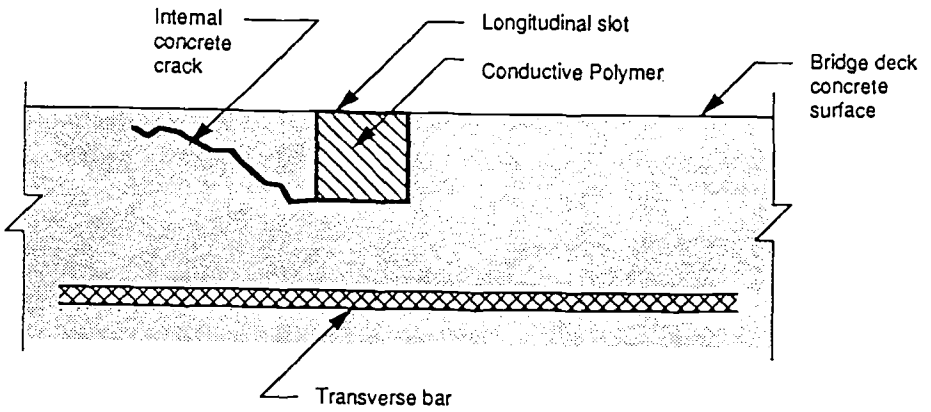

Figure 4 . Development of Internal Concrete Crack from the Corner of the Slot in Slotted Cathodic Protection System

The third problem had occurred in the CP system of Hood Canal Bridge. A visual survey of the slotted system revealed deterioration at the vertical interface of the conductive polymer in the slots and the adjacent concrete in several areas. Both the polymer and concrete had deteriorated in those areas, creating a joint at the interface. The presence of a yellowish substance at the deteriorated areas indicated that acid had been produced at the interface. Apparently, the CP system produced acid at the face of its anode system (i.e., the conductive polymer embedding platinum anode wire) and that acid caused the deterioration. The extreme humidity of the marine environment of Hood Canal Bridge had a definite role in this type of deterioration. The acid deterioration was not noticed in the CP system of Woodinville Interchange, which is exposed to a normal bridge environment.

COST-EFFECTIVENESS OF PROTECTIVE STRATEGIES

The cost effectiveness of concrete overlay and cathodic protection strategies was evaluated on the basis of life-time costs (i.e., assuming 50 years of remaining bridge deck life after protection an annual interest rate of 10 percent and inflation rate of 5 percent) and the unit costs reported in Washington State. Consistent with the test results, it was assumed that the CP system would halt the corrosion but that corrosion-induced deterioration in a concrete overlaid deck would continue at a rate of 0.25 percent of the deck area per year. That rate of deterioration corresponds to a moderate level of LMC overlay surface cracking of about 15 to 20 percent of the deck area (Figure 2). Additionally, it was assumed that major maintenance in the form of deck resurfacing would be required for both overlaid and cathodically protected decks because of reasons other than corrosion. The results are shown in Table 6.

Table 6. Lifetime Cost of Bridge Deck Protective Alternatives

Alternative	Cost per Square Foot of Deck Area					
	Lifetime Cost					Present Worth
	Initial Cost	15 years	25 years	32 years	50 years	
Latex-Modified Concrete	$5.60		Rehab. & Resurface with Latex-modified mortar $6.37			$7.48
Cathodic Protection, Slotted System	$7.71	Resurfaced with Asphalt Concrete $2.21		Remove and Resurface with Asphalt Concrete $2.66		$9.33
Cathodic Protection, Non-slotted, LMC Overlaid system	$12.48		Resurface with Latex-modified Mortar $4.18			$13.71

(1 sq. ft. = 0.3 m^2)

The LMC strategy (or LSDC) was found to be the least expensive strategy, followed by the slotted CP and the non-slotted CP that is covered with a concrete overlay. Note that in Table 6 resurfacing of the slotted CP system is done by asphalt concrete overlay, since a slotted system cannot be scarified for the application of a concrete overlay. The non-slotted CP system consists of wire anode rolls that are rolled out on and fastened to a deck that has already been scarified for the LMC overlay. The present worth of the slotted CP strategy was 25 percent more than that of the LMC strategy, and the present worth of the non-slotted CP strategy was 83 percent more than that of the LMC strategy. The present worth of the slotted CP strategy was still 19 percent more than that of the LMC strategy when the corrosion-induced deterioration in the LMC overlaid deck continued at a rate of 0.4 percent of deck area per year. That deterioration rate was the average deterioration rate obtained for the LMC overlaid decks of this study.

CONCLUSIONS

1. After an average of seven years of service, both LMC and LSDC overlaid decks showed various levels of post-overlay corrosion-induced deterioration rates. Those rates ranged from none to about 1 percent of the deck area per year. The average deterioration rate of LMC decks was 0.4 percent of the deck area per year, and that of LSDC decks was 0.5 percent of the deck area per year. The deterioration rates were about the same in both 1986 and 1988-89 surveys, or they were less in 1988-89 survey.

2. The post-overlay deterioration rates of the LMC and LSDC overlaid decks correlated with the magnitude of overlay surface cracking. The deteriorated areas almost always coincided with surface cracking. However, surface cracking was also found in sound areas. Overlay surface cracking has the potential to accelerate corrosion-induced deterioration by wetting the deck and by periodically facilitating, through drying, the intrusion of new water and oxygen into the concrete.

3. The effect of overlay surface cracking on the deterioration of decks overlaid with LMC seemed to be more severe than the effect of cracking on the deterioration of decks overlaid with LSDC. This difference in behavior is probably related to the thickness of the overlay.

4. The mode of corrosion-induced deterioration in the concrete overlaid decks was internal cracking of the concrete surrounding the corroding bar, propagation of the internal crack diagonally toward the overlay interface, and extension of the internal crack along the overlay interface. This condition had caused the overlay to debond near the corroding bar.

5. After about five years of service, both of the cathodically protected decks showed satisfactory performance with regard to the corrosion of the reinforcing steel.

6. Three problems with the durability of the slotted CP systems were noted. those were

- small and shallow spalls in the concrete adjacent to the slots,
- internal crack in the concrete that originated from the bottom of the slot, and
- acid deterioration at the interface of the slot and deck concrete.

The first two problems were related to the slots and traffic impact. The third problem was related to the humidity of the environment.

7. On the basis of a bridge deck life-time costs and the unit costs used in this study for installing a protective system and rehabilitating/resurfacing the deck, a concrete overlay strategy seems to be more

cost effective than CP systems. However, if any continuation of corrosion or corrosion-induced deterioration cannot be tolerated, because of structural integrity concerns, then cathodic protection may be a better alternative.

ACKNOWLEDGMENT

This paper is primarily based on a research conducted at the University of Washington, Washington State Transportation Center, by the authors, as part of a Federal Highway Administration study. At the time this work was conducted Khossrow Babaei was a senior research engineer with the Washington State Transportation Center. Also, at the time this work was conducted Neil M. Hawkins was a professor of civil engineering at the University of Washington.

REFERENCES

[1] Babaei, K., "Evaluation of Concrete Overlays for Bridge Applications," Report No. WA-RD 137.1, Washington State Department of Transportation, Olympia, WA, October 1987.

[2] Babaei, K. and Hawkins, N. M., "Evaluation of Bridge Deck Protective Strategies," Report No. 297, National Cooperative Highway Research Program, Washington, DC, September 1987.

Koji Homma[1], Nobuhiro Goto[2], Kazumi Matsuoka[2], and Satoshi Ito[3]

UTILIZATION OF ELECTROCHEMICAL IMPEDANCE TECHNIQUES TO ESTIMATE CORROSION DAMAGE OF STEEL INFRASTRUCTURES

REFERENCE: Homma, K., Goto, N., Matsuoka, K., and Ito, S., "Utilization of Electrochemical Impedance Techniques to Estimate Corrosion Damage of Steel Infrastructures," Corrosion Forms and Control for Infrastructure, ASTM STP 1137, Victor Chaker, Ed., American Society for Testing Materials, Philadelphia, 1992.

ABSTRACT: Infrastructures such as bridges, highways, pipelines and harbor piers sometimes suffer from corrosion damage during their service life. To diagnose deterioration of infrastructures and secure effective maintenance, in-situ corrosion monitoring methods based on electrochemical impedance techniques have been developed. This paper reports three examples of new corrosion monitoring sensors: 1) a sensor for detecting corrosion of marine steel structures in seawater, 2) a sensor for detecting corrosion of reinforcing bars in concrete, and 3) a sensor for detecting coating deterioration of painted steel structures in the atmosphere. The effectiveness of these sensors has been verified by experiments both in the laboratory and in the field.

KEY WORDS: corrosion, monitoring, impedance, infrastructure, electrochemistry

Over the years, many infrastructures suffer structural damage due to corrosion. In Japan, some statistics estimate that corrosion losses total more than ¥ 2.5 trillion (approximately $ 20 billion) a year [1]. To meet the increasing need to minimize those losses and prolong the service life of infrastructures, corrosion monitoring techniques have been developed as one of the most essential tools. There are various kinds of infrastructures such as bridges, highways, harbors, and so on. Most of these infrastructures are made of steel structures or reinforced concrete structures. Moreover, there are various environments that affect the corrosion of steel, for example, seawater, concrete, or the atmosphere. To monitor corrosion in these structures, measurement

[1] Researcher of Steel Structure Development Center, [2] Senior Researcher of Steel Structure Development Center, and [3] Senior Research Chemist of Stainless Steel & Titanium Laboratory, respectively. Steel Research Laboratories, Technical Development Bureau, Nippon Steel Corporation, 20-1 Shintomi, Futtsu, Chiba-ken, Japan 299-12

techniques must be developed, that are appropriate to the kind of structures and environments. Electrochemical impedance techniques are known to be useful methods in the laboratories to determine the corrosion rate of metals. In the field, there are still some difficulties in applying these techniques to measure corrosion rates directly. For example, the in-situ electrochemical measurement must be made on a part of the structure. Therefore, one of the most important factors is how to determine the surface area where the measurement is made. Then the measurement techniques, including sensors, must be developed so that they correspond to the structures. This paper discusses the effectiveness of the sensors developed for three kinds of structures: 1) marine steel structures, 2) reinforced concrete structures, and 3) painted steel structures.

Laboratory Experiments

To analyze electrochemical aspects of corrosion on the surface of steel in various environments, we used electrochemical impedance spectroscopy. The test equipment consisted of a potentiostat (Toho Technical Research Model 2000), a frequency response analyzer (NF Circuit Design Block Model S5720), and a computer. The electrochemical cell consisted of a platinum counter electrode (CE), a silver-silver chloride reference electrode (RE), and a working electrode (WE) connected to the specimen. Alternating current (AC) impedance measurements were made as follows:

1) Measurements of Corrosion of Steel in Synthetic Seawater
For this measurement, the test specimens were made from cold-rolled steel sheets. The size of the specimens was 50mm X 50mm X 0.8mm with 4cm^2 bare surface. The remaining surface was completely covered with epoxy. After preparing these specimens, the AC impedance measurements were made in synthetic seawater opened to the air.

2) Measurements of Corrosion of Steel in Concrete
In this laboratory experiment, we used cold-rolled steel sheets embedded in mortar. The size of these mortar-steel specimens was 60mm X 40mm X 10mm, and the steel sheets were embedded in the center of mortar pieces. The size of the embedded steel sheets was 25mm X 50mm X 0.8mm with 10 cm^2 bare surface (25mm X 40mm) and the remaining surface is covered with epoxy. The mortar consists of portland cement, standard Japanese sand, and tap water; the water/cement ratio was 65% (namely, water:cement: sand = 34:52:104). The specimens were removed from the molds after 24 hours and cured in the laboratory atmosphere for 24 hours. Then corrosion was accelerated by wet-dry cycle. The accelerated corrosion test was as follows. The mortar-steel specimens were first immersed in synthetic seawater for 24 hours, and then dried in the air for 24 hours. The test was continued for 30 days in an automatic wet and dry test chamber. After this test, the AC impedance measurements were made on the specimens immersed in synthetic seawater.

3) Measurements of Corrosion of Painted Steel
Painted steel specimens (150mm X 70mm) were prepared using the above mentioned cold-rolled steel sheet and polyamide cationic electrodeposition paint. Thickness of coating was approximately 20 micrometers. Specimens were exposed for a 1,000-hour cyclic corrosion test. This test cycle consisted of salt spray for four hours, drying for two hours, and humidifying for two hours. After this cyclic corrosion

test, the AC impedance measurements were made by using a cylindrical cell containing 0.1M sodium sulfate aqueous opened to the air.

Laboratory Test Results

The results of the tests are shown in Figure 1, Figure 2, and Figure 3. The impedance curves obtained show three patterns corresponding to the kind of specimens. These impedance characteristics represent the combination of resistive impedance and capacitive impedance. In general, when the corrosion reaction takes place on the surface of steel, the electrochemical system can be modeled by an equivalent circuit, which consists of the polarization resistance (Rp) due to a charge transfer process, a double layer capacitance (Cp), and the solution resistance (Rs) [2]. In the case of painted steel, there is also the resistance of the paint film (Rf) and the capacitance of the paint film (Cf). Figure 4, Figure 5 and Figure 6 show the model of the equivalent circuit of the corrosion system of the specimens tested in three conditions respectively.

The theory of the corrosion rate measurement is based on the following relationship:

$$CR(mm/year) = a\ Icorr \qquad (1)$$

where

CR: corrosion rate (mm/year)

Icorr: corrosion current density (A/cm^2)

a ($= 1.167X10^4$): conversion factor

The corrosion current density (Icorr) can be related to the polarization resistance (Rp) through the following Stern-Geary equation [2]:

$$Icorr = \beta a\beta c/2.3(\beta a+\beta c)Rp = K/Rp \qquad (2)$$

where

βa: Tafel slope of an anodic reaction

βc: Tafel slope of a cathodic reaction

K: a constant value.

K is a constant dependent on the Tafel slope of the corrosion system. The value of K can be determined through Tafel measurement and material data.

On the other hand, corrosion rate can be determined through AC impedance measurement by using the above-mentioned relationship. In this equation, the polarization resistance (Rp) is considered to be equivalent to the pseudo-polarization resistance (Rp') measured by AC impedance technique [3].

Practically, the value of K is determined through laboratory experiments. In this experiments, pseudo-polarization resistance (Rp') was defined by the following equation as an assumption.

$$Rp' = Z(4.64mHz) - Z(1kHz) \qquad (3)$$

Where Z(f Hz) means the impedance at the frequency of f Hz. Figure 7 shows the relation between corrosion rate (CR) calculated from weight loss and the reciprocal of the pseudo-polarization resistance (1/Rp'), which was obtained in the synthetic seawater in our laboratory experiment. As the result, K was determined as

$$K = 4.36\ mV \qquad (4)$$

However, there are still some difficulties in the direct measurement of the corrosion rate of existing structures. The problems are as follows:

1) To determine the surface area where the measurement is made, sensors that can be used for AC impedance measurement in the field must be developed instead of using laboratory experimental apparatus.

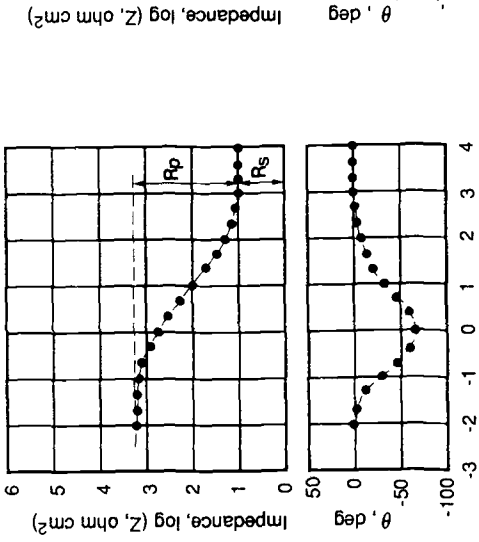

Fig. 1 Typical impedance data for steel in seawater

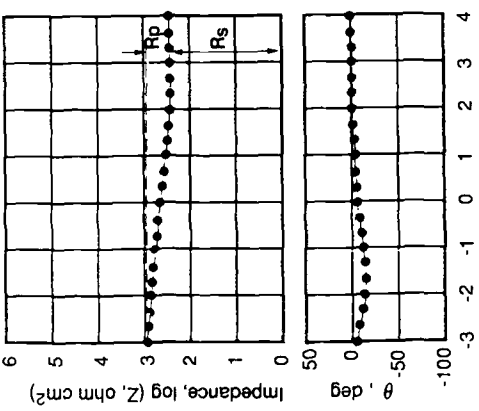

Fig. 2 Typical impedance data for steel in concrete

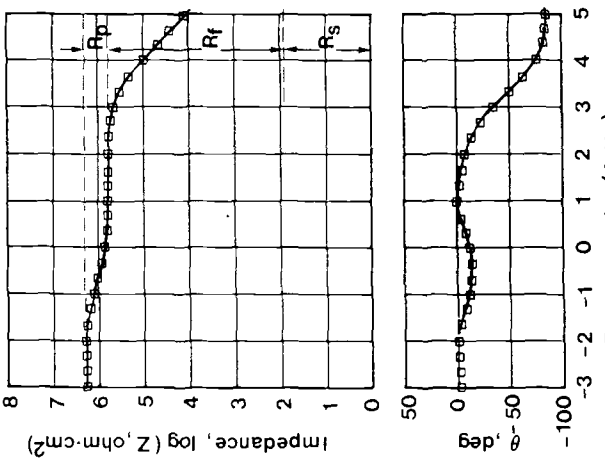

Fig. 3 Typical impedance data for painted steel

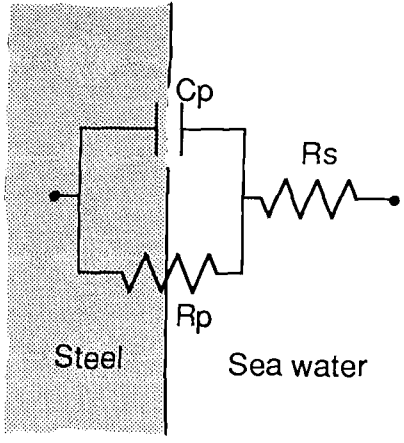

Fig. 4 Equivalent circuit model for steel in seawater

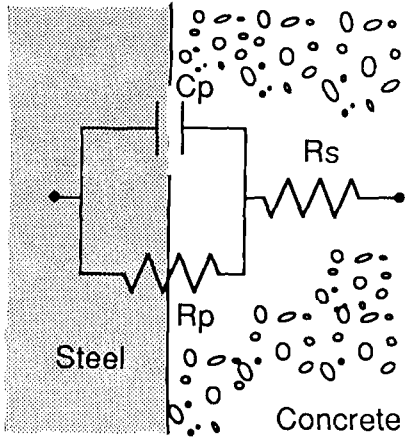

Fig. 5 Equivalent circuit model for steel in concrete

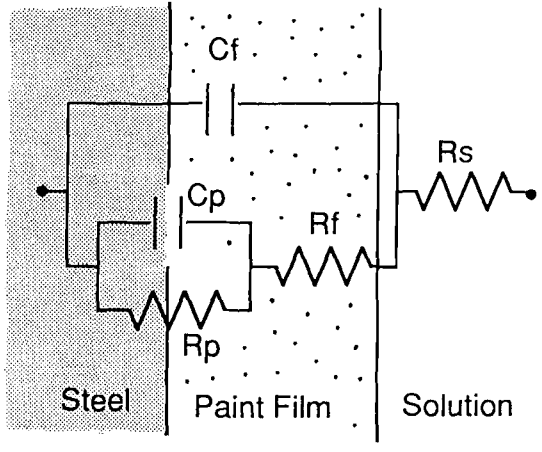

Fig. 6 Equivalent circuit model for painted steel

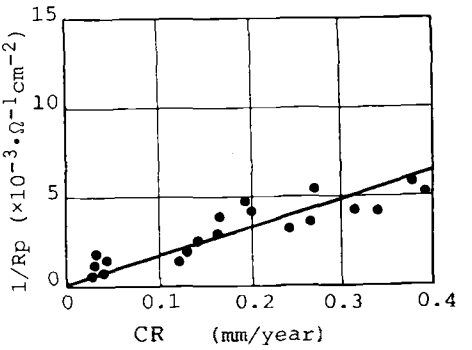

Fig. 7 Relation between the corrosion rate calculated from weight loss and the reciprocal of the pseudo-polarization resistance

2) In the case of measurement of steel embedded in concrete, the sensor cannot be attached directly to the steel surface. Then how to limit the measurement area is an important problem to solve.
3) In the case of measurement of painted steel, the polarization resistance (Rp) cannot be measured easily under the high resistance of paint film (Rf) whose value is usually more than 100,000,000 ohm cm^2 in the practical paint film [4]. Then, especially in the field measurement, another electrochemical parameter that can evaluate the deterioration of painted steel must be studied.

Field Application of AC Impedance Measurement

For the purpose of applying AC impedance measurement to existing structures, the sensors were developed and used in the field.
1) A Sensor for Detecting Corrosion of Marine Steel Structures
Figure 8 shows a schematic illustration of field measurement system.

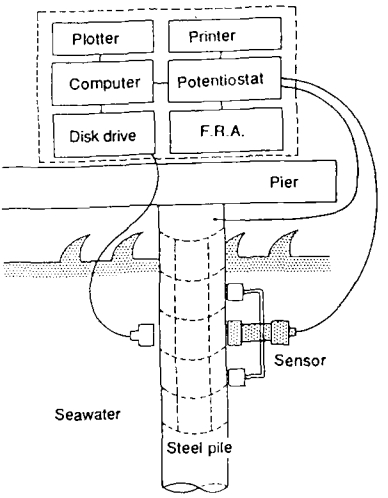

Fig. 8 Schematic illustration of field measurement system

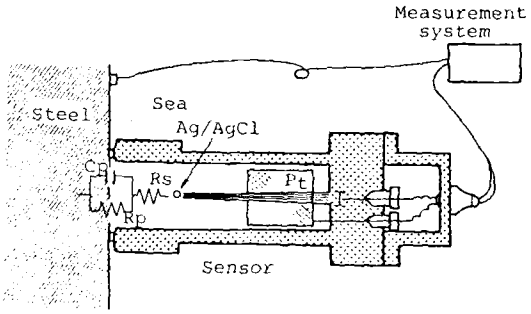

Fig. 9 Detail of sensor

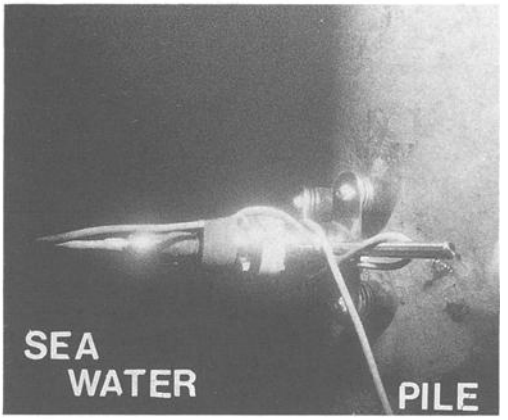

(a) impedance measurement instruments inside the vehicle (b) sensor and steel pile

Fig. 10 Field measurement system for marine steel structure

It consists of the impedance measurement instruments inside the vehicle (Figure 10(a)) and the sensor that consists of a platinum counter electrode and an Ag/AgCl reference electrode as shown in Figure 9. This sensor is made of electrical insulating material and the inner diameter is 30mm. The sensor was taken underwater by divers and attached to the object by a magnetic holder (Figure 10(b)). After a working electrode was connected to the steel structure, a minute alternating current was applied directly to the structure. In this experiment, an eight-year-old steel pile of a pier in a harbor in Japan was used. This steel pile has not been protected by cathodic protection or coating since its construction.

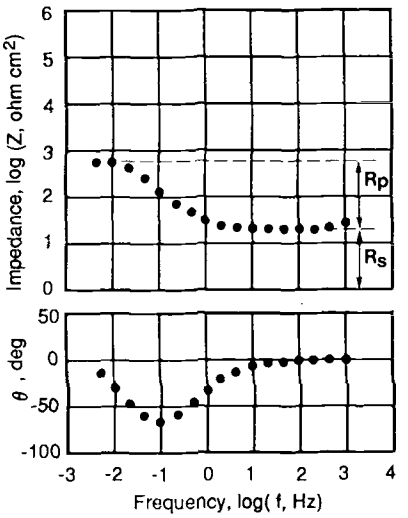

Fig. 11 Result of impedance measurement in the field

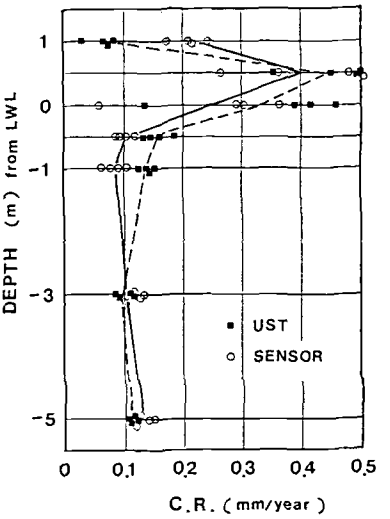

Fig. 12 Corrosion rate of steel pile

The results of impedance measurement in the field are shown in Figure 11. This figure shows the typical impedance spectrum of the steel in seawater. Pseudo-polarization resistance was measured in the same way as during the laboratory experiments, i.e., Rp' = Z(4.64mHz)-Z(1kHz). Corrosion rates were calculated based on the equations:

$$CR = a\ Icorr = a\ K\ 1/Rp'$$

where K = 4.36mV

Figure.12 shows the results of the corrosion rates at different depths on the steel pile. In this figure, the white dots (solid line) represent the corrosion rate calculated from impedance measurements. The black dots (broken line) represent the corrosion rate calculated from the reduction of the thickness of the steel pile, which was measured using an ultrasonic thickness gauge (U.S.T.).

Both corrosion rates are closely correlated although the former is the corrosion rate at the time of measurement and the later is the mean value for eight years. This is in accordance with the report that the corrosion rate in seawater changes little with time when the environmental change is small [5].

2) A Sensor for Detecting Corrosion of Reinforcing Bars in Concrete

In the laboratory experiment, the total area of the steel surface was known before the measurement. In contrast, the existing structure contains a large number of reinforcing bars embedded in concrete, which makes it difficult to determine the surface area where the AC impedance measurement is made. To limit the measurement area, the authors found the effective double counter electrode system, as shown in Figure 13 [4]. The sensor consists of a central counter electrode (CE), a surrounding counter electrode (SE), and a silver-silver chloride reference electrode in the central part. The purpose of this system is to confine the pertubative current distribution into a limited measurement area. By analyzing current distribution based on the numerical simulation method, the double counter electrode system was found to confine polarizing current flow into a constant area [6].

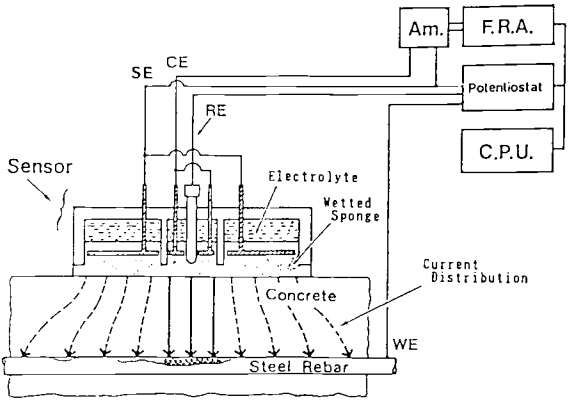

Fig. 13 Sensor for corrosion monitoring of reinforcing bars in concrete

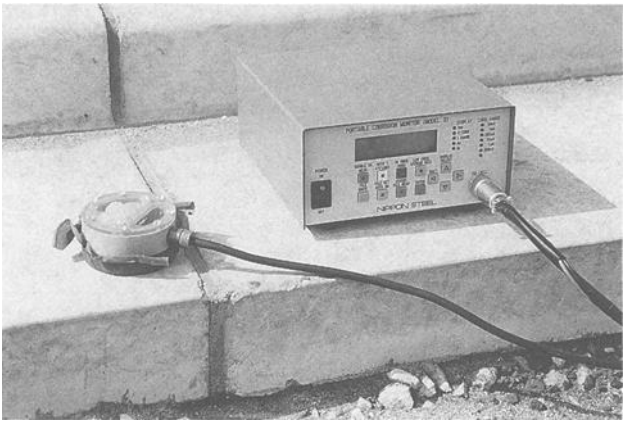

Fig. 14 Field measurement system for reinforced concrete structure

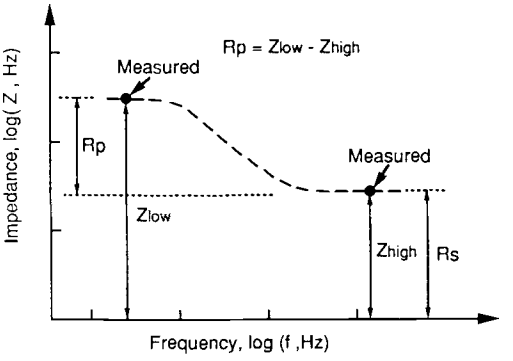

Fig. 15 Concept of measurement of Rp

The authors also developed an impedance measurement instrument for field monitoring (Fig. 14). For convenience, this instrument is designed to apply two kinds of optimum frequency to measure Rs and Rp, respectively. Figure 15 shows the concept of the measurement of Rp. In this field experiment, one frequency was set at 400Hz as the high frequency and the other was set at 0.25Hz as the low frequency.

For the purpose of investigating corrosion of rebar, reinforced concrete blocks have been exposed in a field (residential area) for 1.5 years. One of the concrete blocks contains 6.4 kg NaCl per 1 m^3 to accelerate corrosion. The size of the block is 15cm X 15cm X 45cm. The diameter of the rebar is 9mm and the thickness of the concrete cover is 5mm (Fig. 16). Measurements were made according to the following three methods:

(1) AC impedance measurement by the above-mentioned system,
(2) potential measurement by the Ag/AgCl reference electrode,
(3) and the visual measurement of the corroded area (%) based on Japan Concrete Institute [7], after the rebars are broken out of the concrete.

Figure 17 shows the corroded area at each measurement point Corrosion of reinforcing bars occurred at every point in the concrete

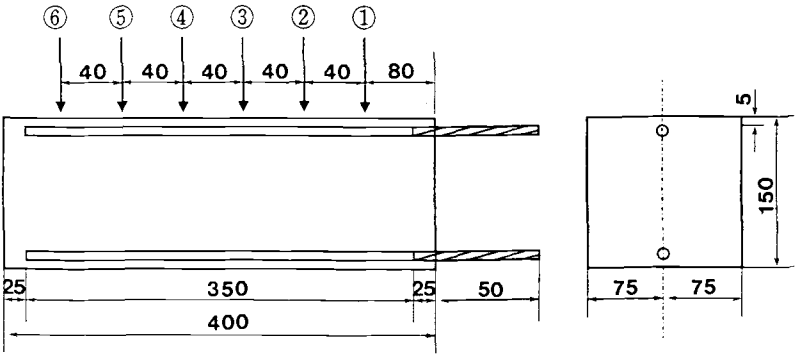

Fig. 16 Reinforced concrete specimen and its measured point

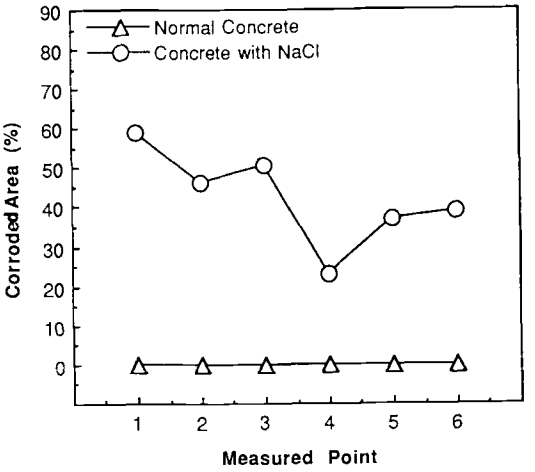

Fig. 17 Visually assessed corroded area at each measured point

containing NaCl. On the contrary, corrosion did not occur in the normal concrete. Figure 18 shows the results of potential measurement at the same points. As shown in this figure, almost all data belong to the "gray zone" defined in the ASTM Test Method "Half Cell Potentials of Reinforcing Steel" (C876-77) [8]. It is difficult to say, in this case, whether the rebar is corroded or not simply by the potential data. Therefore, AC impedance measurement is particularly required in such a case. Figure 19 shows the reciprocal of Rp measured by the field monitoring system. Figure 20 exhibits the relationship between 1/Rp and the ratio of the corroded area, although it does not directly correspond to the corrosion rate, but to the corrosion damage.

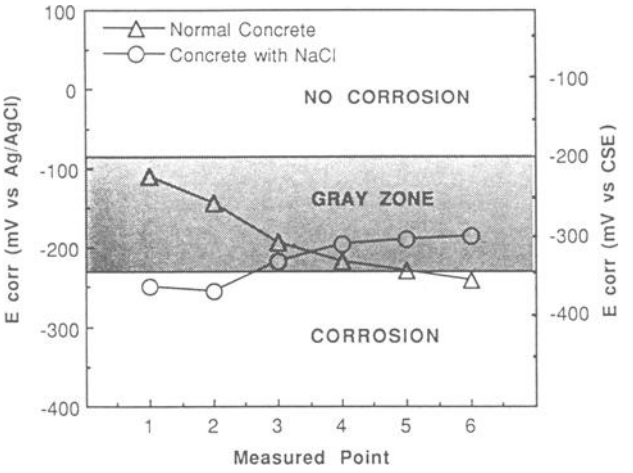

Fig. 18 Result of potential measurement at each measured point

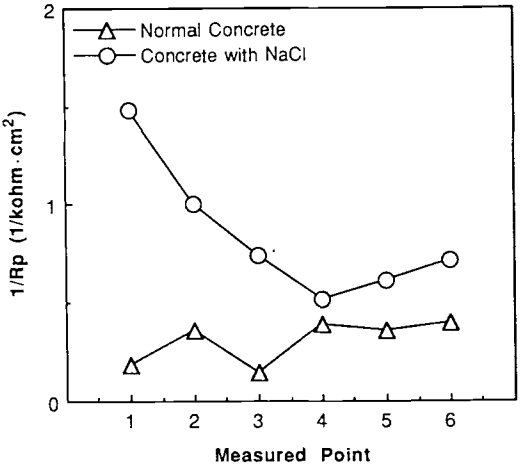

Fig. 19 Inverse of Rp measured by the field monitoring system

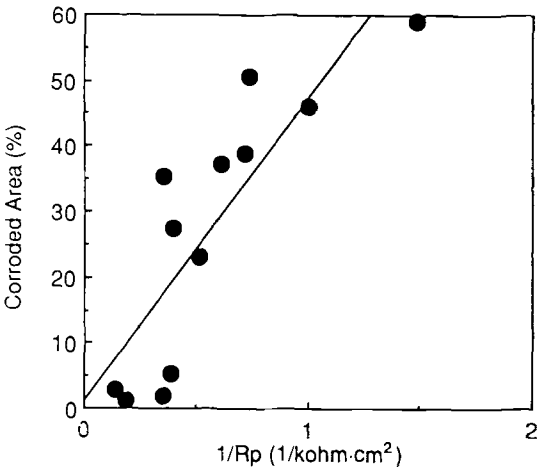

Fig. 20 Relationship between 1/Rp and the ratio of the corroded area

3) A Sensor for Detecting Deterioration of Painted Steel Structures

As mentioned before, it is difficult to detect Rp directly because of the high resistance of paint film especially in a field measurement. Therefore, the other electrochemical parameter related to the deterioration of painted steel was studied. By analyzing the time change of the paint film resistance (Rf) and the paint film capacitance (Cf) (Fig. 21) during the cyclic corrosion test as mentioned in the laboratory experiments, Rf decreases obviously as time progresses, while Cf stays constant. Rf was thought to be the parameter related to the deterioration of painted steel. Figure 22 shows more detailed investigation between the paint film deterioration and the electrochemical parameter Rf. In this figure, the deterioration of the paint film was visually assessed by the adhesion testing method based on JIS K5400 "cross cut test" [9]. According to this figure, the validity of Rf in evaluating the deterioration of paint film was verified. For the purpose of field measurements, a compact instrument was developed (Fig. 23). This instrument consists of a set of electrical circuitry for impedance measurements and a sensor probe in which platinum electrode and super-absorbent polymer are contained.

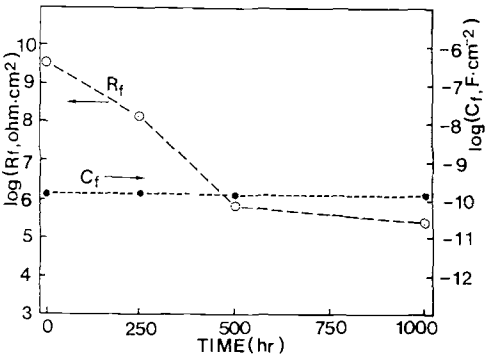

Fig. 21 Time change of paint film resistance (Rf) and paint film capacitance (Cf)

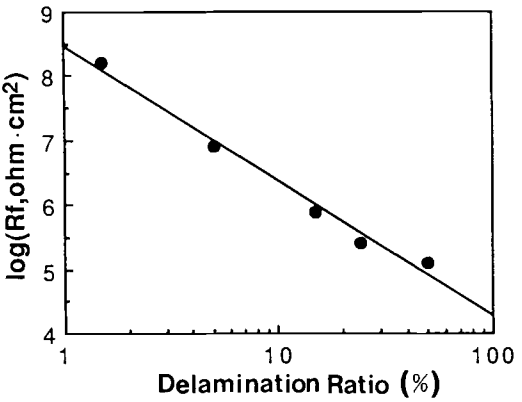

Fig. 22 Relation between Rf and delamination ratio

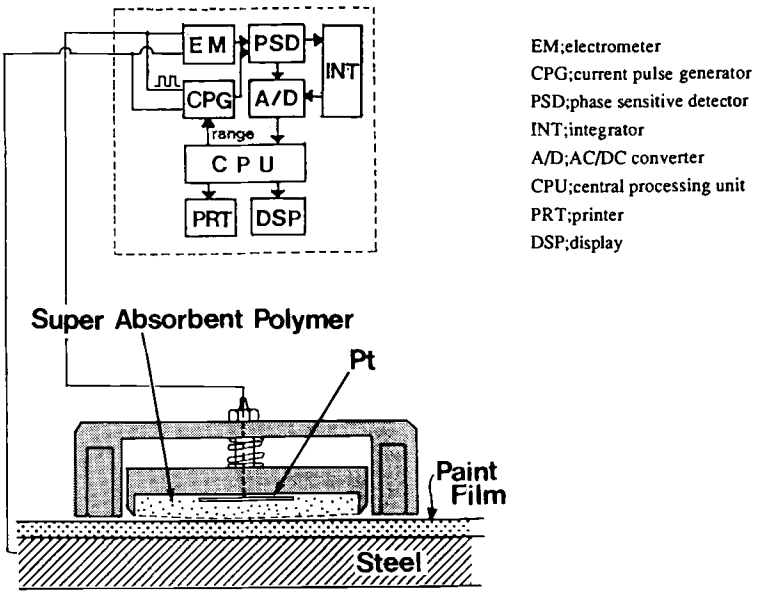

Fig. 23 Schematic illustration of developed instrument for measuring Rf of painted steel

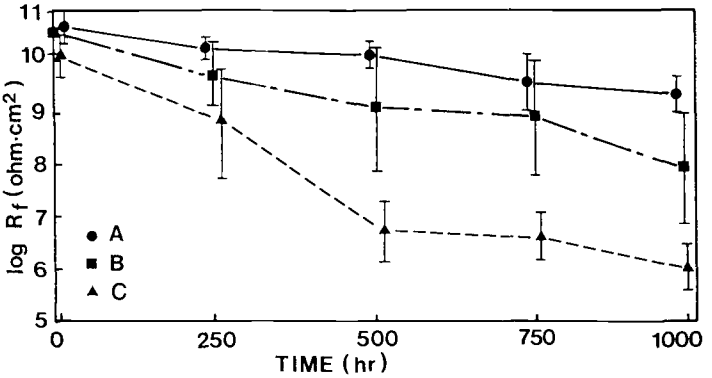

Fig. 24 Time change of Rf for three types of painted steel from different surface preparations

Three specimens were prepared for the application of this instrument. Painted steel panels were made from different surface treatments, which are (A) excellent phosphating steel panel, (B) rough phosphating steel panel, and (C) untreated steel panel. Figure 24 shows the result of Rf measured by this instrument during a 1000-hour cyclic corrosion test. Rf decreased as time progressed all specimens, but the degree of decrease is different. Specimen A, the excellent phosphating sample, kept the highest value during the test, while specimen C, the untreated sample, showed the lowest value. This difference was considered to result from the different surface preparations. Under visual observation, no changes such as blisters or other corrosion products were observed in specimen A in the 1000-hour test period. On the other hand, blisters were seen in specimen B after 1,000 hours and in specimen C after 500 hours. Rf decreased in all specimens before any changes were observed visually.

Conclusions

The three types of corrosion monitoring sensors were developed for the purpose of applying the AC impedance method to existing structures in the field. It was concluded that the sensors reported here have proven their capability as follows:

1) As for the sensor for detecting the corrosion of marine steel structures, the corrosion rate calculated from the reciprocal of pseudo-polarization resistance measured by the AC impedance method has a good correlation with the corrosion rate measured by UST in the steel pile of existing marine structures.

2) As for the sensor for detecting the corrosion of reinforcing bars in concrete, it is possible to estimate corrosion damage by the reciprocal of Rp measured by the double counter electrode system, even if it is difficult to judge from the potential measurement.

3) As for the sensor for detecting the deterioration of painted steel, Rf was found to be an effective parameter for the evaluation of deterioration caused by delamination. As a result, quantitative and nondestructive evaluation of the deterioration of painted steel was established by using the sensor.

References

[1] The Committee for National Corrosion Damage Survey, Bosyoku Gijutsu, Vol. 26, No. 7, pp. 401-428, Japan, 1977.
[2] Hiladky, K., Callow, L., and Dawson,J., "Corrosion Rates from Impedance Measurement," British.Corrosion Journal, Vol. 15, No. 1,1980.
[3] Oka, T., Kihira, H.and Ito, S., "Corrosion Rate Monitoring of Coastal Steel Structures," The 1987 Asian Conference on Inspection and Maintenance for the Offshore and Marine Industries, Indonesia, 1987.
[4] Homma, K., Kihira, H , and Ito, S., "Application of Alternating Impedance Method to Evaluation of Coating Deterioration," NACE Corrosion 91, No. 483, 1991.
[5] Southwell, C., and Alexander, A., Material Protection, Vol. 9, pp. 14, 1970.
[6] Matsuoka, K., Kihira, H., Ito, S., and Murata, T., "Monitoring of Corrosion of Reinforcing Bar in Concrete," NACE Corrosion 87, No. 121, 1987.
[7] Fusyoku-Bosyoku Committee, Concrete Journal, J.C.I., Vol. 23, No. 5, pp. 2, 1985.
[8] ASTM C876-77 "Half Cell Potentials of Reinforcing Steel"
[9] JIS Handbook, K5400, pp. 210-215, Japan, 1990.

Donald Galler and Peter L. Todd

IMPROVED RAIL-FASTENER INSULATION FOR STRAY-CURRENT CONTROL

REFERENCE: Galler, D.,and Todd, P.L., "Improved Rail-Fastener Insulation for Stray-Current Control," Corrosion Forms and Control for Infrastructure, ASTM STP 1137, Victor Chaker, Ed., American Society for Testing and Materials, Philadelphia,1992.

ABSTRACT: In North America, dc powered transit systems use running rails for negative return of traction current. Insulated rail fasteners are used to electrically isolate the rails from earth and structures in order to minimize stray current and the resultant corrosion. The insulating surfaces of the rail fastener can become wet and contaminated in service so that leakage current paths develop. This paper describes the development and testing of improved rail fastener insulation.

KEYWORDS: Corrosion, dc powered, leakage current, negative return, rail fastener, running rails, stray current, traction current.

In this report we discuss development of improved rail fastener insulation. We describe the laboratory apparatus and procedures that we used to simulate rail corrosion and insulating material performance. Observations made in the laboratory and on the operating railroad during prototype development are in excellent agreement.

The fasteners secure steel rails to form a guide along which steel-rimmed transit vehicle wheels roll. The steel and elastomer composite fasteners satisfy the structural requirements for resilient attachment of the rails.

Mr. Galler is a managing engineer at FaAA Electrical Corporation, 115 Flanders Road, Westborough, MA 01581 and Mr. Todd is a supervising electrical engineer at Bay Area Rapid Transit, 800 Madison Street, Oakland, CA 94607.

The fasteners also provide electrical insulation for the rails.

On systems like the Bay Area Rapid Transit (BART) the steel rails are part of the electrical circuit for audio-frequency signals that are used to detect train presence and control train acceleration. The rails are also conductors in the circuit that supplies electrical traction power to the trains. The rail circuit element is called the negative return as it is connected to the negative, anode, side of the traction power rectifiers.

Since the rails are electrical conductors, the rail fasteners must be insulators in order to contain the electrical energy within the circuit. Adequate insulation ensures that power current does not leave the circuit to cause stray current corrosion and that train control signals do not leave the circuit to cause a loss of signal level. Proper design of the elastomer and steel configuration along with proper choice of the elastomer composition assure that the fastener meets both electrical and structural requirements. The procurement specifications require that rail fasteners pass stringent structural and electrical insulation resistance tests.

PROBLEM STATEMENT

Effective electrical insulation limits current flow through as well as across the surface of the insulator. Rail fasteners' surface paths are determined by the structural design requirements and are relatively short for the purpose of electrical insulation in contaminated environments. In tunnels with ground water intrusion, the contamination can greatly reduce the surface path resistance and cause significant stray-current corrosion of the rails and rail fasteners.

The procurement specifications for fasteners require that they have a minimum resistance of 10 MΩ dry and 1 MΩ when wet with demineralized water. The fastener has a height limited to 51 mm (2.0 in.) and the minimum electrical leakage distance of 19 mm (0.75 in.) and meets the resistance requirement. Even so, measurements after the fasteners are installed show less track insulation than expected. This relationship is clearly described in the following evaluation of the measurements of the Washington Metro track-to-earth resistance at start-up.

The more significant problem relative to effective

> *track-to-earth resistance, however, is one of moisture or other materials forming a conductive film across the surfaces of the insulators. Moisture on the surface and absorbed into the timber tie can change the tie from a very good insulator to a very good conductor. These factors must be recognized and reasonable levels of variation in track-to-earth resistance accepted. All of the track presently in service, including the maintenance/storage yards, were tested at least once prior to start-up. It has been possible, and in some areas necessary, to obtain resistance data on some track sections more than once. The resistance values ultimately obtained vary over a wide range. The precise reasons for this variation are not known except to say that the poorer values within the direct fixation sections are generally attributable to various moisture conditions* [1].

At BART we have also experienced wide variations in the measured values of rail insulation. If all installed fasteners had a resistance of 10 MΩ, the track-to-earth resistance would be 13 kΩ per 300 m (1000 ft.). Measured values range from 13 kΩ per 300 m (1000 ft.) to 13 Ω per 300 m (1000 ft.) with most values in the middle of the range. Even the lower levels of track insulation have been adequate for train signalling and stray current control. In wet tunnels, however, the rails and rail fasteners have been corroded by currents straying over surface leakage paths. Under wet and contaminated conditions the surface path resistance has been low enough to permit significant stray current but not low enough to cause problems with the train control signals.

The first idea that occurs to an observer of the deterioration from stray-current corrosion in the tunnels is that the tunnels should be kept dry. In practice water control is difficult, and, therefore, we at BART decided on a program to develop improved rail fastener insulation. In 1984, BART hired Alexander Kusko Inc., now FaAA Electrical Corporation, to develop insulation concepts and to test a prototype insulator.

LABORATORY TESTING

Test Procedure

When the program began in 1984, one of the goals was to develop a test procedure that would simulate the environment of the fastener but allow testing under accelerated conditions. The procedure also needed to simulate the salt-laden moisture of the San Francisco bay area and the

electrical environment of the BART system.

The spray chamber shown in Figure 1 was designed to address these testing requirements. It consists of a polyethylene drain compartment, 4 overhead spray fixtures, and a series of perforated plastic pipes which spray up against the rails. The two spray systems are supplied from separate reservoirs, each having its own pump. The drain compartment has overall dimensions of about 71 by 101 cm (28 by 40 in.) and is designed to accommodate two rail assemblies at a time for comparative testing.

The test procedure involves mounting two rail sections with fastener hardware onto 26.7 x 45.7 x 12.7 cm (10.5 x 18 x 5 in.) concrete blocks. These assemblies are placed in the chamber as shown in Figure 1.

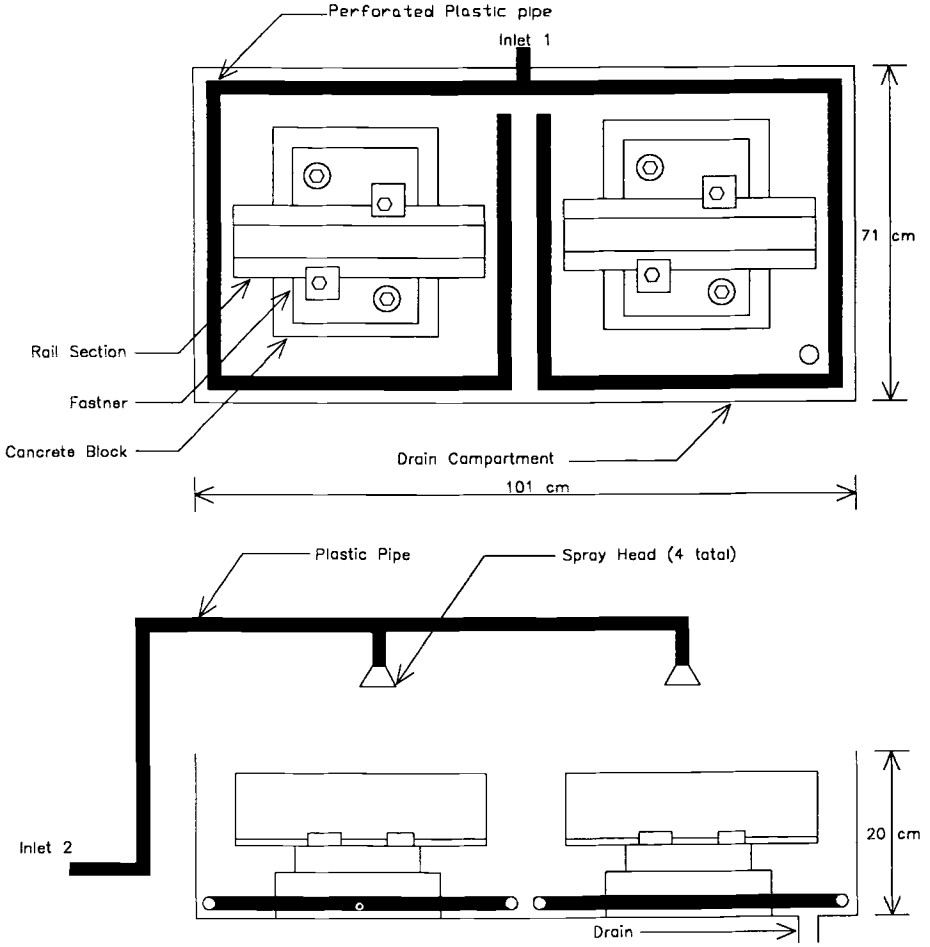

Figure 1. Laboratory Apparatus for Testing Rail Insulators.

The rails are energized at 100 V (positive) by a dc power supply. An aluminum plate at the bottom of the drain compartment is used as the return to the power supply. The rails are sprayed twice a day with a salt solution and the leakage current is measured using sensing resistors in series with each rail.

The spraying procedure consists of two, one-minute sprays twice a day. Each test is run for 7 to 10 days. The solution is adapted from [2] and consists of 40 grams of commercial rock salt dissolved in one liter of tap water. Seven gallons of solution are applied during each one minute spray period. The pumps are independently adjusted prior to testing so that the solution is divided equally between the two spray systems. The runoff is discarded and a new solution is made before each spray application.

Leakage current is measured using the apparatus shown in Figure 2. The rail sections are energized at 100 Vdc continuously during the 7 to 10 day test period. The currents in each rail are independently measured using the current sensing resistors and digital voltmeters. It is possible to have currents in excess of 1 A at times because of the high conductivity of the spray solution and the high applied voltage. The power supply current is limited to 1 A to limit the thermal power applied to the fasteners. The applied voltage declines when this current is reached.

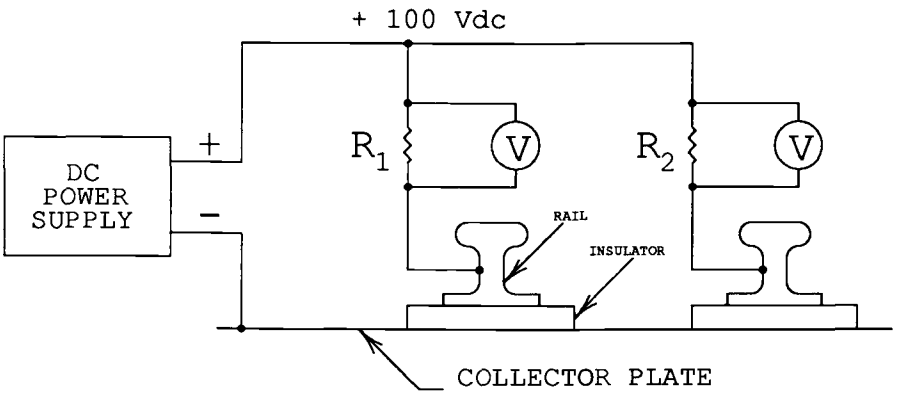

Figure 2. Schematic of Apparatus for Measuring Leakage Currents.

Typical test data is shown in Figure 3. Leakage current data is shown for two fasteners which were tested for a period of 240 hours. The leakage currents for each fastener are recorded just before, and one minute after, spraying. The applied voltage is also recorded. When the power supply is current limited, the applied voltage will be less than 100 V. In this case the data is normalized by scaling the current up to the value that would have occurred at 100 V.

The leakage currents throughout the remainder of this paper are referred to 100 Vdc as described above.

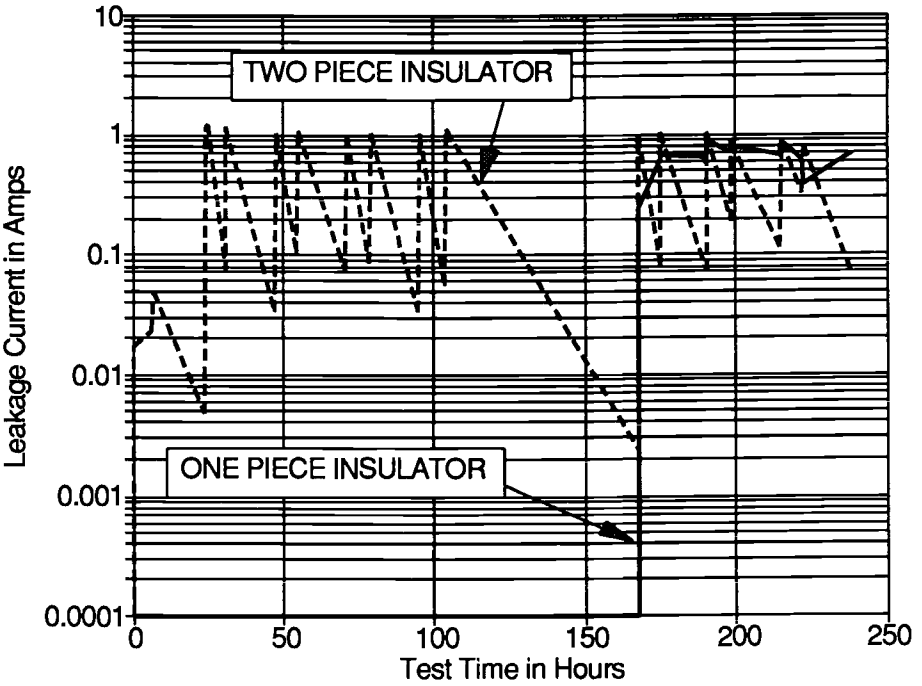

Figure 3. Typical Leakage Current Data From Laboratory Tests.

Insulation Concepts

In 1984, five basic insulation concepts were tested as modifications to the existing BART fastener. The purpose of the tests was to identify the most promising fundamental concepts for further field and laboratory testing. An unmodified (control) fastener was tested on one side of the spray chamber while each of the modifications was tested in turn on the other side. The complete program was conducted over a 9 week period. A brief description of the results of each test is as follows:

Control fastener: Initial leakage currents were on the order of 500 mA. The current increased and stabilized to about 1500 mA after 2 weeks. A small notch appeared on the rail where the rail edge meets the fastener. Corrosion eventually attacked the other metallic parts and ultimately destroyed the fastener.

Spraying rail with silicone oil: The rail and fastener were sprayed with Dow Corning Molykote 4X silicone oil prior to testing. The average leakage currents were about 220 μA but there was some evidence that the spray was being washed off the fastener.

Packing slots with silicone grease: The test fastener was assembled and the slots for the rail clip bolts were packed with Dow Corning 111 silicone grease prior to testing. The average leakage current was about 200 mA.

Clamping rail with insulated blocks: In this test 3.8 mm (0.15 in.) thick polyethylene sheet was placed beneath the rail and between the rail clips and the rail. The initial leakage currents were about 10 mA but gradually increased to about 40 mA.

Plastic skirt modification: Skirts were glued around the edge of the fastener to extend the leakage path to the concrete blocks. Plastic skirts were also added to the bosses for each of the fastener bolts. The average leakage currents were about 1.3 mA.

Wrapping rail with plastic sheet: The rail was wrapped with 4 layers of 5 mil PVC sheet before mounting to the fastener. The sheet extended about 76 mm (3 in.) beyond the fastener on each side. Leakage currents were below 10 μA during the entire test.

As a result of this testing BART has patented the skirt modification [3] and the plastic sheet design [4] for improving rail insulation.

DUPLICATION OF FIELD CONDITIONS

Summary of First Phase of Laboratory Tests

The results of the 1984 tests showed two things. The first is that the laboratory apparatus and test procedure could reproduce corrosion effects encountered in the field environment. Figure 4 shows a corrosion notch in the rail at the edge of the fastener. A similar notch began to appear after a week of accelerated testing and is shown in Figure 5.

The two Mylar pieces were designed to overlap one another beneath the rail. The overlapping region trapped moisture and caused a very short high conductivity path which went right to the edge of the fastener. This negated most of the beneficial properties of the design after a short period of accelerated testing.

Identification of Stress Failure

The testing conducted in 1989 identified a failure condition which had been occurring in the field testing of the insulating device. This condition was a cracking which started at the edge of the fastener and from the area around the rail clips. An insulating device on the BART system exhibited the cracking and is shown in the photo of Figure 7. Figure 8 is a photo of the cracking identified in the laboratory tests. The cracking increases the leakage currents of the fasteners by allowing moisture to collect and by providing a current path between the rail and the rail clip.

The cause of the cracking is a condition known as environmental stress cracking[5]. It is the result of exposure to the combination of the alkali developed by the leakage current and mechanical stress. The presence of the alkali was verified with pH paper during the testing. Mylar does not have long term resistance to alkalis but does not normally exhibit the cracking unless mechanical stress is also applied.

The cracking was reproduced under artificial conditions by placing a small piece of Mylar in a solution of 50% sodium hydroxide. The Mylar was fastened in a small metal clip and began cracking along the bend after one day of exposure. Polyethylene, which was used as an insulator in some of the previous tests, is resistant to both acids and alkalis. This explains why the cracking phenomenon was not observed during the tests performed in 1984.

FUTURE TESTING

A test program is planned to identify suitable materials for implementing the plastic sheet insulating device. The program will include consultation with industry experts on environmental stress cracking and plastics, accelerated aging tests using the laboratory apparatus described in this paper and mechanical testing. The planned result will be an insulator design suitable for long term use on the BART system.

Figure 4. Photograph of Fastener on BART System with Notch in Rail due to Corrosion.

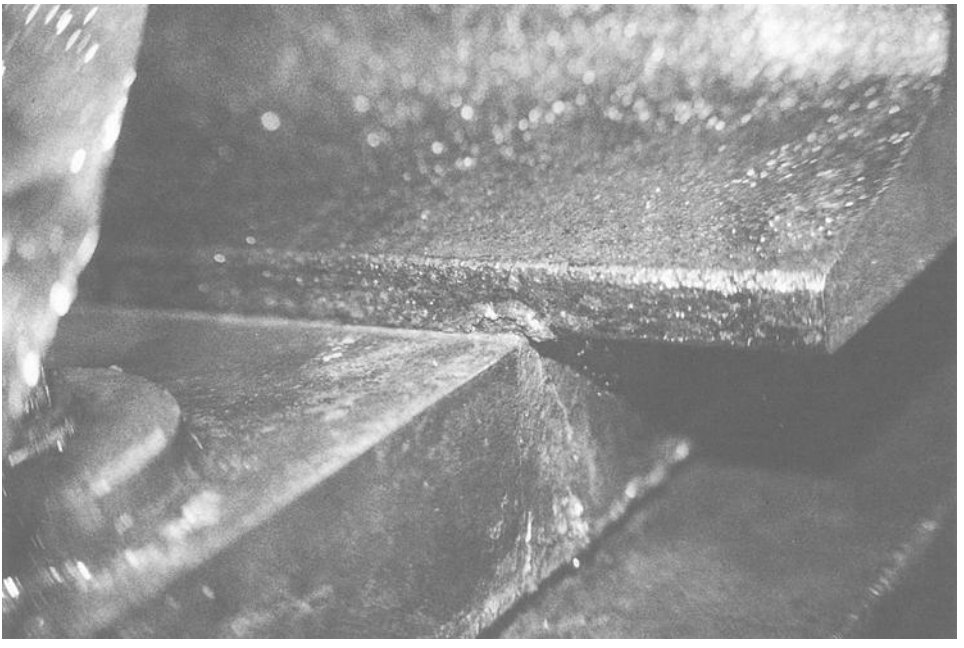

Figure 5. Photograph of Fastener in Test Chamber with Notch in Rail after one week of Accelerated Testing.

The results of the testing also showed that the most promising structure for leakage reduction would be some type of wrap or covering for the rail. Leakage current reductions of more than 4 orders of magnitude with respect to the control fastener were measured during the testing. These currents were about 20 times less than that of the best of the other four concepts tested.

Prototype Testing

Field testing of the plastic wrap concept was conducted by BART beginning in late 1985. The device was constructed of two folded sheets of Mylar and inserted between the rail and the fastener in damp areas on the BART system. Laboratory testing was conducted in 1989 and again in 1990 to identify certain field problems and more precisely identify aging characteristics of the design.

Testing in 1989 involved one of the two piece Mylar devices which had been removed from the BART system. A new device was tested at the same time to compare the aging characteristics. Figure 6 shows the two insulating devices in the spray chamber. Results of the testing showed that the two fasteners would eventually have leakage currents on the order of 1 A. These currents were surprisingly high compared to the initial results on the order of 10 μA. One reason for this is the structure of the two-piece insulating device.

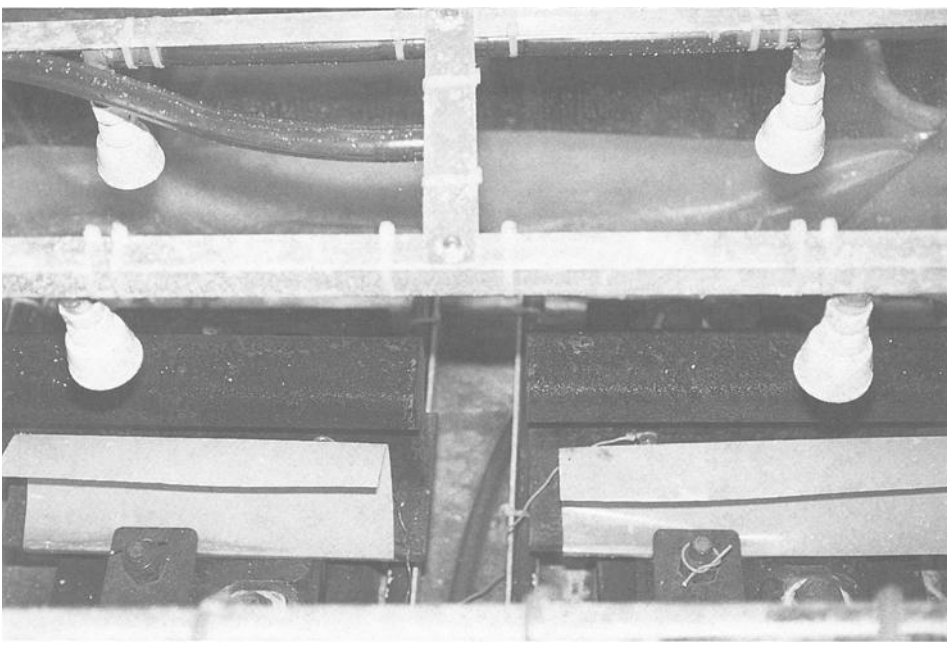

Figure 6. Photograph of Two Rail Sections in Test Chamber.

Figure 7. Photograph of Plastic Insulator on the BART System where Cracking was Common.

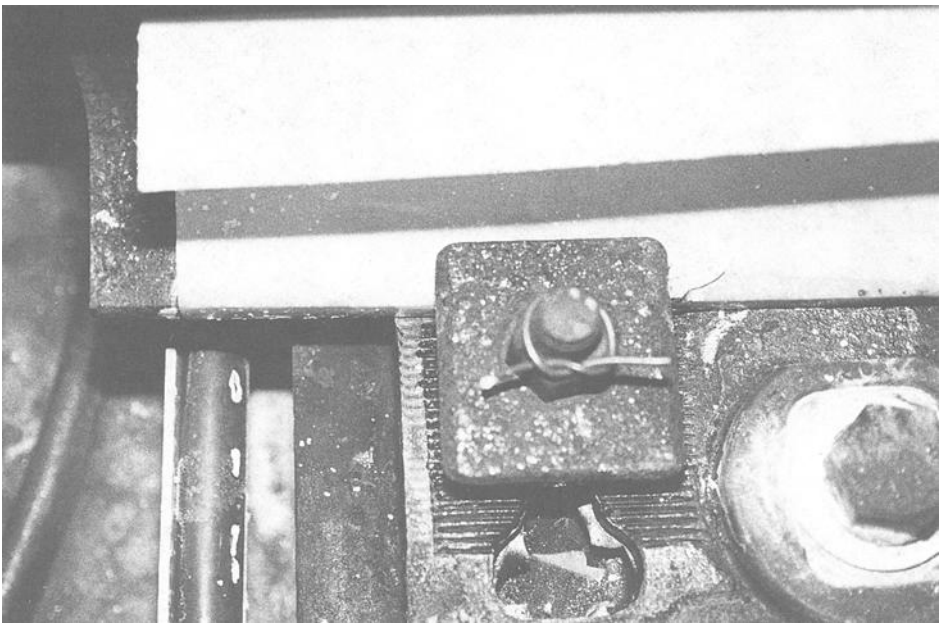

Figure 8. Photograph of Cracking on Plastic Insulator During Laboratory Testing (Right Side of Rail Clip).

CONCLUSIONS

- The laboratory apparatus and procedures reproduce electrochemical and environmental effects observed on the BART system.
- The apparatus can be used as a practical tool for predicting the performance of new rail insulating devices.
- The insulating skirt design can reduce the leakage current by a factor of about 1000 (from 1 A to 1 mA) when compared to an aged, unmodified fastener.
- The one-piece plastic wrap design can reduce the leakage current by a factor of about 100,000 (from 1 A to 10 μA) when compared to an aged, unmodified fastener. The insulation level provided is similar to the minimum allowed by procurement specifications for new fasteners.

ACKNOWLEDGEMENTS

Mr. Todd gratefully acknowledges the support and assistance of Gail Todd and Kim Todd in the preparation of this paper. Mr. Galler would like to thank Donna McGuirk for her efforts in preparing the graphic materials, editing and final formatting of the paper, and Mr. Medora, who conducted most of the testing. The authors would also like to thank Dr. Alexander Kusko who has provided insight into leakage current mechanisms and technical direction since the beginning of the work.

REFERENCES

[1] Shaffer, R.E. and Fitzgerald, J.H., "Stray Earth Current Control Washington, D.C. Metro System," Materials Performance, Vol. 20, No.4, April 1981, pp 9 -15.
[2] IEEE Standard 4-1978, "IEEE Standard Techniques for High Voltage Testing."
[3] United States Patent, Number 4,615,484, Oct. 7, 1986, "Insulative Protective Device for Rail Fastener," Alexander Kusko, Weston, MA.

[4] United States Patent, Number 4,635,846, Jan. 13, 1987, "Insulative Protective Device for Rail Fastener'" Peter L. Todd, Berkeley, CA.
[5] ASM International Handbook Committee, Engineered Materials Handbook: Engineering Plastics, ASM International, Metals Park, OH, 1988.

Melvin F. Kanninen, Krishnan V. Pagalthivarthi, and Carl H. Popelar

A THEORETICAL ANALYSIS FOR THE RESIDUAL STRENGTH OF CORRODED GAS AND OIL TRANSMISSION PIPELINES

REFERENCE: Kanninen, M. F., Palgathivarthi, K. V., and Popelar, C. H., "A Theoretical Analysis for the Residual Strength of Corroded Gas and Oil Transmission Pipelines," Corrosion Forms and Control for Infrastructure, ASTM STP 1137, Victor Chaker, Ed., American Society for Testing and Materials, Philadelphia, 1992.

ABSTRACT: The current regulations governing the integrity of corroded gas and oil pipelines are empirical. In many cases the guidelines are very conservative, but even so they are not reliably conservative in all instances. To improve upon this situation, a theoretical approach was taken within elastic shell bending theory. Preliminary results developed using a maximum hoop stress criterion in an axisymmetric approximation of the metal loss provided a relation for the failure pressure for a pipe with axial direction metal loss. It was found that the form assumed in the existing empirical approach is essentially correct in so far as the axial extent of the damage governs. However, the extension of the shell bending theory approach to the plane strain case indicates that it may be the circumferential dimension of the damage that actually governs the failures of corroded pipes. While this important finding must be confirmed by further analyses and experimentation, this result indicates the usefulness of the type of approach described in this paper. The use of even simple mechanics models where only empirical approaches currently exist can surely be useful to address corrosion-related problems associated with a variety of infrastructural components.

KEYWORDS: Pipelines, Corrosion, Corroded Pipelines, Shell Theory, B31G Guidelines

Dr. Kanninen is program director, Engineering Mechanics, and Dr. Pagalthivarthi is a senior research engineer, both at The Southwest Research Institute, San Antonio, Texas. Dr. Popelar is a professor in the Department of Engineering Mechanics at The Ohio State University, Columbus, Ohio.

INTRODUCTION

Corrosion damage in the form of metal loss is a frequent occurrence in gas and oil transmission pipelines. This can not only cost the industry millions of dollars annually for inspection, repair and replacement of corroded pipes, but, in addition, there is danger to the public; see Fig. 1. Accordingly, guidelines that will preclude pipe rupture, but not force an excessive amount of premature repairs and replacements in so doing, is very important to the public and industry.

The guidance that pipeline engineers currently have is that contained in the ANSI/ASME B31G guidelines [1], which in the United States effectively have the force of law through the U.S. Code of Federal Regulations [2]. While these have been very helpful to the pipeline industry, it is widely believed that they are excessively conservative; for example, see reference [3]. This has led to an improved version [4]. However, as that work retained the original empirical basis [5], it remains unable to address a key condition not included in the current guidelines — circumferential direction metal loss. Of perhaps more importance, because the approach underlying the current and newly proposed guidelines remains empirical, they cannot be reliably extrapolated beyond the data base; e.g. to larger diameter pipes, higher grades of steel.

The current ANSI/ASME B31G guidelines are based on an empirical relation that is drawn from the conceptual view shown in Figure 2. It is commonly written in the form [1, 2]

$$S_F = \overline{S}\frac{A_o - A}{A_o - AM^{-1}} \tag{1}$$

where S_F is the hoop stress in the pipe at failure, $\overline{S}$ is the flow stress of the material, A is the area of through-thickness metal loss in the most severely degraded section of the pipe wall, A_o is the nominal (undamaged) area corresponding to A, and M is a dimensionless parameter called the bulging factor. This relation, commonly known as the "Folias Factor", is given by

$$M = \left[1 + 0.8\frac{L^2}{Dt}\right]^{1/2} \tag{2}$$

Referring to Fig. 2, M is a function of L, the axial length of the metal loss region, D is the mean pipe diameter, and t is the wall thickness. In the B31G guidelines, $\overline{S}$ is taken equal to $1.1\,SMYS$ where SMYS is the specified minimum yield stress of the pipe steel. Note that the circumferential dimension does not affect the result.

The realization that further empirical modifications would be unlikely to achieve any significant increases in accuracy motivated the development of a theoretically based alternative approach [6]. Starting with the theory of elastic shells, a theoretical relation for an axisymmetric metal loss region was obtained. A number of mathematical simplifications were made in that development in order to expedite the work. Encouraged by the success of this development, the shell bending theory was continued to develop solutions that rectify the above cited deficiencies and to

FIG. 1 Photograph of ruptured corroded pipeline.

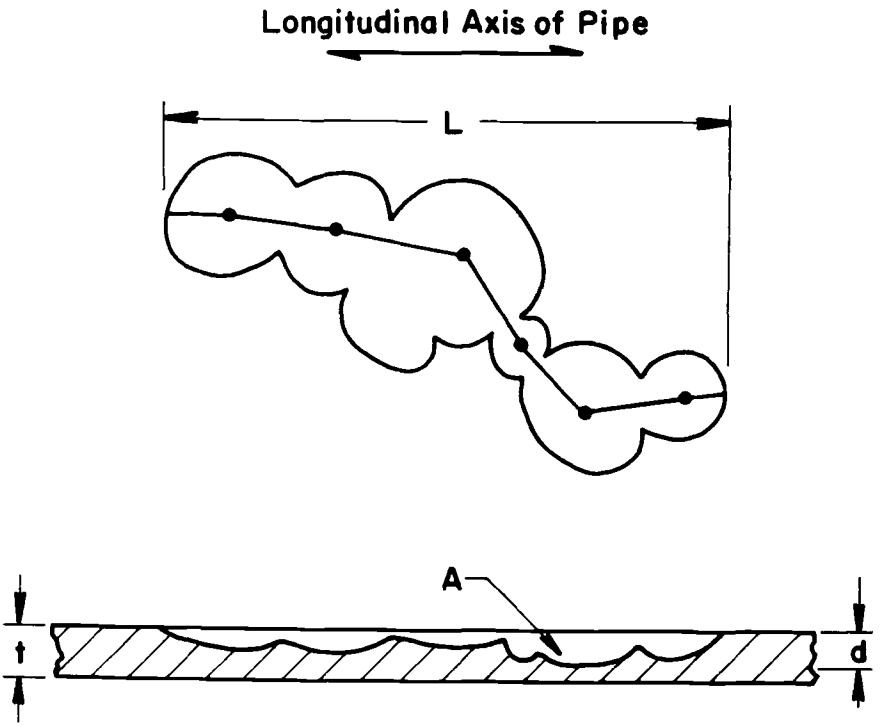

FIG. 2 Conceptual view of a corroded axial pipe wall segment [1].

open the door to even further improvements. The results obtained by considering the circumferential dimension of the damage via a plane strain representation of the metal loss region are provided in this paper.

EXTENSION OF THE ELASTIC SHELL THEORY APPROACH

In this paper the work reported in reference [6] has been extended in two ways. First, the simplifying assumptions in the axisymmetric solution have been relaxed. Second, a solution to the plane strain solution has been developed. These developments are described in this section in conjunction with determining the dominant dimension of a rectangular metal loss region.

Axisymmetric Solution

Recognizing the restrictiveness inherent in an empirical approach, a theoretical alternative was initiated using shell bending theory, [6]. In this approach, the damage in a corroded pipe was considered to correspond to a "ring" of metal loss having a through-thickness depth d and an axial length L. Using Flugge's bending theory equations for a circular cylindrical shell for axisymmetric conditions, the key variable is the radial displacement w which is a function only of the axial coordinate x. If the axial displacement can be neglected the governing equation is the fourth order ordinary differential equation given by

$$\frac{d^4w}{dx^4}+\frac{12}{R^2t^2}w=\frac{12(1-\nu^2)}{Et^3}p \tag{3}$$

where R is the pipe radius ($R=D/2$), t is the wall thickness, p is the internal pressure, E is the elastic modulus, and ν is Poisson's ratio.

In reference [6] the boundary conditions for the problem were those for symmetry conditions at the center of the metal loss region (x = 0) and, for simplicity, that the undamaged portion of the pipe is significantly stiffer than is the damaged portion. Then, by using t^* to denote the effective thickness of the damaged region and t_o, to denote the nominal thickness, the solution to Eq (3) satisfying the simple set of boundary conditions is

$$w(x)=\frac{1-\nu^2}{E}\frac{R^2p}{t^*}\left\{1-\left(1-\frac{t^*}{t_0}\right)[B\,\mathrm{Sinh}\lambda x\sin\lambda x+C\,\mathrm{Cosh}\lambda x\cos\lambda x]\right\} \tag{4}$$

where λ, B and C are known functions of L, D and t_0 [6].

The most important use of this result is to quantify the stress that occurs in the damaged region. If the contribution of the bending stresses to the failure condition is neglected in favor of the membrane stresses, and the criterion for failure is taken to be the achievement of a flow stress at the most highly stressed point in the damaged region, the failure pressure is

$$p_F=\frac{2\bar{S}t^*}{D}\left[1-\left(1-\frac{t^*}{t_0}\right)M^{-1}\right]^{-1} \tag{5}$$

where M^{-1} represents the bulging of the pipe wall. As shown below, this function is not the same as Eq (2).

By introducing $S_F = Dp_F/2t_0$ to denote the nominal hoop stress at failure, and noting that $A/A_o = 1 - t^*/t_o$, Eq (5) can be cast into the form of Eq (1). Thus, the result derived from elastic shell bending theory supports the use of the empirical relation, albeit the relation for M in Eq (4) differs from the relation used in the current empirical approaches. It is a much richer function in that it includes a synergistic dependence upon both the length and depth of the metal loss profile while the "Folias relation," depends only upon the damage length. However, in actuality, the results are not too greatly different.

More recently, the "first cut" simplified solution to Eq (3) developed by assuming that the deformation of the undamaged region could be neglected relative to that of the damaged region, was improved upon. A more realistic approach is to enforce continuity conditions on the displacement, slope, moment and shear force at the transition point. While algebraically intensive, the procedure is straight forward. The result is similar to Eq (4), but containing additional terms. The result gives rise to much greater deformation in the axisymmetric metal loss region.

While the replacement of the rigid condition by continuity conditions affects the stress that occurs to promote failure, the general form of the result is unchanged. This leads to an expression for the failure pressure that is identical to Eq (5). The difference lies in the form of the bulging factor, M. The enhanced shell theory approach gives

$$\begin{aligned} M = &\{(1+\eta^4)(\cosh\alpha \cdot \sinh\alpha + \sin\alpha \cdot \cos\alpha) + 2\eta^{3/2}(\cosh^2\alpha - \cos^2\alpha) \\ &+ 2\eta^2(\cosh\alpha \cdot \sinh\alpha - \sin\alpha \cdot \cos\alpha) + 2\eta^{5/2}(\cosh^2\alpha - \sin^2\alpha)\} \\ &\cdot \{\cosh\alpha \cdot \sin\alpha + \sinh\alpha \cdot \cos\alpha + 2\eta^{5/2}\cosh\alpha \cdot \cos\alpha \\ &+ \eta^2(\sinh\alpha \cdot \cos\alpha - \cosh\alpha \cdot \sin\alpha)\}^{-1}, \end{aligned} \tag{6}$$

where

$$\alpha = \frac{3^{1/4} \cdot L}{2\sqrt{Rt^*}}, \quad \text{and} \quad \eta = t^*/t_o$$

Note that if the undamaged region is assumed to be very stiff, then $\eta \to o$ and the original form of M in Eq (5) is recovered; see reference [6].

Plane Strain Solution

When the length of a corroded region of a pipe is relatively long in the axial direction, the axial variations of the deformations and stresses can be neglected. In this case, the stress analysis reduces to plane strain for which only circumferential or hoop variations of the deformation and stress are present. As in the axisymmetric case, the plane strain analysis is expected to yield conservative predictions for the maximum stress. A plane strain model of a corroded pipe under an internal pressure p is depicted in Fig. 3(a).

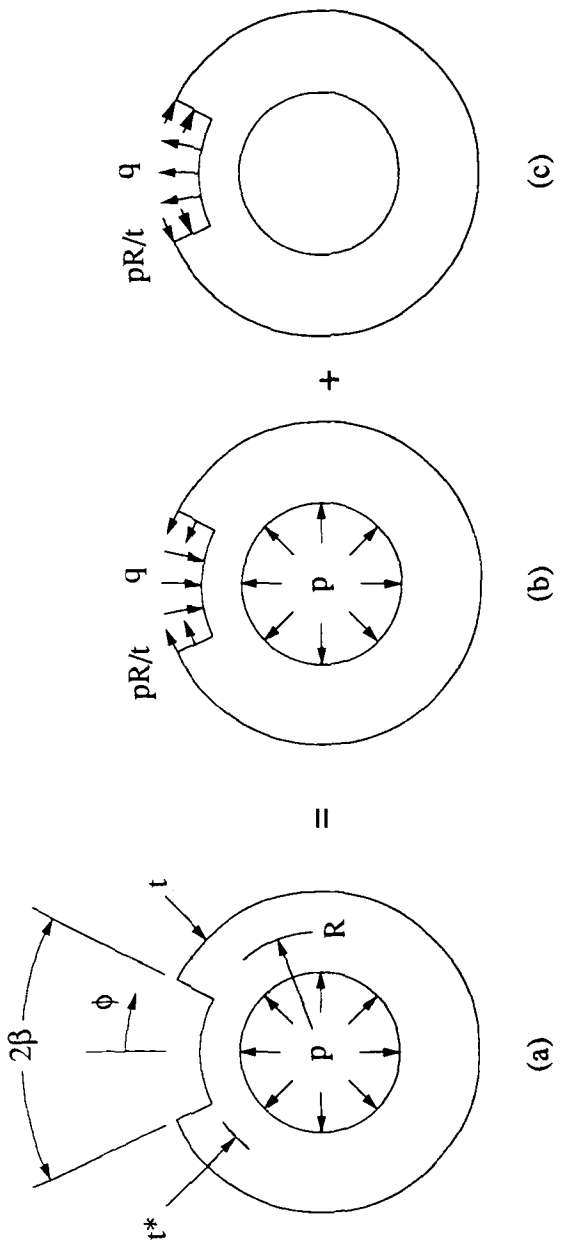

FIG. 3 Plane strain analysis model for corroded pipe

The corroded region in Fig. 3 is assumed to have a uniform reduced wall thickness t^* over the region $0<|\phi|<\beta$. The original wall thickness is t, R is the mean radius, and $t/R \ll 1$ is assumed. Then, the solution to problem (a) in Fig. 3 can be represented by the superposition of the solutions to problems (b) and (c). In this figure $q = p(1 - t^*/t)$ represents the radial stress in an uncorroded thin-walled pipe at a distance t^* from the inner surface. The solution to problem (b) is for an uncorroded pipe under an internal pressure for which the hoop stress is pR/t. Hence, the solution to problem (c) yields the additional stresses produced by the metal loss. The tractions pR/t acting on $|\phi|=\beta$ introduce a significant bending stress due to the resulting mismatch of the midsurfaces in the corroded and uncorroded regions.

The solution to problem (c) is readily effected through the principle of minimum complementary energy (i.e., Castigliano's Theorem). This approach has the advantage that the compatibility (continuity) conditions at the interfaces ($|\phi|=\beta$) of the corroded and uncorroded regions are automatically satisfied. The internal membrane force N and bending moment M are

$$N = (N_o - qr)\cos\phi + qRH(\beta - \phi) \tag{7}$$

and

$$M = M_o + R(N_o - qR)(1 - \cos\phi) - q\frac{Rt^*}{2}H(\phi - \beta) \tag{8}$$

where N_o and M_o are internal membrane force and bending moment at $\phi=0$ and $H(x)$ is the Heaviside step function. Minimizing the complementary energy U^* requires that

$$\frac{\partial U^*}{\partial M_o} = \frac{\partial U^*}{\partial N_o} = 0 \tag{9}$$

where

$$U^* = \int_o^{\pi}\left(\frac{M^2}{EI} + \frac{N^2}{EA}\right)Rd\phi$$

and EI and EA are the flexural and extensional rigidities, respectively.

Omitting the algebraic details, it is found that, to a first approximation (especially for $\eta \to 1$), $N_o \cong qR$ so that the direct stress at $\phi=0$ for problem (a) is then

$$\sigma_m = pR/t^*. \tag{10}$$

The bending moment M_o turns out to be

$$M_o = qRt^*(1 + \varepsilon)/2, \tag{11}$$

where

$$\varepsilon = \frac{B(\beta - \sin\beta) - C\beta}{AC - B^2} \tag{12}$$

In Eq (12), A, B and C are constants defined as

$$A = \beta + (\pi - \beta)\eta^3 \tag{13}$$

$$B = \beta - \sin\beta + (\pi - \beta + \sin\beta)\eta^3 \tag{14}$$

$$C = \frac{3}{2}\beta - 2\sin\beta + \frac{1}{4}\sin 2\beta + \left[\frac{3}{2}(\pi - \beta) + 2\sin\beta - \frac{1}{4}\sin 2\beta\right]\eta^3, \tag{15}$$

where η is the thickness ratio, t^*/t.

The maximum bending stress occurs at $\phi = 0$ and can be written as

$$\sigma_b = 3pR(1 + \varepsilon)(1 - t^*/t)/t^* \tag{16}$$

The variation of the bending stress with β for representative values of t^*/t is shown in Fig. 4. The maximum stress (sum of the direct or membrane stress and the bending stress) also occurs at $\Phi = 0$ and is given by

$$\sigma_{max} = \frac{pR}{t^*}[1 + 3(1 + \varepsilon)(1 - t^*/t)] \tag{17}$$

Michalopoulos [7] performed an elastic finite element analysis for a corroded pressurized pipe in which the width of the corrosion in the circumferential direction was 10t and the length in the axial direction was either 10t (a square patch) or 33t. In general, the finite element analyses indicated that greater hoop stresses were obtained for the longer corroded region. A variety of pipe diameters, wall thicknesses and corrosion depths were investigated. Table 1 compares the maximum stress of Eq (17) with the finite element analysis for a corroded length of 33t since it represents a closer approximation to plane strain. The plane strain analysis yields maximum stress 11 to 32 percent greater than predicted by the finite element analysis. This difference is likely due to the assumed corroded length in the finite element analysis being insufficient to produce plane strain.

Determination of Governing Dimension

Having solutions for the axisymmetric and the plane strain approximations to the finite metal loss regions occurring in a corroded pipe, the next step is determining the regimes in which each is dominant. This could be done by equating the critical pressures obtained in the two solutions to obtain an "indifference" condition. This condition would delimit the metal loss regions in which its axial dimension leads to a lower failure pressure from those in which its circumferential dimension provides the lower value. However, a simpler procedure is to compare the results for a variety of cases. A set of examples demonstrating this conclusion is shown in Figures 5 and 6.

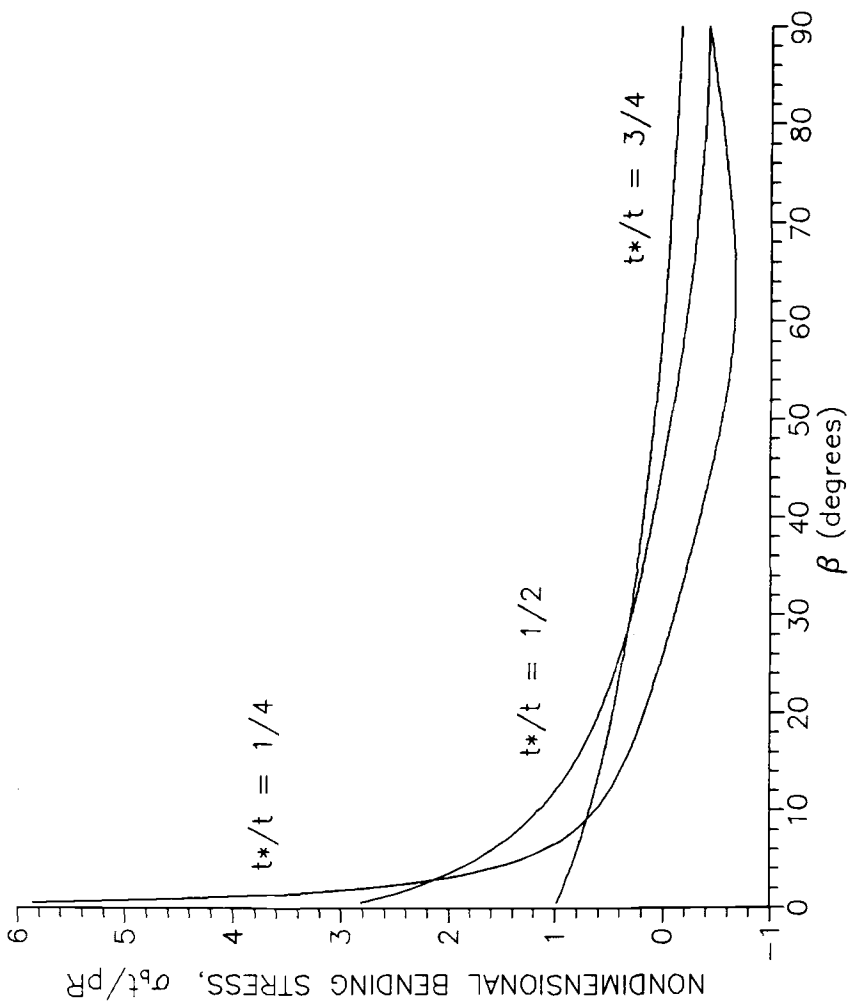

FIG. 4 Variation of non-dimensional outer fiber bending stresses with β

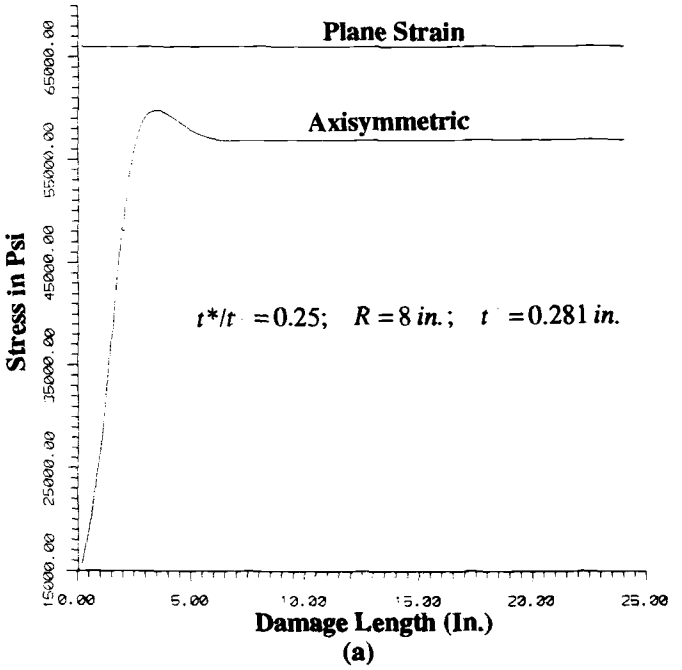

FIG. 5 Maximum outer fiber stress in metal loss region versus damage length
(*a*)$\beta = 90$, (*b*)$\beta \approx 10$

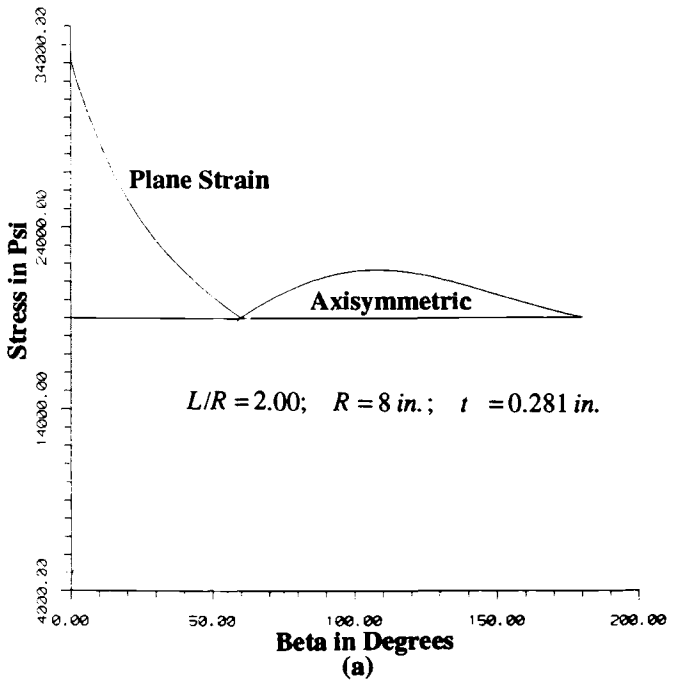

FIG. 6 Maximum outer fiber stress in metal loss region versus damage angle, β

TABLE 1 -- Comparison of model predictions with finite element analysis

Case No.	Outside Diameter (in)	Wall Thickness (in)	$\frac{t^*}{t}$	Pressure (psi)	β (degrees)	σ_{max}* (ksi)	$(\sigma_{max})^{**}_{FEA}$	$\frac{\sigma_{max}}{(\sigma_{max})_{FEA}}$
P1B11L	20	0.3125	3/4	375	8.95	24.1	21.7	1.11
P1B21L	20	0.3125	3/5	375	8.95	32.8	27.1	1.21
P1B31L	20	0.3125	1/2	375	8.95	38.4	34.0	1.31
P2A11L	30	0.3125	3/4	450	5.97	45.5	39.4	1.15
P2A21L	30	0.3125	3/5	450	5.97	63.9	48.4	1.32
P2A31L	30	0.3125	1/2	450	5.97	76.8	58.2	1.32
P3C11L	30	0.360	3/4	450	6.88	38.9	33.8	1.15
P3C21L	30	0.360	3/5	450	6.88	54.1	42.5	1.27
P3C31L	30	0.360	1/2	450	6.88	64.4	50.6	1.27

* Eq 12
** Michalopoulos [7]

DISCUSSION

With the current B31G guidelines for the remaining strength of corroded transmission pipelines it is not possible to meet the need of the industry for a relaxation of the excessive conservatism that is now embodied in the guidelines, nor will it be possible to provide precise predictions for larger diameter pipes and other variables beyond those contained in the data base. While the empirical approach has been taken as far as it possibly can, in contrast, shell bending theory has ample room for generalization. This paper described the generalization of the approach to include the circumferential dimension of the corrosion damage region. It was found that, despite its neglect in the empirical approaches, the circumferential dimension may be the dominant one. However, this potentially very significant conclusion needs further substantiation.

To accomplish this, a more realistic failure criterion can be used to generalize the outer fiber failure criterion used in this work. It is anticipated that this could be accomplished through the incorporation of bending via a failure relation based on a collapse load. This is

$$\left(\frac{N_\phi}{t\bar{\sigma}}\right)^2 + \frac{4M_\phi}{\bar{\sigma}t^2} = 1 \tag{13}$$

where N_ϕ and M_ϕ are the stress resultant and bending moment, respectively, while $\bar{\sigma}$ denotes a collapse stress. Figure 7 shows that this approach would give a higher failure pressure than one based on an outer fiber failure criterion, thus possibly giving rise to a region in which the axial dimension dominates.

While, in general, the analysis of the remaining strength of a corroded pipe is conceptually very simple, practical solutions are very complex. There are many variables, even in idealized conditions; i.e., $D, t, \sigma_y, \sigma_u, L, W, d, p, \sigma_a$. Actual corrosion patches have complex shapes. There is also uncertainty of input data; e.g., the stress-strain behavior of the pipe steel. Because of the complexity that exists, the usefulness of elastic shell theory can be used to translate analysis/experimental results into field useable damage assessment procedures This paper indicates how this can be accomplished. In so doing, a key finding was obtained. This is that the circumferential extent of damage, rather than the axial dimension, governs.

In general, for risk free pipeline operation, consideration of many other factors in addition to wall thinning is needed. These include time dependent increase in corrosion patch dimensions, corrosion in dents and gouged dents and at weldments, competition between fracture and plastic instability failure, leak versus rupture deliminations, and the extension to weld discontinuities and residual stresses. It is conjectured that the elastic shell theory approach might be helpful in addressing these problems also; particularly if the alternative is a purely empirical approach.

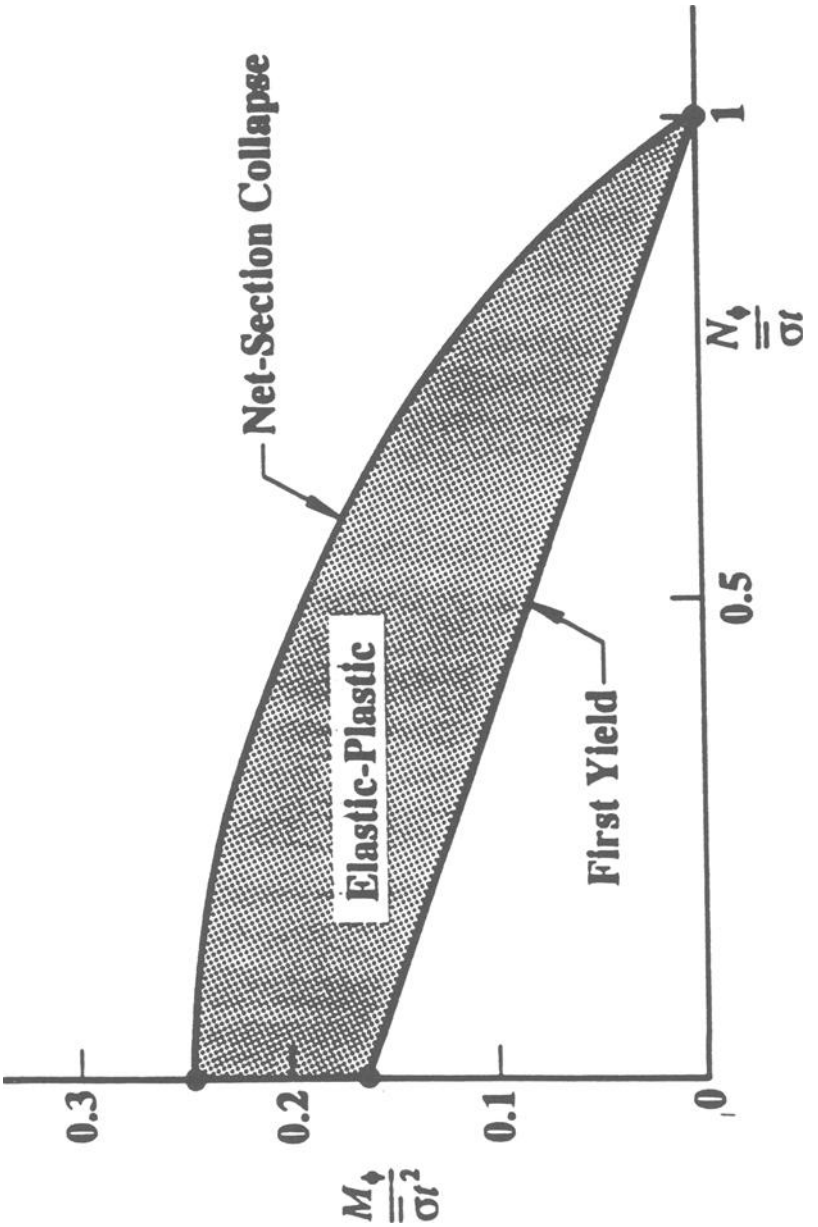

FIG. 7 Failure criteria for shell bending theory

CONCLUSIONS

Because the present and recently proposed guidelines for oil and gas pipelines having corrosion damage are empirical, they are both inefficient and unreliable. Inefficient in the sense that large degrees of built-in conservatism will cause unnecessary repair and replacement operations, unreliable when extrapolated to conditions beyond the data base used to formulate them. These considerations have motivated the development of the theoretical relations by applying elastic shell theory to pipes with idealized metal loss regions given in this paper.

It was found that the solution for an axisymmetric metal loss region supports the general form of the empirical relation. Thus, for cases where the axial dimension of the corroded region is critical, the current guidelines may be appropriate. However, the theoretical solution for the plane strain representation of the corroded region generally provides a lower critical pressure. It can be concluded that the circumferential dimension of the corroded region, which is neglected in the empirical approach, may actually govern corroded pipe integrity.

REFERENCES

[1] Anon., ASME Guide for Gas Transmission and Distribution Piping Systems, B31G, Manual for Determining the Remaining Strength of Corroded Pipelines, American Society of Mechanical Engineering, New York, 1986.

[2] Code of Federal Regulations, 1986, 194.

[3] Coulson, K. E. W., and Worthington, R. G., "Pipe Corrosion," Oil and Gas Journal, 9 April 1990, pp. 54-59.

[4] Kiefner, J. F. and Vieth, P. H., A Modified Criterion for Evaluating the Remaining Strength of Corroded Pipe, American Gas Association, Pipeline Research Committee Report on Project PR3-805, December 22, 1989; see also, Oil and Gas Journal, 6 August 1990, p. 56.

[5] Kiefner, J. F., "Fracture Initiation," Proceedings of the Fourth AGA Line Pipe Research Symposium, American Gas Association, Arlington, VA, Section G, 1968.

[6] Kanninen, M. F., "A Theoretical Basis for Determining the Integrity of Corroded Pipelines," manuscript submitted for publication, September 1990.

[7] Michalopoulos, C. D., "Design Analysis for Fiberglass Reinforced Composite Repair Sleeve," Final Report, Southwest Applied Mechanics, Inc., Houston, Texas, November 1990.

James B. Hinte[1]

THE NUPIPE® RECONSTRUCTION TECHNOLOGY[2]

REFERENCE: Hinte, J. B., "The NUPIPE® Reconstruction Technology", Corrosion Forms and Control for Infrastructure, ASTM STP 1137, Victor Chaker, Ed., American Society for Testing and Materials, Philadelphia, 1992.

ABSTRACT: Increasing awareness of deteriorating infrastructure systems has led to the development of a new pipeline reconstruction method which forms a tight-fitting, new PVC pipe within an existing pipe. This unique process can be used for reconstructing pipes ranging from 4-inch through 12-inch diameter for both municipal and industrial applications. The new PVC pipe provides structural support and isolates the existing conduit from further corrosion from the effluent.

KEYWORDS: PVC, trenchless reconstruction, corrosion protection, infiltration control, thermoplastics

The process involves the insertion of a folded PVC extrusion (Figure 1) into an existing pipeline. Once the folded PVC pipe is fully extended within the host pipe, it is heated to a temperature sufficient to make the plastic soft and pliable.

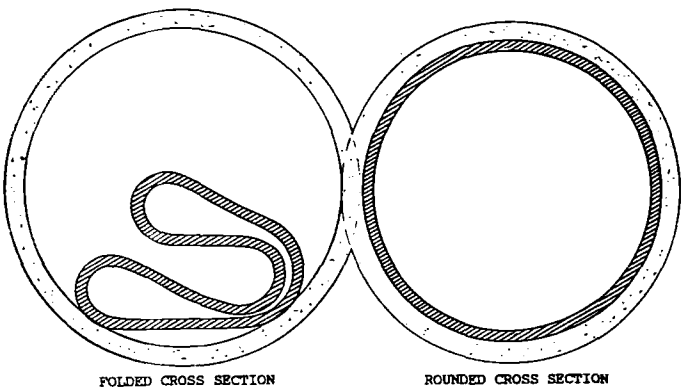

Figure 1. Cross section of pipe showing the folded configuration (left) and the rounded configuration (right).

[1]Registered professional engineer and a Business Development Engineer at NUPIPE, Inc., 3315 Democrat Road, Memphis, TN 38118.

[2]The NUPIPE® technology is a patented process for reconstructing small diameter pipelines without excavation. NUPIPE, Inc., Memphis, TN

The folded pipe is then progressively expanded using a specially designed rounding device that is propelled by low pressure steam. This expansion process develops a tight fit while creating a mechanical lock at joints and offsets as well as forming distinct dimples at lateral connections. The PVC is cooled to a rigid state, the ends are cut off, and service connections are reinstated internally using a remote controlled robotic cutting device (Figure 2).

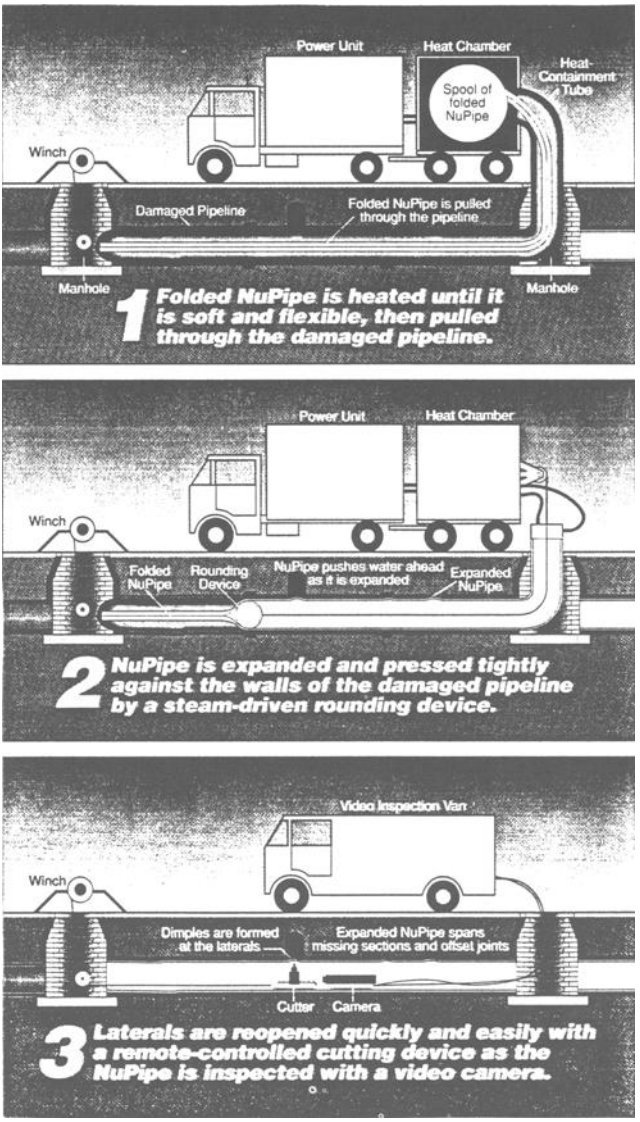

Figure 2.

The finished pipe is fully structural with no joints. Internal corrosion of the host pipe is stopped, and since the new pipe is not dependent on the structural capacity of the existing pipe, external corrosion will not effect the operating life of the system. Structural integrity of the system is reestablished while infiltration through joints or defects in the pipe wall is virtually eliminated. Flow capacity is typically increased due to a combination of the low Manning's coefficient of PVC ("n" = 0.009) [1] and the continuous nature of the pipe which provides smooth transitions at joints, cracks or missing segments in the existing line.

DEVELOPMENT

A key component in the development of the process began with the selection of which material would be most suitable for this technology. Thermoplastic materials, defined as having the property of being able to be repeatedly softened and hardened by heating and cooling through a specific temperature range characteristic for each plastic, per ASTM Standard Definitions of Terms Relating to Plastics (D 883), were the obvious choice; however, selecting the most appropriate thermoplastic was the problem. The most commonly used thermoplastics for sanitary sewer systems are polyvinyl chloride (PVC), polyethylene (PE) and acrylonitrile-butadiene-styrene (ABS). In evaluating materials, some of the more critical characteristics analyzed were temperature necessary to sufficiently soften the plastic, degree of ductility while in the softened state, strength of material in both the pliable and rigid condition, workability of material, and effects on the material as a result of the processing required to install the product.

PVC was selected as the material best fitting these criteria. PVC becomes pliable above 189°F (87.2°C), which allows the pipe to conform to the host pipe and yet maintains sufficient physical characteristics to allow for installation and processing. It was also found through testing [2] that the physical properties of the processed PVC were not altered by the installation and processing, providing a finished pipe that was equivalent to normal PVC. PVC compounds are a mixture of PVC polymers, stabilizers, catalysts, processing agents, modifiers and pigment. This combination of materials aids in the extrusion process as well as ensures a PVC compound with predictable physical and chemical properties. In developing a formulation for this process, the objective was to derive a compound that would fall within the scope of ASTM Standard Specification for Rigid Poly(vinyl Chloride) (PVC) Compounds and Chlorinated Poly(vinyl Chloride) (CPVC) Compounds (D 1784) and applicable portions of ASTM Standard Specification for Type PSM Poly(vinyl Chloride) (PVC) Sewer Pipe and Fittings (D 3034) and was capable of providing the necessary properties required for the process. ASTM D 1784 categorizes PVC into cell classes based upon the physical properties and chemical resistance of each compound. The final properties have been tested and were found to meet or exceed the performance requirements within ASTM D 3034.

The pipe is extruded round and while still hot and flexible is passed through a specially designed folding and calibration unit that carefully transforms the round pipe into the folded configuration. After having the appropriate markings applied to the pipe wall, the folded pipe is slightly heated and is then wound onto wooden spools at which time it is ready for installation.

INSTALLATION

The first stage of an installation is the cleaning and evaluation of the existing pipe. A video camera is pulled through the pipe to determine the extent of deterioration, to see if the current condition

is suitable for the process, and to record the location of side connections. The pipe is then cleaned to remove roots and sediment that would interfere with the expansion of the pipe. Access for gravity systems is typically through existing manholes. If the system must remain operational during the reconstruction process, bypass pumping is established.

Spools of folded pipe are loaded into a trailer-mounted insulated heat chamber. The heat chamber is a self-contained environmental unit that is used for transporting the pipe and which is equipped to provide a closed environment to heat the folded PVC while still on the spool. Once the installation crew mobilizes to the job site, the heat chamber is positioned over the insertion manhole. At this point, necessary hardware and fittings are positioned in the insertion and terminating manholes while heat is applied to the spool in the heat chamber. Heating the material prior to insertion makes the PVC flexible, which reduces the forces needed to pull the PVC in and eliminates damage to both the PVC and the host pipe that might occur during insertion. After the hardware is in place, a winch is positioned over the terminating manhole. The winch is used to pull the heat containment tube (HCT) and folded PVC through the existing pipe. The HCT is a thin reinforced flexible tube that is pulled into the host pipe prior to inserting the PVC. The HCT protects the PVC from damage during the winching process, allows the PVC to be heated from both the inside and the outside in a closed environment, and insulates the PVC from groundwater that may be entering the pipe during the heating and rounding process. Once the HCT is in place and the PVC has become pliable, the winch cable is attached. The folded pipe is then pulled through the HCT and host pipe to the terminating manhole. Once the pipe is completely extended, the ends are cut off and specially designed fittings are attached to each end. The fitting attached at the insertion end is a canister that contains the rounding device and is equipped with two attachments for supplying steam to the pipe. The attachment located in front of the rounding device supplies steam to the interior of the folded pipe, and the attachment behind the rounding device supplies steam to propel the rounding device through the pipe. The fitting at the terminating end is designed to receive the rounding device and act as a controlling valve to regulate pressure and release condensate. Once the fittings are secured, steam is applied until thermocouples indicate the required temperatures have been obtained at both ends of the line, ensuring the material has become soft and pliable.

At this point, steam is transitioned to the line behind the rounding device, propelling it through the pipe. The rate of progress is controlled by a steel cable and winch located on the heat chamber. The rounding device is the vital element of the installation process as it ensures controlled, progressive expansion of the folded pipe. The rounding device forces the PVC tightly against the existing pipe and creates dimples at side connections as well as a mechanical lock at joints and irregularities in the conduit. Progressive expansion, which means the pipe is sequentially rounded from one end to the other, eliminates any trapped air or water that might interfere with the rounding process. If the folded pipe was only inflated using internal pressure, it would round uniformly from end to end possibly trapping air or water in between the new pipe and the existing pipe. Areas that do not round completely would have reduced structural capacity and flow area in that section.

After the rounding device reaches the termination point, heat and pressure are maintained for a predetermined period, and then the system is stabilized with air and quenched by introducing cool water into the pipe. Once the system has cooled, the new pipe becomes a hard, structurally sound PVC pipe. The ends are cut off and trimmed, and the robotic cutting device and CCTV camera are placed in the pipe to

reinstate service connections. The dimples created during the rounding process give the technician a clearly defined outline of the lateral, allowing reinstatement of regular and irregular shaped openings.

STRUCTURAL ANALYSIS

Although the installed pipe will perform like standard PVC pipe, the static and dynamic loads are different than that for a direct buried condition. When reconstructing pipelines in situ, there are two design conditions that have been defined relating to the condition of the existing pipe, and they are the partially deteriorated state and the fully deteriorated state. In the partially deteriorated case, the existing pipe is structurally sound and is capable of sustaining live and dead loads; however, it is suffering from infiltration through separated joints, hairline cracks and other minor defects in the pipeline. Once the line has been reconstructed and groundwater is locked out, the pipe will be subjected to hydrostatic loading while the host pipe carries the other loads. In the fully deteriorated condition, the existing pipe is at or near structural failure and, therefore, cannot be considered as providing any structural contribution. In this case, the pipe must sustain all static and dynamic loads as if it were in a direct burial condition. Therefore, the pipe is designed for the direct burial condition using the AWWA formula for the buckling design of buried flexible pipe, AWWA Standard For Fiberglass Pressure Pipe (AWWA C950) and the Spangler equation to check deflection under load. The application of these equations is conservative since the installation is inside an existing pipe surrounded by consolidated soils.

Tests to assimilate the partially deteriorated condition and subsequent failure modes were developed by Utah State University Civil and Mechanical Engineering Departments. [3]

Test samples were prepared inside an 8-inch (203 mm) schedule 40 steel pipe, 7.98 inches (202.7 mm) inside diameter. The inside surface of the steel pipe received no special treatment or cleaning. No bonding to the steel pipe was intended or achieved, only a typical tight fit.

The ends of the steel pipe were then gasketed and flanged end caps installed so that water pressure could be introduced between the steel casing and the pipe through the wall of the casing. The pressure was then increased until failure occurred. Eight tests were performed, all at ambient air and water temperature of approximately 80°F (26.6°C). Eight test sections were recorded. The average pressure at failure was 172 psi (1,185.9 kPa) (397 feet, or 121 m, of head). Ring compression stress theory appeared to best model the principal failure mode, although the high pressure requirements to cause failure clearly indicate that for almost all installations, external pressure will not be critical, and ring compression stress will not be a performance limit.

Three possible mathematical models were considered in analyzing the test results.

1. Wall buckling from external loading.
2. Ring compression theory.
3. Semi-circular/semi-elliptical theory (gap analysis).

The buckling equation for a flexible pipe is: (1)

$$\frac{P(DR-1)^3\ (1-\nu^2)}{E}=2$$

where

P = external hydrostatic pressure (psi)
DR = standard dimension ratio = 35
ν = Poisson's ratio of pipe material
E = modulus of elasticity of pipe (psi)

This describes the critical buckling pressure for external hydrostatic forces working on an unrestrained pipe. Since the PVC pipe is restrained within an existing host pipe which is further restrained by surrounding soil, this equation does not directly apply. In fact, using this equation will give results for critical buckling pressure of only about 1/7 of the test results.

Performance was further analyzed using the principle of ring compression stress. (2)

$$\sigma=\frac{P\ (OD)}{2t}=S_p$$

where

σ = ring compression stress (circumferential stress) (psi)
P = external hydrostatic pressure (psi)
OD = outside diameter of the pipe (inches)
t = wall thickness (inches)
S_p = proportional limit (stress) (psi) of the PVC

The results are plotted in Figure 3.

A gap analysis was also performed. In this analysis, the structure is examined where the external pressure reduces the circumference of the pipe and forces it into a semi-elliptical shape. Therefore, 180° of the pipe is circular and in direct contact with the host pipe, and the other 180° is in an approximate elliptical shape uniformly stressed by external pressure. Assuming that the pipe in the gap is semi-elliptical, the ring compression stress is increased as shown by the upper portion of the graph in Figure 3. See Figure 4 for a free-body diagram of the restrained pipe as assumed for gap analysis.

Figure 3 shows that the graph of the ring compression stress analysis is almost identical to that of gap analysis. In fact, the ring compression stress analysis best represents the actual test results. For design of SDR 35 pipe, a maximum of 57.33 psi (395.3 kPa) is recommended. This equates to 132 feet (40.2 m) (397′ ÷ 3) of external water pressure at a 3 to 1 safety factor.

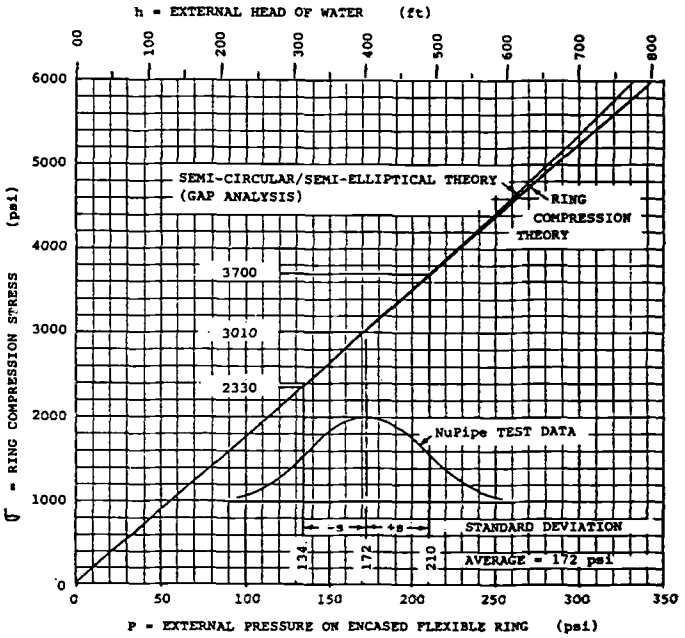

Figure 3. Ring compression stress as a function of external hydrostatic pressure, showing the pure ring compression stress theory for a circular pipe in the lower graph, and the gap-theory (semi-circular/semi-elliptical analysis) in the upper graph. (1 ft = 0.3048 m; 1 psi = 6.8948 kPa)

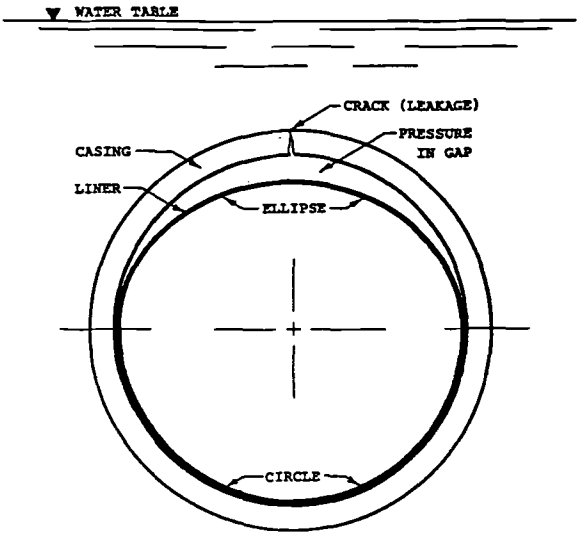

Figure 4. Gap Analysis -- free-body diagram of an encased, flexible pipe showing how external pressure blows half of the flexible pipe against the casing and deforms the other half into an ellipse with a gap between the pipe and casing. This analytical procedure is referred to as gap analysis or as semi-circular/semi-elliptical theory.

SUMMARY

Using the material most widely installed for new construction of sanitary sewers in the United States, PVC, this process provides a means to reconstruct sewers without the need for excavation at a fraction of the time associated with open cut replacement. The finished pipe reestablishes the structural integrity of the deteriorating system with a continuous, corrosion resistant pipe that will significantly extend the useful life of the system.

REFERENCES

[1] Uni-Bell PVC Pipe Association, Uni-Bell Handbook of PVC Pipe Design and Construction, Dallas, Texas, 1982

[2] Moser, A. P. and Shupe, O. K., Buried Structures Laboratory, Utah State University, "ASTM Testing of 8-inch Diameter PVC NuPipe", Logan, Utah, 1991

[3] Watkins, Reynold K., Professor, Civil and Environmental Engineering, Utah State University, "Structural Performance of NuPipe", 1989

Neal S. Berke,[1] and Maria C. Hicks[2]

ESTIMATING THE LIFE CYCLE OF REINFORCED CONCRETE DECKS AND MARINE PILES USING LABORATORY DIFFUSION AND CORROSION DATA

REFERENCE: Berke, N. S., and Hicks, M. C. , **"Estimating the Life Cycle of Reinforced Concrete Decks and Marine Piles using Laboratory Diffusion and Corrosion Data,"** Corrosion Forms and Control for Insfrastructure, ASTM STP 1137, Victor Chaker, Ed., American Society for Testing and Materials, Philadelphia, 1992.

ABSTRACT: Chloride induced corrosion is a major cause of the deterioration of steel reinforced concrete structures in marine environments, and in Northern environments where deicing salts are used. The time-to-corrosion initiation and subsequent corrosion induced damage is related to the time that it takes chloride ions to reach a critical level at the steel. In this paper it is demonstrated that chloride ingress into concrete follows Fick's Diffusion equation for properly cured concretes. It is shown how the diffusion coefficients and chloride surface concentrations can be used to predict the chloride profile as a function of time. The effects of concrete mixture proportioning and concrete admixtures on the diffusivity of chloride and chloride corrosion threshold level are shown. The results of several experiments and models developed show that reducing the water-to-cement ratio and increasing concrete cover over the steel greatly reduce the chloride ingress as recommemded by the American Concrete Institute codes. Furthermore, even more dramatic decreases in chloride penetration can be obtained by the use of microsilica in the concrete mixture. It is also shown that calcium nitrite when admixed into the concrete significantly increases the chloride levels at which severe corrosion will occur. The above results are used to estimate the time to corrosion and failure for different types of reinforced concrete structures. These models can be used by a design engineer to estimate the life of reinforced concrete exposed to chloride ingress.

KEYWORDS: Concrete, steel reinforcing, corrosion, chloride diffusion, design, parking garage, deck, marine structure, marine pile

[1] Research Manager, Construction Products Division, W. R. Grace & Co.- Conn., 62 Whittemore Av., Cambridge, MA 02140.

[2] Senior Research Engineer, Construction Products Division, W. R. Grace & Co.Conn., 62 Whittemore Av., Cambridge, MA 02140.

INTRODUCTION

The durability of steel reinforced concrete is affected by several parameters of which chloride ingress is one of the most important. The natural passivity of steel in the alkaline environment provided by concrete is disrupted by chloride ions and the resulting corrosion products can lead to cracking, spalling, delamination and eventual failure of the structure. Several areas of the infrastructure are subjected to severe chloride ingress. These are bridge and parking structures in locations where deicing salts are used to keep the roads open in the winter, and marine structures which are subjected to a daily severe salt exposure. In the absence of chlorides these structures would last many years longer without need for additional corrosion protection.

One means of combating chloride induced corrosion is to decrease the permeability of the concrete to chloride ingress. This is recognized by the American Concrete Institute (ACI) in the Building Code [1] and in its guide for offshore structures [2]. These documents call for a maximum water-to-cement ratio (w/c) of 0.4 and for minimum concrete covers over the steel of 38 mm (1.5 in.) for nonmarine to 64 mm (2.5 in.) in marine environments. Additional ACI documents address the maximum allowed crack sizes which are 0.15 and 0.18 mm (0.006 and 0.007 in.) for marine and deicing salt environments respectively [3]. For crack sizes under 0.2 mm (0.008 in.) the effect on chloride ingress through the cracks is marginal [4]. Thus for concrete produced according to current recommended practices and codes, a model for chloride ingress based upon diffusion through uncracked concrete may be used.

Several investigators have shown that chloride ingress into good quality concrete can be modeled by a diffusion process [5-15] and have come up with estimates of chloride profiles as a function of exposure and time. In this paper diffusion coefficients determined on one to three year old severely exposed laboratory specimens are used to predict chloride levels after five years of severe exposure. In some cases the effective diffusion coefficient is estimated from concrete resistivity or rapid chloride permeability data as measured by AASHTO T277 [16]. It will be shown that the effective diffusion coefficients can be used to predict chloride levels. Based upon these findings several curves estimating chloride profiles as a function of concrete mixture design, geometry, and exposure conditions are produced.

The effects of silica fume (microsilica) and calcium nitrite on the long-term durability of concrete will be discussed within the context of chloride ingress. Chloride ingress data show that microsilica significantly lowers the effective diffusion coefficient. Modeling of long-term severe chloride exposures predicts that even though the permeability is very low, that significant chloride can reach the reinforcing steel. In this paper data are presented that

supports the modeling, and corrosion behavior shows that corrosion will occur. It will be demonstrated that calcium nitrite treated concrete has no adverse effects on the diffusion of chloride and prevents corrosion in the presence of chlorides.

The above findings are used to demonstrate how an engineer can effectively design a reinforced structure for long-term durability to chloride exposures. In particular, the effects of concrete w/c ratio, concrete cover over the reinforcing steel, microsilica content, and calcium nitrite on chloride ingress and subsequent corrosion behavior will be highlighted.

EXPERIMENTAL

In this paper data are given on the chloride content and corrosion rates of reinforced concrete produced for several long-term studies. The concretes were produced with cements meeting ASTM Specification for Portland Cement (C 150) and the coarse aggregates conformed to ASTM Specification for Concrete Aggregates (C 33) Size 67. The fine aggregates were a natural sand which met the requirements of ASTM C 33.

Admixtures used met the requirements of ASTM Specification for Chemical Admixtures for Concrete (C 494) except for microsilica which is not currently governed by an ASTM specification. The microsilica was added as a slurry. Calcium nitrite was added as a nominal 30% by mass solution.

Concrete specimens discussed were in the form of 102 mm x 203 mm (4 in. x 8 in.) cylinders for compressive strength and were cut to be 51 mm (2 in.) thick for the AASHTO T277 method.

Lollipops were produced for resistivity and polarization resistance tests. These specimens were 76 mm x 152 mm (3 x 6 in.) cylinders with an embedded Number 3 reinforcing bar (9.5 mm (3/8 in.) diameter) positioned 38 mm (1.5 in.) from the cylinder bottom and with the top embedded 13 mm (0.5 in.) protected with electroplater's tape to expose 102 mm (4 in.) of bar.

Minidecks were also produced and were 279 mm x 114 mm x 152 mm (11 in. x 4.5 in. x 6 in.) with top and bottom number 4 (13 mm (0.5 in.) diameter) reinforcing bars. The bottom bar was 25 mm (1 in.) from the bottom and the top bars were 19 to 35 mm (0.75 to 1.37 in.) from the top surface. The reinforcing bars were taped with electroplater's tape to expose 178 mm (7 in.) of bar. A 51 mm (2 in.) high plastic dam with inside dimensions of 230 mm x 70 mm (9 in. x 2.75 in.) was caulked to the top. The four sides of the sample and top surface outside of the dam were coated with a concrete epoxy. Ground clamps were used to attach a 100 Ω resistor between the top and bottom bar.

TEST METHODS

Rapid chloride permeability tests were conducted in accordance with the AASHTO T277 test method on samples cut from 102 mm x 203 mm (4 in. x 8 in.) cylinders. The data shown in this paper were first reported by Berke and Roberts in 1989 [17].

Electrochemical tests were used to determine concrete resistivity and corrosion rates as a function of time. Concrete resistivities were determined at 20 kHz. Each cylinder was submerged in a 3% NaCl solution to within 25 mm (1 in.) of the top surface, in order to provide a high conductivity environment and to minimize resistance drops outside of the concrete. The technique is explained in greater detail in references 18 and 19.

Corrosion rate measurements consisted of polarization resistance (with IR interruption) on the lollipop specimens and macrocell corrosion on the minidecks. Both methods have been successfully used to measure corrosion rates of steel in concrete [6-9,15,17-25]. Both techniques as used in this work are described in detail in references 17 and 25.

Chloride analyses were performed using the method outlined in the Florida DOT Research Report 203 PB 289620 [27]. Powder from dry drilling with a 13 mm (0.5 in.) bit was collected and crushed to pass a 300 μm sieve (No. 50). The powder was then digested with a boiling solution of 10% by volume nitric acid, filtered, and the chloride content analyzed using the silver nitrate titration method.

DETERMINATION OF CHLORIDE DIFFUSION COEFFICIENTS

Before one discusses the results of new data presented in this paper and models predicting the service life of several structures exposed to chloride ingress, a brief description of how effective chloride diffusion coefficients (D_{eff}) were determined is in order. The exact rate of chloride diffusion through concrete cannot be determined due to the heterogeneous nature of concrete and the differences between concreting materials. However, a reasonable approximation can be obtained and can be used to estimate the ingress of chloride as a function of time, depth and environment. D_{eff} values can be determined for various concrete mixture designs by analyzing chloride contents in laboratory and field concretes as a function of time and depth. Similar mixture designs would be expected to have approximately the same D_{eff} values. Furthermore, in this paper data will be presented that indicate that a determination of concrete resistivity and/or rapid chloride permeability can be used to provide a reasonable estimate of D_{eff}.

Chloride data from numerous laboratory and field studies [7-9] were analyzed using a nonlinear regression analysis technique available on a mainframe computer with SAS [26]. The model used was Fick's diffusion equation for a semi-infinite slab:

$$C=C_o \{1-erf[x/(2\sqrt{(D_{eff} \cdot t)})]\} \quad (1)$$

Where C is the concentration at depth x and time t, D_{eff} is the effective diffusion coefficient and C_o is the surface concentration. The program solves for C_o and D_{eff} with no assumptions other than that Fick's Law is applicable.

This model has been used by others [11,12] and was shown to fit our data well [7-9]. D_{eff} values determined previously as well as newer coefficients based upon additional work will be given later.

The above diffusion coefficients were determined on concretes exposed to constant temperatures of 22°C (72°F). Assuming that the diffusion is an exponential function of the temperature, a change in temperature of 10 °C will affect the coefficient by a factor of 2.33. This is a reasonable approximation, since $D=D_o e^{-Q/RT}$ for solids, where D_o is essentially constant over a wide temperature range and Q is an activation energy [28].

Once D_{eff} is known, it is possible to use Fick's Law to develop a chloride profile for a given surface concentration and exposure time. In this paper an average yearly temperature is used for the selection of D_{eff} based upon the mixture design and correlation found between diffusion and bulk concrete resistivity and AASHTO T277 rapid chloride permeability. It should be noted that specimens that were ponded for chloride analysis were moist cured for 28 days and as such concretes with less curing might not be as impermeable at the same mixture design. Determination of the resistivity or rapid chloride permeability on specimens with the same cure as the exposed concrete could provide a better indication of D_{eff}. Also of note is that ionic admixtures such as calcium nitrite can change the correlation between D_{eff} and resistivity or rapid chloride permeability. This is addressed below and a relationship for use with calcium nitrite is provided.

Three models based upon Fick's Law and using D_{eff} values as determined above are used in this paper to predict long-term chloride ingress. The first model is the straightforward one-dimensional model in which the surface is quickly saturated to a constant chloride concentration. This is used for minideck laboratory specimens which are severely exposed and can be used for sea walls. The second model is also one dimensional but realizes as

pointed out in reference 7 that the pseudo surface chloride surface concentration increases in time until it levels off at a constant value. Based upon numerous test specimens and severe field exposures we have found this value to be approximately 17.8 kg/m^3 (30 lb/yd^3). Higher chloride analysis values are only found after severe cracking and spalling has occurred and salt has filled the cracks.

The third model is two-dimensional in nature and is used to predict the ingress along the diagonal of a square pile. This gives much more ingress than the one-dimensional model. For typical piles the center of a face would essentially be the one-dimensional model. Since the splash-tidal zone is subjected to the most severe exposure, a value of 17.8 kg/m^3 (30 lb/yd^3) is used for the surface concentration.

It will be shown that the two-dimensional model can be used to provide a reasonable approximation for ingress into a cylinder. A cylindrical model requires the use of spherical Bessel functions and is difficult to use. A cylinder was approximated by averaging the chloride contents at a given depth from a square piles, with a side equal in length to the cylinder diameter.

RELATIONSHIPS BETWEEN RESISTIVITY, RAPID CHLORIDE PERMEABILITY, AND DIFFUSIVITY AND THEIR EFFECT ON CORROSION

Development of Equations Relating Resistivity, Rapid Chloride Permeability and Diffusivity

As can be surmised, determination of diffusion coefficients by measuring chloride concentration profiles in concrete is a time-consuming process in that it requires long-term chloride exposures and sample analysis. It is therefore of interest to determine whether the diffusion coefficient can be estimated more readily. Two parameters that can be measured easily are the rapid chloride permeability and the resistivity. These parameters are frequently used in quality control and as such might be related to the diffusivity of the concrete.

The rapid chloride permeability is frequently included in the concrete specifications for a construction project. The resistivity of concrete is an electrochemical parameter which is measured in the course of monitoring the corrosion behavior of concrete samples with embedded reinforcing bars.

Resistivity data are shown in Table 1 together with diffusion coefficients calculated from chloride concentrations using Eq.(1). The relationship between the resistivity and diffusion coefficient is seen in Figure 1, which also shows that the correlation between the two parameters is affected by the pres-

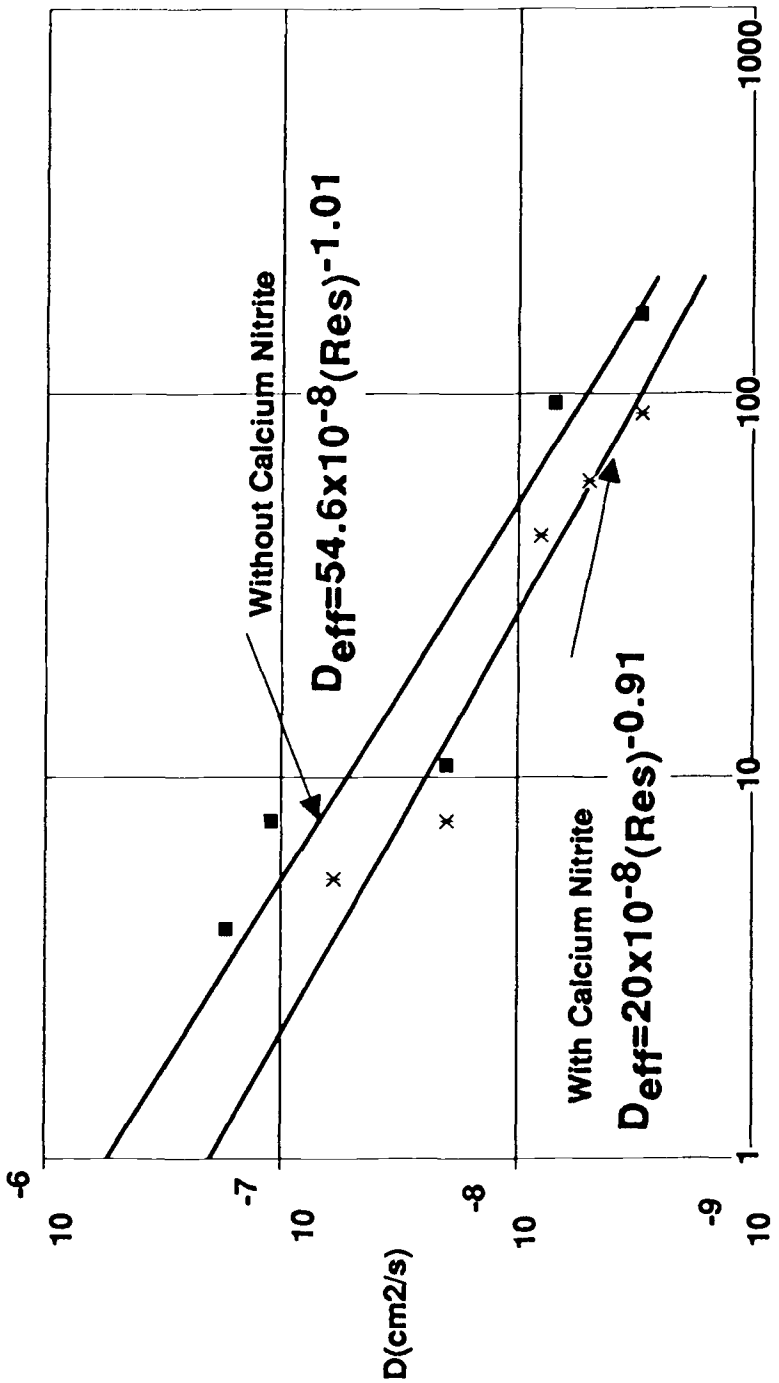

FIG. 1–Variation of the diffusion coefficient with resistivity

ence of calcium nitrite in the concrete. This is to be expected as the presence of conductive additives decrease the resistivity whereas these additives do not adversely affect the diffusion coefficient.

TABLE 1-- Chloride diffusion coefcients for concrete samples ponded in 3% NaCl for two years.

Mix	Cement (kg/m3)	%CSF	30% $Ca(NO_2)_2$ (l/m3)	W/C	AASHTO T277 Coulombs	D_{eff} (10-8 cm2/s)	ρ (kohm•cm)
1	347	0	0	0.48	3663	11	7.7
2	343	0	20	0.48	4220	6	5.4
5	350	15	0	0.48	198	0.7	94.7
6	359	15	20	0.48	253	0.5	59.3
11	363	7.5	10	0.43	308	0.8	42.6
13	338	0	0	0.38	3485	2.0	10.8
14	352	0	20	0.38	1838	2.0	7.7
17	354	15	0	0.38	75	0.3	161
18	343	15	20	0.38	119	0.3	88.6
...	348	0	0	0.46	...	17	4.0

It is important to note that the resistivity data are the values taken before significant corrosion has occurred. Once the rebars are corroding, the resistivity values can be affected by the corrosion process, and can no longer be expected to reflect the permeability of the concrete.

The data yielded the following correlations between the effective diffusion coefficient and the resistivity:

No calcium nitrite

$$D_{eff} = 54.6 \cdot 10^{-8}(\text{Resistivity})^{-1.01} \qquad r^2=0.95 \qquad (2)$$

With calcium nitrite

$$D_{eff} = 20.0 \cdot 10^{-8}(\text{Resistivity})^{-0.91} \qquad r^2=0.97 \qquad (3)$$

Where the resistivity is given in kohm•cm, and D_{eff} is given in cm^2/s.

It has previously been shown that the resistivity is related to the permeability of the concrete [17]. This relationship is shown in Figure 2 and can be expressed by the following correlation:

$$\text{Resistivity} = 4887\ (\text{Rapid Permeability})^{-0.832} \qquad r^2=0.97 \qquad (4)$$

Where resistivity is once again in kohm•cm, and the rapid permeability is in coulombs as determined by AASHTO T277.

Data for permeabilities above 2000 Coulombs were not included in the correlation because at these high currents the resistance heating of the concrete becomes significant, and the specimen can no longer be assumed to be at ambient temperature. The current increases and the resistivity decreases with increasing temperature, thus giving a higher value for the permeability.

Equations (2) to (4) can be used to derive correlations between the effective diffusion coefficient and the rapid chloride permeability:

No calcium nitrite

$$D_{eff} = 0.0103 \cdot 10^{-8}(\text{Rapid Permeability})^{0.84} \qquad (5)$$

With calcium nitrite

$$D_{eff} = 0.0088 \cdot 10^{-8}\ (\text{Rapid Permeability})^{0.76} \qquad (6)$$

The few permeability data available (Table 1) are shown plotted in Figure 3, and give an indication of the accuracy with which the above correlations can predict diffusion coefficients from permeabilities.

In observing Figure 3, it is seen that the correlations show that calcium nitrite specimens have lower diffusion coefficients at the same rapid permeability values. Thus, even though calcium nitrite might reduce resistivity or increase the rapid permeability value of a given concrete, it does not increase the rate of chloride ingress.

Variation of Diffusivity with Time

Chloride concentration profiles for the concrete minidecks were measured after two and three years of exposure. The diffusivities calculated using Eq. 1 are shown in Table 1 (for two years) and Table 2 (for three years) and show little change.

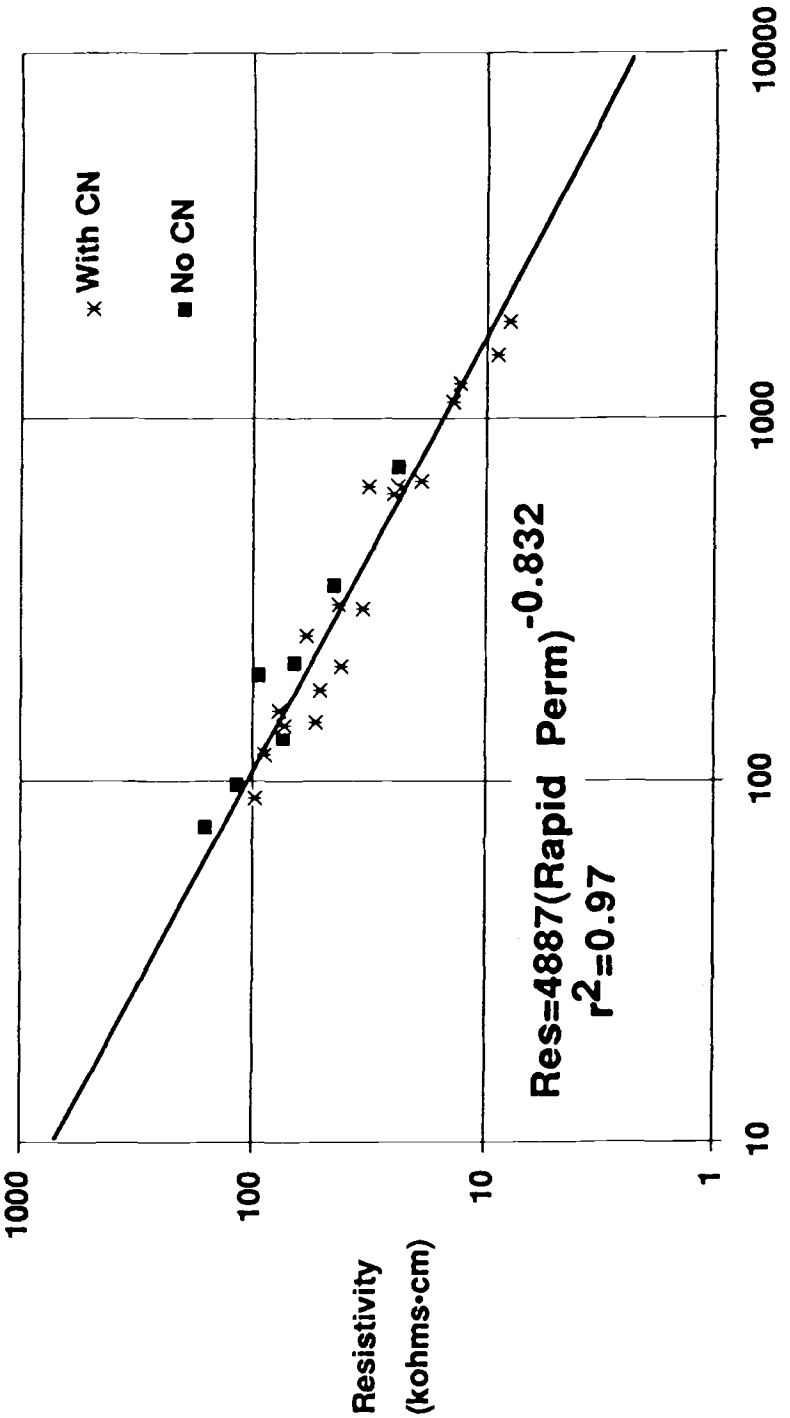

FIG. 2–Variation of the resistivity with rapid permeability

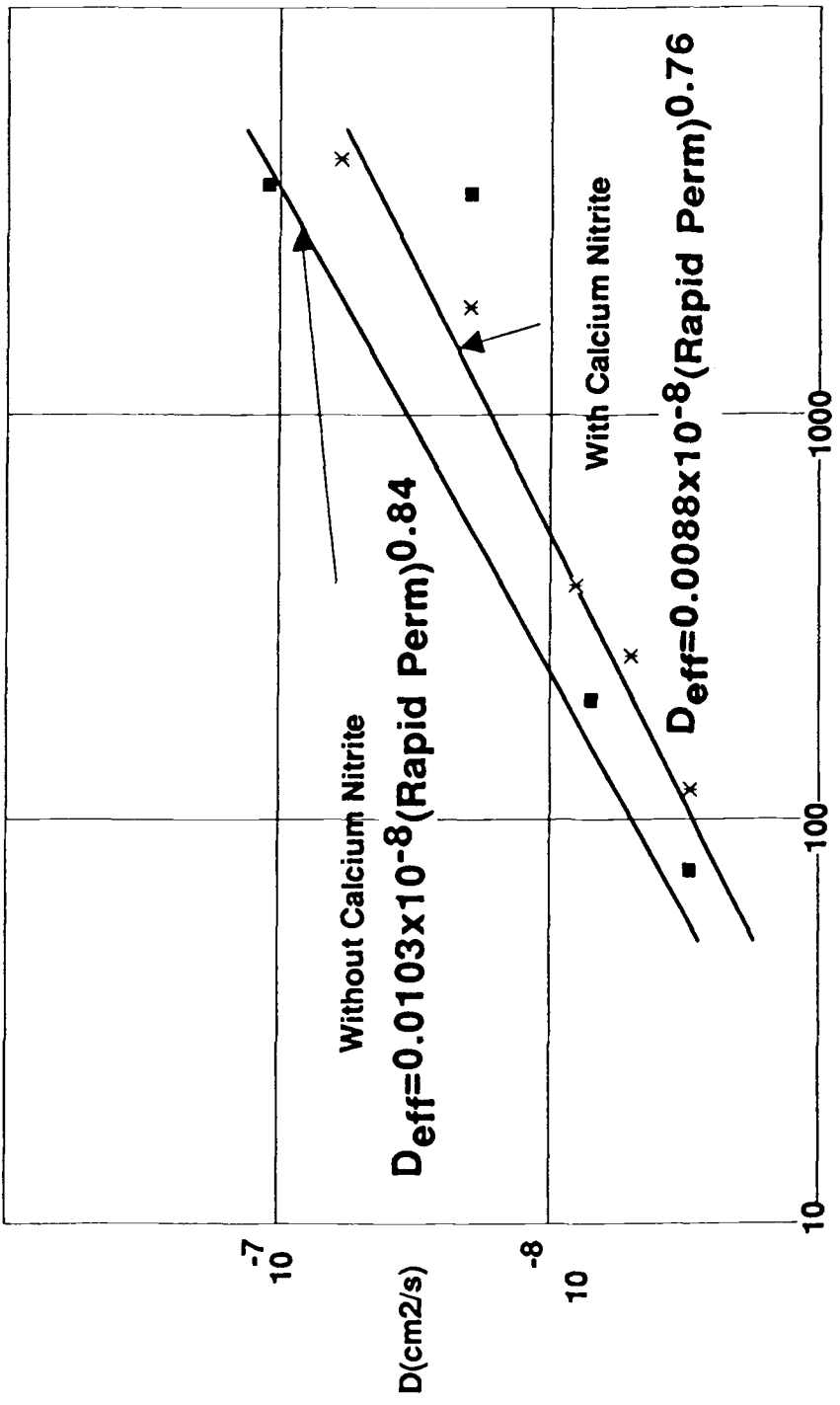

FIG.3—Dependence of the diffusion coefficient on rapid permeability

TABLE 2--Chloride diffusion coefficients for concrete samples ponded in 3% NaCl for three years.

Mix	Cement (kg/m3)	%CSF	30% $Ca(NO_2)_2$ (l/m3)	W/C	AASHTO T277 Coulombs	D_{eff} (*10-8 cm2/s)
1	347	0	0	0.48	3663	11
5	350	15	0	0.48	119	0.6
11	363	7.5	10	0.43	380	0.6
13	338	0	0	0.38	3485	3.2
18	343	15	20	0.38	119	0.3

Comparison of Calculated and Actual Chloride Values

The same concrete mixtures were used to prepare lollipops that have now been exposed to chloride solutions for five years. In this case, chloride concentrations were measured in one location (between 13 mm and 33 mm (0.5 in. and 1.3 in.)) only. The diffusion model was applied to determine the accuracy with which the chloride concentration after five years can be predicted using diffusion coefficients determined after two years (from concentration profiles) and from resistivity and permeability data.

This was done using a two dimensional model for cylindrical specimens (76 mm x 152 mm (3 in. x 6 in.)) in which chloride concentrations were calculated assuming equivalence with a square pile with a side equal to the cylinder diameter (76 mm (3 in.)).

The calculated and measured chloride concentrations are given in Table 3. The agreement between the predicted and measured data, is remarkably good.

TABLE 3--Chloride concentrations of 76 mm x 152 mm cylindrical samples at depths between 1.3 and 3.3 cm (specimens ponded for 5 years).

W/C	%CSF	Measured Cl^- (kg/m^{3*})	Calculated Cl^- (kg/m^{3*})
0.48	3.75	11.0	14.6
0.38	0	10.1	11.6
0.38	3.75	7.3	12.0
0.48	7.5	6.7	7.9

* To convert to lb/yd^3 multiply by 1.7

Of interest here is that silica fume decreases permeability and slows down chloride ingress but eventually the chloride reaches the reinforcing bars and corrosion takes place. Note that it takes about 0.9-1 kg/m^3 (1.5-2 lb/yd^3) chloride for corrosion initiation and at 3 kg/m^3 (5 lb/yd^3) cracking and staining occurs.

Measured and calculated chloride concentrations were similarly done for the minidecks. The data are given in Table 4. Equation (1) was used for the determination of C, with C_o = 18 kg/m^3 (30 lb/yd^3) or 12.5 kg/m^3 (21 lb/yd^3) as found for the specimens at w/c = 0.46 [10]. Here the agreement of calculated and measured values for samples containing calcium nitrite is poor, probably due to the fact that the nitrite specimens had reduced permeabilities, even more so than calculated. Nevertheless, equation 3 relating diffusivity to resistivity might have a built in safety factor.

Corrosion Results

Some researchers believe that corrosion in not possible at high concrete resistivities [29]. Recent studies show that even in low permeability, high resistivity concrete, the embedded reinforcing steel goes into corrosion after 5 years of accelerated laboratory testing [30] (controls without microsilica failed within two years). The long-term data showed that calcium nitrite significantly improved the corrosion resistance of steel in concrete containing microsilica. This occurred even though rapid chloride permeability values were almost doubled and initial resistivities were almost a factor of two lower.

Figure 4 shows new corrosion data for minidecks with 0.46 w/c ponded for 5 years. The chloride data for these specimens are given in Table 4, and clearly show that chloride levels are well beyond normal threshold values of 0.9 to 1 kg/m^3. The total corrosion is the integrated macrocell current measured with time. The specimens without calcium nitrite were severely corroding within one year. Here the beneficial effect of the calcium nitrite addition can clearly be seen as with over a four-fold increase in performance even at concrete covers below those recommended.

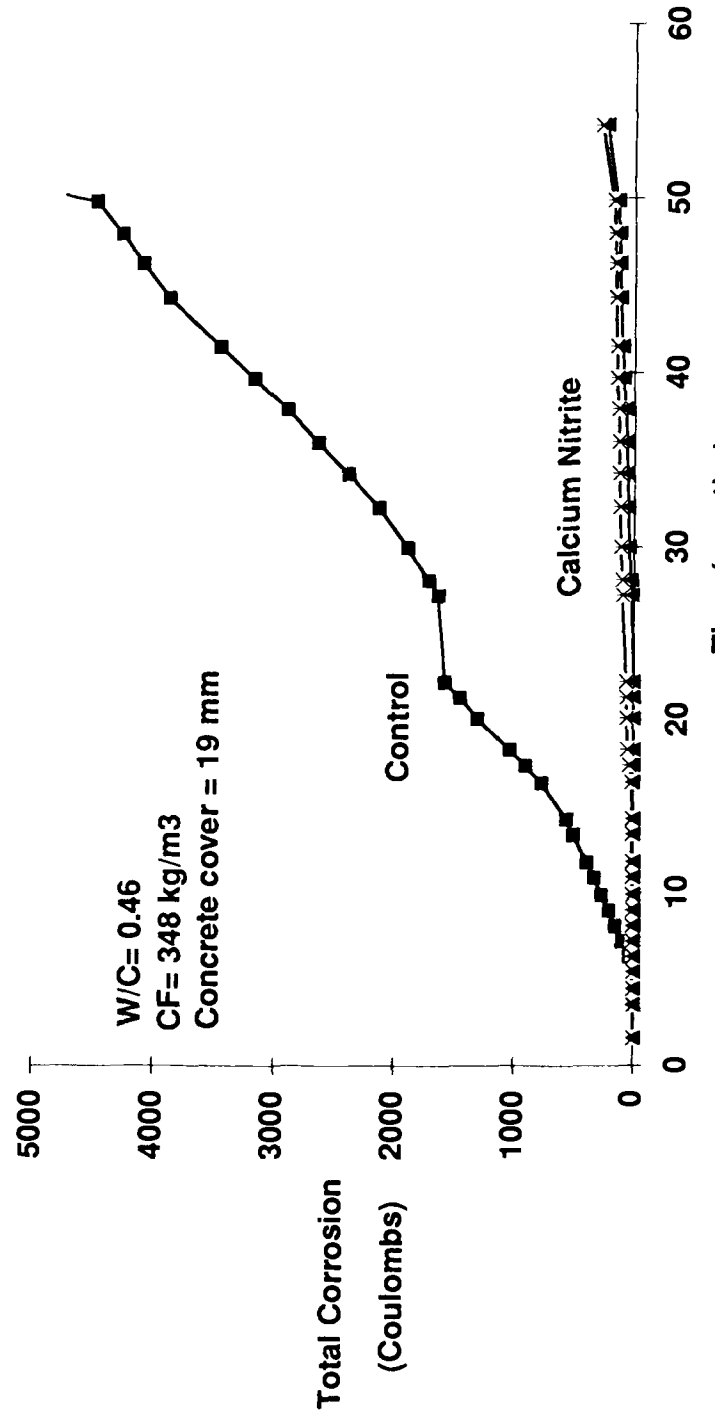

FIG. 4--Minideck corrosion vs. time

TABLE 4--Chloride concentration at the rebar level of minidecks (279 mm x 114 mm x 152 mm) (5 year samples).

W/C	Depth (mm)	30% $Ca(NO_2)_2$ (l/m^3)	D_{eff} ($*10^{-8}cm^2/s$)	Measured Cl^- (kg/m^3)	Calculated Cl^- using Eq.(1) (kg/m^3)
0.48	35	0	11	9.8	9.8
0.46	19	0	17	17.2	10.0
0.46	19	10	5.7*	5.8	8.2
0.46	19	20	5.7*	7.8	8.2
0.46	35	0	17	4.4	7.9
0.46	35	10	5.7*	1.6	5.1
0.46	35	20	5.7*	1.4	5.1

*Calculated from equation 3 relating diffusion coefficient to resistivity.

Improved benefits of increasing cover to 35 mm (1.4 in.) are seen in Figure 5 in which case the control specimens started to corrode at 18 months and the specimens with calcium nitrite are not corroding after 5 years.

PRACTICAL APPLICATIONS

Because there is a well-established relationship between permeability and concrete quality, the diffusion coefficients can be calculated for any specific concrete of interest. The diffusion coefficient must be corrected for the yearly average temperature prevailing at the proposed site, and then may be used to predict chloride profiles as a function of time. The examples given below are based upon estimates of chloride diffusivity calculated and extrapolated from laboratory and field data. Local materials, workmanship, curing conditions and structural history (e.g., dynamic loads, one time events such as earthquakes) can affect the chloride ingress. These examples are thus a useful prediction guide, and obviously do not give the exact values of chloride at the reinforcement at a given time.

Parking Garage

The first example is a parking garage with a design life of 40 years situated in an area where the average temperature is 10 C (50 F) and the local roads have heavy applications of deicing salts. This is comparable to the case of a slab where chloride ingress is one-dimensional. Estimated chloride concentrations at various depths for concrete with W/C=0.4 over a period of time are given in Figure 6. Assuming a 38 mm (1.5 in.) concrete cover over the re-

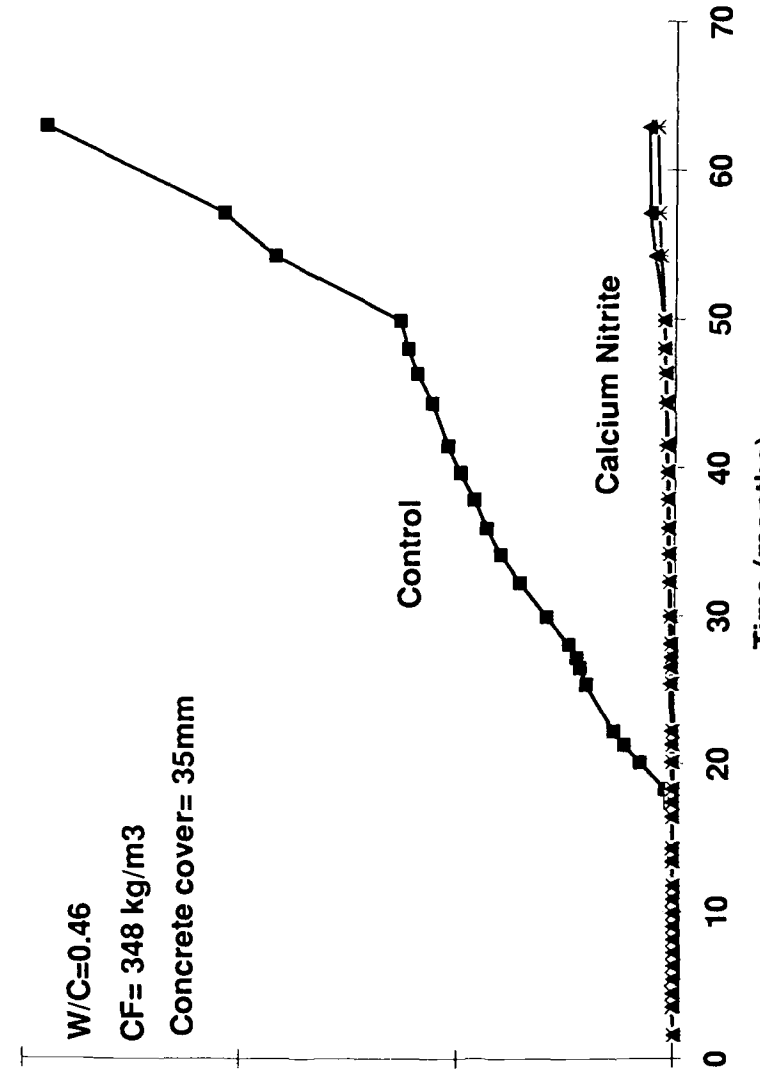

FIG. 5--Minideck corrosion vs. time

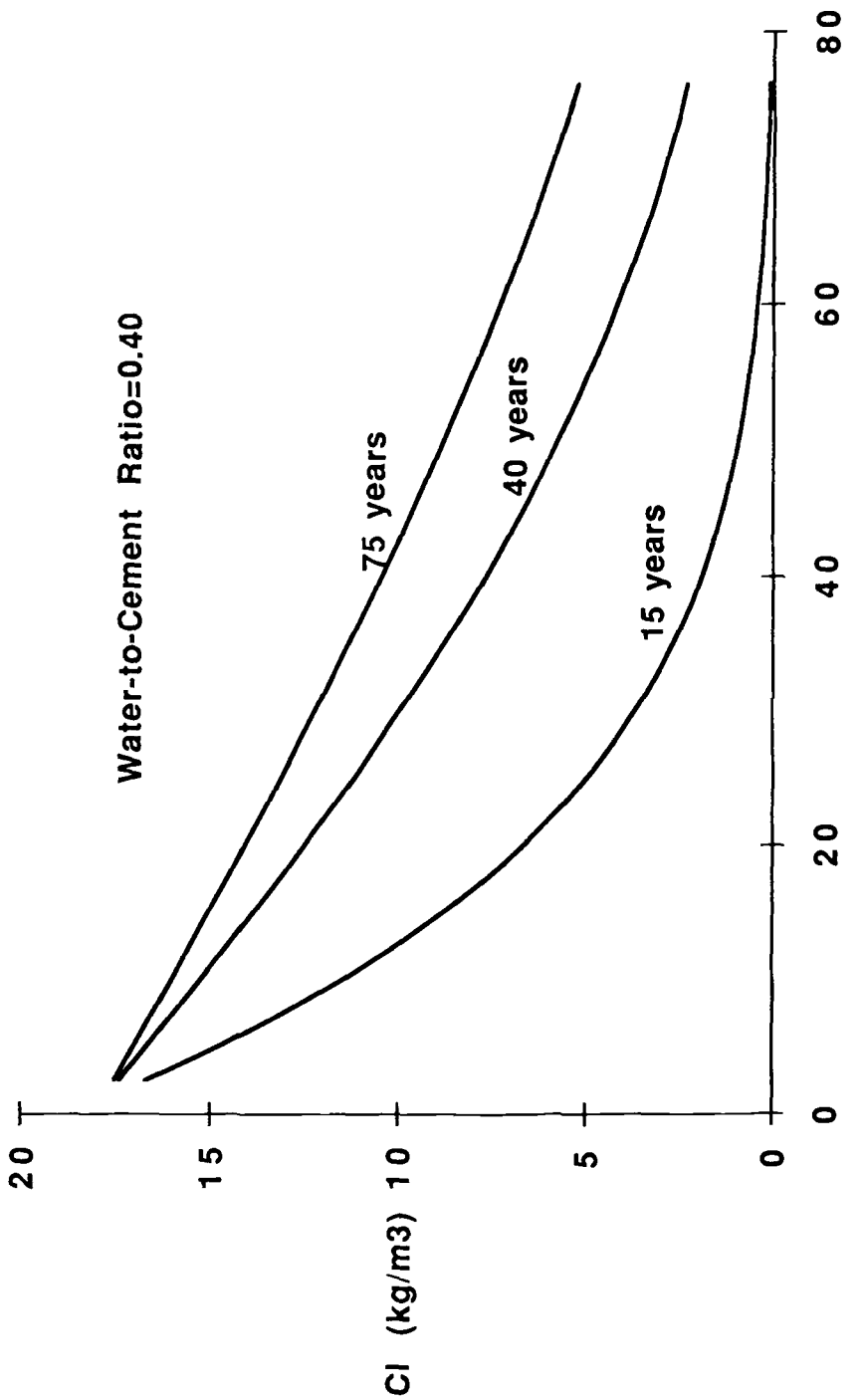

FIG. 6--Estimated parking deck chloride profiles (10°C)

inforcement, the amount of chloride at the bar after 40 years is estimated to be about 7.7 kg/m^3 (13 pcy). Using better quality concrete (Figure 7), for example adding 30 kg/m^3 (50 pcy) microsilica, will lower the chloride concentrations to a level of 4 kg/m^3 (7 pcy).

The unprotected structure would have to be repaired after 15 years whereas the addition of microsilica would considerably extend the life of the structure. The corrosion data presented show that the addition of calcium nitrite would further improve the corrosion resistance of the structure for both concretes. As can be seen in Table 5, approximately 10 l/m^3 (2 gal/yd^3) of 30% calcium nitrite solution would provide for the 40 year design life with microsilica, and 20 l/m^3 (4 gal.yd^3) would protect the structure without microsilica [7].

TABLE 5--Calcium nitrite dosage rates vs. chloride protection.

Calcium Nitrite (30% solution) l/m3 (gal/yd3)	Chlorides kg/m3 (lb/yd3)
10 (2)	3.6 (6.0)
15 (3)	5.9 (9.9)
20 (4)	7.7 (13)
25 (5)	8.9 (15)
30 (6)	9.5 (16)

Square Pile in a Marine Environment

Consider a square pile with a side dimension of 356 mm (14 in.) exposed to a marine environment where the yearly average temperature is 18 °C (65 °F). The chloride concentration profiles along the diagonal after 50 years are represented in Figure 8 for three types of concrete. Assuming a design concrete cover of between 64 mm and 76 mm (2.5 and 3 in) was specified, chloride concentrations could be halved by the addition of 30 kg/cm^3 (50 pcy) microsilica (600 Coulombs concrete).

At 76 mm (3 in.) the chloride contents are 10.2 kg/m^3 (17.1 lb/yd^3) for a 0.4 w/c concrete, 7.5 kg/m^3 (12.6 lb/yd^3) for a 1000 coulomb concrete and 5.1 kg/m^3 (8.6 lb.yd^3) for concrete having a rapid chloride permeability value of 600 coulombs. Using Table 5, for a 50 year design life, the 0.4 w/c concrete could just make it with about 30 l/m^3 (6 gal/yd^3) of 30% calcium nitrite, whereas the 1000 coulomb concrete would need 20 l/m^3 (4 gal/yd^3), and the 600 coulomb concrete would need 12.5 to 15 l/m^3 (2.5 to 3 gal/yd^3) [7]. Thus, once

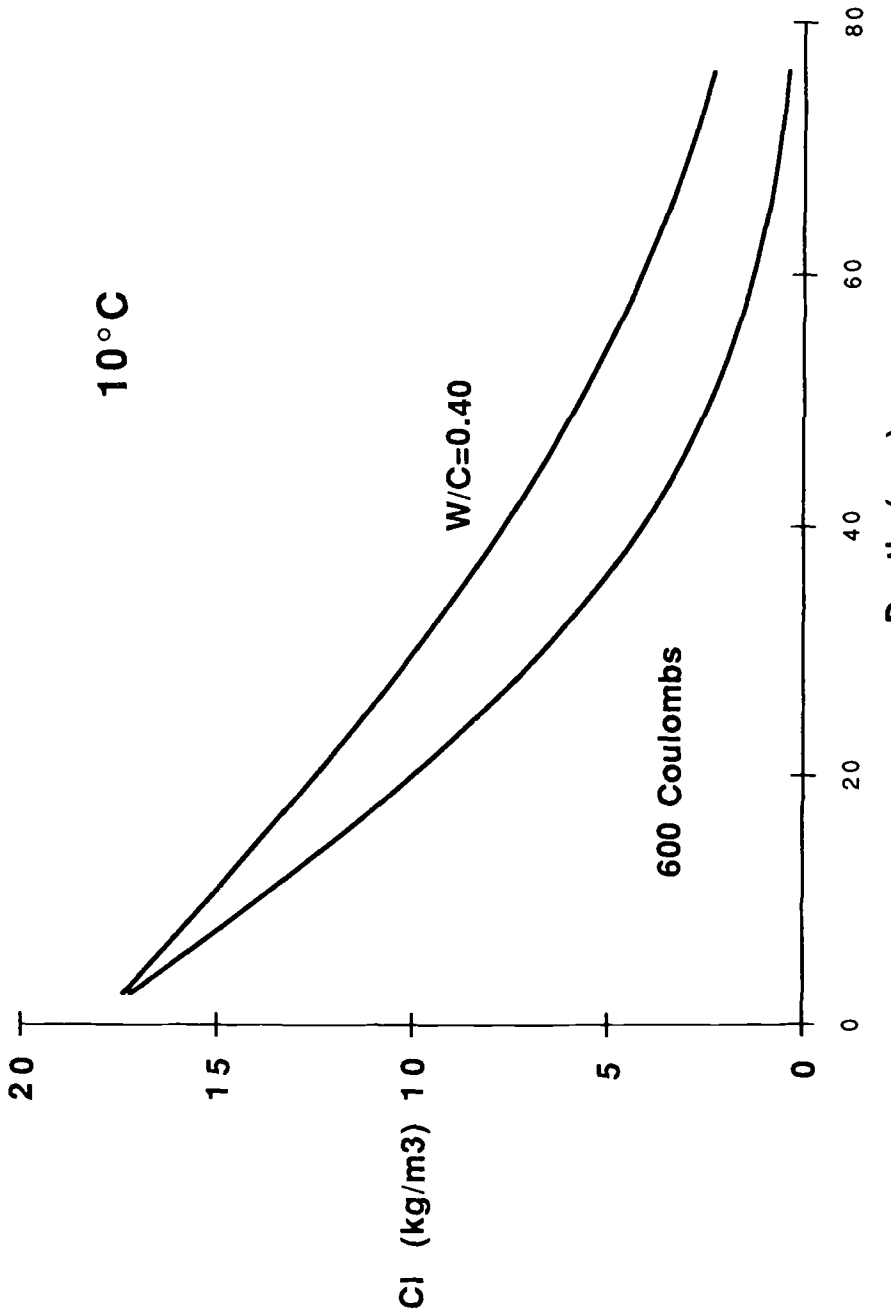

FIG. 7--Estimated parking deck chloride profiles at 40 years

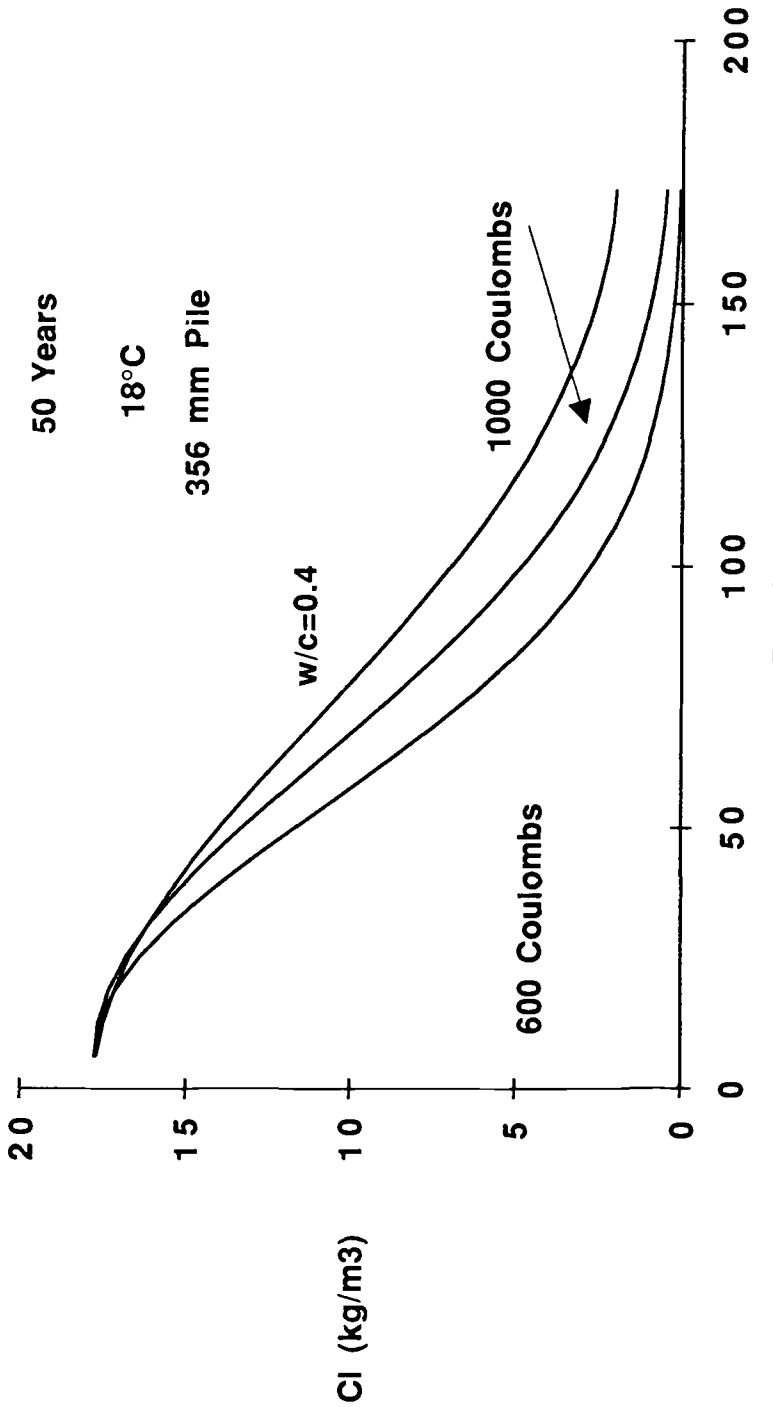

FIG. 8--Square pile profiles at the splash/tidal zone

again it is seen how calcium nitrite with low permeability concrete can provide long-term protection in a severe exposure in which the low permeability concrete alone would not be sufficient to meet the design life.

Sea Wall

Consider a sea wall where chloride enters the concrete structure from one direction and where the average temperature is at 18°C (65°F) as used in the square pile example. In the splash tidal zone the chloride surface concentration would quickly reach the 18 kg/m^3 (30 lb/yd^3) as in the pile case. The chloride concentration profiles after 50 years, for similar concretes as discussed in the square pile example, are given in Figure 9.

Assuming a design concrete cover of between 64 mm and 76 mm (2.5 in. to 3 in.) was specified, chloride concentrations could be halved by the addition of 30 kg/m^3 (50 lb/yd^3) of microsilica (estimated to provide 600 coulomb concrete). At 76 mm (3 in.) the chloride contents are 6.2 kg/m^3 (10.5 lb/yd^3), for a 0.4 w/c concrete, 4.2 kg/m^3 (7 lb/yd^3) for a 1000 coulomb concrete and 2.8 kg/m^3 (4.7 lb/yd^3) for a 600 coulomb concrete. Table 5 shows for a 50 year design life, the 0.4 w/c concrete could be protected with 15 l/m^3 (3 gal/yd^3) of 30% calcium nitrite, whereas the 1000 coulomb concrete would need 12.5 l/m^3 (2.5 gal/yd^3) and the 600 coulomb concrete would need 10 l/m^3 (2 gal/yd^3) [7].

Comparing the sea wall to the square pile structures (Figures 8 and 9), it is seen that the latter is a more severe chloride ingress situation. In both cases the benefits of adding calcium nitrite and/or microsilica are apparent.

CONCLUSIONS

1. Diffusion coefficients estimated from resistivity or permeability data can be useful in estimating the design life of a concrete structure.

2. Silica fume and calcium nitrite significantly improve the durability of structures subjected to severe chloride environments.

3. Silica fume does not prevent corrosion once sufficient chloride has reached the steel reinforcing

4. Calcium nitrite initially reduces resistivity and increases rapid chloride permeability values in concrete with silica fume, but this has no adverse effect on actual concrete permeability and improves the durability of concrete in corrosive environments.

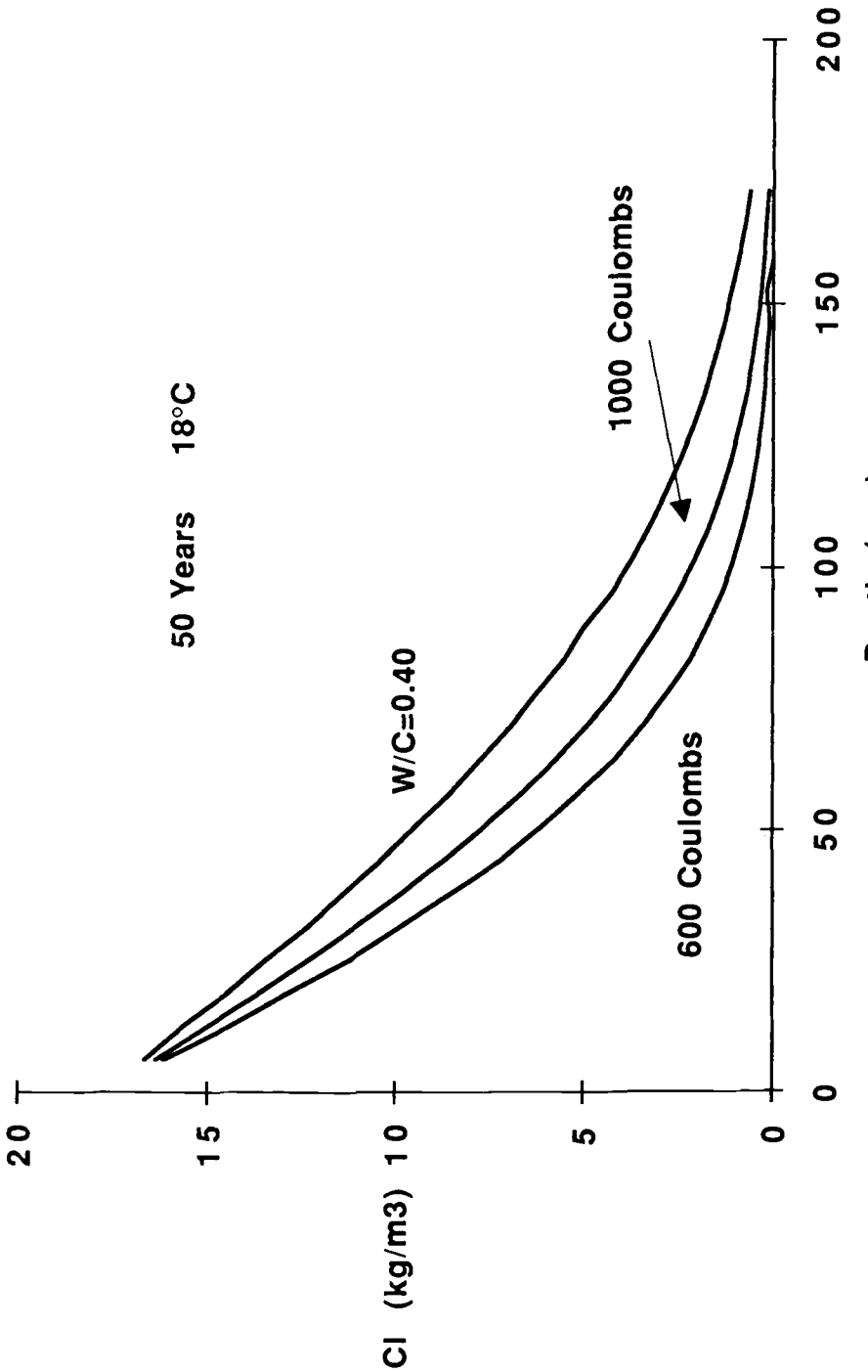

FIG. 9--Sea wall profiles at the splash/tidal zone

ACKNOWLEDGEMENT

We thank S. Y. Lee and D. Myers for writing the computer programs necessary for determining diffusion coefficients and diffusion profiles.

REFERENCES

1] ACI 318 "Building Code Requirements for Reinforced Concrete", 1989.

2] ACI 357, "Guide for the Design and Construction of Fixed Offshore Concrete Structures", American Concrete Institute, 1982.

3] ACI 224R-89, "Control of Cracking in Concrete Structures".

4] Mangat, P.S., and Gurusamy, K., Cement & Concrete Research, Vol. 17, p. 385-396, 1987.

5] Browne, R.D., "Design Prediction of the Life for Reinforced Concrete in Marine and Other Chloride Environments," Durability of Building Materials, V. 1, pp. 113-125 (1982).

6] Tuutti, K., "Corrosion of Steel in Concrete", Swedish Cement and Concrete Research Institute, pp. 469, Stockholm, 1982.

7] Berke, N.S., Pfeifer, D.W. and Weil, T.G., "Protection Against Chloride-Induced Corrosion", Concrete International, Vol. 10, No. 12, pp. 45-55, 1988.

8] Berke, N.S., Sundberg, K.M. and Shen, D.F., "Comparison of the Polarization Resistance Technique to the Macrocell Corrosion Technique," ASTM STP-1065, Corrosion Rates of Steel in Concrete," N.S. Berke, V. Chaker and D. Whiting eds., 1990.

9] Berke, N.S., "Resistance of Microsilica Concrete to Steel Corrosion, Erosion and Chemical Attack," in Fly Ash, Silica Fume, Slag and Natural Pozzolans in Concrete, Proceedings Third International Conference, Trondheim, Norway, SP-114, ed. Malhotra, V.M., American Concrete Institute, Detroit, p. 861, 1989.

0] Hansson, C.M. and Berke, N.S., "Chloride in Concrete", MRS Symposium Proceedings, Pore Structure and Permeability of Cementitious Materials, L.R. Roberts and J.P. Skalny eds., Vol. 137, pp. 253-270, November 1988.

1] West, R.R. and Hime, W.G., NACE Corrosion/85, Paper No. 256, National Association of Corrosion Engineers, Houston, 1985.

2] Weyers, R. and Cady, P., Concrete International, p. 15, January 1987.

3] Dhir, R.K. Jones, M.R. and Ahmed, H.E.H, Magazine of Concrete Research, Vol. 43, No. 154, pp. 37-44, March 1991.

4] Uji, K., Matsuokas Y. and Maruya, T., "Formulation of an Equation for Surface Chloride Content of Concrete Due to Permeation of Chloride" Corrosion of Reinforcement in Concrete, C.L. Page, K.W.J. Treadaway and P.B. Bamforth editors, pp. 258-267, May 1990.

[15] Berke, N.S. and Sundberg, K.M., "The Effects of Calcium Nitrite and Microsilica Admixtures on the Corrosion Resistance of Steel in Concrete", SP 122, P. Klieger Symposium, pp. 265-280, 1990.

[16] AASHTO T277-83, "Rapid Determination of the Chloride Permeability of Concrete," Standard Specification for Transportation Materials and Methods of Sampling and Testing, Vol. II, American Association of State Highway and Transportation Officials, Washington D.C., August 1986.

[17] Berke, N.S. and Roberts, L.R., "The use of Concrete Admixtures to Provide Long-Term Durability," Proceedings, Third CANMET/ACI International Conference on Superplasticizers and Other Chemical Admixtures in Concrete, Ottawa, Canada, October 4-6, 1989, ACI SP 119, 1989 (Ed. V.M. Malhotra) p. 383.

[18] Berke, N.S., Shen, D.F. and Sundberg, K.M., "Comparison of Current Interrupt and Electrochemical Impedance Techniques in the Determination of the Corrosion rates of Steel in Concrete," presented at the ASTM Symposium on Corrosion Rates of Steel in Concrete, Baltimore MD, June 29, 1988.

[19] Berke, N.S., "Corrosion Rates of Steel in Concrete," ASTM Standardization News, March, pp. 57-61 (1986).

[20] Pfeifer, D.W. and Landgren, J.R. "Protective Systems for New Prestressed and Substructure Concrete", Report No. FHWA/RP-86/193, Federal Highway Administration, Washington DC, April 1987, p. 113.

[21] Virmani, Y.P., Clear, K.C. and Pasko, T.J., "Time-to-Corrosion of Reinforcing Steel in Concrete Slabs, Vol. 5 - Calcium Nitrite Admixture and Epoxy-Coated Reinforcing Bars as Corrosion Protection Systems" Report No. FHWA/RD-83/012, Federal Highway Administration, Washington DC, September 1983, p. 71.

[22] Berke, N.S. and Sundberg, K.M., "The Effects of Admixtures and Concrete Mix Designs on Long-Term Concrete Durability in Chloride Environments", Paper No. 386, NACE CORROSION/89, April 1989, NACE, HOUSTON.

[23] Dawson, J.L., Callow, L.W., Hardky, K. and Richardson, J.A., "Electrochemical Impedance Measurements Applied to the Corrosion of Reinforcing Steel in Concrete," NACE CORROSION/78 Paper No. 125, NACE, Houston 1978.

[24] Gonzalez, J.A., Molina, A., Esadero, M. and Andrade, M.C., "A Comparison of Linear Polarization and A. C. Impedance in the Determination of Corrosion Rates of Reinforcement Embedded in Concrete," NACE CORROSION/85, Paper No. 257, NACE, Houston 1985.

[25] Gonzalez, J.A., Alyaba, S. and Andrade, C., Br. Corrosion J., Vol. 15, p. 135 (1980).

[26] Dawson, J.L., "Corrosion Monitoring of Steel in Concrete," Corrosion of Reinforcement in Concrete Construction, A.P. Crane, ed., Ellis Horwood LTD., London, England, p. 175, 1983.

[27] Kessler, R.J., "An Interlaboratory Study of the Test Method for Determining Low-levels of Chloride in Concrete and Raw Materials," Florida Department of Transportation, Bureau of Materials Research, FL/DOT/BMR-82/253, April 1982.

[28] Berke, N.S. and Hicks, M.C. "Electrochemical Methods of Determining the Corrosivity of Steel in Concrete," ASTM G-1 50th Anniversary Volume, ASTM STP-1000, R. Baboian and S.N.W. Dean, eds., American Society for Testing and Materials, Philadelphia, 1990 pp. 425-440.

[29] SAS Institute Inc., Cary, North Carolina

[30] Geiger, A.H. and Poirier, D.R., Transport Phenomena in Metallugy, Addison-Wesley, Reading, MA, 1973 p. 445.

[31] Hope, B.B., Ip, A.K., and Manning, D.A., "Corrosion and Electrical Impedance in Concrete", Cement and Concrete Research, Vol. 15, 1985, p.523.

[32] Berke, N.S., Dallaire, M.P. and Hicks, M.C., "Plastic, Mechanical, Corrosion and Chemical Resistance Properties of Microsilica Concretes", to be presented at the 4th CANMET-ACI International Conference on Fly Ash, Silica Fume, Slag and Natural Pozzolans in Concrete, Istanbul, Turkey, May 3-8, 1992.

Miki Funahashi, Kuan-Foung Fong, and N. Dennis Burke

INVESTIGATION OF REBAR CORROSION IN PARTIALLY SUBMERGED CONCRETE

REFERENCE: Funahashi, M., Fong, K., Burke, N. D., "Investigation of Rebar Corrosion in Submerged Concrete," Corrosion Forms and Control for Infrastructure, ASTM STP 1137, Victor Chaker, Ed., American Society for Testing and Materials, Philadelphia, 1992.

ABSTRACT: A large number of ocean and harbor concrete structures have been in service for more than a century. However, the cost associated with repair of these structures damaged by corrosion of steel in concrete is a major maintenance expense for the owners. Due to wave and tidal action of sea water, these structures are divided into atmospheric, tidal, and submerged zones. The most devastating corrosion damage occurs at the splash area which is somewhere between the lower part of the atmospheric zone and upper part of the tidal zone. However, it is generally believed that steel corrosion in the submerged concrete is stifled because the oxygen concentration in the concrete is too low to sustain the corrosion activity. To investigate the corrosion mechanism in partially submerged concrete structures, the corrosion potentials, total corrosion current, and macro-cell corrosion current of the steel in concrete specimens were monitored. The results obtained from the three zones (submerged, tidal, and atmospheric zones) were compared and discussed.

KEYWORDS: rebar, corrosion, submerged concrete, corrosion potentials, corrosion rates, macro-cell corrosion, passive film.

A large number of ocean and harbor concrete structures have been in service for more than a century. Offshore platforms, piers, wharfs, oil drilling rigs, sea walls, concrete barges, docks, and oil storage stations are examples. Many of these structures have experienced corrosion of steel reinforcement in concrete caused by chloride ions from the marine environment.

Mr. Funahashi is a senior corrosion engineer at Corrpro Companies, Inc., 610 Brandywine Parkway, West Chester, PA 19380; Dr. Fong is a research engineer and Mr. Burke is a Vice President of Corrpro Companies, Incorporated.

The costs associated with repair of these structures damaged by corrosion of steel in concrete is a major maintenance expense for the owners. One of the techniques to detect corrosion activity on the steel in concrete structures is the half-cell or corrosion potential measurements along the concrete surface. This technique was investigated and developed by the Federal Highway Administration (FHWA) in order to detect corrosion of reinforcing steel in a bridge deck [1]. However, the applicability of this measurement technique to marine structures, which are quite different from the bridge deck environments, has had little study. To avoid misinterpretations of corrosion condition for partially submerged reinforced concrete structures, it is important to understand the corrosion mechanism.

Backround

In 1980, P. K. Mehta [2] presented a schematic diagram from the case histories of concrete deterioration in seawater as shown in Fig 1. Generally, a marine structure can be divided into three zones, which are atmospheric, tidal, and submerged:

Atmospheric zone--above the high tide line;
In this zone, accumulation of salt near the concrete surface occurs due to wetting and evaporation cycles. Freeze and thaw cycles also occur on structures located in the northern climates. Abundant atmospheric oxygen is available on the steel surface if the oxygen diffusion flux of the concrete is sufficiently high.

Tidal zone--between the high and low tide line;
In this zone, the concrete is mainly water saturated. The concrete is not only vulnerable to damage due to corrosion of steel, but also to loss of material due to chemical reactions and the impact of waves, sand, gravel, or floating ice [2].

Submerged zone--below the low tide line;
In this zone, the concrete is vulnerable to strength degradation and loss of material as a result of chemical reactions between seawater and hydrated cement [2]. Oxygen availability is limited (that is, 7 ppm at the water surface decreasing to 3 ppm at 100 m water depth), but the hydrostatic pressure of seawater can cause more rapid penetration of seawater into the concrete [3].

The severest corrosion damage is generally observed in the splash area, which includes parts of both atmospheric and tidal zone, due to the high chloride concentrations caused by successive wetting and evaporation cycles and sufficient oxygen availability. It is known that oxygen and water are essential for the corrosion process. Many researchers have reported that corrosion normally becomes more negligible in the submerged zone due to the lack of oxygen, even though high chloride concentrations exist at the rebar and concrete interface [3-8].

Oxygen diffusion into concrete with various moisture contents was studied by some researchers [7-9]. They reported that oxygen

diffusion is greatly influenced by the moisture content of the concrete because the moisture fills capillary pores suppressing oxygen diffusion. Therefore, oxygen diffusion into the water saturated concrete is minimized. On the other hand, oxygen diffusion into various water-cement (W/C) ratio, composition of concrete mixtures, and properties of concrete has less effect, especially for the concrete containing high moisture [9].

For corrosion of steel embedded in chloride contaminated concrete, the anodic and cathodic reactions are

$$Fe \rightarrow Fe^{++} + 2e^{-} \quad \text{(anodic reaction)} \qquad (1)$$

$$O_2 + 2H_2O + 4e^{-} \rightarrow 4OH^{-} \quad \text{(cathodic reaction)} \qquad (2)$$

As seen from the above electrochemical reactions, oxygen reacts not at the anode, but at the cathode. In other words, steel in the concrete submerged under the water line can act as an anode to the steel in the above water concrete, where more oxygen is available. Generally, two types of corrosion cells, micro- and macro-cells, are observed on steel in concrete associated with chloride ions [20]. These corrosion cells are defined [16-21].

Micro-corrosion cell--The anode and cathode are microscopically separated. Micro-couples resulting from local breakdown of the passive film on the steel surface cause the formation of pitting corrosion. Operation of micro-corrosion cell is determined by the anodic and cathodic processes and depends little on the ohmic resistance. The corrosion potential measured on the concrete surface is a mixed potential of a number of microscopic anodes and cathodes on the steel surface in concrete.

Macro-corrosion cell--Both the anodic and cathodic reactions frequently take place in different places with some distance apart. Macro-electrochemical heterogeneity causes macro-corrosion cells. Macro-cells depend not only on the kinetics of anodic and cathodic processes, but also on the ohmic resistance of the anode and cathode couples. A corrosion potential measured on a concrete surface is a mixed potential of a few anodes and cathodes on the steel surface.

R. D. Browne [7] stated that macro-corrosion cell is not likely to be due to the high resistivity of the above water concrete which restricts the corrosion current. However, his statement can not explain how steel embedded in atmospheric exposed concrete can corrode by forming macro-cell corrosion. In addition, some degree of steel corrosion has been reported on concrete piles continuously submerged [10].

Steel in concrete is normally protected from corrosion by a passive film formed on the steel surface due to the highly alkaline pore water of the hydrated cement paste [6-11]. Composition of the pore water is essentially a mixed solution of sodium hydroxide, potassium hydroxide, and very little calcium hydroxide [12]. The pH of concrete pore water is typically above 13 unless the concrete is

carbonated [6,13]. The alkalinity of portland cement extracted water did not drop below a pH of about 12 even with the presence of 20% sea salt to a total volume of the extracted water [14]. It should be noted that this amount of salt is much larger than what actually has been observed in concrete, even from very old marine structures [15]. The continuous passive film is not an inert coating, but is in a state of dynamic electrochemical equilibrium with the electrolyte [16]. The passivity without external polarization is maintained by the corrosion current of self-dissolution. The anodic process taking place within the film, and the cathodic process occurring on the film surface are [16]

$$Fe + 2OH^- \rightarrow FeO + H_2O + 2e^- \quad \text{(anodic process)} \qquad (3)$$

$$O + 2e^- \rightarrow O^{2-} \xrightarrow{H_2O} 2OH^- \quad \text{(cathodic process)} \qquad (4)$$

To initiate corrosion of the steel, the protective film must be destroyed or the steel depassivated. As is well known, depassivation is caused by chloride ions existing at the steel-concrete interface. On the other hand, as seen from the above equations, to maintain the stability of the passive film, constant oxygen access to the steel surface is necessary to induce self-dissolution and cathodic reaction [8,16]. Therefore, a decrease of oxygen access to the steel surface due to blocking of concrete pores by water may reduce the cathodic current needed to maintain the passive film and eliminate it. If this protective film is eliminated, anodic reactions shown in Eq 1 may be able to develop and cause corrosion.

It is generally recognized that the transition potential of steel from the passive state to the active is between -200 and -350 mV to a copper/copper sulfate reference electrode (CSE), which is specified by ASTM C 876, Section 7, titled, Standard Test Method for Half-Cell Potentials of Uncoated Reinforcing Steel in Concrete. This specification was written for rebars in bridge decks based on the study performed by the FHWA [1]. To determine the corrosion condition of the steel embedded in concrete, a number of concrete slabs were tested to simulate bridge decks and the corrosion potentials were monitored with time. The top surface of the slabs were subjected to ponding with a 3% sodium chloride solution each afternoon. However, as previously mentioned, moisture content of the concrete may influence the passive film condition on the steel due to blocking of oxygen access. In other words, the corrosion potential of the steel in concrete may be dependent not only on the chloride ion concentration but also the moisture content of concrete. Few studies have been performed on the relationship between the corrosion potential and the concrete moisture content.

Some researchers [17-19] noted that indications of high negative corrosion potentials of steel in concrete may be associated with either breakdown of the passive film by chloride ions or instability of passive film by reducing oxygen supply. They explained that this high negative corrosion potential may result in misinterpretations of corrosion conditions of steel due to various moisture contents.

If such high negative potentials are developed by wetting the concrete, a question arises as to why such a great potential difference (electromotive force) between the steel submerged in fresh water or seawater and atmospherically exposed concrete does not cause a large galvanic macro-cell corrosion.

Based on the information discussed above, the authors of this paper investigated the corrosion mechanism of steel in partially submerged concrete in fresh water and seawater.

Experimental Procedure

Concrete Specimens

Two different types of concrete specimens were cast. One type of the specimens, concrete block as shown in Fig. 2, was used to determine relative moisture contents of concrete. The other, concrete beam as shown in Fig. 3, was to measure various corrosion parameters for reinforcing steel.

Four concrete blocks were cast with various chloride concentrations (0, 0.125, 0.25, and 0.3% of the concrete weight). Each concrete block contains two titanium electrodes to determine relative moisture contents of the concrete using an AC resistance measurement method. The two electrodes, 1-in. (2.54 cm) long and 1/8-in. (0.32 cm) in diameter, were mounted on a plastic ring with 1-in. (2.54 cm) apart as also shown in Fig. 2. The concrete was made with Type I portland cement, 1/2-in. (1.27 cm) maximum size crushed limestone and river sand. The water-cement ratio was 0.4.

Two concrete beams (Specimen Nos. 1 and 2) having dimensions 7 x 4.5 x 18 in. (17.8 x 11.4 x 45.7 cm) were cast. Each beam contained two 1-in. (2.54-cm) diameter reinforcing steel bars positioned 1-in. (2.54 cm) from the nearest concrete surface. One rebar was cut into three sections (A, B, and C) and electrically isolated using plastic washers located between the rebar sections. A copper wire was connected by a screw to each rebar section and covered with a heat shrinkable tube at each rebar isolated section. In addition, a total of three titanium counter electrodes, 2-in. (5.08 cm) long and 1/4-in. (0.64 cm) in diameter, were embedded near each rebar section to measure the corrosion current of Rebars A, B, and C, utilizing a linear polarization technique. Three moisture gauges were also embedded near each rebar section.

The concrete beam (Specimen No. 1), as shown in Fig. 4, was cast with the same concrete mix ratio as the concrete blocks. Four portions of the concrete beam were mixed with four different chloride concentrations (0.25, 0.3, and 0.125% for Rebar sections A, B, and C, respectively, and no chloride for the continuous rebar). These chloride concentration variations were utilized based on the findings of chloride concentration profiles from this type of structure [14,16,28].

One concrete beam (Specimen No. 2) was cast with chloride free

Type I portland cement concrete. Section Rebars A, B, and C were embedded in water/cement (W/C) ratio of 0.6 concrete and continuous Rebar D was embedded in 0.4 water/cement concrete. Rebar D was not connected to Rebars A, B, and C during the test period.

Moisture Content Measurements of Concrete Blocks

After the concrete blocks containing the two titanium electrodes were cured in the plastic concrete mold for 30 days, the blocks were immersed in 3% artificial sea water (ASTM Specification for Substitute Ocean Water, D 1141). Using an AC resistance meter (12 volts with 97 Hertz square wave), the concrete resistance between the electrodes was monitored with time until the resistance reached a steady minimum. It was assumed that the lowest resistances were indicative of water saturated (100%) concrete containing various chloride concentrations. The concrete blocks were then successively dried out at 50°C in a oven. The concrete resistances were measured with time until they reached a steady maximum. The hydrated cement contains a network of capillary pores, gel pores, and air voids. The larger pores, which are usually referred to as capillary pores, are the remains of water-filled spaces [22]. The capillary pores occupied from 0 to 40% of concrete volume, depending on the water-cement ratio and the degree of hydration [23,24]. The gel pores constitute about 26 to 28% of the past volume, even if the cement paste is completely hydrated [23,24]. At low relative humidities, the water in the capillary pores can evaporate but it is not possible to remove the water from the gel pores [22]. Therefore, it was assumed that the highest concrete resistance measured at the end of the drying period was indicative of 20% of the relative moisture content, which was also used by Gjorv and Vennesland [13]. To compensate for the resistances measured at the different temperatures, the Hinrichson-Rash Law was used

$$d_1 = d_2 \, e^{a(1/T1 - 1/T2)} \qquad (5)$$

Where d_1 and d_2 are resistivities at absolute temperatures T_1 and T_2, and "a" is a constant. The value of 2885 for the constant "a" was used based on the findings by B. B. Hope et al. [17] and K. C. Clear [25]. Resistivities of each concrete block which contains various chloride concentrations were measured.

Measurements of Corrosion Parameters for Concrete Beams

After concrete beams were cured in the mold for 90 days, the lower half of Specimen No. 1 was vertically immersed in 3% of artificial sea water, and the lower half of Specimen No. 2 was submerged in tap water. All rebar sections were connected with 10 ohm resistors to measure macro-cell corrosion current flow between the rebars. A switch was connected between Rebars C and D to isolate Rebar D from Rebars A, B, and C.

The following corrosion parameters were measured to investigate the corrosion mechanisms of these experimental specimens:

- Magnitudes and directions of macro-corrosion current

flowing between the rebars with respect to the time immersed.

- Corrosion potentials on the concrete surface of each rebar section immediately after the specimens were lifted from the water using a portable copper/copper sulfate reference electrode. The locations of the potential measurements are A1, A2, B1, B2, C1, C2, and D1 through D6 as shown in Fig. 4.

- Corrosion rates of each rebar section utilizing a linear polarization resistance technique with a potentiostat, immediately after the specimens were lifted from the water. The IR-drop free potentials were obtained using a computer control current interruption.

The above measurements were taken in the condition that all Rebars A, B, and C are either connected or disconnected from Rebar D. Relative moisture contents of the various sections of the concrete beams were determined based on the resistance measurements of the concrete blocks.

Results and Discussion

The variation of the relative moisture contents with respect to the time immersed is shown in Fig. 5. Before the specimens were partially immersed in water, the concretes were still holding high moistures. Therefore, the corrosion parameters of steel in drier environments were not obtained.

The concrete containing Rebar A in Specimen No. 1 became saturated after the specimen was immersed for approximately 100 h. The concrete containing Rebar A in Specimen No. 2, which was partially submerged in tap water, became saturated after approximately 150 h immersion. It is known that concrete mixed with chloride ions is generally more porous and holds higher moisture contents in a dry environment than the chloride-free concrete. Therefore, the chloride mixed concrete, Specimen No. 1, was saturated in a shorter period than Specimen No. 2.

The concrete containing Rebar B, which was partially submerged in the water became highly saturated in short periods. It appears that the concretes above 1 in. from the water line became saturated after approximately 150 h immersion for Specimen No. 1 and approximately 250 h for Specimen No. 2.

Figure 6 shows the corrosion potential variation of Rebars A, B, and C of Specimen No. 1 with respect to time. The potentials of Rebars A and B shifted in a more negative (anodic), direction immediately after the specimen was immersed and then drifted in a more positive (cathodic), direction up to and after 20 h. Thereafter, the potentials shifted again in the more anodic direction up to approximately 500 h immersion.

The potentials of Rebars A and B during the saturating period did not vary significantly and did not appear to be a function of the moisture content in a highly moist concrete. The corrosion potential

of steel is expressed by the Nernst equation:

$$E = E^{\circ} - (RT/nF) \ln [Fe^{++}]/[Fe] \quad (6)$$

where $[Fe^{++}]$ represents the activity of iron ions. [Fe] is the activity of metallic iron, the latter being a pure solid and equal therefore to unity, and E° is the standard oxidation potential of iron [29].

During the saturating period, the ferrous ion activity $[Fe^{++}]$ appeared to fluctuate with increasing moisture content. However, after the concrete was saturated, the rate of the anodic reaction shown in Eq 1 may slowly increase; consequently, the ferrous ion activity may increase. When Rebar D was connected to Rebars A, B, and C, the potentials of Rebars A, B, and C did not significantly change.

Figure 7 shows the potential variation of Rebar D in Specimen No. 1 with respect to the time immersed. After the specimen was immersed for approximately 150 h, the potentials measured on the wet concrete area, under the condition of Rebars A, B, and C connected to Rebar D, shifted to approximately -400 mV (CSE). On the other hand, when Rebars A, B, and C were disconnected from Rebar D, the potentials measured at the wet surface shifted largely in the more positive direction and fluctuated between -200 and -300 mV. It was noted that the potentials measured on the wet surface were generally, approximately 100 mV more negative than those measured at the dry surface, regardless of the Rebar D connection.

The potentials were measured along Rebar A, B, and C and Rebar D at 2 in. intervals after Specimen No. 1 was immersed for 510 h. The potential profiles are shown in Fig. 8. As discussed above, the potentials measured above the wet line on the concrete were more positive with increasing distance from the wet line for Rebars A, B, and C, and Rebar D. On the other hand, the potentials measured below the water surface were more negative for both rebars. In addition, the potentials measured at 2 in. above the water surface of Rebars B and Rebar D, which is the boundary of the wet and dry surfaces, were mostly negative.

When Rebars A, B, and C were connected to Rebar D, the entire potential profile of Rebar D shifted approximately 120 mV in the negative direction, and the potentials measured on the wet surface became approximately -400 mV even though Rebar D was not corroding. This was confirmed by visual inspection of the rebars by destroying the specimen at the end of the tests. On the other hand, the potential profile of Rebars A, B, and C shifted approximately 10 to 20 mV in the positive direction. Therefore, the small potential shift of Rebars A, B, and C in the positive direction resulted in the large potential shift of Rebar D in the negative direction. Thus, when the concrete is heavily moist by water and noncorroding rebars are electrically continuous to corroding steel, the potential measurements cannot distinguish the condition of steel in concrete.

Figure 9 shows the potential variation of Rebars A, B, and C and Rebar D for Specimen No. 2, with respect to the time immersed in tap water. The potentials of the rebars, except these measured at the boundary of the wet and dry concrete surface (B1 and D3), slowly shifted to the more positive potentials with time, and became more positive than -100 mv (CSE). As observed on Specimen No. 1, the potentials measured at the interface of the wet and dry surfaces were distinctively more negative than those measured on the other areas. L. L. Shreir [30] described that when the pH of an electrolyte is between 10 and 13, differential aeration causes a significant increase in the potentials of both aerated and non-aerated areas without appreciable current flow. These high negative potentials at the interface may be due to the local differential aeration cells developed between the rebar embedded in the wet and dry concrete.

As discussed in the "Background" section, the potentials of rebars measured on the submerged concrete surface did not indicate passive film breakdown even after the specimen was immersed for over 400 h. To dilute the oxygen concentration in the concrete and influence the condition of the passive films, it may require an increased exposure period. Testing will be continued to determine this long term influence. The potentials of the rebars embedded in the different water/cement ratio concrete (W/C = 0.4 and 0.6) did not indicate any difference over the test period.

Figure 10 shows the corrosion rate variation of Rebars A, B, and C in Specimen No. 1 with respect to time. The corrosion rate of each rebar was measured in both Condition I, where Rebar D was connected, and Condition II, where Rebar D was disconnected.

The corrosion rate of Rebar A increased with time regardless of Rebar D connection. When Rebar D was connected, higher corrosion rates of rebar A were always measured due to increasing cathodic surface area.

The corrosion rate of Rebar B varied with time, and was influenced by the connection to Rebar D. When the specimen was immersed in water, the corrosion rate increased immediately. However, the corrosion rate became relatively steady until the concrete was highly moist. This indicates that the moisture content of the concrete greatly influences the corrosion rate of rebar which is embedded in a drier concrete. With increasing moisture content, the corrosion rate became less sensitive.

The corrosion rates of Rebar C were relatively steady and low over the test period. When Rebar D was connected, the corrosion rate of Rebar D was not significantly different. This indicates that Rebar C is not strongly anodic to Rebar D.

Figures 11 and 12 show the variation and magnitude of the total corrosion current and macro-cell corrosion current produced between the rebars. Figure 11 shows the corrosion current of Rebars A, B, and C without connecting Rebar D. The direction of the macro-cell corrosion indicated that Rebar A was initially cathodic to Rebar B

which was embedded in the concrete containing 3000 ppm of chloride concentration. However, after the concrete containing Rebar A was saturated, the direction of the macro-cell corrosion current was reversed, which indicated that Rebar A had become anodic to Rebar B. The macro-cell anodic current continuously increased with time over the test period. As discussed in the "Background" section, this is due to the absence of oxygen in the anodic reaction which does not need oxygen. However, the magnitudes of the macro-cell anodic currents (current flowing to Rebar A through the resistor) were less than those of the total corrosion current (micro and macro corrosion current) of Rebar A.

In addition, this type of structure has a large steel surface area in the submerged concrete. Therefore, these macro-cell anodic currents can be distributed to the entire surface due to the low resistance path of sea water. Therefore, the macro-cell anodic current density would be very low. This low anodic current density indicated that the rebar embedded in the water saturated concrete corroded due to micro-cells that existed on the steel surface during the test period. It is unknown whether or not these high corrosion rates of Rebar A would continue for a long term period.

The macro-cell anodic current on Rebar B developed by Rebar C slowly increased with time. It seems that the upper portion of Rebar B is anodic to Rebar C and the lower portion of Rebar B is cathodic to Rebar A. However, these macro-cell currents were again, much less than the micro-cell corrosion current.

Until the concretes of Rebars A and B were saturated, the macro-cell cathodic current of Rebar C (flowing from Rebar C), developed by Rebars A and B, increased and then became relatively steady over the test period. The magnitude of this macro-cell cathodic current on Rebar C was approximately 20 to 30% of the total corrosion current. In addition to the lower chloride concentration of the concrete containing Rebar C, this macro-cell cathodic current reduces the corrosion rate of Rebar C.

The variation and magnitudes of the corrosion currents of Rebars A, B, and C with connecting Rebar D are shown in Fig. 12. Similar results were obtained for Rebar A, without connecting Rebar D. Obviously, when Rebar D was connected, larger macro-cell anodic currents were developed on Rebars A, B, and C due to increasing cathodic surface area. However, the magnitudes of macro-cell currents were still small compared with the total corrosion currents.

Macro-cell corrosion current flows between the rebars in Specimen No. 2 were monitored over the test period. There was no macro-cell current flow developed, indicating that if the oxygen concentration in the concrete submerged is lower than that of the concrete exposed to air, differential aeration does not produce current flow, as indicated by Shreir [30].

Corrosion rate versus potential for Rebars A, B, and C over the test period were plotted in Fig. 13. The corrosion rates of Rebar A

are widely scattered in the range between -230 (CSE) and -500 mV. Even though the potentials were more positive than -250 mV, high corrosion rates were measured. On the other hand, low corrosion rates were measured at approximately -400 mV. The corrosion rates of Rebar B are scattered in the range between -200 and -300 mV. When the potentials of Rebar B were more negative than -400 mV, the corrosion rate was always high. The corrosion rates of Rebar C were low when the potentials were more positive than -250 mV.

As seen in these graphs, the data points are more scattered with higher moisture contents of concrete. When the potentials were more positive than -200 mV, the corrosion rates are always low regardless the moisture and chloride concentrations.

After the tests were terminated, the rebars in Specimen No. 1 were exposed to visually observe the surface condition. Corrosion was observed on Rebars A, B, and C. Even though the magnitude of the corrosion rates on Rebars A and B did not vary significantly, the corrosion appears to be more concentrated in the region of the wet and dry concrete of Rebar B. For actual structures, this observed concentrated corrosion area on Rebar B should be greater due to the wave and tidal action. Therefore, the highly concentrated corrosion areas can be expanded and most extensive in the splash area of the structure.

Conclusions

1. When concrete contains high moisture contents, non-corroding rebars are electrically continuous to corroding rebars, and the potentials are more negative than -200 mv (CSE), the potential measurements can not distinguish the corroding or non-corroding condition of the rebars.

2. Corrosion potentials of rebars in the concrete containing less moisture appear to follow the ASTM 876 standard.

3. Rebars embedded in chloride-free concrete did not show any sign of passive film breakdown after the concrete was immersed in tap-water for more than 400 h.

4. Local differential aeration cells appear to be developed on the rebars embedded at the interface of the wet and dry concrete, which is not contained chloride. However, these cells did not develop corrosion at the interface during the test period.

5. Large differential aeration cells were not developed on the passivated rebar embedded in the wet and dry concrete over the test period.

6. In chloride contaminated concrete, rebar located under the sea water was anodic to the rebar in concrete exposed to atmosphere. However, the magnitude of the corrosion current developed by the corrosion cell was far less than that of the total corrosion current.

7. The corrosion rate of rebar embedded in a drier, chloride mixed concrete was more influenced by the moisture content. On the other hand, the corrosion rate in a highly moist concrete became less sensitive to the moisture content.

8. Water-cement ratio did not create significant potential differences on the rebar embedded in chloride-free concrete regardless of the moisture contents.

References

[1] Clear, K. C. and Hay, R. E., "Time-to-Corrosion of Reinforcing Steel in Concrete Slabs, Vol. 1, Effect of Mix Design and Construction Parameters," Federal Highway Administration Report FHWA-RD-73-32, April 1973, p. 98.

[2] Mehta, P. K., "Durability of Concrete in Marine Environment - A Review," Performance of Concrete in Marine Environment, SP 65-1, American Concrete Institute, Aug. 1980, p. 20.

[3] Browne, R. D. and Domone, P. L. J., "The Long-Term Performance of Concrete in the Marine Environment," Off-Shore Structures, ICE, London, 1975, pp. 49-59.

[4] Gjorv, O. E., "Durability of Reinforced Concrete Wharves in Norwegian Harbors," The Norwegian Committee on Concrete in Seawater, Ingeniorforlaget A/S, Oslo, 1968, p. 208.

[5] Gjorv, O. E., "Control of Steel Corrosion in Concrete Sea Structures," American Concrete Institute, SP 49-1, 1975, pp. 1-9.

[6] Hausman, D. A., "Steel Corrosion in Concrete, How Does It Occur?," Material Protection, Nov. 1967, pp. 19-23.

[7] Browne, R. D., "Mechanisms of Corrosion of Steel in Concrete in Relation to Design, Inspection, and Repair of Offshore and Coastal Structures," American Concrete Institute, SP 65-11, Aug. 1980, pp. 169-204.

[8] Fidjestol, P. and Nilsen, N., "Field Test of Reinforcement Corrosion in Concrete," American Concrete Institute, SP 65-12, Aug. 1980, pp. 205-221.

[9] Kobayashi, K. and Shuttoh, K., "Oxygen Diffusivity of Various Cementitious Materials," Cement and Concrete Research, Vol. 21, 1991, pp. 273-284.

[10] Beaton, J. L., Spellmann, O. L., and Stratfull, R. F., "Corrosion of Steel in Continuously Submerged Reinforced Concrete Piling," California Division of Highways, Research Report M&R 635116, 1967, p. 32.

[11] Ashfold, J. H., Garnsey, R., and Mann, G. M. W., "Corrosion of

Mild Steel Under Heat Transfer in High Temperature Sodium Chloride Solutions," Corrosion Science, Vol. 14, 1974, pp. 515-525.

[12] Monteiro, P. J. M., Gjorv, O. E., and Mehta, P. K., "Microstructure of the Steel-Cement Paste Interface in the Presence of Chloride," Cement and Concrete Research, Vol. 15, 1985, pp. 781-784.

[13] Gjorv, O. E. and Vennesland, O., "Electrical Resistivity of Concrete in the Ocean," Offshore Technology Conference, OTC 2803, 1977, pp. 581-588.

[14] Gjorv, O. E. and Vennesland, O., "Sea Salts and Alkalinity of Concrete," American Concrete Institute Journal, Vol. 73, No. 9, 1976, pp. 512-516.

[15] Gjorv, O. E., "Durability of Concrete Structures in the Ocean Environment," Proceedings, Symposium on Concrete Sea Structures, London, 1973, pp. 141-145.

[16] Tomashov, N. D., Theory of Corrosion and Protection of Metals, The MacMillan Company, New York, 1966, pp. 325-361.

[17] Hope, B. B., Ip, A. K., and Manning, D. G., "Corrosion and Electrical Impedance in Concrete," Cement and Concrete Research, Vol. 15, 1985, pp. 525-534.

[18] Arup, H., The Mechanisms of the Protection of Steel by Concrete in Corrosion of Reinforcement in Concrete Construction, Ellis Horwood, Ltd., 1983, p. 393.

[19] Cheng, T. P., Lee, J. T., and Tsai, W. T., "Corrosion of Reinforcements in Artificial Sea Water and Concentrated Sulfate Solution," Cement and Concrete Research, Vol. 20, 1990, pp. 243-252.

[20] Funahashi, M., Corrosion of Steel Reinforcement in Concrete: Threshold Chloride Ion Concentration for Corrosion in Type I Portland Cement Concrete, Florida Atlantic University, Thesis, 1985, p. 109.

[21] Okada K. and Miyagawa, T., "Chloride Corrosion of Reinforcing Steel in Cracked Concrete," American Concrete Institute, SP 65-14, 1980, pp. 237-254.

[22] Hansson, I. L. H. and Hansson, C. M., "Electrical Resistivity Measurements of Portland Cement Based Materials," Cement and Concrete Research, Vol. 13, 1983, pp. 675-683.

[23] Neville, A. M., Properties of Concrete, Pitman Publishing Ltd., London, 1981.

[24] Power, T. C., "Structure and Physical Properties of Hardened

Portland Cement Paste," Journal of The American Ceramic Society, Vol. 41, No. 1, 1958, pp. 1-6.

[25] Clear, K. C., F. C. P. Annual Progress Report, Federal Highway Administration, 1980.

[26] Nagano, H. and Naito, T., "Application of Diffusion Theory to Chloride Penetration into Concrete Located in Splash Zones," Transactions of Japanese Concrete Institute, Vol. 7, 1985, pp. 157-164.

[27] Kaneko, Nagano, Sakurai, and Yasu, "Chloride Content and Cement Hydrate Minerals in Concrete in Sea Environment," Transactions of the Japanese Concrete Institute, Vol. 6, 1984, pp. 147-154.

[28] Aguilar, A., Saynes, A. A., and Powers, R. G., "Corrosion Measurements of Reinforcing Steel in Partially Submerged Concrete Slabs," Corrosion Rates of Steel in Concrete, ASTM STP 1065, Neil S. Burke, Victor Chaker, and David Whiting, Eds., 1990, pp. 66-85.

[29] Uhlig, H. H., Corrosion and Corrosion Control, Second Edition, John Wiley & Sons, New York, 1971, p. 21.

[30] Shreir, L. L., Corrosion, Vol. 1, Newmes-Butterworths, London, 1963, p. 1:137.

Gareth John, Karel Hladky, Patrick Gaydecki and John Dawson

RECENT DEVELOPMENTS IN INSPECTION TECHNIQUES FOR CORROSION DAMAGED CONCRETE STRUCTURES

REFERENCE: John, D.G., Hladky, K., Gaydecki, P.A. and Dawson, J.L., "RECENT DEVELOPMENTS IN INSPECTION TECHNIQUES FOR CORROSION DAMAGED CONCRETE STRUCTURES", Corrosion Forms and Control for Infrastructure, ASTM STP 1137 Victor Chaker, Ed. American Society for Testing and Materials, Philadelphia, 1992.

ABSTRACT: Improved procedures for inspecting both reinforced concrete and prestressed concrete structures, with regard to determination of the embedded steel components are discussed. Prototype ultrasonic procedures recently developed to determine the condition of prestressed pretensioned tendons in concrete will be discussed. The application of electrochemical surface mounted systems for estimating the rate of corrosion of reinforcing steel and other embedded steel components in large concrete structures will also be described. In particular, the ability to obtain rate of corrosion data over the concrete surface and presenting it as iso-corrosion rate contours will be highlighted.

KEYWORDS: Corrosion monitoring, ultrasonics, reinforced concrete, prestressed concrete, inspection.

INTRODUCTION

Deterioration of reinforced concrete structures resulting from corrosion of the reinforcing steel and prestressing steel has become an increasing problem worldwide. A number of techniques have been used to ascertain the corrosion condition of embedded steel. Methods of inspection currently used to determine structural condition, existence or otherwise of corrosion, and the likelihood of further damage, include half-cell (iso-potential) mapping to ASTM C876-87, cover surveys, chloride profiles, core sampling and electromagnetic/infra-red scanning. Although useful and accepted throughout the industry, these techniques only give an indication of the extent or likelihood of damage due to corrosion occurring, they do not provide any data about the rate

Dr. D.G. John is Technical Development Manager, Dr. K. Hladky is a Senior Project Officer and Dr. J.L. Dawson is a Senior Consultant at CAPCIS Ltd., Bainbridge House, Granby Row, Manchester, M1 2PW, U.K. Dr. P.A. Gaydecki is a Lecturer at the Department of Instrumental & Analytical Science, UMIST, Sackville St., Manchester, U.K.

of corrosion process at the time of the measurement and with the exception of electromagnetic systems the standard techniques cannot give an indication of the amount of corrosion/metal loss already occurred.

Research into electrochemical methods of obtaining rates of corrosion in concrete has been carried out by numerous workers. Various methods have been applied including embedded test cell arrangements, wet surface mounted probes, guard ring probes, electrochemical linear polarization resistance measurements, electrochemical (a.c.) impedance measurements, monitoring and analysis of electrochemical potential noise and others. Discussion of these different techniques and procedures is outside the scope of this paper, but a summary is available in the literature [1-4]. The measurement of corrosion rates on steel reinforcement in concrete is fraught with difficulties [3,4]. Our experience indicates that a number of compromises must be made in the design of a practical system, trading off precision of the resulting data against speed of measurement, reliability of the hardware and 'usability' in the field.

In the case of prestressed concrete structures failures can occur without necessarily external signs of damage or deterioration being apparent. Examples of such failures are covered in the literature [5,6]. Prestressed structures also have a particular problem associated with inspection [7,8]. A NCHRP contract in 1985 reviewed options for non-destructive inspection of pre-cast structures [7] and indicated that there were several techniques available for the inspection of some, but not all, types of prestressed structures. In particular it identified the SCORPION system developed in France that essentially consists of a lorry mounted mobile X-ray radiography system for the inspection of specific bridge and concrete structures.

Electromagnetic systems were also identified as being capable of providing some information with regard to the condition of embedded components. However, one generic system which, at the time, did not appear to have been investigated to any great degree was the possible use of ultrasonics to inspect the embedded components in prestressed members.

A research proposal was prepared and awarded by the National Academy of Sciences to look into the possibility of developing an ultrasonic inspection system for pre-cast pre-tensioned and pre-cast post-tensioned structures. This work was carried out at CAPCIS in conjunction with the Department of Civil Engineering and the Department of Instrumentation and Analytical Science (DIAS), UMIST.

The work involved an assessment of the fundamentals of ultrasonic propagation in concrete, the reflective nature of ultrasound waves from embedded components and scatter, the practical investigations incorporated measurements on various laboratory test samples and full scale pre-cast beams.

RATE OF CORROSION MEASUREMENT

Equipment

The corrosion rate measuring system employs suitably designed electrochemical instrumentation and interface, data logger and a dry surface mounting probe as shown in Figure 1.

Figure 1. Rate of Corrosion Probe and Monitoring Instrumentation.

The probe comprises a circular auxiliary electrode, formed by a 'sandwich' of carbon loaded conductive plastic foam, a backing pad of flexible polyurethane foam and a rigid polypropylene support [9]. The foam assembly is held in place by a set of radially placed stainless steel retaining wires that also provide electrical connection to the probe face. A standard 'potential measuring' Ag/AgCl/KCl gel type reference electrode is located at the centre of the probe assembly. In use, the probe is simply pressed against the concrete surface at the desired measurement location. Moderate hand pressure or vacuum suction is then maintained for the duration of the measurement (some 2 to 3 minutes). No special surface preparation is normally necessary, apart

from the removal of dust and loose debris from the surface of the concrete by a hand held wire brush prior to placement of the probe.

The electronic measurement system has been described before [3,10] and is shown in Figure 1. It comprises a battery powered electrochemical interface based on a low power potentiostat and a data logger. The measurement is carried out using a three electrode arrangement; the system measures the potential of the reinforcement with respect to the reference electrode (E_{corr}) and applies an anodic overpotential of 20mV via the auxiliary electrode. The resulting current is then recorded. The measurement sequence is controlled by a program resident in the data logger, user interface is via the logger display and key pad. Data from each measurement location is stored as location identifier (usually a grid reference code entered by the user), E_{corr} reading and two readings of the polarising current. Data and time information may also be stored.

At the end of each measurement session the data is downloaded from the data logger to an IBM PC compatible computer for storage and analysis using Corrsoft™ POTMAP program. This package handles data transfers to and from the data logger and gives a plotter or graphics printer hard copy output in the form of contour maps, in numerous colours, as required.

The area of rebar surface being polarised must be known in order to obtain a quantitative estimate of the corrosion rate. In practice this area will depend not only on the rebar diameter but also on the particular rebar surface profile, on the distribution of aggregate and on the geometry of the reinforcement cage. The effects of these may be modelled and their contributions compared in a computer simulation, but they are very difficult to ascertain in practice. Practical results, however, indicate that areas where active corrosion is occurring usually give corrosion rate readings up to several orders of magnitude higher than areas where the steel is not actively corroding. Reinforcement density and rebar sizing do not usually vary by as much as this amount across any particular structure, making it possible to use the 'raw', qualitative, data as a good predictor of the distribution of the corrosion attack. Further calibration may then be made for particular locations, based on a careful examination of drawings, cover meeting readings, etc., and possibly aided by a computer simulation of the current distribution based on the geometry of those locations.

Applications

The system as described above has been applied to several structures in Europe and the Middle East. The corrosion monitoring system was originally developed to take some 300 spot readings on the structures of the Sea Water Cooling canal in Al-Jubail, Saudi Arabia [3,11]. Several means of probe mounting were tried, including retaining bolts and a vacuum operated skirt. Valuable lessons were learned from the exercise and the system was modified accordingly.

The system has also been tested on several reinforced concrete bridges in Finland, using a simplified design of the probe, without the

retaining stainless steel wires. The Finnish structures exhibited excessive carbonation and in many cases a sufficiently good electrical contact could not be made between the probe face and the concrete surface. It should, however, be noted that in this application the probe was mounted on the top of a long (5 metre) telescopic pole that made it difficult to apply sufficient pressure to the probe; also it was not possible to access the surface of the structure to remove the carbonated deposit or thin but highly resistive on to film to ensure a good contact between the reference electrode tip and the concrete surface.

Recently, the system was applied to a large reinforced concrete marine structure in the Middle East. In this application it was necessary to carry out a fairly detailed survey of a number of large (approx. 13 x 17 metres) vertical retaining walls. Two operators working from a hydraulic platform and measuring a 1 metre grid could comfortably survey one of these walls over each 6 hour working period. Measurements have also been taken on several bridges in the U.K.

Results

The present corrosion rate measuring system can be used to obtain iso-potential contour maps of the surface of the surveyed structure, together with iso-corrosion rate contour maps covering the same area. Figure 2 shows the equipotential contour maps obtained on a bridge support pier, U.K. The spread of the potential values and their distribution across the surface of the structure does not give any clear indication of corroding or passive areas. The corresponding corrosion rate contour maps are shown in Figure 3. The corrosion rate data is plotted on a logarithmic scale since the measured corrosion rates spanned a range of nearly three decades. Relative corrosion rate values are shown, although absolute rate values could also be calculated and plotted by the software if the conversion constant was known.

Figure 2a shows the half cell potentials obtained on the north face of the crosshead. Figure 3a shows the corresponding relative corrosion rate map. An area of a high corrosion rate is apparent near the top of the crosshead, centred at approx. 5,-1 metres. Interestingly, the area of relatively low (more negative) potentials near the ground level (e.g. 8,-6) does not appear to be associated with a particularly high corrosion rate.

Figures 2b and 3b show corrosion potential and corrosion rate contour maps for the south face of the crosshead. Again, the area of more negative potential near ground level does not appear to be associated with a corresponding area of high corrosion rate. A relatively high corrosion rate was measured on the right side of this crosshead face (approx. 11,-2). This appeared to correspond to an area previously wetted by leakage from the road deck.

The results of the corrosion rate survey were in general agreement with those of the present half-cell survey. The major exception was found in areas near the ground level where low (more negative) half cell potentials relative to the majority of readings of the order of -105 to

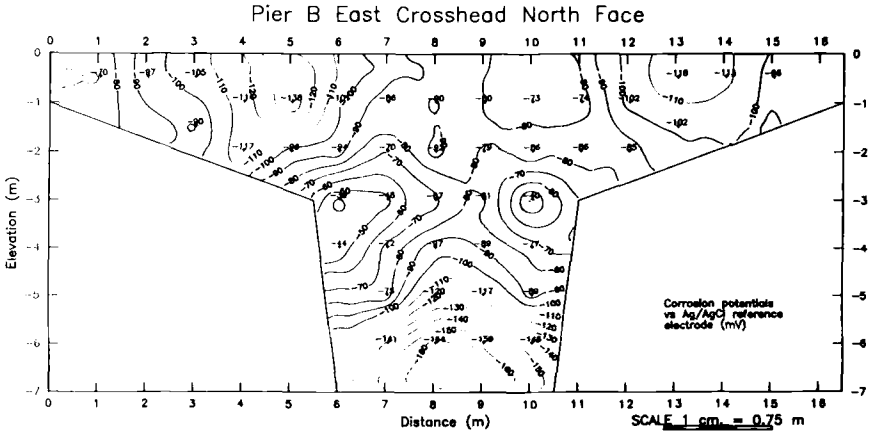

Figure 2a. Iso-potential contour map, North Face of Crosshead. (potentials mV; Ag/AgCl/KCl)

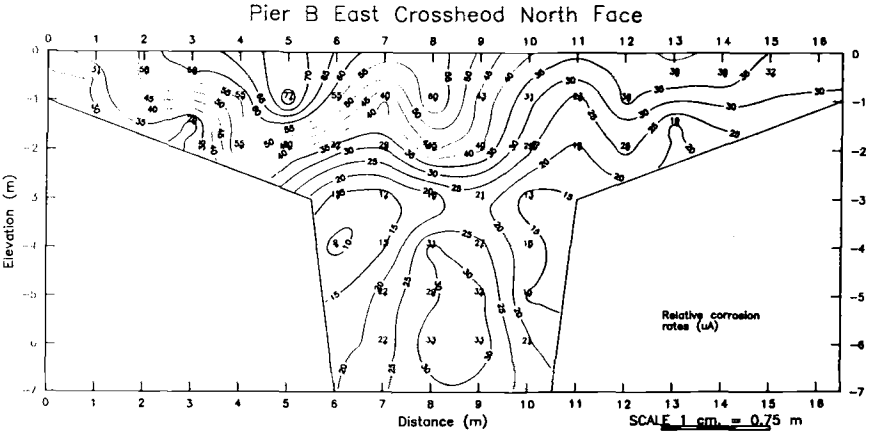

Figure 2b. Iso-corrosion current contour map, North face of crosshead. (corrosion currents uA)

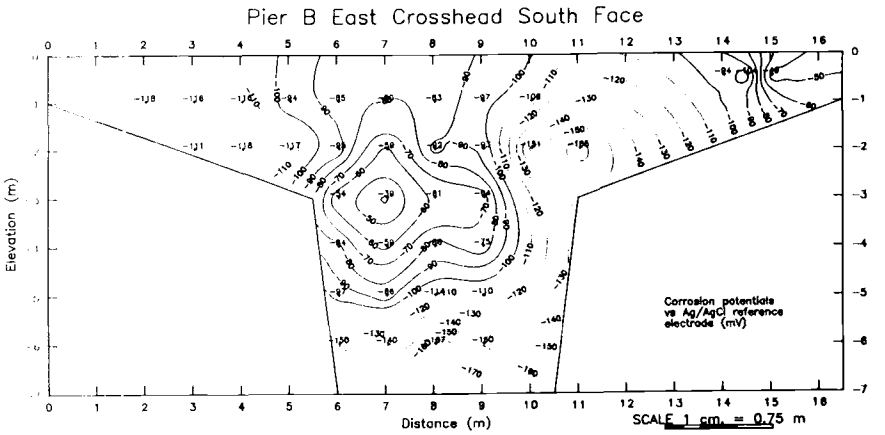

Figure 3a. Iso-potential contour map, South Face of crosshead. (potentials mV; Ag/AgCl/KCl)

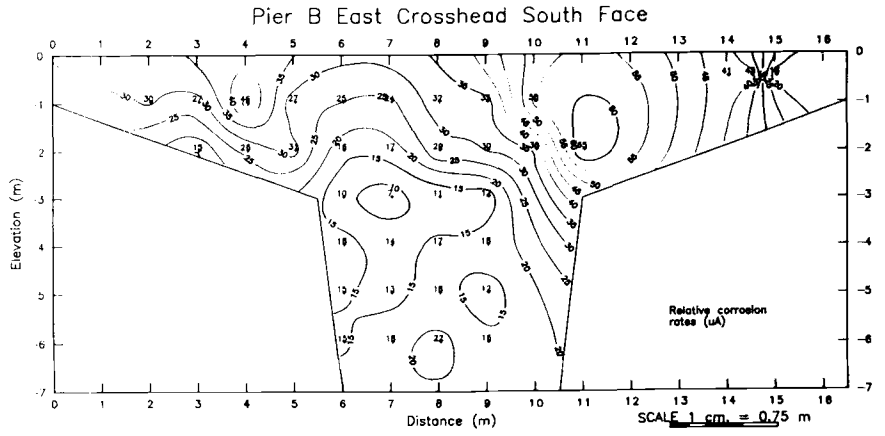

Figure 3b. Iso-corrosion current contour map, South face of crosshead. (corrosion currents uA)

-170mV vs Ag/AgCl/KCl were observed without corresponding high corrosion rates.

DEVELOPMENT OF ULTRASONIC INSPECTION SYSTEM

Background

The ultrasonic inspection of concrete has traditionally been limited to rather simple measurements conducted in the time domain, such as the time required for an acoustic pulse to travel through a know distance or depth of the material. Since the propagation velocity is related to the strength of concrete, the pulse-velocity technique has been established as possibly the only standard method of non-destructive testing of concrete using ultrasonic systems. Pulse-echo techniques, which provide detailed information regarding the internal defects in materials whose composition is essentially homogeneous with respect to the interrogating wavelength (such as metal castings etc.), are unsuitable for use with concrete [12]. Concrete is so inhomogeneous in its composition that the scatter of ultrasound waves normally precludes the use of frequencies extending beyond 150kHz. These low frequencies cannot provide sufficient spatial resolution for conventional imaging purposes.

The need to develop an ultrasonic inspection system capable of providing information not only with respect to the internal integrity of the concrete but also the condition of any steel reinforcing components, led to the detailed analysis of the waveforms that were received having travelled through concrete samples and structures of various types. A thorough understanding of these waveforms, which contain components arising from a number of sources, ultimately led to the development of an instrument (for which a patent application has been filed) that can successfully detect various internal conditions of the concrete under inspection [13, 15].

System Operation

The final prototype system that operated successfully in laboratory trials is described in detail elsewhere [16, 17]. A general arrangement is shown in Figure 4. In practice, the system operates with 400kHz rolling probes (see Figure 5), that move along the surface of the concrete beam to be analysed, firing and receiving pulses at regular intervals. For example for a 5m concrete beam, that is interrogated every 50mm, one hundred waveforms will be acquired, i.e. $x_1(n)$ to $x_{100}n$ (each waveform comprises 512 data points, i.e. n = 1...512). Each waveform is then transformed to the frequency domain by an FFT algorithm and the energies in 8 bands are calculated.

The bands that are calculated are 500kHz in width and range from 0-5kHz to 350-400kHz. The energy for the first band of the first waveform is labelled E_{11}. The energy for the second band of the first waveform is labelled E_{12} etc. Hence, for each waveform, 8 separate energy values are calculated. The way in which the energies are combined for each waveform determine the kind of defect that can be detected, since the scattering equations show that the amount of energy scattered (and hence received) is determined by the dimensional relationship of the

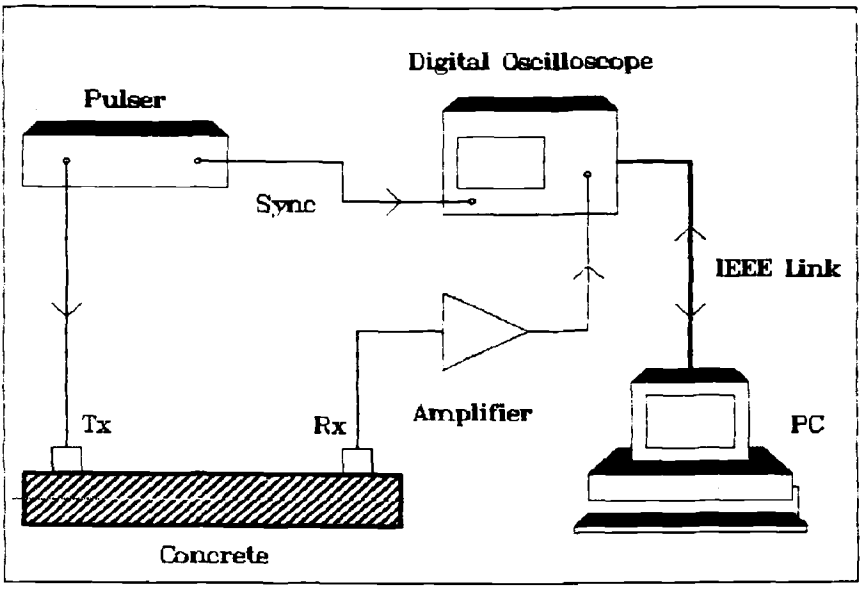

Figure 4. Schematic Experimental Arrangement.

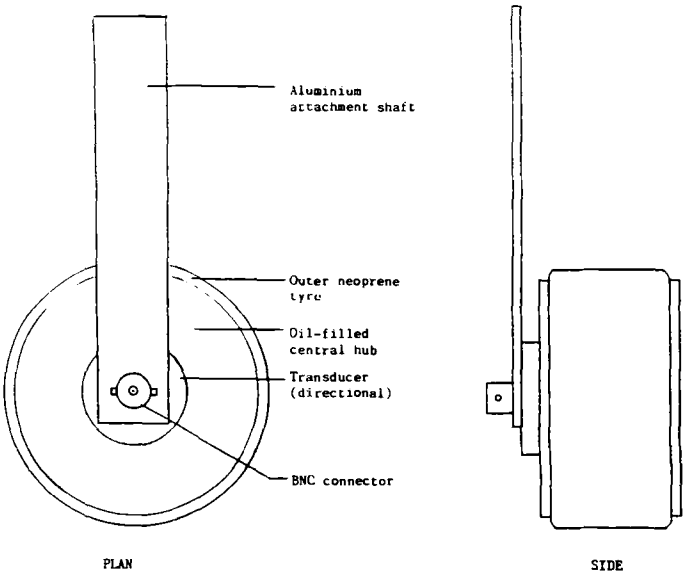

Figure 5. Details of Rolling Transducers

wavelength and scatterer. For instance, if a major void was being sought, the energies in each band for a given waveform are simply multiplied together (an operation similar to cross-correlation), since all bands will show greater energy levels due to reflection. In this case, a new function Z(k) is synthesised that represents the combined (multiplied) energies as a function of the scan position.

A major void in the middle of the beam would be revealed by plotting Z(k) against k, as shown in Figure 6. The result was obtained on a laboratory cast beam containing a know defect, located actually under the observed "spike" [16]. If smaller defects are being sought, such as areas of delamination due to the corrosion of steel reinforcing components, then experiment has shown that only high frequency components respond. In this case, the energies of the low frequency bands are used to correct for coupling variation.

Once the method of signal processing has been established, the computer based digital signal processor was replaced with a dedicated signal analyser. In the final prototype, the analyser performed the data acquisition and the signal processing and the computer acted as system supervisor, informing the analyser what operations it should perform and acting as a mass storage device for the data.

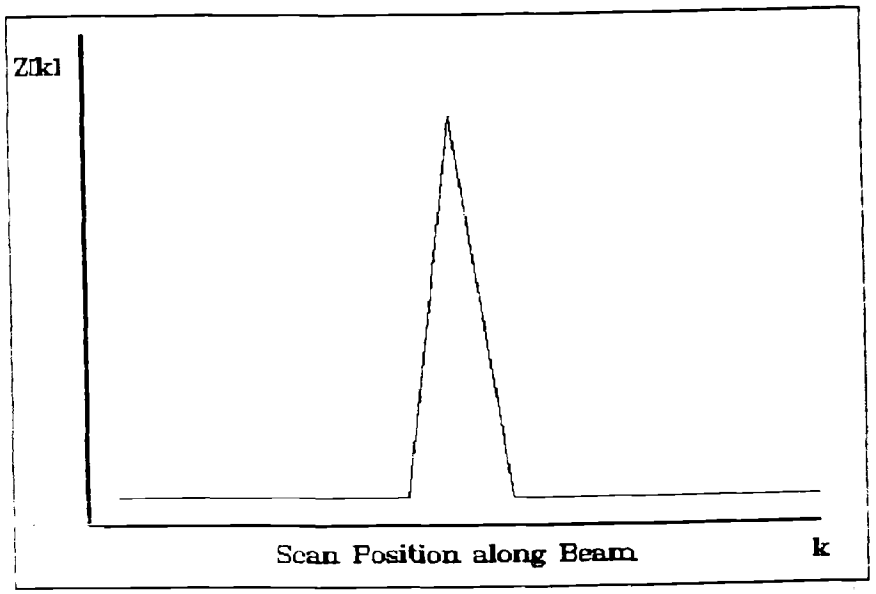

Figure 6. Typical Output of System, after analysis. "Spike" indicates location of defect.

SUMMARY

The rate of corrosion measurement system as described above makes it possible to electrochemically determine the rates of corrosion of steel reinforcement in concrete. Both E_{corr} and corrosion rates are determined at each grid location and stored, making it possible to draw both corrosion potential and corrosion rate contour maps of the surveyed structure. Corrosion rate variation is usually greater than that of corrosion potential on any particular structure, making it easier to identify areas at risk. This is not unreasonable as corrosion rates for steel in concrete appear to follow an E vs log i_{corr} relationship [18]. Absolute corrosion rates may also be computed if the reinforcement size and density are known at each location, and may be used to accurately assess the extent of the corrosion damage.

The development carried out to date on ultrasonic inspection systems indicates that it has the potential for providing information with regard to the present condition of the prestressed components without the need for destructive examination. However, it should be pointed out that it would be anticipated that such a system would be used in conjunction with other inspection procedures and not as a sole criterion for structural integrity. Given the possible speed of any such survey it would enable regular and rapid scanning of structures to identify potential problem areas for further assessment by other techniques including, where necessary, break out and direct physical examination.

ACKNOWLEDGEMENTS

The authors wish to express their thanks to The National Academy of Sciences, Transportation & Research Board, National Co-operative Highway Research Programme, for permission to reproduce some of the work carried out and to colleagues in CAPCIS and the Department of Civil Engineering and Department for Instrumentation & Analytical Science, UMIST, for assistance in the ultrasonic work.

REFERENCES

1. DAWSON, J.L., Chapter 12 in Corrosion of Reinforcement in Concrete Construction, ed. A.P. Crane, Pub. Ellis Horwood, U.K., 1983.

2. ESCANTE, E, NBS Report NBSIR 86-3456, October 1986.

3. HLADKY, K., JOHN, D.G. & DAWSON, J.L., Paper No. 169, presented at NACE/Corrosion '89, New Orleans, April 1989.

4. DAWSON, J.L., JOHN, D.G., JAFAR, M.I., HLADKY, K. & SHERWOOD, L, paper presented at Corrosion of Reinforcement in Concrete, Belfry Hotel, May 1990, published by Elsevier Applied Science, eds. C.L. Page, K.W.J. Treadaway & P.B. Bamforth.

5. ISECKE, B, Chapter 5 in Corrosion in Reinforcement in Concrete Construction, ed. A.P. Crane, Pub. Ellis Horwood, U.K., 1983.

6. WOODWARD, R.J., "Conditions within ducts in post-tensioned and prestressed concrete bridges". TRRL Laboratory Report 980, 1981.

7. "Non-destructive methods for field inspection of embedded or encased high strength steel rods and cables". NCHRP Project 10-30 (1), October, 1986.

8. "Detecting Defects and Deterioration in Highway Structures", ed. D.C. Manning, NCHRP, Syn. of Highway Practice No. 118, 1985.

9. HLADKY, K. & JOHN, D.G., UK Pat. Appl. 87 22088, PCT and Canadian Pat. Appl. 1988.

10. JOHN, D.G. & HLADKY, K, paper presented at UK Corrosion '90, Sandown Park, Esher, November 1990, pub. Institute of Corrosion, Leighton Buzzard, U.K., 1990.

11. HEJJI, J.A., JOHN, D.G. & SULLIVAN, R.K., paper no. 388, presented at NACE/Corrosion '89, New Orleans, April 1989.

12. CARLETON, H.R. & MURATORE, J.F., IEEE Ultrasonics Symposium, Vol. 2, pp 1017-1020 (1986).

13. GAYDECKI, P.A., BURDEKIN, F.M., DAMAJ, W., JOHN, D.G. & PAYNE, P.A., IEE Collquium on Measurements, Modelling and Imaging for Non-Destructive Testing. Digest No. 1991/054, 27 March, 1991.

14. GAYDECKI, P.A., BURDEKIN, F.M., DAMAJ, W, JOHN, D.G. & PAYNE, P.A., A detailed feature extraction from concrete media using medium frequency ultrasound and digital signal processing methods. Proc. I.O.A. Vol. 13, Part 2, pp. 195-202.

15. GAYDECKI, P.A., BURDEKIN, F.M., DAMAJ, W, JOHN, D.G. & PAYNE, P.A., The propagation and attenuation of medium-frequency ultrasonic waves in concrete; a signal-analytical approach. (Measurement Science and Technology. Accepted for publication).

16. BURDEKIN, F.M., JOHN, D.G., PAYNE, P.A., SMITH, T.A. & GAYDECKI, P.A., CAPCIS-UMIST, Manchester, U.K. Non-destructive methods for field inspection of embedded or encased high strength steel rods and cables. NCHRP project 10-30(3) Final Report, June 1991.

17. JOHN, D.G. & GAYDECKI, P.A., paper presented at UK Corrosion '91, Manchester, October 1991, pub. Institute of Corrosion, Leighton Buzzard, U.K.

18. JAFAR, M.I., DAWSON, J.L. & JOHN, D.G., paper presented at ASTM symposium on Electrochemical Impedance, San Diego, Nov. 5-6, 1991.

Mitsuru Shimizu[1], Norimitsu Mukai[1], Masahiro Hamada[2], Junichi Shimamura[2]

AN AUTOMATIC PIPE CORROSION INSPECTION SYSTEM

REFERENCE: Shimizu, M., Mukai, N., Hamada, M., and Shimamura, J., **"An Automatic Pipe Corrosion Inspection System,"** Corrosion Forms and Control for Infrastructure, ASTM STP 1137, Victor Chaker, Ed., American Society for Testing and Materials, Philadelphia, 1992.

ABSTRACT: Corrosion in various buildings and factory piping has been a serious concern for many industries. Corrosion-related leaks or pipeline bursts may cause expensive damage to property and result in shutting down the operation. Therefore, nondestructive corrosion inspection of inside piping has become more important. Utilizing ultrasonic waves, internal corrosion and metal loss can be measured. However, existing inspection techniques were not satisfactory to determine the accurate condition. In this scenario, an automatic pipe corrosion inspection system was developed, utilizing state-of-the-art electronics technology. The system consists of an inspection device and a data processing unit. The inspection device travels on the external pipe surface, while the data processing unit displays the condition of both the internal surface and a cross section areas of the pipe. The data collected by the robot is also numerically analyzed to calculate the pipe thickness distribution, the minimum thickness, metal loss percent and corrosion rate and to estimate the remaining service life of the pipe based on proper theory. This inspection can also be applied on the threaded pipe section to determine the allowable metal loss. To verify the performance and accuracy of the data collected using the robot, partifical corroded pipes are tested. This paper will discuss the abilities and limitations of the automatic pipe corrosion inspection system and the results of the verifications tests.

KEYWORDS: pipe corrosion, internal corrosion, inspection system, ultrasonic wave, robot, verifications tests

[1]Deputy General Manager and Deputy Manager, Facilities Planning Deparmtment, OBAYASHI CORPORATION, 2-2-2, Kanda Tsukasa-cho, Chiyoda-ku, Tokyo 101, Japan.

[2]Managers, Production Technology Center, Osaka Gas Co., Ltd. 1-1-16 Hokko, Konohana-ku, Osaka 554, Japan.

INTRODUCTION

A new trend of using nonmetallic or compound pipes for the piping of building facilities has recently been prevailing. However, metallic pipes, particularly the pipes made of carbon steel, are still widely used. In Japan, the raw water with low hard component is subjected to purification before being supplied as the service water for building facilities. Because of the increasing amount of coagulant and chlorine added to the raw water for purification to cope with the deteriorating quality of the raw water, the corrosive environment in building facilities has been worsened in these recent years, leading to the problem of corrosion of the facility pipes in existing buildings.

Furthermore, the evaluation of the condition and durability of a piping system, largely influencing the improvement plan of the laid pipes throughout the building, has become an important factor under the social background calling for an improved facility system to meet with the new functional demand. Therefore, it has become indispensable to carry out corrosion diagnosis of the pipes to grasp the corrosion status of the existing metallic pipes.

To cope with the present situation, "Automatic Pipe Corrosion Inspection System" as a method of corrosion diagnosis has developed. This system is capable of carrying out automatic non-destructive diagnosis by using ultrasonic wave.

This paper describes the details of the development of the such system, the purpose of development, its outline and functions.

DETAILS OF DEVELOPMENT AND PURPOSE OF DEVELOPMENT

The existing pipe diagnostic methods have numerous problems apparently with no solutions yet, calling for a systematized diagnosis method. In the process of development the vital factors demanded in the actual corrosion diagnosis were extracted. These factors and the corresponding measures thereby are given below:

1) Shall not involve the stoppage of carrying (transmission) function of a piping system - Shall be limited to the "non-destruction diagnosis" on the outer surface of a pipe.

2) Minimum residual wall thickness of the carbon steel pipes can be firmly detected. - "The ultrasonic measurement technique" shall be applied.

3) The pipe corrosion form can be grasped. - The "automation of measurement" shall be carried out to collect a large quantity of data regarding the wall thickness, position, etc.

4) Measurement at narrow place is possible. - The apparatus to be installed to a pipe shall be preferably compact.

5) Shall have the data analyzing function. - The personal computer shall be connected to analyze.

6) Measurement at the bent (elbow) portion shall be possible.

7) Measurement can be made on the coated pipe.

8) Lamination can be detected.

9) Remeasurement shall be possible if the collected data turns out to be defective.

The development of "Automatic Pipe Corrosion Inspection System" was commenced in order to cope with the factors mentioned above.

OUTLINE OF "AUTOMATIC PIPE CORROSION INSPECTION SYSTEM

The block diagram of the system is shown in Fig. 1. The system is composed of a "pipe inspection robot unit" that carries out the field measurement and simple analysis, and a "data processing system unit" that carries out precise data analysis and image representation.

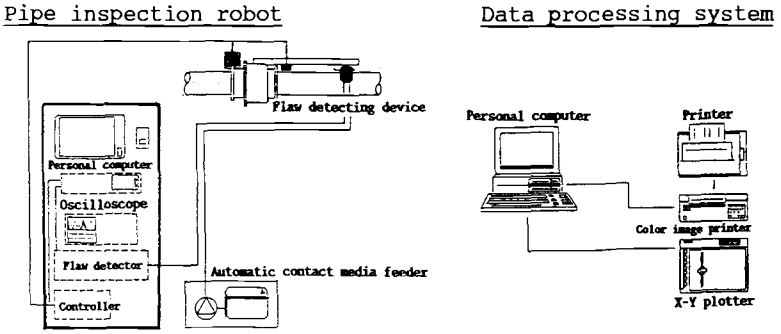

FIG. 1 -- System block diagram.

1. Pipe Inspection Robot Unit

The Photo. 1 shows the pipe inspection robot carrying out field measurement.

(1) Flaw detecting device

Installed to the pipe, the flaw detecting device is composed of the pipe fixing jig, rolling unit and ultrasonic probe holder.

1) Pipe fixing jig

The pipe fixing jig is used for ensuring the fixing strength of the system and for carrying out pipe centering. The jig is divided into two sections, one section equipped with the pulse motor (with pinion gear) to carry out rotation and control of the rolling unit. The rotary rail is also installed in the circumferential direction to allow the rolling unit to travel along the appropriate orbit.

The centering for fixing and piping is carried out by engaging and integrating the pipe fixing jig to the pipe by means of a clamp, and then tightening the spacer block, installed at the tip with the adjusting screws inserted into the flanges at both ends of the jig toward the center. Three types of pipe fixing jigs (for small aperture: 20 - 100 A, for medium aperture: 125 - 200 A, and for large aperture: 225 - 300 A) are available to enable measurement even at narrow places.

2) Rolling unit

The rolling unit, on receiving the driving force from the pulse motor, rolls over the pipe fixing jig, and shifts the probe holder appropriately over the pipe axis. The contact with the pipe fixing jig is made by means of the built-in driven wheel. The rolling unit is divided into two sections, with one section equipped with a scanner in the Y-axis where the probe holder makes axial movement.

The movement of the probe holder in the axial direction of the pipe is made by the driving force from the concerned pulse motor, transmitted to the holder connector through the built-in belt in the

Y-axis scanner. Furthermore, the Y-axis scanner is equipped with an original position sensor at the foremost end, and with a terminal point stopper at the tip end to prevent malfunction.

PHOTO. 1 -- Field measurement using pipe inspection robot.

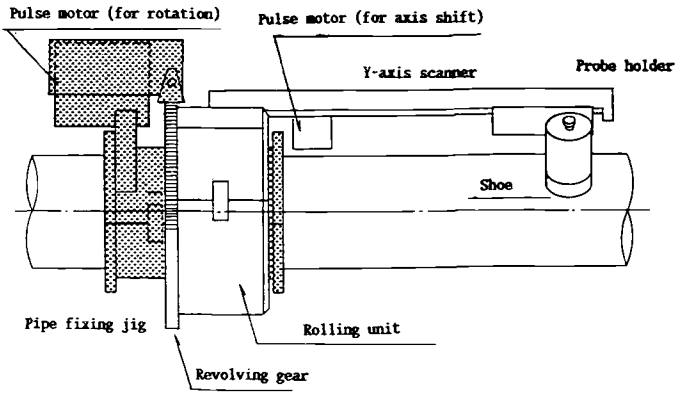

FIG. 2 -- Outline of flaw detecting mechanism.

3) Detecting probe holder

Photo. 2 shows a set-up probe holder. The probe holder is composed of the ultrasonic probe, shoe befitting with the pipe curvature, displacement absorbing mechanism with various springs, etc. The shoe enables smooth movement (shifting) of the probe in the circumferential direction, and is also used for retaining the contact media in the specified space between the probe and the pipe to appropriate quantity. The displacement absorbing mechanism, on the other hand, absorbs the unevenness on the outer surface of the wall and the three-dimensional displacement on the curved section to allow smooth follow-up.

(2) Operation control panel

The operation control panel is composed of a controller that carries out the scanning control of the ultrasonic probe, an ultrasonic flaw detector that carries out measurement, a lap-top personal computer that controls the above-mentioned apparatuses in addition to carrying out data collection, storage and analysis.

The operation control panel is also equipped with an oscilloscope to enable the real time verification and monitoring of the propriety of the obtained data, and a monitor screen on the CRT to monitor the data during measurement. The data, judged appropriately at the field, is stored in the FD before being transmitted to the data processing system unit. However, the operation control panel is also possessed with the function of making basic analysis. As an example of the image representation at the operation control panel, the "pipe section indication" is shown in Photo. 3.

(3) Automatic contact media feeder

This system applies the gap submerged coupling system (the system that enables indirect contact rather than the direct contact by interposing the contact media between the probe and the pipe). In this system the contact media is fed automatically into the probe holder by using the variable speed, geared pump pressure-feed system.

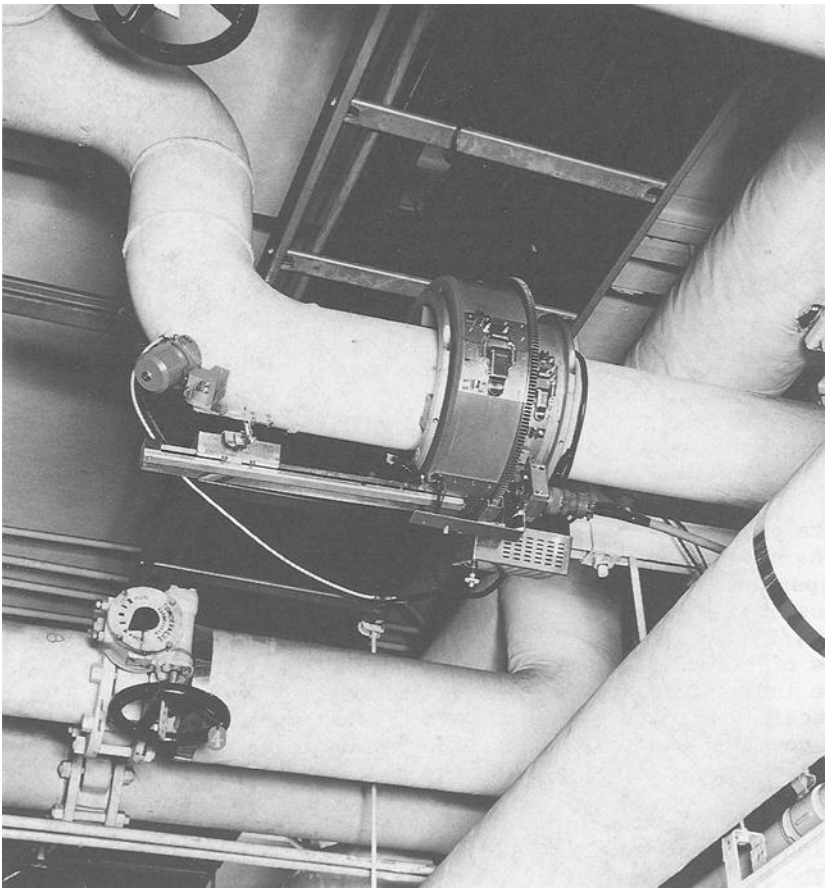

PHOTO. 2 -- Installation of detecting probe

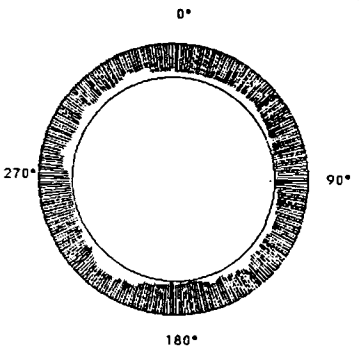

PHOTO. 3 -- Example of image output on operation control panel

2. Data processing system unit

As shown in Fig. 1, the data processing system unit is composed of a personal computer, a printer and a plotter, and carries out processing of the data, stored by the pipe inspection robot, through the 3 1/2" floppy disc. In order to give a clearer vision of the status of corrosion, the following image representations are made: "plane indication of residual wall thickness," "vertical and horizontal section indication of pipe," "estimated section indication of the screw coupling section," etc. In addition to the above processings, the following numerical processings can also be made: "residual wall thickness degree distribution and analysis," "estimation of the remaining life of the pipe," and "statistic processing of several testpieces in the same piping system."

The actual examples of the "plane indication of residual wall thickness" and the "residual wall thickness degree distribution and analysis" are shown respectively in Figs. 3 and 4. The system outline chart and the specifications for measurement are summarized in Tables 1 and 2 respectively.

RESULTS OF TESTS

Various tests were made to verify the functions of this system regarding the measurement. The results of the tests are given in this Chapter.

1. Functional verification at the pipe resorted to natural corrosion

To verify the functions enabling secured detection of complicated forms of corrosion, the results obtained by the measurements of the cold and hot water pipes actually laid in a certain office building, and the actual results obtained by overhaul and analysis of the pipes on which the measurements were made are presented here for comparison. The image representation of the "plane indication of

residual wall thickness," obtained through this system, is given in Fig. 3.

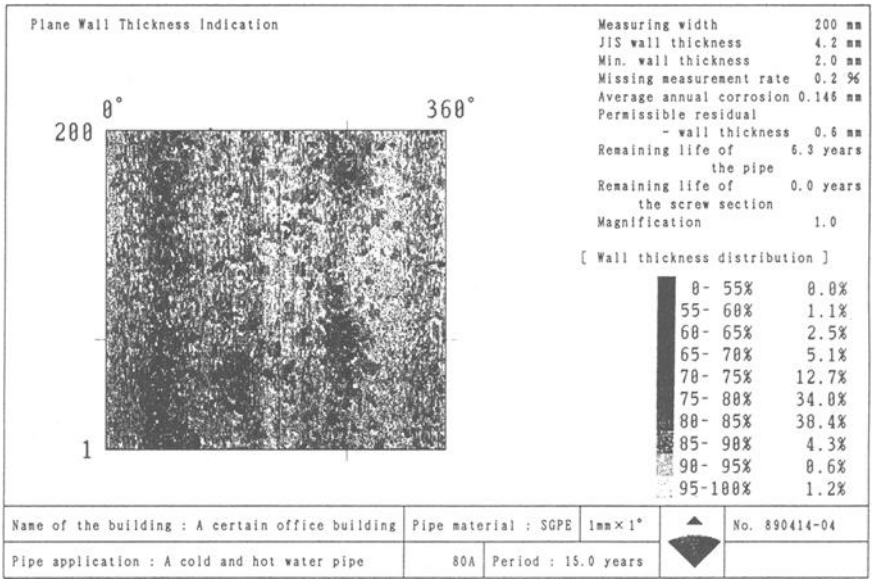

FIG. 3 -- Plane indication of residual wall thickness.

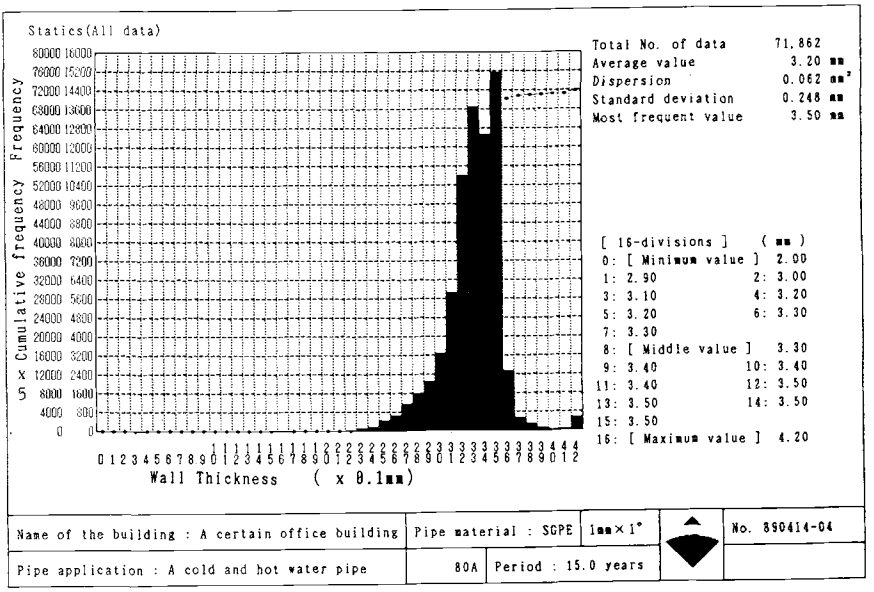

FIG. 4 -- Analysis of frequency distribution of wall thickness.

TABLE 1 -- System outline chart

Item	Outline
Deterioration diagnosis procedure	Deterioration diagnosis through evaluation of corrosion due to the automatic measurement of residual wall thickness by using ultrasonic wave
Ultrasonic flaw detecting mechanism	Ultrasonic flaw detector: Pulsar output over 200 V Repeat frequency 625 Hz Detecting probe : Separate-type vertical probe Frequency 10 MHz Trembler diameter 5 mmϕ Flaw detecting cable: Double-layer shielded
Drive and transmission system	Circumferential direction: Gear transmission due to pulse motor Pipe axial direction: Belt transmission due to pulse motor
Data sorting system	The minimum values are extracted out of the several wall thickness data collected during measurements. Number of data: N = PL x PRF/V where; PL: Distance between the points of measurement (mm) PRF: Repeat frequency (Hz) V : Circumferential scanning speed (mm/s)
Measurement of curved pipe	Measured by installing the extension adjusting jig to the flaw detecting mechanism * Indefinite position accuracy
Measurement through paint Detection of lamination	Original point correction due to B1-B2 system * Paint thickness at the original point shall be uniform as the premise
Detection of lamination	The analytic program, obtained through the analysis of lamination characteristics, is used.

TABLE 2 -- Specifications for measurement using the system

Item	Specifications
Measurable pipe	Carbon steel pipes for piping [JIS-G 3452, G 3454, ASTM-A 120, A53 (F), A 135, A 53 (A, B)], etc.
Measurable range	The measurement can be made within the following range. Axial direction of pipe : Max. 200 mm Circumferential direction: Max. 360°
Applicable curved pipe	Pipes above 100 A of JIS B 2311 and JIS B 2312 can be measured.
Measurable pitch	Circumferential direction: 1.0 mm or 2.0 mm (20 A - 150 A) 2.0 mm (175 A - 300 A) 1.0 mm is also possible in the case of partial measurement Axial direction (of the pipe): 1.0 mm or 2.0 mm
Number of measurable points	103,600 points for 1.0 mm x 1.0 mm in 150 A pipe
Scanning speed	Circumferential direction: 10, 20, 30 mm/sec Axial direction : 20 mm/sec
Time required for measurement	55 - 60 minutes for 100 A pipe at the scanning speed of 30 mm/sec
Fault detecting mechanism installation space	Axial direction: 650 mm Pipe periphery : Unit mounting surface 1,000 mm (approximately) Other three surfaces: 110 mm

Furthermore, the internal corrosion of the pipes arranged in plane after subjecting to pickling and rust removing is given in Photo. 4.

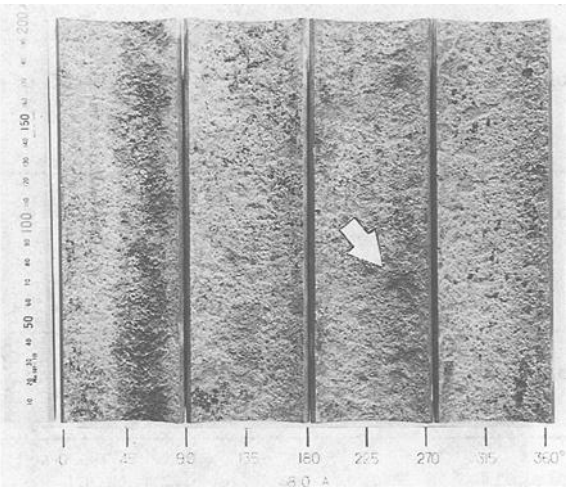

PHOTO. 4 -- Internal corrosion on the pipe subjected to overhaul and analysis

The degree of corrosion is given in terms of color-stage-tone in Fig. 3, indicating distinctly the banded corrosion in the pipe axial direction (near 60°) and the two pin-hole corrosion spotted near 45° in Photo. 4. The results of comparison of the maximum corroded section (pin-hole corrosion: arrow mark) of the concerned pipe are given below.

[Results of Overhaul and Analysis]
Position: 245° in circumferential direction, 65 mm in pipe axial direction
Residual wall thickness: 2.0 mm

[Results of measurement using this system]
Position: 249° in circumferential direction, 69 mm in pipe axial direction
Residual wall thickness: 2.0 mm (measured with a point micro meter)

Since the concerned pin-hole corrosion size is approximately 5 mmø, it can be safely judged that the fault detecting function has been almost verified.

2. Functional verification at the pipe subjected to artificial fault (defect)

The cylindrical corrosion model under the assumption of "hole corrosion," normally considered hard to detect, and the V-corrosion model under the assumption of "groove corrosion on the electro-unite pipe" were artificially made on the inner surface of 20 A and 300 A carbon steel pipes by means of electro spark machining.

The plane development diagram of the 300 A pipe subjected to artificial fault is shown in Fig. 5.

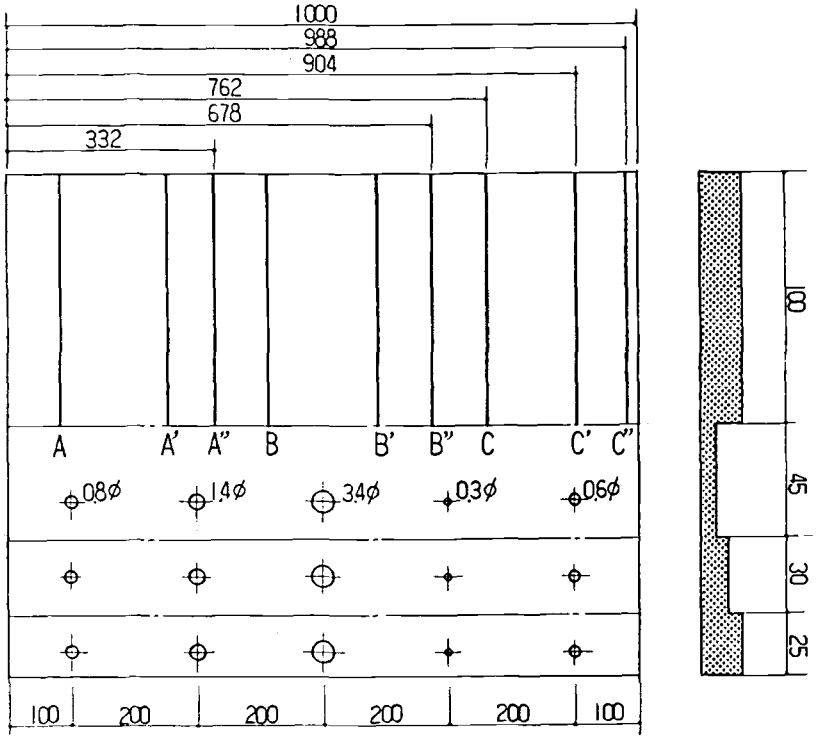

[Tip-end shape of V-corrosion model]
ABC: R < 0.1 mm, A'B'C': R = 0.1 mm A"B"C": R = 0.25 mm

[V-corrosion model]
A: tx = 0.9 x t0 B: tx = 0.5 x t0 C: tx = 1.1 mm
tx: Residual wall thickness(mm) t0: Wall thickness of base metal(mm)

FIG. 5 -- Plane development diagram of artificially corroded 300 A pipe

(1) Functional verification of V-corrosion model

An example of the image output of the "plane developed and enlarged indication" of the V-corrosion model, obtained through the experiment made on the 300 A model pipe by using this system, is shown in Fig. 6, while the results of the analysis of the data on V-corrosion model, obtained through the experiment made on the 20 A and 300 A model pipes are given in Table 3.

The above results make the following point clear.

1) In the case of V-corrosion model the fault with the tip end size 0.25 mmR was detected at 2 points in the 20 A model pipe, while all faults with tip end size 0.25 mmR, faults with tip end size 0.1 mmR and below 0.1 mmR were found at one point each in the 300 A model pipe.

2) The detection position accuracy in all cases remains within the range of -0.1 - +2.0 mm.

3) The measured wall thickness accuracy in all cases remains within the range of -0.4 - +0.1 mm.

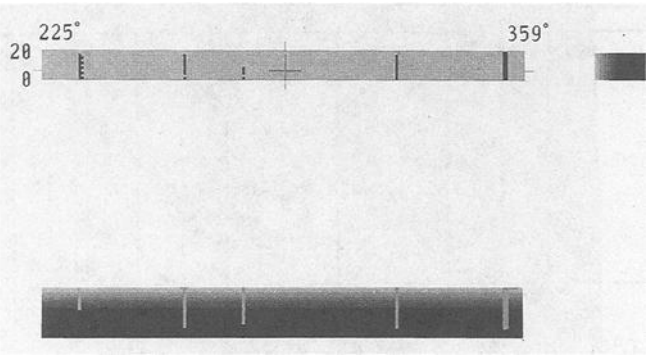

FIG. 6 -- Plane development diagram (plan) of V-corrosion model.

TABLE 3 -- Analysis result of V-corrosion model

Aperture	Tip-end shape	Standard value		Data obtained through the system				
		Wall thickness	Circumferential position	Detecting position	Minimum value	Most frequent value	Maximum value	Average value
20 A	A"	1.4 mm	4 mm	5/5 mm 4	0.7 mm 1.0	1.5 mm 1.2	2.0 mm 1.2	1.6 mm 1.2
	B"	0.9 mm	46 mm	48/48 48	0.5 0.5	1.0 0.5	1.4 0.6	1.0 0.5
300 A	A"	6.0	320	320/322	5.6	5.7	6.8	5.7
	B"	3.1	652	654/656	3.2	3.4	3.4	3.3
	C	1.1	736	736/738	0.7	0.8	0.8	0.8
	C'	1.1	904	902/904	0.7	0.8	0.8	0.8
	C"	1.1	987	986/988	0.8	0.8	0.8	0.8

(2) Functional verification of cylindrical corrosion model

Fig. 7 shows an example of the image output of the "plane developed and enlarged indication" of the cylindrical corrosion, obtained through the experiment made on the 20 A model pipe, while Table 4 shows the results of the data analysis regarding the cylindrical corrosion model of the 20 A and 300 A model pipes.

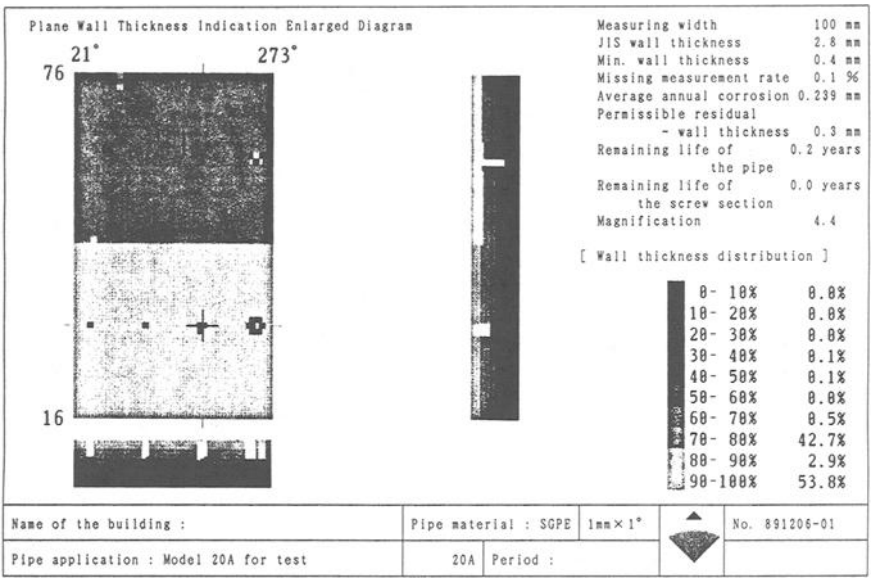

FIG. 7 -- Plane developed and enlarged indication of cylindrical corrosion model

The results make the following points clear.

1) In the case of cylindrical corrosion model, all faults of size 0.6 mmϕ - 3.4 mmϕ in the 20 A model pipe and the faults ranging from 0.8 mmϕ - 3.4 mmϕ in the 300 A model pipe were detected.

2) The detection position accuracy (error range) remains within ±1.5 mm in the case of 20 A, and within 0 - +1.0 mm in the case of 300 A model pipe.

3) The measured wall thickness accuracy remains within 0.6 mmϕ: ±0.1 mm, 0.8 mmϕ: 0 - +0.3 mm in the case of 20 A, 0 - +0.1 mm in the case of 300 A, and 0.1 - +0.5 mm in the case of the other model pipes. Through the above experiment results, it can be deduced that the inspection (diagnosis) system can be safely put to practical use.

3-3. Other functional verifications

(1) Measurement through paint

This experiment, made on the partially painted pipe subjected to artificial corrosion, showed the same result as in the case of a pipe without paint Therefore, it has been proved that the measurement can be made through the paint, provided that the paint thickness on the wall is uniform.

(2) Measurement on curved pipe (elbow) sections

Although the wall thickness measurement accuracy, etc. have not yet been confirmed since the obtained result has not yet been put to comparison (verification) with the result of overhaul and analysis of the actual curved pipe, it is found that the measurable range is roughly ±15° with the back of the curved pipe as standard, and approximately 80 - 120 mm in the axial direction of the pipe.

TABLE 4 -- Analysis result of cylindrical corrosion model

Aperture	Hole (pitting) corrosion dia.	Standard value		Data obtained through the system				
		Wall thickness	Circumferential position	Detecting position	Minimum value	Most frequent value	Maximum value	Average value
20 A	0.6ø	1.7 mm 1.2	8.5 mm 8.5	8/11 mm 9/10	1.6 mm 1.2	1.8 mm 1.2	1.8 mm 1.2	1.8 mm 1.2
	0.8ø	1.7 1.2	25.5 25.5	26/27 27/27	1.5 1.2	1.5 1.2	1.5 1.2	1.5 1.2
	1.4ø	1.5 1.2	42.5 42.5	43/45 44/44	1.6 0.9	1.7 0.9	1.7 0.9	1.7 0.9
	3.4ø	1.4 0.9	59.5 59.5	55/59 59/63	1.4 1.2	1.5 1.2	1.5 1.3	1.5 1.3
300 A	0.8ø	5.6 3.4 1.2	100 100 100	99/100 99/100	5.5 3.8	5.5 3.8	5.7 3.9	5.6 3.8
	1.4ø	5.5 3.3 1.1	300 300 300	296/299 295/299 298/300	5.6 3.8 1.1	5.6 3.8 1.1	5.8 3.9 1.2	5.7 3.8 1.2
	3.4ø	5.3 3.3 1.0	500 500 500	494/500 494/498 496/500	5.6 3.7 1.0	5.6 3.8 1.0	5.9 3.9 1.7	5.7 3.8 1.4

(3) Recollection of data

Measurements were made several times on the same section of a pipe resorted to natural corrosion, and the results were compared to indicate that the reproduction of data is possible with accuracy of ±0.1 mm, provided that the flaw detecting device is normally installed.

CONCLUSION

Through the various experiments made to verify the functions of the system, the system seems to have achieved the object set at the initial stage of development. However, there are some problems left unsolved yet, such as the diagnosis limited to certain pipes, applicable partially to the curved section only, etc. We are determined to continue making effects to find some solutions to these problems.

Jey K. Jeyapalan, Ph.D, P.E.

PREDICTION AND CONTROL OF SULFIDE INDUCED CORROSION IN CONCRETE SEWER INFRASTRUCTURE AND REHABILITATION TECHNIQUES

REFERENCE: Jeyapalan, J. K., "Prediction and Control of Sulfide Induced Corrosion in Concrete Sewer Infrastructure and Rehabilitation Techniques," Corrosion Forms and Control for Infrastructure, ASTM STP 1137, Victor Chaker, Ed., American Society for Testing and Materials, Philadelphia, 1992.

ABSTRACT: Most cities, counties, and sanitary districts have used concrete pipe for sewer construction during the past 100 years. Many of these pipelines under certain site conditions have been corroded by sulfuric acid formed from sulfide gas. Despite this track record, many design engineers are still selecting concrete pipe with some allowance for corrosion using the somewhat outdated sacrificial wall thickness method. There are numerous agencies which do not even include sulfide corrosion prediction and control as part of the sewer structure material selection process. Even when sulfide corrosion studies are undertaken, no engineering considerations are given for the potential of corrosion in structures such as wet wells, manholes, drop structures, and metering stations. Deteriorated concrete pipe in some cases is replaced with new concrete pipe with no provisions for corrosion and such practices will lead to premature failure of the sewer system and excessive rehabilitation budgets. This paper presents the state-of-the-art of prediction and control of sulfide corrosion in sewers and rehabilitation methods available for repairing such sewer systems.

KEYWORDS: sanitary, sewers, concrete, rehabilitation, sulfide, coatings, liners, admixtures, corrosion

INTRODUCTION

The most common sanitary sewer pipe material is reinforced concrete. Unfortunately many agencies have experienced serious problems of concrete sewer deterioration due to sulfuric acid attack resulting from hydrogen sulfide gas. The sulfide induced corrosion is normally in the part of the sewer that is exposed to atmosphere and moisture. Corrosion caused by acidic discharges found in the industrial effluent affect the lower half of the sewer pipe carrying the discharge. Under severe conditions, the concrete wall thickness close to the crown of pipe can

Dr. Jeyapalan is an Engineering Consultant, 21310 NE 101st Court, Redmond, Washington, USA 98053. Phone 206-868-6998

disappear at the rate of 1.0 to 3.0 cm per year due to sulfide corrosion. In corrosive soils, the outside of the concrete pipe also could be attacked by salts such as sulfates and chlorides. States having severe problems of sulfide corrosion in four or more municipalities are Washington, California, Arizona, Texas, Lousiana, Florida, Iowa, Illinois, Indiana, Ohio, Michigan, Wisconsin, Pennsylvania, New York, and Massachussets. Some of the worst corrosion problems have been reported in Seattle, Boise, Milwaukee, Casper, Albuquerque, Baton Rouge, Fort Worth, Los Angeles, San Diego, Sacramento, New Orleans, and Tampa. The survey by the Los Angeles County Sanitation Districts indicated that of the 89 cities responded, about 30 % reported sewer collapses due to sulfide corrosion, and 63 % have taken some steps to control this problem.

Although much is known about the sulfide problem, engineers are still designing sanitary sewer systems either with no evaluation for sulfide corrosion or with the sacrificial wall thickness, most commonly known as the "Az" method. Even when some sulfide corrosion predictions are made, the structures such as manholes, drop structures, wet wells, metering stations, etc. are usually not protected. Deterioration of a sewer system can result in loss of ability to transport sewage, contamination of ground and the groundwater supply, excessive ground settlements, and cave ins. The design engineer and the owner should recognize the adverse consequences of improper engineering practices and must undertake appropriate measures during planning and design of sewer systems for their communities. The practice of selecting the most suitable pipe material based solely on the review of pipe material suppliers' product literature will result in early rehabilitation of the sewer infrastructure.

PREDICTION OF SULFIDE BUILDUP

Evaluation of corrosion caused by hydrogen sulfide in concrete sewers require some understanding of the chemical behavior of sulfides. The conditions necessary for hydrogen sulfide corrosion are as follows:

- o Reduction of sulfates to sulfides
- o Dissolved sulfides in the wastewater
- o Release of hydrogen sulfide from the water to gas form
- o Bacterial conversion of hydrogen sulfide to sulfuric acid
- o Sulfuric acid in contact with the exposed concrete surface

Three approaches have been tried over the years by engineers practicing in this area of environmental engineering to forecast the likelihood of sulfide buildup in certain classes of sewers and these are namely:

- o limiting velocity
- o flow-slope relationship
- o Pomeroy's Z formula

These methods do not give reliable indications of sulfide buildup potential and therefore, it is recommended that the design engineer proceeds to predicting sulfide buildup using more rational equations which would model the problem better.

The rate at which hydrogen sulfide is generated by the slime layer formed on the inner surface of the concrete pipe or structure is controlled by factors such as:

- o Biological Oxygen Demand
- o Concentration of Sulfates
- o Dissolved Oxygen
- o pH
- o Temperature
- o Flow Velocity
- o Exposed Surface Area
- o Detention Time
- o Slope

It is necessary to simulate varied conditions of flow in order to get reliable estimates of sulfide buildup. Numerous mathematical models have been reported in the literature for this purpose and the most commonly used equation is that by Pomeroy-Parkhurst[1] for partially filled sewers. This model is based on research conducted primarily in the collection systems of Los Angeles County. This model is applicable only when the conditions satisfy the basic criteria for sulfide buildup. The model is not applicable when the DO level exceeds 0.5 mg/L. The model is given by

$$dS/dt = M'[EBOD]/r - N\,(sv)^{0.375}\,[S]/d_m$$

where S = total sulfide concentration
t = time
M' = empirical constant to account for sulfide generation
N = empirical constant to account for sulfide loss
EBOD = effective BOD
r = hydraulic radius
s = slope of energy gradient
v = mean velocity
d_m = mean hydraulic depth

At equilibrium, when the gain is equal to the loss of sulfide, the limiting sulfide concentration, S_{lim} is obtained using the equation

$$S_{lim} = 1.56\,M'[EBOD](sv)^{-.375}\,p/(b\,N)$$

where p = wetted perimeter
b = surface width of flow

Thus, the sulfide generation in a series of pipe reaches with varying hydraulic properties can be obtained with the use of an integrated form of the governing equation and this is

$$t_2 - t_1 = 1.1 d_m \{\log (S_{lim} - S_1) - \log (S_{lim} - S_2)\}(sv)^{-.375}/N$$

Numerically applying this equation, with the assumption that S_2 for the first reach could be used as the S_1 for the next reach, it is possible to calculate the sulfide levels for a series of reaches. One such effort is the computer program SULF.BAS by Kienow and Kienow[2]. When the characteristics of the effluent varies substantially from tributaries to the primary interceptor, the sulfide conditions at the junctions should be carefully modelled using mass balance equations.

In a force main or surcharged sewer trunk line, the pipe is flowing full, thus minimizing

surface reaction, sulfide oxidation potential, and sulfide losses to the sewer atmosphere. Furthermore, the DO is assumed to be zero. Thus, the sulfide predictions are normally done using the EPA equation[3] which is given by

$$S_2 = S_1 + M\,t\,[EBOD(4/d + 1.57)]$$

where d = pipe diameter

Even at this stage of the prediction, the equations have too many empirical constants and result in uncertainties in the calculation of sulfide buildup in sanitary sewers. Field calibration of calculated results using observed values on representative reaches are always required in order to make reliable predictions in the remaining reaches of any given sewer.

CORROSION EVALUATION

Hydrogen sulfide buildup eventually leads to corrosion of the sewer structures which can be visually documented. Thus, physical inspections, close circuit televising, and some concrete core samples are always necessary. Once these data become available numerical modelling should follow to verify field results. The rate of corrosion of concrete can be predicted based on the assumption that the rate depends on the rate at which sulfuric acid is generated in the sewer, the alkalinity of the concrete, and the hydraulic considerations. Pomeroy assumed that the total amount of hydrogen sulfide reaching the wall and the amount that will be oxidized and made available for reaction with the pipe material will control the corrosion rate. The equation he developed is given by

$$C_{avg} = 0.45\,k\,PHI_{sw}/A$$

where C_{avg} = average rate of penetration of corrosion in m/yr
k = coefficient of efficiency for acid reaction
PHI_{sw} = flux of sulfide to the pipe wall in g/m^2-hr
A = alkalinity of the concrete wall in calcium carbonate equivalent

It should be emphasized that the PHI value used in this equation is the annual average sulfide concentration and not either the peak or climactic value. The peak corrosion rates are calculated using factors such as those in the equation

$$C_{peak} = C_{avg} \cdot CCF \cdot TCF$$

where CCF = crown corrosion factor
TCF = turbulence corrosion factor, when the flow is nonuniform
C_{peak} = peak corrosion rate in m/yr

When the design and construction of a new sewer system is in the planning stage, the sulfide buildup evaluation of the existing system verified by field data will provide valuable insight into trouble spots. If the existing collection system can be repaired,

it still requires engineering studies to determine the extent to which sulfide would buildup in the future years. Such an evaluation of the existing system requires careful planning and execution. A strategy should be developed to get the most for the tax dollars available for

investigation of the sulfide problem. The field work should be done methodically with the appropriate level of planning, preparation, and inspection. Concrete coring, effluent sampling, and analytical work to determine the characteristics of the effluent are all time consuming and expensive. Thus, sampling locations should be carefully selected to optimize the fieldwork and data collection.

CONTROL OF SULFIDE CORROSION

It is necessary to design to avoid sulfide buildup and the related corrosion in sewer structures. Many efforts could be undertaken by the designer and the owner to avoid future problems of corrosion. For small sewers, proper flow velocities and slopes are chosen to minimize sulfide buildup. Proper ventilation, periodic cleaning of the sewer, limiting the length of force mains, grinding the solids before it enters the sewer, providing pretreatment at a septic system, and using either pressurized or vacuum for driving the effluent are all prudent practices to consider for improving the design life of the sewer structures.

For trunk sewers, velocities should be chosen to avoid excessive deposits of solids. Proper ventilation is equally important. Special structures and manholes should be carefully designed to avoid excessive deposition of solids and to avoid too long a detention time. Adequate maintenance and monitoring should be part of the O & M budget of the owner.

Most concrete pipe designs are still done using the Az method, where

$$Az = 0.45\ PHI_{sw}.\ L.\ CCF.\ TCF$$

in which L is the design life of the concrete sewer structure with the assumption that the sacrificial wall thickness at a certain alkalinity level will provide the necessary protection against loss of use of the concrete sewer ahead of its intended design life. This practice unfortunately has not yielded any meaningful engineering solutions to the hydrogen sulfide induced corrosion in concrete sewer structures for most cases. Although, the steel pipe industry and the ductile iron pipe industry have somewhat similar corrosion problems, these industries have developed better engineering solutions to address the corrosion problems than simply follow the outdated sacrificial wall thickness design philosophy. Pipe materials should be carefully evaluated and pipe made of HDPE, PVC, PP, PB, RPM, lined steel, lined ductile iron, vitrified clay should be compared with the performance of Az designed concrete pipe and plastic lined concrete pipe. Many plastic pipe products, when properly engineered, will provide better materials for sites which are likely to generate high levels of sulfide. There are several admixtures which have improved the performance of concrete in sulfide situations in France, Germany and Norway. Research reported by Fidjestal[4], Durning [5], Mehta [6], Luther [7], Bock [8], Compagnie Nationale Du Rhone [9] indicate that the presence of high alumina cement and/or silica fumes in concrete increase the resistance to acids due to the reduction of permeability of the concrete pipe wall and in turn the depth of penetration of the sulfuric acid. Furthermore, these admixtures tend to reduce or completely eliminate the free calcium hydroxide in concrete. Furthermore, the calcium silicate hydrate paste formed with silica fume is more stable in low pH environments.

Other methods which are used for sulfide control include oxygen injection, chlorination, hydrogen peroxide dosing, iron salt addition, sodium hydroxide shock dosing, potassium permanganate addition, sodium nitrate addition, ozone treatment, and growing bacterial/enzyme cultures.

CHEMICAL RESISTANCE TESTING

Some form of sulfide corrosion testing needs to be undertaken by design engineers on a routine basis as part of QA/QC measures for either proper protection of traditional pipe materials with plastic liners and coatings or use of new materials. The Standard Specifications for Public Works Construction (known as the Greenbook) developed by the Joint Cooperative Committee of the Southern California Chapter of the American Public Works association and Southern California Districts of the Associated General Contractors of California[10] is the only public document that outlines a procedure for testing various sewer structure materials for chemical resistance. In this procedure, the physical properties of the specimens are measured after exposure to chemical solutions of the following types:

o sulfuric acid	20 % by volume
o sodium hydroxide	5 %
o ammonium hydroxide	5 %
o nitric acid	1 %
o ferric chloride	1 %
o soap	0.1 %
o detergent (LAS)	0.1 %
o bacteriological	BOD not less than 700 ppm

At 28 day intervals, specimens are removed from each chemical solution and tested. If any specimen fails to meet the 112 day requirements set by the committee before completion of the 112 day exposure, the material is subject to rejection. It is recommended that public agencies adopt a procedure similar to this to be able to screen pipe/structural materials to be used in sewer systems.

LIFE CYCLE COST STUDIES

It is important that life cycle cost studies be undertaken following procedures similar to those given in Kerr and Ryan [11], by sewer system designers to account for the costs associated with planning, engineering, construction, maintenance, rehabilitation and replacement, and deductions for any residual value at the end of the proposed project design life. Such studies should include realistic service life estimates for various sewer structure materials considered based on actual track record and field performance rather than on testimonies of consultants on vendor's payrolls or public officials who might bring their own biases in defiance of sound engineering principles. Sulfide induced corrosion and its impact on service life of unprotected concrete pipe should be given equal consideration as the significant role installation and inspection plays in structural performance of flexible pipe materials in the calculation of service life.

REHABILITATION METHODS

Before a public agency and the engineering consultant embark on a rehabilitation program of a deteriorated sewer system, the pros and cons of replacement v. rehabilitation should be carefully studied. Schrock[12] provides a detailed account of various factors to consider in the proposed chapter for the City of Los Angeles Specifications. The well-defined tangible factors to consider are as follows:

o inspection

- o engineering
- o rights-of-way
- o easements
- o cost to business/government
- o construction time/cost
- o cost of disruption
- o mobilization
- o savings in O and M
- o costs of detour and flow bypass/rerouting
- o mapping

Intangible items usually ignored are as follows:

- o noise, dirt
- o safety
- o ground settlement/damage to buildings
- o reputation of the agency
- o inconvenience
- o complaints
- o liability
- o emergency
- o traffic rerouting

Economic evaluations between the options of replace or rehabilitate should include realistic estimates of costs associated with the above items. The most suitable rehabilitation methods for repairing concrete pipe should be carefully chosen by weighing the following factors:

- o pipe shape and size
- o soil conditions
- o groundwater conditions
- o additional loads
- o corrosion conditions
- o accessibility
- o flow quantity
- o possible bypassing/rerouting flows
- o type and level of damage to the sewer system
- o cause of damage to the sewer system

Most methods require some form of initial cleaning, close circuit televising, root control, and groundwater monitoring. The pipe material considerations should include the following factors:

- o availability
- o track record
- o quality control
- o engineering support
- o future repair
- o abrasion resistance
- o durability
- o hydraulic resistance
- o structural capability
- o installation rate/cost
- o ease of use

- availability of standards

Some repair techniques are applied on the outside of the concrete pipe while others attempt to repair the inside. Brief descriptions of some of such methods are given here.

Cement Grouting

Portland cement grout can also be used to form extra layers of material to repair deteriorating sewer structures provided proper mixes and alkalinity are provided. The amounts of water and cement used are carefully controlled based on the final physical properties and workability requirements. Micro-fine cement is usually used in subsurface conditions where the grain size characteristics of the site would not permit efficient pumping of the regular portland cement grout. Cement mortar is used for consolidation grouting where the ground needs to be packed to avoid excessive settlements due to a deteriorating sewer structure.

Chemical Grouting

Chemical grouting is used to repair usually from the ground surface, after some excavation, or by using drilled holes from the inside of the pipe. Chemical grouts consist of a mixture of several substances which stiffen after some time once placement is achieved within a selected time period. Typical grouts used are acrylamide base gel, acrylic base gel, acrylate base gel, urethane base gel, and urethane base foam.

Segmented Liners

Segmented liners are available in many convenient shapes and sizes to fit the specific purpose. These are also made of different materials. The designer should be careful in selecting the material to ensure that the chemical resistance is adequate to handle the level of corrosion anticipated. The work is accomplished in a dry condition and therefore bypassing the flow is always required. These liners are combined with either concrete placement or pressure grout.

Sliplining

Sliplining takes place in the form of inserting a pipe of smaller size into a deteriorating sewer using planned hole in the ground as the access port. This is accomplished either using a continuous slipliner pipe or segmented pipe with appropriate OD controlled joints. The insertion pit is used to pull the slipliner pipe with a mechanical winch which relies on rollers to cut down the friction against the exterior of the liner pipe wall. Pipe pulls of over 300 m are fairly common in small sizes. Materials such as ductile iron, steel, clay, HDPE, PVC, PB, PP, and RPM are used for slipliner pipe. Some of these materials are available in the market with profiles and cores. Buckling is a major consideration during the installation process, grouting, and in service. Therefore, the design engineer needs to make appropriate calculations to ensure that the wall stiffness of the slipliner pipe chosen could withstand the loads. It is uneconomical to design these slipliner pipe materials without taking advantage of the buckling strength enhancement provided by grouting.

Deformed Lining

An extruded PVC or HDPE pipe that is folded into a U shape is pulled into a broken sewer and with the aid of hot water or steam with pressure the deformed pipe is stretched back to its original shape to conform to the shape of the sewer.

Spiral Wound Lining

A PVC strip is pulled through a winding machine that is placed at the bottom of a manhole and this machine pushes the pipe made at site into the broken sewer. This spiral pipe essentially is the formwork for the cement grout to be either pumped in or placed using grout tubes in the annulus between the liner and the existing pipe. Man entry size lining is done using mechanically interlocking PVC panels either in segment form or a continuous coil delivered from a spool dragged inside the pipe.

Cured-In-Place Inversion Lining

Cured in place pipe uses a thermosetting resin that is used to saturate the fabric felt initially. Once the pipe is inverted into its final location inside a sewer using hydrostatic pressure or air pressure, either hot water, hot air, or steam is used to initiate the hardening process of the resin used in the liner pipe. A catalyst is always used in the resin matrix to control the processing time. The felt could be woven, nonwoven, or a combination of both. Reinforcements of various types are also being tried at the present time to be able to handle higher internal working pressures.

Specialty Concrete

Shotcrete, gunnite, high alumina cement spray on, silica fume mixes, latex modified cement all provide better corrosion protection than regular Portland cement concrete, if the mixes are very carefully designed and applied.

Coatings

The success of any form of coating depends on the adequacy of the cleaning of the initial concrete surface, the effectiveness of the bond between the concrete surface and the coating/lining, and the chemical resistance of the lining/coating material. An ongoing evaluation of protective coatings for concrete is carried out by John Redner and his colleagues at the Los Angeles County Sanitation Districts and the most recent results are reported in Redner, Hsi, and Esfandi[13].

Spot Repair

Spot repair is done at areas where damage is far more severe than the rest of the sewer structure. The method allows several forms of grouts, liners, seals, mechanical, etc.

SUMMARY

1. Most prediction models in use for estimating sulfide buildup rely on too many empirical constants, which need to be carefully chosen to get reasonable answers. Some level of field calibration of all calculated results are always essential before an engineer can claim some degree of confidence in the forecasts. The prediction of corrosion rates in concrete sewer structures is even worse when it comes to reliability due to most models having not done enough characterization of fundamental processes contributing to corrosion in concrete sewers.

2. More research is required on the various physico-chemical phenomena involved in concrete corrosion due to sulfide buildup.

3. It is important for the design engineer and the owner to invest some funds into evaluating the sulfide buildup potential during the planning stages of either a new system or an existing structure proposed for repair work.

4. Numerous methods have been in use for some time for controlling sulfide buildup and in turn to prolong the service life of sewer structures and the design engineer and the owner should consider using one or more of such techniques. Trials should start with bench scale tests to screen for the best among several methods and the final protoype also should deserve some testing, before public money is spent in large amounts on the final design and construction for the whole sanitary district.

5. When a sewer system is deteriorated enough to consider either replacement or rehabilitation, many factors should be taken into consideration in deciding which route to take.

6. In designing new sewer systems, the choice of the pipe material should be given careful consideration. Carefully engineered and tested concrete mixes with proper admixtures can prolong the service life of the sewer system in as much as the use of plastic liners or other pipe materials.

7. Failure of an unprotected manhole, drop structure, junction structure, or wet well due to sulfide corrosion can cause as much an expenditure to the public as that from the failure of the main sewer itself. Therefore the design engineer need to pay some attention to selecting proper materials for the construction of these structures as well.

8. Design engineers need to pay enough attention to the fundamental principles governing the generation and release of sulfide gas in our sewer systems and more importantly the corrosion damage caused to a vital part of our infrastructure. While continuing our practice of applying the existing design tools to provide some answers to this problem, we need to expend more of our efforts to research further into the fundamental mechanisms of sulfide buildup and the associated corrosion. If they fall short of this mission, the taxpayers will question their ability to solve a problem which is so well known for so long in the pipe industry. In this pursuit, the concrete pipe industry has a fundamental obligation, far more than anyone else, to the public to work with those in engineering so that reliable answers are found for this pressing problem.

REFERENCES

[1] Pomeroy, R. D. and Parkhurst, J. D., "The Forecasting of Sulfide Buildup Rates in Sewers, Prog. Wat. Tech., Vol. 9, Pergamon Press, London, England, 1977, pp. 621-628.
[2] Kienow, K. K. and Kienow, K. E., "Sulf.Bas-Sulfide Prediction Program," Proceedings of the International Conf. on Advances in Underground Pipeline Engineering," Jey K. Jeyapalan

Ed. Madison, Wisconsin, 1985, pp. 466-476.
[3] EPA, "Design Manual on Odor and Corrosion Control in Sanitary Sewerage Systems and Treatment Plants," Cincinnati, Ohio, 1985.
[4] Fidjestol, P., "Silica-Concrete in Sewage Installations, " Proceedings of the First International Conference on Pipeline Construction, Hamburg, Germany, 1987, pp. 509-516.
[5] Durning, T. A. and Hicks, M. C., "Using Microsilica to Increase Concrete's Resistance to Aggressive Chemicals," Concrete International, 1991, pp. 42-48.
[6] Mehta, P.K., "Studies of Chemical Resistance of Low Water-Cement Ratio Concretes," Cement and Concrete Research, V. 15, 1985, pp. 969-978.
[7] Luther, M. D., "Microsilica Concrete Durability in Severe Environments," Proceedings of the ASCE Structures Congress, San Francisco, California, 1989, pp. 95-105.
[8] Bock, E., "Examination of the Resistance of Cement Mortar Linings of Ductile Iron Pipes to Sulfuric Acid Corrosion," Research Report of the Hamburg University, Germany, 1989.
[9] Compagnie Nationale Du Rhone, "Testing of Wear Preventive Coatings for Existing Sewer Structures," Research Report to Paris City Council, Lyons, France, 1986.
[10] Greenbook, "Specifications for Public Works Construction," Published by Building News, 3055 Overland Ave, Los Angeles, CA 90034.
[11] Kerr, W. O. and Ryan, B. A., "Taking the Guesswork out of Least-Cost Analysis," Consulting Engineer, March 1986, pp 1-4.
[12] Schrock, B. J., "Chapter on Pipeline Rehabilitation Methods," City of Los Angeles Specifications for Public Works, 1991.
[13] Redner, J. A. Hsi, R. P. , and Esfandi, E. J., "Evaluation of Protective Coatings for Concrete, Research Report of the Los Angeles County Sanitation Districts, Whittier, California, 1991.

Vladimir Novokshchenov[1]

CORROSION-RELATED DETERIORATION OF REINFORCED CONCRETE STRUCTURES AT OIL REFINERIES IN THE PERSIAN GULF REGION

REFERENCE: Novokshchenov, V., **"Corrosion-Related Deterioration of Reinforced Concrete Structures at Oil Refineries in the Persian Gulf Region,"** Corrosion Forms & Control for Infrastructure, ASTM STP 1137, Victor Chaker, Ed., American Society for Testing and Materials, Philadelphia, 1992.

ABSTRACT: This paper cites specific examples of corrosion-related distress of reinforced concrete exposed to aggressive environments of the Persian Gulf region. Several case histories are described involving structures at various oil refineries situated along the Gulf coast. The paper outlines major factors affecting the development of a particular failure and depicts repair techniques implemented to eliminate the damage and to prevent the future occurrence of the failure.

KEYWORDS: reinforcing steel, corrosion, concrete, chlorides, oil refineries, Gulf region

Conventionally reinforced concrete deteriorates rapidly in the hostile environments of the Persian Gulf coast region, one of the most difficult areas in the world for construction of durable concrete structures [1,2].

While the causes of distress are numerous, corrosion of reinforcing steel and particularly the chloride-induced corrosion is most frequent, being responsible for about 85% of all deteriorations [3]. Chloride ions accelerate corrosion of the steel either by preventing the formation of the passivating film, or by destroying it after it has developed on the surface of rebars. This results in a loss of cross section and a buildup of the voluminous rust with subsequent cracking, spalling, and delamination of concrete cover [4].

One of the most frequent sources of chlorides in concrete in the Gulf coast region are concrete aggregates

[1]Consultant, Concrete Clinic International, 5204 Karrington Drive, Gibsonia, PA 15044.

quarried from the chloride-bearing surface deposits of sand and gravel. Chlorides can also be introduced into concrete with brackish or sea water which may be specified for mixing and/or curing concrete, especially in areas where potable water is not readily available. The groundwater and subsoil, frequently containing chloride salts in concentrations exceeding 3000 ppm and 6.5%, respectively are likely to become a vast source of chlorides in below ground structures, unless preventive measures are implemented. Other sources of chlorides include the sea water spray carried by prevailing winds, saline water, particularly in the splash zone of reinforced concrete structures, and moisture condensates in combination with the windborne salt-laden dust from surface crusts of salt playas and sabhas.

In the Gulf region near the coast, the mean monthly temperature is in the range of 18 to 32°C. In the summer months, daytime temperatures frequently exceed 40°C. The average relative humidity is about 62% in June and July, and 78% in December and January, and may rise to 90% and higher. These conditions promote corrosion-related reactions with the sharp increase in the rate of corrosion at an ambient temperature of about 30-40°C and a relative humidity approaching 70% [5].

Elevated temperatures and humidity also significantly increase the penetration of CO_2 and SO_2 into the pores of concrete, which results in the neutralization of concrete cover and a subsequent loss of its protective power.

Poor concrete practices commonly encountered on concrete-related projects along the Gulf coast are also among the major contributors to the corrosion of reinforcing steel. This includes, the lack of control over the water-cement ratio, poor consolidation of freshly-placed concrete, excessive cracking of concrete cover, inadequate hydration of portland cement, poor workmanship, as well as the lack of proper maintenance of reinforced concrete structures. This leads to a sharp increase in the permeability of hardened concrete and creates favorable conditions for penetration of corrosion-inducing agents into the concrete.

With the concentration of sulfates up to 4500 ppm in ground-water and about 20% in subsoil, it is a common practice in the Gulf region to specify sulfate resistant portland cement (SRPC) for almost all subsurface concrete. Since SRPC has a lower amount of the tricalcium aluminate (C_3A), its chloride-binding capacity, and consequently the degree of protection provided to the reinforcing steel against chloride-induced corrosion, is lower than that of ordinary cement. To provide an adequate protection the amount of C_3A should not be less than 4%, and preferably 5-6% [6-7].

All these and other factors make reinforced concrete in the Gulf coast region highly vulnerable to deterioration due to chloride-induced corrosion of embedded steel.

LIQUIFIED NATURAL GAS STORAGE TANK FOUNDATION

Constructed in 1974, the storage tank is a steel double-skinned 83-m diameter and 31-m high vessel with a fixed dome roof. The tank is supported by a ring 2.4-m wide and 2.0-m deep foundation having an outside diameter of 84.8 m. The heating to the tank is provided by means of electric elements placed in stainless steel tubes. The tubes were installed by inserting them through steel sleeve pipes embedded in the foundation during construction.

The concrete showed cracking, spalling, and delamination within a few years after construction. Most damage was noted along the plane of the heater tube sleeves (Fig. 1). In areas where the sleeves were absent, the deterioration of concrete was rated as minor, being represented mainly by fine vertical drying shrinkage cracks on the side surface, and some plastic settlement hairlines on the top surface of the foundation.

FIG. 1--Deterioration of concrete in areas of the heater tubes.

A number of spalled areas of the top surface were removed to reveal severe corrosion of the sleeves. On one occasion, a sleeve was found to be totally corroded exposing the inner tube. Unlike the sleeves, all examined steel bars of the main reinforcement were in a perfect condition, with an exception of some bars located in the vicinity of hair cracks that exhibited minor corrosion. Examination of the holding-down bolts in areas where they pass through the top

surface of the foundation did not reveal any significant corrosion. A coating of the bitumen paint on the top surface of the foundation beam was found to be severely weathered exposing the original concrete. The vertical surface of the beam was also weathered, but to a lesser extent. On one occasion during the inspection, a moisture condensate was noted to have ponded on the top surface of the foundation. Water streak marks readily visible on the tank walls as well as on the foundation surfaces suggested that the amount and frequency of the moisture condensation were quite significant. Despite severe corrosion of the sleeves and corrosion-related deterioration of the top concrete cover, there was no evidence indicating that the load-carrying capacity of the foundation was significantly affected.

Measurements showed that concrete cover to the heater tube sleeves and to the main reinforcement was approximately equal to the specified value of 50 and 75 mm, respectively. The concrete in the foundation beam was generally sound and well consolidated with the depth of carbonation varying from 1 to 15 mm. The average cement content was about 380 kg/m^3. Based on the amount of C_3A the cement appeared to be sulphate resistant. Compressive strength of concrete cores obtained vertically was in the range of 23.4 to 36.6 MPa, as compared with the minimum specified cylinder strength of 17.2 MPa.

Concentration of water soluble chlorides by weight of cement determined on vertical cores varied from 0.77-0.88% at the top surface to 0.41-0.56% at the level of the heater tube sleeves. This is far in excess of the maximum value of 0.15% allowed by ACI 318 for reinforced concrete structures exposed to moisture in service [8]. The concentration of chlorides at the level of rebars was much lower, an average being about 0.26%. A similar pattern of distribution of chloride ions was recorded in horizontal cores, although the surface concentrations were somewhat lower. Test results showed the concentration of chloride ions in samples of the moisture condensate collected from the top surface of the foundation varied from 85 to 4100 ppm. The manner in which concentration of chlorides varied in the concrete suggested they originated externally on the foundation surfaces, most likely from the windblown dust, and migrated to the level of the sleeves via the saline condensate through the weathered bitumen coat and the concrete cover.

After removing unsound concrete to a depth of about 100 mm below the main reinforcement, the corroded sleeves were cut off and replaced with split stainless tubes. All exposed rebars, the outer edge of the tank annular base plate, the tank wall to a height of 75 mm, and the holding-down bolts were shotblasted to bare metal, and then treated with two coats of zinc phosphate primer, followed by two coats of micaceous iron paint (Fig. 2).

Prior to placing new concrete the existing concrete surface was thoroughly cleaned and then coated with an epoxy adhesive. Examination of cores obtained upon completion of

the repairs showed that there was a good bond between newly-placed and existing concretes. To prevent penetration of salt-laden moisture, the ends of the newly-installed heater sleeves were sealed with silicone sealant, and the entire horizontal surface of the foundation as well as the top 175 mm of the vertical surface were treated with two coats of epoxy paint.

FIG. 2--Preparation of embedded steel and concrete for repairs.

ACID FLARE FOUNDATION

The foundation plinths of the acid flare tower were about 7 years old when severe cracking developed in concrete cover. Most damage was observed to occur in the top of the plinths, where holding-down bolts were located (Fig. 3).

A series of tests conducted to determine the cause and extent of deterioration showed that cracking of concrete cover was due to corrosion of reinforcing steel bars induced by chloride ions from the surrounding concrete. Concentration of water soluble chlorides measured at various depths up to 650 mm was in the range of 1.1 to 1.7% by weight of cement. The manner in which chlorides were distributed throughout the mass of concrete indicated that the source of chlorides was internal. The concrete in the plinths was made using sulfate resistant cement with the cement content varying from 210 to 355 kg/m^3. The estimated water-cement ratio was in the range of 0.48 to 0.57. There was no indication of adverse reactions involving the mortar

matrix of the concrete. An average compressive strength of concrete cores was 29.8 MPa.

Structural analysis showed that if concrete were removed and steel bars exposed in the top of the plinths, there was a possibility that the tower supports would not be able to withstand wind loads and the whole tower could overturn.

FIG. 3--Cracking of concrete cover in the plinth.

Therefore, instead of replacing the unsound concrete and corroded steel, it was proposed to construct a reinforced concrete jacket around each damaged plinth which would also encapsulate the bottom portion of steel legs and hold-down bolts. Prior to repair works a temporary protective shelter was erected over the work area, comprised of a roof insulated with a reflective cover against radiant heat from the flare. The paving around each plinth was removed and the soil excavated down to the base slab of a plinth. The top mat of the base slab reinforcement was then

exposed and new reinforcement fixed around each plinth, with vertical bars being installed and resin-grouted in the base slab. To prevent appearance of reflective cracks and migration of chlorides from the old structure into the newly-placed concrete, each plinth was covered with a compressible material.

After curing, all concrete surfaces below the ground level were treated with two coats of a bituminous paint and above the ground level with two coats of a chlorinated rubber paint. Joints between concrete and steel legs were sealed with a two-part polysulfide sealant.

COOLING WATER OUTFALL FLUME

Designed to discharge plant cooling water into the sea, the flume is a monolithic U-shaped 5-m wide, 3-m deep and 250-m long reinforced concrete structure (Fig. 4).

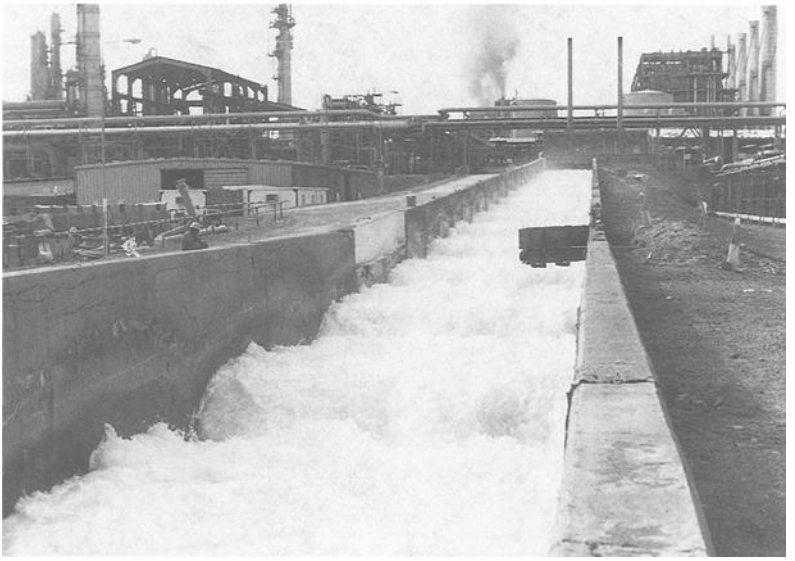

FIG. 4--The cooling water outfall flume.

Inspection of the flume conducted seven years after its construction revealed severe cracking, spalling, and delamination of concrete cover along the whole length of the structure. The most significant damage was observed at the top of the flume walls where concrete in many areas completely debonded from the main body of the wall and could easily be removed (Fig. 5). The exposed rebars exhibited severe uniform and localized pitting corrosion being in some cases completely rusted through. The extent of deterioration

of the reinforced concrete was less severe lower down the wall, but corrosion of steel and cracking of concrete were still apparent. No visible signs of corroded reinforcement, except for some minor hairline cracks, were observed on the outside surface of the wall below the ground level. Concrete in this area was found to have a coating of a bituminous paint, apparently applied at the time of construction. Inside the flume, large areas of delaminated concrete cover were well visible, extending the full height of the wall. In some cases, the concrete cover has fallen away exposing heavily corroded reinforcing steel bars. The wall sections below the waterline were found to be in a better condition than those above the waterline. The thickness of concrete cover throughout the flume varied from 0 to 100 mm, as measured in areas of exposed reinforcement.

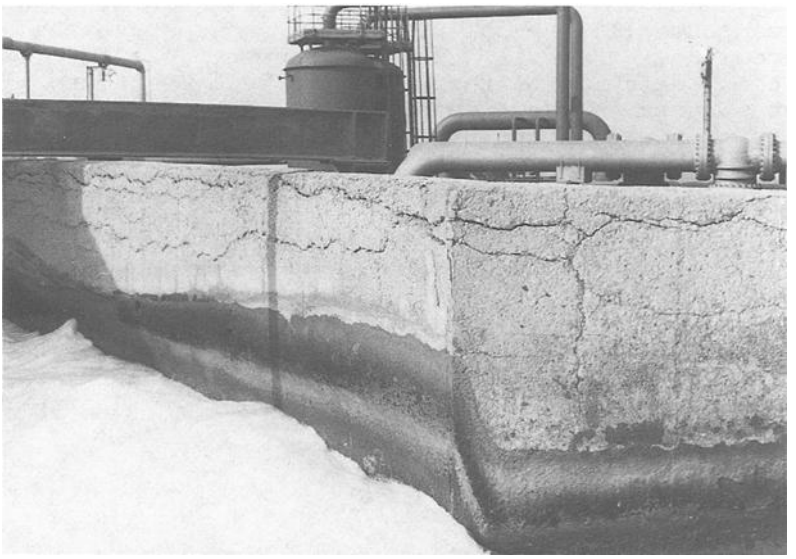

FIG. 5--Deterioration of concrete in the flume walls.

The concentration of water soluble chloride ions in the flume walls varied from 1.22 to 2.18% by weight of cement. There was no appreciable difference in concentrations of chlorides determined at various depths of the concrete.

Compressive strength of concrete cores obtained from various portions of the flume was in the range of 36.6 to 44.1 MPa. There was no evidence of any deleterious reactions in the concrete. The depth of carbonation normally did not exceed 15 mm. An average cement content was about 365 kg/m^3.

Half-cell potential survey conducted in areas above the ground and water levels, where the concrete cover was intact, indicated a greater than 90% probability that active

corrosion of rebars was occurring at the time of the survey.

Based on results of the investigation, it was concluded that the singular most significant factor responsible for corrosion of steel and corrosion-related deterioration of concrete was the presence of chlorides at the level of the reinforcement. The pattern of distribution of chlorides in the concrete suggested that the source of chlorides was internal, most likely, contaminated concrete ingredients. The other possible source of chlorides was the hot salt-laden discharge water. Also, since the flume was situated in close proximity to the sea, it was possible that chlorides, at least in some portions of the structure, were introduced with the sea water spray.

The condition survey showed that the flume walls have deteriorated to such an extent that the probability of the collapse occurring within the next five years was rated as extremely high. In addition to blocking the channel and the downstream outfall, the failure of the walls would also cause erosion of the soil with a consequent loss of ground around the foundation of the flume, as well as around adjacent structures. Any remedial works to restore the integrity of the existing structure would be costly and still only of a temporary nature. Therefore, the decision was made to demolish the existing water outfall and to replace it with a new structure. To ensure the operational safety of the flume until the new structure is commissioned, a buttress wall was constructed along excavated existing walls. This was done by placing concrete against existing walls in 4-m long and 1-m wide sections, extending to the outfall base. The sections were separated from each other by means of expansion joints. To prevent migration of chlorides, the new wall was isolated from the old structure by installing polythene sheathing.

SULFUR PIT

Constructed in 1977 the sulphur pit is a rectangular 11-m wide, 14-m long, and 3-m deep reinforced concrete monolithic structure. The roof of the pit is a 250-mm thick slab resting on 6 simply supported beams. Eight years after completion the roof slab of the pit has collapsed (Fig. 6). Since the sulfur pit has never been used, no loads other than the weight of the roof system were applied to the supporting beams.

Visual inspection showed the failure happened in beam sections located at approximately 2.5-3.0 m away from supporting walls of the pit. Prior to collapse, large deflections occurred causing numerous cracks to develop in the slab and in the beams. It appeared the beams collapsed as a result of a domino effect. Initiated in the end beam, the first failure induced the other failures by a sudden transmission of the weight load. Even though the reinforcing steel in the fractured beams was highly corroded, no rupture

was noted in exposed rebars, except for some stirrups.

Petrographic analysis carried out on cores extracted from the roof slab showed the concrete was adequately consolidated and was, in general, of good quality. The cement paste was hard, dense, and well-bonded to aggregate particles. An average cement content was about 341 kg/m^3. No evidence of deleterious alkali-aggregate reactions was observed in any of the examined cores. The depth of the cement paste carbonation measured from the top and bottom surfaces of the slab did not exceed 10 mm. The estimated water-cement ratio of the concrete was about 0.53. Compressive strength of concrete cores was in the range of 27.3 to 31.2 MPa.

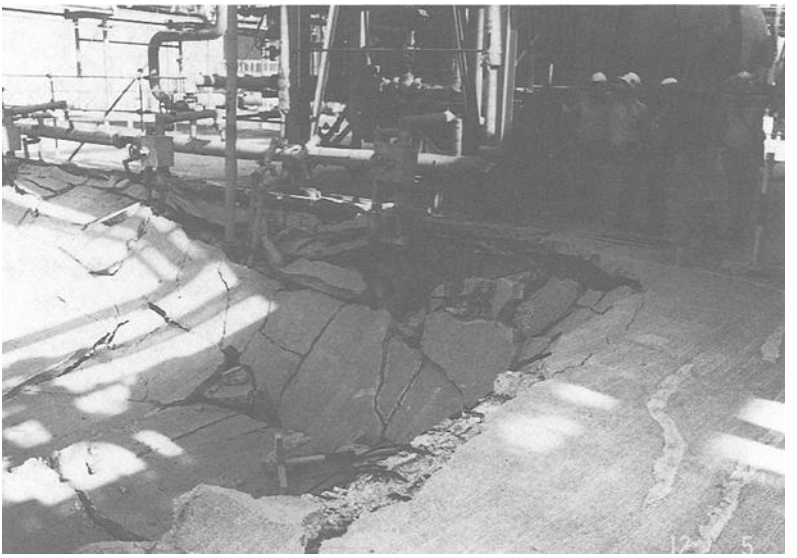

FIG. 6--Collapse of the sulfur pit roof slab.

A total of 7 samples were obtained from the failed beams to determine concentration of chlorides in concrete at varies depths. Tests showed percent of chlorides varied from 1.0 to 1.7 by weight of cement. The pattern of distribution of chloride ions throughout the mass of concrete suggested that the source of chlorides was internal. Review of construction documents showed that concrete for the sulfur pit was mixed using sea water. This was in accordance with the project specification which stated: "sea water shall be used for all concrete."

Based on results of the investigation, it appears the collapse of the roof has occurred as a result of the bond failure caused by severe chloride-induced corrosion of reinforcing steel bars, and a consequent deterioration of

concrete cover. Corrosion of reinforcing bars has weakened beams to such an extent that they could no longer support their weight and the weight of the slab on top. When deflections developed, the main bottom rebars separated from a beam without failure. The remaining bottom section consisting of concrete and some stirrups was not able to resist tensile stresses causing a beam (apparently the end beam) to fail in tension. When the beam collapsed adjacent beams also collapsed, due to a sudden application of an excessive load.

VESSEL SUPPORTS

Visual examination of vessel supports carried out during the routine inspection in 1984, after 7 years in service, revealed extensive cracking and spalling of concrete cover caused by corrosion of reinforcing steel and holding-down bolts (Fig. 7).

FIG. 7--Deteriorations in a typical vessel support.

Potential survey conducted on areas where steel could not be visually examined showed there was more than 90% probability that active corrosion of steel was occurring in all the investigated structures (Table 1).

Laboratory examination indicated that the concrete surrounding reinforcing steel contained a significant amount of chlorides, varying from 0.13 to 0.22% by weight of cement. Chloride ions were distributed rather uniformly throughout the mass of the concrete, thus implying that chlorides may have been added during construction either with chloride-bearing aggregates, or mixing water, or a combination of both. Concentration of chlorides in vessel supports not exhibiting signs of deterioration was only 0.02-0.04%. Quality of concrete as well as the thickness of concrete cover in all the examined supports were adequate.

TABLE 1--Results of the investigation of vessel supports.

Equipment foundation	Concrete deterioration			Steel corr	Cl^- %	Half cell
	Crack	Spall	Delam			
Separator	VS	S	S	VS	-	+
Receiver#1	VS	M	S	S	0.21	+
Flash drum	VS	S	S	VS	0.20	+
Boiler #3	VS	S	M	S	0.24	+
Boiler #2	VS	M	S	S	0.19	+
Reboiler#1	S	M	M	S	0.26	+
Reboiler#2	VS	M	S	S	0.29	+

Note: VS-very severe, S-severe, M-moderate, +-active

To repair the damage, the defective concrete was first cut with a disc-cutter and than removed to sound concrete to a depth of 10-50 mm behind the reinforcement. Where cracks in the concrete originated from the anchor bolts the concrete was removed over the full length of the bolt to a maximum of 300 mm from the end face of a plinth. All embedded steel was cleaned by chipping and wire-brushing. Two coats of a slow-set epoxy based bonding agent were applied to all exposed steel, one after cleaning, and the other one prior to placing concrete. The existing concrete surface was also treated with one coat of the same bonding agent (Fig. 8).

To ensure that the load-carrying capacity of the supports was not significantly decreased, only one half of a support was repaired at a time. The other half was repaired after the newly-placed concrete gained a sufficient strength. The concrete used for repairs was a 25 MPa mix

modified with styrene-butadiene. The maximum size of coarse aggregate was 10 mm. After curing, all the repaired supports were treated with two coats of low viscosity penetrating epoxy resin.

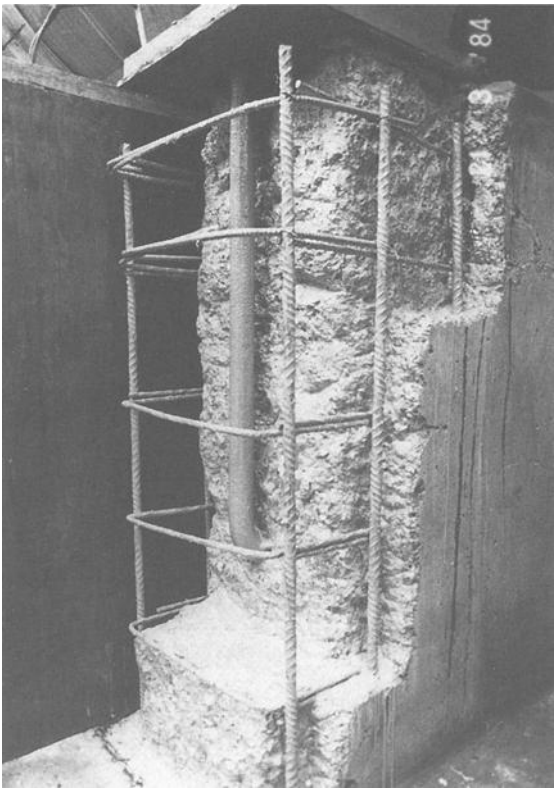

FIG. 8--Vessel support ready for concreting.

Inspection of the same structures conducted 3 years after repairs showed that corrosion of reinforcing steel was occurring again, though at a lower rate. This may have happened if chloride-contaminated concrete was not removed completely during repairs and chloride ions migrated into the newly-placed concrete. Also, because of various rates of corrosion, deterioration is likely to surface in areas where the rate of corrosion was low at the time of repairs. And finely, if not all anodic sites were removed from the chloride-contaminated member, the replacement of unsound concrete with fresh, chloride-free, high-oxygen concrete could accelerate the macrocell action and, consequently, the rate of corrosion by introducing potential cathodic sites into the system.

In the case of a very severe damage, a vessel was lifted off its foundation, after necessary modifications to the connected pipework, and the foundation was demolished. The ground was then compacted and a 100-mm thick slab was cast. After positioning a new precast foundation to the previously recorded lines, the surrounding areas were backfilled and the paving reinstated.

SUMMARY AND DISCUSSION

In all the reported cases the most important single factor responsible for corrosion of reinforcing steel was the presence of chloride ions at the level of the reinforcement.

Chlorides were introduced into concrete with contaminated aggregates, sea water that was used for mixing concrete, sea water spray, cooling sea water, as well as with the moisture condensate contaminated with salt-laden dust.

In most examined structures the deterioration was noticed within the first 5-7 years of their service life.

No evidence was observed of any deterioration of concrete which may have been attributed to atmospheric pollution.

Pachometer surveys and inspection of cores indicated that the thickness of concrete cover over embedded reinforcement in the majority of investigated structures was generally equal to or in excess of the specified value.

The most common repair method used to eliminate corrosion-related damage was the replacement method. It should, however, be remembered that this method is effective only when contamination of concrete with chlorides is of a localized nature. For repairs to be effective, it is important not only to remove unsound concrete but also all concrete contaminated with chlorides in concentrations exceeding the corrosion threshold value.

When all concrete is contaminated with chlorides the replacement method in combination with a routine inspection can be an effective temporary measure. For permanent repairs the cathodic protection and the full replacement of contaminated concrete, preferably with precast concrete, are the only alternatives.

Installation of a jacket over a structure which is heavily contaminated with chlorides does not appear to be a sound repair technique. A jacket will not eliminate corrosion but promote it by sealing corrosion-inducing agents inside the affected structure.

Since normally rehabilitation works require the shutdown of the equipment operations, most oil refinery structures are difficult to repair. Because of this, more attention must be paid to the development of design criteria, the selection of concrete materials, and to the quality of concrete operations to prevent the deterioration

of reinforced concrete.

Because moisture plays an important role in chloride-induced corrosion of reinforcing steel, a structure must be designed in such a way that the accumulation of chloride-laden water on concrete surfaces will be kept to a minimum.

Concrete aggregates must be free from contamination with chlorides. In no case should sea water be used for making and/or curing concrete.

Testing concrete for the concentration of chlorides and the chloride permeability, prior to acceptance of a concrete mix design, will assist in keeping the concrete chloride-free, before and after placing.

Low water-cement ratio, proper compaction and curing are important to ensure that hardened concrete will be dense and resistant to carbonation and penetration by chloride ions.

Field observations of structures in service have shown that a bitumen coating applied to the above ground concrete surface may become weathered and therefore, may not provide an adequate corrosion protection to reinforcing steel.

It is generally accepted that the use of an epoxy-based coating properly applied to the surface of a concrete structure is one of the best means of shielding the structure against intrusion of chloride ions. It should, however, be noted that an epoxy coating is more effective when used as a post-construction rather than as a post-repair treatment. When utilized in rehabilitation projects, an epoxy coat may promote corrosion of reinforcing steel by sealing corrosion-inducing agents inside the structure.

Lack of maintenance is responsible for a vast majority of corrosion-induced damage in reinforced concrete. It is a common practice to repair a structure only after corrosion of steel and corrosion-related deterioration of concrete become very severe. In many instances the implementation of a preventive maintenance may be much more cost-effective. This includes: a) regular inspections to identify potential areas of corrosion-induced distress, b) removing accumulations of salt-laden dust, c) sealing cracks to prevent ingress of corrosion-inducing agents, d) minor patching, and e) renewal or application of protective coats in critical locations.

REFERENCES

[1] Novokshchenov, V., "Cracking in Hot Climates," Concrete International: Design & Construction, Vol. 8, No. 8, August 1986, pp. 27-33.

[2] Novokshchenov, V., "Investigation of Concrete Deterioration Due to Sulfate Attack," Proceedings of the Katherine and Bryant Mather Conference on Concrete Durability, ACI SP-100, American Concrete Institute, Detroit, MI, 1987, pp. 1979-2006.

[3] Rasheeduzzafar, Fahd H. Dakhil and Ahmad Saad Al-Gahtani, "Deterioration of Concrete Structures in the Environment of the Middle East," ACI Journal, Proceedings V. 80, No. 1, January 1984, pp. 13-20.

[4] Novokshchenov, V., "Stopping the Cracks," ASCE Civil Engineering, Vol. 56, No. 11, November 1987, pp. 54-56.

[5] Shallon, R., "Corrosion of Reinforcing Steel in Hot Countries," RILEM Bulletin, No. 24, September 1964, pp. 29-45.

[6] ACI Committee 357R-84, Guide for the Design and Construction of Fixed Offshore Concrete Structures, ACI Manual of Concrete Practice, Part 4, 1989, pp. 357R-3.

[7] Gerwick, B. C., Jr., "Practical Methods Ensuring Durability of Prestressed Concrete Ocean Structures," ACI SP-47 Durability of Concrete, 1975, pp. 317-324.

[8] ACI Committee 318-83, Building Code Requirements for Reinforced Concrete, ACI Manual of Concrete Practice, Part 3, 1989, pp. 318-17.

Neal. S. Berke[1], Michael. P. Dallaire[2], Richard E. Weyers[3], Mark Henry[4], John. E. Peterson[4], and B. Prowell[4]

Impregnation of Concrete With Corrosion Inhibitors

REFERENCE: Berke, N. S., Dallaire, M. P., Weyers, R. E., Henry, M., Peterson, J. E., and Prowell, B., **"Impregnation of Concrete With Corrosion Inhibitors"**, Corrosion Forms and Control for Infrastructure, ASTM STP 1137, Victor Chaker, Ed., American Society for Testing and Materials, Philadelphia, 1992.

ABSTRACT: Corrosion of steel in concrete is a major problem in the U. S. infrastructure. Approximately half of the bridges in the interstate highway system are in need of repair, and a significant cause is the corrosion of the embedded steel due to chloride ingress. A similar problem is found in parking structures throughout the northern regions of the United States due to deicing salts brought in from automobiles.

As of now the only commercial means of arresting corrosion without replacing concrete is the application of cathodic protection. Calcium nitrite has been shown to be an effective corrosion inhibitor when admixed into plastic concrete. In this paper an experiment to impregnate a bridge deck and support column with calcium nitrite is discussed.

Two methods were used to impregnate the concrete with calcium nitrite. The first involved drying a bridge deck by heating it above the boiling point of water, and then slowly cooling to ambient temperature to avoid thermal and drying shrinkage cracking. The deck was then successfully impregnated with liquid calcium nitrite.

The column was impregnated by removing delaminated concrete and drilling holes. A calcium nitrite rich latex modified grout was placed in the drill holes and a calcium nitrite rich latex modified concrete was produced to replace the removed concrete. Nitrite migration into the sound concrete left in place is to be measured over time.

Corrosion rates determined by polarization resistance, and corrosion potentials were measured before the above processes were performed. The steel was definitely cor-

[1] Research Manager,W.R. Grace & Co.-Conn, Construction Products Division,Cambridge Ma., 02140

[2] Senior Research Engineer,W.R. Grace & Co.-Conn. Construction Products Division,Cambridge Ma., 02140

[3] Professor,Civil Engineering Department, Virginia Polytechnic and State University, Blacksburg, Va.

[4] Student, Civil Engineering Department, Virginia Polytechnic and State University, Blacksburg, Va

roding in some areas and the corrosion behavior is to be monitored over time.

KEYWORDS: concrete, corrosion, corrosion rate measurements, inhibitors, calcium nitrite, rehabilitation, heating, concrete/mortar overlay

INTRODUCTION

The two most common means of repairing concrete in which steel corrosion has caused distress are the removal of the concrete and/or the use of cathodic protection. In cases where delaminated and spalled areas are a small percentage of the deck area and the steel has not lost appreciable cross sectional area, cathodic protection is the current method of stopping corrosion without concrete removal. In this project the feasibility of adding a known corrosion inhibitor, calcium nitrite, to repassivate the reinforcing steel in concrete was examined. This would represent a repair method that would not require removal of sound concrete, nor would it require long-term maintenance of a cathodic protection system.

Initial laboratory testing was performed by W. R. Grace & Co.-Conn. in the mid 1980s to determine the conditions needed to impregnate hardened concrete with calcium nitrite to below the reinforcement level. Methods examined included vacuum impregnation, pressure impregnation, ordinary soaking and drying the concrete by heating above the boiling point with subsequent soaking with an aqueous calcium nitrite solution. Only the last method was successful in impregnating the concrete with calcium nitrite to below the reinforcement level. It was also determined that the cooling of the concrete had to be controlled to prevent thermal shock.

In August 1985 a large scale bridge deck impregnation was performed at the University of Texas at Austin (1). A 6.1 by 18.3 m bridge deck section was made available for treatment. Two 3 by 6 m sections were dried to above 100 ℃ to approximately mid depth and slowly cooled. Detailed analyses of the heating and cooling profiles as well as the crack distribution before and after heating were performed. There were no new cracks due to the heating and cooling process and there was no growth in existing cracks. Analysis of the concrete and measurement of liquid consumed in the soaking process both indicated that 10.7 kg/m^3 of nitrite penetrated 51mm into the deck. Thus, the posttreatment process was successful and a patent was issued in 1991(2).

In the summer of 1987 a 3 by 6 m section of a parking garage was subjected to the posttreatment procedure. This structure was approximately 18 years old and severe delamination was present. Chloride levels were over 8.9 kg/m^3 in the top 32 mm. The deck was successfully heat treated and slowly cooled without creating cracks. However, nitrite analysis of cores showed that only 1.9 kg/m^3 of nitrite penetrated to the 25- 38 mm depth. It was concluded that the reduced penetration was due to surface contamination and high surface chloride concentrations which blocked the nitrite.

Laboratory experiments showed that removing a contaminated surface layer on other field specimens improved ingress. Thus, in future posttreatment of field concrete it was considered desirable to either scarify the surface, or to cut grooves below the surface.

In this work a 6 by 2.4 m section of a bridge deck breakdown lane was posttreated during the week of July 23, 1990. The location of the test site was on U.S. Route 460 Bypass West, outside of Christiansburg and Blacksburg Va.,spanning Va. Rt. 732. The bridge consisted of three simple spans, with two travel lanes of 3.6 m each, and a 3 m breakdown lane. The test area was a 2.4 by 6 m long section of the breakdown lane in the north span. The deck was grooved parallel to the expansion joints between the spans. (Figure 1) Based upon experience of R. Weyers and P. Cady grooves were precut in the deck to allow the calcium nitrite to ingress without having to penetrate surface impurities (3). Corrosion measurements (polarization resistance and corrosion potentials) and chloride determinations were performed. The section was demonstrating both active and passive corrosion rates which correlated well with the chloride concentrations. There were also a few delaminated areas.

In addition to performing the posttreatment on the deck section a severely corroded column was treated (Figure 1). This involved filling drilled holes with a calcium nitrite rich grout, and replacing spalled concrete with a calcium nitrite rich concrete. It is felt that over time the calcium nitrite will diffuse into the surrounding concrete providing corrosion protection for the embedded steel.

This report describes the procedures used and results to date on the posttreatment of the bridge deck and treatment of the column. Initial analysis showed that nitrite was impregnated into the deck, and that grouts and concrete at high nitrite levels could be field applied. Approximately six months after the posttreatment corrosion potentials and corrosion rates were measured. Further analysis over time will need to be performed.

CORROSION MEASUREMENTS AND CHLORIDE CONCENTRATIONS BEFORE POSTTREATMENT

Preliminary corrosion measurements and drillings for chloride analysis were taken before posttreatment.

Test Procedures

Corrosion measurements included corrosion potentials and the measurement of corrosion rates by the polarization resistance method. These were performed as a function of position on the deck or column and serve as a baseline number for the corrosion activity.

Corrosion potentials were measured against a copper-copper sulfate (CSE) reference electrode according to ASTM Standard Test Method for Half-Cell Potentials of Uncoated Reinforcing Steel in Concrete (C876).

One set of deck polarization resistance data was collected using a portable computer controlled potentiostat (Thompson Autostat-Software Controlled Potentiostat) which used a potentiostatic technique without compensation for IR drop. A copper wire mesh/sponge counter electrode (152 mm x 76 mm) was used. A 51 mm hole was in the center for a CSE reference. The polarization resistance, $R_p=\Delta E/\Delta I$ at $I= 0$, where E is the potential and I is the current was determined. R_p is inversely proportional to the corrosion rate. A complete description of the polarization resistance method is given in reference 3.

Another set of polarization resistance data was collected using a portable unit produced by KCC Inc.. The use of this instrument is described in reference 4. This instru-

ment corrects for the IR drop in the concrete using a current interruption technique. Galvanostatic control is used and three points are measured from which a straight line is determined.

Chloride analyses were performed on specimens from roto-hammer drillings. A method outlined in Florida DOT Research Report 203 PB 289620 was utilized.

Results

Pretreatment chloride data are given in Table 1 and correspond to positions in a deck schematic in Figure 1. Location 1-2 is at the guardrail and increasing letter values indicate moving towards the traffic line. Chloride levels are in general much higher near the guardrail (1-2, A4, A26) as snow and slush containing salt buildup at that point due to traffic. Chloride levels at the 57 mm nominal reinforcement depth are above 0.9 kg/m^3, which is considered a lower limit for chloride induced corrosion at several locations.

Chloride results for two positions in column 1 are in Table 1. The chloride values are at the borderline for corrosion initiation at the 44 mm depth. The corrosion potential analysis indicated that corrosion was not occurring since potentials were more noble than -100 mV vs. CSE.

Corrosion potential and corrosion rate measurements were performed within the 2.4 by 6 m posttreatment area on July 23, 1990 before drying the deck. It rained the day before so there wasn't any difficulty in obtaining stable corrosion potential readings. The corrosion potentials versus CSE are shown in Figure 2. Locations of high negative potential occurred near the guardrail in good agreement with the chloride data.

Polarization resistance values at several locations are shown in Figure 2. They are not corrected for the area of steel polarized, and as such serve as a relative comparison between corroding and noncorroding sections that can be monitored over time. The need for area correction is not great since the reinforcement pattern is not expected to change, and we are more interested in changes over time than absolute values. Note that it is likely that at least 100 cm^2 of rebar area is involved (based upon a 150 mm long counter electrode and 16 mm rebars with current spreading 25.4 mm on each side). Laboratory studies indicate that R_p values greater than 66,000 ohm•cm^2 are indicative of passivity, while those less than 40,000 ohm•cm^2 are indicative of severe corrosion (5), so if an arbitrary 100 cm^2 area was used corrosion was occurring at several locations where $R_p < 400$ ohms, Figure 2. The low R_p values occur in regions of high negative corrosion potential and thus there is good agreement between the methods. Note that no correction was made for the concrete resistance, but since the concrete was moist and of moderate w/c ratio (above 0.45) the correction is minor in the noncorroding regions, and would mask higher corrosion rates in the corroding regions (6).

The above measurements are in relatively good agreement with data from March 1990 which were used to assess the condition of the bridge. Figure 3 shows the corrosion potential and corrosion rate values determined on the deck. A total area of 92 cm^2 was used for the bar area exposed which is probably low considering current spread. Corrosion rates were calculated using the KCC method for which values less than 0.22 μA/cm^2 indicate that no corrosion damage is expected; between 0.22 and 1.08 μA/cm^2 damage is possible in 10 to 15 years; and for rates between 1.08 to 10.8 μA/cm^2 damage is expected in 2 to 10 years (5). Values in Figure 2 can be compared to those in Figure 3

FIGURE # 1

Sketch of Post Treatment Test Site

US Rt 460 Bypass West between Christiansburg and Blacksburg Va.

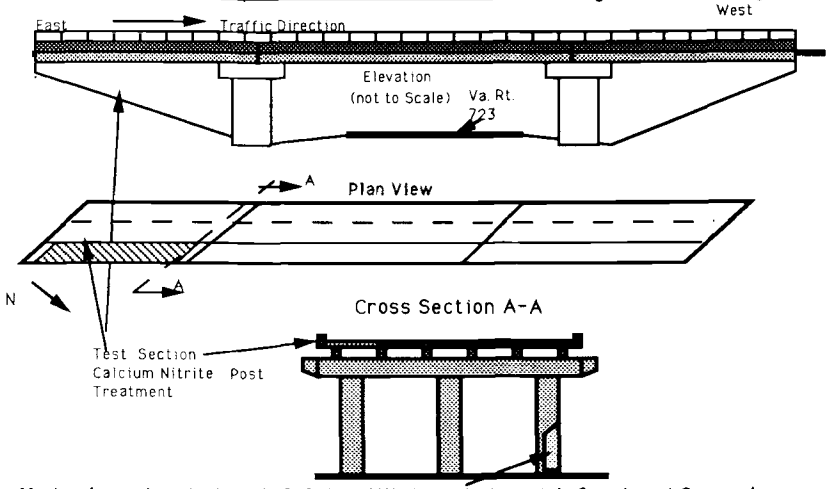

Spalled column treated with Calcium Nitrite - Latex rich Grout and Concrete

Corrosion Testing Coordinate Map

3/90, 7/90, 2/91, 7/91

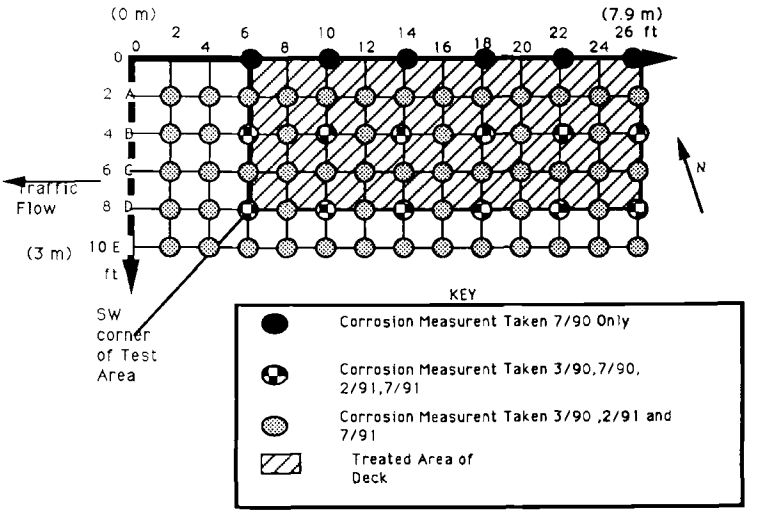

Table 1 Chloride analyses of bridge deck samples. (In kg/m^3.)

	Location						Column	
Depth (mm)	**1-1**	**A4**	**A26**	**B14**	**E14**	**E24**	**CO1-1**	**CO1-2**
6-19	4.4	10.7	4.0	4.5	4.1	1.1	1.4	2.0
19-32	2.8	6.3	3.1	2.2	2.2	1.4	1.2	1.1
32-44	2.4	4.0	2.0	1.2	1.0	0.9	1.0	1.0
44-57	---	3.5	1.4	1.2	0.7	1.1	---	0.8
57-70	---	2.4	0.9	0.90	0.5	0.7	---	0.5

(Based on concrete unit weight of 140 pounds/ cu. ft [2237 kg/m^3] .)

Table 2 Calcium nitrite grout mixes used to fill grooves in deck.

MIX #	CEMENT (kg/m^3)	LATEX FINE AGGREGATE (kg/m^3)	(DOW) ' @ 48% solids (kg/m^3)	DCI-S ' @ 35% solids (kg/m^3)	Daratard- HC (l/m^3)	Water (ICE) (kg/m^3)
1	483	1459	149 (15% s/s cement)	64 (5% s/s cement)	3.2 (0.3% s/s cement)	50
2	483	1459	149 (15% s/s cement)	64 (5% s/s cement)	3.2 (0.3% s/s cement)	50
3	483	1512	107 (11% s/s cement)	64 (5% s/s cement)	3.2 (0.3% s/s cement)	72

Figure 2

CSE Potential Measurements Prior to Post Treatment 7/90

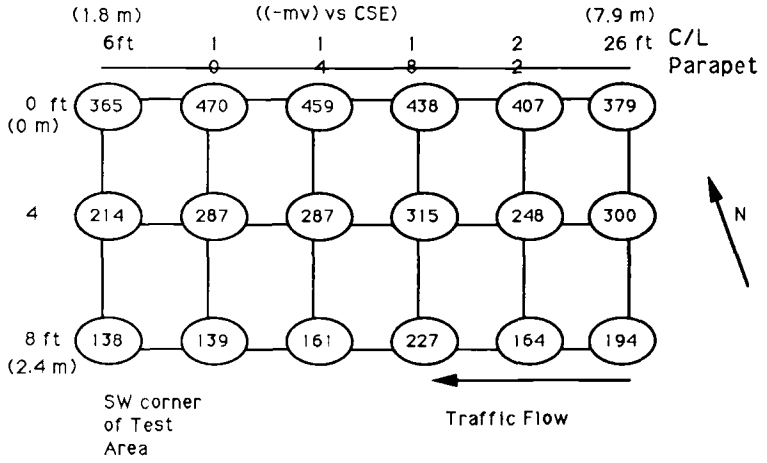

Rp Measurements

Prior to Post Treatment 7/90

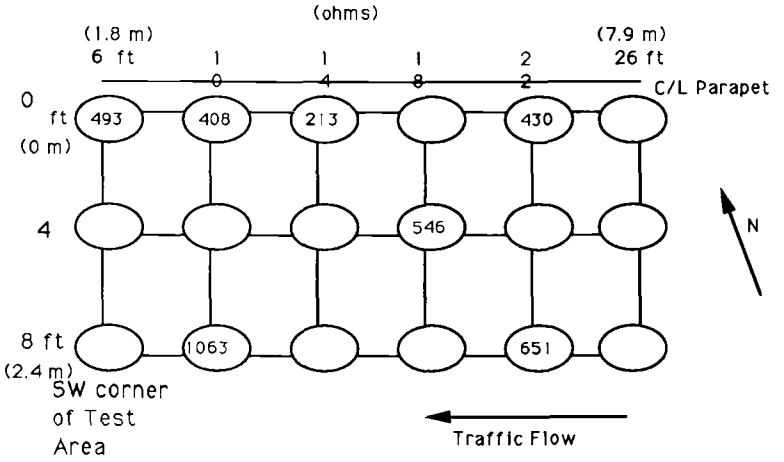

FIGURE 3

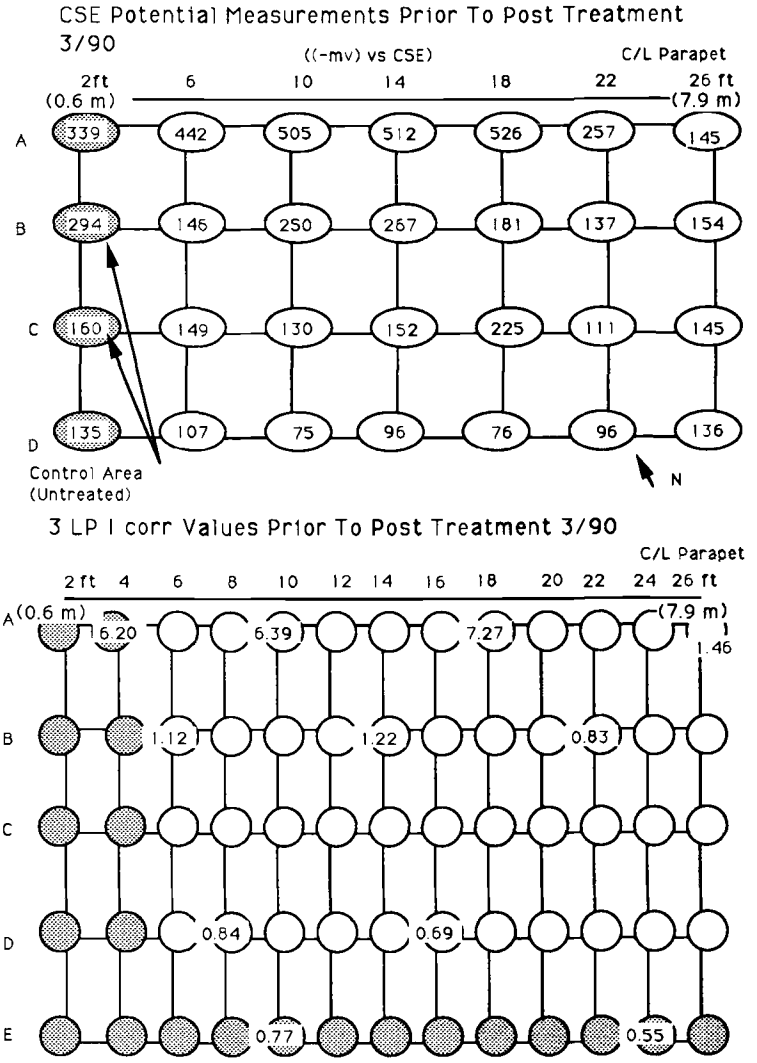
CSE Potential Measurements Prior To Post Treatment
3/90
((-mv) vs CSE)
C/L Parapet
2ft (0.6 m)
6
10
14
18
22
26 ft (7.9 m)
A
B
C
D
339
442
505
512
526
257
145
294
146
250
267
181
137
154
160
149
130
152
225
111
145
135
107
75
96
76
96
136
Control Area (Untreated)
N
3 LP I corr Values Prior To Post Treatment 3/90
C/L Parapet
2 ft
4
6
8
10
12
14
16
18
20
22
24
26 ft
(0.6 m)
(7.9 m)
A
B
C
D
E
6.20
6.39
7.27
1.46
1.12
1.22
0.83
0.84
0.69
0.77
0.55

by multiplying the inverse of the R_p value in Figure 2 by 320 to give a value in $\mu A/cm^2$.

The chloride analyses, corrosion potential, and corrosion rate data are in good agreement. The posttreated area definitely had locations undergoing active corrosion and others that appear to be in the passive state. As such the ability of the posttreatment process to arrest or reduce corrosion activity should be measurable.

THE POSTTREATMENT PROCESS

Posttreatment of the Deck

Equipment--A plan view of the bridge deck and the treated area is presented in Figure 4. A series of 19 mm diameter holes were drilled into the underside of the deck for placement of thermocouples to monitor the heating/cooling of the bridge deck. The approximate location of the holes is shown in Figure 4. A pair of holes were drilled at each location. The deepest hole penetrated 102 mm into the concrete from the underside of the deck. The distance between the deepest penetration of the hole and the deck surface was 51 mm. A Type K and Type T thermocouple was inserted into the hole, and then sealed with a clay plug. The thermocouple leads were then taped to the underside of the deck and brought over the side to temperature measuring instrumentation on the deck surface. The second hole was drilled to a depth of 51mm from the underside into the concrete. A Type T thermocouple was placed in this hole and sealed and taped in the same manner as previously discussed.

A multichannel digital thermometer was used to measure all Type K thermocouples. A total of 9 Type K thermocouples were used, with 4 being placed on the surface of the concrete deck, in addition to the 4 being placed in the holes drilled into the underside of the deck. The surface thermocouples were held in place with clay and blocks to insure solid contact with the surface of the deck. The ninth thermocouple was used to measure the heated air temperature inside insulating shell. The eight Type T thermocouples were attached to a portable data logger and serial printer that was programmed for measuring up to 12 temperatures at 15 minute intervals. Due to battery discharge/damage during transit, the data logger did not function properly. A backup hand held two channel digital thermometer was used instead, to take reading from the eight thermocouples at 15 minute intervals.

To provide fast, effective heating to the deck, a Dayton 6.33 x 10^8 J/hr. kerosene heater was utilized. The heater was modified to incorporate a centrifugal blower for an increased throughput of air (CFM) in comparison to the original blower. A high temperature controller with adjustable on/off setpoint provided a constant air temperature inside the shell. A Type K thermocouple placed 152 mm above the deck surface at the center of heated deck furnished the temperature signal.

A lightweight modular heating shell was fabricated to trap the heated air above the concrete deck. The shell was built in a layered construction, with reflective aluminum sheeting attached to an inner frame of aluminum angle. Four 12.5 mm thick high temperature fiberglass boards/sheets were glued together with high temperature silicone caulking, and was then glued to the inside frame. An outside frame of aluminum was then glued to the panels. The outside fiberglass panel had a foil facing for water resistance. (See Figure 4) Field assembly of the shell went slowly at first, since some of the panels were damaged during shipment and initial handling. (More silicone caulking was need-

Figure 4

Plan View of Calcium Nitrite Post Treatment Test and Thermocouple Placement

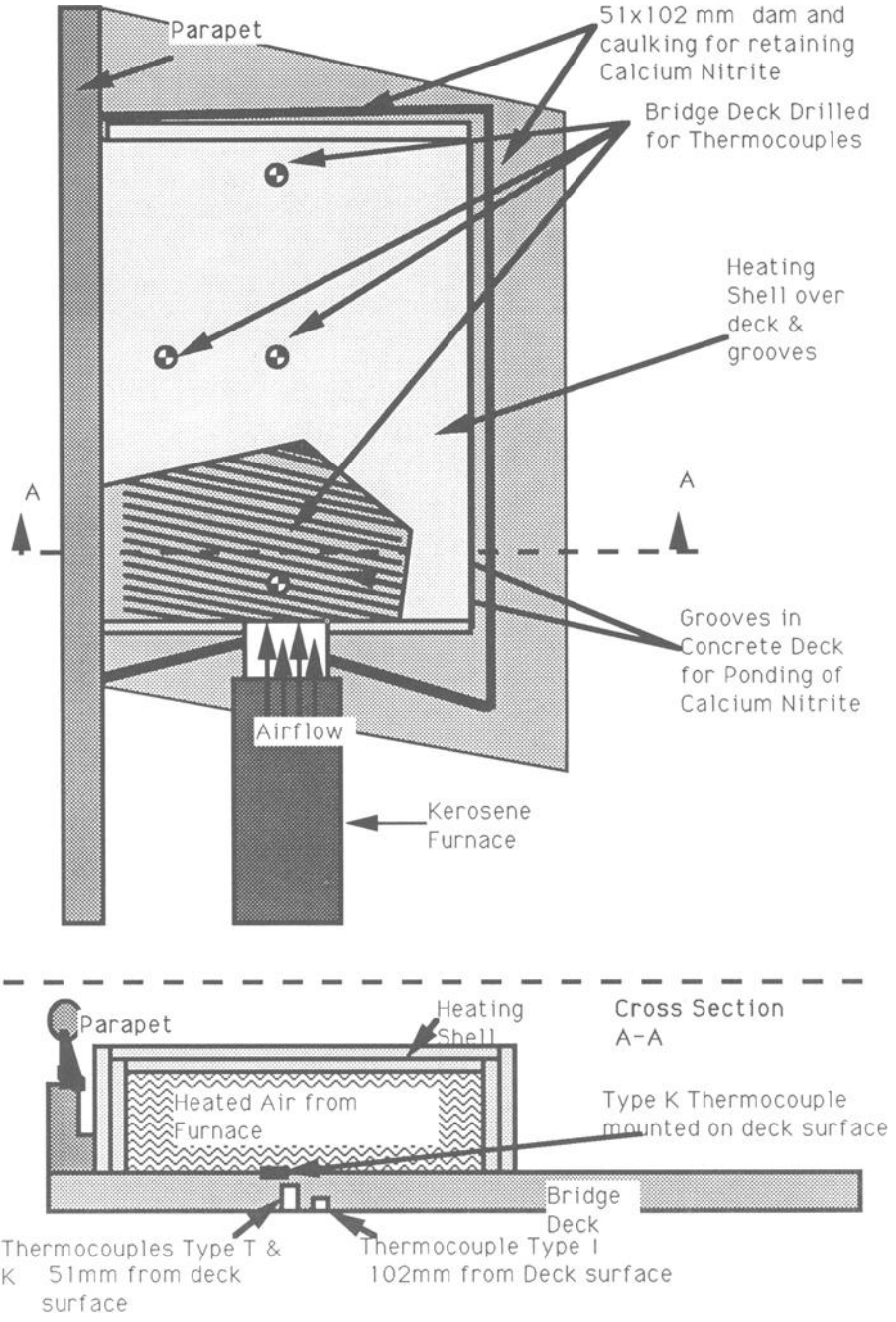

ed). The use of aluminum pop rivets to attach the panels and additional panels together did not go as well as planned. Additional bracing and modifications were made to hold the structure together. A connecting duct between the furnace and the shell was assembled and pop riveted onto the shell. In commercial use a more rugged and more easily assembled shell would be used. Figure 4 gives a schematic of the drying setup and thermocouple locations.

A 0.1 cubic meter gas powered drum mixer was used for grouting and concreting operations. A scale was used for batching materials for the grout and concrete mix designs by mass.

Procedure--The method of impregnating the concrete with calcium nitrite involved driving the free water out of the concrete by heating the deck surface. A major concern during the heating and subsequent cooling process was the temperature gradient that existed throughout the slab. Instrumentation of the deck was critical for monitoring any temperature gradients that developed, since the deck was being heated from one surface. Temperature monitoring capabilities were provided by a series of Type K and T thermocouples as described in the Equipment section. The thermocouples provided critical information on the depth of dry concrete and temperature gradients for the prevention of thermal cracking, especially during the cooling down process.

Plots of temperature of the concrete slab at various depth as a function of time are presented in Figures 5-8. Furnace shutdown is marked on each plot to delineate between the heating and cooling cycles of the test. Figure 5 is a plot of the surface temperatures of the concrete under the heating shell. Temperatures ranged from over 240 °C next to the duct from the furnace to 146 °C at the far end of the shell prior to furnace shutdown. Note that temperature differences between the various locations within the test area have dropped dramatically after 1 hour of cooling. The differential is less than 55 °C versus over 110 °C prior to furnace shutdown. After 8 hours of cooling, the temperature differential is only 11 °C. Figures 6 and 7 plot temperatures at 51 mm depth and 102 mm depth of the concrete slab. An indication of how successful the heating and expulsion of free water from the concrete at various locations can be found in Figures 6 and 7. The boiling point was reached at 51 mm depth except at the far end of the slab. Boiling was reached at the four inch depth for the center region of the slab. Figure 8 is a temperature profile of center region of the slab, with surface, 51mm depth, and 102 mm depth plotted at the same time. During the heating cycle, the concrete at any appreciable depth into the slab was at a relatively constant temperature, with little temperature difference between 51 mm and 102 mm depth. When the furnace was turned off and the cooling cycle began, within three hours the three temperatures varied by only 8 °C. A large temperature gradient which could cause cracking during the cooling of the deck was avoided by judicious opening of vents and by extending the cooling period until the concrete was slightly above ambient temperatures.

After the deck had been cooled, the heating shell was removed. The 51 mm x 102 mm dam for ponding the calcium nitrite was caulked, and a 15% calcium nitrite solution was siphoned from a holding drum onto the deck. The calcium nitrite solution was applied with a hose and poured into each of the grooves until the groove was full. The level of calcium nitrite solution was measured in the holding drum prior to application and after the grooves had been filled to estimate the amount applied to the deck. A few small cracks were noticed during application of the calcium nitrite, but it was not known if these cracks were a result of the heating of the deck, since a survey of any existing cracks prior to heating had not been done. However, there were several delaminated areas caused by

Figure 5

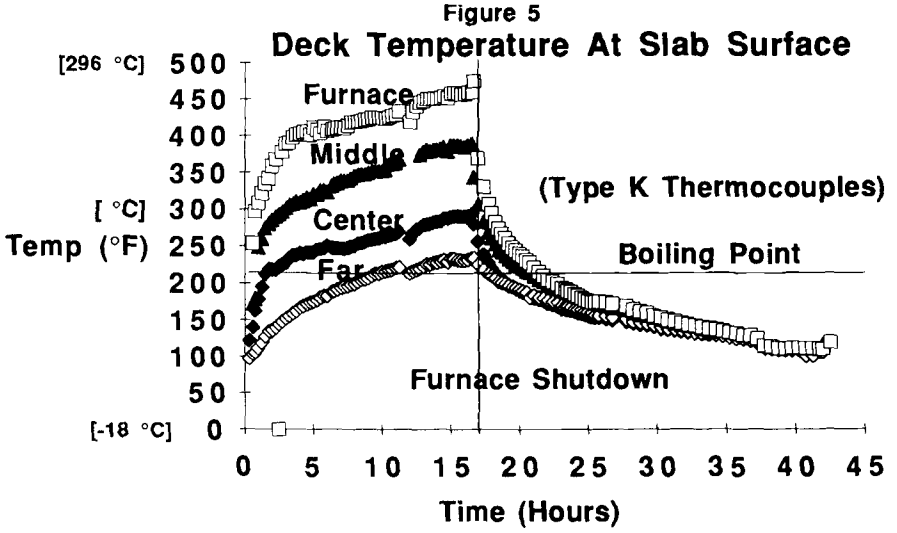
Deck Temperature At Slab Surface
[296 °C]
500
450
400
350
[°C]
300
Temp (°F)
250
200
150
100
50
[-18 °C]
0
Furnace
Middle
Center
Far
(Type K Thermocouples)
Boiling Point
Furnace Shutdown
0 5 10 15 20 25 30 35 40 45
Time (Hours)

Figure 6

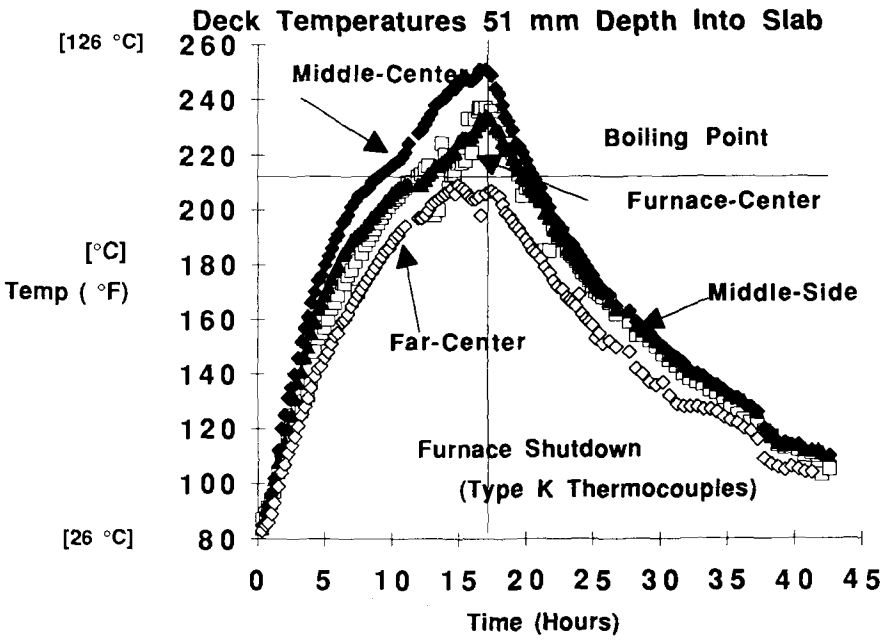
Deck Temperatures 51 mm Depth Into Slab
[126 °C]
260
240
220
200
[°C]
Temp (°F)
180
160
140
120
100
[26 °C]
80
Middle-Center
Boiling Point
Furnace-Center
Middle-Side
Far-Center
Furnace Shutdown
(Type K Thermocouples)
0 5 10 15 20 25 30 35 40 45
Time (Hours)

Figure 7

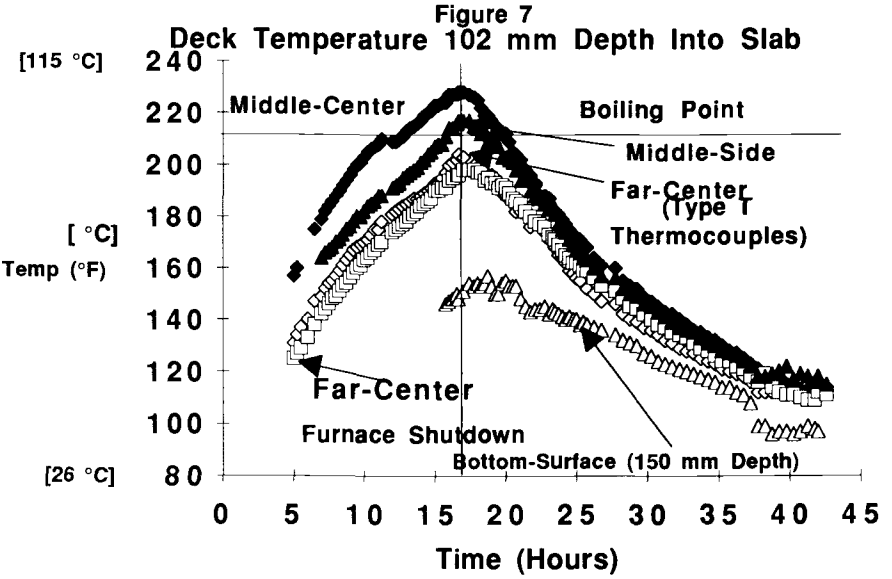
Deck Temperature 102 mm Depth Into Slab
[115 °C]
240
220
200
180
160
140
120
100
80
[26 °C]
[°C]
Temp (°F)
Middle-Center
Boiling Point
Middle-Side
Far-Center
(Type T
Thermocouples)
Far-Center
Furnace Shutdown
Bottom-Surface (150 mm Depth)
0
5
10
15
20
25
30
35
40
45
Time (Hours)

Figure 8
Deck Temperature Profile at Center Middle Theromcouple Location

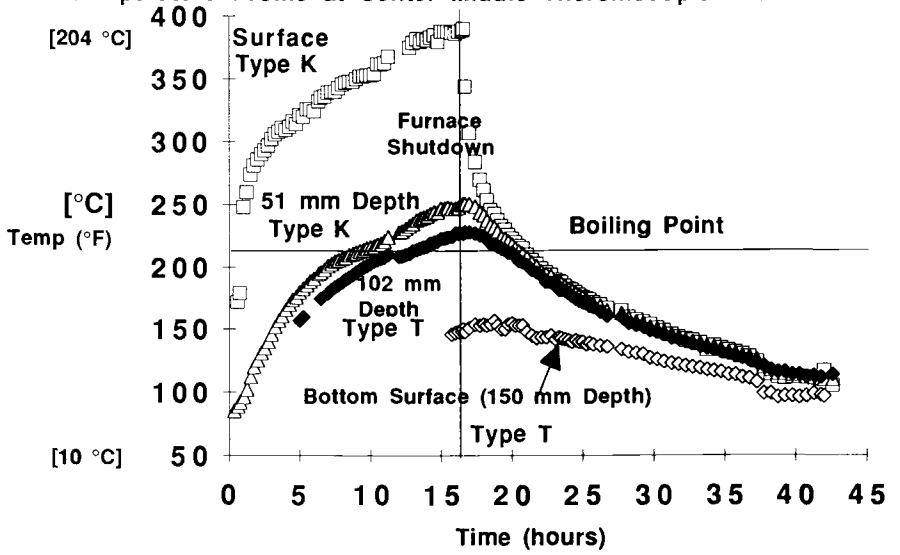

the corrosion of the steel within the test section. The deck was then covered with a polyethylene tarp to prevent evaporation of the calcium nitrite solution.

Ponding of the calcium nitrite solution was over a period of 24 hours. At the end of the 24 hour period the tarp was removed from the concrete. An inspection of the underside of the bridge deck slab, revealed two small cracks that had leaked some calcium nitrite. The cracks were inspected, and the amount of calcium nitrite lost was determined to be minimal. Again, there was no crack survey done prior to the test to determine if these cracks were already present. The calcium nitrite was then removed from the grooves with a wet-dry shop vacuum.

The volume of 15% calcium nitrite that was ponded was 120 liters. The recovered product was 40 liters. Therefore, approximately 80 liters was absorbed by the deck. This is equivalent to 40 liters of of 30% calcium nitrite which is the nominal composition of a commercial admixture, DCI Corrosion Inhibitor™.

The treated deck was rinsed down with plain water using burlap as an applicator. This was in preparation for filling the grooves of the treated area with a calcium nitrite rich latex -modified grout. This provided an acceptable riding surface containing nitrite to be compatible with the treated concrete.

The calcium nitrite-latex modified grout was mixed using a 0.1 cubic meter gas powered drum mixer. The mix design data is in Table 2. Due to the combination of the reactivity of the cement, relatively high ambient temperatures on the bridge deck, and the high addition rate of calcium nitrite (5% s/s vs. 2% s/s at normal addition rates) required extra precautions not normally necessary. Ice and a large quantity of retarder was required to prevent flash set, and more importantly, preserve initial workability until the grout could be applied by squeegee into the grooves. The retarder that was used was Daratard-HC™, at a an addition rate of 3.2 l/m^3. This was required even with the use of neutral set calcium nitrite (at normal addition rates), DCI-S Corrosion Inhibitor™. The addition of latex (DOW Chemical (48% solids) at an addition rate of 15% s/s cement) resulted in a smooth, pourable, but homogeneous grout which was ideal for application with a squeegee. Mix #3 had a reduction in latex content (11 % s/s) due to the end of the supply, and the reduction in latex reflected in the reduced workability of mix #3.

Wet burlap was applied to the deck after the application of the grout. The burlap was covered with a polyethylene tarp and allowed to wet cure 24 hours. The tarp and burlap were removed after the 24 hour wet curing period.

Column Repair

Equipment--Equipment necessary for the repair of the column with calcium nitrite-latex concrete and grout was minimal in comparison to the bridge deck post treatment. The 0.1 cubic meter gas powered drum mixer was also utilized for mixing the concrete for the column repair. A plywood form was banded to the column for the concrete patch. A metal chute was used for placing the concrete at the top of the form into the patch cavity. A small Hobart mixer was used for the mixing of the grout. Other equipment required was a scale, batching pails, accurate liquid measuring containers such as measuring cups for admixture dispensing, and concrete/grout finishing tools.

Procedure--A series of 25 mm diameter holes had also been drilled in a pattern outside the spalled area to the depth of the reinforcement. The area drilled also represented

an area with corrosion problems. A calcium nitrite rich grout was mixed to fill the holes. The mix was based on several trial mixes performed at Grace. Mix design information can be found in Table 3. DCI-S Corrosion Inhibitor™, a neutral set corrosion inhibitor (containing 30% calcium nitrite) at normal dosage levels (2% s/s), was to be used at 7.5 times the normal dosage rate. Latex (DOW chemical 48% solids) was to be used at 15% s/s cement. Requirements for the grout were that it had to have some workability but be stiff enough to remain in the drill holes. The first mix, with 15% latex was too fluid during the first 20 minutes after mixing with the Hobart mixer.

The best mixes for the grout were mixes 4 and 5 in Table 3. A skim coat of mortar was place over the hole pattern to prevent drying out of the grout and for cosmetic purposes.

A concrete patch mix based on the grout was designed and batched. Mix design data are in Table 4. Cement content for the mixes were in the 444 kg/m³ range, with a design w/c ratio of approximately 0.4. Mixture 2 with 10% calcium nitrite % s/s gave the best results. Ice was obtained for mix water, and retarder was added to the mix water to be present at the start of hydration. During the mixing of the revised mix, additional retarder was added (3.8 l/m³) and the w/c ratio was increased by 0.02 (final w/c= 0.40) to obtain the desired workability for the repair. The concrete had an estimated slump of approximately 200 mm, with no noticeable segregation. The concrete was then rapidly placed inside the form by the chute. The outside of the form was vibrated with a hand held vibrator to facilitate consolidation of the concrete.

INITIAL FOLLOWUP DATA ON THE POSTTREATMENT PROCESS

Chloride and Nitrite Analyses

The concrete deck was drilled in three locations to determine the chloride and nitrite contents. The data are in Table 5 and Figure 9. The nitrite penetration is the lowest in the southwest corner for possibly three reasons. These are (1) that the deck was sloped towards the northeast and liquid moved in that direction even though the grooves were cut at equal contours to minimize this; (2) the corner could have received less temperature increase since it was in contact with the large unheated deck mass and not in the direct air flow of the heater; and (3) chloride contents were the highest in that location making it more difficult to impregnate.

The average calcium nitrite content at the 51 to 64 mm level was equivalent to 25.6 l/m³ of a 30% calcium nitrite solution. The liquid that was absorbed was 78.6 liters or 39.3 liters of 30% calcium nitrite solution. This works out to a dosage of 52 l/m³ for a uniform distribution between 0 and 51 mm or 26 l/m³ from 0 to 102 mm. These values are consistent with the analyzed nitrite with the exception being that the distribution was not uniform.

Typically, 20 l/m³ of 30% calcium nitrite solution will protect against 7.7 kg/m³ of chloride (7). Thus, it appears that sufficient nitrite is present to lower corrosion rates over time.

Corrosion Data

Table 3 Grout mixes for the column repair

MIX #	CEMENT (kg/m^3)	FINE AGGREGATE (kg/m^3)	LATEX (DOW) @ 48% solids (kg/m^3)	DCI-S @ 35% solids (kg/m^3)
1	488	1464	151 (15% s/s cement)	162 (11.6% s/s cement)
2	517	1553	108 (10% s/s cement)	172 (11.6% s/s cement)
3	497	1508	133 (12.5% s/s cement)	167 (11.6% s/s cement)
4	480	1440	164 (16.7% s/s cement)	159 (11.6% s/s cement)
5	472	1416	157 (18.3% s/s cement)	157 (11.6% s/s cement)

Table 4 Concrete mixes used in column repair

MIX #	CEMENT (kg/m^3)	COARSE AGGREGATE (kg/m^3)	FINE AGGREGATE (kg/m^3)	LATEX (DOW) @ 48% solids (kg/m^3)	DCI-S @ 35% solids (kg/m^3)	Daratard-HC (l/m^3)	WATER (ICE) (kg/m^3)
1	449 (w/c=0.38)	888	669	89 (10% s/s cement)	192 (15% s/s cement)	1.5 (0.2% s/s cement)	7
2	444 (w/c=0.40)	880	663	89 (10% s/s cement)	127 (10% s/s cement)	9.2 (1.0% s/s cement)	51

(aggregate absorption at 0.5%)

Table 5 Chloride and Nitrite Analyses (Chloride values in kg/m^3, nitrite in l/m^3 of 30% solution)

	Core A Southwest Corner		Core B Center		Core C Northeast Corner	
Depth (mm.)	Chloride	Nitrite	Chloride	Nitrite	Chloride	Nitrite
0 - 12	3.6	29.6	1.3	46.4	2.1	36.1
12-25	3.55	27.2	2.25	44	0.4	51.9
25-38	2.1	30.6	0.95	51.9	0.25	62.2
38 -51	2.55	12.4	1.2	26.2	0.6	39.5
51-64	1.8	10.4	0.9	32.6	0.55	39.5
64-75	2.2	9.4	0.9	33.6	0.45	45.9
75-89	1.55	4.5	0.65	19.3	0.45	47.4
89-102	1.3	3.0	0.35	11.9	0.55	20.7
102-114	0.75	1.5	0.45	10.9	0.55	11.4
114-127		0.5		4.0		4.5
127-140				3.0		1.0
140-152				0.5		3.0

Note that there are 0.27 kg of nitrite in a liter of 30% calcium nitrite solution.

FIGURE 9

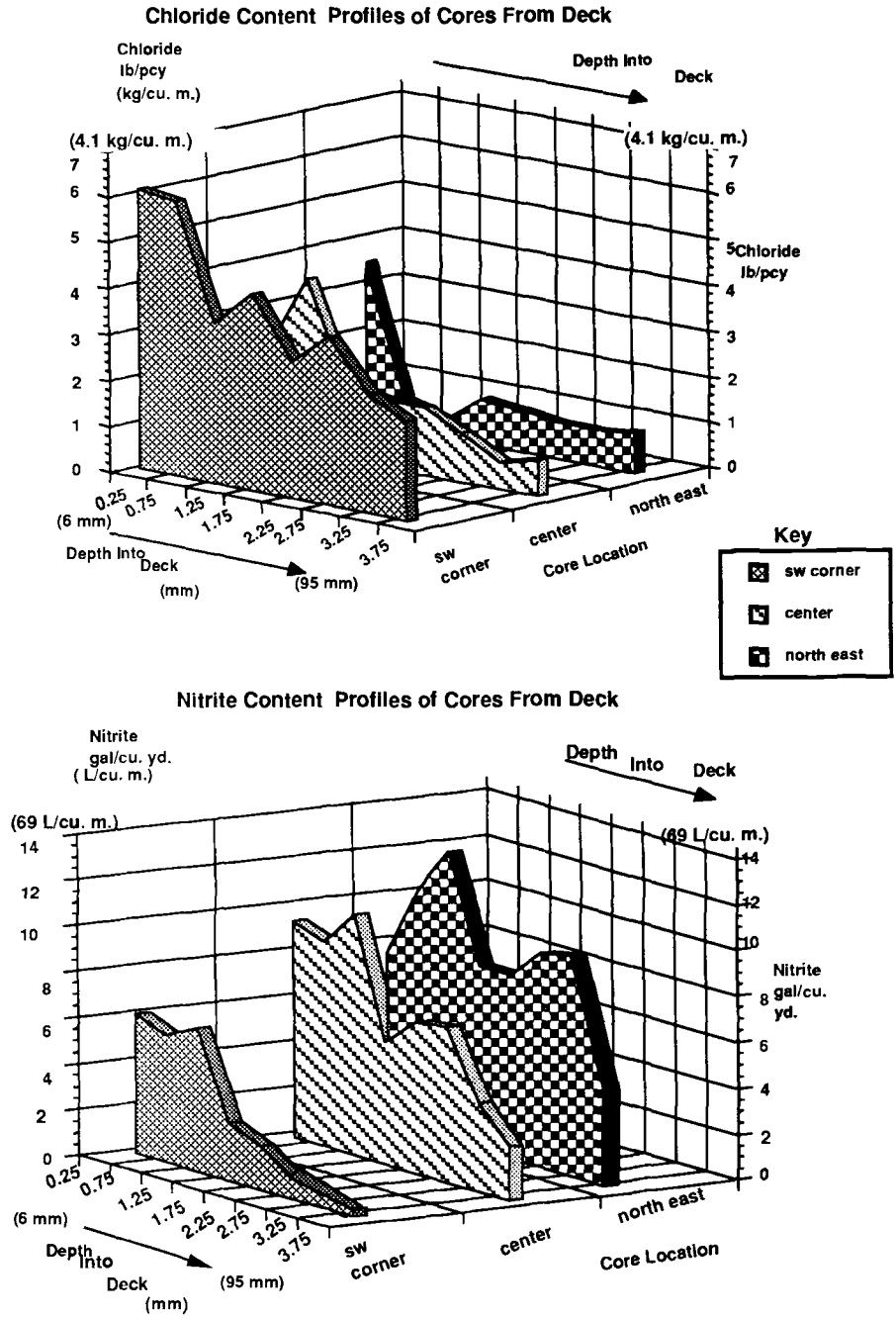
Chloride Content Profiles of Cores From Deck
Chloride lb/pcy (kg/cu. m.)
Depth Into Deck
(4.1 kg/cu. m.)
(4.1 kg/cu. m.)
Chloride lb/pcy
0.25 0.75 1.25 1.75 2.25 2.75 3.25 3.75
(6 mm)
Depth Into Deck (mm)
(95 mm)
sw corner
center
north east
Core Location
Key
sw corner
center
north east
Nitrite Content Profiles of Cores From Deck
Nitrite gal/cu. yd. (L/cu. m.)
Depth Into Deck
(69 L/cu. m.)
(69 L/cu. m.)
Nitrite gal/cu. yd.
0.25 0.75 1.25 1.75 2.25 2.75 3.25 3.75
(6 mm)
Depth Into Deck (mm)
(95 mm)
sw corner
center
north east
Core Location

Corrosion rates and potentials were remeasured in February 1991 and are compared to March 1990 data using the KCC Inc. instrument. Repeat measurements were performed on the Deck in July 1991. At this time polarization resistance measurements were determined using polarization with a guard ring counter electrode (Geocisa) to better define the polarized area (8). These values are compared to the KCC Inc. 3LP values.

Corrosion potentials measured in February 1991 are in Figure 10 for the deck and Figure 11 for the column. In both cases the standard deviations are substantially reduced in the treated concrete areas versus the pretreated values. Also, the standard deviations are less than in the control areas. Reduced potential gradients are generally considered to be indicative of less corrosion activity.

Absolute deck potentials are more negative in both the treated and untreated deck areas. This might be due to higher moisture contents leading to reduced oxygen reduction activity. The column shows more positive corrosion potentials after treatment.

Corrosion rates for the deck and column are given in Figures 12 and 13. Comparing the March 1990 to February 1991 values shows that the treated deck had a 17% reduction in corrosion rates and 47% reduction in standard deviations. The control area had a 22% increase in corrosion rates and a 134% increase in standard deviations. Thus, the treated deck appears to be improving relative to the untreated deck. Since calcium nitrite can decrease resistivity (9), and because passive areas are known to correspond to a larger area of bar being polarized (8), it is likely that the corrosion rates in the treated area are much lower than indicated.

Deck measurements made in July 1991 tend to support the trends noted in February 1991. There is a slight negative increase in corrosion potentials in the treated area, however, the increase is much higher in the untreated area (Figure 10). Considering that July temperatures are at least 10°C warmer than February-March temperatures this might be a temperature effect. Furthermore, corrosion potential measurements do not directly relate to corrosion activity and the continual reduction in standard deviations in the treated area tends to show that macrocell activity has significantly decreased.

The most negative potentials in the treated areas are at the boundaries where the drying would have been the least efficient in the posttreatment process. This is supported by further examining the July 1991 data where the average corrosion potential in the treated area boundary was-306 mV vs. CSE with a standard deviation of 44 mV, whereas the interior of the treated section had an average corrosion potential of -265 mV vs. CSE with the standard deviation being 23 mV. Therefore, better results are probable if larger areas are treated.

Corrosion rate measurements made in July 1991 are shown in Figure 12. The 3LP results show that corrosion rates in the treated area which were originally larger than in the untreated area were lower. This indicates that the treated section is showing improved corrosion performance compared to the untreated section. The slight increase in rates from February 1991 to July 1991 is much less than what could be attributed to a temperature increase (rates approximately double for every 10°C increase in temperature) which implies that corrosion activity is decreasing more than indicated.

There is a large discrepancy between the 3LP measurements, and those determined with the guard ring Geocisa instrument. The Geocisa data indicate that no corrosion is taking place (that is, all rates are below 0.22 $\mu A/cm^2$). As mentioned earlier an extremely

FIGURE 10

CSE Potential Measurements After Post Treatment 7/91

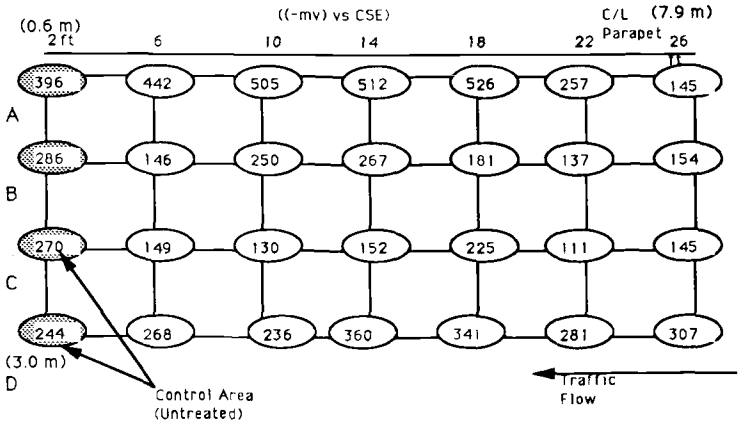

CSE Potential Measurements After Post Treatment 2/91

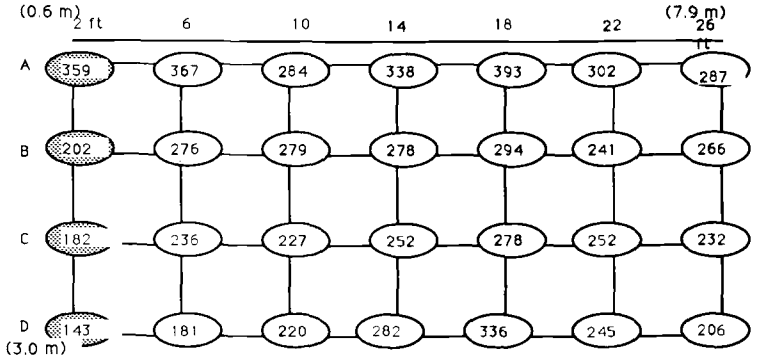

		Mean	Std Dev
3/90	Area To Be Treated (see Figure 3)	222	153
	Untreated Area	189	80
2/91	Treated Area	278	51.3
	Untreated Area	236	68
7/91	Treated Area	286	44
	Untreated Area	313	48

FIGURE 11

CSE Potential Measurements Prior To Post Treatment 5/90

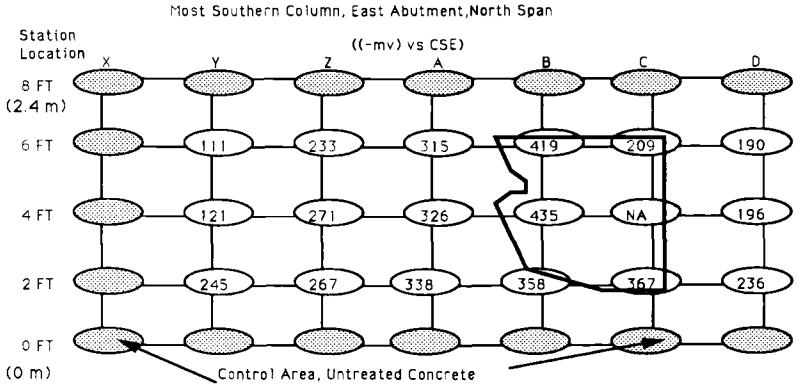

CSE Potential Measurements After Post Treatment 2/91

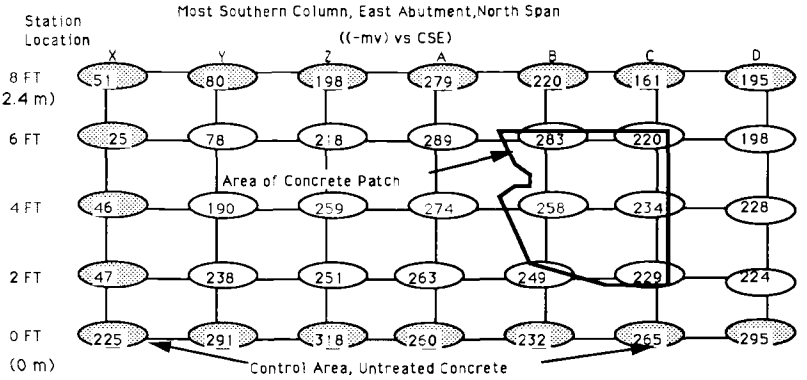

		Mean	Std Dev
5/90	Treated ,Concrete Removed	358	89.3
	Treated,Calcium Nitrite Plugs	237	73.6
2/91	Control, Untreated	188	100
	Treated ,Concrete Removed	246	22.9
	Treated,Calcium Nitrite Plugs	226	55.2

FIGURE 12

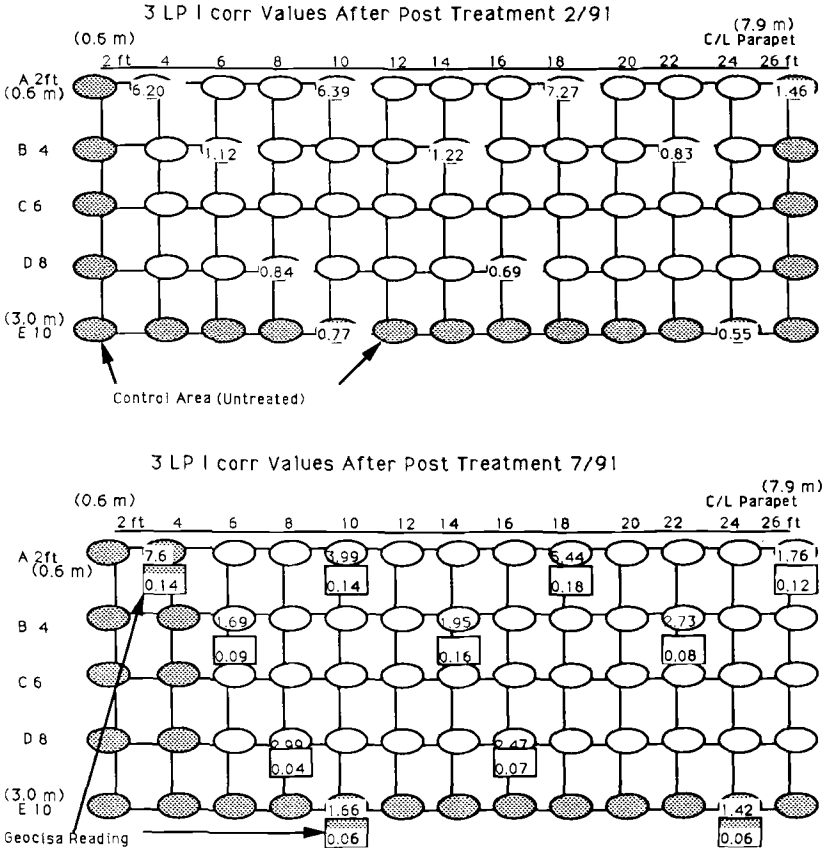

			Mean	Std Dev
3/90	Area To Be Treated (see Figure 3)		3.07	2.96
	Untreated Area		0.93	0.47
2/91	Treated Area		2.75	1.55
	Untreated Area		1.13	1.10
7/91	Treated Area		3.61	2.01
	Untreated Area		1.61	0.17
7/91	Geocisa Reading	Treated Area	0.11	0.05
	Geocisa Reading	Untreated Area	0.08	0.03

FIGURE 13

3 LP I corr Values After Post Treatment 2/91

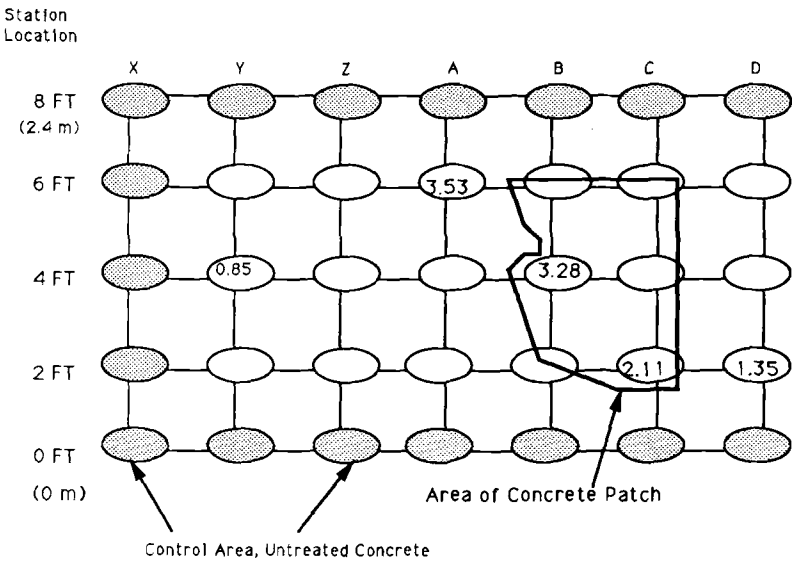

		Mean	Std Dev
2/91	Treated ,Concrete Removed	2.70	0.83
	Treated,Calcium Nitrite Plugs	1.91	1.43

conservative value was chosen for the polarized area using the 3LP KCC instrument, and this can explain some of the difference. Further work beyond the scope of this project is suggested to address the differences between the techniques. Nevertheless, the corrosion activity in the treated area is decreasing relative to that in the untreated area.

Corrosion rates were not determined in the column before treatment due to time constraints. Corrosion rate data after treatment are shown in Figure 13. Due to the higher density of steel in the column, and for reasons outlined above the rates are much higher than the actual corrosion rates.

The initial posttreatment corrosion measurements don't necessary reflect the ultimate performance of the posttreatments. The corrosion activity will need to be monitored in time to get a more accurate assessment.

CONCLUSIONS

The ability to dry out a concrete bridge and successfully impregnate it with a known corrosion inhibitor was demonstrated. It appears to be a viable method of bridge rehabilitation that does not require the large-scale removal of sound concrete. The equipment employed is relatively unsophisticated and can easily be scaled up to treat larger areas.

The practicality of using grouts and concretes with high calcium nitrite inhibitor contents was confirmed. This technology can be used in column repair where it is difficult to remove the column or apply other means of protection.

Initial posttreatment corrosion and nitrite analysis data indicate that the treated areas are outperforming adjacent untreated areas and have reduced corrosion activity compared to pretreatment values.

The next steps should be an economic assessment of the cost per square foot of the processes and the treatment of a larger area. The corrosion behavior of the deck and column should also be monitored over time to determine the benefits of the treatment.

ACKNOWLEDGMENTS

We wish to acknowledge the contributions of Ding Feng Shen who participated in the field test. We also wish to thank Maria Hicks and Paul Toner who did preliminary work on the grout mixes used in the field. Special acknowledgement to Ray Henderson for designing and building the heating shell used and in packaging our equipment. Also, we wish to thank Management at W. R. Grace & Co.-Conn., and Virginia Polytechnic and State University for their support.

Original work on the calcium nitrite posttreatment process was initiated by Dr. Joseph Cogliano, of the Washington Research Center of W. R. Grace & Co.-Conn., and he was instrumental in transferring the technology to us.

We also gratefully acknowledge the support of this research by the Strategic Highway Research Program under contract SHRP-87C-103.

This paper represents the views of the authors only, and is not necessarily reflec-

tive of the views of the National Research Council, the views of SHRP, or SHRP's sponsor. The results reported here are not necessarily in agreement with results of other SHRP research activities. They are reported to stimulate review and discussion within the research community.

REFERENCES

1. R. L. Carrasquillo, "Evaluation of a Posttreatment Procedure of an Existing Reinforced Concrete Bridge Structure," Final Report Prepared for W. R. Grace & Co. Austin, TX, January 15, 1986.

2. J. Cogliano and A. Rosenberg, "Treating Concrete Structures to Inhibit Corrosion by Heating the Structure, Cooling Same Under Controlled Temperature Gradient and Applying an Inhibiting Agent to an Internal Portion of the Structure," United States Patent #5039556, August 13, 1991.

3. R. E. Weyers and P. D. Cady, "Deep Polymer Impregnation of Concrete Bridge Decks," Paper No. 870185, TRB, National Research Council, Washington, D.C., 1988.

4. N. S. Berke and M. C. Hicks, "Electrochemical Methods of Determining the Corrosivity of Steel in Concrete," In Silver Anniversary Symposium on Corrosion Testing and Evaluation. ASTM STP 1000. R. Baboian and S. W. Dean Eds. American Society for Testing and Materials, Philadelphia, PA, 1990, p. 425.

5. K. C. Clear, "Measuring Rate of Corrosion of Steel in Field Concrete Structures," In Transportation Research Record 1211. TRB, National Research Council, Washington, D.C., 1989, pp. 28-37.

6. N. S. Berke, D. F. Shen, and K. M. Sundberg, "Comparison of Current Interruption and Electrochemical Impedance Techniques in the Determination of Corrosion Rates of Steel in Concrete," In The Measurement and Correction of Electrolyte Resistance in Electrochemical Tests. ASTM STP 1056. L.L. Scribner and S. R. Taylor, Eds. American Society for Testing and Materials, Philadelphia, PA, 1990, pp. 191-201.

7. N. S. Berke and A. Rosenberg, "Technical Review of Calcium Nitrite Corrosion Inhibitor in Concrete," In Transportation Research Record 1211. TRB, National Research Council, Washington, D.C., 1989, pp. 18-27.

8. S. Feliu, J. A. Gonzales, M. L. Escudero, S. Feliu, Jr., and M. C. Andrade, "Possibility of the Guard Ring for the Confinement of the Electrical Signal in Polarization Measurements of Reinforcements," Corrosion 89, National Association of Corrosion Engineers, Houston, Paper No. 623, 11 pp.

9. N. S. Berke and L. R. Roberts, "The Use of Concrete Admixtures to Provide Long-Term Durability from Steel Corrosion," Proceedings, Third CANMET/ACI International Conference on Superplasticizers and Other Chemical Admixtures in Concrete, ACI SP 119 American Concrete Institute, Detroit, MI (1989), p. 863.

Philip D. Cady and Richard E. Weyers

PREDICTING SERVICE LIFE OF CONCRETE BRIDGE DECKS SUBJECT TO REINFORCEMENT CORROSION

REFERENCE: Cady, Philip D. and Weyers, Richard E., "Predicting Service Life of Concrete Bridge Decks Subject to Reinforcement Corrosion," Corrosion Forms and Control for Infrastructure, ASTM STP 1137, Victor Chaker, Ed., American Society for Testing and Materials, Philadelphia, 1992.

ABSTRACT: The deterioration of the nation's highway infrastructure is proceeding at an alarming rate. A major element of the problem involves chloride-induced corrosion of reinforcing steel in concrete bridge components. In order to rationally implement bridge management strategies, it is generally recognized that life-cycle cost analyses of viable alternatives are required. This necessitates the development of reliable means for predicting the service lives of alternative procedures. The major components of a rational model for predicting service life in this scenario center on the time for the chloride ion concentration to reach the corrosion threshold level at reinforcement locations and the corrosion reaction time necessary to produce loss of serviceability. Obviously, the definition of the terminal serviceability in terms of deterioration level also constitutes an important element of the model. This paper examines a semi-empirical deterioration model for predicting service life based on fundamental concepts, augmented with historical data.

KEYWORDS: service life, bridge decks, reinforcement corrosion, chloride diffusion, corrosion rate

INTRODUCTION

According to a recent U.S. Department of Transportation report, 39 percent of the 576,665 bridges on the nation's federal aid highway system are structurally deficient or functionally obsolete [1]. In prepared testimony before the Investigation and Oversight subcommittee of the House Public Works committee, Federal Highway Administrator Thomas D. Larson recently reported that spending on bridge repair and replacement needs to increase from the current $3.5 billion per year to $4.2 billion just to keep up with the rate of deterioration [2].

Dr. Cady is professor of civil engineering and Distinguished Alumni Professor of Engineering at Penn State University, 212 Sackett Building, University Park, PA 16802. Dr. Weyers is professor of civil engineering at Virginia Polytechnic Institute and State University, 200 Patton Hall, Blacksburg, VA 24061.

The riding surfaces, or decks, of bridges are the primary focal point of problems related to loss of serviceability due to deterioration. Furthermore, it has been repeatedly documented over the past 30 years that the primary deteriorative mechanism involved is chloride-induced corrosion of reinforcing steel in concrete bridge decks. The high pH environment present in portland cement concrete (about 12.5) normally causes embedded steel to become passivated by the formation of gamma ferric oxide on the metal surface. However, chlorides present in quantities greater than about 0.025 to 0.050 percent by weight of concrete [3] depassivate the steel, promoting corrosion and subsequent destruction of the concrete through the wedging action of voluminous corrosion reaction products. The primary sources of the chlorides are deicing chemicals (sodium and calcium chlorides) and brine or brackish ground- and surface-waters and aerosols from the bridge environment.

The use of epoxy coated reinforcing steel in bridge decks that are liable to exposure to chlorides (which has been standard practice in the U.S. for about a decade) should greatly reduce problems in the future. However, a very large percentage of the approximate 577,000 bridge decks in this country are over ten years old and do not contain epoxy coated reinforcement. Regarding bridge demographics, the average life of a bridge, in terms of overall site serviceability (which includes rehabilitation and component replacements), is estimated to be 70 years [4]. Forty-five percent of the nation's bridges are over 35 years old, the average age when major bridge rehabilitation is usually required [4].

Increasingly, highway agencies are endeavoring to embark upon fiscally responsible bridge management strategies based on minimization of life-cycle costs. For the matter of existing bridge decks that do not contain epoxy coated steel, this involves the evaluation of a range of possible alternatives for the protection, maintenance, repair, rehabilitation, or replacement of the deck. The base line, against which the various active strategies are compared, is the passive (do nothing) alternative. Therefore, it is essential that means be available to estimate the service lives of bridge decks containing black (i.e. non-epoxy coated) reinforcing steel as a function of those factors that promote deterioration by corrosion of the reinforcing steel.

THE MODEL

In 1984, the authors published a predictive model for the deterioration of unprotected bridge decks subject to chloride-induced corrosion of the reinforcing steel [5]. It is an hybrid theoretical/heuristic approach that attempts to simplify the highly complex interactions of myriad variables involved in the deterioration versus time relationships into a practical and workable, yet sufficiently sensitive process model. It considers only the effect of chloride-induced reinforcement corrosion. That is, effects of carbonation are ignored. Carbonation can depassivate reinforcing steel in concrete by reducing the pH in the concrete below the protective 11.5-level needed to form and maintain the protective gamma ferric oxide coating. However, the time required for carbonation to proceed to the depth of the reinforcing steel, under most circumstances, can be expected to be much longer than the probable useful life of the structure. Under typical conditions, the time versus carbonation depth relationship can be approximated from [6]:

$$t = [0.40 - 0.5(w/c)]\, d^2 \qquad (1)$$

where: t = time, years
w/c = water/cement ratio of concrete (by mass)
d = carbonation depth, mm

Thus, for example, at a water/cement ratio of 0.50 (which is at or above the values typically allowed by specification for bridge deck concrete) and a concrete cover depth of only 25 mm (1 in.), it would typically take over 90 years for the concrete to become carbonated to the level of the top of the reinforcing steel. Furthermore, at this shallow cover of 25 mm, there exists a better than 70% chance that subsidence cracking (see below) will produce immediate access of chlorides to the steel anyway. Therefore, the effect of carbonation in the bridge deck case was considered by the authors to be of no practical consequence.

Morphology and Chronology of the Process

Several field studies on the performance of bridge decks, along with complimentary laboratory evaluations and ever-constant vigilance of the technical literature on the subject, led the authors to formulate a typical morphology and chronology for the deterioration of concrete bridge decks due to reinforcement corrosion. The process often begins during construction when "subsidence" cracking (to be discussed in more detail below) causes immediate exposure of some of the reinforcing steel to access by chlorides at the first contact with chloride salts in the environment. Reinforcement exposed in this manner will corrode and produce fracture planes within a few months to a few years after construction.

The movement of chlorides through uncracked concrete occurs almost exclusively by the process of diffusion, which begins with the first contact of chloride salt solutions with the surface of the concrete. Diffusion is a time-dependent process driven by concentration gradients. For the typical bridge deck, constructed to specification in the 1970's, the deterioration model developed by the authors indicates that it takes about five years for the chloride content to reach the corrosion threshold concentration at the level of the shallowest reinforcing steel. Then, approximately two more years are needed for the wedging action of corrosion produces to produce fracture planes and spalls. It is at this point that patching of small spall areas on bridge decks begins. The process continues as successively deeper steel becomes infected by chloride diffusion. During the latter period, the proportion of the bridge deck surface afflicted with fracture planes and spalls increases at the rate of about 2% per year. Finally, the deck surface becomes so badly damaged that it is necessary to remove the deteriorated concrete and to overlay the deck, usually with latex-modified or low-slump, dense concrete or with asphalt paving mixture. This action is typically taken at the point when the deck surface displaying fracture planes, spalls, and previously patched areas is about 40% of the total deck area. Figure 1 graphically portrays the scenario just described.

Subsidence cracking: The body forces resulting from the sedimentation (bleeding) process in fresh concrete produce tensile stresses above stationary embedded objects (i.e. reinforcing bars) due to the resistance that they provide to subsidence of the fresh concrete during that period. This can result in cracking of the fresh concrete. Subsidence cracking was found to be a probabilistic function of the consistency of the concrete (slump), the diameter of the reinforcing bars, and the depth of concrete cover over the reinforcement [7]. The cracking probability is directly related to slump and bar size, and inversely related to cover. Notice that this type of cracking is parallel to and directly above the reinforcing steel, as opposed to stress-induced cracking which typically runs perpendicular to the reinforcement and the exposes very little rebar to the environment. Bar cover is the most significant factor of the three cited factors, as demonstrated in Figure 2.

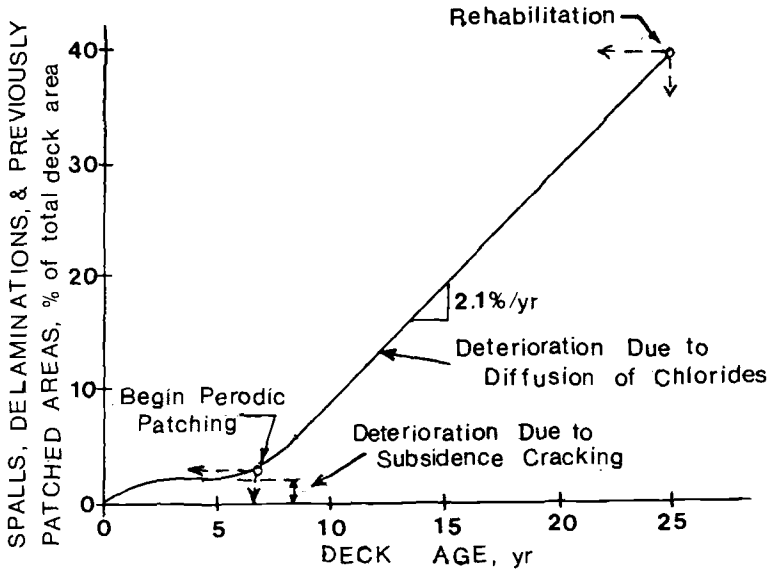

FIG. 1 -- Typical Deterioration Curve for Bridge Deck Having About 5 cm (2 in.) Average Rebar Cover.

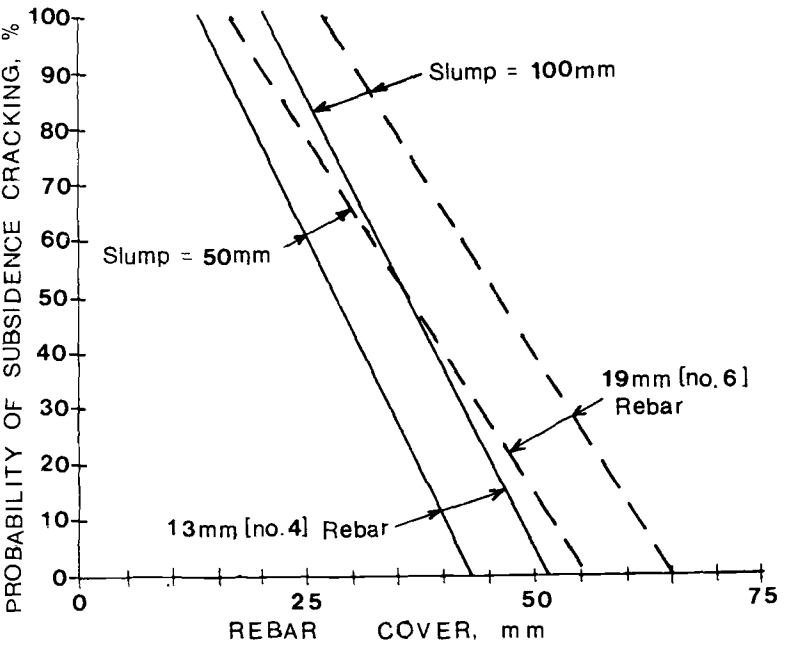

FIG. 2 -- Probability of Subsidence Cracking Versus Cover, Bar Size, and Slump.

Chloride diffusion: The process of diffusion, by which chlorides infiltrate sound concrete, can be expressed mathematically in terms of Fick's second law:

$$\partial C/\partial t = D_c \, (\partial^2 C/\partial x^2) \qquad (2)$$

where: C = concentration
x = distance
t = time
D_c = diffusion constant

Using the error function solution for this partial differential equation and imposing conditions typical of the concrete bridge deck scenario, the following relationship was used in the model [5, 8]:

$$t = 0.4918 \, (L - 2.0)^2 \qquad (3)$$

where: t = time to the initiation of reinforcement corrosion due to diffusion of chloride ions, years
L = mean reinforcement cover, cm

The value assumed for the diffusion constant D_c, was 3 x 10^{-8} cm^2/s. The diffusion constant varies with the water/cement ratio of the concrete and with temperature. In this instance a water/cement ratio of 0.45 by mass and an average ambient temperature of 15°C were assumed [8]. More recently, in research carried out under the direction of one of the co-authors, analysis of chloride profile data from ten bridges in three states (PA, VA, WI) gave mean chloride diffusion constants that averaged 1.5 x 10^{-8} cm^2/s (range 0.5 x 10^{-8} to 3.8 x 10^{-8} cm^2/s) [9]. This indicates that the assumed value for D_c in the model may be too high, possibly due to lower mean ambient temperatures than that assumed, lower water/cement ratios than the 0.45 assumed (unlikely), the greater maturity of the field concrete, or a combination of these. For given surface and corrosion threshold chloride concentrations and cover depth, time to diffusion varies inversely and linearly with D_c. Therefore, accurate determination of the diffusion constant is imperative for reckoning service life. Also, since D_c appears to vary over about one order to magnitude in our sampling of typical bridge decks, it appears that it is necessary to consider the chloride diffusion constant as a site-specific variable which needs to be determined for each bridge deck.

Corrosion threshold chloride content: In developing the expression for time-to-corrosion based on the error function solution to the diffusion equation, the authors assumed the value of the corrosion threshold chloride content to be 0.2% by mass of the portland cement content of the concrete [8], following the work of others. For a typical bridge deck concrete [cement content 363 kg/m^3 (6 1/2 sacks per cubic yard)] this works out to about 0.73 kg/m^3. In a summary of findings by a number of researchers published in a recent paper [3], that figure is approximately mid-range of the values presented. As was the case with the diffusion constant, the reported range of corrosion threshold chloride contents is sufficient to produce significant variations in the calculated time-to-corrosion values. The magnitude of the error, if 0.73 kg/m^3 is assumed to be a correct and constant value for the threshold chloride content, will range from +20% for a true value of 0.60 kg/m^3 to -135% for a true threshold of 1.30 kg/m^3. More research is needed to more precisely quantify the magnitude of the corrosion threshold chloride content. Intuitively, its value should be relatively constant for the ranges of the variables that define the bridge deck scenario.

Cracking caused by corrosion: The cracking of the bridge deck surface produced by the wedging action from the increasing volume of

corrosion products may occur either as inclined (trench) cracks or horizontal fracture planes, depending on the depth of concrete cover. The relationships that quantify the period of time from the initiation of corrosion to the occurrence of cracking for these two cases were adopted, in the deterioration model, from work published by Bazant [10]. Time to cracking is a function of concrete cover over the reinforcement, rebar diameter, spacing of rebars, corrosion rate, and the tensile strength, modulus of elasticity, and Poisson's ratio of the concrete. For the bridge deck scenario, rebar cover and corrosion rate would be expected to be the primary independent variables. This was substantiated in recent work carried out under the direction of one of the authors on a Strategic Highway Research Program project [11]. In the model, we assumed a corrosion rate of 1.2×10^{-3} g/cm^2/yr based on information from one literature source [12]. In recent research carried out under the direction of one of the authors [13], corrosion rates were determined on six bridges located in three states (PA, VA, FL) and on removed sections of deteriorated bridge deck slabs. Corrosion current (I_{corr}) readings, were obtained using a sophisticated galvanostatic linear polarization device which employs special guard ring procedures to clearly define the polarized area of the reinforcement. Sixty-three readings were obtained in areas where corrosion potentials were more negative than -350 mV (CSE), indicative of 90% or greater probability of active corrosion. After eliminating three of the readings as obvious outliers, the mean corrosion current value obtained and converted to metal loss for the remaining 60 readings was 5.9×10^{-3} g/cm^2/yr (range: 1.4×10^{-3} to 20.2×10^{-3} g/cm^2/yr). This mean value is about five times the value assumed in the original deterioration model. Once the chloride concentration of the concrete in the vicinity of the reinforcement reaches the corrosion threshold level, the time to cracking of the concrete is linearly and inversely proportional to corrosion rate. Therefore, corrosion rate is an important parameter in the deterioration model. The range of values found in the field study, just cited, would suggest that corrosion rate is a site-specific variable. Therefore, it is a variable that should be evaluated on a case by case basis.

Service Life

The service life of a building component or material is defined in ASTM E632 [14] as: "the period of time after installation during which all properties exceed the minimum acceptable values when routinely maintained." For the purpose of life-cycle cost analyses in the bridge deck scenario, we are confronted with at least three types of service life. First we have the useful life of the structure, which will be terminated by either the serviceability of the structure as a whole or cessation of its need (which almost never happens). That time period constitutes the planning horizon over which the strategies for maintaining the shorter-lived bridge components must be evaluated. Since that time period will be quite long for bridges, perhaps 60 to 100 years, it's determination is relatively unimportant due to the only minor differences between discounted cash flows for the actual service life versus an assumption of perpetual service. Two other "service lives" associated with the deck component of the bridge, however, are important and need to be determined in order to evaluate life cycle costs for the bridge. Recalling Figure 1, there is a period of time following the initial bridge construction (or deck replacement) when no maintenance is required. That period is followed by a period of approximately steady-state deterioration until the point is reached at which the deck requires major rehabilitation or replacement. The durations of the two periods just described must be determined in order to carry out meaningful life-cycle cost evaluations.

In the original deterioration model developed by the authors [5], the maintenance-free period (T_m) and the deck age at rehabilitation (T_r) were derived from a single parameter, viz., the clear cover of

concrete over the reinforcement (L). However, as demonstrated earlier in this paper, the chloride diffusion constant (D_c) and corrosion rate (J_r) are both sufficiently site specific and influential on service life so as to require that they be incorporated into service life determinations. Figures 3 and 4 present the maintenance-free period (T_m) and deck age at rehabilitation (T_r), respectively, as functions of mean rebar cover for the maximum, minimum, and mean values of the chloride diffusion constant and corrosion rate reported earlier in this paper.

PERFORMANCE OF THE MODEL

A review of the technical literature and data from a current research project yielded some information on the time-to-corrosion (i.e. maintenance-free period) and time-to-rehabilitation for bridge decks to compare with the predictions of the model. For the time-to-corrosion period, the data plotted in our earlier paper [8] were found to reasonably match the results shown on Figure 3. For example, at a mean rebar cover value of 4 to 6 cm (typical range for bridge decks), T_m varies from about 3 to 20 years for the Clear [15] data, and from about 6 to 12 years for the Stratfull equation (as modified by Clear) [15], versus the approximate range of 4 to 16 years shown for mean D_c and J_r values on Figure 3.

NCHRP Report 297 [16] presents an equation relating the number of salt-applications-to-corrosion to rebar cover and water/cement ratio. When combined with deicer chemical application rate data from the same report, the water/cement ratios at which the indicated time-to-corrosion values for 5 cm rebar cover occurred for the maximum, minimum, and mean values of D_c and J_r on Figure 3 are 0.60, 0.43, and 0.49, respectively. Again, these values seem reasonable for typical bridge deck conditions.

Regarding bridge deck life to rehabilitation, the statement of an FHWA spokesman was referred to earlier in this paper alleging that the average age when major bridge rehabilitation is usually required is 35 years [4]. In our deterioration model it is assumed that major rehabilitation occurs, averagely, when about 40% of the deck surface is affected with delaminations, spalls, and previously patched areas, as previously mentioned. If that criterion is applied to first figure in a recent paper by Carter [17], it reveals that the average age of bridge decks at rehabilitation in the Alberta primary highway system is about 27 years.

Researchers at MIT attempted to model bridge deterioration by statistical evaluation of data from the 1983 Federal Highway Administration National Bridge Inventory [18]. Using the data from the two states in that study in which deicing chemicals would have been routinely employed (NY and MI), we extrapolated bridge deck condition versus age information to provide an estimate of bridge deck life at rehabilitation. This was accomplished by plotting ages of bridges having specific deck conditions against the cumulative percent of bridges affected, expressed in terms of the normal probability function. The specific condition code evaluated here was "Code 4" which is described as: "marginal condition - potential exists for major rehabilitation." The condition indicators, in terms of % of deck area, for Code 4 were given as: > 5% spalls, or the sum of all deteriorated and/or contaminated deck concrete 40 to 60%. The results are shown on Figure 5. Notice that the extrapolation is based on the initial slope of the data plots. The break in slope at about 15 years occurred with all of the data sets in the MIT study and was attributed to a systematic fault in the NBI data acquisition procedure ("... unobserved bridge deck maintenance and/or repairs ... ") [18]. The

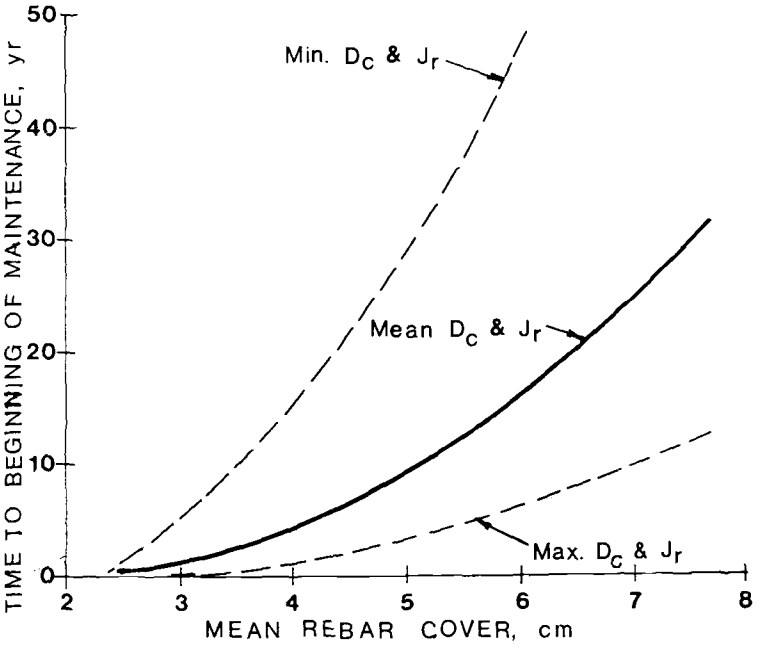

FIG. 3 -- Time to Beginning of Maintenance.

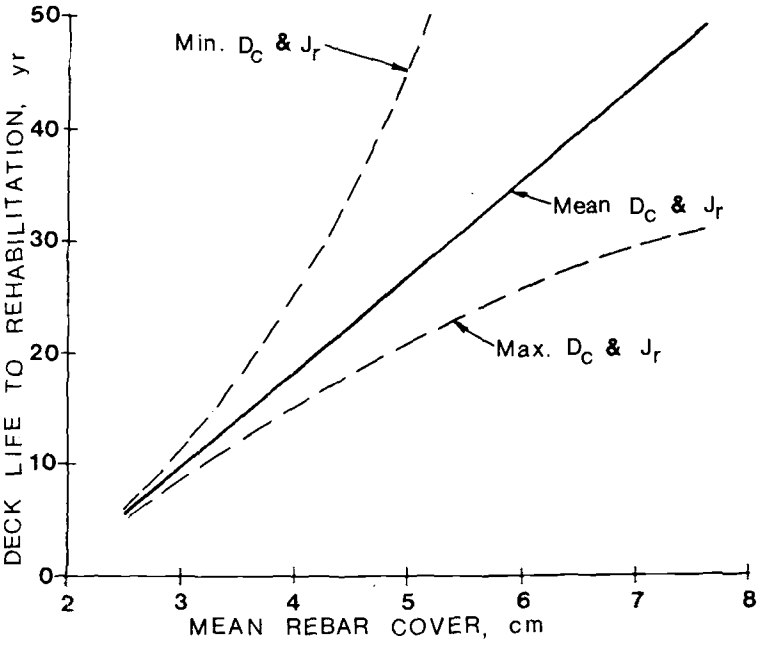

FIG. 4 -- Deck Life to Rehabilitation.

resulting mean (50% probability) age, as shown on Figure 5, is about 39 years.

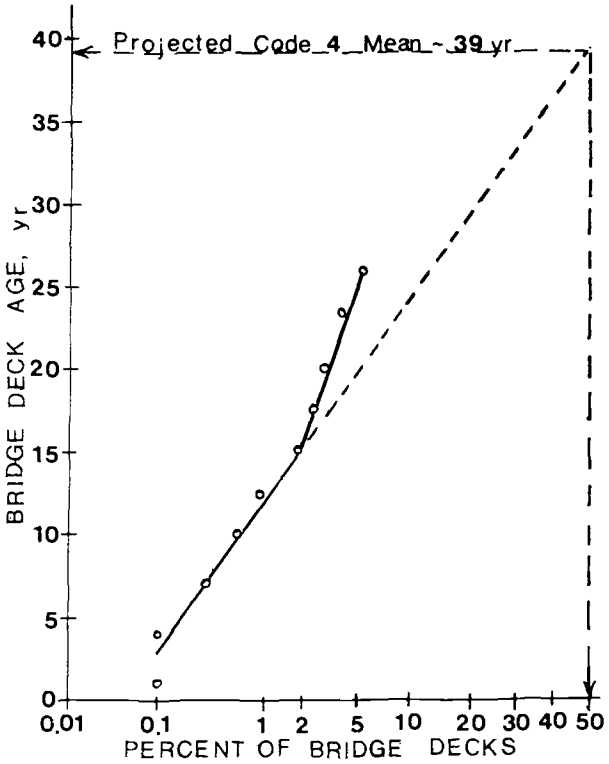

FIG. 5 -- Prediction of Mean Deck Age for Code 4 Deck Conditions Based on Normal Probability (New York State and Michigan Bridges).

Finally, bridge deck condition data from three states (NY, PA, VA) were analyzed in a current research project under the direction of one of the authors of this paper in order to determine average bridge lives to rehabilitation [19]. The analysis technique used here was the same as that employed with the NBI data from the MIT report. The determined mean ages at rehabilitation are 16, 23.5, and 34 years, respectively, for NY, PA, and VA.

In summary, the actual bridge deck life to rehabilitation mean values cited range from 16 to 39 years with a mean of 29. Since these numbers, in general, represent mean values for fairly large samples, one might expect that the effects of site-specific influences which produce the scatter anticipated with the model (Figure 4) should be mitigated. However, in most instances the "actual" values represent specific highway agencies, indicating possible effects of environment (traffic and climate) and policies (deicing practices and definition of conditions precipitating rehabilitation). Even the two factors taken into account in the model (diffusion constant and corrosion rate) may actually be relatively more constant within jurisdictions (states or provinces) than universally due to influences of climate and policy. For example, the results presented above for NY, PA, and

VA in the SHRP C-103 research were found to correlate very well with freezing indices and road salt usage in the respective states [19]. All of this serves to point to the requirement for detailed description of the terminal conditions that define service life and for the identification of the variables that must be assessed in order to satisfy site specificity for individual case studies.

ACKNOWLEDGMENTS

Some of the data used in developing the theme of this paper evolved from current research funded by the Strategic Highway Research Program (National Research Council). The presentation of that material does not necessarily indicate approval or endorsement by the National Academy of Science, the United States Government, or the American Association of State Highway and Transportation Officials (or its member states), of the findings, opinions, conclusions, or recommendations either inferred or specifically expressed herein.

REFERENCES

[1] ENR Washington Observer, Engineering News Record, Vol. 227, No. 2, July 15, 1991, pp. 7.
[2] "Subcommittee Leader Pushes Bridge Funding," Engineering News Record, Vol. 226, No. 20, May 20, 1991, pp. 13-14.
[3] Funahashi, M., "Predicting Corrosion-Free Service Life of a Concrete Structure in a Chloride Environment, ACI Materials Journal, Vol. 87, No. 6, November-December 1990, pp. 581-587.
[4] "Plight of Aging Bridges Decried Anew," ASCE News, American Society of Civil Engineers, February 1990, pp. 8.
[5] Cady, P. D. and Weyers, R. E., "Deterioration Rates of Concrete Bridge Decks," Journal of Transportation Engineering, Vol. 110, No. 1, American Society of Civil Engineers, January 1984, pp. 34-44.
[6] Somerville, G. "The Design Life of Concrete Structures," The Structural Engineer, Vol. 64A, No. 2, February 1986, pp. 60-71.
[7] Dakhil, F. H., Cady, P. D., and Carrier, R. E., "Cracking of Fresh Concrete As Related to Reinforcement," Journal of the American Concrete Institute, vol. 72, No. 8, August 1975, pp. 421-428.
[8] Cady, P. D. and R. E. Weyers, "Chloride Penetration and the Deterioration of Concrete Bridge Decks," Cement, Concrete, and Aggregates, Vol. 5, No. 2, American Society for Testing and Materials, Winter 1983, pp. 81-87.
[9] Weyers, R. E., "Concrete Bridge Protection and Rehabilitation: Chemical and Physical Techniques," Project Quarterly Report No. 8 of 18, SHRP Contract C-103, Virginia Polytechnic Institute, September 15, 1990, 34 p.
[10] Bazant, Z. P., "Physical Model for Steel Corrosion in Concrete Sea Structures," Proceedings, Journal of the Structural Division, Vol. 105, No. ST6, American Society of Civil Engineers, June 1979, pp. 1137-1167.
[11] Weyers, R. E., "Concrete Bridge Protection and Rehabilitation: Chemical and Physical Techniques," Project Quarterly Report No. 11 of 18, SHRP Contract C-103, Virginia Polytechnic Institute, July 15, 1991, 11 p.
[12] Escalaute, E., Ito, S., and Cohen, M., "Measuring the Rate of Corrosion of Steel in Concrete," Paper No. 44, International Corrosion Forum, National Association of Corrosion Engineers, April 6-10, 1981, Toronto, Ont.
[13] Cady, P. D., "Assessment of Physical Condition of Concrete Bridge Components," Project Quarterly Report No. 12 of 15, SHRP Contract C-101, Penn State University, July 12, 1991, 109 p.

[14] ASTM E632-82, "Standard Practice for Developing Accelerated Tests to Aid Prediction of the Service Life of Building Components and Materials," American Society for Testing and Materials, Philadelphia, PA, 1991.
[15] Clear, K. C., "Time-to-Corrosion of Reinforcing Steel in Concrete Slabs," Report No. FHWA-RD-76-70, Federal Highway Administration, Washington, D.C., April 1976.
[16] Babaei, K. and Hawkins, N. M., "Evaluation of Bridge Deck Protective Strategies," NCHRP Report 297, Transportation Research Board, Washington, D.C., September 1987, 80 p.
[17] Carter, P. D., "Preventive Maintenance of Concrete Bridge Decks," Concrete International, Vol. 11, No. 11, American Concrete Institute, November 1989, pp. 33-36.
[18] Busa, G. D., Jr., Ben-Akiva, M. E., and Buyukozturk, O., "Modelling Concrete Bridge Deterioration," Report Prepared for the U.S. DOT Transportation Systems Center, Cambridge, MA, September 1985, 193 p.
[19] Weyers, R. E., Chamberlin, W., and Hoffman, P., "Concrete Bridge Protection and Rehabilitation: Chemical and Physical Techniques Task 1 - Field Survey," SHRP C-103, Task 1, First Year Annual Report, Virginia Polytechnic Institute, October 24, 1989, 45 p.

Edward Escalante*

MEASURING THE UNDERGROUND CORROSION OF STEEL PILING AT TURCOT YARD, MONTREAL, CANADA - A 14 YEAR STUDY

REFERENCE: Escalante, E., "Measuring the Corrosion of Steel Piling at Turcot Yard, Montreal, Canada - A 14 year study, "Corrosion Forms and Control for Infrastructure, ASTM STP 1137, Victor Chaker, Ed., American Society for Testing and Materials, Philadelphia, 1992.

ABSTRACT: This paper describes a 14 year study of the corrosion of steel H-piles in soil at Turcot Yard, Montreal, Canada. The program was directed at evaluating the corrosion of these piles in disturbed and undisturbed soils. Three sets of steel H-piles were placed in the ground, one set without protection, a second set coated in the disturbed soil region, and a third set with concrete caps. Each set consisted of six vertical piles driven to bedrock and one pile placed horizontally in an excavation which was then backfilled. A steel pier, supporting a portion of the Transcanadian Highway, was included in the study. Electrochemical polarization measurements were made annually during the period of exposure, and periodically, selected piles were extracted for examination and physical measurements. The results show that corrosion of the steel piles in undisturbed soil is less than 0.33 mils per year (8.1 μm/y), but in all cases, corrosion is low. The electrochemical polarization measurements indicate that corrosion of the steel piles supporting the pier has decreased by more than an order of magnitude over the 14 year period.

KEYWORDS: bare steel, coated steel, concrete capped steel H-piles, disturbed soil, instantaneous corrosion rate, polarization resistance, underground corrosion, undisturbed soil

*Metallurgist, Corrosion Group,
National Institute of Standards & Technology,
Gaithersburg, MD 20899.

Construction of the Transcanadian Highway at the Turcot Yard interchange, Montreal, and concern about the corrosivity of the soil in that area, resulted in a long term program to study the corrosion of steel H-piles at that site. Previous information, based on visual examination of extracted piles, had suggested that corrosion of steel piles in undisturbed soil was negligible [1]. The limited amount of information on this subject provided motivation for this effort. This paper describes the design of the test site, the procedures used in making the corrosion measurements, and a discussion of the results obtained.

APPROACH

The need for monitoring the corrosion of steel piles in soil over a long period of time, provided an opportunity to use a nondestructive electrochemical method to obtain corrosion data that could later be compared to similar data obtained by physical measurements, before and after exposure, to determine changes in flange thickness during exposure. The technique of polarization resistance was chosen because it is supported by extensive laboratory studies and the requirements for its application to a field situation can be met [2]. These requirements include: 1) a measurement that can be performed in less than one hour per pile, and preferably in less than 15 minutes; 2) uses equipment that is easily transported, rugged, and is battery operated; 3) provides data that can be verified in the field during the measurement period.

EXPERIMENTAL PROCEDURE

Twenty-one steel H-piles, 12 in x 12 in x 74 lb/ft (30 cm x 30 cm x 110 kg/m) were used in the study, and all were characterized by measuring the flange thicknesses of each pile with micrometers at 1 ft (30 cm) intervals, 1 in (2.5 cm) from the flange edge. Seven steel piles were placed in the ground at each of three test sites, as illustrated in Figure 1a. A wide area of soil was excavated to a depth of 7 ft (2.1 m), and six piles were driven vertically in the excavation to bedrock, so that the top of the piles were 2 ft (0.6 m) below the original soil surface. A seventh pile was buried by placing it horizontally in the excavation, followed by backfilling the excavation. Note that one of the vertical piles is located in the center of the other five, which are arranged around the central pile at a radius of 6 ft (1.8 m). The horizontal pile was placed tangential to the circle and 10 ft (3.1 m) from the piles. Figure 1b dipicts the placement of the piles relative to the excavated, disturbed soil and the undisturbed soil underneath. The piles at each of the three sites were treated differently, in the following manner. The steel piles at site A were placed in the ground, bare, without any form of protection. At site B, the top 4 ft (1.2 m) of the six vertical piles was coated, after being driven into the ground, and one end of the horizontal pile

was coated for the same distance as the vertical piles. The six vertical piles at site C were concrete capped for their top 4 ft (1.2 m), after being driven into the ground, and the horizontal pile was capped on one end, simulating the vertical piles. To allow electrical contact to the H-piles, each had a 1 in (2.5 cm) diameter steel reinforcing bar welded to to the top of the vertical piles and to the center of the horizontal piles, so that the top of the rebar was a few inches below the surface of the soil. A removable cylindrical concrete marker, approximately 6 in (15 cm) in diameter and 24 in (60 cm) long, rests on the rebar serving as a marker to locate the rebar to each pile. All piles were marked with a letter-number identifier welded to the top and bottom.

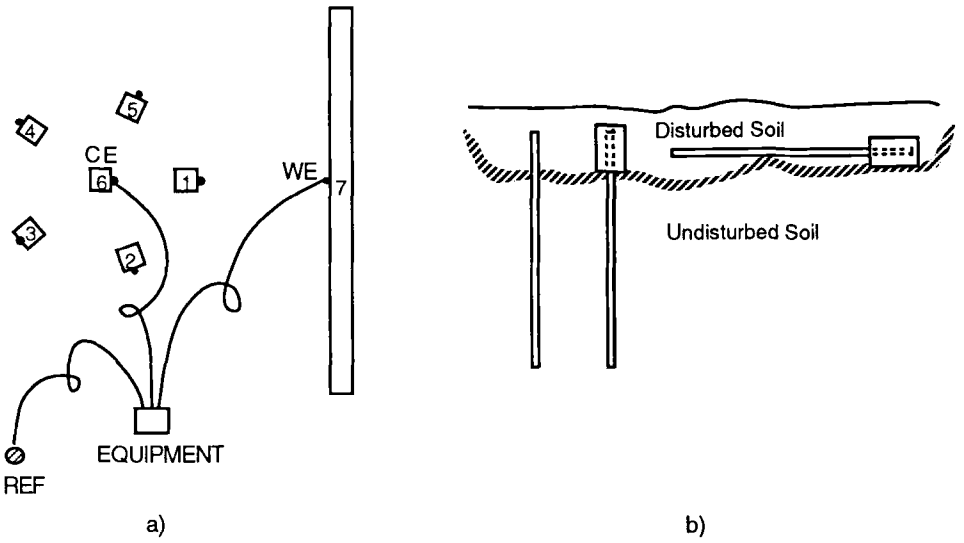

Figure 1 - a) Top view of a test site with typical placement of equipment, electrodes, and cables. b) Side view of a test site with disturbed and undisturbed soil regions.

In addition to the controlled test site piles, measurements were made on one of the piers supporting the highway overpass located in the area of Site B. This particular pier, Pier A-10, rested on 32 steel H-piles driven into the ground. All piles were electrically connected together in anticipation to the possible future use of cathodic protection. Two 2 in (5.1 cm) steel reinforcing bars were brought to the surface, allowing an electrical connection to the piles.

Soil samples were collected by borings made at Sites A and B, and the soil type, soil resistivity, and soil pH were determined at different depths. A perforated plastic pipe

was imbedded at each of the three sites, so that the water table could be measured. This measurement was made with an ohm-meter and a two-wire conductor that was lowered into the pipe until conductivity increased. The length of the conductor when conductivity was detected was then determined, providing a measure of the depth of the water line. These measurements were made approximately once every two months for a period of two years.

Electrochemical Measurements

After emplacement, electrochemical polarization measurements were made on the piles every year for 14 years. The corrosion measurement is made using the Stern-Geary method, where the working electrode (WE) is polarized to not more than 20 mV, and the applied current necessary to achieve that change is noted [3]. The Stern-Geary equation relates the corrosion current, i_{corr}, of the WE as an inverse function of the slope of the potential-current polarization curve in the following way:

$$\left(\frac{dv}{di}\right)_{v \to o} = - \frac{\beta_a \beta_c}{2.3 i_{corr} (\beta_a + \beta_c)}$$

Where v is the potential of the WE, i is the applied current, amd β_a and β_c are the anodic and cathodic tafel slopes, respectively, assumed to equal 100 mv/decade.

Because of time constraints, measurements could not be made on every pile during the annual measurement period. In general, the measurement is made in the following way. Consider three electrodes, where the first electrode, the working electode (WE), is the pile to be measured. The second electode, the counter electrode (CE), is a nearby pile, serving as the source of polarizing current. A copper/copper sulphate reference electrode is the third electrode. Thus, through polarization measurements on the steel piles in the ground, it is possible to calculate a corrosion current. The surface area of the piles is known, and is used to calculate corrosion current density. Using an average of the corrosion current density, corrosion rate is calculated for the period of exposure. Measurements were typically made in the late summer or early fall, and the effect of temperature at other times of the year is not known.

In preparation for the electrochemical measurements, the concrete cylinders, marking the location of the reinforcing steel bar to each steel pile, are removed and each rebar cleaned with a wire brush. Locking pliers that have been modified to accept an electrical wire connection make the electrical contact to the rebar. Fifty foot (15.2 m) wire conductors with a minimum 16 gage size are used to connect

the electronic equipment to the electrodes, as illustrated in Figure 1a.

A polarizing current is applied to the steel pile of interest, (WE). The center pile in the group of six is normally chosen as the counter electrode (CE) for application of polarizing current, i, to the WE. A copper-copper sulfate reference electrode is placed 50 ft (15.2 m) from the WE at the soil surface. When conditions are very dry, it is sometimes necessary to moisten the soil where the reference electrode is positioned, to make certain that the electrode makes good contact with the soil. Poor soil contact often manifests itself by erratic or drifting potential readings.

For the first several years, measurements were made using a Holler bridge circuit, which is reliable, rugged, and versatile. The circuit is especially useful for this application, because it is designed to allow compensation for IR error, the error in the potential measuremnt when current is passing across the working and reference electrodes [4,5]. The major disadvantage of the Holler bridge is that balancing the bridge circuit is slow and sometimes difficult, leading to over or under estimation of IR and an error in the measurement.

More recently, in addition to the Holler bridge measurements, a portable computerized system has been used for making the polarization resistance measurements. This system is made up of a portable computer, a data logger, a disk drive for file storage, and a printer, all with self-contained batteries, or powered from an automobile battery. The system was originally designed for measuring the corrosion of reinforcing steel in bridge decks and has been described in detail [6]. Briefly, this system uses current interruption for eliminating IR error, and applies a cathodic polarizing current to the steel pile sufficient to change its potential by 10 mV from its corrosion potential. This information is printed out for immediate inspection and, at the same time, stored for future reference. A digital storage oscilloscope is used to monitor the wave form of the current and potential signals. From these measurements, an average corrosion rate is calculated for each of the piles.

Physical Measurements

Periodically, during the period of exposure, selected piles are extracted for examination. The piles are visually examined and photographed after each cleaning procedure in order to document the condition of the pile. When capped with concrete, the concrete is removed with jack hammers. This is followed by cleaning with a water jet to remove loose debris or debonded coating, when coated. The piles are then sand blasted to bare metal. The final step in this procedure is a repetition of the flange thickness measurements made prior to initial burial, which is measurement of the flange

thickness every foot (30 cm) one inch (2.5 cm) from the edge of the flange. These measurements provide a means for evaluating the extent of corrosion along the length of the steel pile, and from these measurements the corrosion rate at any level is determined. The flange thickness represents two surfaces, and the rate of corrosion for one surface is calculated using half of the flange thickness.

One problem in this type of program is the need to repeat measurements consistently over a long period of time. It is important to avoid changes in procedure that may have a detrimental affect the data, but over a period of 14 years some changes were unavoidable. The major changes were an improvement in the equipment used, such as the incorporation of high impedance voltmeters, and more recently, the use of a computer controlled system. Though the author was not present at the initial emplacement of the piles, he was directly involved in all aspects of the program thereafter.

RESULTS AND DISCUSSION

A listing of all the piles in the program and a summary of the results obtained from the electrochemical polarization measurements is shown in Table 1. Piles were extracted after 2.8, 6.8 and 12.9 years, but ten of the H-piles are still in place at the test sites, as identified by missing data in the table. A report on the polarization data after the first removal of piles was published by Schwerdtfeger and Romanoff [7]. Because of the extensive amount of data obtained over the 14 years, only an overview of the results can be provided here. The emphasis of these data is on the piles that have been extracted, providing physical information for comparison to the the electrochemical data. A significant fact, revealed in this table, is that the average corrosion rate in every case is less than 1 mpy (25.4 μm/y).

Information on the soil at different depths for Sites A and B are shown in Tables 2 and 3 respectively. Unfortunately, there are no similar data for Site C. The pH is near neutral or slightly alkaline in all cases, and is not considered a source of corrosion problems to steel. The soil resistivity at Site A varies between 1170 Ω-cm and 4570 Ω-cm, and past experience suggests that it is not an aggressive soil. In general the same is true at site B, except for sections with a soil resistivity below 600 Ω-cm, where soil conditions can be corrosive to steel. As will be shown, this low resistivity region at Site B was the most aggressive of the soils.

TABLE 1 - Summary of electrochemical data.

Pile ID	Average Corrosion Current Density mA/sq ft	Number of Corrosion Current Measurements over 14 y	Exposure Time* years	Average Corrosion Rate From Corrosion Current* mils/yr (μm/y)
A-1	1.12	6	6.8	0.55 (14.0)
A-2	1.05	12		
A-3	0.75	10	12.9	0.37 (9.4)
A-4	0.42	11		
A-5	0.30	2	2.8	0.15 (3.7)
A-6	0.24	2		
A-7	0.40	10		
B-1	1.04	2	2.8	0.51 (13.0)
B-2	1.42	6	6.8	0.70 (17.7)
B-3	1.56	12	12.9	0.77 (19.5)
B-4	1.98	12		
B-5	1.40	12		
B-6	0.88	2		
B-7	1.11	2	2.8	0.55 (13.9)
A-10	0.26	8		
C-1	0.66	2	2.8	0.32 (8.2)
C-2	0.86	12		
C-3	0.92	11	12.9	0.45 (11.5)
C-4	0.51	5	6.8	0.25 (6.4)
C-5	0.94	12		
C-6	0.77	4		
C-7	0.53	10	12.9	0.26 (6.4)

*Note: Missing data indicate that piles are still in place. Multiply mA/sq ft by 10.76 to obtain mA/sq m.

TABLE 2 - Soil properties as a function of distance from the soil surface at Sites A.

Site A Soil Samples	Depth ft	Soil Type	Resistivity Ω-cm	pH
1	3 - 4.5	Fill	2030	7.8
2	5 - 6.5	Fill	2130	7.6
3	6.5 - 8	Boulder	-	-
4	8 - 9.5	Shale	-	-
5	9.5 - 10	Peat	1170	7.0
6	10 - 10.5	Peat	-	-
7	10.5 - 11.5	Marle	1630	7.4
8	11.5 - 13	Marle	1880	7.3
9	13 - 13.9	Clay	1470	7.2
10	13.9 - 14.5	Silt-Gravel	-	-
11	15 - 15.9	Silt-Gravel	4570	8.2
12	15.9	Boulder	-	-

Note: Multiply ft by 0.3 to obtain m.

TABLE 3 - Soil properties as a function of distance from the soil surface at Site B.

Site B Soil Samples	Depth ft	Soil Type	Resistivity Ω-cm	pH
1	2 - 3.5	Fill	510	7,2
2	3.5 - 5	Fill	400	7.2
3	5 - 6.5	Fill	1020	7.5
4	7 - 8.5	Fill	1220	6.9
5	8.5 - 10	Peat	-	-
6	10 - 11.5	Peat	-	-
7	11.5 - 12	Marle	460	6.8
8	12 - 13.5	Marle	600	7.3
9	13.5 - 14.5	Clay	1120	7.1
10	14.5 - 15	Silt-Gravel	-	-
11	15 - 16.5	Silt-Gravel	4570	7.8
12	16.5 - 18	Gravel	-	-
13	18 - 20	Silt-Sand	-	-
14	20 - 21.5	Silt-Sand	4830	7.7
15	22	Silt	-	-

Note: Multiply ft by 0.3 to obtain m.

The location of the water table is of interest, because it is expected that oxygen diffusion is limited in water saturated soil, reducing the rate of corrosion. Table 4 lists the average distance from the soil surface to the level of the water table.

TABLE 4 - Distance from the soil surface to the water table.

Site	Average Depth ft	Minimum Depth ft	Maximum Depth ft
A	7.7	6.5	8.7
B	10.3	7.6	11.8
C	13.0	11.0	13.6

Note: Multiply ft by 0.3 to obtain m.

Electrochemical Measurements

Figure 2 illustrates the electrochemical data obtained on the three piles extracted from site A. Only two data points were obtained on Pile A-5, because it was removed from the site after three years. However, 10 data points, representing measurements over a 10 year period, were obtained on Pile A-3, since it remained in the ground for almost 13 years. The data on Pile A-1 indicates that it was undergoing the highest corrosion of the three piles extracted from this site. Even though there are fluctuations in the corrosion current density from year to year, the greatest fluctuation for any given pile at the three sites is less

than a factor of four, indicating that corrosion remains fairly constant. Table 1 reveals the corrosion rate calculated from these data and the corrosion current density for the piles that remain in the ground.

The piles at site B, coated in the disturbed soil region, on the average showed a higher rate of deterioration than the piles at the other two sites, including the bare piles. This is not unexpected, since the soil analysis data indicated the soil resistivity at this site was low, <600 Ω-cm in some regions, as revealed in Table 3. The corrosion current density data for the four piles extracted from this site is shown in Figure 3.

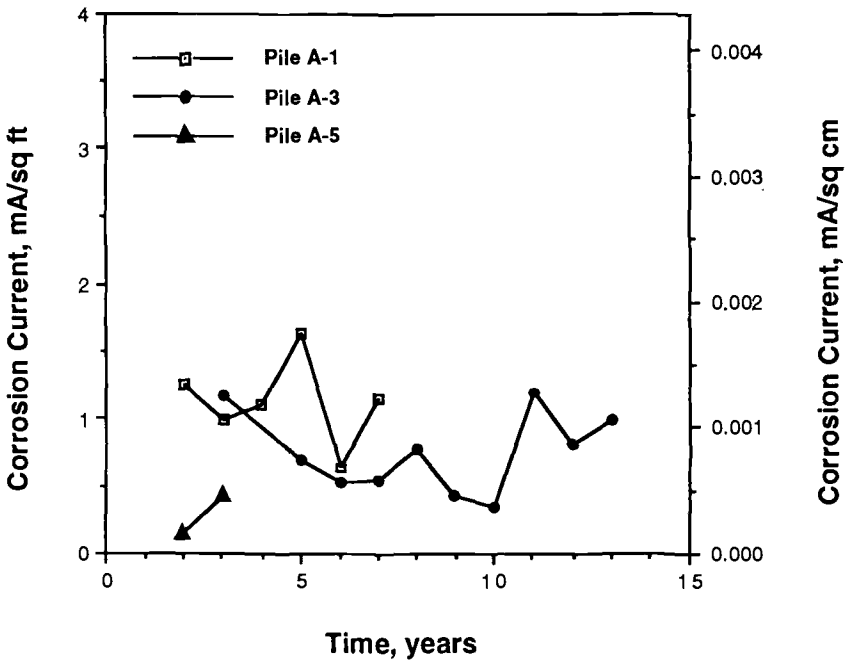

FIGURE 2 - Corrosion current density data on three piles extracted from Site A.

The concrete capped piles at Site C, which more realistically resembled the piers supporting the highway, showed the lowest corrosion of the piles at all three sites. Figure 4 is a plot of the corrosion current density data for the four piles removed from this site, and shows that corrosion was much lower than that at the other two sites as indicated by electrochemical polarization measurements.

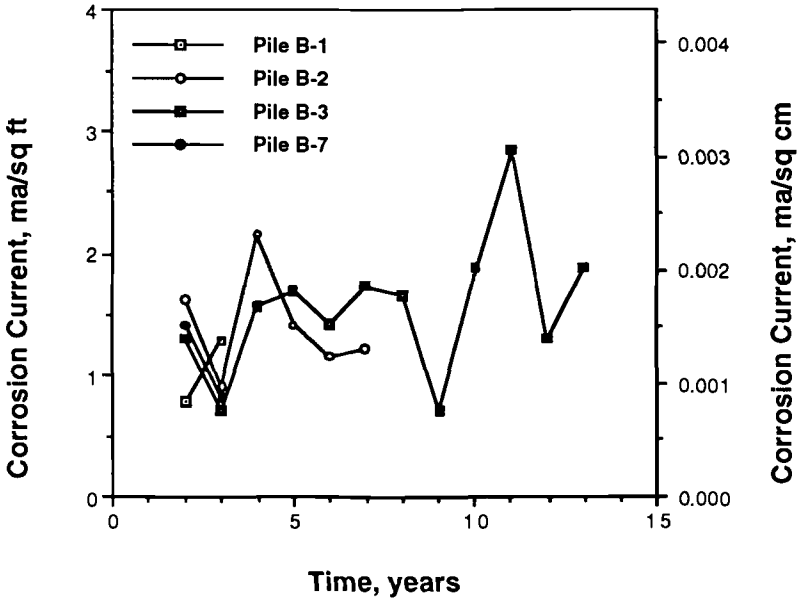

FIGURE 3 - Corrosion current density data on four piles extracted from Site B.

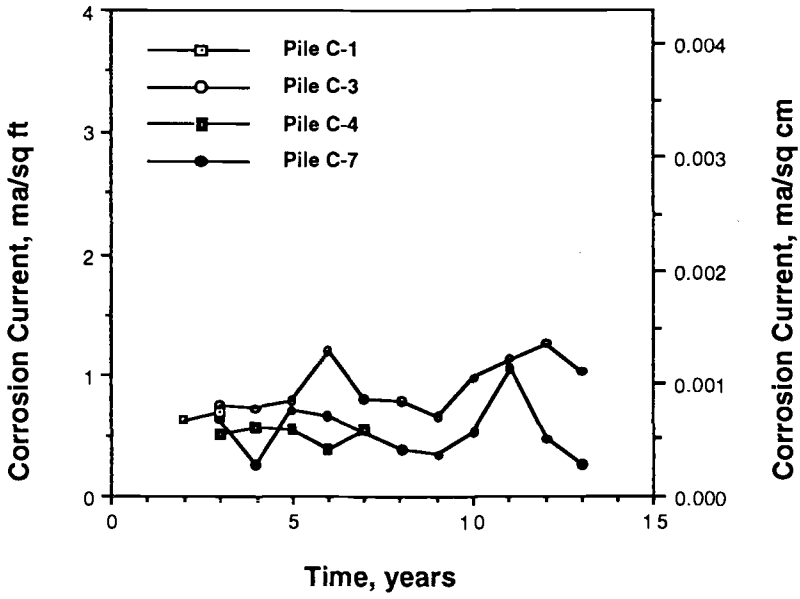

FIGURE 4 - Corrosion current density data on four piles extracted from Site C.

The results of the electrochemical data collected from Pier A-10 are interesting because this was the only real structure included in the study. It has already been mentioned that the pier is supported by 32 interconnected steel H-piles, and the total surface area of these piles is reflected in the calculated corrosion current density. Figure 5 illustrates the corrosion current density for Pier A-10. Two features are immediately apparent. First, the corrosion current is a approximately a factor of 3 less than the corrosion current density for the concrete capped piles and about a factor of 5 less than that for the piles at Site B. This low corrosion current is probably due to a shielding effect, where the applied polarizing current is only reaching the piles on the outer fringes of the pile cluster. These data suggest that the polarizing current is only polarizing between 1/3 to 1/5 of the piles in the cluster. The second noticeable feature is that the corrosion current density for Pier A-10 is decreasing significantly with time. The maximum current density is 0.65 mA/sq ft (7.0 mA/sq m)) and the minimum, after 14 years, is 0.03 mpy (0.32 mA/sq m), resulting in a corrosion current density decrease of more than one order of magnitude. This may be due to the larger surface area of steel in the cluster that has depleted the oxygen concentration in its immediate vicinity, reducing the rate of corrosion more rapidly than is occurring with the test piles. Physical measurements could not be made on these piles.

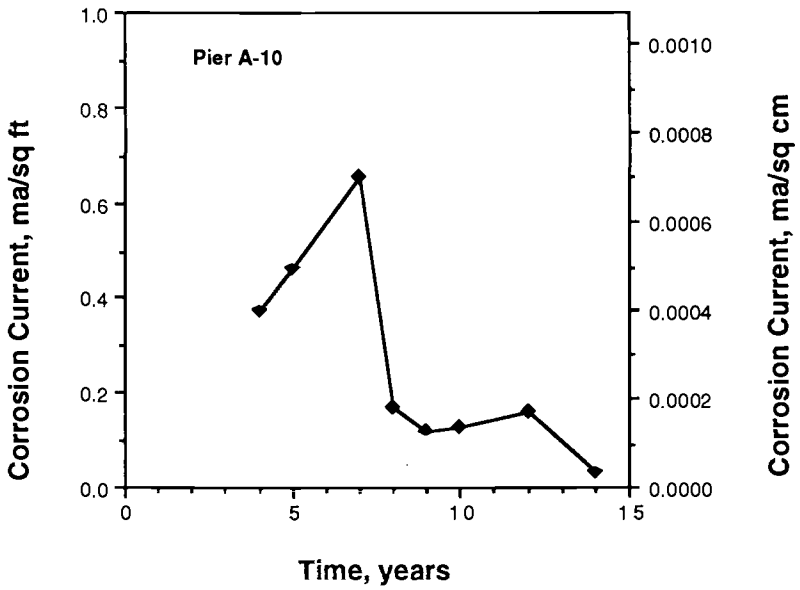

FIGURE 5 - Corrosion current density data on Pier A-10 at Site B.

Physical Measurements

The electrochemical polarization data provides information on the total corrosion on a pile, but does not reveal how it is distrubuted over its surface. This detailed information was obtained by visual examination and physical measurements on the extracted piles. The physical measurements also serve as a reference for the electrochemical polarization measurements. A summary of the corrosion rate of all the piles in three soil zones calculated from the physical measurements and an average of the total corrosion obtained from these data is listed in Table 5. The corrosion rate calculations in this table are based on the decrease in thickness of the flange that exceeds the standard deviation of the original thickness of the piles. The three soil zones in this table are 1) the top 4 ft (1.2 m) of the pile in the disturbed soil, 2) a 2 ft (0.6 m) section of the pile in the soil interface between the disturbed soil and the undisturbed soil, and 3) the undisturbed soil below the soil interface. Because of the variability in the level of the water table, its effects are not specifically emphasized in this table, but examination of these data for the unprotected piles at Site A clearly indicate that the corrosion rate of the piles in the undisturbed soil is much lower than in the upper soil regions. The undisturbed soil region includes the water saturated soil below the water table.

TABLE 5 - Average corrosion rate of the extracted piles at three soil levels calculated from physical measurements

Pile ID	Disturbed Soil Top 4 ft mils/y*	Interface Soil Mid 2 ft mils/y*	Undisturbed Soil Below Mid mils/y*	Overall Average mils/y	(μm/y)
A-1	0.72	1.01	0.26	0.42	(10.6)
A-3	0.51	0.07	0.23	0.27	(6.8)
A-5	0.77	1.72	0.11	0.35	(8.9)
B-1	0.80	0.00	0.52	0.53	(10.9)
B-2	0.27	1.49	0.55	0.58	(14.7)
B-3	0.13	0.65	0.55	0.50	(12.8)
B-7	1.88	0.00	0.17	0.43	(10.9)
C-1	0.00	0.69	0.30	0.28	(7.2)
C-3	0.00	0.55	0.34	0.31	(7.9)
C-4	0.00	2.32	0.22	0.33	(8.4)
C-7	0.00	0.41	0.30	0.27	(6.9)
Average		0.81	0.32	0.39	(9.9)

*Note: Multiply mils/y by 25.4 to calculate μm/y.

A plot of the flange profile, before and after exposure, graphically displays the effects of corrosion on the piles. Profile data for a "representative" pile from each of the sites is provided to give the reader an indication of the

differences in corrosion attack at different soil levels. These profiles also reveal the effects of a coating, a concrete cap, and no protection, on the corrosion of a pile.

Figure 6 is a plot of the average flange thickness of Pile A-1, exposed for 6.8 years without corrosion protection at Site A. The dashed vertical line is the average original flange thickness of the steel H-piles, and the two parallel lines on either side respresent the standard deviation of the average. It is evident from this profile that most of the corrosion attack occurred in the top 14 ft (4.3 m) of the pile with negligible attack below that level. Table 5 shows that the average corrosion rate measured for the top 4 ft (1.2) section of this pile is 0.72 mils per year (mpy) or 18.3 μm/y. At the soil interface, between the disturbed soil and the undisturbed soil, the average corrosion is 1.01 mpy (25.7 μm/y), and the same table shows that in the undisturbed soil region, average corrosion rate is 0.26 mpy (6.6 μm/y). The average corrosion rate over the entire pile is 0.42 mpy (10.6 μm/y).

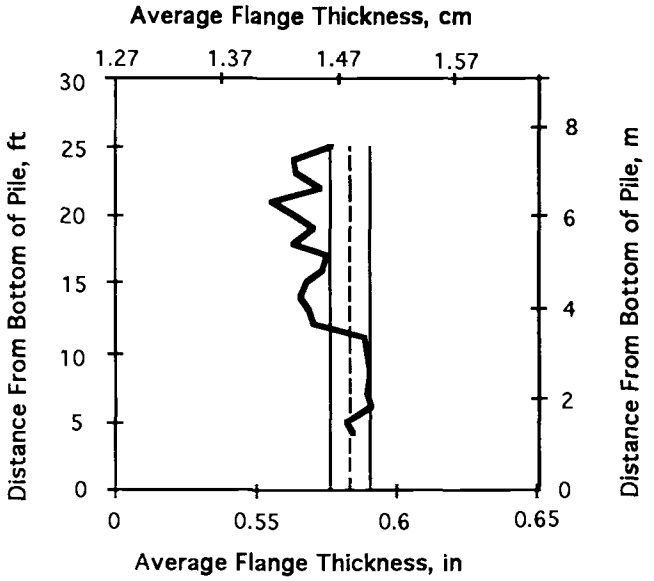

FIGURE 6 - Profile of the flange thickness of pile A-1 (unprotected) after 6.8 years at Site A.

The steel piles at Site B suffered more corrosion attack in the undisturbed soil region than the piles at the other three sites. This is clearly reflected in the data of Table 5, which reveals that corrosion in the undisturbed soil region for the piles at Site B was twice that observed at the other sites. The soil property measurements at Site B showed that portions of the soil near the surface and approximately 12 ft (3.7 m) below the soil surface had a soil resistivity less than 600 Ω-cm, which is considered a highly corrosive

soil. In general, coating the top of the pile in the disturbed soil region was beneficial, but where the coating failed, corrosion attack was severe. This is reflected in the variability in the corrosion observed for this region as shown in Table 5, where the corrosion rate ranged from 0.13 to 1.8 mpy (3.3 to 45.7 μm/y). Figure 7 illustrates the profile data for Pile B-2. The average corrosion rate of this pile in the undisturbed soil region was 0.55 mpy (14 μm/y). On removal of this pile it was noticed that the pile was wet up to 21 ft (6.4 m) from the bottom of the pile, which is just below the interface region where high corrosion was observed. In the soil interface region corrosion was calculated to be 1.49 mpy (37.8 μm/y). The average corrosion rate in the coated region, was 0.27 mpy (6.9 μm/y).

The piles at Site C were capped with concrete to simulate the actual pier structure, and the effect of the concrete on the corrosion process is especially interesting for this reason. Removal of the concrete cap clearly indicated that the concrete had protected the steel H-pile from any corrosion attack. However, visual examination revealed shallow pitting in the area immediately below the concrete cap, and the data in Table 5 supports this observation. The table shows that the most severe corrosion on the piles at Site C occurred in the soil interface region, which in this case, is immediately below the concrete cap. It was also observed that corrosion on the rest of the pile surface was less than that developed at the other two sites, as indicated by the data in Table 5. The profile data for Pile C-4 is illustrated in Figure 8.

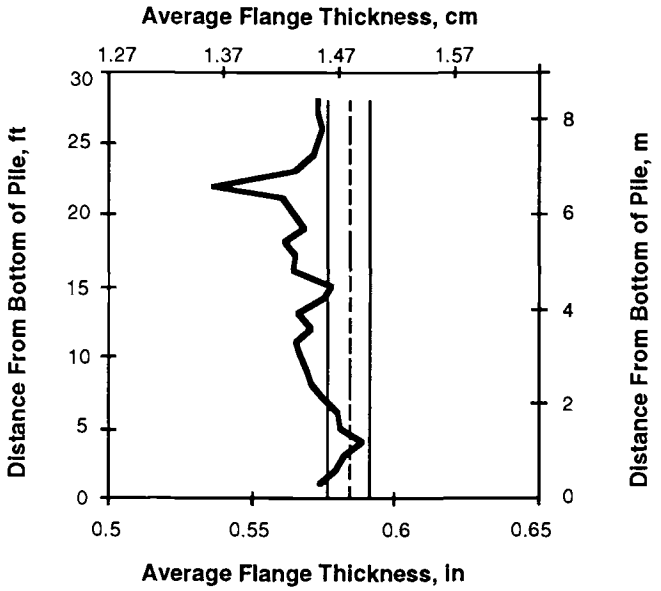

FIGURE 7 - Profile of the flange thickness of pile B-2 (coated in disturbed soil region) after 6.8 years at Site B.

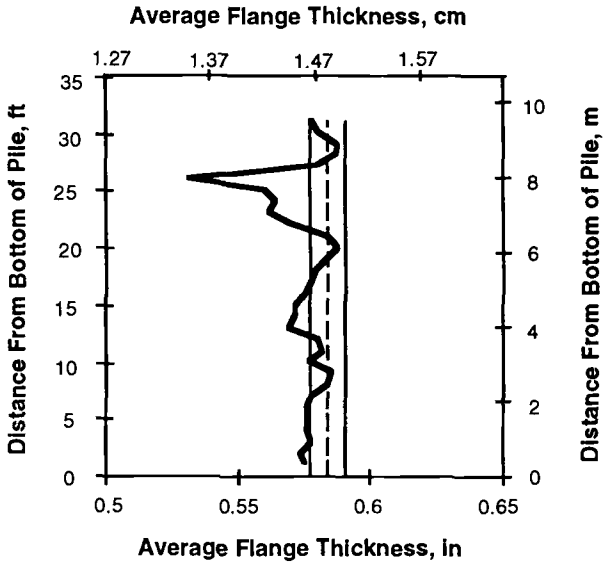

FIGURE 8 - Profile of the flange thickness of pile C-4 (concrete capped) after 6.8 years at Site C.

CONCLUSIONS

Two questions are of importance in this program. First, how reliable are polarization measurements for measuring the corrosion rate of steel H-piles in soil, and second, what is the corrosion rate of these steel H-piles. In this study, the physical measurements are the primary reference for determining rate of corrosion, and the reliability of the electrochemical polarization data is determined by comparison. The corrosion rate data in Table 1, obtained by electrochemical polarization, and similar data in Table 5, obtained through physical measurements, are plotted and shown in Figure 9. Each point is labeled for the pile it represents, and the straight line is a least-squares best fit to the data. The equation of the line and the coefficient of determination, R^2, are shown. This equation, based on eleven data points, indicates that the electrochemical polarization technique tends to overestimate corrosion rate by approximately 30%, for values greater than 0.25 mpy (6.3 µm/y). The dashed line, $y = x$, represents where the data would lay, if there were perfect agreement between the two measurements.

These data show that the average corrosion rate of the steel H-piles in the three soil regions is low for all three sites. As Table 5 shows, the average corrosion rate for the bare piles in the disturbed soil region is 0.67 mpy (16.9 µm/y). In the soil interface region, the average corrosion for all the piles is 0.81 mpy (20.6 µm/y), and in the

undisturbed soil region, their average corrosion rate is 0.32 mpy (8.1 μm/y). The average corrosion rate for all the piles over their entire surface is 0.39 mpy (9.9 μm/y).

SUMMARY

1) Electrochemical polarization measurements are useful for evaluating the corrosion of steel H-piles in soil, even though the measurement overestimates the rate of corrosion by approximately 30 percent.

2) This 14 year study reveals that the average corrosion rate of the steel H-piles at Turcot Yard is low in all cases, and is especially low in undisturbed soil where the average corrosion rate is less than 0.33 mpy (8.4 μm/y).

3) The electrochemical measurements also show that the corrosion current of piles supporting a pier has decreased by more than an order of magnitude over the 14 year period.

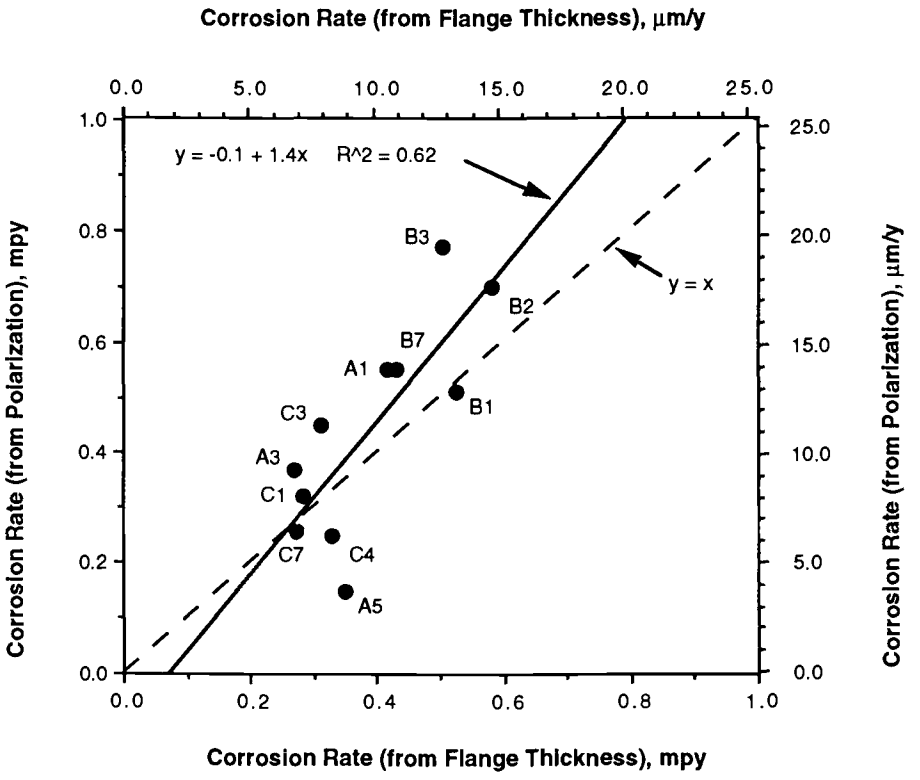

FIGURE 9 - Comparison of corrosion rate calculated from flange thickness and electrochemical polarization data.

REFERENCES

1. Romanoff, M., "Corrosion of Steel Piling In Soils", NBS Monograph 58, National Institute of Standards & Technology, 1962.

2. Mansfeld, F., "The Polarization Resistance Technique for Measuring Corrosion Currents", Advances in Corrosion Science and Technology, v6, Plenum Press, New York, 1976, p 163-262.

3. Stern, M., Geary, A.L., "Electrochemical Polarization, 1. A Theoretical Analysis of the Shape of Polarization Curves," J. Electrochemical Soc., v104, 1957, p 56-63.

4. Holler, H.D., "Studies On Galvanicl Couples - 1. Measurement of Electromotive Force and Internal Resistance of Cells During Current Flow," J. Electrochemical Soc., v97, 1950, p 271.

5. Jones, D.A., Lowe, T.A., "Polarization Methods for Measuring the Corrosion of Metals Buried Underground," J. Materials Science, 8, 1969, p 600-617.

6. Escalante, E., Ito, S, "Measuring the Rate of Corrosion of Steel in Concrete," Corrosion Rates of Steel in Concrete, ASTM STP 1065, American Society for Testing and Materials, Philadelphia, 1990, p 86-102.

7. W.J. Schwerdtfeger, M. Romanoff, "Corrosion Rates on Underground Steel Test Piles at Turcot Yard, Montreal, Canada - Part 1," NBS Monograph 128, National Institute of Standards & Technology, 1972.

Bernard H. Hertlein (1)

ASSESSING THE ROLE OF STEEL CORROSION IN THE DETERIORATION OF CONCRETE IN THE NATIONAL INFRASTRUCTURE : A REVIEW OF THE CAUSES OF CORROSION AND CURRENT DIAGNOSTIC TECHNIQUES

REFERENCE : Hertlein, B.H. "Assessing the Role of Steel Corrosion in the Deterioration of Concrete in the National Infrastructure : A Review" Corrosion Forms and Control for Infrastructure, ASTM STP 1137, Victor Chaker, Ed., American Society for Testing and Materials, Philadelphia, 1992.

ABSTRACT : Concrete forms a major component of the national infrastructure. The interaction between corrosion of embedded steel and deterioration of concrete is of concern to the engineers involved with infrastructure maintenance. If an effective repair and maintenance strategy is to be planned, it is important to understand the forms and causes of deterioration and corrosion damage in concrete structures. Equally important is an understanding of the range of test methods available to diagnose the cause and determine the extent of such damage.

KEYWORDS : concrete, corrosion currents, rusting, pitting, destructive testing, non-destructive testing, passive monitoring.

Concrete is an important component in infrastructure. Many structures rely on concrete to give them rigidity, and to bear compressive loads. Concrete itself relies on steel reinforcing to take tensile and shear loads, and distribute them to suitable support points. Concrete also has the vital function of providing a protective cover to this steel, to prevent corrosion. Conditions that reduce the effectiveness of the 'cover concrete' as a barrier to the corrosive effects of environment and weather increase the risk of corrosion damage, higher maintenance costs, and shortened structural life. It is in the national interest to minimize maintenance costs and maximize the service life of infrastructure.

---

(1) Bernard Hertlein is Project Scientist, STS Consultants Ltd, 31 College Place, Suite 306D, Asheville, NC 28801, USA.

There are now many techniques available to help predict the onset of corrosion, assess corrosion damage, and identify the cause. However, if they are to be effectively employed, it is important to understand the variety of processes that can initiate corrosion, and how this corrosion may affect the structure. Only by knowing the effects and interactions of these processes can the Engineer decide on the combination of inspection and test methods that will provide the information needed to make a correct diagnosis, and to plan an effective maintenance or repair program.

CORROSION FORMS

Corrosion of metals can take many forms, and for those unfamiliar with this topic, Schweitzer [1] provides a good general introduction to the subject. Being concerned with the effects of corrosion on steel in concrete structures, this paper will focus on those forms caused by normal weathering and environmental influences:-

a) General rusting,
b) Pitting corrosion,
c) Galvanic corrosion,
d) Erosion caused by physical and biological action.

This paper reviews the most common forms and causes of corrosion of embedded steel, and their effect on concrete. It then summarizes the more commonly used methods that are currently available for evaluation of damage, determination of cause, and assessment of repairs. This is an international problem, and experience in both Europe and the United States are drawn on to describe the available methods, and the current status of research and development in this field.

Concrete Properties and their Effects on Corrosion

General rusting is the most readily recognised form of steel corrosion, and is often described as a simple chemical reaction that occurs when steel is exposed to air and water. In fact it is a complex electrochemical process that can be controlled if certain conditions are maintained.

When rusting takes place, small electrical currents flow between areas of differing voltage potential on the steel, through a surrounding medium, or 'electrolyte'. In doing this, they transport ions of metal from anodic to cathodic areas, reducing the steel cross-section at the anode, and depositing material at the cathode, where it forms rust. For these corrosion currents to occur on steel in concrete, three essential conditions must be met :-

- There must be a difference in voltage potential between points on the steel surface or the surrounding material.

- The concrete must be conductive to form the electrolyte.

- The concrete must have electrical contact with the steel.

The engineer has little control over the first condition, for variations in the steel, surface impurities, and stresses from bending or fabrication all induce potential differences. Cover concrete, however, provides an opportunity to control the latter two conditions.

Fresh concrete is alkaline, in excess of pH 13.5. This alkalinity oxidizes the surface of embedded steel, forming a chemically and electrically inert layer of ferric oxide. Dry, hardened concrete has a high electrical resistance, so if it can be kept dry, and the oxide coating on the steel can be kept intact, neither of the latter conditions can be met. Even if the concrete is saturated, but the oxide coating is maintained, the potential corrosion currents cannot flow.

To control corrosion, the engineer must be concerned with maintaining the conditions that prevent the flow of corrosion currents. This requires knowledge of the physical, chemical, and electrical properties of the materials.

Concrete: Typical concrete is a mixture of cement, sand, coarse aggregate, and water. Cement itself is a mixture of calcium, aluminum, silicon and iron. Aggregate is usually crushed rock, or gravel. Most gravel is a mixture of rocks, depending on where they were drawn from by river or glacier. Sand is often also a mixture of different rock particles. The water must be of drinkable quality, but usually contains some trace minerals, organic matter, fluoride and chloride.

The range of materials present in concrete is important, because they will determine it's permeability, density, and reactivity. They affect the type and rate of corrosion that may occur. Where admixtures are used, they may well introduce further variables. An example in this case is the once common use of calcium chloride to accelerate setting. This released free chlorides into the concrete, which were later found to be a key catalyst in the corrosion process.

Which Corrosion Form ?

Depending on the moisture and gases available to form an electrolyte, corrosion may take the form of general rusting, or localised, severe attack known as 'pitting'. Thus external or environmental conditions will also influence the type and rate of corrosion.

General Rusting : Once corrosion starts, it tends to be self-accelerating. In general rusting, the metal is oxidised in a chemical reaction triggered by contaminants, such as chlorides, and the resulting rust typically occupies eight times the volume of the original steel. This increase in volume creates stresses that crack the concrete, and thus

facilitate the ingress of more air, water and contaminants to speed up the rusting. The cracks will worsen until pieces of concrete break off or spall. The cracks often bleed corrosion products onto the surface as rust stains, so signs of damage can be readily visible. Unfortunately, such signs indicate that the damage is already well-established and deep-rooted.

Pitting corrosion : However, not all forms of attack are so readily visible. A much more insidious form is localised 'pitting'. This is often a result of chloride ions in the concrete being concentrated in small depassivated areas by the ionic current flow, increasing the conductivity of the electrolyte locally, and so accelerating the pitting process at the small anodic point. The corrosion products are usually deposited over the larger remaining cathodic area, and rapid metal loss occurs at the corrosion pit, but rust may not form sufficient thickness to cause cracking.

In this way, a complete loss of steel cross-section can occur at the corrosion site with no external sign of damage, a potential disaster in such items as pre-stress wires, or in post-tension tendons in floors, columns, and decks.

Galvanic corrosion : Each metal and metal alloy occupies a given position in the 'Galvanic Series'[1], signifying an anodic or cathodic nature relative to other metals in the series. Two dissimilar metals, in a suitably electrolytic environment, form an electrical cell. Electrolytic action removes material from the anode, and the further apart metals are in the galvanic series, the more aggressive is this reaction. Therefore two dissimilar metals embedded close together in concrete will react in the same way as steel with surface potential differences, if the concrete is suitably conductive.

Forms of Attack

As stated, for corrosion of embedded steel to take place, the protective, passivating properties of overlying concrete must be destroyed, and this can happen in many ways, though they can be summarised in three broad categories :-

- Chemical attack on concrete from environment or spillage
- Chemical attack on steel of internal or external nature
- Physical damage, such as cracks from impact, settlement, overloading, or fire damage, and erosion or stripping.

Chemical attack on Concrete - Carbonation : As an example of an atmospheric or environmental attack, the carbonation process also shows the interaction which occurs during the deterioration of concrete. Cement paste has a submicroscopic pore matrix, and absorbs moisture by capillary action. It 'breathes' with changes in humidity, atmospheric pressure, and temperature. Carbon dioxide penetrates the concrete, to

react with the pore moisture, forming carbonic acid. This in turn reacts with the alkaline calcium hydroxide in the cement to form calcium carbonate, reducing the pH of the matrix to around 9.4. By reducing the alkalinity of concrete in this way, Carbonation can destroy the concrete's ability to maintain the protective oxide layer on any embedded steel, and so open the way for corrosion.

Chemical attack on Steel - Chlorides : A secondary effect of carbonation involves chloro-aluminates, which are harmless in concrete. However these compounds are stable only at high pH levels, so carbonation, in reducing the alkalinity of the concrete, also causes the breakdown of chloro-aluminates, releasing chloride ions.

Free chlorides increase the electrical conductivity of moisture present in the carbonated concrete, and by chemical reaction promote depassivation of the steel. In doing so, they create both of the conditions with which the engineer is concerned -conductive concrete, and good electrical contact between concrete and steel. The chlorides thus take an active part in both destroying the protective properties of the concrete, and in the corrosion process itself.

Other Chemicals : Airborne sulfates, or 'acid rain' can be highly aggressive to concrete, and may seriously affect the integrity of structures. Sulfates penetrate concrete in a similar way to carbon dioxide. They react with certain calcium compounds in the cement paste to form gypsum and ettringite. These products weaken the paste structure, and reduce the strength of the cement. This process also is expansive, generating stresses that crack the weakened concrete, creating easier ingress for additional moisture and contaminants. When the steel is reached, the access created for air and moisture almost inevitably induces corrosion. In advanced attack concrete can be reduced to loose rubble.

It is not only airborne contaminants that cause problems, and many substances are aggressive enough to damage concrete. Milk, fruit juices, some brewery products, and a number of oils and animal fats, for example, will attack concrete if regular or untreated spills occur. A booklet by the Portland Cement Association, 'The Effects of Substances on Concrete' [2], gives a comprehensive list, useful for any engineers concerned with transportation or industrial infrastructure.

Alkali-Silicate Reaction (ASR) : ASR is reasonably well understood and documented. It occurs between certain types of silicate aggregate and free alkalis in the concrete. The product of the reaction is a hygroscopic gel that absorbs available moisture to expand, cracking the concrete as it does so. Less often found is Alkali-Carbonate Reaction, (ACR) where carbonate aggregates are involved, but the result is virtually identical, although earlier to develop. The cracks may lead to an early onset of corrosion, for they increase permeability of the concrete, allowing easier access for both oxygen and moisture to the embedded steel.

If all the free alkali or reactive aggregate is used up, the process may halt before visible damage occurs. If repairs are carried out for some other purpose, however, they may re-introduce the exhausted reagent, and so restart the process locally, causing failure of the repair bond. The rate of ASR deterioration will depend on the quantity and reactivity of the reagents, available moisture, and temperature, but severe structural damage can occur in as little as three years. If ACR is the problem, damage usually occurs in less than three years. At the other extreme, ASR can take more than thirty years to create any visible damage. The number of structures affected by ASR or ACR is uncertain, though believed to be considerable. ACR damage is very limited in geographical extent, unlike ASR.

Modern concrete mixes consider potential reactivity, and theoretically avoid the problem in newer structures, but the Strategic Highway Research Program (SHRP) published a note of caution in a recent report [3]. Research from SHRP shows that inadequate curing can lead to ASR. If fresh concrete is left unprotected from sun or warm wind excessive evaporation of water from the surface will occur, causing migration of more water up to the surface. As this also evaporates, alkali build-up occurs that can reach critical levels even with low-alkali cements. This process can also cause concentration of any contaminants or additives in the mix water.

Physical and External Damage

Most literature on the subject of cracking in plain and reinforced concrete considers it in terms of strength and stability, concentrating on drying shrinkage, deflection under load, and structural movement. There is little that addresses problems of durability caused by cracking. Some standards have been set for assessment of crack sizes, and for reporting on crack patterns, distribution, etc.[4] but in general they deal with large, visible cracks. There is little information available on micro-scale cracking.

Cracking and Permeability : Fine, micro-scale cracking, or micro-fissuring is often almost invisible. In the Author's experience, engineers have often discounted micro-fissuring as being of no significance to structural stability. Whilst this may be true for stability in the short term, it is not so when durability is considered. Micro-fissuring can often be found in heavily loaded slabs adjacent to support beams, where the slab flexes over the support. It is found in the underside of concrete beams for similar reasons, particularly if there are heavy cyclic loads. It is also caused by the early stages of sulfate attack and ASR.

The long term effects are that the concrete integrity is compromised, and permeability is increased. Thermal stresses from sunlight/shade patterns, or freezing and thawing will aggravate micro-fissuring, facilitating ingress of air and moisture.

Erosion and Surface Stripping : There are processes that will gradually strip away the surface layers of concrete, so progressively reducing the amount of cover protecting the steel. Apart from abrasion by traffic tires on bridge-decks etc, erosion can be caused by air-borne debris and dust, or water-borne particles. Two other important processes cause surface stripping that reduces cover concrete over a period of time, and may eventually expose embedded steel.

Freeze/Thaw Cycle : Moisture in concrete will freeze if the temperature is low enough, and ice occupies more volume than the original water. If the surface layer of concrete is saturated, the expansion forces generated by freezing can be enough to crack the concrete, and the outer layer will flake off as the ice melts. Typically it will only affect a few millimetres of concrete at a time, but the cumulative effects of repeated freeze and thaw cycles will eventually remove significant amounts of concrete.

Where such action is anticipated, its effects can be controlled or eliminated by using air-entrained concrete. In this material small air voids are deliberately created, to provide room for the expansion of any ice.

Cavitation : Structures exposed to fast-flowing turbulent water can be subjected to cavitation. This occurs when small momentary pockets of low pressure or vacuum are created by the turbulence. Bubbles of water vapour form, and collapse again as the flow carries them out of the low pressure area. In collapsing, they create pockets of very high pressure that is capable of pitting the surface of any steel or concrete on which it impinges. The rate of deterioration depends on the water volume and turbulence, but is capable of producing significant damage in periods of months, rather than years.

Electrically induced Corrosion : Most engineers are aware of the principle of cathodic protection, but not as many are aware that it can be a double edged weapon. In practice, a structure can be protected from corrosion by connecting it, via an electrolyte, to a suitable anodic material that will become the corrosion site. Electrical current flows between the now cathodic structure, and the anode. This over-rides any internal electrolytic currents, and forces corrosion to occur outside the structure, at the anode site. The method is often used on marine structures and lock gates etc., where the anode is immersed close to the structure. An 'impressed current' system is where a power supply creates a controlled flow of current between the structure and the anode, allowing the engineer to control the efficiency of the system.

In the great majority of cases, such cathodic protection systems have proven to be a safe and effective way to control corrosion, but care is needed to prevent the creation of any inadvertent cathodic systems. Steel pipeline, for example, is often protected by an impressed current system. If the pipe crosses a highway or other obstacle by bridge, and is not totally insulated from it, the system can leak stray current

that will force the steel in the bridge to become anodic, and corrode. Whilst such occurences are rare, they can cause a significant amount of damage if undetected.

Impressed current systems use direct current (dc), and processes that use large dc currents can leak stray current into the surrounding structures, creating accidental cathodic protection systems. There have been cases where stray current from dc railway systems have damaged nearby structures. Many chemical and industrial plants have suffered similar damage through stray current effects. The corrosion process requires only milliamps of current at low voltages, and such small currents can be very difficult to detect and remedy.

Biological attack : A concern for engineers working with sanitation infrastructure, but also of importance to other structures under some circumstances, is biological damage to concrete and steel. Raw sewage and some animal wastes are naturally aggressive to concrete, but it is less well-known that bacteria can cause significant damage. There are some bacteria, for example, that can digest organic sulfates and produce a waste product rich in hydrogen sulfide (H_2S).

This compound erodes concrete by reacting with calcium hydroxide, weakening the cement paste in much the same way as sulfate attack. The combination of this weakening, allied with abrasion by water and sewage flow over the concrete, can eventually strip it back to expose reinforcing steel. If cast iron pipes are exposed, hydrogen sulfide will directly attack the metal, reacting with it to form iron sulfide.

Interdependence

The aim of these first pages has been to make it clear that corrosion of embedded metal in concrete will eventually cause damage to the concrete. Conversely, any damage to, or deterioration of the concrete can lead to the corrosion of embedded metal. They are interdependent processes, and it is futile to treat the symptoms of decay without first having identified and remedied the cause. Structural and cosmetic repairs often suffer early failure because the cause of the original damage has not been identified and corrected.

The term 'embedded metal' has been deliberately used here to emphasise that the risk of corrosion is not limited only to reinforcing steel. A common source of damage to concrete on bridges is where parapet rails have been added after the main construction, and fixing holes are drilled into the concrete. If ordinary steel anchor bolts are used, and not effectively sealed into the concrete, corrosion will occur. The rusting will eventually burst open the concrete, and the rail will become detached. Similar damage is frequently found on concrete balconies, where the safety rail has been fitted by bolts or cast sockets. Drainpipes, guttering, conduit and their fixings are also common points for corrosion attack.

TEST METHODS

There is now a wide range of methods available to the engineer to determine the true causes of damage, and measure its extent and the rate of progress. These methods can be used to predict the likelihood of corrosion taking place, and identify the areas of a structure most at risk. They can be loosely grouped into two categories :

- Destructive (Coring, sampling, drilling, etc.)
- Non-Destructive (In-situ tests with no damage to the structure or disfigurement of the concrete surface)

Generally speaking, the destructive tests involve testing a sample to failure, and rely on laboratory facilities for full analysis. Non-destructive tests are usually carried out on site, although complete analysis of the test data may be done subsequently at an office or laboratory.

Space does not allow a full description of every method here, but the following is a review of the more commonly used tests with a brief summary of methodology, and information obtained. It should assist in determining which methods would be relevant to a given set of circumstances. There is also a cautionary note about limitations of some methods. If a test is incorrectly applied, ambiguities or measurement errors can occur which may make the test data inconclusive. Though some of the methods described here were developed in Europe, they are all available in the USA through specialist companies.

Destructive Tests

Core sampling : A sample of concrete is core-drilled from the structure, and analyzed by a selected combination of the following laboratory procedures :-

- Visual inspection for aggregate size and type, cracks, voids, depth of surface deterioration, presence of steel.
- Physical measurements for density, moisture content, rate of water absorption, and air permeability. Testing for compressive, tensile, and shear strength, elastic modulus and Poissons ratio.
- Ultrasonic Pulse Velocity (UPV) tests to be correlated with in-situ test results from the rest of the structure. (UPV testing is described in the next section)
- Petrographic (microscopic) examination for mix type and proportions, presence of ASR or sulphate products etc. Accelerated growth test to determine if ASR is active
- Chemical analyses for cement content, presence and depth

of any contaminants, carbonation depth, identify High Alumina Cement (HAC), and measure degree of conversion.

Note : Cores should be kept moist until analysed unless specified otherwise. E.g. sealed in plastic film, or a sample box with water retaining packing such as sawdust.

Drilled samples : Concrete sampled by collecting the dust from a masonry drill can be analysed in a Laboratory for :-

- Percentage cement content and alkalinity .
- Percentage and depth of penetration of contaminants such as chlorides or sulfates.
- High Alumina Cement (HAC) and degree of conversion.

The drill hole can be used to check depth of reinforcing steel, and to carry out carbonation depth tests.

Note : Careful control of drill depth and cleaning of the drill bit and hole between samples is essential when sampling from specific depths. For HAC testing a low speed drill or chisel is used to avoid pre-heating the sample, destroying evidence of HAC conversion.

Steel sampling : Reinforcing steel is exposed by removing cover concrete. This permits visual assessment of corrosion damage, and measurement of residual thickness. Samples of the steel may be taken for laboratory tests to determine steel type, tensile strength, corrosion resistance etc.

Carbonation Depth : Usually carried out with the previous tests. Requires a fresh broken concrete face perpendicular to the outer face. A small chisel is used to flake off the side of a drilled or cored hole. A chemical indicator sprayed onto the test face indicates alkalinity or acidity of the cement by color change. Though not as accurate as laboratory testing, it is a good site guide to the depth of carbonation.

Pull-out test : Determines approximate concrete strength by measuring the force required to pull a set of standard expansion anchors out of standard drilled holes. Provides a good approximation if a large enough number of samples are used, and correlated with crushing tests on a core sample taken from the same area.

Non-destructive Tests (NDT)

Rebound Hammer : Also known as the Schmidt, or the Swiss hammer. It measures the rebound distance of a standard steel projectile, propelled against the concrete with a standard force. A scale on the tool shows the rebound distance as a 'Rebound Number'. This number can be used to check concrete uniformity by comparison of the test data. If calibrated with laboratory tests, it can give an indication of strength.

Note : The actual property of the concrete measured is surface hardness. The comparatively small cross-section of the projectile tip may mean that impact is on a piece of hard aggregate at the surface, whereas a subsequent test may be on softer cement paste between aggregate particles. This creates measurement disparity which can only be resolved by making a large number of tests and averaging the data. Processes that have a surface hardening effect, such as curing membranes or carbonation, may give rise to optimistic strength estimates.

Surface finish, curvature, and presence of water affect the uniformity of the impact, therefore the degree of rebound recorded. The method also assumes a standard velocity for the projectile at impact, but this will be affected by gravity, and friction. A difference will be noted between measurements made by the same instrument, in the vertical and horizontal planes, on the same test piece.

Ultra-sonic Pulse Velocity (UPV) : Two transducers, a transmitter and a receiver, are placed on the test piece. An electronic trigger/timer device measures the transit time of an ultrasonic pulse through material between the transducers.

UPV is calculated from the transit time and measured path length. Since UPV is a function of the modulus and density of the material, it provides comparative data for the assessment of concrete uniformity. Cracks, inclusions, honeycombing, and voids affect transit time by diverting the pulse, or reducing its velocity. UPV can also measure crack depth and direction in some circumstances. Correlation with compressive strength tests on core samples will enable estimates of strength in other parts of a structure cast from the same concrete.

Note : UPV should not be used to estimate the concrete strength without correlation on a laboratory test sample. If repeatability is required for long term monitoring, the UPV transmission path must be precisely duplicated, using fixed, permanent reference points. Accuracy of calculated velocity depends on the accuracy of path length measurement, angle between transducers, and diameter of transducer faces. Most accurate when transducers are on opposite, parallel faces of test piece (direct path). Less accurate on faces at 90° to each other, ie. corners (semi-direct). Least accurate when both transducers are on the same face, (indirect path).

Steel close to, and parallel to the transit path can cause error due to its higher UPV, compared with concrete. Steel extending across a crack can transmit the pulse and 'hide' the crack if the test is made too close to the steel.

Sonic-logging : Can be used to apply the UPV test in many inaccessible areas, underwater etc. Transducers are sealed probes lowered down preplaced access tubes or coreholes. The probe cables are drawn over a special winch, which measures and records the probe depth.

Sonic logging provides a continuous profile of transit

time between the probes as they are withdrawn. Measurement densities of up to two per vertical inch make the method less susceptible to repeatability error caused by normal variation in concrete quality than conventional UPV. It can be used in coreholes extending through the foundation base to assess the quality of the contact between bedrock and the foundation.

Mechanical Impedance : The test point is struck with a small hammer containing a load-cell (force). The response is monitored by geophone (velocity). The transducer signals are captured by a data acquisition system, and processed by PC computer. In the frequency domain, velocity is divided by force to give the transfer function, or mechanical impedance response graph, providing information on dynamic stiffness, structural resonance, concrete quality and integrity.

The method can detect low density or honeycombed concrete micro-cracking or delamination due to deterioration, and loss of support or voids beneath concrete pavements, floors, dam spillway linings and runways. It can be used to assess the bonding of screeds, finishes, tiles, and asphalt overlays on concrete.

Note: Specialist experience is needed for application and and interpretation of the data. Transducers must be used on a clean, sound surface, with no debris or flaking concrete.

Re-bar locator : Several proprietary devices use similar methods to locate and map reinforcing and embedded steel. A sensor coil, generating an electromagnetic field, is passed over the surface of concrete or masonry. Magnetic material entering the field will cause variations in the magnetic flux that can be measured electronically.

From these measurements, the location and orientation of the material can be determined. Some devices enable the size and depth of cover to steel bars to be determined by using spacer shims of known dimensions to increase the distance between the transducer and the reinforcing steel, and then comparing the measurements.

Note : The method uses electro-magnetism to detect the target and can be 'blinded' by magnetic mass (steel beams, columns or plates, magnetic aggregate). It may be unable to discriminate individual bars if re-bar is bundled, or the steel misplaced, and the bars are too close together.

Ground Penetrating Radar (GPR) : GPR systems send pulses of microwave energy through the test piece. Some pulse energy is reflected from the interfaces between different materials, back to the surface, where it is recorded.

The method can be used to determine layer thicknesses if correlation with a known depth sample is made. It can locate embedded conduits and steel too deep for, or not detectable by re-bar locators. In certain circumstances GPR can locate or map the extent of voids or delaminations.

Note: The pulse energy reflected depends on difference in the dielectric constants of the materials at the interface, and bulk conductivity. High conductivity materials dissipate pulse energy as heat. The dielectric constant is the ratio of pulse velocity in air to velocity through the test material.

Conductivity and velocity vary with moisture content and density, therefore radar may not be able to detect interfaces between saturated materials.

Half-cell Potential Test : Typical Half-cell probes may be either a copper electrode in copper sulfate electrolyte, or silver in silver chloride. Half-cells generate a known reference voltage that can be used to assess the electrical potential difference of any point on a concrete structure's reinforcing steel.

Empirical evidence from research and commercial testing has not yet proven any specific voltage at which corrosion will occur, but it has been shown that the likelihood of corrosion is proportional to potential difference. Mapping of 'potential contours' for a structure readily identifies the most 'active' areas, and so provides a focus for other test and evaluation methods. Test results are usually analysed in conjunction with Resistivity test data.

Bulk Resistivity : Resistivity testing measures the bulk resistance of the concrete to the flow of the electrical currents necessary for electrolytic corrosion. An array of two or four electrodes in contact with the concrete surface pass an alternating current using the concrete to complete the electrical circuit. According to the type, the device may use a constant current, and measure voltage loss, or measure the amount of current required to maintain constant voltage.

Resistivity measurements should be correlated with half-cell potential data to determine the likelihood of corrosion activity. Again, the data is empirical, but experience has shown that high resistivity is associated with low corrosion risk and vice-versa.

Note : Electrical resistance of a material is affected by moisture content. In dry conditions, Half-cell or resitivity tests may show no evidence of corrosion risk, even where the process is well advanced. Tests should planned for wet parts of the year, or after thorough wetting of the structure.

Caution must be used when using the methods on structures with post-tensioning tendons. Usually the tendons do not have intimate contact with the concrete. Test results for concrete and reinforcing steel around tendon ducts may not be relevant to the condition of the tendons themselves.

Passive monitoring

If effective repairs are to be made, the engineer must

know if any cracks in the structure are still active as load or climate condition changes, and therefore likely to recur in any repair material at some later date. Much information can be gathered from visual inspection and what are referred to as 'Passive' monitoring methods. These include devices such as tell-tale plates, crack monitoring gages, and other movement measurement instruments.

Visual inspection : A key part of a structural evaluation is the visual inspection. It is used to establish reference points and select sites for other tests. The comparison of test results from apparently sound areas with those from the damaged areas will often provide much useful information in later analysis. Exposure conditions, the prevailing weather patterns and construction details such as overhangs, ledges and joints are all considered when analysing test results.

In addition to noting surface anomalies such as spalling, stains, pitting, and effloresence (furry or scaly deposits) crack size should be measured, using a calibrated pocket microscope. Any deposits or gel in the cracks will also be seen with this device.

Tell-tale plates : The simplest crack monitors are thin glass plates glued across the crack. Any crack movement will break the glass. A more sophisticated unit is the Avongard monitor, which consists of two acrylic plates. One is etched with a fine grid pattern, the other with a simple cross-hair marking. The plates are glued either side of the crack, the cross-hairs overlappping the grid, and centered on it. Any subsequent movement of the sides of the crack can be measured from the position of the cross-hairs on the grid.

Strain gages : These may be electrical or mechanical, and are used to monitor relatively slow movement across or around cracks as load or thermal stresses change. They can therefore provide 'spot' measurements, or record a history of movement over time, when coupled to a suitable data-logging system.

Acoustic Emission : Change in load or temperature induces stresses in a structure that can result in minute movements of the structural material around such anomalies as cracks, voids, or inclusions. These movements generate acoustic noise that can be monitored and recorded. Analysis of the data can characterize each noise source 'signature', by amplitude for a given stress, and frequency content. Once the base-line signature for a point on the structure has been established, changes in the signature, either in frequency content or in amplitude, will indicate a corresponding change in structural condition, such as an increase in crack length.

Settlement : If settlement may have caused cracking, more complex devices, ie. extensometers or inclinometers, may be used to monitor the movement over time, to determine if it is on-going, before an effective repair strategy can be planned.

Recent Developments

There have been significant developments in this field, particularly in the last two to three years. The increasing power and portability of PC type computers has had a profound effect on test methods, increasing speed, data accuracy and reliability, and reducing costs. Data processing methods on modern PC's have greatly increased the information available in the field from techniques such as Sonic Logging, Ground Penetrating Radar, and Mechanical Impedance tests. Data from methods such as Half-cell Potential and Resistivity tests can be presented as simple 'contour' maps of the structure, that show areas of high and low activity with clarity.

Researchers at Cornell University, funded in part by the Strategic Highway Research Program, have developed a simple in-situ test to identify the presence of ASR without the need for core-drilling. [5] The method can provide an important 'early warning' of ASR before visible damage occurs. A number of researchers are also currently evaluating methods for the determination of the chloride content of in-situ concrete.

There are ongoing research and development programs for high-speed pavement condition measurement systems, some of which have shown the capability of locating the cracks and delamination caused by corrosion in bridge decks etc. The methods under investigation include Infra-Red Radiation, Radar, Stress Wave Analysis and Deflection. Several papers were given on the subject at the Transportation Research Board meeting in Washington DC, January 1991. [6]

One of the difficulties facing the engineer in trying to carry out a preliminary inspection on a large structure is that of access. Where parts of the structure are beyond the reach of mobile platforms, and scaffolding is too costly, such surveys are often carried out solely by observation through binoculars. A number of agencies and universities in the USA, England, and France are currently working on the development of robotic devices that can not only carry a video-camera to record surface detail, but also carry out a number of other sampling procedures or non-destructive tests.

CONCLUSION - PLANNING AN INSPECTION PROGRAM

Though not a complete list of methods or capabilities, this paper has presented a brief review of the techniques currently available in the United States to predict and evaluate corrosion damage to concrete, and the reasons for their use. An informed choice of test and inspection methods can make assessments more accurate and economical, and can make maintenance more effective. An article in Hydro-review Journal recently gave some case histories and typical test program combinations for concrete structures.[7]

With an understanding of the causes of deterioration, and

by knowing the capabilities and limitations of the technology available, the engineer can plan an inspection program that will yield a maximum of information. Quality of construction and repairs can be monitored, and scheduling of maintenance needs can be carried out more objectively with information gathered by such programs.

Though the general deterioration of infrastructure is of widespread concern, local circumstances can mean that some structures face unique construction and operational problems, such as composition of locally mined aggregates, impact from marine vessels, or chemically contaminated atmosphere. Having identified the cause and mechanism of deterioration on any particular structure, the engineer is better able to design the rehabilitation works or replacement project specifically to counter the local influences of environmental conditions, materials properties, or unusual operational requirements.

REFERENCES

[1] Schweitzer, P.A."What Every Engineer Should Know about Corrosion," Marcel Dekker Inc. New York and Basel ISBN:0-8247-7755-7

[2] Portland Cement Association "Effects of Substances on Concrete and Guide to Protective Treatments" 5420 Old Orchard Rd, Skokie, IL 60077. Pub.No.IS001.08T, 1989.

[3] Strategic Highway Research Program "Concrete & Structures Progress and Products Update," 818 Connecticut Ave.NW, Ste 400, Washington DC 20006. Published Nov.1989.

[4] American Concrete Institute."Manual of Concrete Practice" 22400 West Seven Mile Road, Detroit MI 48219.

[5] Strategic Highway Research Program, 1991."Handbook for Identification of Alkali-Silica Reactivity in Highway Structures' Pub.No. SHRP-C/FR-91-101. 818 Connecticut Ave.NW, Suite 400, Washington DC 20006

[6] TRB 70th annual meeting, 13-17 January, 1991. Session Nos. 22, 40, 44, 231. National Research Council, Transportation Research Board, 2101 Constitution Avenue, Washington, DC 20418

[7] Hertlein, B.H."Predicting and Prioritizing Maintenance for Concrete Structures," Hydro-Review Journal, June 1991. vol.X, No.3, pp.70-81. HCI Publications, 410 Archibald St. Kansas City MO 64111

Luis A. Maldonado[1], Pedro Castro[1], José H. Marrufo[2], Wilberth González[2] and Alvaro Zapata[2].

BOND LOSS BETWEEN EPOXY AND ALKYD COATED REINFORCEMENT REBARS AND CONCRETE.

REFERENCE: Maldonado, L. A., Castro, P., Marrufo, J. H., Gonzalez, W., and Zapata, A., "Bond Loss Between Epoxy and Alkyd Coated Reinforcement Rebars and Concrete," Corrosion Forms and Control for Infrastructure, ASTM STP 1137, Victor Chaker, Ed., American Society for Testing and Materials, Philadelphia, 1992.

ABSTRACT: Organic coatings are increasingly being used to control corrosion of reinforcing bars but relatively little importance has been given to their effect on the mechanical properties of reinforced concrete elements. This study evaluates the bond loss of coated rebars with respect to uncoated rebars using pull-out tests on 0.15 m x 0.30 m. cylinders and in 0.66 m (length) x 0.15 m (width) x 0.20 m.(height) beams. Three thicknesses of epoxy coatings were tested in both, cylinders and beams. Six thicknesses of alkyd coatings were tested only in cylinders. There were also tests on cylinders and beams with uncoated rebars. Average losses of bond strength for #3 and #4 bar sizes with respect to the uncoated ones were, respectively, 13% and 15% for beams, 25% and 27% for cylinders using epoxy coatings and, 29% and 35% for cylinders using alkyd paints.

KEYWORDS: epoxy coatings, alkyd paints, bond loss, pullout test, flexion test, bond stress, anchorage length.

Premature deterioration of concrete structures due to corrosion is very common in bridge decks, parking garages, building structures and in general, where de-icing salts may occur [1]. In coastal regions the problem is of particular importance because the infrastructure is exposed to salt spray or to sea water during practically all the year. In tropical countries the problem is very complicated, because the corrosion damages are accelerated due to very high temperatures which may reach 40°C in the shade and very high levels of relative humidity, which can range from 100% to 60% depending on the time of day and on the season of the

[1] Research Scientist, Corrosion Group, Centro de Investigación y de Estudios Avanzados, A.P. 73, Cordemex, C.P. 97310 Mérida, Yucatán, México.

[2] Profesional Engineer, Universidad Autónoma de Yucatán, Calle 14 s/n ex-terrenos del Fenix, Mérida, Yucatán, México

year.

Organic coated bars are being used increasingly to provide protection against corrosion. Epoxy coated reinforcing bars are especially recommended for marine environments. Although the performance to date in highway bridge decks has been reported to be successful [2,3], severe corrosion of epoxy-coated rebars has been described in the substructure of four major bridges in the Florida keys after six to ten year of service [4].

The coating aplication is specified by the ASTM Standard Specification for Epoxy-Coated Reinforcing Steel Bars (A775/A775M). Section A1.2 of this specification states that other organic coatings may be used provided they meet the appropiate requirements. Because alkyd paints are cheaper than epoxy, the former are prefered, particularly in the Yucatan, for repairing small houses of private users where no large buildings or companies are involved. In each case, a strong bond between concrete and steel is essential. The ASTM A775/A775M recommends that the mean critical bond for coated bars shall not be less than 80% of the mean strength for uncoated bars. Coating effects which decrease the bond performance might be corrected by anchorage. In Mexico arbitrary criteria are followed of painting rebars and there are no regional studies to investigate the corrosion performance of the applied coating to inform the engineers if there is an effective protection against corrosion or, on the contrary, if the bond between concrete and steel is affected in a critical manner. In any case, the coatings are increasingly being applied by local operators and the scope of this study is to evaluate the loss of adherence when the reinforcing steel is painted.

Previously Treece and Jirsa [5] studied the bond between concrete and coated reinforced steel. They tested 21 beams comparing the bond strength of coated bars with respect to that of uncoated bars. They used spliced bar sizes #6 or #11. In our case #3 and #4 non-spliced bar sizes were used (most common sizes used in dwellings here). Thicknesses of epoxy coatings were the same in both cases. We prepared 9 beams to be tested for each size of bar, three with 0.100 mm coating, three with 0.182mm coating and three without coating.

Mathey and Clifton [6] tested 28 #6 bars embedded in large concrete prisms and subjected them to axial pull out tests. In our case, 11 #3 and 11 #4 bars embedded in short cylinders of concrete were subjected to similar pull out tests. Three thicknesses of epoxy coatings (between 0.100mm and 0.182 mm) were tested. In both, beams and cylinders we used NAPKO 4326 epoxy with 25% thinner (NAPKO 4026).

Previous studies related to the application of alkyd paints to protect the steel were not found in the literature. In this work, 42 cylinders were tested, 21 for each bar size. We used 6 different thicknesses of coatings (between 0.070 mm and 0.232mm) and they were selected on the

basis of their most common use in our region.

EXPERIMENTAL

Material

Portland cement type I was used. Reinforcing steel and the aggregates for the concrete were provided by local factories. The material characteristics were obtained from the suppliers.

Coating Preparation and Application

An alkyd paint from a local producer (REX) was used.

The epoxy paint is based on a vinyl-epoxy primer NAPKO 4161 and a finish layer-NAPKO 4326. The sample surface was cleaned in accordance with the Specification SSPC-SP Near-White Blas Cleaning and after that the samples were suspended with a cord. With the nozzle of an air gun 30 cm away from the samples, the application of the paint was carried out. The application rate was always uniform beginning at the top and ending at the botton of the bars. In order to measure the coating thickness obtained after the paint application, small cylindrical samples (2 cm long) were put on the bars immediatly before they were coated, Fig. 1. The coating thicknesses on the bars were measured with help of these cylindrical samples using a microscope with micrometer.

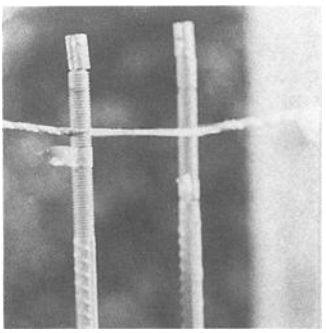

FIG. 1- Sample position during the paint operation.

Preparation and Cure of Samples

Cilinders--The sample preparation was performed using iron molds for standard cylinders. A device was placed on the top of the cylinder in order to maintain the bar on the cylinder axis during the casting operation. The diameter of the cylinder was 15 cm and its length was also 15 cm, e. g.

a length-diameter ratio equal to 1:1. Dimensions like these are recommended by Basant [7], in order to assure adherence failure for the specimens. The length of the bars (70 cm) was selected due to the requirements for the placement of the specimens during the pull out tests on the test machine.

A mixture was designed to obtain a concrete strength of 200 Kg/cm^2. The concrete mixture was prepared in a mixing machine with capacity for 12.5 Kg of cement and the necessary quantity of aggregates and water. A different batch was prepared for each coating thickness. Six specimens were prepared for pull out tests and two for compresion tests. Previous to the casting of the specimens a 5 cm x 5 cm plate was put in the mold bottom, to be used to fix a micrometer during the mechanical tests. After casting the specimens, the concrete length was recorded.

The samples were removed from the molds after 24 hours and cured by immersion in a solution of water and 2% NaCl for 27 days. Immediately after the curing period the specimens were removal from the curing bath, their surfaces were dried and they were prepared for the mechanical tests.

Beams--The preparation of the beams was carried out using wooden molds and two sets of concrete castings. The cure procedure for the beam specimens consisted of wetting them continously for 27 days.

Mechanical Tests

The mechanical tests were performed using a Universal Machine from Forney Testing Machines with a capacity of 180 ton.

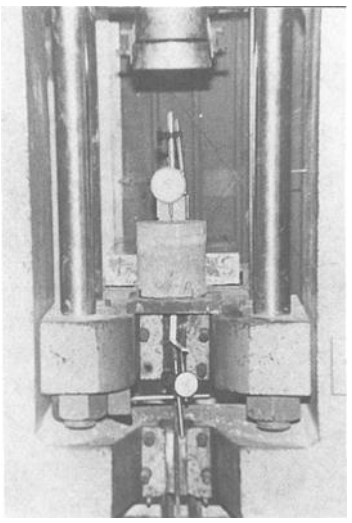

FIG. 2- Experimental arrangement for pull out tests.

Cylinders--For the pull out test the cylinder bases, were leveled with sulphur powder [6]. A square plate with a drilled hole in the center was put on the loaded-end of the specimen in order to get a better distribution of the applied load. Through the hole of the plate a device was fixed to the bar, which was in contact with a micrometer used to measure the bar slips. The specimens were positioned on the test machine at the same time that a micrometer was installed on the free-end of the specimen Fig. 2.

The standard ASTM A775/A775M specifies that the critical bond strength is the smaller of the stress corresponding to a free-end slip of 0.05 mm or to a loaded-end slip of 0.25 mm. Nevertheless, it is important to remark that some authors [8] consider the ultimate bond stress as important as the critical stress, because at least in theory, this is the largest stress that the element can resist.

Initially 100 Kg was applied through the test machine, by this load the micrometers were calibrated to zero and a constant load of 200 Kg per min [9] was then applied. This procedure allowed to take readings from the micrometers for each load increment of 100 Kg.

Beams--Flexure tests were performed only on beams. The test was conducted applying the load to two-thirds of the beam length. A device, shown in Fig. 3, which includes an I-beam and load plates (supports), was used to assure that the applied loads were vertical to the beams, e.g. without eccentricities.

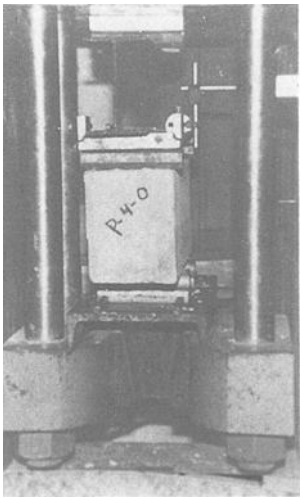

FIG. 3- Experimental arrangement for flexure tests.

After placing the specimen on the test machine a load was applied which was 50% less than the calculated value of the necessary load to produce a specimen failure, followed by load increments of 100 Kg each min. The beam deflections in the center of the beam length, the maximum applied load, the failure type and the crack patterns were recorded.

RESULTS AND DISCUSSION

Cylinders

The cylinders failed by fracturing into 2 or 3 parts. Cases of failure by slipping appeared with more frequency in the cylinders with alkyd coating than in the epoxy coated ones. To evaluate the bond loss during the test, the critical load corresponding to slips of 0.05 mm in the free end of the specimens were used. Tables 1 and 2 show these results.

The average length the cylinders was obtained for each bar size and thickness of coating. This average corresponds to the anchorage length (ld). With these data and the pull out loads the bond stresses, μ were obtained from [8],

$$\mu = \frac{T}{ld\ \Sigma o} \qquad (1)$$

where:

μ = Bond stress, Kg/cm^2,
T = Pull out critical load, Kg,
ld = Anchorage length, cm,
Σo = Summation of Perimeters of the cross-sections of the embedded bars in the cylinder, cm.

The average of the critical bond stresses obtained from three specimens with the same thickness of coating in the steel were corrected by a normalizing factor for the concrete strength, given as

$$fc = [\bar{f'c}/f'c]^2 \qquad (2)$$

where:

fc = Normalizing factor,
$\bar{f'c}$ = Average compression strength of concrete, Kg/cm^2,
f'c = Indiyidual compression strength of concrete, Kg/cm^2.

TABLE 1.- Specimen data and bond loss for alkyd coated reinforcing bars (cylinders).

Bar Num.	coating Thick., μm	ld, cm	load (Crit.), Kg	f'c, Kg/cm^2	μ, Kg/cm^2	B.L., %	B.L. (Corr.), %
	0	15.6	3176	185	68	0	0
	70	15.5	2517	226	54	20	13
	103	15.6	2266	210	48	28	24
3	137	15.5	2333	193	50	26	26
	168	15.6	2266	224	48	28	28
	197	15.6	1467	216	31	54	54
	233	15.8	1500	210	32	53	53
	0	15.7	3500	185	51	0	0
	70	15.6	2600	226	42	27	15
	103	15.5	2133	210	34	40	25
4	137	15.5	2500	193	40	29	30
	168	15.4	2033	224	33	42	42
	197	15.6	2033	216	33	43	43
	233	15.7	1633	210	27	54	54

Table 2.- Specimen data and bond loss for epoxy coated reinforcing bars (cylinders).

Bar Num.	coating Thick., μm	ld, cm	load Kg	f'c, Kg/cm^2	μ, Kg/cm^2	B.L. %
	0	15.3	3176	185	71	0
	100	15.4	2700	193	60	15
3	132	15.2	2276	212	52	25
	182	15.2	2250	226	47	34
	0	15.7	3500	185	52	0
	100	15.6	2466	193	42	19
4	132	15.6	2500	212	39	25
	182	15.2	2250	226	35	33

This factor was used because the concrete strength has a strong influence between the concrete and the steel. As it can be seen in tables 1 and 2, values for f'c varied to some extent.

After correcting for the concrete strength, rebars with the critical bond strength for epoxy, alkyd coated and uncoated samples were calculated and the relative bond loss was evaluated according to

$$B.L. = \left[1 - \frac{EC}{WEC} \right] \times 100 \qquad (3)$$

where:

B.L. = Relative percentage of bond loss, %,
E.C. = Bond stress in bars with epoxy coatings, Kg-cm^2,
W.E.C.= Bond stress in bars without epoxy coatings, Kg-cm^2.

The relative bond loss due to alkyd paints are shown in table 1. It seems in some cases that there is no influence of the coating thicknesses. For example we have coatings of 103 μm and 137 μm with bond loss of 28% and 26% respectively for bars of 9.5 mm (3/8"). However, a careful analysis of the tested specimens made clear that there were two effects not considered in the calculated relative bond stresses. One of these effects is the angle θ that can exist between the cylinder axis and the embedded bar, Fig. 4.

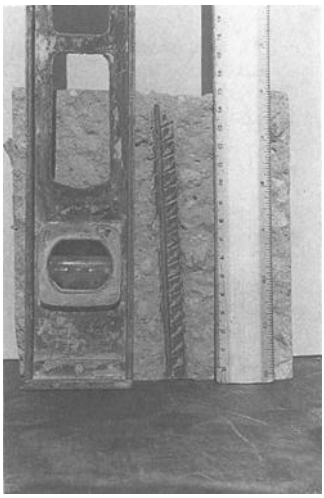

FIG. 4- Eccentricity of bars in concrete cylinders.

This causes the anchorage length (ld) to be increased to a value given by l'd = ld/cosϕ. In other cases it was observed that a bar portion was smooth in the region where the manufacturer placed the trade mark. In these cases the anchorage length was diminished by a factor that could be measured and that in some cases reached up to 25% of ld.

Using the corrected anchorage length in eq.1, in the cases where the described effects were observed, the data in table 1 were reevaluated. The bond loss versus alkyd coating thickness for #3 and #4 bars are given in Fig. 5 and 6. The straigth lines fitted to the experimental points by the least square method are:

$$B.L. = 0.21x - 1.24 \quad \text{for \#3 bars} \tag{4}$$
$$B.L. = 0.23x - 0.61 \quad \text{for \#4 bars} \tag{5}$$

where:

B.L. = Percentage of relative bond loss, %,
X = Coating thickness, μm.

the relation 4 has a correlation coefficient of r=0.97, while the correlation coefficient for the relation 5 is r=0.95

It can be observed that the relative bond losses were less than 20% for thicknesses up to 100 μm and 85 μm for bars #3 and # 4, respectively. According to ASTM A 775/A 775M anchorage corrections are not necessary for these coating thicknesses, while for large coating thicknesses, they are necessary.

As can be seen in table 2, the relative bond losses for epoxy coatings increase gradually as the thickness increases. This tendency is repeated in both bar sizes. Fig. 7 and 8 show a linear regression for the #3 and #4 bars respectively. The straight line obtained by the least square method are:

$$B.L. = 0.19x - 0.99 \quad \text{for \#3 bars} \tag{6}$$
$$B.L. = 0.18x + 0.33 \quad \text{for \#4 bars} \tag{7}$$

The coeficient of correlation in both cases is 0.99. These data suggest a linear dependence for the bond losses as a function of coating thickness. However, the quantity of the studied specimens was relatively small and it will be necessary to study more coating thicknesses to revalidate equations 6 and 7. We believe that the bar becomes more "smooth" as the thickness of the coating is increased and the bond loss will tend to 100%. This tendency can not be verified from the data in tables 1 and 2.

As can be seen, the relative bond losses are practically independent of the bar sizes. This observation agrees with the results of Treece and Jirsa [5]. Using this fact a general average of 34% is obtained for the bond loss for the bar sizes taken together. It is necessary for these cases, to multiply the anchorage length by the factor fo

where

$$fo = \frac{1}{\% \text{ B.L.}} \tag{8}$$

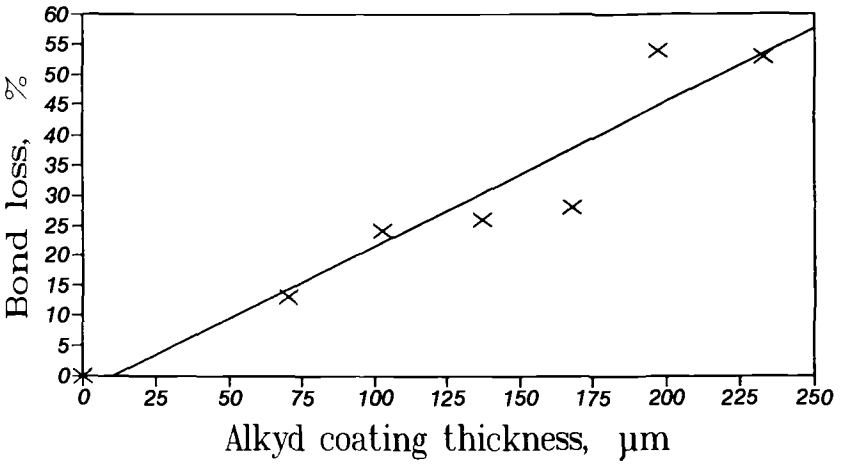

FIG. 5 - Bond loss versus alkyd coating thickness for # 3 bars.

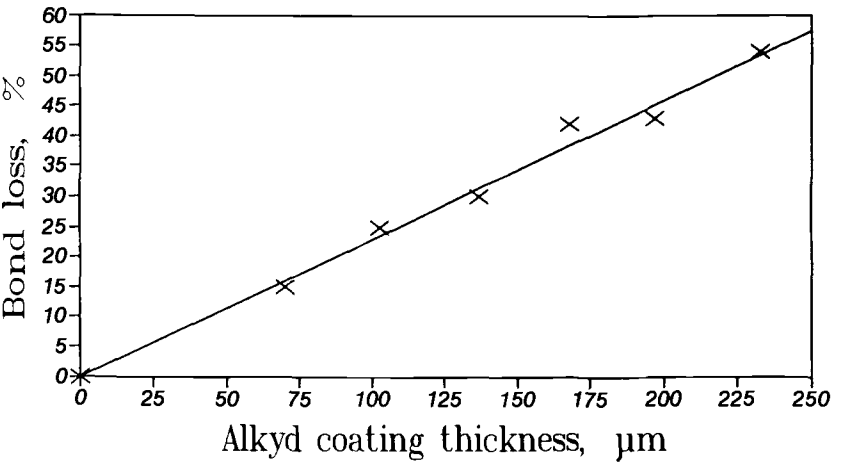

FIG. 6 - Bond loss versus alkyd coating thickness for # 4 bars.

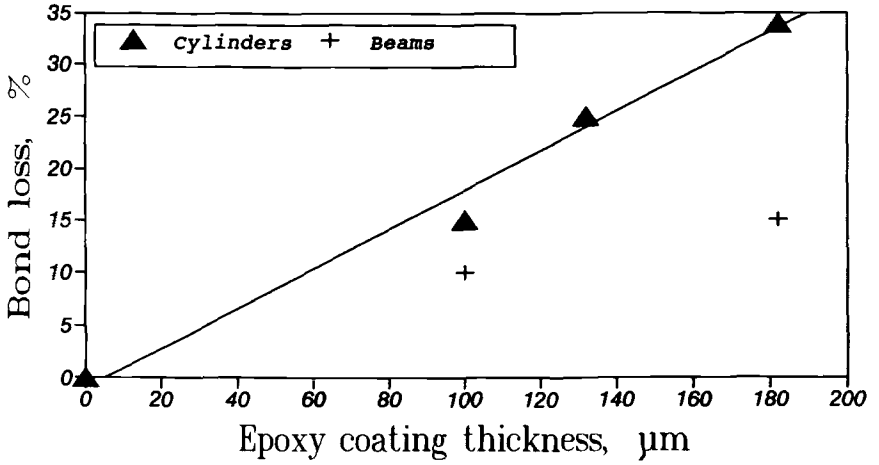

FIG. 7 - Bond loss versus epoxy coating thickness for # 3 bars. Fitting was done only for cylinders.

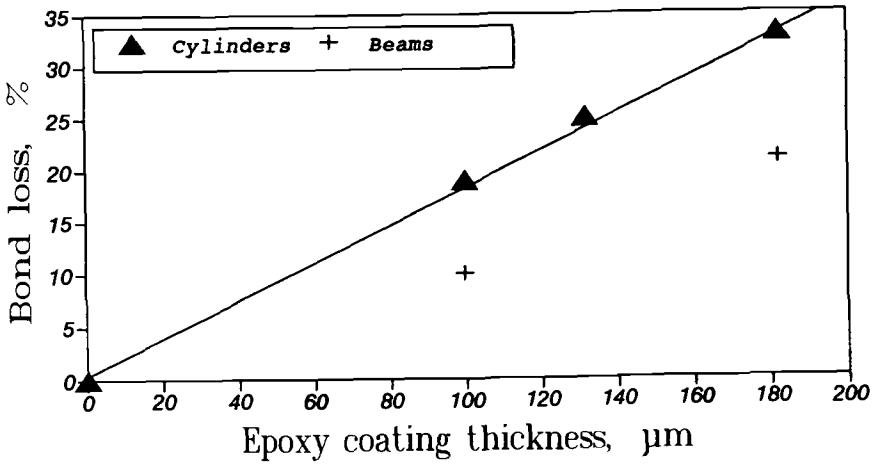

FIG. 8 - Bond loss versus epoxy coating thickness for # 4 bars. Fitting was done only for cylinders.

Beams (Flexure test)

Eighteen flexure tests were made in beams and the epoxy coating thicknesses were 100 μm and 182 μm for each bar size. The theoretical stress μ_t that the beams should resist was calculated by [8,10]

$$\mu_t = \frac{Mu}{Z1d\Sigma o} \tag{9}$$

In the equation (9) Z is the length of the torque that forms the components of the tension and compression forces acting on the beam.

and

Mu = Ultimate theoretical moment, Kg-cm,
b = Average beam width, cm,
d^2 = Beam cross-section where reinforcing bars are embedded, cm2,
W = Reinforcement index (Rebar cross-section to Beam cross-section ratio).

The bond stress μ_t for the tested beams was obtained using equation (1). The average bond stress from the three specimens studied with the same thickness of coating on the rebars was corrected by a normalizing factor for the concrete strength through equation (2). Then the bond efficiency (B.E.) was calculated from

$$B.E. = \frac{\mu \text{ (test)}}{\mu_t \text{ (theorical}} \tag{10}$$

Finally, the relative percentage of bond loss (B.L.) of the beams can be defined as

$$B.L. = \left(1 - \frac{B.Ec.}{B.Ew.}\right) \times 100 \tag{11}$$

where

B.Ec. = bond efficiency of beams with coated rebars.
B.Ew. = bond efficiency of beams with uncoated rebars.

The resulting relative bond losses for the beams are given in table 3.

Figs. 7 and 8 show the experimental points for beams. Because we have only investigated two coating thicknesses, it was not possible to verify if there is any correlation between the coating thicknesses and the relative bond losses. It can be seen that, in both cases, the relative bond loss is less than 20%.

Table 3.- Specimen data and relative bond loss for epoxy-coated reinforcing bars (beams).

Bar Num.	coating (Thick.) μm	ld cm	f'c Kg/cm^2	load (Theo.) Kg	load (Exp.) Kg	μ_T (Theo.) Kg/cm^2	μ B.L. (Exp.) Kg/cm^2	%
	0	22	167	4125	5000	43	53	-
3	100	22	167	4220	4333	43	47	10
	182	22	167	4304	3966	44	45	15
	0	22	167	7328	5866	56	45	-
4	100	22	167	7439	4850	56	40	10
	182	22	167	7338	4200	56	36	21

CONCLUSIONS

Average bond losses for #3 and #4 bar sizes with respect to the uncoated ones were, respectively, 13% and 16% for beams, 25% and 26% for cylinders using epoxy coatings and 33% and 35% for cylinders using alkyd paints.

The relative bond losses for alkyd and epoxy coated rebars in cylinders are a linear function of the coating thicknesses.

REFERENCES

[1] Locke, C.E. and Siman, A., "Electrochemistry of Reinforcing Steel in Salt-Contaminated Concrete", in Corrosion of Reinforcing Steel in Concrete, ASTM STP 713 D.E. Tonini and J.M. Gaidis, Eds., American Society for Testing and Materials, 1980, pp. 3-16.

[2] Gustafson, D., "Epoxy Update", Civil Engineering 58, October 1988, pp. 38.

[3] Malasheskie, G., Mauer, D., Mellot, D., Arellano J. "Bridge Deck Protective Systems" Report FHWA-PA-88-001+85-17, Pennsylvania Dept. of Transportation, National Tech. Info. Center, Springfield, VA, July, 1988.

[4] Sagüéz, A.A., Pérez-Durán, H.M. and Powers, R.G. "Corrosion Performance of Epoxy-Coated Reinforcing Steel in Marine Substructure Service", Corrosion, Nov. 1991, pp. 884-893.

[5] Treece, R.A. and Jirsa, J.O. "Bond Strength of Epoxy-Coated Reinforcing Bars". ACI Material Journal, 1989, pp. 162-167.

[6] Mathey, G.R. and Clifton, R.J. "Bond Strength of Epoxy-Coated Reinforcing Bars" in Concrete, Journal of the Structural Division. Proceedings, ASCE, Vol. 102 STI, Jan. 1976, pp. 215-229.

[7] Bazant, P.Z. and Siddik Sener. "Size Effect in Pull out Tests", ACI Materials Journal, Sep/Oct, 1988, pp. 347-351.

[8] Johnston, W., and Zia, P., "Bond Characteristics of Epoxy Coated Reinforcing Bars", Report No. FHWA-NC-82-002, Federal Highway Administration, Washington, D.C., 1982, pp. 163.

[9] Park, R. and Paulay T. Reinforced Concrete Structures, first Ed. 1978 (in Spanish).

[10] Bresler, B. Reinforced Concrete in Engineering, Vol. I, LIMUSA, México, 1981 (in Spanish).

Gareth John, Bill Leppard & Brian Wyatt.

REPAIR AND CATHODIC PROTECTION OF CORROSION DAMAGED REINFORCED CONCRETE WHARVES IN THE MIDDLE EAST

REFERENCE: John, D.G. Leppard, N.W. & Wyatt, B.S., "REPAIR OF CORROSION DAMAGED REINFORCED CONCRETE WHARVES USING CATHODIC PROTECTION IN THE MIDDLE EAST", Corrosion Forms and Control for Infrastructure, ASTM STP 1137, Victor Chaker, Ed. American Society for Testing and Materials, Philadelphia, 1992.

ABSTRACT: The deep water port of Mina Zayed, Abu Dhabi, was constructed between 1970 and 1978 and consists of pre-cast reinforced concrete beams and slabs with in situ concrete topping, supported by tubular steel piles. The first signs of deterioration were recorded in 1977, evidenced by cracking of the lower corners of the pre-cast beams. A number of detailed inspections were carried out during 1979, 1983, 1985 and 1987, allowing a study of the progressive deterioration to be recorded.

This paper summarises the construction of the port, the deterioration that occurred and the repair/rehabilitation procedure used. An impressed current cathodic protection system incorporating metal oxide coated titanium mesh in a sprayed concrete overlay was used to prevent further deterioration. The system incorporated 83 individual units providing protection to over 11,000 m^2 (121,000 ft^2) of concrete.

A particular problem associated with interference in the polarisation/de-polarisation of the reinforcing steel due to large repaired areas was noted during the repair work and is summarised in this paper.

KEYWORDS: Repair of reinforced concrete, cathodic protection, sprayed concrete, performance criteria.

Dr. D.G. John, CChem, MRSC, FICorr, is Technical Development Manager for CAPCIS Ltd, Bainbridge House, Granby Row, Manchester, M1 2PW, UK. N.W. Leppard, CEng, MICE, is Technical Director, Transportation & Marine Group, Sir Alexander Gibb & Partners, Earley House, London Road, Reading, RG6 1BL, UK. B.S. Wyatt, CEng, MIM, FICorr, is Cathodic Protection Manager, Tarmac Global, Tarmac Structural Repairs, Ward Street, Wolverhampton, WV2 2PJ, UK.

HISTORICAL BACKGROUND

The deep water port of Mina Zayed, Abu Dhabi in the Arabian Gulf coast was designed in 1968 and was planned to be built in phases, with the first phase utilising a dredged channel, serving an existing jetty, whilst the deep water channel was dredged on a new alignment. It was planned that the port would eventually comprise 29 wharves with a berthing face of approximately 6 kilometres. The present layout is shown in Figure 1.

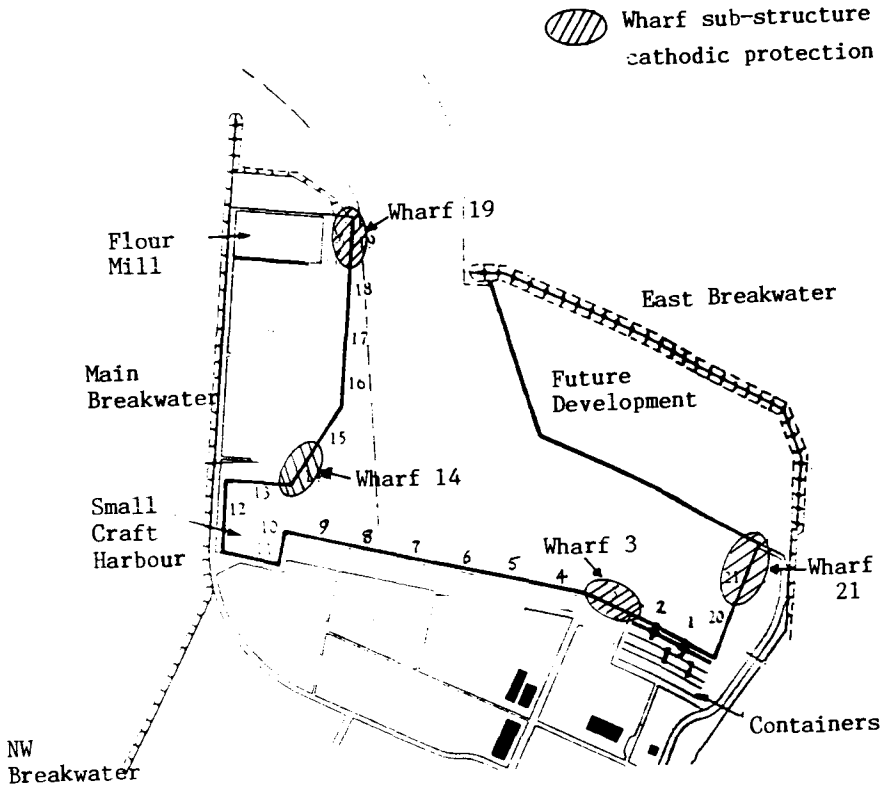

Figure 1. General Layout of Mina Zayed

Construction started in 1971 and continued in phases until 1979. In order to minimise the construction period, it was decided to construct the wharves of pre-cast units supported on tubular steel piles with in situ concrete pile caps. This basic concept was used on all wharves with the exception of 10, 11, 12 and part of 13 which form the shallower small craft basin.

Having driven the tubular steel piles pile caps (which incorporate a pre-cast annular pile muff) were cast onto the piles. The pre-cast beams were then placed on the caps and the slabs on the beams. Additional top steel was then placed in the in situ upper part of the beams. The concrete infill above the pile cap and between the slabs was then placed allowing the slabs to be cast integral with the beams and the beams to become continuous over the pile caps. The space between the annular muffs and the piles was filled with grout. The space between the wharf surfacing and the structural slab was filled with dredged fill. A typical wharf section is shown in Figure 2.

The front of all wharves have a pre-cast vertical coping unit from the deck surface at elevation of +3.66m with respect to Abu Dhabi Chart Datum (ACD) down to +0.5m ACD and this unit supports the tubular rubber fender. To the rear, beneath the wharf structure, there is a sloping rubble bank on wharves 1, 2, 4, 13 to 17, 20 and 21. On wharves 3, 18 and 19, there is a sheet pile retaining wall. On wharves 5 to 9 the natural dredged slope is protected by a sheet pile wall driven behind the cope beam. The North East 26 m of wharf 19 is constructed slightly differently in that the supporting beams (equivalent to beams B2, B4 and B5 in Figure 2), the lower level slabs and the pile caps are all cast in situ.

The soffits of all the supporting beams (except for the North East end of wharf 19) are at an elevation of +2.13m ACD. A study of the tide tables shows that high water level is above the beam soffit for several days during eight months of each year, that is the beam soffits are submerged for short periods regularly. The base of the pile muffs and front coping are below mean low water level and remain immersed on all but a few tides per year. Mean high water level is above the base of all the pile caps and is also above the soffits of the low level beams under Wharf 19, hence these sections of the structure are wetted on the majority of tides.

In summary, the coping units, pile caps and muffs and the low level beams of wharf 19 are all regularly immersed and, given the high relative humidity in the enclosed substructure and the tidal intervals, do not dry out. The beams are cycled through the immersion and draining process regularly while the slabs are only wetted in exceptional circumstances.

During the construction of Mina Zayed, stringent quality control standards were maintained. Particular care was taken with respect to the prevention of chloride contamination in the cement, sand, coarse aggregate and water. Chloride tests were carried out on all aggregates used from early 1974. Typical values for chloride content of fine and coarse aggregates used during the period 1974-78 were between less than 0.01% and 0.02% (expressed as NaCl) by weight of aggregate. In addition, water:cement ratio requirements were maintained to rigorous standard (especially low for the years the wharves were constructed) and were generally kept below 0.45. Finally, a minimum of 60 mm of concrete cover

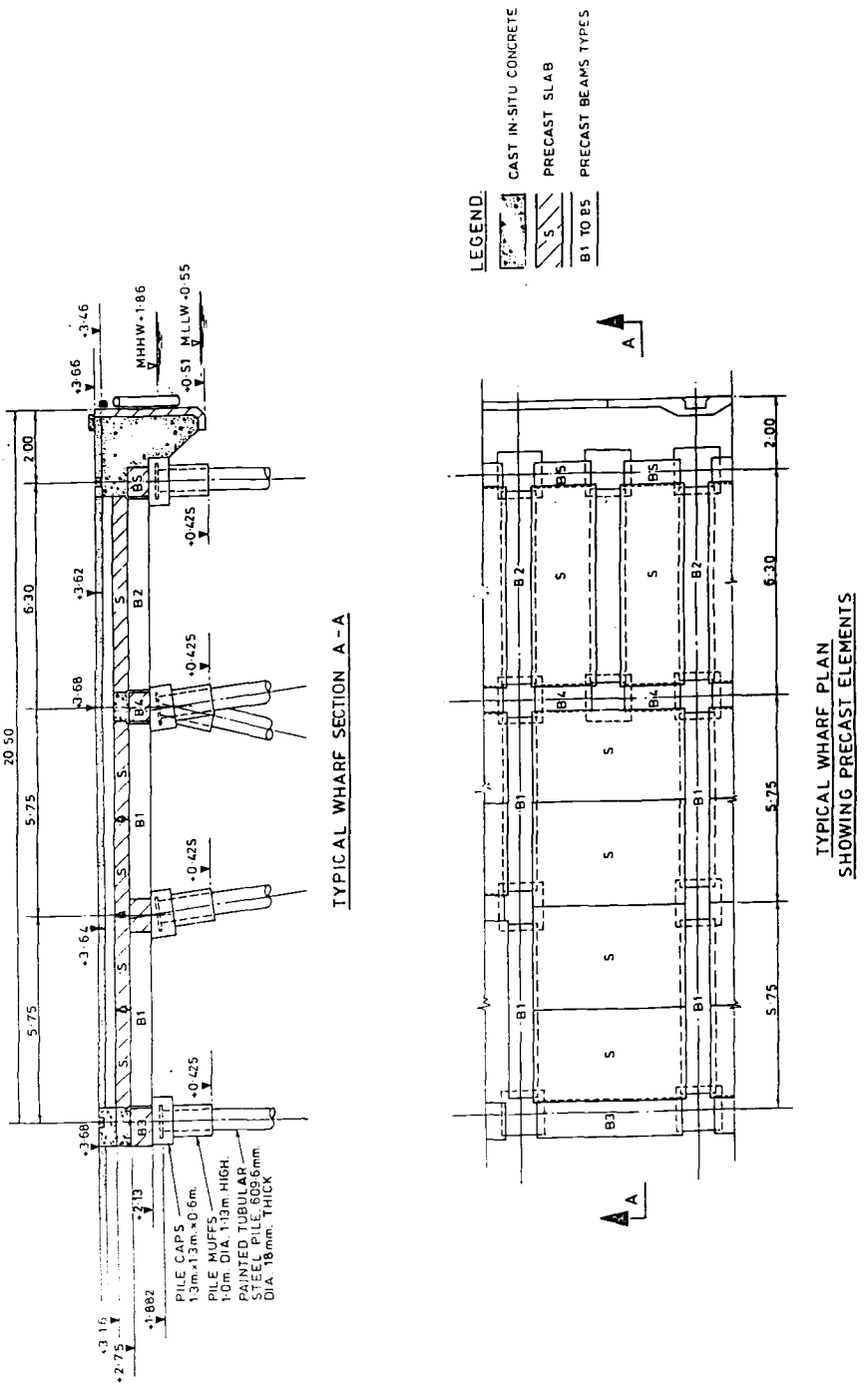

Figure 2. Typical Layout of Wharf

was provided for on all substructure members. This was increased to 80 mm for wharves 1, 2, 3, 20 and 21. However, from the mid 1970's onwards it was apparent that these measures would not necessarily prevent the intrusion of chloride ions into the concrete and to the steel reinforcement surfaces with time.

Unfortunately, the environmental conditions surrounding the port are probably as severe as can be expected anywhere in the world. During the summer months the day time temperature approaches 45°C (114°F) with an atmospheric humidity approaching 100%. Temperatures under the wharf structure appear to remain at a constant 40°C to 43°C (105°F to 110°F) and due to the cope beam preventing effective ventilation the relative humidity remains high all year.

DETERIORATION

The first indication of distress to the pre-cast beams was noticed in 1977. This was evident by cracking of the lower corner of a number of beams under wharf 4. A typical example of such damage is shown in Figure 3.

Detailed inspections were carried out in 1979, 1983, 1985 and 1987. These allowed a clear picture of the progressive rates of the deterioration, since the wharves are of different ages, but all constructed to similar standards. Full details of the result of the inspection have been presented elsewhere [1]. The general results and conclusions from the 1987 survey are summarised below for the different components forming the wharves.

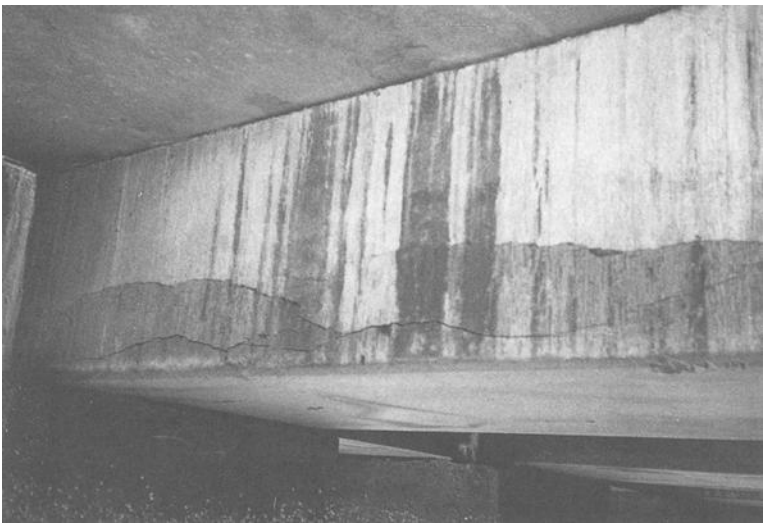

Figure 3. Example of typical damage to lower corner of reinforced concrete beams. Note cracking.

Pre-cast Beams

The main deterioration was to the pre-cast support beams located in the higher tidal range, as shown in Figure 3. The soffit of these beams is located at +2.13m ACD and the lower reinforcing steel all show active corrosion due to chloride ingress. The older the beam, the most severe the corrosion damage. For the newer wharves (1, 2, 3, 20 and 21) only limited cracking and delamination of the beams has occurred. However, for the older wharves (14 to 19 and 4 to 9) the extent of cracking and delamination is severe, with concrete spalling off some beams from the oldest wharves (4 to 9).

The reinforcing steel in the top of the beam is in an essentially chloride free environment (being above the highest high water) and consequently is not corroding. This was confirmed by examination of beams removed from wharf 4 for other works, which show clean, passivated steel at the top of the beam (see Figure 4.)

Figure 4 Pre-cast beam removed after 15 years exposure showing clean, passivated rebar in top portion of beam (left hand side of photograph).

Pile Caps and Pile Muffs

The pile caps and pile muffs are located in the lower tidal range. That is they are almost entirely located below mean water level, as shown by the barnacle line in Figure 5. The high humidity condition under the deck means that the pile caps and pile muffs never dry out. Therefore whilst the reinforcing steel is situated in a very high chloride environment, it is oxygen starved. The result is no corrosion taking place. This was confirmed by visual examination of pile caps and pile muffs removed from wharf 4 as part of other works.

These conditions also relate to the cast in situ beams located at the north east end of wharf 19. These beam soffits are at an elevation of +1.25m ACD and also exhibit no signs of deterioration. Additional inspection carried out during the cathodic protection contract (see below) confirmed these conclusions.

Figure 5. General Condition under wharves (Note barnacle line on pile caps).

Exterior Face of Coping Unit

The concrete forming the coping units, ladders and fender supports of a number of wharves exhibited cracking particularly around the ladder recesses (Figure 6) but also near the slab joints (Figure 7). The cracking did not extend below the level of extensive barnacle growth, i.e. concrete is only distressed in the regions where it is regularly dried by the sun and wind. It was also observed that cracking generally originated from metal inserts, e.g. the cast in sockets for the fender supports, although some of the damage was apparently due to impact on the rubber fenders. The concrete on the facia of newer wharves did not show signs of distress.

In 1989 it was decided to replace the cope facing on wharf 5 in order to re-fender with larger fender units. During this exercise it was discovered that the reinforcement below an elevation of +2.0m ACD showed no signs of deterioration. The concrete and reinforcement was therefore only replaced from +1.7m ACD to +3.66m ACD elevation.

Pre-cast Slab Soffits

Because the slabs generally are located well above the highest high water level, there is no corrosion related damage to any slabs under any of the wharves. However, as part of the detailed inspection carried out during the repair cathodic protection contract under the end of wharf 19,

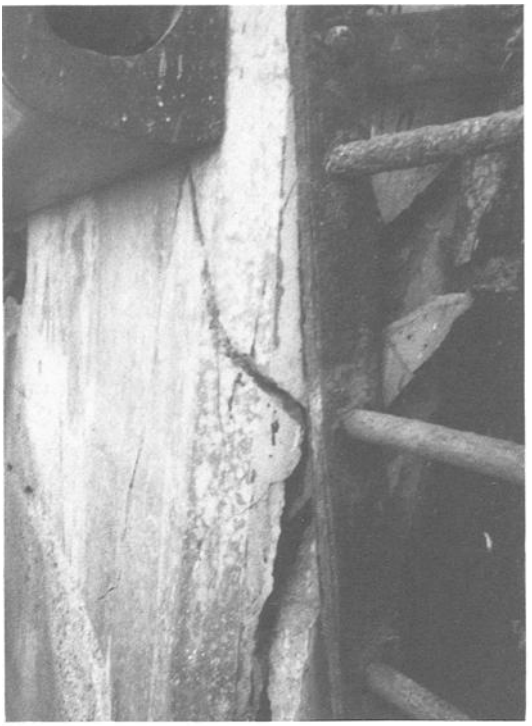

Figure 6.

Cracks formed at Ladder reccess.

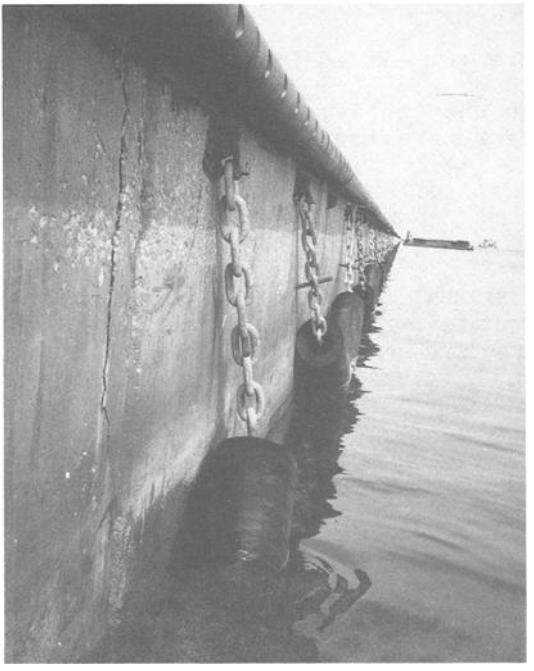

Figure 7.

Cracks formed at edge of Pre-cast cope face.

it was noted that the pre-cast slab soffits in the end bays exhibited significant delaminations. Consequently, a further investigation into the condition of the present slabs under Wharf 19 was carried out during 1989/90.

The results from the 1989/90 investigation gave very high chloride levels were obtained for the slabs at the rear of wharf 19 in bays 1 to 8 and in the front in bays 6 to 15 (bays 1 to 5 have low level in situ slabs between the front pile rows). Potential surveys carried out on the pre-cast slabs gave results in the range -213 mV to -752 mV silver/silver chloride for all slabs tested.

The above results are consistent with wave conditions observed under wharf 19, where the waves at right angles to the berthing face are restrained by the cut off at the end of the wharf. These waves are generated by the wash from pilot and tug boats leaving and entering the port.

RECOMMENDATIONS FOR REPAIR AND PROTECTION

Based on the various investigations it was decided in 1987 to proceed with a contract to repair and cathodically protect the under deck beams on wharves 14, 19, 3 and 21. A further phase to undertake similar works on wharves 1, 2 and 20 is currently under consideration.

The repairs recommended were as follows:

Pre-cast beams with soffits at elevation +2.13m ACD: Repair of all cracked and delaminated concrete by removal of concrete, cleaning of reinforcement and replacement if necessary and replacement of concrete cover with sprayed concrete, and installation of an impressed current cathodic protection system utilising either a conductive polymeric wire or metal oxide coated titanium mesh encased in sprayed concrete.

In situ beams and slabs under Wharf 19: Additional testing to confirm no repair work or cathodic protection required.

Pre-cast Pile Caps, Pile Muffs and Interior Faces of Coping Units: No repair work, impressed current Cathodic protection or concrete surface sealant to be applied.

Exterior Face of Coping Units: Undertake conventional repairs to ladder recesses by breaking out concrete and replacing reinforcement with epoxy coated rebar. The replacement concrete to be coated with a monomeric alkoxy silane. It was considered, at the time, that sprayed concrete repairs would not be durable enough on the cope face.

Pre-cast Slabs: No protection/rehabilitation was required for the majority of pre-cast slabs, with the exception of the slabs at the north eastern ends of Wharves 19 and 21. This is because the slabs of the ends of Wharves 19 and 21 exhibit different exposure conditions. In these cases further testing was required to identify which slabs need application of protective surface sealant (to prevent further ingress of chlorides) and which need repair/rehabilitation.

The repair works for Wharves 14, 19, 3 and 21 were carried out during 1989/91 and are detailed below:

DESCRIPTION OF REPAIR & CATHODIC PROTECTION SYSTEM ADOPTED

General

The rehabilitation system selected for the pre-cast beams under wharves 3, 14, 19 and 21 was designed to incorporate sprayed concrete (gunite) repair to the beams together with metal oxide coated titanium mesh anodes placed on the repaired concrete surface and embedded in a sprayed concrete overlay. The pre-cast slabs above the beams, together with the pile caps & pile muffs below the beams were not included in the system since they were not deteriorating (see above).

For convenience of control, the four wharves were sub-divided into essentially similar units, each unit consisting of the beam forming two bays, see Figure 8. The number of beams forming each unit varied from wharf to wharf. Wharf 3 had three pile rows (hence typically 16 beams), wharf 21 had four pile rows (hence typically 18 beams), whilst wharves 14 & 19 had five pile rows (hence typically 20 beams per unit). The number of units in each wharf were 20 for wharf 3, 19 for wharf 14, 18 for wharf 9 and 26 for wharf 21. The total concrete surface area being protected was over 11,000 m^2 (121,000 ft^2).

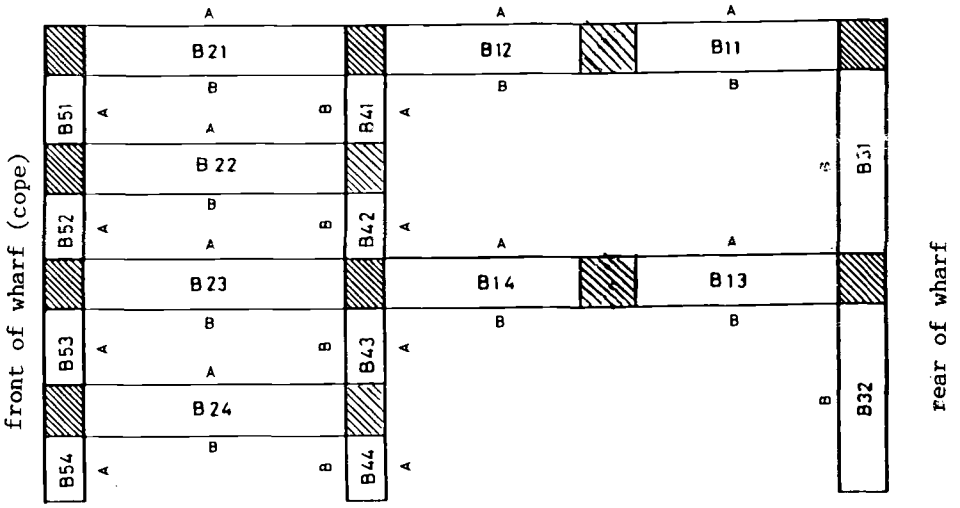

Figure 8. Typical 'unit' for wharf 21. Each unit comprises 2 bays, shaded areas are in-situ concrete over pile caps. Anode mesh was applied to accessible side and soffit surfaces of the beams.

Each unit is powered by independent transformer-recifiers, each rated at 3 amps and 12 volts. Twelve transformer-rectifier units are located in each housing, two each for wharves 3, 14 and 19 and three for wharf 21.

The system is based on a design protection current density of 20 mA/m² for embedded steel to be protected. This included steel in the main beam, plus the additional steel located above the pile caps. It did not include the back, inaccessible steel in beams B3 and B5 (see Figure 2). The maximum current density for the anode was set at 110 mA/m² anode surface.

Up to six test electrodes (graphite) and one reference electrode (double junction silver/silver chloride/potassium chloride) are installed in each unit to allow measurement of polarisation and depolarisation. Independent negative test cables are used to minimise any ohmic effect in measurement. The design called for a 100 mV depolarisation test over 5 to 25 hours. However, problems associated with extensive repairs (see later) led to the performance criteria being modified to allow "instantaneous off" (IR) polarised potentials as an alternative.

To prevent possible problems with current dumping from the soffit anode at high tides a current cut-off "float switch" was incorporated for all wharves. The repair and installation process has been detailed elsewhere [2] and is summarised below.

Preparation of Concrete

Prior to the application of the impressed current cathodic protection system the support beams of the structure were surveyed to locate delaminations in the concrete. Delaminations were removed by mechanical breaking. Electrical continuity provisions for the reinforcing steel were made as described below. All surfaces were then abrasive blast cleaned to expose aggregate and present a suitably roughened surface for subsequent sprayed concrete adhesion, see Figure 9. All loose material was pressure washed from the surface and the beams were pre-wetted in preparation for a sprayed concrete repair or overlay.

Figure 9. Damaged lower corner of beam removed and blast cleaned. Bonding straps installed between beams

Electrical Continuity and Negative Connections

Electrical continuity of bar to bar was found to be inadequate in wharves 14, 19 and partially so in wharf 21. Continuity bars were welded in place to ensure beam to beam continuity, bottom bar to bar continuity and top to bottom bar continuity on all beams of wharves 14 and 19 and part of wharf 21. For the remaining parts of wharf 21 and all of wharf 3 exposed bars were tested for continuity and the small number of these showing bar to bar resistances in excess of 1 ohm had their continuity restored by welded connections.

For each unit four negative power connections were made to the main lower longitudinal steel. The four connections were linked by cable to form a "negative ring main". The two ends of the ring main cable were then terminated at a dc junction box installed above the deck in suitable pits.

For each unit, two further cables were attached to the steel reinforcement in the same manner as the negative power cables, for use as a non-current carrying cable for steel/concrete potential monitoring. These two cables were then terminated at another junction box termed the "reference electrode junction box", also installed above the deck in suitable pits.

Concrete Repairs

The previously delaminated areas were repaired using sprayed concrete (gunite). The surface preparation (as described above) ensured a clean, non-friable, fully saturated surface prior to sprayed concrete repairs. All sprayed concrete "nozzlemen" (the skilled operators with control of water content and direction of placement of the sprayed concrete) were previously subjected to individual approval for work on both soffits and sides of beams to a high standard, as defined by the specification. The repaired areas were cured for 7 days by covering with hessian (jute sack cloth) and repeated wetting, with potable water. Over-spray and laitance were removed by grit blasting and washing the surfaces with potable water to remove any contamination left on the surface of the beams.

Installation of Monitoring Equipment

As noted above, graphite test electrodes and silver/silver chloride/potassium chloride (Ag/AgCl/KCl) electrodes, were installed in the substrate concrete. The reference electrodes were placed in pre-drilled holes, 25 mm dia. x 100 mm deep into the existing concrete and fixed a nominal 10 mm from the reinforcement steel with shrinkage compensated mortar containing 3% chloride by weight of cement added as sodium chloride.

Wherever possible reference electrodes were located at least 0.5 m remote from areas of concrete repair. However, in many beams the amount of corrosion damage and delamination was extensive and made this optimum spacing impossible. The consequences of this are discussed later.

Installation of Anode

The anode material used was the Eltech Systems Corporation Elgard mesh Types 150 and 210. The anode material is expanded titanium coated with a proprietary mixed metal oxide coating. Type 150 provides up to 16.3 mA/m^2 current per concrete surface and Type 210 up to 23.1 mA/m^2 at maximum anode current densities of 110 mA/m^2.

The anode mesh was secured to the beams by means of non-conductive push pins fitted into pre-drilled holes in the concrete thus holding the mesh firmly in place. Type 150 mesh was applied to the sides of beams, wherever possible in a continuous length. Type 210 mesh was applied to all soffits and corners of beams. At some locations of corners and joints more than one layer of Type 210 mesh was applied over the Type 150 mesh already installed on the beam sides, in order to provide adequate cathodic protection current to the greater density of reinforcing steel in these areas.

A positive ring main cable was established within each Unit with 4-6 (dependent on Unit size) separate anode/cable positive connections made using a proprietary design of cable termination which utilised solid round titanium rod spot welded to the conductor strip (see Figure 10).

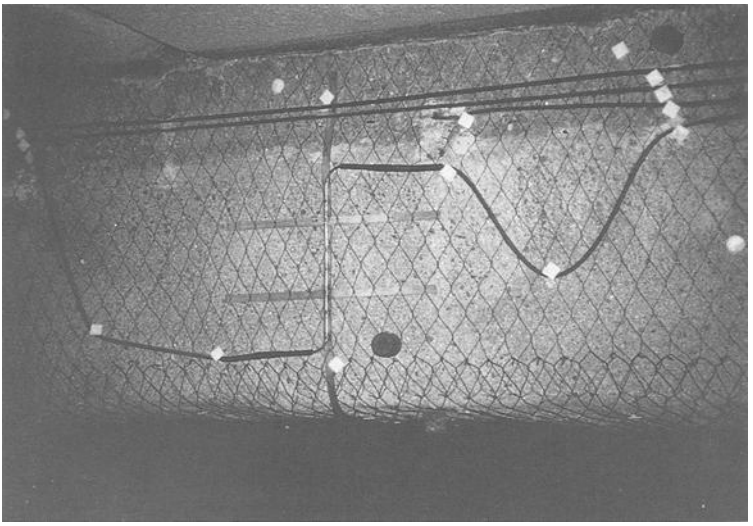

Figure 10. Anode mesh installed with power feed.

Cable Installation

All cables were fixed to the sides of the beams over the anode mesh using the non-metallic push pins as fixings. All cables were spaced at least 25 mm from each other to enable good sprayed concrete application. Ten core instrument cable was run in ducts above the wharf from each Reference Electrode Junction Box on each Unit and connected to the appropriate Test Box located in suitable test pits.

Final Inspection/Approval Before Overlay

After installation of all monitoring equipment, anodes and cables, a detailed inspection of each completed unit was undertaken. This comprised a visual inspection of all installed items, measurements of "natural" steel/concrete potentials using all reference electrodes and continuity/insulation measurements for all power and test cables.

Sprayed Concrete Overlay Material

Upon approval of the installed cathodic protection for each unit from the Resident Engineer, all the beams were coated with a sprayed concrete overlay, incorporating the monitoring equipment, anode and cables, to a nominal overlay thickness of 30 mm, minimum 25 mm. Prior to application of the overlay all surfaces to receive it were saturated with fresh water. The overlay was allowed to cure for 14 days prior to energising the cathodic protection system. The curing period included 7 days under wet hessian. The final system is shown in Figure 11.

Figure 11. Condition of beam after repair and installation of anode in sprayed concrete overlay.

Transformer-Rectifier

Each unit on each wharf is powered from an individually controlled 3 ampere 12 volt transformer-rectifier. These transformer-rectifiers are housed in large transformer-rectifier cabinets, each containing 12 individual units. In order to ensure that reverse current between anode and steel could not occur a proprietary circuit was incorporated into each unit which would detect the fault and disable the output if incorrectly connected.

Data Logging Equipment

A Global Surveyor™ portable data logger was provided for data logging interrogation of transformer-rectifier dc voltage and current outputs and steel/concrete potentials. The data logger drives remote ON/OFF switching circuits of the transformer-rectifier using a trailing cable.

The unit can collect 4 channels of data at the same time and is provided with a manually switchable interface unit to allow interrogation of the maximum 9 channels of data available at the cathodic protection test boxes. The data logger is switchable between 10 and 1000 ohm input impedance and has a data capacity of 256 Kb, sufficient for some 28,000 four channel data sets.

An IBM personal computer-based data management system was provided in order to assist in the compilation and presentation of the commissioning and operating data for the Mina Zayed Protection Systems.

Special Provisions

As a result of the early commissioning work on some units with greater than anticipated concrete repairs, it was considered advisable that additional electrodes and some corrosion coupons should be installed in selected units. This was to enable additional data required for the confirmation of satisfactory performance in the light of the difficulties caused by the extensive concrete repairs as discussed before. The additional electrodes and coupons were placed in selected beams within the various units at locations selected to be; remote from concrete repairs, close to concrete repairs, within concrete repairs.

The additional electrodes in these locations facilitated the easy collection of additional ON, Instant OFF and Potential Decay data from within these three categories within the beams.

Installation Programme

The working conditions under the wharf were very difficult. Access was limited to designated entry points cut through the wharf deck at nominal 30 metre intervals, all access being via temporary access platforms that were submerged for some 10-18 hours/day, and by small boats at low tide. Tidal working dictated as many as three separate working periods in each 24 hour day.

Delamination Surveys

Delamination surveys were undertaken at 1 month, 3 months and in some cases 12 months after completion of the sprayed concrete operations with a final survey some 16 months after commissioning the cathodic protection systems. These surveys detected very limited and isolated delaminations, generally between the primary (repair) and secondary (overlay) sprayed concrete.

The delaminations were corrected with resin injection following surface potential measurements which proved that even at the largest delamination full cathodic protection would be provided to the reinforcement steel behind the resin injected area, due to the current from adjacent areas of anode.

The total extent of all delaminations was under 10 m^2, with the largest individual delamination measuring some 0.5-0.8 m^2 in size. Hence, the delaminations were less than 0.1% of the total area of sprayed concrete.

There was no instance of either new delamination or growth of previously detected delamination at the final delamination survey some 16 months after initial commissioning.

COMMISSIONING & PERFORMANCE OF CATHODIC PROTECTION SYSTEM

Commissioning Procedure

The commissioning procedure essentially followed that advised by the Concrete Society/Institute of Corrosion 'Model Specification' [3] with the as found potentials from the embedded test and reference electrodes being recorded and system energised to produce a potential shift of typically 300mV (measured with current ON, i.e. without IR correction). The extent of polarisation was checked at 7, 10, 21 days before the contract required test of 28 days.

After 28 days energisation the ON and instantaneous OFF (IR corrected) potentials were recorded from all embedded electrodes. The system was powered off and the resulting depolarisation was then determined after 4-5 and 24-25 hours.

The original specification called for either a minimum 100 mV depolarisation after 5 hours or 120 mV depolarisation after 25 hours. For the majority of the test electrodes in the units this was achieved. However, there were a number of test electrodes and units which, in the early period following energisation were not meeting this requirement. Detailed analysis of the results indicated that the extent of depolarisation achieved could be related to the extent of repairs carried out.

Effect of Repairs on Polarisation

In order to determine the cause of the variations in depolarisation from unit to unit, a detailed survey was carried out on a number of beams using surface mounted (portable) reference electrodes (silver/ silver chloride/potassium chloride).

Measurements when carried out on both sides and soffits of selected beams at the location of the embedded test electrode and at other points at beams. Beams were selected based on records of extent of repairs. Also, as mentioned above, in some of the later units additional test electrodes, including macro cell (pick-up) probes were also installed.

The results of the detailed survey clearly confirmed the relationship between extent of repair and polarisation/ depolarisation. Areas which had only limited repair showed good levels of depolarisation (typically 100 mV to 200 mV) of the 5 to 25 hours, whilst areas with large repaired sections often show little depolarisation (typically less than 30 mV) after 5 to 25 hours, but did indicate highly negative instantaneous off potential (typically more negative than -800 mV Ag/AgCl/KCl).

Of specific interest were areas adjacent to large repaired sections. In these cases the potential shift was sometimes negative (i.e. increasing cathodic) on de-energising the system.

The "pick-up" probe results confirmed that repaired areas and areas adjacent to repair were receiving cathodic protection current.

It was concluded that the extent polarisation was influenced by the nature of the repairs, since these often left large areas of reinforcing steel which had had chloride contaminated corrosion product removed and were now located in chloride free concrete. This compared to reinforcing steel in unrepaired, original concrete containing high chloride concentrations.

This resulted in a large macro cell between the reinforcing steel in the repaired area acting as a cathode (oxygen reduction reaction predominating) and the reinforcing steel in the unrepaired/original concrete acting as the anode (iron dissolution reaction predominating) [4]. On application of cathodic protection the macro cell is suppressed and corrosion of the rebar, in the original (unrepaired) concrete, halted. On turning the cathodic protection current off (to obtain depolarisation results) the macro cell switches back on. This had the effect of either the measured depolarisation being very 'sluggish' or, in some cases, being reversed (i.e. potential became more negative).

Revision of Performance Criteria

Based on the detailed results, a revised performance criteria was devised. This stated that satisfactory protection was being afforded to the embedded steel provided that one or more of the following criteria are achieved for each unit.

a) depolarisation of at least 100 mV was achieved after 5 hours, or

b) depolarisation of at least 120 mV is achieved after 25 hours, or

c) an instantaneous off potential of more negative than -750 mV as measured against a Ag/AgCl/KCl surface mounted reference electrode, or

d) an "instantaneous off" potential of more negative than -600 mV as measured against an embedded Ag/AgCl/KCl reference electrode.

CONCLUSIONS

The repair and cathodic protection system installed to the support beams at Mina Zayed have been completely successful. All 83 units throughout wharves 3, 14, 19 and 21 of Mina Zayed are operating consistently and satisfactorily.

The effect of large areas of repairs on the subsequent polarisation/depolarisation can significantly affect the results obtained for both the repaired and non-repaired and interface regions and should be considered in any performance criteria.

The Mina Zayed C49 Cathodic Protection System Contract can be considered one of the most successful large cathodic protection system integrated into a contract for the repair of corrosion damaged reinforced concrete structures, especially when the difficulties of access and working conditions are taken into account. The major key to this success was the extraordinary extent of co-operation that existed between all parties during the work.

ACKNOWLEDGEMENTS

The authors acknowledge with thanks the permission of the Director of Services and Communications, Department of Public Works, Emirate of Abu Dhabi, to publish this paper and the assistance of the Director and his Engineers during the planning and execution of the works.

Furthermore, the authors are indebted to their many colleagues in their respective organisations who have helped throughout the work and especially during the early investigations, design and installation.

REFERENCES

1. LEPPARD, N.W., and JOHN, D.G. "Repair and Cathodic Protection of Reinforced Concrete Substructures to Four Wharves at Mina Zayed, Abu Dhabi, Part I: History, Inspection & Deterioration", paper presented at UK Corrosion '91, Volume 3, Manchester, October 1991, pub. by Institute of Corrosion, Leighton Buzzard, England.

2. WYATT, B.S., SCHOLS, A.J.H, LEPPARD, N.W.. and JOHN, D.G. "Repair & Cathodic Protection of Reinforced Concrete Substructures to Four Wharves at Mina Zayed, Part II: Concrete Repairs & Application of Cathodic Protection System", paper presented at UK Corrosion '91, Volume 3, Manchester, October 1991, pub. by Institute of Corrosion, Leighton Buzzard, England.

3. "Model Specification for Cathodic Protection of Reinforced Concrete", Technical Report TR37, pub. by Concrete Society/ Institute of Corrosion, Wrexham Springs, England, 1990.

4. ANDRADE, C., "Electrochemical Aspects of Repair Methods", paper presented at Structured Improvement Through Corrosion Protection of Reinforced Concrete Conference, June 1992, published by Institute of Corrosion, Leighton Buzzard, England.

SUMMARY

Eugene J. Fasullo, Deputy Director of Engineering and Deputy Chief Engineer of The Port Authority Of New York And New Jersey gave the keynote address entitled "Infrastructure: The Battlefield Of Corrosion." His presentation offered the attendees examples of successful projects using new technology coupled with reasonable risks and support of management. His paper covers the cost of corrosion of infrastructure to the U.S.A. and the reasons for this serious problem. He covered the role of corrosion in the infrastructure arena, the causes of corrosion, prevention methods, and the main causes of rebar corrosion. In his paper he focuses on the major problems in transportation and offers some advanced technology for each segment. While many innovative technologies are available to help infrastructure managers, their acceptance requires a sharing of the financial and technical risks among designers, manufacturers, builders, and government agencies. In his conclusion he challenged the engineering societies, universities, scientists, and constructors to come up with innovative solutions that can benefit future generations.

Robert Baboian, Principal Fellow and Head of the Electrochemical and Corrosion Laboratory at Texas Instruments, Inc. presented a paper entitled "Synergistic Effects Of Acid Deposition And Road Salts On Corrosion". Mr Baboian stated that "the importance of corrosion in our modern, high-tech society can be measured by the magnitude of the direct and indirect problems that result from this degradation process." His paper covers the effect of acid deposition and road salts individually and synergistically. He tabulates in his paper the atmospheric corrosion rates of zinc and iron at various sites. He also compares the corrosion rate of auto bodies when bare steel is used versus galvanized steel. In his conclusion he advises to consider the "real world" environment in solving the most serious infrastructure problems to reach the most economic and safe solutions.

Thomas R. Menzies, Research Associate at the Transportation Research Board, National Research Council presented a paper entitled "National Cost Of Damage To Infrastructure From Highway Deicing." His paper addresses the impact of deicing salt on bridge decks, bridge components, highway components, and parking structures. In the summary of bridge deck costs, he stated that "during the next 10 years, the total cost of protecting newly-constructed decks and restoring currently sound decks that become damaged by salting will be roughly $125 million to $325 million per year." In the summary of other bridge components costs, he mentioned that their repair can be very difficult and expensive. The cost is estimated to be as high as deck costs so the range is between $125 million to $325 million per year. In the summary of impacts on other highway components, the cost is about $100 million per year. As for the parking structures the cost is estimated to be in

the range of $75 million to $175 million per year for the next 10 years.

With the increased use of atmospheric resistant steels, known as weathering steels, for infrastructure, the need for estimating the rate of corrosion penetration at the end of the service life arose. To address this topic Richard H. McCuen et al, Professor, Department of Civil Engineering, University of Maryland, College Park, Maryland presented a paper on "A New Approach To Power Model Regression." Two mathematical formula were given: The upper bound and the log-log fitting of power model. Indices for assessing models are also given. The proposed formula are backed up with data from an atmospheric exposure test. The paper concluded that Goodness-of-fit statistics obtained from the linear model based on logarithms do not reflect the prediction accuracy of the nonlinear model, which is the model used for design. Also, the correlation coefficient as traditionally calculated should only be applied to linear unbiased models, not the power model.

Computer simulation in corrosion control engineering is one of the new tools emerging. Directions for proper use and application is discussed in a paper entitled "A Review Of Computational Simulation Techniques" presented by V. Gensheimer De Giorgi et al, Research Engineer, Mechanics of Material Branch, Naval Research Laboratory, Washington, D.C. The paper outlines the necessary steps for the design of accurate computational simulation. An example is given for the simulation of an impressed current cathodic protection system for the surface of a ship. The paper concluded by emphasizing the need for complete detailed understanding of the corrosion process by the analyst as well as the computational simulation procedure used.

The next paper was by Fred H. Haynie, Consultant, formerly with Atmospheric Research and Exposure Assessment Laboratory, U.S. Environmental Protection Agency, Research Triangle Park, N.C."Evaluation Of An Atmospheric Corrosion Rate Monitor" introduces a tool to measure the rate of corrosion in the atmosphere based on the polarization resistance technique. An atmospheric corrosion rate monitor (ACRM) that could be attached to a point on a structure to measure corrosion rate as a function of time would be a valuable tool for the corrosion engineer to use. The results and responses of the new sensor sere compared with other methods of measuring corrosion such as the mass loss and the time of wetness.
The new sensor can measure the time of wetness in a few hours rather than days. In the conclusion, Mr Haynie mentioned that the experimental work can be turned into a valuable tool by changing some of the hardware and software to measure polarization resistance.

Pedro Albrecht, Professor, Department of Civil Engineering, University of Maryland, College Park, Maryland presented a

paper entitled "Corrosion Control Of Weathering Steel Bridges." The forms of corrosion of bare weathering steel bridges were enumerated, and their effects on bridge performance were discussed. Numerous examples are cited in the paper to drive the point home.
This paper is a detailed description of the types of weathering steels and includes a historical data of their applications and experience results. Mr Albrecht included a method for site analysis to determine the suitability of using weathering steel. Also included in the paper are design details for the enhancement of the material performance. Recommendations for construction, inspection, maintenance, and rehabilitation are added.

Jean-Jacques Hechler, Senior Research Officer and Program Manager at the Industrial Materials Research Institute,National Research Council of Canada, boucherville, Province of Quebec, Canada presented a paper entitled "Wetness Monitoring on the Exterior of Infrastructures." This paper describes the results of a comprehensive study on the effects of the design and orientation on the corrosion of metals on buildings using an existing ASTM time of wetness sensor. In the conclusion Mr Hechler stated that the ASTM sensor for measuring the time of wetness can provide more information besides its original intent. The nature of wetness, the speed of deposition, and drying are some of the important information provided. Thus, it is valuable in studies related to degradation, restoration & design of building material to withstand atmospheric deterioration, corrosion, and weathering.

Corrosion of steel reinforced concrete is the topic of the following paper:"Performance of Rehabilitated\Protected Concrete Bridge Decks" the title of the paper by Khossrow Babaei et al., which compares the results of three protective systems to determine their effectiveness. Latex modified concrete overlay, (LMC), low-Slump dense concrete overlay (LSDC), and a Cathodic protection (CP) were the three systems studied. The results showed that after an average of seven years of service, the LMC and LSDC showed various levels of post-overlay corrosion-induced deterioration. On the other hand, after about five years of service, the CP system showed satisfactory reinforcment of steel.

Electrochemical Impedance is an important technique to determine the rate of corrosion of metals. Advancement in computer science allowed the use of that technique in the field. The next paper, entitled "Utilization of Electrochemical Impedance Techniques to Estimate Corrosion Damage of Steel Infrastructures" was presented by Koji Hamma et al of Nippon Steel Corporation, Japan.
The paper introduces three new sensors: all are using AC impedance method for field application. The first sensor can be used for measuring the corrosion rate of marine steel

structures. The second sensor enables the estimate of corrosion damage of reinforcing bars in concrete. The third sensor can be used for detecting the deterioration of painted steel.

The impact of stray current corrosion can be serious if ignored. The next paper "Improved Rail Fastener Insulation For Stray Current Control" presented by Peter L. Todd of the Bay Area Rapid Transit, Oakland, California, describes the laboratory tests conducted on a prototype rail fastener and the actual field conditions. Effective electrical insulation limits current flow through as well as across the surface of the insulator. A contaminated environment can reduce the resistance of the current path leading to significant stray current corrosion.The conclusion reported that successful simulation of field conditions by the laboratory apparatus can be used as a practical tool for predicting the performance of new rail fasteners. One of the new rail fasteners can reduce the leakage current by a factor of 100,000 , which is very effective.

The integrity of gas and oil pipelines are very important. Corrosion of these pipelines can cause loss of life as well as loss of precious material. They are controlled by empirical and conservative regulations. However, they proved deficient in some cases. The next paper "A Theoretical Analysis For The Residual Strength Of Corroded Gas And Oil Transmission Pipelines" was prepared by Melvin F. Kanninen et al, Program Director, Engineering Mechanics at the Southwest Research Institute, San Antonio, Texas, and Carl H. Poplar, Professor, Department Of Engineering Mechanics, Ohio State University, Columbus, Ohio. This paper used a maximum hoop stress criterion in an axisymmetric approximation of the metal loss to provide a relation for the failure pressure for a pipe with axial direction metal loss. The paper suggests that if the shell bending theory approach is extended to the plane strain case, then it may be the circumferential dimension of the damage that actually governs the failures of corroded pipes. Similar models can be developed and used in addressing corrosion-related problems associated with other infrastructure components.

Underground pipelines constitute a significant segment of the infrastructure. Replacement of such pipes is costly and produces a lot of inconveniences when streets have to be closed for construction. New technology was developed to reconstruct small diameter pipes without excavation. The next paper "The NUPIPE Reconstruction Technology" presented by James B. Hinte of NUPIPE, Inc, Memphis, TN. describes the procedure and necessary equipment to insert a PVC pipe inside existing, deteriorated underground pipes without excavation. The new PVC pipe provides structural support and isolates the effluent from the corroded pipe. The new technology can also be used for lining non-metallic pipes such as concrete. In

conclusion it was stated that the new technology reestablishes the structural integrity of deteriorated systems with a continuous, corrosion resistant pipe that will extend the useful life of the system.

Tools to predict accurately the life expectancy of structures are very valuable. One of the major problems in reinforced concrete infrastructure is the corrosion of steel rebar due to chloride penetration into the concrete. The next paper "Estimating The Life Cycle Of Reinforced Concrete Decks And Marine Piles Using Laboratory Diffusion And Corrosion Data" prepared by Neal S. Berke et al of W.R.Grace & Co, Cambridge, MA. presents the results of a laboratory study showing that chloride ingress into concrete follows Fick's Diffusion equation for properly cured concrete. Several models were presented. One model showed reducing water-to-cement ratio and increasing concrete cover over the steel to reduce the chloride ingress. Another model demonstrated the use of microsilica in the concrete mixture, resulting in drastic reduction of chloride penetration. A third model showed that calcium nitrite initially reduces resistivity and increases rapid chloride permeability values in concrete with silica fume. However, it has no adverse affect on actual concrete permeability and improves the durability of concrete in corrosive environments.

Cyclic conditions are known to cause high corrosion rates. One of these is the tidal zone in marine structures. Thus, it is important to identify the mechanism of corrosion in this zone. The next paper "Investigation Of Rebar Corrosion In Partially Submerged Concrete" was prepared by Miki Funahashi, et al, of Corrpro Companies,Inc.
The paper discusses the results of potentials, total corrosion current, and macro cell corrosion current of steel in concrete in three zones, namely submerged, tidal, and atmospheric. The paper concluded that in chloride contaminated concrete, the rebar was found to be anodic in the submerged zone and cathodic in the atmospheric zone. Moisture content influenced the corrosion rate of a drier concrete and visa versa.

Reinforced concrete and prestressed structures are used widely in infrastructure. Thus, inspection techniques are very important to determine accurately their conditions. The next paper "Recent Developments In Inspection Techniques For Corrosion Damaged Concrete Structures prepared by Gareth John, et al, of CAPCIS Ltd, Manchester, UK and P.A. Gaydecki of UMIST, Manchester, UK. Introduces prototype ultrasonic procedures to determine the condition of prestressed, pretentioned tendons in concrete. The paper also describes the application of electrochemical impedance for estimating the rate of corrosion of reinforcing steel using surface-mounted sensors. The system features iso-potential contour maps of the surveyed surface and corresponding iso-corrosion rate contour maps of the same area. The results of the corrosion rate

survey were in general agreement with the corresponding half-cell survey. As for the ultrasonic procedure, the paper describes a computerized system capable of determining the necessary level of signal and frequency. The paper points out that this technique must be used in addition to other inspection procedures and not as a sole criterion for structural integrity.

Internal corrosion of piping systems in buildings and factories is a major concern. Equipment to indicate the condition of the internal surfaces without dismantling the pipe would be very valuable. The next paper "An Automatic Pipe Corrosion Inspection System" prepared by Mitsuru Shimizu, et al of Obayashi Corporation, Tokyo, Japan, and Masahiro Hamada, et al of Osaka Gas Company, Osaka, Japan describes in detail a new robotics computerized system to perform accurate inspection of the internal surface of the pipe. It utilizes ultrasonic waves and the state-of-the-art in electronics technology to complete the inspection automatically. The robot, which carries the ultrasonic device, moves on the outside of the pipe and transfers the data collected to a computer. The computer analyzes the data and calculates the pipe thickness distribution, the minimum thickness, the percent of metal loss, and the rate of corrosion of the metal. From this information the remaining life expectancy of the pipe is estimated based on proper theory. This new inspection technique is conducted while the pipe is operational, which is a real advantage in minimizing the down time for any operation without compromising the safety of a building in case of sprinkler pipes. The data collected gives a clear cross-section of the pipe on a 360 degree basis, not a one-spot measurement. The results of the new system were verified and deemed successful.

Sewer pipes are an important segment of the infrastructure. Reinforced concrete pipe is used frequently for this application. The next paper "Prediction And Control Of Sulfide Induced Corrosion In Concrete Sewer Infrastructure And Rehabilitation Techniques" presented by Jey K. Jeyapalan, Engineer Consultant, Redmond, Wa.describes the chemical behavior of sulfides and the conditions necessary for hydrogen sulfide corrosion to occur. It also gives a formula to calculate the corrosion rate based on the amount of generated sulfuric acid and the alkalinity of concrete.The paper recommends steps to control corrosion and rehabilitation methods for existing pipes with this problem. In the summary, recommendations are made for more research on the various physico-chemical phenomena involved in concrete corrosion due to sulfide buildup. Advice is also offered to the design engineers to consider the impact of that problem during the design phase.

Oil refineries use frequently reinforced concrete structures. The environment of these refineries is very corrosive. The

next paper "Corrosion Related Deterioration Of Reinforced Concrete Structures At Oil Refineries In The Persian Gulf Region" prepared by Vladimir Novokshchenov, Consultant, Gibsonia, Pennsylvania includes several case histories of corrosion failures of reinforced concrete structures in an aggressive environment. The single most important cause of rebar corrosion was found to be the presence of chloride ions at the level of the reinforcement. Contaminated aggregates and sea water were used during the mixing of concrete. The conditions were aggravated by the flow of sea water in the concrete system and the moisture condensate contaminated with salt-laden dust. The paper reported the recommended methods for rehabilitation in each situation, which could be used as a guide in similar cases.

One of the most important problems in infrastructure is the corrosion of steel in concrete. Chlorides were identified as the major cause of this problem. Chemical inhibitors are one of the methods generally used for corrosion control. The next paper "Impregnation Of Concrete With Corrosion Inhibitors" was prepared by Neal S. Berke et al of W.R. Grace & Co, Cambridge, Massachusetts, and Richard E. Weyers et al of Virginia Polytechnic and State University, Blacksburg, Virginia reports the results of impregnating chloride contaminated concrete with liquid calcium nitrite an effective corrosion inhibitor. Two different procedures were used: One involved heating a bridge deck to above-boiling point of water, then slowly cooling it to ambient temperature, and impregnating liquid calcium nitrite. The second involved placing calcium nitrite rich latex modified grout in predrilled holes and calcium nitrite rich latex modified concrete to replace removed delaminated concrete. Polarization resistance was used to determined the rate of corrosion of steel. Potential measurements were also collected before and after the process. The preliminary results of the two procedures indicate the successful arrest of corrosion. However, more time is needed to determine the effectiveness over a long period as well as a feasibility study to determine the cost for large structures.

Bridges are a vital element of the infrastructure. Bridge management strategies are based on life cycle cost analyses of viable alternatives. The next paper "Predicting Service Life Of Concrete Bridge Decks Subject To Reinforcement Corrosion" was prepared by Philip D. Cady Professor at Penn State University, University park, Pennsylvania, and Richard E. Weyers, Professor at Virginia Polytechnic Institute and State University, Blacksburg, Virginia and presents a mathematical model to predict the service life of a bridge deck. Two main factors control the model. The first is the time for the concrete ion concentration to reach the corrosion threshold level at the reinforcement locations. The second is the time necessary for the corrosion reaction to produce loss of serviceability. The two factors are controlled by the chloride

diffusion through concrete and the rate of corrosion of the reinforcement steel. The paper concluded that the model proved that the actual bridge deck life is influenced by specific site elements such as climate, traffic, and policies.

Steel Piles are used in the support of many infrastructures. The steel piles are usually driven in a variety of soils. Thus, it is important to have a method to measure the rate of corrosion of piles in situ. The next paper "Measuring The Underground Corrosion of Steel Piling At Turcot Yard, Montreal, Canada - A 14 Year Study" was prepared by Edward Escalante, Metallurgist, National Institute of Standards & Technology, Gaithersburg, Maryland.
This paper gives the results of using electrochemical polarization to measure the rate of corrosion of H steel piles in both disturbed and non disturbed soils. These results were compared with the actual physical measurements of metal loss. The paper concluded that the electrochemical polarization technique is useful even though it overestimates the rate of corrosion. The same technique showed that the corrosion current decreased over the-14-year-period of the test.

Steel reinforced concrete is an important component in infrastructure. Thus, it is essential to understand the causes, the forms, and identify the available techniques to assess the deterioration of concrete. The next paper "Assessing The Role Of Steel Corrosion In The Deterioration Of Concrete In The National Infrastructure: A Review Of The Causes Of Corrosion And Current Diagnostic Techniques" was prepared by Bernard H. Hertlein, Project Scientist, STS Consultants, Ashville, North Carolina explained the different elements of concrete and their sources. It also mentioned that the corrosion products of steel occupy 8 to 10 times its original volume. Thus causing the concrete to crack and expose the steel to air, water, and contaminants leading to increase of the corrosion rate. The paper described the forms of concrete deterioration and its impact on corrosion of imbedded steel. The test methods were subdivided into destructive such as coring, sampling, and drilling and non-destructive such as rebound hammer, ultrasonic pulse velocity, ground-penetrating radar, and half-cell potential. The monitoring systems mentioned included strain gages, acoustic emission, and tell-tale plates.

Epoxy-coated rebars are used to control their corrosion. However, coatings could compromise the bond between concrete and the reinforcement. The next paper "Bond Loss Between Epoxy And Alkyd Coated Reinforcement Rebars And Concrete" prepared by L. Maldonado et al, Research Scientist, Centro de Investigacion Y de Estudios Avanzados, Yucatan, Mexico describes the tests performed to determine the bond strength between epoxy coated rebars and concrete. The study showed that there is considerable loss of bond strength. The bond

losses varied with the different type of coating. On the other hand, they increased linearly with thickness in all cases. In the case of epoxy coating, it was found that the bond losses were independent of the bar size.

Cathodic protection has been used successfully to protect the steel rebar in concrete from corrosion. The next paper "Repair Of Corrosion Damaged Reinforced Concrete Wharves Using Cathodic Protection In The Middle East" was prepared by Gareth John, Technical Development Manager of CAPCIS Ltd, Manchester, UK, and Bill Leppard, Technical Director of Sir Alexander Gibb & Partners, Reading, UK, and Brian Wyatt, Cathodic Protection Manager of Tarmack Global, Tarmack Structural Repairs, Wolverhamptor, UK.
This paper describes the steps taken to investigate the cause of corrosion of the reinforced concrete. Regardless of the tightness of specifications and construction, the high chloride induced environment was the main reason determined. Impressed current cathodic protection system was carefully designed using a mixed metal oxide coated titanium mesh as an anode. Gunite (sprayed concrete) was used as an overlay since the protected structure was made of beams and the site conditions were difficult to select another method. Graphite and silver/silver chloride reference electrodes were embedded in concrete below the anode mesh for potential measurement. The final criteria used to control the system include achieving at least 100 mv depolarization after 5 hours, or at least 120 mv depolarization after 25 hours, or an instantaneous off potential of more negative than 750 mv measured against surface mounted Ag/Agcl/Kcl, or an instantaneous off potential of more negative than 600 mv measured against embedded Ag/Agcl/Kcl.

Victor Chaker,P.E.
Editor & Symposium Chairman
Corrosion Control Engineering
The Port Authority Of NY & NJ
One World Trade Center,
New York, New York.

Author Index

Subject Index

ISBN 0-8031-1432-X